land

Special Issue Reprint

Eco-Sensitive Areas

Ecosystem Services, Protected Lands, and Current Challenges (Second Edition)

Edited by
Shicheng Li, Lanhui Li and Mingjie Song

mdpi.com/journal/land

MDPI

Eco-Sensitive Areas: Ecosystem Services, Protected Lands, and Current Challenges (Second Edition)

Eco-Sensitive Areas: Ecosystem Services, Protected Lands, and Current Challenges (Second Edition)

Guest Editors

Shicheng Li
Lanhui Li
Mingjie Song

MDPI

Basel • Beijing • Wuhan • Barcelona • Belgrade • Novi Sad • Cluj • Manchester

Guest Editors

Shicheng Li
School of Public Administration
China University of Geosciences
Wuhan
China

Lanhui Li
School of Computer and Information Engineering
Xiamen University of Technology
Xiamen
China

Mingjie Song
College of Public Administration
Central China Normal University
Wuhan
China

Editorial Office
MDPI AG
Grosspeteranlage 5
4052 Basel, Switzerland

This is a reprint of the Special Issue, published open access by the journal *Land* (ISSN 2073-445X), freely accessible at: https://www.mdpi.com/journal/land/special_issues/6Q82PUWQZ5.

For citation purposes, cite each article independently as indicated on the article page online and as indicated below:

Lastname, A.A.; Lastname, B.B. Article Title. *Journal Name* **Year**, *Volume Number*, Page Range.

ISBN 978-3-7258-4593-4 (Hbk)
ISBN 978-3-7258-4594-1 (PDF)
https://doi.org/10.3390/books978-3-7258-4594-1

© 2025 by the authors. Articles in this book are Open Access and distributed under the Creative Commons Attribution (CC BY) license. The book as a whole is distributed by MDPI under the terms and conditions of the Creative Commons Attribution-NonCommercial-NoDerivs (CC BY-NC-ND) license (https://creativecommons.org/licenses/by-nc-nd/4.0/).

Contents

About the Editors . . . . . **vii**

Zongmei Li, Wang Man, Jiahui Peng, Yang Wang, Qin Nie, Fengqin Sun and Yutong Huang
Spatiotemporal Variation in Ecological Environmental Quality and Its Response to Different Factors in the Xia-Zhang-Quan Urban Agglomeration over the Past 30 Years
Reprinted from: *Land* **2024**, *13*, 1078, https://doi.org/10.3390/land13071078 . . . . . **1**

Pingping Zhang, Mingjie Song and Qiaoqi Lu
Mapping Ecological Security Patterns Based on Ecosystem Service Valuation in the Qinling-Daba Mountain Area, China: A Multi-Scenario Study for Development and Conservation Tradeoffs
Reprinted from: *Land* **2024**, *13*, 1629, https://doi.org/10.3390/land13101629 . . . . . **24**

Pengtao Wang, Guan Huang, Le Chen, Jing Zhao, Xin Fan, Shang Gao, et al.
Spatio-Temporal Variations of Soil Conservation Service Supply–Demand Balance in the Qinling Mountains, China
Reprinted from: *Land* **2024**, *13*, 1667, https://doi.org/10.3390/land13101667 . . . . . **53**

Zhongqian Zhang, Huanli Pan, Yaqun Liu and Shuangqing Sheng
Ecosystem Services' Response to Land Use Intensity: A Case Study of the Hilly and Gully Region in China's Loess Plateau
Reprinted from: *Land* **2024**, *13*, 2039, https://doi.org/10.3390/land13122039 . . . . . **81**

Lei Wang, Xufeng Mao, Hongyan Yu, Baowei Zhao, Wenjia Tang, Hongyan Li, et al.
Identifying the Key Protection Areas of Alpine Marsh Wetlands in the Qinghai Qilian Mountains, China: An Ecosystem Patterns–Characteristics–Functions Combined Method
Reprinted from: *Land* **2024**, *13*, 2115, https://doi.org/10.3390/land13122115 . . . . . **104**

Yanqing Lang, Heng Chao and Jingyu Xiao
The Relationship Between Carbon Emissions and Ecosystem Services in Guangdong Province, China: The Perspective of Ecological Function Zones
Reprinted from: *Land* **2024**, *13*, 2227, https://doi.org/10.3390/land13122227 . . . . . **123**

Qin Nie, Wang Man, Zongmei Li and Xuewen Wu
From Policy to Practice: Assessing Carbon Storage in Fujian Province Using Patch-Generating Land Use Simulation and Integrated Valuation of Ecosystem Services and Tradeoffs Models
Reprinted from: *Land* **2025**, *14*, 179, https://doi.org/10.3390/land14010179 . . . . . **142**

Fuliang Deng, Wenhui Liu, Wei Liu, Yanxue Xu, Yuanzhuo Sun, Chen Zhang, et al.
Regional Differences in the Impact of Land Use Pattern on Total Phosphorus Concentration in the Yangtze River Basin
Reprinted from: *Land* **2025**, *14*, 210, https://doi.org/10.3390/land14020210 . . . . . **165**

Jia Xiang and Junjun Niu
Ecological Compensation and Comprehensive Zoning of Cultivated Land Based on Ecosystem Service Value and Extended Three-Dimensional Ecological Footprint Model: A Case Study of Shandong Province
Reprinted from: *Land* **2025**, *14*, 316, https://doi.org/10.3390/land14020316 . . . . . **182**

Yuchun Wang, Yufeng Ang, Yingying Zhang, Yunfeng Ruan and Bingyi Wang
Identification of Ecological Functional Areas and Scenario Simulation Analysis of the Wanjiang Urban Belt from a Trade-Off/Synergy Perspective
Reprinted from: *Land* **2025**, *14*, 444, https://doi.org/10.3390/land14030444 . . . . . **216**

Victoria-Eugenia Guáqueta-Solórzano, César Enrique Ortiz-Guerrero and Edna Castañeda Salazar
Do Small Livestock Producers Adapt to Climate Variability? An Approach to the Case of the Upper Fonce River Páramo in Santander, Colombia
Reprinted from: *Land* **2025**, *14*, 1068, https://doi.org/10.3390/land14051068 . . . . . **244**

Mingjie Song, Shicheng Li, Basanta Paudel and Fangjie Pan
A Framework for Multifunctional Green Infrastructure Planning Based on Ecosystem Service Synergy/Trade-Off Analysis: Application in the Qinling–Daba Mountain Area
Reprinted from: *Land* **2025**, *14*, 1287, https://doi.org/10.3390/land14061287 . . . . . **261**

Fangfang Sun, Chengcheng Dong, Longlong Zhao, Jinsong Chen, Li Wang, Ruixia Jiang and Hongzhong Li
Spatiotemporal Variation and Influencing Factors of Ecological Quality in the Guangdong-Hong Kong-Macao Greater Bay Area Based on the Unified Remote Sensing Ecological Index over the Past 30 Years
Reprinted from: *Land* **2025**, *14*, 1117, https://doi.org/10.3390/land14051117 . . . . . **283**

Zhanhao Dang, Baoqing Hu, Chunlian Gao, Shaoqiang Wen, Jinrui Ren and Yunfei Liang
Construction and Optimization of the Ecological Security Pattern of Pinglu Canal Economic Zone Based on the InVEST-Circuit Theory Model
Reprinted from: *Land* **2025**, *14*, 1103, https://doi.org/10.3390/land14051103 . . . . . **307**

About the Editors

Shicheng Li

Shicheng Li, PhD, is an Associate Professor at the School of Public Administration, China University of Geosciences. His research interests include protected area evaluation and planning, ecosystem services, and reconstruction of historical land use/cover change and its ecological effects. He has served as Principal Investigator on various projects, including the National Natural Science Foundation of China, the Second Tibetan Plateau Scientific Expedition and Research Program, and the Project of Humanities and Social Sciences of the Ministry of Education, China. He has published more than 60 peer-reviewed papers, many of which are highly cited papers.

Lanhui Li

Lanhui Li is an Associate Professor at the College of Computer and Information Engineering, Xiamen University of Technology. His research focuses on the combined effects of human activity and climate change on vegetation; remote sensing-based monitoring of rice cropping patterns; and spatial statistical analysis methods, including geographically weighted regression. Within the field of vegetation response to climate change and human activities, his work has yielded significant insights, providing a scientific foundation for global climate change adaptation strategies. He has led research projects funded by the National Natural Science Foundation of China (NSFC) and the Natural Science Foundation of Fujian Province.

Mingjie Song

Mingjie Song is an Associate Professor at the College of Public Administration, Central China Normal University. Her research interests include smart land space governance, land use and ecological protection, and geographic information systems and spatial analysis. She has served as Principal Investigator on projects supported by the National Natural Science Foundation of China, the Hubei Provincial Social Science Fund, and the Mitacs Globlink research program. Her research on ecological protection and poverty alleviation in key ecological function areas has provided scientific insights for ecosystem management and poverty reduction initiatives.

land

MDPI

Article

Spatiotemporal Variation in Ecological Environmental Quality and Its Response to Different Factors in the Xia-Zhang-Quan Urban Agglomeration over the Past 30 Years

Zongmei Li [1,2], Wang Man [1,*], Jiahui Peng [1], Yang Wang [3], Qin Nie [1], Fengqin Sun [1] and Yutong Huang [1]

[1] School of Computer and Information Engineering, Xiamen University of Technology, 600 Ligong Road, Jimiei District, Xiamen 361024, China; lizongmei@xmut.edu.cn (Z.L.); 1913206322@stu.xmut.edu.cn (J.P.); nieqin@xmut.edu.cn (Q.N.); fengqinsun@xmut.edu.cn (F.S.); huangyt@xmut.edu.cn (Y.H.)
[2] Institute of Remote Sensing and Digital Earth, Chinese Academy of Sciences, 9 Dengzhuang South Road, Haidian District, Beijing 100094, China
[3] College of Geography and Planning, Nanning Normal University, 508 Xining Road, Wuming District, Nanning 530100, China; wangy.10b@igsnrr.ac.cn
* Correspondence: manwang@xmut.edu.cn

Abstract: The interactions between economic development, environmental sustainability, population growth, and urbanization are vital in assessing the ecological dynamics of urban agglomerations. This study explores the relationship between economic development, environmental sustainability, population growth, and urbanization within the Xia-Zhang-Quan urban agglomeration in Fujian Province from 1989 to 2022. Utilizing Landsat remote sensing images, we calculated the Remote Sensing Ecological Index (RSEI) to evaluate changes in ecological quality. The results show that the average RSEI values for 1989, 2000, 2010, and 2022 were 0.5829, 0.5607, 0.5827, and 0.6195, respectively, indicating an initial decline followed by a significant increase, culminating in an overall upward trend. The spatial distribution of RSEI classification shows that the study area has the largest proportion of mainly "good" ecological quality. The proportion of areas with "excellent" ecological environmental quality has increased (13.41% in 1989 and 25.12% in 2022), while those with "general" quality has decreased (28.03% in 1989 and 21.21% in 2022). Over the past three decades, Xiamen experienced substantial ecological degradation (RSEI change of −0.0897), Zhangzhou showed marked improvement (RSEI change of 0.0519), and Quanzhou exhibited slight deterioration (RSEI change of −0.0396). Central urban areas typically had poorer ecological conditions but showed signs of improvement, whereas non-central urban regions demonstrated significant environmental enhancement. The factor detector analysis identified land use as the dominant factor influencing ecological environmental quality, with precipitation having a relatively minor impact. Interaction analysis revealed that all other factors demonstrated bi-variable enhancement or nonlinear enhancement, suggesting that the interactive effects of these factors are greater than the effects of individual factors alone. Land use consistently showed solid explanatory power. Temperature also exhibited significant influence in 2022 when interacting with other factors. Due to urban planning that can plan for land use, these findings suggest that effective urban planning can harmonize economic development with ecological protection within the Xia-Zhang-Quan urban agglomeration.

Keywords: remote sensing; central urban area; ecological and environmental protection; geodetector

1. Introduction

The global urbanization rate is projected to increase from 50% in 2009 to 69% by 2050 [1]. Over the past four decades, China has achieved significant milestones in urbanization, mirroring the developmental processes that took Western developed countries over a century to accomplish [2]. This rapid urbanization has been instrumental in driving the country's economic and social progress and remains a critical force for current and future

development [3]. However, traditional urbanization driven by functionalism and growth supremacism has led to extensive and unsustainable expansion, exacting a substantial environmental toll. Issues such as imbalanced development and resource misallocation are prevalent [4]. The ecological environment is a complex system of interaction among society, economy, and nature, forming the bedrock of healthy societal development and regional survival. Ecological challenges now pose significant obstacles to sustainable human development [5]. The rapid economic growth and accelerated urbanization of our country have led to the swift expansion of urban areas and changes in land use patterns. Population growth and climate change exert immense pressure on regional ecosystems, exacerbating ecological issues. Problems such as soil erosion, air pollution, climate change, biodiversity loss, and declining urban livability have intensified the scrutiny of the interplay between urban development and the ecological environment [6]. The ecological environmental quality evaluation involves a qualitative or quantitative assessment of the conditions within a specific ecological system using an objective index system over a defined time and space. This evaluation reflects the impacts of sustainable human development on living environments. Essentially, it explores the relationship between environmental quality and human social behaviors and activities, assessing the suitability of a regional environment for human survival and social development.

Ecological environment assessment methods have evolved significantly, incorporating advanced technologies and interdisciplinary approaches. With the continuous development of Remote Sensing (RS) and Geographic Information System (GIS) technology, the acquisition and collection methods of land surface information are gradually diversified, which provides new means and ideas for carrying out regional ecological environment assessment [7]. Remote sensing techniques form the backbone of modern ecological assessments, providing continuous, large-scale, and high-resolution data. These techniques are often complemented by GIS, which facilitates the integration and spatial analysis of diverse environmental data. In the past 20 years, researchers have used RS and GIS methods to study basin environmental desertification [8], water pollution assessment [9], lake water prediction [10], ecological environment (forest, farmland, garden, etc.) evaluation [11], etc. Research areas, such as Egypt, Italy, Hainan Island, Lianyungang, Hangzhou, etc., have had good results.

Over the past five decades, significant advancements have been achieved in ecological environment assessment. Researchers have developed various indices and models to quantify ecological conditions and monitor environmental changes. The ecological environment index is key in these assessments, serving as the foundation for evaluating ecological environment quality. Selecting appropriate evaluation indices is fundamental to constructing effective index evaluation systems and calculating the ecological environment index. As nations increasingly engage in quantitative and qualitative analyses of ecological environmental quality, various evaluation index systems have emerged and are continuously evolving. In 1969, the National Wildlife Federation of the United States introduced the Environmental Quality Index, which utilized six factors to assess air, water, soil, forest, wildlife, and mineral resources, assigning grades to each environmental category from good to poor. In 1974, the Canadian Ministry of Environment proposed the "Total Environmental Quality Index" [12]. Over the subsequent decades, the selection of evaluation indicators has increasingly embraced comprehensiveness and diversity. In 2006, Marull et al. [13] developed the Land Suitability Index (LSI), while in 2012, Dizdaroglu et al. [14] introduced the Sustainable Urban Ecosystem Assessment Index Model (ASSURE), aimed at evaluating and monitoring the interactions between human activities and urban ecosystems. These innovations reflect the evolution of methods to understand and manage our ecological environments better.

Research on ecological environment quality evaluation indices in China has been significantly influenced by the development of the Eco-Environmental Status Index (EESI). In 2006, the Ministry of Environmental Protection of the People's Republic of China issued the industry standard, "Technical Specifications for Ecological and Environmental Status

Assessment". This standard introduced the EESI, reflecting the overall status of regional ecological environments. Despite its widespread use, Xu (2013) [15] argued that the EESI could not effectively visualize the ecological status of a region. Xu introduced the Remote Sensing Ecological Index (RSEI) to address this limitation in 2013. The RSEI integrates four key indices—greenness, humidity, dryness, and heat—extracted from high spatial resolution images and combines them using principal component analysis. This approach provides a clear spatial distribution of varying regional ecological conditions. It facilitates the study of ecological changes over different periods, thereby overcoming some of the limitations of the EESI. The RSEI's objective and accurate evaluation results have led to its widespread adoption by scholars for assessing ecological environment changes at regional [16], provincial [17], city [18,19], and district scales [20]. Studies have demonstrated the RSEI's effectiveness in capturing spatiotemporal variations in ecological conditions and its responsiveness to natural and anthropogenic influences [21,22]. Numerous studies have undertaken modifications of the Remote Sensing Ecological Index (RSEI) to suit better the specific characteristics of their respective study areas [23–25]. These advancements underscore the RSEI's value in enhancing our understanding and management of ecological environments.

The spatiotemporal variations in ecological environment quality are influenced by a multitude of factors, including land use and land cover changes [26], Digital Elevation Model (DEM) data [19], and the interactions of natural factors such as precipitation and temperature [21]. Methods such as univariate and interaction factor analysis using geographical detectors are primarily employed to analyze these variations. These techniques help explain the spatial heterogeneity in ecological environment quality changes, offering a deeper understanding of the underlying dynamics. Moreover, advancements in remote sensing technology and geospatial analysis have enabled high-resolution monitoring of ecological changes at multiple scales, enhancing our knowledge of urban ecological dynamics.

Despite these advancements, several gaps remain in the current research on ecological environment assessment. One major limitation is the insufficient consideration of socioeconomic factors, which are critical to understanding human–environment interactions and their implications for ecological health. Current research mainly focuses on one city and lacks research on the ecological environment change of urban agglomerations. It is now starting the economic development mode of city clusters in China. In this context, it is worth studying whether the economic development of city clusters will affect the ecological environment. In addition, urban centers are centers of economic growth, and the majority of people live in this area, which plays a vital role in the lives of its residents. So, the central city is highly influenced by human activities for the longest time. In general, its ecological environment should be declining, and it is worth studying whether its ecological environment has become better under urban planning.

The Xia-Zhang-Quan urban agglomeration is located in the rapidly developing urbanization area on the southeast coast of China. The rapid development of the economy and urbanization will impact the ecological environment to a certain extent. Based on the Landsat remote sensing influence and ecological environment index (RSEI), this paper evaluates the ecological environment change of the Xia-Zhang-Quan urban agglomeration and studies the impact of urbanization on the ecological environment change, which is of great significance for the protection of the ecological environment under economic development.

This paper aims to analyze the ecological environment changes in the urban development process in the Xia-Zhang-Quan urban agglomeration. The details are as follows: (1) Using remote sensing images in 1989, 2000, 2010, and 2022, we calculated the RSEI to analyze the ecological environment changes in the Xia-Zhang-Quan urban agglomeration. (2) An analysis of changes in ecological quality in central and non-central urban areas was performed. (3) Using the geographical detector method, this study analyzed the factors influencing the spatial heterogeneity of ecological environment quality. These findings are significant as they provide empirical evidence supporting the notion that targeted

environmental interventions and sustainable urban development practices can lead to measurable ecological benefits.

2. Materials and Methods

2.1. Study Area

The Xia-Zhang-Quan urban agglomeration (Figure 1) is located in Fujian Province, a rapidly urbanizing region in southeast China, often called the "Golden Triangle of Southern Fujian". This area encompasses the cities of Xiamen, Zhangzhou, and Quanzhou, covering approximately 26,000 square kilometers. According to data released by the Bureau of Statistics in March 2023, the permanent population in 2022 was 5.308 million for Xiamen, 5.068 million for Zhangzhou, and 8.879 million for Quanzhou. Additionally, the Fujian government reported that the GDPs for Xiamen, Zhangzhou, and Quanzhou in 2022 were 730.66 billion CNY, 570.66 billion CNY, and 1220.97 billion CNY, respectively, collectively accounting for about 48.22% of the province's GDP. Overall, the Xia-Zhang-Quan urban agglomeration is the most economically developed and densely populated region in Fujian Province.

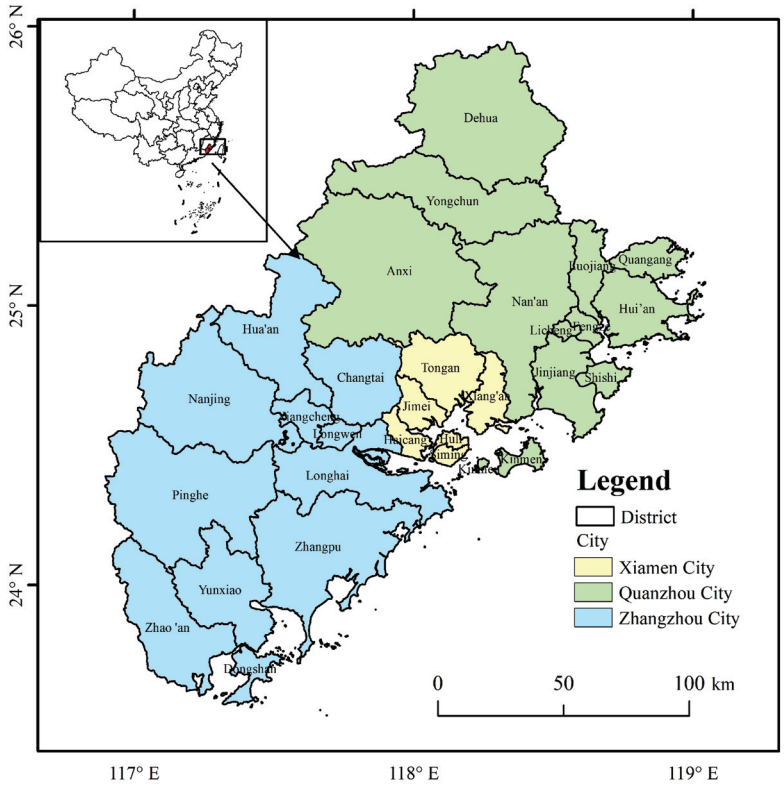

Figure 1. Study area.

2.2. Data

2.2.1. Remote Sensing Images

In this study, remote sensing image data were downloaded from the United States Geological Survey (USGS) website (https://landsatlook.usgs.gov (accessed on 3 January 2023)). We selected four remote sensing images from 1989, 2000, 2010, and 2022 (Table 1). The images contain data from Landsat TM and Landsat OLI/TIRS sensors. All remote sensing data products have been subjected to systematic radiometric and geometric corrections. The spatial resolution of the images is 30 m × 30 m, with a revisit period of 16 days and an imaging swath width of 185 km × 185 km.

Table 1. Information of remote sensing images in the study area.

Path and Row Number		1989	2000	2010	2022
11,9 42	Data	15 June 1989	29 June 2000	6 June 2009	17 May 2022
	Degree of cloud cover	1.00%	4.00%	0.00%	9.23%
119 43	Data	15 June 1989	29 June 2000	6 June 2009	17 May 2022
	Degree of cloud cover	1.00%	6.00%	1.00%	1.68%
119 44	Data	15 June 1989	29 June 2000	6 June 2009	17 May 2022
	Degree of cloud cover	0.00%	2.00%	1.00%	0.41%
120 42	Data	3 June 1988	4 June 2000	3 August 2010	6 April 2022
	Degree of cloud cover	0.00%	7.00%	1.00%	13.08%
120 43	Data	3 June 1988	4 June 2000	3 August 2010	6 April 2022
	Degree of cloud cover	0.00%	8.00%	3.00%	12.53%
120 44	Data	3 June 1988	4 June 2000	3 August 2010	6 April 2022
	Degree of cloud cover	0.00%	3.00%	6.00%	0.20%
Type		Landsat TM	Landsat TM	Landsat TM	Landsat OLI

Since the ecological environment quality is closely related to the amount of vegetation, the surface reflectance data of the growing season of plants should be used for calculation [27]. The images with little or no cloud should also be selected for research as much as possible to reduce the influence of cloud cover on the results. In summary, remote sensing images taken in summer when the cloud cover is below 15% were selected as data sources in this study. Table 1 shows the acquisition time, cloud cover, and data types of remote sensing images in the study area.

2.2.2. Influencing Factors Data

The influencing factors data (Table 2) selected for this study include fractional vegetation cover, climate data (average annual precipitation and average annual temperature), topographic data (DEM), population density, vegetation coverage, and land use data.

Table 2. Influencing factors data source.

Factors Data	Spatial Resolution	Date	Source
Fractional vegetation cover (FVC)	500 m	2000, 2010, 2022	https://data.tpdc.ac.cn/ (accessed on 3 January 2023)
Average annual precipitation (Pre)	1 km	2000, 2010, 2022	https://www.geodata.cn/ (accessed on 20 June 2024)
Average annual temperature (Temp)	1 km	2000, 2010, 2022	https://www.geodata.cn/ (accessed on 20 June 2024)
Population density (LandScan)	1 km	2000, 2010, 2022	https://landscan.ornl.gov/metadata (accessed on 20 June 2024)
Land use data (LUCC)	30 m	2000, 2010, 2022	http://doi.org/10.5281/zenodo.4417809
DEM	30 m	2000	NASA.NIMA (accessed on 3 September 2022) (http://srtm.csi.cgiar.org/srtmdata/) (accessed on 1 January 2020)

2.3. Methods

2.3.1. RSEI Index

In this paper, the remote sensing images of the study area will be used to extract its humidity index (Wet), greenness index (NDVI), heat index (LST) and dryness index (NDBSI), analyze the Ecological Environmental Quality Evaluation Index (RSEI), and quantitatively evaluate the ecological environmental change of the Xiamen-Zhang-Quan urban agglomeration in Fujian Province.

(1) Humidity index

There is a large amount of remote sensing band data information contained in remote sensing images, from which four main component features can be obtained after a tassel-cap transformation of remote sensing images: soil brightness (BI), greenness (GVI), humidity

(wI), and yellowness. The humidity index in this study is represented by the moisture component after the tassel-cap transformation [28]. The formula is as follows:

$$\mathrm{WET_{TM}} = 0.0315\rho_{blue} + 0.2021\rho_{green} + 0.3012\rho_{red} + 0.1594\rho_{nir} - 0.6806\rho_{swir1} - 0.6109\rho_{swir2} \quad (1)$$

$$\mathrm{WET_{OLI}} = 0.1511\rho_{blue} + 0.1973\rho_{green} + 0.3283\rho_{red} + 0.3407\rho_{nir} - 0.7117\rho_{swir1} - 0.4559\rho_{swir2} \quad (2)$$

In Equations (1) and (2), ρ_{blue}, ρ_{green}, ρ_{red}, ρ_{nir}, ρ_{swir1}, ρ_{swir2} represents the blue band, green band, red band, near-red band, mid-infrared band 1, and mid-infrared band 2 of remote sensing images, respectively.

(2) Greenness index

In ecological monitoring work, the normalized vegetation index (NDVI) is the most widely used vegetation index, which is closely related to plant biomass, leaf area index, and vegetation cover and can be used to monitor the growth status of vegetation. Therefore, NDVI was chosen to represent the greenness index [29], and the formula is as follows.

$$\mathrm{NDVI} = \frac{(\rho_{nir} - \rho_{red})}{(\rho_{nir} + \rho_{red})} \quad (3)$$

In Equation (3), ρ_{red} and ρ_{nir} represent the red band and the near-infrared band, respectively.

(3) Heat index

Land surface temperature (LST) is an essential hydrological and meteorological parameter of the earth's surface. Since only the atmospheric transmittance parameter after 2000 is published on the NASA website, this paper simplifies the atmospheric correction method and retrieves the LST [30].

$$\mathrm{LST} = \frac{T}{\left[1 + \left(\frac{\lambda T}{\xi}\right)\right]} - 273 \quad (4)$$

$$\mathrm{T} = \frac{K_2}{\ln \frac{K_1}{L_6} + 1} \quad (5)$$

$$\mathrm{L_6} = gain \times DN + bias \quad (6)$$

$$\varepsilon_{\mathrm{surface}} = 0.9625 + 0.0614F_v - 0.0461{F_v}^2 \quad (7)$$

$$\varepsilon_{\mathrm{building}} = 0.9589 + 0.0860F_v - 0.0671{F_v}^2 \quad (8)$$

$$\mathrm{F_v} = \begin{cases} 0, & NDVI < 0 \\ \frac{NDVI - NDVI_s}{NDVI_v + NDVI_s}, & 0 \le NDVI \le 0.7 \\ 1, & NDVI > 0.7 \end{cases} \quad (9)$$

In Equations (4)–(9), LST is the surface temperature, T is the temperature at the sensor, and L_6 is the thermal infrared band reflectance after radiometric calibration. For the Landsat5 TM sensor, $K_1 = 607.76$ W·m^{-2}·sr^{-1}·μm^{-1} and $K_2 = 1260.56$ K. For the 10th band of the Landsat9 TIRS sensor, $K_1 = 774.89$ W·m^{-2}·sr^{-1}·μm^{-1} and $K_2 = 1321.08$ K. λ is the central wavelength of the thermal infrared band, $\lambda_{TM} = 11.435$ μm, $\lambda_{b10} = 10.900$ μm, $\xi = 1.438 \times 10^{-2}$ m·K, ε is the surface emissivity, $\mathrm{NDVI_v} = 0.7$ represents the NDVI value of the area completely covered by vegetation, and $\mathrm{NDVI_s} = 0$, represents the NDVI value of the area without vegetation.

(4) Index of dryness

The dryness factor is expressed by the dryness index NDBSI. The bare soil index SI and the building index IBI are used to calculate the mean value [23].

$$\mathrm{SI} = \frac{(\rho_{swir1} + \rho_{green}) - (\rho_{nir} + \rho_{blue})}{(\rho_{swir1} + \rho_{red}) + (\rho_{nir} + \rho_{blue})} \tag{10}$$

$$\mathrm{IBI} = \frac{\frac{2\rho_{swir1}}{\rho_{swir1}+\rho_{nir}} - \left(\frac{\rho_{nir}}{\rho_{nir}+\rho_{red}} + \frac{\rho_{green}}{\rho_{green}+\rho_{swir1}}\right)}{\frac{2\rho_{swir1}}{\rho_{swir1}+\rho_{nir}} + \left(\frac{\rho_{nir}}{\rho_{nir}+\rho_{red}} + \frac{\rho_{green}}{\rho_{green}+\rho_{swir1}}\right)} \tag{11}$$

$$\mathrm{NDBSI} = \frac{SI + IBI}{2} \tag{12}$$

$\rho_{blue}, \rho_{green}, \rho_{red}, \rho_{nir}, \rho_{swir1}$ represent the blue band, green band, red band, near-infrared band, and mid-infrared band of remote sensing images.

(5) RSEI index

The four indexes calculated above have different dimensions and units. If it is directly used in the calculation of RSEI index, the weight of each index will be unbalanced. To avoid this situation and also to reduce the differences in remote sensing images caused by different seasons, it is necessary to normalize the original calculation results of the four indicators and unify their range between [0, 1].

$$\mathrm{BI_i} = \frac{b_i - b_{min}}{b_{max} - b_{min}} \tag{13}$$

In Formula (13), $\mathrm{BI_i}$ is the normalized pixel value of an index, $\mathrm{b_i}$ is the original pixel value of the index, and $\mathrm{b_{max}}$ and $\mathrm{b_{min}}$ represent the maximum and minimum value of the index, respectively.

In this study, the principal component analysis (PCA) method was used to calculate the RSEI index, and the four indexes that had been normalized were synthesized into an image, and the first principal component was extracted to calculate $\mathrm{RSEI_0}$.

$$\mathrm{RSEI_0} = \begin{cases} PC1[f(NDVI, WET, LST, NDBSI)] \\ 1 - PC1[f(NDVI, WET, LST, NDBSI)] \end{cases} \tag{14}$$

The RSEI calculated PC1, when RSEI has high values for representing excellent ecological conditions. If the high RSEI values represent ecologically poor conditions and low values represent good ones, the RSEI would be subtracted from one to let higher values represent better ecological status as usually expected [27].

To compare the change in the RSEI index in each period more intuitively, $\mathrm{RSEI_0}$ should be normalized to obtain the final RSEI:

$$\mathrm{RSEI} = \frac{RSEI_0 - RSEI_{0min}}{RSEI_{0max} - RSEI_{0min}} \tag{15}$$

$\mathrm{RSEI_{0max}}$ and $\mathrm{RSEI_{0min}}$ represent the maximum and minimum values of $\mathrm{RSEI_0}$, respectively.

Principal component analysis can eliminate the correlation between indicators and is not affected by indicator units. Also, it can retain the vast majority of information and select a few comprehensive indicators. Therefore, principal component analysis is widely used in many fields, and it is more used in the geoscience field for statistical analysis but less used in comprehensive index construction. In this paper, applying principal component analysis in constructing ecological indicators can weaken the correlation between indicators and better evaluate the ecological environment.

2.3.2. Classification of RSEI Index

In order to better visualize the ecological quality of the Xia-Zhang-Quan urban agglomeration, this study refers to the "Quality Evaluation of Ecological Environment Quality

in China", and divides the normalized RSEI index into five grades at an interval of 0.2. The RSEI index within the range of [0, 0.2] means that the ecological environment quality is "poor". The RSEI index in the range of (0.2, 0.4) means that the ecological environment quality is "worse". The RSEI index in the range of (0.4, 0.6) means that the ecological environment quality is "average". The RSEI index in the range of (0.6, 0.8) means that the ecological environment quality is "good". The RSEI index in the range of (0.8, 1] means that the ecological environment quality is "excellent". A description of each level is as follows:

- Poor: $0 \leq \text{RSEI} \leq 0.2$. Conditions are harsh and not suitable for long-term human survival.
- Worse: $0.2 < \text{RSEI} \leq 0.4$. The vegetation coverage is poor. There is drought and little rain, few species, and obvious factors limit human life.
- General: $0.4 < \text{RSEI} \leq 0.6$. The vegetation coverage is at a medium level, and the biodiversity is at an average level, which is more suitable for human survival. Still, occasionally, some constraints are not suitable for human survival.
- Good: $0.6 < \text{RSEI} \leq 0.8$. The vegetation coverage and biodiversity are good, and it is suitable for human survival.
- Excellent: $0.8 < \text{RSEI} \leq 1.0$. Good vegetation coverage, good biodiversity, and stable ecosystems are most suitable for human survival.

2.3.3. Classification of RSEI Index Changes

To study the ecological environment change of the Xia-Zhang-Quan urban agglomeration, we will refer to the grading table of the ecological environment change degree of the environmental protection standard "Technical Specification for Ecological Environment Condition Evaluation" promulgated by the state and divide the ecological environment change situation into seven levels (Table 3): significantly worse, obviously worse, slightly worse, no obvious change, slightly better, obviously better, and significantly better.

Table 3. Levers of RSEI changes.

Id	Levels	Change in RSEI
1	Significantly worse	<−0.1
2	Obviously worse	−0.1~−0.05
3	Slightly worse	−0.05~−0.02
4	No obvious change	−0.02~0.02
5	Slightly better	0.02~0.05
6	Obviously better	0.05~0.1
7	Significantly better	>0.1

2.3.4. Geographic Detector

(1) Parameter Optimization

To optimize the parameters, the study area's data were divided into a 1 km × 1 km grid, with the data from the center of each grid cell used as the raw data points. Continuous driving factors (vegetation coverage, precipitation, temperature, DEM, and population density) were discretized using several classification methods, including equal intervals, natural breaks, quantiles, geometric intervals, and standard deviation classification. The number of categories ranged from 3 to 8. An optimization model was then employed to select the most suitable classification method and the optimal number of categories [31].

(2) Geodetector

The geodetector [31] consists of factor detector, interaction detector, risk detector, and ecological detector. We chose the factor and interaction detectors to detect the spatial heterogeneity of RSEI. The factor detector is used to analyze the explanatory power of individual factors on ecological environment quality. In contrast, the interaction detector method assesses the combined explanatory power of two factors acting together on ecological environment quality.

1) Factor detector

$$q = 1 - \frac{1}{N\sigma^2}\sum_{h=1}^{L} N_h \sigma_h^2 \tag{16}$$

The q-statistic ranges from 0 to 1, with larger q-values indicating stronger explanatory power. In this method, L represents the stratification of factors. N_h is the number of units corresponding to the ecological environment quality and factors in layer h, and N is the total number of units corresponding to the ecological environment quality and factors across the entire study area. ${\sigma_h}^2$ denotes the variance of ecological environment quality within layer h while σ^2 represents the variance of ecological environment quality for the whole of the study area.

2) Interaction Detector

The interaction detector explores the interactions between different factors, assessing whether the combined effect of two independent variables enhances or diminishes their explanatory power on the dependent variable. It also accounts for cases where the influence of each independent variable on the dependent variable is mutually independent. The interaction effects between factors are detailed in Table 4.

Table 4. Interaction relationship [31].

Interactive Relationship Description	Interactive Relationship
$q(X_1 \cap X_2) < \mathrm{Min}[q(X_1), q(X_2)]$	Nonlinear weakening: Impacts of single variables are nonlinearly weakened by the interaction of two variables.
$\mathrm{Min}[q(X_1), q(X_2)] \leq q(X_1 \cap X_2) \leq \mathrm{Max}[q(X_1), q(X_2)]$	Uni-variable weakening: Impacts of single variables are uni-variable weakened by the interaction.
$\mathrm{Max}[q(X_1), q(X_2)] < q(X_1 \cap X_2) < q(X_1) + q(X_2)$	Bi-variable enhancement: Impacts of single variables are bi-variable enhanced by the interaction.
$q(X_1 \cap X_2) = q(X_1) + q(X_2)$	Independent: Impacts of variables are independent.
$q(X_1 \cap X_2) > q(X_1) + q(X_2)$	Nonlinear-enhance: Impacts of variables are nonlinearly enhanced.

To identify the primary factors influencing spatial differentiation, the study utilized the optimized parameters of the geographical detector (R package). This approach is advantageous as it determines the optimal discretization classification method and the number of classifications. The factors selected for analysis include DEM, land use and land cover (LUCC), fractional vegetation cover (FVC), average annual precipitation (Pre), yearly average temperature (Temp), and population density (LandScan). Data for these factors were derived from a 1 km × 1 km grid, using the center point of each grid cell as the data source.

3. Results

3.1. Rationality of RSEI

The RSEI index is widely used in ecological environmental assessment research, and studies have been conducted in different regions. This paper calculated heat, humidity, dryness, and greenness (Figure 2) from remote sensing images to perform principal component analysis. From four years of principal component analysis (Table 5), the following can be obtained: The contribution rates of the first principal component (PC1) eigenvalues in 1989, 2000, 2010, and 2022 were 75.45%, 70.01%, 78.00%, and 76.58%, respectively, which were greater than 70%, indicating that the first principal component contained most of the information of the four indicators. Therefore, PC1 can replace the original RSEI index, composed of the humidity index, greenness index, dryness index, and heat index. It indicates that the RSEI constructed by PC1 is reasonable.

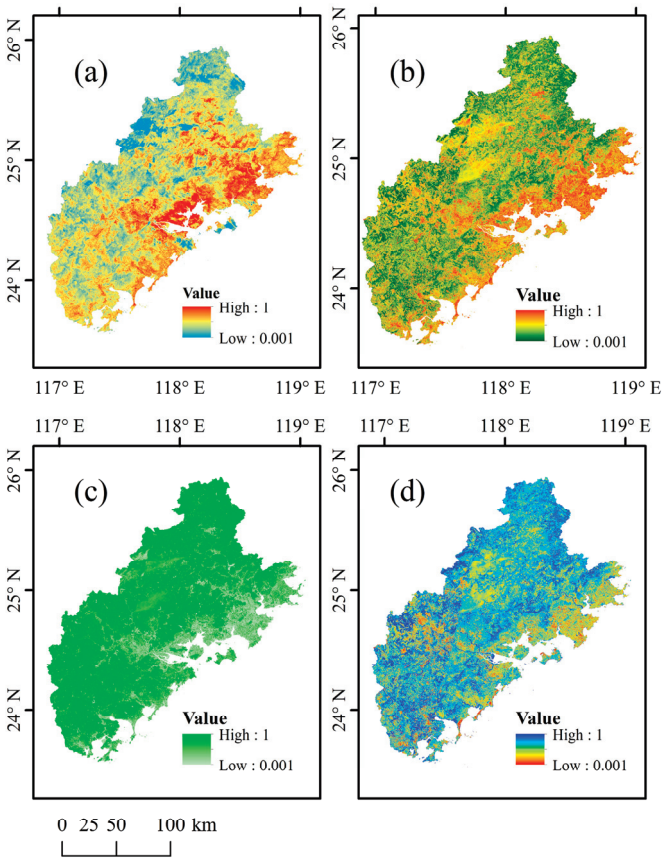

Figure 2. The normalized index of the heat, humidity, dryness, and greenness in 2022: (**a**) the heat, (**b**) dryness, (**c**) greenness, and (**d**) humidity.

Table 5. Principal component analysis table of humidity index, greenness index, heat index, and dryness index.

Principal Component	1989	2000	2010	2022
PC1	75.45%	70.01%	78.00%	76.58%
PC2	15.00%	17.60%	11.54%	12.11%
PC3	7.31%	9.93%	8.82%	10.72%
PC4	2.24%	2.46%	1.65%	0.60%

3.2. Analysis of RSEI

3.2.1. RSEI Index of the Xia-Zhang-Quan Urban Agglomeration

By analyzing the RSEI index, it is possible to study the ecological environmental changes in the Xia-Zhang-Quan urban agglomeration from 1989 to 2022. It can be concluded that the ecological environmental quality index RSEI of the Xia-Zhang-Quan urban agglomeration was 0.5829, 0.5607, 0.5827, and 0.6195 in 1989, 2000, 2010, and 2022, respectively, showing a trend of first decreasing and then increasing; the overall trend was still increasing (Figure 3). Compared with 1989, the RSEI in 2022 increased from 0.5829 to 0.6195. With an increase of 6.3%, the ecological environment quality of the Xia-Zhang-Quan urban agglomeration has improved in the past 30 years.

The average value of the RSEI index of each county-level administrative region of the Xia-Zhang-Quan urban agglomeration was calculated, and the statistical results are shown in Figure 4. Among the three prefectural-level administrative regions of the Xia-Zhang-Quan urban agglomeration, the average value of the RSEI index of Zhangzhou is the highest, which is 0.5532, indicating that its ecological environmental quality is the best among the three cities. The mean value of the RSEI index in Quanzhou is 0.5228. The

average RSEI index of Xiamen is the lowest among the three cities, which is 0.4546, and its ecological environmental quality is the worst among the three cities. From the four periods of the RSEI index and its mean value of each district and county from 1989 to 2022, it can be found that during the 30 years, the mean value of the RSEI index of Hua 'an County, Nanjing County, Pinghe County, and Changtai County in Zhangzhou City, and Dehua County and Yongchun County in Quanzhou City are all higher than 0.6, indicating that the ecological environmental quality is at a relatively high level. However, the average RSEI index of Siming District and Huli District in Xiamen City, Dongshan County in Zhangzhou City, Jinjiang City, and Shishi City in Quanzhou City is lower than 0.4, indicating that the ecological environmental quality is of a relatively low level.

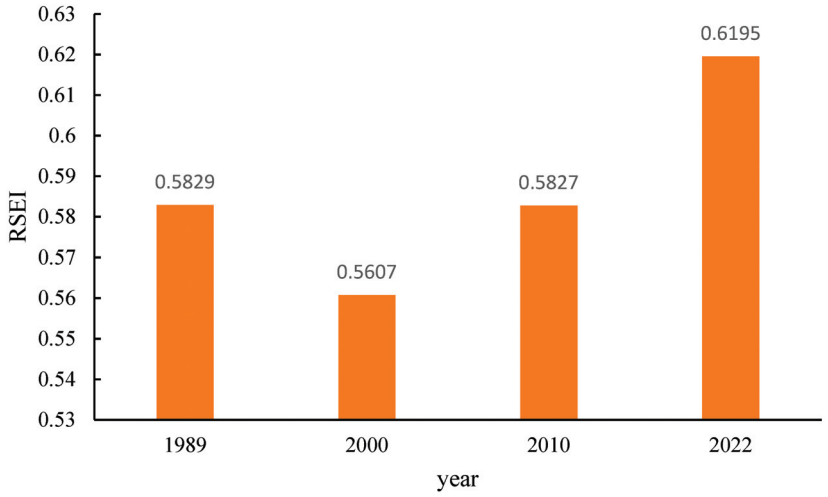

Figure 3. RSEI index of Xia-Zhang-Quan Urban agglomeration in 1989, 2000, 2010, and 2022.

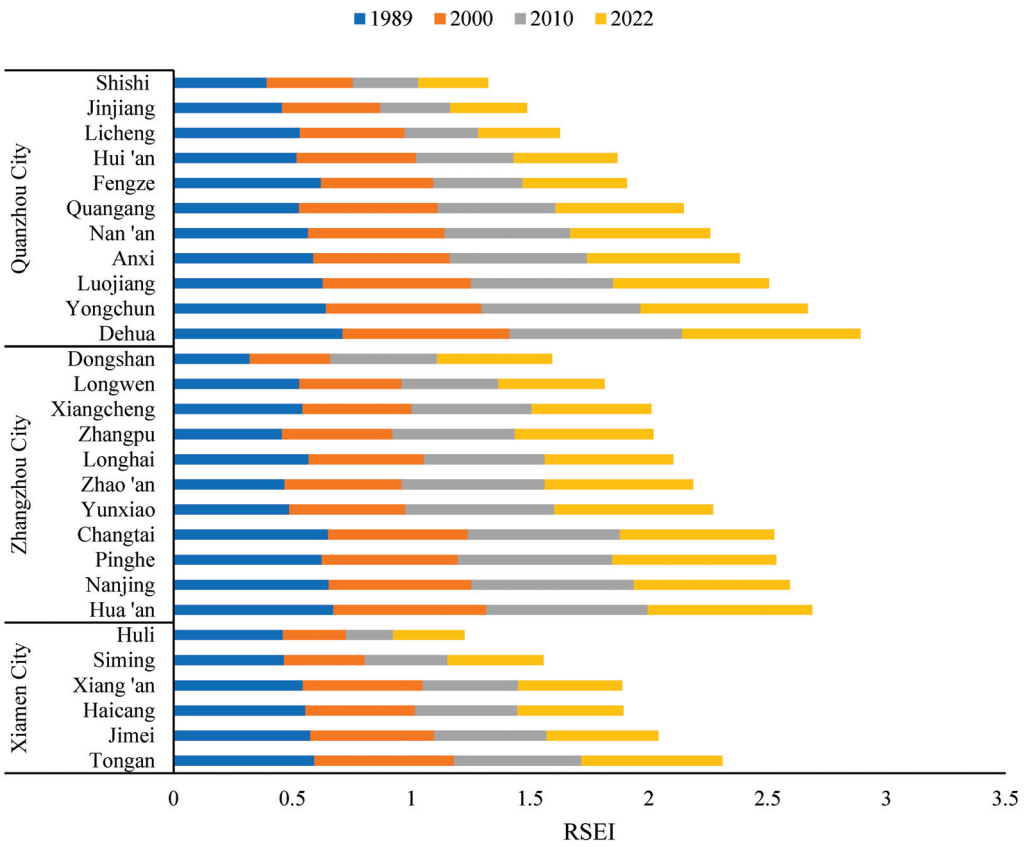

Figure 4. The RSEI in district scale in 1989, 2000, 2010, and 2022.

Combined with the relative geographical location distribution of each county-level administrative region of the Xia-Zhang-Quan urban agglomeration, it can be found that the Siming District and Huli District of Xiamen City, Dongshan County of Zhangzhou City, Jinjiang City, and Shishi City of Quanzhou City are all located in the urban center. Compared with other county-level administrative regions around them, the buildings are relatively dense, and the population density is relatively large. Therefore, the RSEI index is relatively low, and the ecological environment quality is poor. Hua'an County, Nanjing County, Pinghe County, Changtai County in Zhangzhou City, Dehua County, and Yongchun County in Quanzhou City have relatively high elevation values and belong to mountainous areas, so the vegetation coverage rate is high. In addition, due to their geographical location far from the urban center, human activities are relatively less, and their impact on the ecological environment is also less. The RSEI index is relatively high, and the ecological environment quality is good.

3.2.2. Classification of RSEI Index

The normalized RSEI index is classified, and the statistical results (Figure 5) show that the ecological environmental quality of the Xia-Zhang-Quan urban agglomeration is "good". That is, the proportion of the regions in the range of RSEI index (0.6, 0.8) is large, and the proportion of each stage is above 30%. The ecological environment quality is "poor" and "worse". That is, the proportion of the area in the RSEI index in the range of [0, 0.4] is small, and the highest proportion is 15.46% in 2000. Through the analysis of other levels, it was found that the proportion of "excellent" ecological environmental quality in the Xia-Zhang-Quan urban agglomeration showed an overall upward trend. The proportion of "general" ecological environmental quality showed a downward trend. To sum up, the overall ecological environment quality of the Xia-Zhang-Quan urban agglomeration is relatively good and has been improved in the past 30 years.

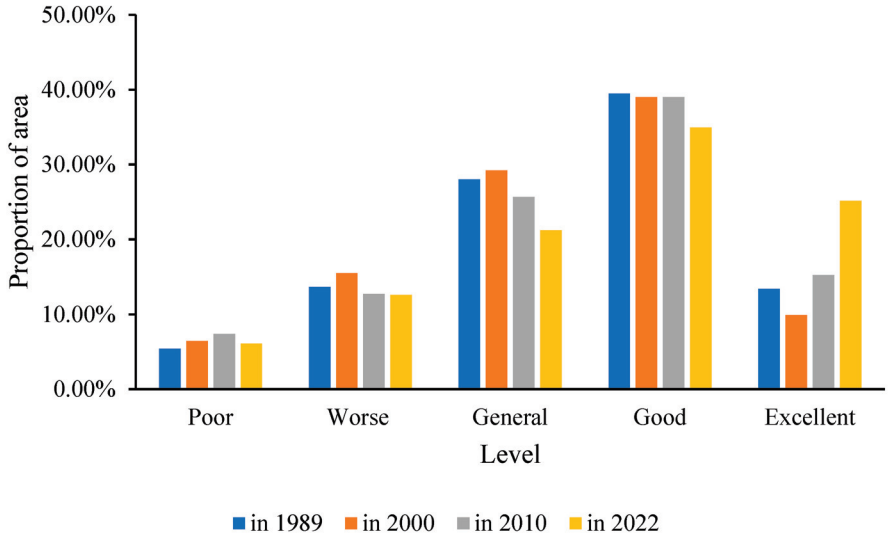

Figure 5. Statistical figure of hierarchical RSEI in 1989, 2000, 2010, and 2022.

The areas of "poor" and "worse" ecological quality were mainly concentrated in the southeast coastal urban building land and other bare soil and wasteland areas (Figure 6). As early as in the early 1980s, Xiamen, Zhangzhou and Quanzhou had proposed jointly building the "Golden Triangle Metropolitan Circle in southern Fujian". In the 1990s, southeast Fujian began to develop with rapid industrial development, increasing the demand for industrial land. The ecological environment quality of the Xia-Zhang-Quan urban agglomeration also decreased, which was the reason for the degradation of ecological environment quality in 2000 compared with that in 1989.

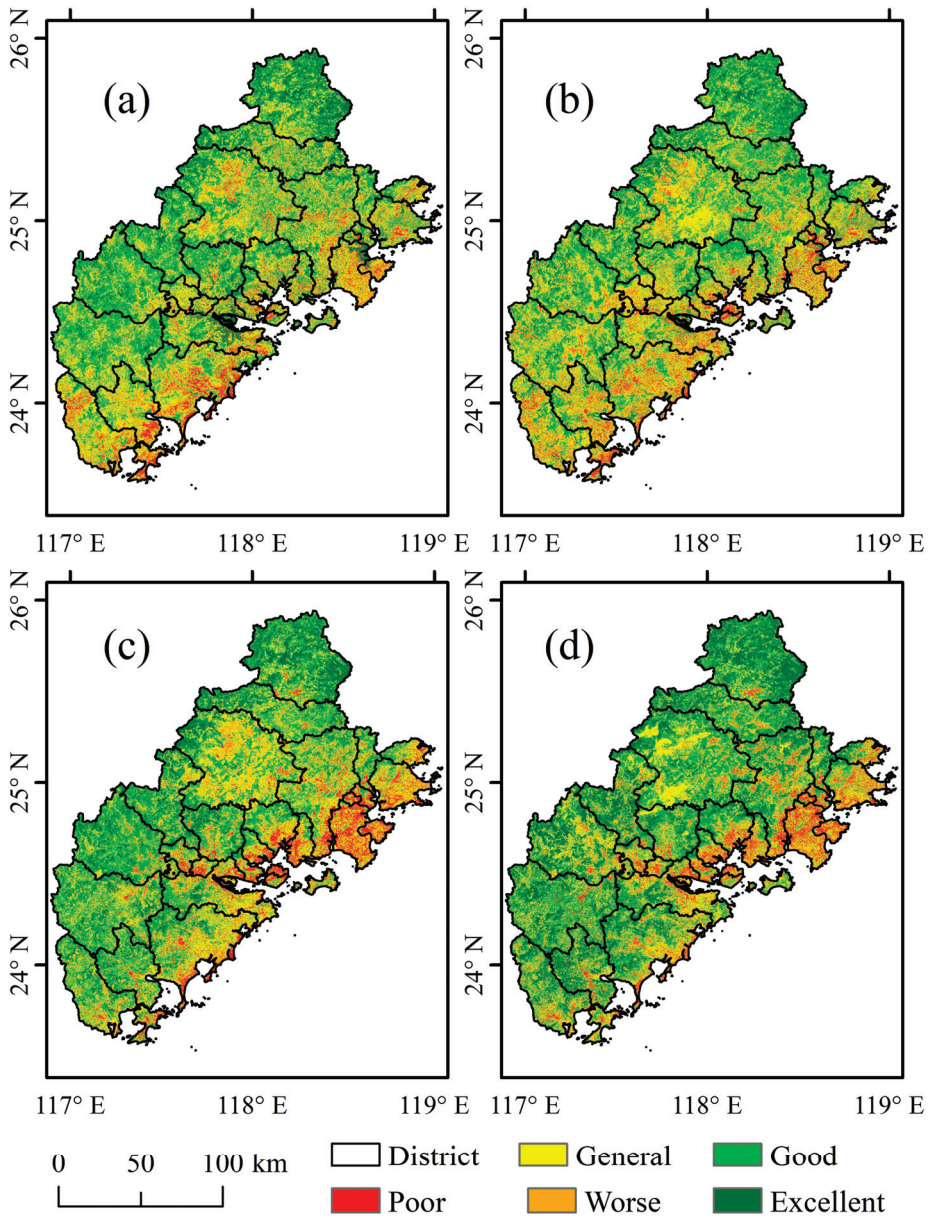

Figure 6. RSEI classification map of the Xiamen-Zhang-Quan urban agglomeration in 1989, 2000, 2010, and 2022. (**a**) 1989, (**b**) 2000, (**c**) 2010, and (**d**) 2022.

3.3. Changes in Ecological Environment Quality

The spatial distribution of the RSEI index from 1989 to 2022 was calculated according to prefectural and county-level administrative regions, and the results are shown in Figures 7 and 8, and Table 6. From 1989 to 2000, the change in the value of the RSEI in Xiamen was −0.0854, indicating that the ecological environment was significantly worse. The change in the value of the RSEI in Zhangzhou was −0.0379, indicating that the ecological environment was slightly worse. The change in the value of the RSEI in Quanzhou was −0.0258, the ecological environment was slightly worse, and the overall trend is worse. Among them, the RSEI change values of the Huli District and Siming District of Xiamen City were −0.1953 and −0.1259, respectively, indicating that the ecological environment was significantly worse. From 2000 to 2010, the change value of RSEI in Xiamen was −0.0499, indicating that the ecological environment was slightly worse. The change value of RSEI in Zhangzhou was 0.0640, indicating that the ecological environment was significantly improved. The change value of RSEI in Quanzhou was −0.0597, indicating that the ecological environment was significantly worse. Among them, the RSEI values of Xiang 'an

District in Xiamen City, Jinjiang City, and Lizheng District in Quanzhou City were −0.1031, −0.1175, and −0.1326, respectively, indicating that the ecological environment was significantly worse. The RSEI values of Dongshan County, Yunxiao County, and Zhao'an County in Zhangzhou City were 0.1106, 0.1375, and 0.1078, respectively, indicating that the ecological environment was significantly improved. From 2010 to 2022, the change value of RSEI in Xiamen was 0.0455, indicating a slight improvement in the ecological environment. The change value of RSEI in Zhangzhou was 0.0258, indicating that the ecological environment was slightly better. The change value of RSEI in Quanzhou is 0.0459, the ecological environment is slightly better, and the overall trend is better. Among them, the RSEI change value of Huli District in Xiamen City is 0.1048, indicating that the ecological environment has significantly improved.

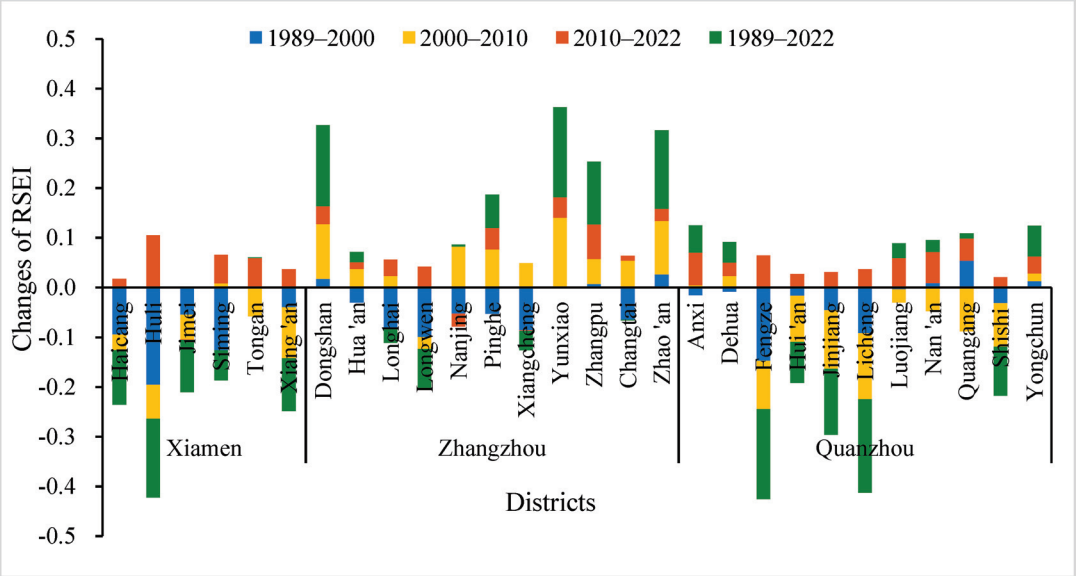

Figure 7. RSEI changes average in the districts of the Xiamen-Zhang-Quan urban agglomeration from 1989 to 2022.

From 1989 to 2022, the change in the value of the RSEI in Xiamen was −0.0897, indicating that the ecological environment was significantly worse. The change in the value of the RSEI in Zhangzhou was 0.0519, indicating that the ecological environment was improved considerably. The change in the value of the RSEI in Quanzhou was −0.0396, and the ecological environment was slightly worse. The RSEI values of Haicang District, Huli District, Jimei District, and Xiang'an District in Xiamen City, Fengze District, Jinjiang City, and Licheng District in Quanzhou City were −0.1092, −0.1589, −0.1053, −0.1061, −0.1806, −0.1328, and −0.1881, respectively, indicating that the ecological environment was significantly worse. The RSEI values of Dongshan County, Yunxiao County, Zhangpu County, and Zhaoan County in Zhangzhou City were 0.1633, 0.1814, 0.1267, and 0.1580, respectively, indicating that the ecological environment was significantly improved.

Also, we find that the ecological environment of the Xia-Zhang-Quan urban agglomeration is slightly better from 2010 to 2022, so the government has formulated policies to pay attention to ecological and environmental protection.

We find ecological environment changes are worse in central urban areas from 1989 to 2020, such as the Huli District and Siming District of Xiamen City, Xiangcheng District of Zhangzhou City, and Licheng District of Quanzhou City. However, the ecological environment of the central urban area has improved from 2010 to 2022, for example, the Huli District, Siming District, and Licheng District. The ecological environment in the Xiangcheng District of Zhangzhou City improved from 2000 to 2010 but worsened from 2010 to 2022. That means the ecological environment of the central city can be improved with economic development if the protection of the environment is enhanced. Otherwise, it gets worse.

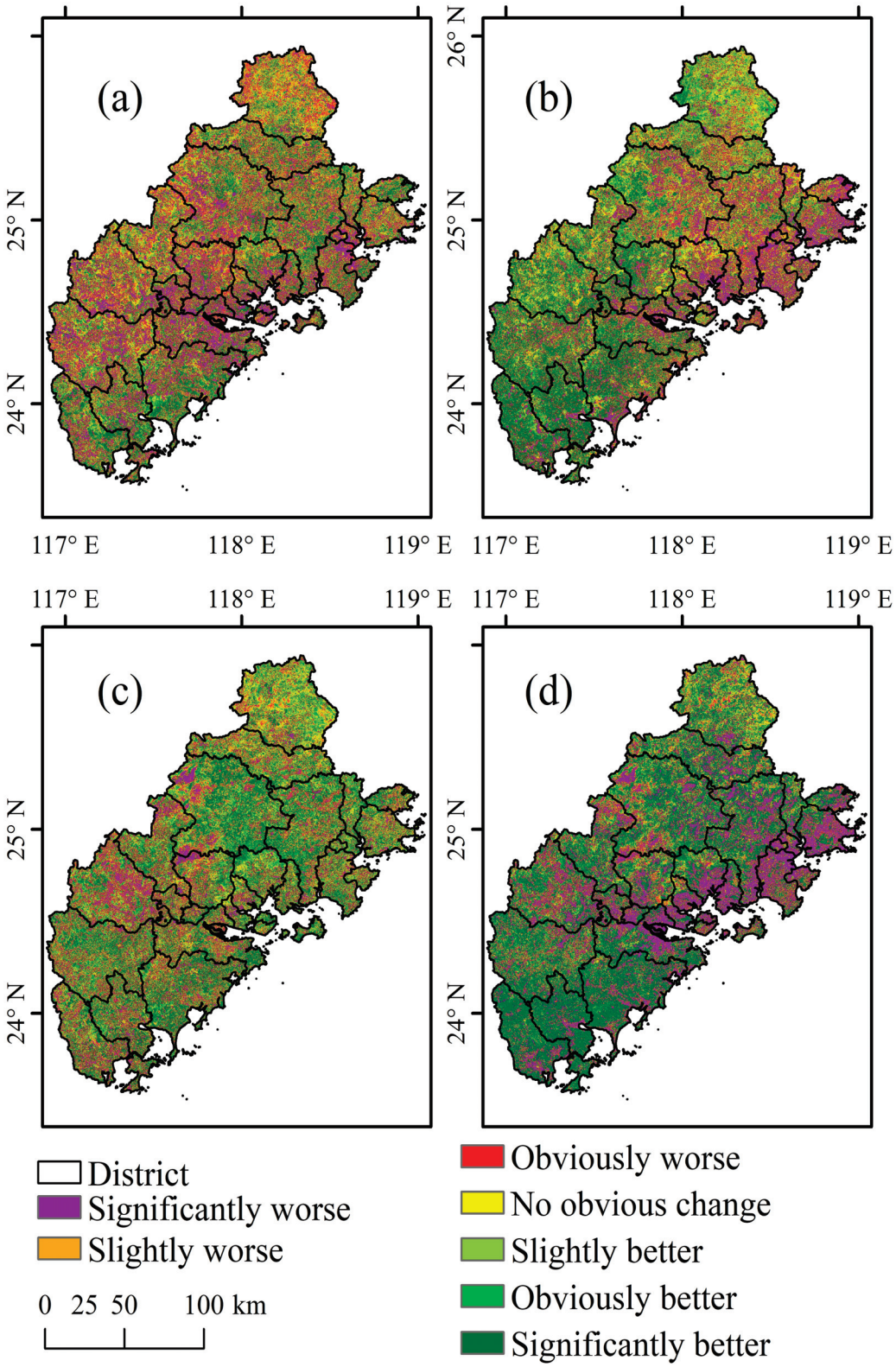

Figure 8. Levels of RSEI changes in the Xiamen-Zhang-Quan urban agglomeration from 1989 to 2022. (**a**) 1989–2000, (**b**) 2000–2010, (**c**) 2010–2022, and (**d**) 1989–2022.

Table 6. Average and level of RSEI changes in Xiamen, Zhangzhou, and Quanzhou from 1989 to 2022.

City	1989–2000 Average	Level	2000–2010 Average	Level	2010–2022 Average	Level	1989–2022 Average	Level
Xiamen	−0.0854	obviously worse	−0.0499	slightly worse	0.0455	slightly better	−0.0897	obviously worse
Zhangzhou	−0.0379	slightly worse	0.0640	obviously better	0.0258	slightly better	0.0519	obviously better
Quanzhou	−0.0258	slightly worse	−0.0597	obviously worse	0.0459	slightly better	−0.0396	slightly worse

3.4. Analysis of Factors Influencing the Spatial Heterogeneity of the RSEI in the Xia-Zhang-Quan Urban Agglomeration

3.4.1. Factor Detector Analysis

Using the factor detector, we analyzed the explanatory power of each factor on the spatial heterogeneity of ecological environment quality. As shown in Table 7, all factors except for the 2022 temperature data significantly impact the spatial differentiation of ecological environment quality. A larger q-value indicates a greater contribution of the driving factor to the spatial heterogeneity of ecological environment quality in the study area. In 2000, FVC > LUCC > DEM > Temp > LandScan > Pre. In 2010, LUCC > FVC > DEM > LandScan > Temp > Pre. In 2022, LUCC > LandScan > DEM > FVC > Pre. Overall, the explanatory power of land use on the spatial differentiation characteristics of RSEI has become increasingly significant, precipitation has the weakest explanatory power, and the influence of vegetation coverage has also diminished over time. This indicates that with the progression of urbanization, the explanatory power of land use for spatial heterogeneity in ecosystem quality changes accordingly. In 2000, vegetation coverage was the primary determinant of spatial differentiation in ecological environment quality. By 2022, land use had become the dominant factor, with the influence of precipitation being relatively minor.

Table 7. Results of single factors detection.

Driving Factors	In 2000		In 2010		In 2022	
	q	p	q	p	q	p
FVC	0.331	0.00	0.362	0.00	0.266	0.00
DEM	0.192	0.00	0.286	0.00	0.322	0.00
Pre	0.106	0.00	0.175	0.00	0.216	0.00
Temp	0.191	0.00	0.194	0.00	0.533	1.00
LandScan	0.135	0.00	0.278	0.00	0.393	0.00
LUCC	0.263	0.00	0.449	0.00	0.518	0.00

3.4.2. Interaction Detector Analysis

We used the interaction detector to explore the relationship between the interaction of various factors and the spatial heterogeneity of the RSEI (Figure 9). The results indicate that in 2000, 2010, and 2022, vegetation coverage and other factors did not exhibit interactive effects. In contrast, all other factors demonstrated bi-variable enhancement or nonlinear enhancement, suggesting that the interactive effects of these factors are greater than the effects of individual factors alone.

The analysis shows that with rising temperatures, the combination of land use and elevation had the strongest interaction in 2000 and 2010. By 2022, the combination of average annual temperature and elevation emerged as the most significant interaction. Land use consistently showed high q-values when interacting with other factors, and the temperature also displayed high q-values in 2022 when interacting with other factors.

We found that the explanatory power of the interactions was greater than that of individual factors. This suggests that the impact of various influencing factors on ecological environment quality is neither unilateral nor a simple additive effect of two factors. Instead, it is characterized by mutual or nonlinear enhance, indicating that the synergistic effects of multiple factors influence ecological environment quality.

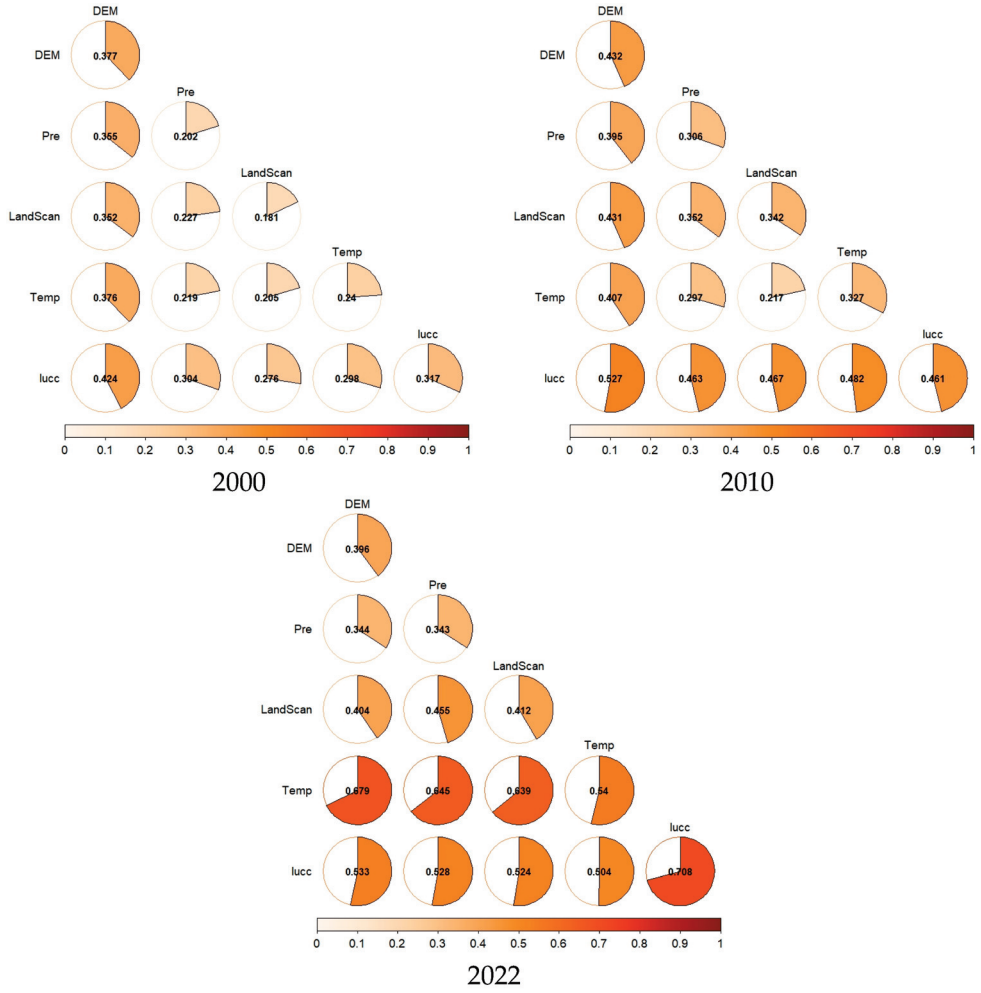

Figure 9. Results of interaction detection.

4. Discussion

This paper mainly studies the ecological environment change of urban agglomeration. We hypothesize that, with the help of urban planning, economic development does not necessarily lead to ecological degradation. Therefore, we study the ecological environment change of the Xia-Zhang-Quan urban agglomeration to verify our research purpose. We found that the Xia-Zhang-Quan urban agglomeration's ecological environment improved from 1989 to 2022. The ecological quality of the non-central urban areas is better than that of the central urban areas. The central urban areas have improved their ecological quality, although in less favorable conditions. The factor detector analysis identified land use as the dominant factor influencing ecological quality, with precipitation having a relatively minor impact. Interaction analysis revealed that all other factors demonstrated bi-variable enhancement or nonlinear enhancement, suggesting that the interactive effects of these factors are greater than the effects of individual factors alone. Land use consistently shows explanatory solid power. Temperature also exhibited significant influence in 2022 when interacting with other factors.

4.1. Changes in RSEI

The average RSEI of the Xia-Zhang-Quan urban agglomeration has an overall upward trend, and the ecological environment quality has improved in the past 30 years, similar to the study's finding [32]. The overall ecological environment index of Fujian Province has increased, and the ecological environment quality has improved [33]. In recent years, the poor ecological environments have been concentrated in the Siming District and Huli District of Xiamen City, Dongshan County of Zhangzhou City, Jinjiang City, and Shishi

City of Quanzhou City. The ecological environment index of urban centers is small, and the ecological environment is poor but exhibiting signs of improvement. During the more than 30 years, the ecological environment of Xiamen Island was significantly worse, which was different from the results of the study [34] from 1995 to 2016, which may be because the ecological environment of Xiamen Island continued to decline from 2016 to 2022. The ecological environment of Zhangzhou was significantly improved. The ecological environment of Quanzhou was slightly worse. This is similar to the results of the study [35] on the ecological environment change in Quanzhou City from 1989 to 2018.

The overall upward trend in the RSEI index from 1989 to 2022 demonstrates that it is possible to achieve both economic growth and ecological improvement simultaneously. This strengthens the finding that challenges the commonly assumed trade-off between development and environmental health. It suggests that urban agglomerations can improve their ecological conditions while promoting economic vitality with appropriate planning and management strategies. Our findings reveal differences in ecological quality between central and non-central urban areas. While central areas of urban cities typically exhibited poorer ecological conditions, there was a trend towards improvement, suggesting that targeted interventions in these densely populated regions are beginning to bear fruit. Urban planners should continue to focus on central areas by promoting green roofs, urban forestry programs, and sustainable building practices to mitigate the urban heat island effect and enhance ecological quality.

4.2. Analysis of Driving Factors of Ecological Environment Changes in the Xia-Zhang-Quan Urban Agglomeration

Ecological environment improvements are influenced by land use changes, elevation, and temperature variations, emphasizing the complex interplay between natural and anthropogenic factors in shaping urban ecological environment conditions.

Both natural and anthropogenic factors influence the ecological environment quality of the Xia-Zhang-Quan urban agglomeration. In 2022, the region experienced extremely high temperatures [36]. During these periods, the interactions between temperature and DEM, precipitation, and population density had a strong explanatory power for the spatial heterogeneity of ecological environment quality. Conversely, under non-extreme temperature conditions, the interaction between land use changes and other factors showed a stronger explanatory power for the spatial heterogeneity of ecological environment quality. This indicates that during extremely high temperatures, human interventions are insufficient to counteract the impact of natural factors. However, effective land use planning is essential to maintain ecological quality under non-extreme temperature conditions.

Similar conclusions have been drawn from studies in other regions of China. The research found that the interaction between land use and other factors provided a stronger explanatory power for the spatial heterogeneity of ecological environment quality in Taojiang County, Hunan Province [37]. The explanatory power of different interacting factors with land use varies by region. For example, in Shandong Province, the interaction between humidity changes and land use showed explanatory solid power for the spatial heterogeneity of RSEI, with an increasing trend in RSEI for cropland and forest land [22]. On Northwest China, vegetation, soil, and land use types were positively correlated with the RSEI, in the Lanxi urban agglomeration [18]. Natural factors are the primary influencers on the RSEI of the Tibetan Plateau, such as temperature, soil moisture, and precipitation [21]. And the interaction between temperature and precipitation showed a positive effect on RSEI.

When natural factors predominantly influence ecological environment quality, interactions with land use exert significant impact. Conversely, when natural factors play a lesser role, the interactions between land use and other factors remain influential. Therefore, changes in land use types play a key role in shaping ecological environment quality. This emphasizes the need to promote economic development while adhering to green and sustainable development principles. The dominance of land use as a factor influencing

ecological quality underscores the critical role of effective land use planning in urban environments. Urban planners should prioritize green spaces, implement stringent zoning regulations to prevent excessive urban sprawl, and encourage the development of eco-friendly infrastructure. The high explanatory power of land use interactions with other factors, such as temperature, indicates that multifaceted strategies that address various environmental components simultaneously can yield significant ecological benefits.

4.3. Planning Implications of Changes in RSEI

Our study is consistent with several previous studies that have reported positive ecological outcomes due to effective urban planning and environmental management. For instance, some studies [21,38] documented similar trends of ecological improvement in other regions, attributing these changes to the successful implementation of green policies and enhanced land use practices. However, our study extends the existing knowledge by explicitly focusing on the Xia-Zhang-Quan urban agglomeration, providing a localized understanding of ecological dynamics in this economically and environmentally significant region. Unlike some studies that report mixed or negative trends in urban ecological quality due to rapid urbanization [39–41], our results indicate that ecological conditions can improve even in highly urbanized areas with appropriate management and planning. Compared with other urban agglomerations, the Pearl River Delta (PRD) is one of the most economically dynamic regions in China, characterized by rapid industrialization and urbanization similar to the Xia-Zhang-Quan urban agglomeration. Both regions have experienced significant ecological changes due to urban expansion. However, while the PRD has seen considerable environmental degradation, the Xia-Zhang-Quan urban agglomeration has shown an overall improvement in ecological quality, as indicated by the RSEI trends from 1986 to 2019 [42]. This contrast underscores the effectiveness of the environmental policies and land use planning implemented in Xia-Zhang-Quan, suggesting that similar strategies could benefit other rapidly urbanizing areas.

Despite the rapid economic development of the Xia-Zhang-Quan urban agglomeration, Zhangzhou City launched the "three-year Action Plan to Win the Blue Sky Defense War" in 2018, deepened the treatment of industrial pollution, and vigorously cultivated green environmental protection industries, which reduced the damage caused by industrial pollution to the ecological environment. In addition, Zhangzhou has promoted land afforestation and forest quality improvement, fully tapped the potential of afforestation, scientifically expanded the afforestation space, and strengthened and improved the ecological advantages of Zhangzhou.

The implications of these findings for urban planning are profound. The demonstrated improvement in ecological quality within central urban areas suggests that it is possible to achieve ecological sustainability even in densely populated and developed regions. Urban planners and policymakers can leverage these insights to design and implement strategies that balance development with ecological preservation. Key strategies may include promoting green infrastructure, enhancing land use efficiency, and integrating climate adaptation measures into urban planning. Additionally, understanding the specific impacts of land use changes, elevation, and temperature on ecological quality allows for more targeted and effective interventions, optimizing resource allocation and maximizing environmental benefits.

The results of this study should inform policy frameworks at both local and regional levels. Policies that incentivize sustainable practices, penalize ecological degradation, and promote community engagement in environmental stewardship can drive broader adoption of eco-friendly practices. Furthermore, integrating ecological indicators like RSEI into regular monitoring and reporting systems can provide ongoing feedback to policymakers and planners, ensuring that urban development remains aligned with ecological sustainability goals.

4.4. Limitations and Future Study

This study selected images taken during the summer months (April to August) as the original data [43]. However, the prevalence of clouds during this season can affect remote sensing images, potentially introducing errors when calculating various indices, including the RSEI index. The remote sensing image data for the same month is challenging to obtain, so we chose the remote sensing images from April to August as the remote sensing images for the study area. Additionally, some remote sensing images from 1989 were missing for the study area, and these gaps were supplemented with images from 1988. Future research should aim to mitigate these errors by seeking data with less cloud cover or by exploring advanced cloud removal techniques in remote sensing imagery to reduce inaccuracies caused by cloud cover.

The final ecological environment quality index (RSEI) obtained in this study only uses four factors relatively related to the ecological environment as indicators, which reflect the ecological environment quality status and the development trend of the study area in the past 30 years to a certain extent. Still, the ecological environment quality is closely related to regional urbanization and atmospheric levels. In future studies, other factors related to ecological environmental quality will also be integrated to evaluate the ecological environmental quality of the study area more comprehensively.

Despite the valuable contribution of this research, there are some limitations that need to be recognized. First, reliance on remotely sensed data, while providing comprehensive spatial coverage, may lack the granularity required for detailed ground-based ecological assessments. Combining remotely sensed data with ground-based observations can improve the accuracy and depth of ecological assessments. Second, although this study identified the key factors affecting ecological quality, it did not fully explore the causal mechanisms of these relationships. Future research should aim to develop more sophisticated models that depict the direct and indirect pathways through which land use change, elevation, and temperature affect ecological conditions. Finally, the time frame of this study, from 2000 to 2022, may not capture longer-term ecological trends and potential lagged effects of environmental policies and interventions. Expanding the time frame and including more recent data would provide a more comprehensive understanding of ecological dynamics.

In the future, multi-source indicators reflecting the natural and human development of the region can be included, and the multi-scale geographically weighted regression model (MGWR) can be utilized to explore the spatial and temporal relationships between ecological environment quality and the factors affecting it. Expanding the analysis to include more granular data and incorporating machine learning techniques could further enhance the precision and applicability of RSEI as a tool for urban planning.

5. Conclusions

Utilizing three Landsat5 TM images from 1989, 2000, and 2010, along with the first phase of Landsat9 OLI images from 2022, We calculated the humidity index, greenness index, dryness index, and heat index to construct the Remote Sensing Ecological Index (RSEI) in the Xia-Zhang-Quan urban agglomeration in Fujian Province. The ecological environment quality was evaluated at four time periods, and the spatial and temporal trends of ecological environment quality and the factors affecting spatial heterogeneity were analyzed.

The average RSEI indices for the study area were 0.5829, 0.5607, 0.5827, and 0.6195 in 1989, 2000, 2010, and 2022, respectively. This indicates an initial decline followed by an increase, reflecting an overall upward trend in ecological quality from 1989 to 2022. The ecological environment of the Xia-Zhang-Quan urban agglomeration was generally classified as "good", with the proportion of areas achieving "excellent" quality showing a rising trend. Over the past 30 years, the ecological environment quality in Zhangzhou has significantly improved, while Xiamen and Quanzhou experienced notable deterioration. Non-central urban areas demonstrated better ecological quality compared to central urban areas, which, despite poorer conditions, exhibited signs of improvement.

Our findings reveal that both natural and anthropogenic factors influence the ecological environment of the Xia-Zhang-Quan urban agglomeration. Land use emerged as the dominant factor, with precipitation having a relatively minor impact. Interaction analysis showed that the combined influence of various drivers on the RSEI was greater than their individual effects. Land use consistently exhibited high explanatory power when interacting with other factors, and temperature also showed a strong influence in 2022 in combination with different variables.

In summary, the study underscores the significant role of land use and the synergistic effects of multiple factors in shaping the ecological environment of the Xia-Zhang-Quan urban agglomeration. These insights can guide future urban planning efforts to harmonize economic development with ecological sustainability.

Author Contributions: Conceptualization, Z.L.; methodology, Z.L. and J.P.; software, J.P.; validation, Y.W., F.S. and Y.H.; writing—original draft preparation, Z.L. and J.P.; writing—review and editing, Z.L.; visualization, supervision, Q.N.; funding acquisition, W.M. All authors have read and agreed to the published version of the manuscript.

Funding: This research was funded by the Xiamen City Open Competition for Leadership Project, grant number 3502Z20231038, the National Natural Science Foundation of China, grant number 41501448, and Xiamen University Technology, grant number XPDKT20029.

Data Availability Statement: Remote sensing data is from USGS (https://landsatlook.usgs.gov (accessed on 3 January 2023)).

Acknowledgments: Thanks for the remote sensing data from USGS (https://landsatlook.usgs.gov (accessed on 3 January 2023)). I (Zongmei Li) would like to thank my mother (Chengshan Chang) for a lifetime of hard work.

Conflicts of Interest: The authors declare no conflicts of interest.

References

1. Liu, F.; Zhang, Z.; Zhao, X.; Wang, X.; Zuo, L.; Wen, Q.; Yi, L.; Xu, J.; Hu, S.; Liu, B. Chinese cropland losses due to urban expansion in the past four decades. *Sci. Total Environ.* **2019**, *650*, 847–857. [CrossRef] [PubMed]
2. Sun, T. Reflection on the leading strategy and practice of urbanization development in China in the past 40 years. *Lingnan J.* **2023**, *2023*, 19–27.
3. Fan, J.; Guo, R. Re-recognition of precondition and driving mechanism of new-type urbanization. *Geogr. Res.* **2019**, *38*, 3–12. [CrossRef]
4. Liang, C.; Zeng, J.; Ding, S. Research on Coupling Coordination Development Between Regional Ecological Civilization Construction and Urbanization: A Case Study on Fujian Province. *J. Hum. Settl. West China* **2022**, *37*, 112–118.
5. Cheng, P.G.; Tong, C.Z.; Nie, Y.J.; Chen, X.Y.; Ding, Y. Design and Application of Urban Ecological Environment Monitoring and Evaluation System using Remote sensing and GIS. *J. East China Inst. Technol.* **2015**, *38*, 314–318.
6. Shi, Y.; Lv, J. China's Urbanization Advancement and Ecological Environment. *Tax. Econ.* **2022**, *2022*, 98–105.
7. Luck, M.A.; Jenerette, G.D.; Grimm, W.N.B. The Urban Funnel Model and the Spatially Heterogeneous Ecological Footprint. *Ecosystems* **2001**, *4*, 782–796. [CrossRef]
8. Basso, F.; Bove, E.; Dumontet, S.; Ferrara, A.; Pisante, M.; Quaranta, G.; Taberner, M. Evaluating environmental sensitivity at the basin scale through the use of geographic information systems and remotely sensed data: An example/1 covering the agri basin southern Italy. *Catena* **2000**, *40*, 19–35. [CrossRef]
9. Chalkias, C.; Petrakis, M.; Psiloglou, B.; Lianou, M. Modelling of light pollution in suburban areas using remotely sensed imagery and GIS. *J. Environ. Manag.* **2006**, *79*, 57–63. [CrossRef]
10. Hossen, H.; Negm, A. Sustainability of water bodies of Edku Lake, Northwest of Nile Delta, Egypt: RS/GIS approach. *Procedia Eng.* **2017**, *181*, 404–411. [CrossRef]
11. Ma, R.H.; Hu, M.C. Accessment of the ecological environment in hainan island and based on RS & GIS. *Trop. Geogr.* **2001**, *21*, 198–201.
12. Hai, R.T.; Wang, W.X. *Ecological Environment Assessment, Planning and Management*; China Environmental Science Press: Beijing, China, 2004.
13. Marull, J.; Pino, J.; Mallarach, J.M.; Cordobilla, M.J. A Land Suitability Index for Strategic Environmental Assessment in metropolitan areas. *Landsc. Urban Plan.* **2007**, *81*, 200–212. [CrossRef]

14. Dizdaroglu, D.; Yigitcanlar, T.; Dawes, L. A micro-level indexing model for assessing urban ecosystem sustainability. *Smart Sustain. Built Environ.* **2012**, *1*, 291–315. [CrossRef]
15. Xu, H.Q. A remote sensing index for assessment of regional ecological changes. *China Environ. Sci.* **2013**, *33*, 889–897.
16. Zhang, X.; Fan, H.; Zhou, C.; Sun, L.; Xu, C.; Lv, T.; Ranagalage, M. Spatiotemporal change in ecological quality and its influencing factors in the Dongjiangyuan region, China. *Environ. Sci. Pollut. Res.* **2023**, *30*, 69533–69549. [CrossRef] [PubMed]
17. Zongfan, B.; Ling, H.; Huiqun, L.; Xuhai, J.; Liangzhi, L. Spatiotemporal change and driving factors of ecological status in Inner Mongolia based on the modified remote sensing ecological index. *Environ. Sci. Pollut. Res.* **2023**, *30*, 52593–52608. [CrossRef] [PubMed]
18. Lv, Y.; Xiu, L.; Yao, X.; Yu, Z.; Huang, X. Spatiotemporal evolution and driving factors analysis of the eco-quality in the Lanxi urban agglomeration. *Ecol. Indic.* **2023**, *156*, 111114. [CrossRef]
19. Liu, Y.; Zhou, T.; Yu, W. Analysis of Changes in Ecological Environment Quality and Influencing Factors in Chongqing Based on a Remote-Sensing Ecological Index Mode. *Land* **2024**, *13*, 227. [CrossRef]
20. Li, Y.; Yuan, H.; Luo, J.S.; Liu, Y.; Gou, K. Study on the Evaluation of Ecological Environment Quality Based on RSEI Model. *Geomat. Spat. Infomation Technol.* **2021**, *44*, 117–124.
21. Airiken, M.; Li, S. The Dynamic Monitoring and Driving Forces Analysis of Ecological Environment Quality in the Tibetan Plateau Based on the Google Earth Engine. *Remote Sens.* **2024**, *16*, 682. [CrossRef]
22. Ma, L.; Liang, Y.; Zhang, Y.; Li, Y. Spatiotemporal Change and Driving Factors of the Eco-Environment Quality of Different Land Covers in Shandong Province Based on RSEI. *Res. Soi Land Water Conserv.* **2024**, *31*, 389–400. [CrossRef]
23. Zhang, W.; Du, P.J.; Guo, S.C.; Lin, C.; Zheng, H.R.; Fu, P.J. Enhanced remote sensing ecological index and ecological environment evaluation in arid area. *Natl. Remote Sens. Bull.* **2023**, *27*, 299–317. [CrossRef]
24. Zhong, A.; Hu, C.; You, L. Evaluation and Prediction of Ecological Restoration Effect of Beijing Wangping Coal Mine Based on Modified Remote Sensing Ecological Index. *Land* **2023**, *12*, 2059. [CrossRef]
25. Chen, N.; Cheng, G.; Yang, J.; Ding, H.; He, S. Evaluation of Urban Ecological Environment Quality Based on Improved RSEI and Driving Factors Analysis. *Sustainability* **2023**, *15*, 8464. [CrossRef]
26. Nguyen, C.T.; Kaewthongrach, R.; Channumsin, S.; Chongcheawchamnan, M.; Phan, T.; Niammuad, D. A regional assessment of ecological environment quality in Thailand special economic zone: Spatial heterogeneous influences and future prediction. *Land Degrad. Dev.* **2023**, *34*, 5770–5787. [CrossRef]
27. Xu, H.; Deng, W. Rationality Analysis of MRSEI and Its Difference with RSEI. *Remote Sens. Technol. Appl.* **2022**, *37*, 1–7. [CrossRef]
28. Huang, C.; Wylie, B.; Yang, L.; Home, C.; Zylstra, G. Derivation of a Tasseled Cap Transformation Based on Landsat 7 At-Satellite Reflectance. *Int. J. Remote Sens.* **2002**, *23*, 1741–1748. [CrossRef]
29. Schwartz, M.D. Green-wave phenology. *Nat. Int. Wkly. J. Sci.* **1998**, *394*, 839–840. [CrossRef]
30. Yang, Y.; LI, H.; Chen, J.; Han, Y.; Zhong, S. Regional ecological quality assessment based on remote sensing ecological index: A case study of Chuanshan District, Suining City, Sichuan. *Yangtze River* **2019**, *50*, 71–76. [CrossRef]
31. Song, Y.; Wang, J.; Ge, Y.; Xu, C. An optimal parameters-based geographical detector model enhances geographic characteristics of explanatory variables for spatial heterogeneity analysis: Cases with different types of spatial data. *Gisci. Remote Sens.* **2020**, *57*, 593–610. [CrossRef]
32. Wang, S.; Zhang, M.; Xi, X. Ecological Environment Evaluation Based on Remote Sensing Ecological Index: A Case Study in East China over the Past 20 Years. *Sustainability* **2022**, *14*, 15771. [CrossRef]
33. Cheng, N.; Gao, W.J.; Yang, H.F.; Wang, F.; Lai, R.W. Dynamic change and driving factors of ecological environment quality in Minjiang River basin. *Bull. Soil Water Conserv.* **2023**, *43*, 310–318.
34. Liu, C.; Yang, M.; Hou, Y.; Zhao, Y.; Xue, X. Spatiotemporal evolution of island ecological quality under different urban densities: A comparative analysis of Xiamen and Kinmen Islands, southeast China. *Ecol. Indic.* **2021**, *124*, 107438. [CrossRef]
35. Pan, W.; Wang, S.; Wang, Y.; Yu, Y.; Luo, Y. Dynamical changes of land use/land cover and their impacts on ecological quality during China's reform periods: A case study of Quanzhou city, China. *PLoS ONE* **2022**, *17*, e0278667. [CrossRef] [PubMed]
36. Zhou, B.; Hu, S.; Peng, J.; Li, D.; Ma, L.; Zheng, Z.; Feng, G. The extreme heat wave in China in August 2022 related to extreme northward movement of the eastern center of SAH. *Atmos. Res.* **2023**, *293*, 106918. [CrossRef]
37. Chen, C.; Nie, P.J.; Huang, F.C.; Fan, D.; Xiang, L.; Ceng, J.; Chen, F.W.; Hu, G.X. Ecological Environmental Quality Evaluation and Driving Mechanism Using Modified RSEI Model. *Bull. Soil Water Conserv.* **2024**, *44*, 1–13.
38. Zhang, C.Y.; Yang, S.K.; Dong, X.H.; Zhao, C.M.; Bo, H.J.; Liu, J. Research on Spatiotemporal Evolution and Influencing Factors of Ecological Environment Quality in the Upper Yangtze Rive rBasin Based on RSEI Index. *Res. Soil Land Water Conserv.* **2023**, *30*, 356–363. [CrossRef]
39. Das, M.; Das, A.; Pereira, P. Impact of urbanization induced land use and land cover change on ecological space quality-mapping and assessment in Delhi (India). *Urban Clim.* **2024**, *53*, 101818. [CrossRef]
40. Fan, X.; Zhang, L.; Yuan, L.; Guo, B.; Zhang, Q.; Huang, H. Urbanization and water quality dynamics and their spatial correlation in coastal margins of mainland China. *Ecol. Indic.* **2022**, *138*, 108812. [CrossRef]
41. Li, J.; Jiang, C.; Xing, Z. Multi-dimensional influence measurement of urbanization on the quality of natural living environment in China. *Environ. Dev. Sustain.* **2021**, *23*, 12151–12168. [CrossRef]

42. Li, T.; Dong, Y. Evolution of ecological security pattern and its influencing factors in the Pearl River Delta from 1986 to 2019 based on RSEI and landscape function. *J. Shaanxi Norm. Univ.* **2022**, *50*, 69–80.
43. Huang, S.; Li, Y.; Hu, H.; Xue, P.; Wang, J. Assessment of optimal seasonal selection for RSEI construction: A case study of ecological environment quality assessment in the Beijing-Tianjin-Hebei region from 2001 to 2020. *Geocarto Int.* **2024**, *39*, 2311224. [CrossRef]

Disclaimer/Publisher's Note: The statements, opinions and data contained in all publications are solely those of the individual author(s) and contributor(s) and not of MDPI and/or the editor(s). MDPI and/or the editor(s) disclaim responsibility for any injury to people or property resulting from any ideas, methods, instructions or products referred to in the content.

land

MDPI

Article

Mapping Ecological Security Patterns Based on Ecosystem Service Valuation in the Qinling-Daba Mountain Area, China: A Multi-Scenario Study for Development and Conservation Tradeoffs

Pingping Zhang, Mingjie Song * and Qiaoqi Lu

College of Public Administration, Central China Normal University, Wuhan 430079, China; zhangpingping0210@mails.ccnu.edu.cn (P.Z.); luqiaoqi@mails.ccnu.edu.cn (Q.L.)
* Correspondence: smingjie@ccnu.edu.cn

Abstract: When focusing on biodiversity maintenance, ecological security pattern (ESP) planning gradually becomes a multi-objective planning strategy for sustainable development; wildlife conservation and ecosystem health maintenance should be balanced with local economic development and people's livelihood enhancement goals. This study focuses on ESP mapping in the Qinling-Daba Mountain area, which is an ecologically significant and socioeconomically underdeveloped area. The tradeoff between conservation and development is made by varying the area of ecological sources and incorporating ecosystem service tradeoffs into ecological source identification through multi-scenario designation. ESPs under six scenarios were generated based on the minimum resistance model, and the important ecological corridors and strategic points in each scenario were identified and compared. The results show the following: (1) The scenario that sets around 30 percent of the study area as ecological sources maintains the integrity of natural ecosystems and leaves space for food and material supply to residents. (2) In this scenario, the ecological sources are connected by 60 corridors that cross 137 townships with high population densities (>100 people/km^2) and intersect with major traffic lines at 71 points. Engineering, management, or education strategies must be taken in these townships or intersections to avoid human–wildlife conflicts. (3) The study area needs to construct both short (north–south) corridors linking proximate ecological sources for species' daily movement and long (west–east) corridors connecting large and distant sources for species' seasonal migration and gene flow. (4) The multi-scenario approach turns out to be an effective strategy for ESP planning with considerations for development–conservation tradeoffs.

Keywords: core conservation areas; ecological corridors; minimum resistance model; mountainous areas

1. Introduction

The Aichi Biodiversity Target 11 and the 30 × 30 Biodiversity Goal at COP28 proposed the construction of well-connected conservation systems to achieve global biodiversity conservation goals. The construction of connected conservation areas is also the focus of a few environmental and spatial planning approaches for sustainable development, such as greenways, green infrastructure, and ecological security patterns. Although taking care of biodiversity maintenance, these planning approaches are multifunctional. Greenways are corridors of land conserved for recreation, environmental protection, or both objectives. They emphasize the aesthetic and recreational services of ecosystems [1,2]. Green infrastructure is a strategically planned network of natural and semi-natural areas and other environmental features designed and managed to deliver a wide range of ecosystem services (ES) [3]. It recognizes the need to plan land use for specific purposes, such as farming, nature protection, and development, but also provides the tools and methods to identify

needs and opportunities to enhance the environment and its functions [4]. Ecological security pattern (ESP) is similar to GI in regards to the connected conservation system and multifunctionality, but it emphasizes the landscape pattern–process interactions [5,6]. ESP is widely implemented by Chinese scholars and practitioners to ensure urban ecological security and achieve sustainability at different spatial scales [7–10]. In addition, ecological networks are also relevant to biodiversity conservation, representing the interactions between species within a community [11]. Simulating and understanding ecological networks will support environmental and spatial planning for biodiversity conservation. This study focuses on mapping ecological security patterns in the Qinling-Daba Mountain (QLDAM) area in China.

ESP is composed of ecological sources, ecological corridors, and strategic points [9,12]. Ecological sources are habitats for target species or areas that provide a wide range of ecosystem services (ESs) for human well-being [13,14]. Ecological corridors connect ecological sources, allowing for species migration or matter and energy delivery among them [14,15]. The least cost path analysis (minimum cumulative resistance model), connectivity analysis, and circuit theory have been used for identifying the potential corridors [6,16,17]. Strategic points are sites that are critical for ecological process maintenance and species dispersal or vulnerable to risks [18], including stepping stones and possible barriers. Possible barriers are sections of ecological corridors in which human activities are frequent, while stepping stones are locations that provide resting spots for species during long-distance migrations and therefore require particular attention [19] (Figure 1).

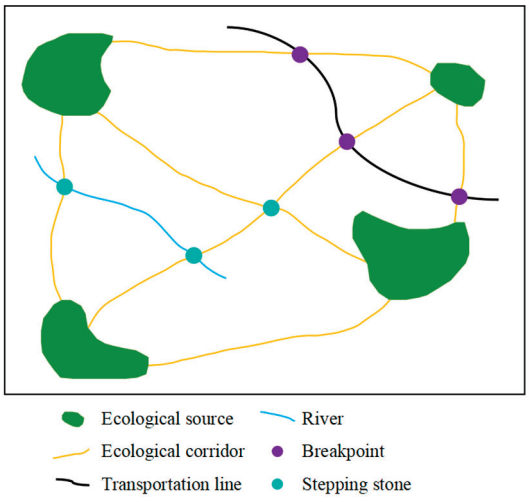

Figure 1. Schematic diagrams of ecological security pattern (ESP).

Early ESP construction usually focuses on biodiversity conservation, focusing on established protected areas (PAs) and creating their linkages [8,20]. Many documents, including Aichi Target 11 and the 30 × 30 Biodiversity Goal at COP28, propose incorporating the areas of particular importance for ecosystem services into the connected conservation system. As a result, ecosystem services gradually become an integral part of ESP planning [6,21]. Ecosystem services (ESs) are the benefits people obtain from ecosystems, which are categorized into provisioning, regulating, supporting, and cultural services in the MA framework [15]. Under many circumstances, the different categories of ESs are not in synergy in an area; ecosystem governance that aims to maintain and improve regulating services or biodiversity for distant stakeholders and future generations often leads to short-term losses of provisioning services for food, fuel, and other basic needs to local populations [22,23]. Under such circumstances, ESP becomes a multi-objective planning problem that needs to be made a tradeoff between conservation for biodiversity and ecosystem safety maintenance and development for local livelihood maintenance and improvement [24]. The tradeoffs were often made through multi-scenario designation by varying the weights or ranking of different categories of ES in ecological source identifica-

tion [25–27]. As a result, the number, area, and spatial distribution of ecological sources, as well as the spread of ecological corridors, differ in different scenarios, which provide decision-makers alternatives to compare.

So far, most research has concentrated on the urban scale, taking specific administrative boundaries as the scope [28–30]. However, many protected areas cover multiple administrative units, and the corridors that connect them also cross the administrative boundaries. Moreover, most ecological processes, such as species dispersal and hydrological and climatic processes, are impacted by natural barriers instead of administrative boundaries. Therefore, ESP study in a physical geographical region is necessary. Except for the above reason, the physical and socioeconomic specificity of the Qinling-Daba Mountain area also highlights the significance of this study. This area is one of China's National Key Ecological function areas for biodiversity conservation. Many endemic species are disturbed in this area, including the Sichuan golden monkey, crested ibis, giant panda, and takin. Meanwhile, it used to be a spatial contiguous poverty-stricken area, where people's livelihoods depended significantly on the products provided by forests and slope farmlands. Setting a high percentage of conservation areas and restricting slope farming will promote supporting, regulating, and cultural (especially aesthetic and scientific value) services of ecosystems but possibly harm the livelihoods of the local residents. Therefore, setting an appropriate proportion of core conservation areas and making tradeoffs between provisioning services and other services are challenging but of vital importance in ESP planning in the study area. Multi-scenario designation is a feasible approach for solving both problems.

This study focuses on ESP in the Qinling-Daba Mountain area based on ecosystem service valuation. Multiple scenarios were designed by varying the total area of core conservation areas (ecological sources) and making tradeoffs between provisioning services and other services. This study will provide multiple alternatives for decision-makers to balance ecosystem conservation and socioeconomic development goals.

2. Materials and Methods

2.1. Study Area

The Qinling-Daba Mountain area in central China spans the following six provinces and cities: Gansu, Shaanxi, Henan, Hubei, Chongqing, and Sichuan. Covering an area of about 300,000 km^2, it extends from the eastern edge of the Qinghai-Tibet Plateau to the southwestern part of the North China Plain (Figure 2). This area includes the Qinling Mountain, Hanjiang River Valley Basin, and Daba Mountain. The Qinling Mountain marks its northern boundary, while the Micang-Daba Mountain forms the southern boundary. The area is characterized mainly by mountainous and hilly landforms interspersed with basins like Hanzhong, Ankang, Shangdan, and Huicheng. This region serves as China's north–south transitional zone, delineating the boundaries between China's northern and southern regions, the subtropical and warm temperate zones, and the Yangtze River and Yellow River basins. Recognized as one of China's biodiversity hotspots, the Qinling-Daba Mountain area is rich in the distribution of endemic species, including the Sichuan golden monkey, crested ibis, giant panda, and takin. Furthermore, it is a large-scale ecological corridor linking the Qinghai-Tibet Plateau with plains in east China, affecting the nation's biodiversity. Spanning the Yangtze, Yellow, and Huai River basins, this area is the source of several rivers, including the Huai, Hanjiang, Danjiang, and Luo rivers. The Qinling-Daba Mountain area was once an area of concentrated and contiguous poverty. Although it has been lifted out of poverty, it still faces critical economic and social development tasks. It is necessary to weigh conservation and development objectives in the ESP planning.

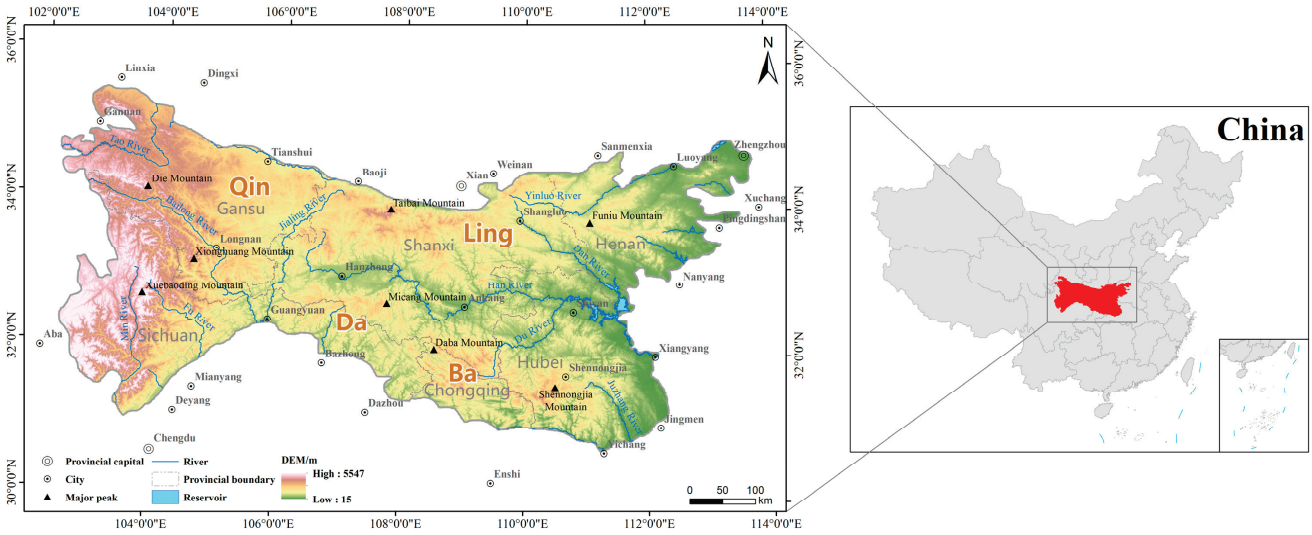

Figure 2. Location of the Qinling-Daba Mountain area, China.

2.2. Data Sources

The datasets used in this study include vector, raster, and statistical data, as shown in Table 1. All datasets were resampled to 1000 m × 1000 m to maintain data consistency, and the projected coordinate system was standardized to WGS_1984_UTM_Zone_49N.

Table 1. Data sources and processing method.

Data	Resolution/Year	Source	Processing
Digital elevation model (DEM)	30 m/2020	NASA https://www.nasa.gov (6 October 2024)	Processed with ArcGIS10.8 to obtain elevation and slope.
Land use and land cover	30 m/2020	CAS Earth Data Sharing and Service Portal https://data.casearth.cn (6 October 2024)	Reclassified into 12 ecosystems.
Normalized difference vegetation index (NDVI)	30 m/2020	Resources and Environmental Science Data Center https://www.resdc.cn (6 October 2024)	
Net primary production (NPP)	500 m/2020	United States Geological Survey (USGS) https://www.usgs.gov (6 October 2024)	
Precipitation	1000 m/2020	National Earth System Science Data Centre http://www.geodata.cn (6 October 2024)	
Soil retention data	300 m/2020	https://www.scidb.cn/en [31] (6 October 2024)	
Built-up areas of Chinese cities	10 m/2020	https://www.scidb.cn/en [32] (6 October 2024)	
Rivers and roads	/	Open Street Map, National Geomatics of China https://www.openstreetmap.org (6 October 2024) https://www.webmap.cn (6 October 2024)	
Natural reserves (NRs)	/	Geographic remote sensing ecological network platform http://www.gisrs.cn/index.html (6 October 2024)	
Population	1000 m/2019	OakRidge National Laboratory https://landscan.ornl.gov (6 October 2024)	
A-level scenic spots	/	Official website of Culture and Tourism Bureau	Converted to points with geographic coordinates in ArcGIS

2.3. Methodology

We started the empirical study with the scenario design and followed the "source-corridor" framework for ESP mapping that comprised the following four main procedures: identifying ecological source identification, constructing ecological resistance surfaces, simulating ecological corridors, and identifying strategic points [14,33]. The workflow of this study is shown in Figure 3. The methods for each procedure are explained in detail below.

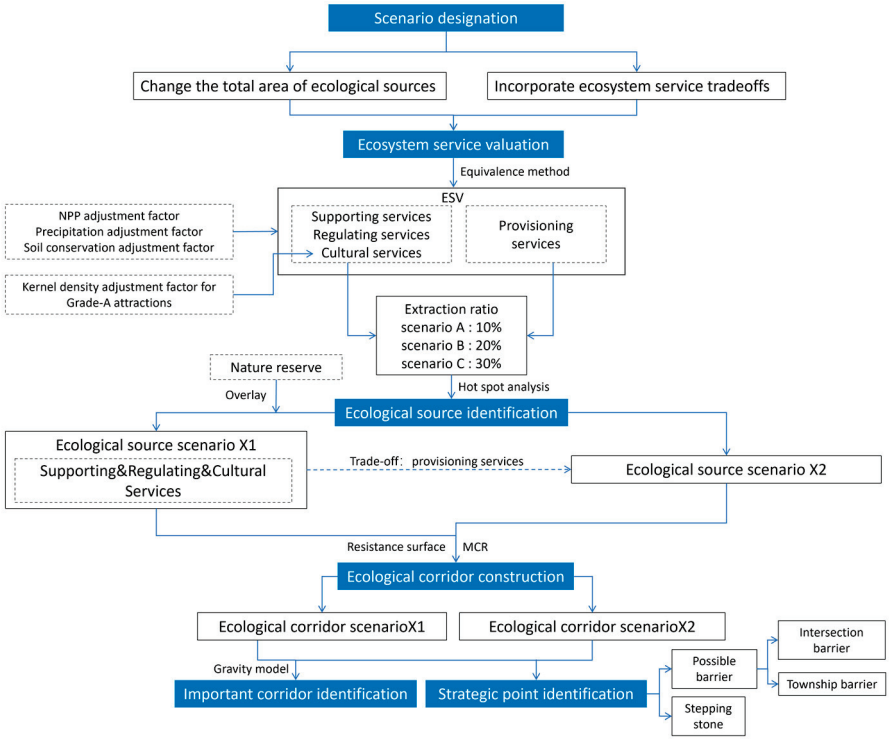

Figure 3. Research workflow.

2.3.1. Scenario Designation

We handled the conservation–development tradeoff problem by mapping the ecological security patterns in multiple scenarios. Since the area and spatial distribution of ecological sources shape the structure and function of ESPs, we designed six scenarios by modifying the area and spatial distribution of ecological sources (Table 2). Referring to many studies on ESP, we regarded the areas with high regulating, supporting, and cultural service values as ecological sources [14,34,35].

Table 2. Six scenarios for ecological security pattern mapping.

Scenario	Scenario	Scenario Note
A	A1	Extract the top 10 percent of the study area regarding the integrated value of supporting, regulating, and cultural services. The extracted regions and natural reserves are set as ecological sources.
	A2	The top 10 percent of the area for provisioning service values is removed from the ecological sources in Scenario A1, and the remaining regions are set as ecological sources.
B	B1	Extract the top 20 percent of the study area regarding the integrated value of supporting, regulating, and cultural services. The extracted regions and natural reserves are set as ecological sources.
	B2	The top 20 percent of the area for provisioning service values is removed from the ecological sources in Scenario B1, and the remaining regions are set as ecological sources.
C	C1	Extract the top 30 percent of the study area regarding the integrated value of supporting, regulating, and cultural services. The extracted regions and natural reserves are set as ecological sources.
	C2	The top 30 percent of the area for provisioning service values is removed from the ecological sources in Scenario C1, and the remaining regions are set as ecological sources.

On the one hand, the total area of ecological sources impacts the tradeoff between conservation and development. More and larger areas of ecological sources set for conservation will limit the space for human development. Many ESP mapping and planning studies extract the top 20 percent of areas for ES values and set them as ecological sources [36–39].

We use the 10%, 20%, and 30% extraction ratios for the following three reasons: (1) The area of established nature reserves (NRs) accounts for about 12 percent of the study area. (2) The area of protected areas (PAs) (including NRs, forest parks, geological parks, and wetland parks) accounts for about 21% of the study area [40]. (3) According to the Blue Book of China's Ecological Protection Red Line (2023) [41], the Chinese government set around 30 percent of the terrestrial area as the ecological redline area (core conservation area). In the scenario designation, the total area of ecological sources increases with the rise in the extraction ratio from Scenario A to C.

On the other hand, the tradeoff between provisioning services and other services is also relevant to the development–conservation tradeoff. Food and raw materials supplied by ecosystems support local people's livelihoods and provide them with development opportunities. However, establishing protected areas to maintain support, regulation, and cultural services may hinder the acquisition of these resources, thereby adversely affecting local communities' livelihoods and potentially slowing economic development. In the scenario designation, the tradeoff between provisioning services and other services is made in Scenarios A2, B2, and C2, which impacts both the area and spatial distribution of ecological sources.

2.3.2. Methods for Ecosystem Service Valuation

The unit-based method was implemented to assess ES value in the study area, by which ESV was estimated based on the ecosystem types and adjusted with the biophysical and socioeconomic characteristics of a specific unit. The ESV evaluation comprises the following four main steps: (1) establishing an equivalent coefficient table, (2) estimating the value of a standard equivalent factor, (3) estimating the ecosystem-based ES value, and (4) amending ecosystem-based ES values by applying spatial adjustment factors. The methods for each step are illustrated below.

(1) Equivalent coefficient table establishment

The equivalent coefficient table provides the relative value of ES provided by different ecosystems [42]. Based on Costanza et al.'s worldwide study, Xie et al. established the equivalent coefficient table for the 11 ESs of 14 ecosystems in China (Appendix B) [42]. We applied this table for this study. The coefficient for each service indicates its relative value to the standard equivalent factor.

(2) Standard equivalent factor (SEF) valuation

The value of the SEF is estimated based on the food production service value of farmland, which is relatively easier to estimate with the available market data. Xie et al. estimated the SEF value as the net profits obtained through cultivating 1 hm^2 of farmland for grains. However, since the profit data are hard to obtain at the national level and vary significantly among different regions, Xie et al. also proposed to set the SEF value as 1/7 of the national average market value of grains yielded by 1 hm^2 of farmland [43].

We referred to Xie et al.'s research but estimated SEF value based on the market value of grains in the QLDBM area rather than that in the whole country [43]. The value of SEF in the QLDAM area was calculated based on the grain yield, planting, and market data with Formula (1). The data of three major grain crops (rice, wheat, corn) in the 31 prefecture-level cities in the QLDAM area were used for the calculation. The value of the SEF is estimated as CNY 1794.31/hm^2.

$$E_a = \frac{1}{7}\sum_{i=1}^{n} \frac{m_i p_i q_i}{M}, i = 1, 2, \ldots, n \quad (1)$$

In the formula, E_a is the economic value of food production services per unit area of farmland ecosystem; i is the variety of food crop; n is the number of grain crop varieties; m_i is the planting area with i^{th} grain crop variety; p_i is the average national price of i^{th} grain crop variety; q_i is the yield per unit area of i^{th} grain crop variety; and M is the total planting area with all varieties of grain crops.

(3) Ecosystem-based ES value estimation

Based on the equivalent coefficient table (Appendix B), ecosystem map (Appendix A), and SEF value in the QLDBM area, the ecosystem-based ES values were estimated using Formulas (2) and (3), and the results are shown in Table 3.

$$VC_{ij} = \sum e_{ij} E_a \quad (2)$$

In the formula, VC_{ij} is the value coefficient of the j^{th} ES for the i^{th} ecosystem type; e_{ij} is the equivalent factor of the j^{th} ES in the i^{th} ecosystem type; i is the ecosystem type; and j is the type of individual ES function.

$$ESV_j = \sum (A_i \times VC_{ij}) \quad (3)$$

In the formula, ESV_j is the value of each unit's j^{th} ES, and A_i is the area of the i^{th} ecosystem type within each unit.

(4) Ecosystem-based ES value adjustment

The ecosystem-based ES values overlook the spatial heterogeneity of other biophysical and socioeconomic factors, except for the ecosystem type. Xie et al. proposed adjustment methods based on some natural factors, such as biomass (NPP), precipitation, and soil conservation [42]. However, they failed to consider the impact of socioeconomic factors on ES values, particularly cultural service values.

This study considers the spatial heterogeneity of cultural services within the study area. We use the kernel density value of A-level scenic spots to adjust the cultural service value (Formula (4)). An A-level scenic spot is certified by the Chinese government, indicating that the area has high aesthetic, recreational, or educational value for developing tourism. The kernel density map of A-level scenic spots was produced in ArcGIS, and the scenic spot adjustment factor (C_{ij}) was calculated based on Formula (4).

$$C_{ij} = A_{ij} / \overline{A} \quad (4)$$

In the formula, C_{ij} is the adjustment factors of A-level scenic spots in the j^{th} year in the i^{th} region of the ecosystem type; A_{ij} is the value of kernel density of A-level scenic spots in the j^{th} year in the i^{th} region of the ecosystem type; and $\overline{A}$ denotes the national annual average kernel density of A-level scenic spots per unit area in the j^{th} year.

Then the NPP, precipitation, soil conservation, and scenic spot adjustment factors were applied to adjust the ecosystem-based ES values based on Formula (5).

$$ESV_{nij} = \begin{cases} P_{ij} \times ESV_{n1} & \text{or} \\ R_{ij} \times ESV_{n2} & \text{or} \\ S_{ij} \times ESV_{n3} & \text{or} \\ P_{ij} \times C_{ij} \times ESV_{n4} & \end{cases} \quad (5)$$

In the formula, ESV_{nij} is the ES value of the n^{th} type of ES function in the j^{th} year of the i^{th} region; ESV_n is the n^{th} type of ES value of that ecosystem type; P_{ij} is the NPP adjustment factor in the j^{th} year of the i^{th} region of that ecosystem type; R_{ij} is the precipitation adjustment factor in the j^{th} year of the i^{th} region of that ecosystem type; S_{ij} is the soil conservation adjustment factor in the j^{th} year of the i^{th} region of that ecosystem type, and the formula for calculating the three adjustment factors is described in the study by Xie et al. [42]; n1 denotes the service of food production, raw material production, gas regulation, climate regulation, environment decontamination, and maintenance of nutrient cycling; n2 denotes the service of hydrological regulation; n3 denotes the service of soil conservation; and n4 denotes the service of aesthetic landscapes.

Table 3. Ecosystem service value coefficient per unit area of the QLDAM Area.

Ecosystems		Provisioning Services		Regulating Services				Supporting Services			Cultural Services
Category	Subcategory	Food Production	Raw Material Production	Gas Regulation	Climate Regulation	Decontaminate Environment	Hydrological Regulation	Soil Conservation	Maintaining Nutrient Cycling	Biodiversity Protection	Aesthetic Landscape
farmland	dry land	1525.17	717.73	1202.19	645.95	179.43	484.46	1848.14	215.32	233.26	107.66
	paddy field	2440.27	161.49	1991.69	1022.76	305.03	4880.53	17.94	340.92	376.81	161.49
forest	coniferous forest	394.75	933.04	3050.33	9097.17	2673.53	5993.01	3696.28	287.09	3373.31	1471.34
	broadleaved forest	520.35	1184.25	3893.66	11,663.04	3463.02	8505.04	4754.93	358.86	4324.29	1901.97
	bush	340.92	771.55	2529.98	7589.94	2296.72	6010.95	3086.22	233.26	2817.07	1238.08
grassland	prairie	179.43	251.20	915.10	2404.38	789.50	1758.43	1112.47	89.72	1004.82	448.58
	shrubs	681.84	1004.82	3534.80	9348.37	3086.22	6854.28	4306.35	322.98	3911.60	1722.54
wetland	wetland	915.10	897.16	3409.19	6459.53	6459.53	43,476.21	4144.86	322.98	14,121.24	8487.10
bare land	bare land	0.00	0.00	35.89	0.00	179.43	53.83	35.89	0.00	35.89	17.94
water area	waterbody	1435.45	412.69	1381.62	4108.98	9958.44	183,450.57	1668.71	125.60	4575.50	3391.25
	glacier and snow	0.00	0.00	322.98	968.93	287.09	12,793.45	0.00	0.00	17.94	161.49
construction area	construction area	0.00	0.00	0.00	0.00	0.00	0.00	0.00	0.00	0.00	0.00

2.3.3. Method for Ecological Corridor Construction: Minimum Cumulative Resistance Model

The minimum cumulative resistance model (MCR) [44] is used to simulate the ecological corridors linking ecological sources. The formula is as follows:

$$MCR = f_{min} \sum_{j=n}^{i=m} (D_{ij} \times R_i) \quad (6)$$

In the formula, MCR is the minimum cumulative resistance value; D_{ij} is the spatial distance of the species from the source j to the landscape unit i; R_i is the resistance value to the migration of the species at the landscape unit i; and f_{min} is a positive function, indicating that the MCR value is positively correlated to the value of D_{ij} and R_i.

The resistance value is obtained from the comprehensive resistance surface. The topography, water systems, and vegetation of the QLDAM area are the most important ecological attributes, with human activities posing ecological stress and soil erosion representing ecological risk [44]. Therefore, this study uses land use types, elevation, slope, vegetation coverage, and distances to major roads, railways, water systems, and built-up areas as indicators to construct a comprehensive resistance surface based on the review and reflection of the following related studies [10,45–48]. Referring to previous research results [44,49,50], resistance coefficients and weights were assigned (Table 4), and a raster calculator was used to perform weighted summation to obtain the comprehensive resistance surface of the QLDAM area.

Table 4. Ecological resistance surface coefficients and weight settings.

Resistance Factor	Weight	Grading Standard	Resistance Value	Resistance Factor	Weight	Grading Standard	Resistance Value
Land Use Type	0.4	Forest, Wetland	1	Elevation (m)	0.15	<700	10
		Grassland, Water	20			1000	30
		Cropland	50			1500	50
		Desert	70			2000	70
		Construction Land	90			>2000	90
Distances from Main Roads (m)	0.03	1000	90	Slope (°)	0.1	0°–8°	10
		3000	70			8°–15°	30
		5000	50			15°–25°	50
		10,000	30			25°–35°	70
		>10,000	10			>35°	90
Distances from Main Railways (m)	0.03	1000	90	Vegetation Cover (%)	0.21	0–20	90
		3000	70			20–40	70
		5000	50			40–60	50
		10,000	30			60–80	30
		>10,000	10			80–100	10
Distances from Main Water Bodies (m)	0.05	1000	10	Distances from Main Urban Areas (m)	0.02	1000	90
		2000	30			3000	70
		5000	50			5000	50
		10,000	70			10,000	30
		>10,000	90			>10,000	10

2.3.4. Method for Important Ecological Corridor and Strategic Point Identification

Gravity models quantitatively evaluate the interaction strength between ecological sources to assess the importance of ecological corridors. The stronger the interaction, the more important the ecological corridor [51]. When using the gravity model to select important ecological corridors, corridors that link authentic, neighboring, or large-scale ecological sources are more likely to be selected as important corridors. This selection strategy is based on several considerations. First, ecological sources with lower ecological

resistance typically reflect better environmental integrity and naturalness, presenting fewer barriers to species migration and dispersal. Second, species prefer paths that minimize distance and migration costs during migration, enhancing the path's prominence in the EN. Third, large-scale ecological sources often support diverse ecosystems and richer biological communities. Corridors linking large-scale sources are therefore evaluated as more important. Additionally, the area of ecological sources is logarithmically transformed to increase the model's sensitivity to small-area sources.

In this study, the gravity model was utilized to classify the ecological corridors into important ecological corridors and general ecological corridors. The formula is as follows:

$$G_{ab} = \frac{N_a N_b}{{D_{ab}}^2} = \frac{\left[\frac{1}{P_a} \times lnS_a\right]\left[\frac{1}{P_b} \times lnS_b\right]}{\left(\frac{L_{ab}}{L_{max}}\right)^2} = \frac{{L_{max}}^2 lnS_a lnS_b}{{L_{ab}}^2 P_a P_b} \quad (7)$$

In the formula, G_{ab} is the interaction strength between ecological sources a and b; N_a and N_b are the weight values of ecological sources a and b, respectively; D_{ab} is the standard value of ecological corridor resistance; $P_a(P_b)$ and $S_a(S_b)$ denote the average value of resistance and area of ecological sources a(b), respectively; L_{ab} is the cumulative value of the corridor resistance between the two sources; and L_{max} is the maximum value of corridor resistance in the study area. The threshold value was set to 5; the corridor with the G_{ab} value higher than 5 is regarded as important ecological corridors.

As for strategic point identification, this study identifies the intersections of two ecological corridors or those of ecological corridors and waterbodies as "stepping stones" facilitating species migration [52]. In contrast, the intersections between ecological corridors and the sites with intensive human activity are taken as "possible barriers", which hinder species movement and increase migration challenges between different ecological sources. Specifically, this study sets the intersections of ecological corridors and transportation lines (mainly highways and railways) as "intersection barriers" [53] and identifies townships on ecological corridors and with high population density (population density > 100 people/km^2) as "township barriers".

3. Results

3.1. Ecosystem Service Values

This study uses the equivalence factor method and relevant factor adjustments to calculate the value of various ESs. Based on the natural breakpoint grading method, these ESs are divided into five levels. As shown in Figure 4, in 2020, the value of four types of ESs in the QLDAM area exhibited significant spatial heterogeneity. High-value areas for provisioning services are mainly distributed in Mianyang City of Sichuan, eastern and southwestern Hubei, and southern Chongqing. In Mianyang City, the primary land use type is forest, which is dominated by raw material supply, while other high-value regions are primarily farmland in plains with high food supply service value. High-value areas for supporting services are mainly located in the southwestern QLDAM area, Micang Mountain, and western Daba Mountain. These areas have rich forest resources, high vegetation coverage, higher altitudes, and minimal human disturbance, which better support soil conservation, nutrient cycling, and biodiversity maintenance functions. High-value areas for regulating services are mainly in Mianyang City of Sichuan, Daba Mountain, Shennongjia, Funiu Mountain, and the northern part of the Hanzhong Basin. These areas have high NPP, significant terrain undulation, dense vegetation, and favorable hydrothermal conditions, which enhance the ecosystem's gas regulation, climate regulation, environment purification, and hydrological regulation functions. High-value areas for cultural services are mainly in Funiu Mountain, Shiyan City of Hubei, western Zuoshui County of Shaanxi, and northeastern Ningshan County. These areas have a high density of national A-level scenic spots, with diverse natural and cultural landscapes, providing higher value for ecological tourism and scientific research.

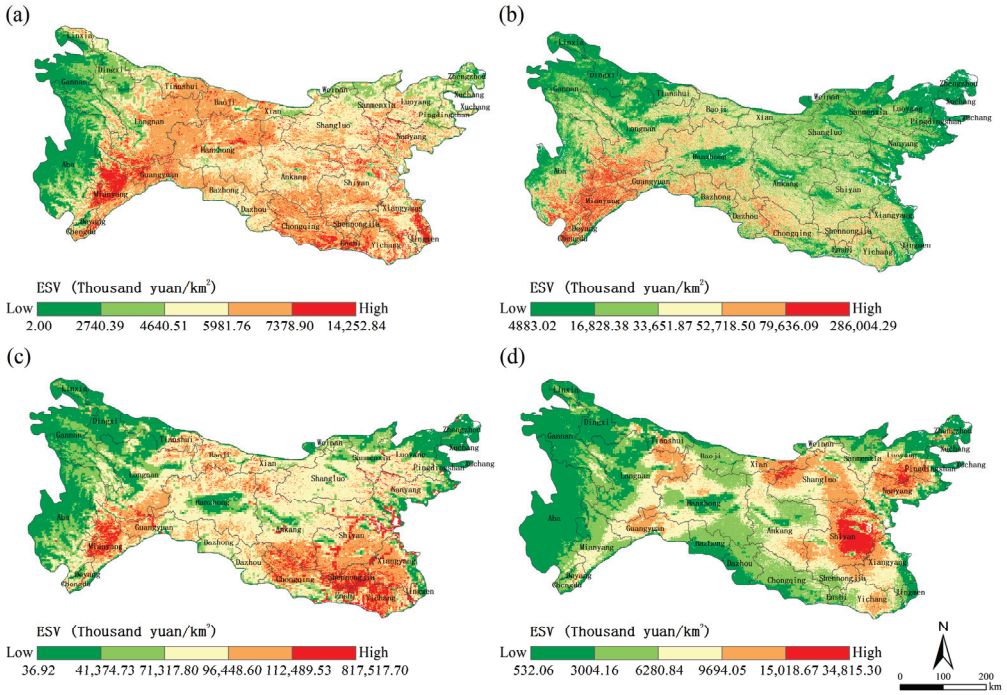

Figure 4. Spatial distribution of four ESVs in the Qinling-Daba Mountain area: (**a**) provisioning service, (**b**) supporting service, (**c**) regulating service, (**d**) cultural service.

The spatial distribution of the aggregated values of ecosystem support, regulation, and cultural services is illustrated in Figure 5. Overall, the ES values exhibit a trend of being higher in the south and lower in the north. High-value regions are primarily concentrated in the northern part of the Hanzhong Basin, near the Taibai Mountain, the southeastern Daba Mountains and Shennongjia forest area, the southern Micang Mountain, and the southwestern Mianyang area. Low-value regions are mainly located in the Hanzhong Basin, the northeastern areas around Zhengzhou, Xuchang, and Luoyang, the eastern edge regions, the northwestern areas along the Tao River, and the regions west of the Min River.

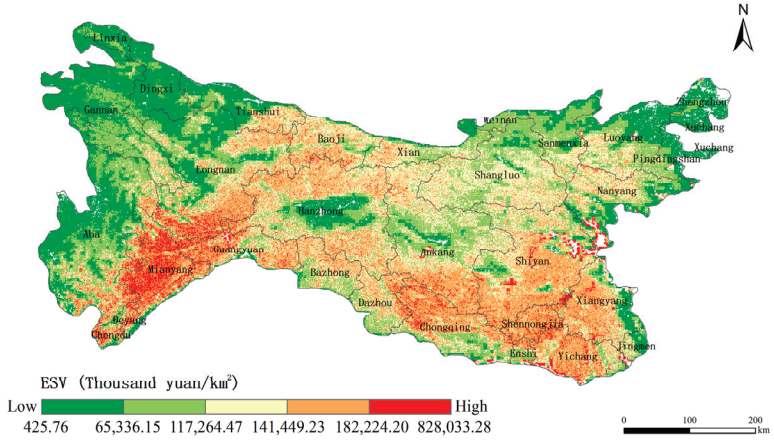

Figure 5. Spatial distribution of aggregated supporting, regulating, and cultural ecosystem service values in the Qinling-Daba Mountain area.

3.2. Distribution of Ecological Sources in Different Scenarios

Based on the results of ES valuation, we identified the ecological sources in six scenarios and mapped them in Figure 6. The statistics of the ecological sources in each scenario are summarized in Table 5.

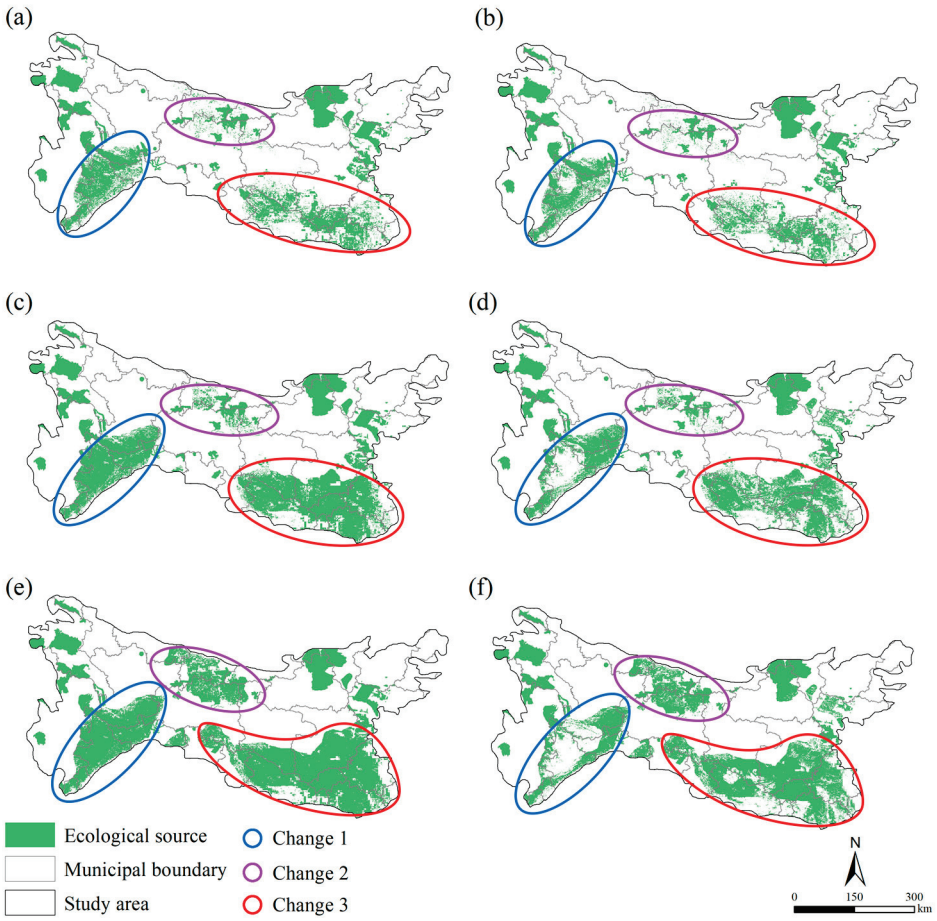

Figure 6. Spatial distribution of ecological sources in different scenarios in the Qinling-Daba Mountain area: (**a**) Scenario A1, (**b**) Scenario A2, (**c**) Scenario B1, (**d**) Scenario B2, (**e**) Scenario C1, (**f**) Scenario C2. Change 1 indicates the change in ecological sources in the Min Mountain area, Change 2 indicates the change in ecological sources in the Qinling-Daba Mountain area, and Change 3 indicates the change in ecological sources in the Micang-Daba-Shennongjia Mountain area.

Table 5. Statistics of source indicators in each scenario.

Sight	Number of Source Sites	Total Source Area (km^2)	Total Area of the Study Area (%)	Forested Land in Total Source Area (%)	Grassland as a Percentage of Total Source Area (%)	Cultivated Land in Total Area of Source Land (%)
A1	26	67,884.64	21.76	82.65	8.04	8.02
A2	27	62,743.81	20.11	82.21	8.66	7.77
B1	32	91,354.42	29.28	84.88	6.15	7.83
B2	34	75,942.13	24.34	84.01	7.27	7.46
C1	23	114,748.14	36.78	86.40	5.08	7.54
C2	26	92,956.31	29.79	85.83	6.10	7.00

In terms of spatial distribution (Figure 6), the ecological sources were mainly located in the areas of the Die, Min, Qinling, Micang-Daba-Shennongjia, and Furniu mountains. According to the data in Table 4, from the perspective of land use types of ecological sources, forest is the main component of the ecological sources, accounting for more than 80% of the total source area, and the percentage increases from Scenario A to C. The percentage of grassland and farmland follows that of the forest, accounting for 5%~9% and 7%~8% of the total source area in the study area, respectively. However, their percentages decrease from Scenario A to C.

The total area of ecological sources impacts their spatial patterns. In Scenario A1, ecological sources are fragmented and scattered; some patches with high ecosystem values are not included in ecological sources. In Scenario B1, more scattering patches are included in ecological sources. In Scenario C1, ecological sources become spatial contiguous; the number of ecological sources decreases, but their average area increases, and fragmentation decreases. This trend can be easily observed in the Min Mountain area (blue circle), the Qinling Mountain area (purple circle), and the Micang-Daba-Shennongjia Mountain area (red circle). Large-scale ecological sources provide diverse ecosystems and are more resilient to natural and human disturbance, and their ecological values are higher than those of small-scale ecological sources. Therefore, the ecological sources in Scenario C1 are preferable to those in Scenarios A1 and B1.

ES tradeoffs also affect the patterns of ecological sources. When Scenarios A1, B1, and C1 are compared to Scenarios A2, B2, and C2, the spatial pattern of the ecological sources mainly differs in the Min Mountain and Daba Mountain areas. These two areas feature diverse terrains and ecosystems. Some farmlands and forests in valleys or basins provide local residents with food and raw materials. These areas are unsuitable as ecological sources when considering their provisioning service values. In contrast, the spatial pattern of ecological sources in the Qinling Mountain area remains similar, indicating that these areas' provisioning service values are not high. This area is more suitable to be conserved for biodiversity and ecological safety.

3.3. Distribution of Ecological Corridors in Different Scenarios

Considering the undesirable pattern and function of ecological sources in Scenarios A1 and A2, we only constructed ecological corridors for ecological sources in Scenarios B1, B2, C1, and C2 based on the cumulative resistance surface (Figure 7) and MCR model.

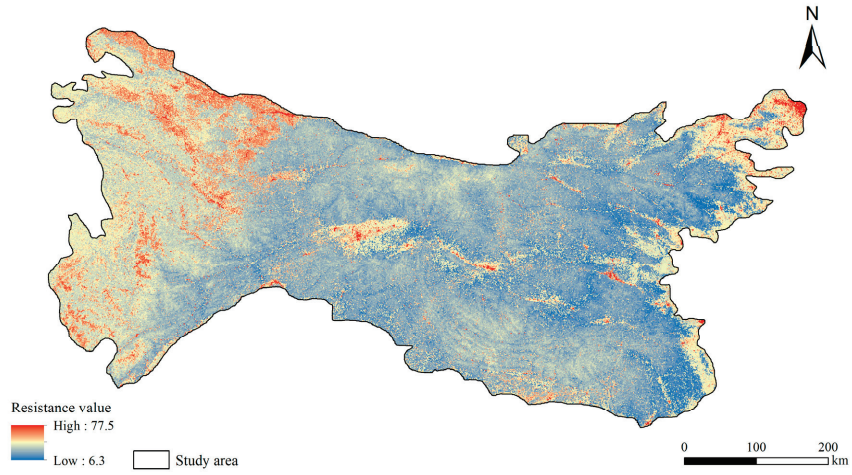

Figure 7. The cumulative resistance surfaces for ecological corridor identification in the Qinling-Daba Mountain area.

The spatial pattern of ecological sources significantly impacts the number and distribution of ecological corridors. In Scenario B1, the corridors are densely distributed because of the small-scale and scattered ecological sources. Their construction cost will be very high. With the decreasing number of ecological sources, there are 16 fewer corridors in Scenario C1 than in Scenario B1; the total length of corridors is also 1451.40 km shorter (Table 6). This implies that the cost of their construction is much lower. Similar changes also happen from Scenario B2 to C2. The abovementioned change in ecological corridors can be observed in the Min Mountain, Qinling-Micang Mountain, Funiu Mountain, and Micang-Daba-Shennongjia Mountain areas (Figure 8).

Table 6. Statistics of ecological corridors in each scenario.

Scenario	Number of Corridors	Total Length of Corridor (km)	Average Length (km)	Corridor Density (km/km^2)
B1	68	8812.95	129.60	2.82
B2	74	9212.25	124.49	2.95
C1	52	7361.55	141.57	2.36
C2	60	8384.43	139.74	2.69

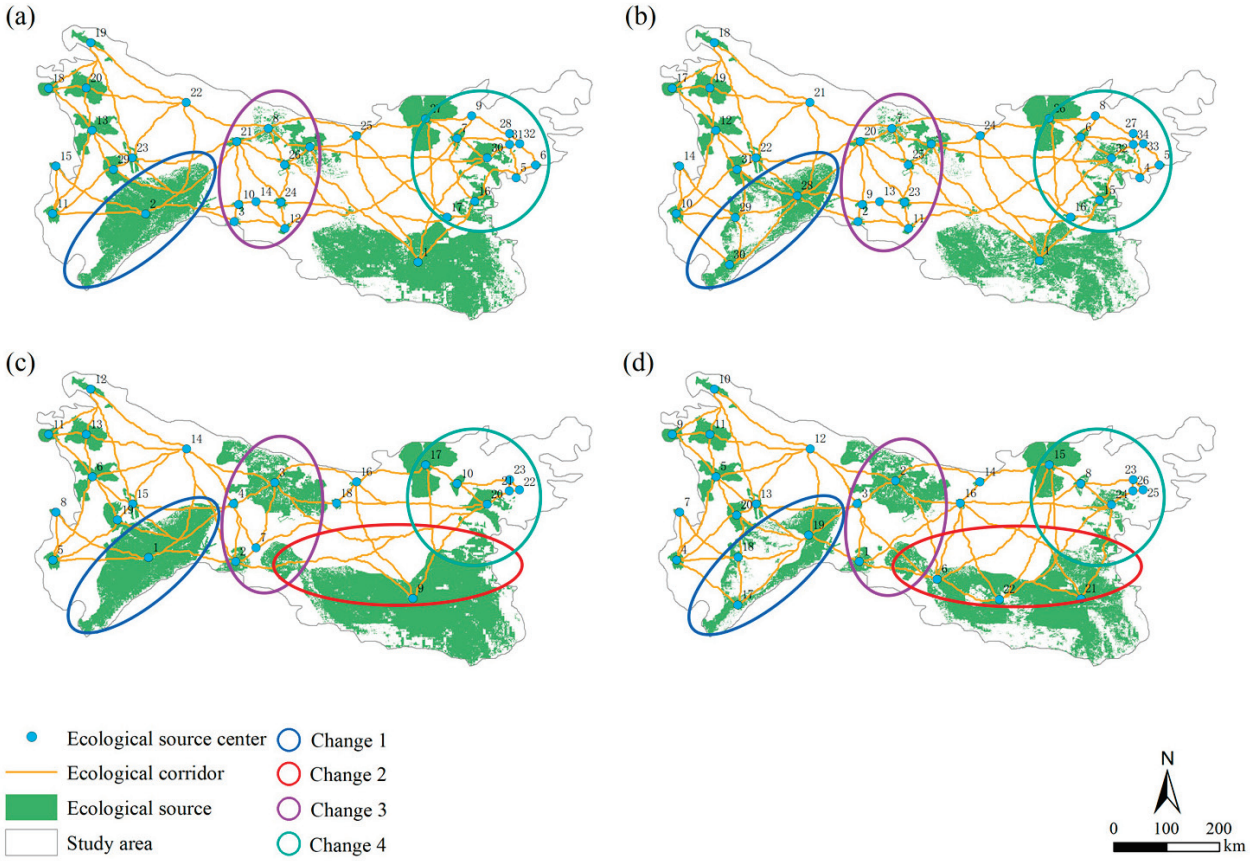

Figure 8. Ecological corridors in different scenarios in the Qinling-Daba Mountain area: (**a**) Scenario B1, (**b**) Scenario B2, (**c**) Scenario C1, (**d**) Scenario C2. Change 1 indicates the change in ecological corridors in the Min Mountain region, Change 2 indicates the change in ecological corridors in the Daba-Shennongjia Mountain area, Change 3 indicates the change in ecological corridors in the Qinling Mountain and Micang Mountain, and Change 4 indicates the change in ecological corridors in the Funiu Mountain.

When Scenarios B2 and C2 are compared to Scenarios B1 and C1, the main differences in the ecological corridors are distributed in the Min Mountain (blue circle), Qinling Mountain (purple circle), Micang Mountain (purple circle), Daba-Shennongjia Mountain (red circle), and Funiu Mountain (cyan circle). When the large-scale ecological sources are divided into a few small-scale ones, corridors are constructed to link them.

3.4. Important Ecological Corridors and Strategic Points

The important ecological corridors were identified with the gravity model. As shown in Table 7, the average length of important ecological corridors is much shorter than that of all corridors in all scenarios.

Table 7. Statistics of key ecological corridors and strategic point indicators for each scenario.

Sight	Number of Ecological Corridors of Importance	Total Length (km)	Average Length (km)	Number of Intersection Barriers	Number of Township Barriers	Number of Stepping Stones
B1	30	2122.72	70.76	98	162	28
B2	31	2200.76	70.99	94	149	31
C1	18	1588.36	88.24	66	125	38
C2	17	1461.59	85.98	71	137	42

The spatial distribution (Figure 9) of important ecological corridors in Scenarios B1 and B2 is similar; they are mainly distributed in the central Qinling and Micang Mountain areas and the eastern Funiu Mountain, Shennongjia, and Daba Mountain areas. The direction of most corridors is north–south, and their lengths are shorter, connecting smaller-scale and proximate ecological sources. In Scenarios C1 and C2, the spatial distribution of important ecological corridors notably differs. In Scenario C1, they are mainly distributed in the northwestern Die Mountain, central Qinling and Micang Mountain, and eastern Funiu Mountain, Shennongjia, and Daba Mountain areas, mainly forming north–south connections. In Scenario C2, they are mainly distributed in the southwestern Min Mountain, southern Micang-Daba-Shennongjia Mountain, and northeastern Funiu Mountain areas, forming both north–south and east–west connections. Many of these corridors link large-scale ecological sources that are far away.

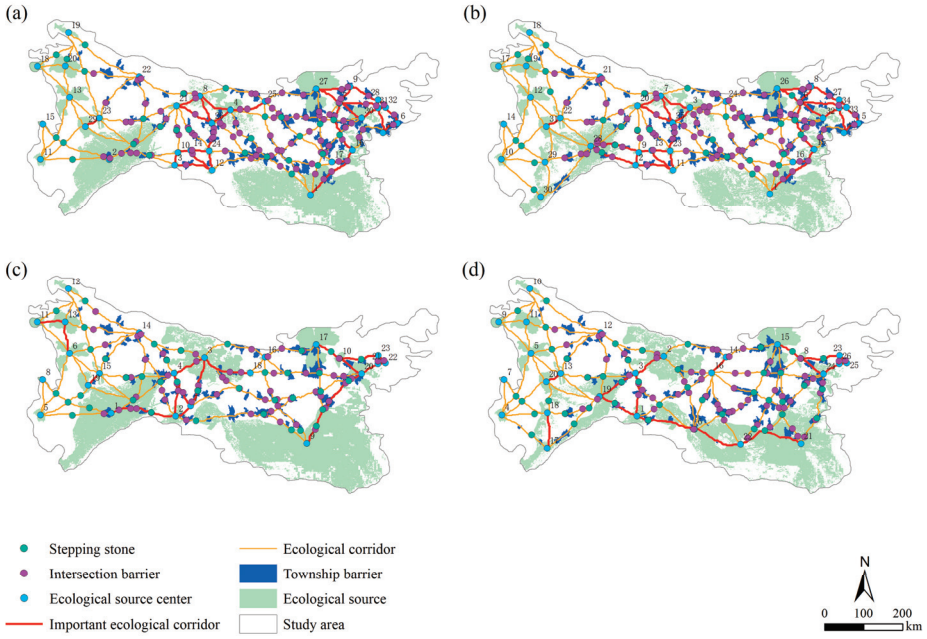

Figure 9. Distribution of important ecological corridors and strategic points in the Qinling-Daba Mountain area: (**a**) Scenario B1, (**b**) Scenario B2, (**c**) Scenario C1, (**d**) Scenario C2.

The following two types of strategic points were identified: possible barriers and stepping stones. The possible barriers include the intersection barriers and the township barriers. The statistics of strategic points in different scenarios are summarized in Table 7. The number of intersection barriers and township barriers in Scenario C is much less than that in Scenario B, especially in Scenario C1. Meanwhile, the number of stepping stones in Scenario C is higher than that in Scenario B. More barriers in Scenario B indicate more human interference in the ecological corridors, resulting in a higher cost for corridor construction and management. In contrast, Scenario C's fewer barriers and more widely distributed stepping stones indicate better ecological connectivity and lower ecological maintenance costs. The location of the strategic points is provided in the Appendices C–E.

4. Discussion

4.1. Tradeoffs between Conservation and Development in Ecological Security Pattern

With the challenging tasks of conserving biodiversity and promoting people's livelihoods, the tradeoff between conservation and development has to be cautiously handled in ESP planning in the QLDBM area.

Ecological sources, as the core elements of ESP, can be regarded as protected areas or core conservation areas. Setting an appropriate percentage of ecological sources is vitally important and challenging in ESP planning. At the global scale, The Aichi Target 11 set the goal of conserving at least 17% of terrestrial and inland areas. The 30 × 30 Biodiversity Goal at COP28 calls for conserving 30% of Earth's land and seas for global biodiversity conservation. In our study, the percentage of ecological sources ranges from 10 to 30%. With the increasing percentage, the integrity and connectivity of ecological sources improve. It will benefit biodiversity. However, the increase in the area of ecological sources also reduces the land available for human development and utilization. In areas dominated by forests, grasslands, and farmlands, setting large areas of ecological sources may restrict forestry, animal husbandry, and agricultural development and, therefore, negatively impact people's incomes and livelihoods. Nonetheless, the construction of ecological infrastructure creates opportunities for developing tourism, thereby providing new prospects for local economic development and the transformation of farmers' livelihoods [54]. Setting different types of ecological sources might be a feasible measure to balance protection and development; core ecological sources prohibit human activities, while supplementary sources allow for the development of ecotourism and eco-agriculture.

The length and density of ecological corridors are also relevant to conservation and development tradeoffs. Densely distributed ecological corridors will support wild animal migration and species dispersal. However, constructing and maintaining ecological corridors require a large financial investment. It might reduce the funds for other public services and infrastructure, weakening the local government's ability to improve public welfare [55,56]. Therefore, it is advisable to use natural forests, grasslands, and rivers as ecological corridors to minimize the cost of ecological corridor construction. Meanwhile, it is of vital importance to identify risk points in the corridors.

4.2. Strategic Points Identification and Management

Strategic points play an essential role in ensuring the connectivity of ESPs. Identifying the locations of significant strategic points is necessary for implementing preventive measures. In addition, management measures should be given priority and supplemented with engineering measures to avoid or mitigate the risks.

Previous studies have mainly focused on the intersections of corridors with major transportation lines or water sources, considering the former as possible barriers and the latter as stepping stones. In addition to these two types of strategic points, this paper identifies the intersections of ecological corridors with townships where the population density exceeds 100 people/km^2 and regards them as possible barriers to ecological processes, especially for terrestrial animal migration. Aside from directly implementing ecosystem restoration and management programs in these townships, the local government is suggested to provide ecological education to the public, making them realize the importance and the suitable approaches for biodiversity and ecosystem conservation.

4.3. Limitations of This Study and Future Directions

Traditional ESP planning often regards established nature reserves as ecological sources, overlooking other areas with significant ecological functions. Applying ES evaluation to identify ecological sources has become a research trend, with significant supporting, regulating, and cultural services being regarded as ecological sources. However, practical applications face challenges in determining appropriate proportions or thresholds for high-value ES areas. If the thresholds are too small, they result in fragmented ecological

sources; if they are too large, they lead to excessively expansive sources, thereby increasing construction and protection costs.

This study proposes a solution by setting different proportions and mapping ESPs in multiple scenarios. The scenario that maintains the integrity of ecosystems and takes care of residents' dependency on the provisioning services of ecosystems is preferred. However, such an approach also has limitations.

Firstly, this study chose a resolution of 1 km^2 for research based on the following two considerations: limitations of the data and feasibility of data analysis and network construction. On the one hand, the precipitation, population, and other data are only available with a resolution of 1 km^2. On the other hand, the research area involved in this project is very large. Using higher-resolution data would increase the complexity and processing time of the network construction and make it challenging to apply the results to support ecosystem management at the regional level. In the future, we will consider partitioning the research area into some subzones, simulating the ecological security pattern in each zone, and discussing scale effects.

Secondly, in this study, the tradeoff between ecological conservation and people's livelihoods was made by varying the area and number of ecological sources and considering the tradeoff between provisioning and other services. This study did not explicitly incorporate socioeconomic indicators (e.g., income, employment dependency on land). Incorporating these data into ESP will provide a clear understanding of the tradeoffs between ecological and social benefits. However, it is feasible to include these factors in ESP mapping at smaller scales (such as the city level) rather than in large-scale studies since such data often need to be collected through surveys.

Thirdly, one scenario has a fixed percentage, while the optimal percentage might be a range rather than a fixed value. In addition, the method assumes a competitive relationship between provisioning services and other services. However, in actual ecosystems, the relationships between various services may be more complex than synergistic or competitive. Future research could consider using multi-objective optimization methods to produce a few Pareto optimal alternatives for ESPs instead of a single solution so that decision-makers can compare the strengths and shortcomings of each solution to make a final selection.

Finally, this study uses a spatial planning perspective to map the ecological security pattern. Lacking knowledge in ecology and zoology, we did not consider and handle migration differences among terrestrial animals, birds, and aquatic animals or those between large and small animals in the ecological corridors. This is a common limitation of most ESP studies, which can only be overcome through collaboration among researchers and practitioners from multiple scientific fields.

5. Conclusions

This study maps ESPs in the Qinling-Daba Mountain area based on the valuation of ESs. The tradeoff between conservation and development was handled through multi-scenario designation and ES tradeoffs. The main conclusions are as follows:

First, about 30 percent of the study area is suitable for being set as ecological sources based on their values for provisioning, regulating, supporting, and cultural ESs. Such planning helps maintain the integrity of natural ecosystems and leaves space for human living and development, thereby balancing ecological protection and livelihood needs in the Qinling-Daba Mountains Area.

Second, development and conservation tradeoffs need to be made, especially in the Min Mountain and Daba Mountain areas. Establishing large-scale and spatial contiguous ecological sources in these regions may impact the livelihoods of local residents. The tradeoff can be made by setting sources with smaller sizes but constructing corridors to connect them to support species migration and other ecological processes.

Third, both shorter corridors in the north–south direction and longer corridors in the west–east direction need to be constructed in the study area to better maintain biodiversity and regional ecological security. The former connects proximate ecological sources for the

daily movements of biological populations; the latter links large-scale and distant ecological sources to facilitate the seasonal migration of species, gene flow, and large-scale ecological processes.

Fourth, possible barriers in ecological corridors include both the intersections of corridors and major traffic lines and townships with high population density (>100 people/km^2). Engineering, management, and education measures should be integrated to address these possible barriers and reduce human interference with wildlife dispersal or other ecological processes.

In conclusion, referring to the control measures proposed by previous studies [57], we offer the following recommendations for consideration:

1. Governments should make policies and take action to encourage farmers to adopt sustainable agricultural practices. For example, they could provide financial subsidies to offset the initial costs, offer tax incentives to reward environmentally friendly farming methods, and organize technical training programs to educate farmers on sustainable techniques. These measures would encourage more farmers to transition to eco-friendly practices, ultimately benefiting both the environment and agricultural productivity.
2. Establish a robust implementation mechanism for managing ecological corridors. Detailed planning for ecological corridors should be developed and endorsed by local governments and relevant departments. A cross-departmental coordination mechanism is crucial; departments responsible for environmental protection, transportation planning and management, and agricultural development and management should be involved in the decision-making process for ESP planning and construction.

Author Contributions: Conceptualization, M.S., P.Z. and Q.L.; methodology, M.S., P.Z. and Q.L.; software, P.Z. and Q.L.; validation, P.Z. and Q.L.; formal analysis, M.S., P.Z. and Q.L.; data curation, P.Z. and Q.L.; writing—original draft preparation, M.S., P.Z. and Q.L.; writing—review and editing, M.S. and P.Z.; visualization, P.Z.; supervision, M.S.; project administration, M.S.; funding acquisition, M.S. All authors have read and agreed to the published version of the manuscript.

Funding: This research was funded by the Research Project of Humanities and Social Sciences of the Ministry of Education, China (grant number 23YJA630046), and the National Natural Science Foundation of China (grant number 42001229). We acknowledge the founders for their support.

Data Availability Statement: No new data were created or analyzed in this study. Data sharing is not applicable to this article.

Conflicts of Interest: The authors declare no conflicts of interest.

Appendix A

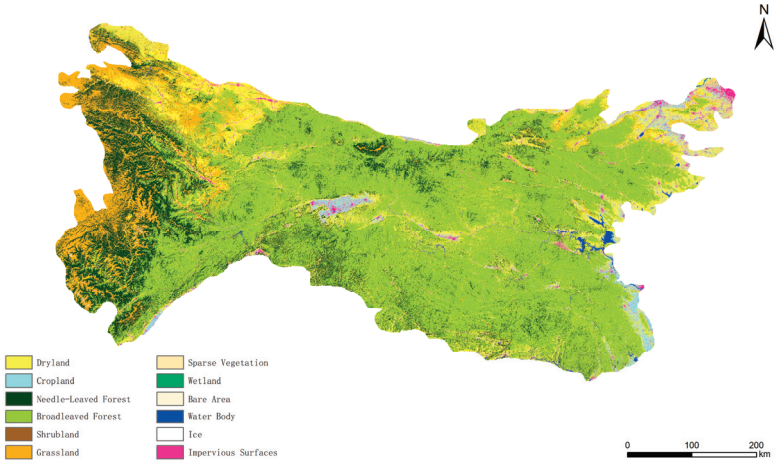

Figure A1. Classification of ecosystem.

Appendix B. The Equivalent Coefficient Table for This Study

Ecosystems		Provisioning Services		Regulating Services				Supporting Services			Cultural Services
Category	Subcategory	Food Production	Raw Material Production	Gas Regulation	Climate Regulation	Decontaminate Environment	Hydrological Regulation	Soil Maintenance	Maintaining Nutrient Cycling	Biodiversity Protection	Aesthetic Landscape
farmland	dry land	0.85	0.40	0.67	0.36	0.10	0.27	1.03	0.12	0.13	0.06
	paddy field	1.36	0.09	1.11	0.57	0.17	2.72	0.01	0.19	0.21	0.09
forest	coniferous forest	0.22	0.52	1.70	5.07	1.49	3.34	2.06	0.16	1.88	0.82
	broadleaved forest	0.29	0.66	2.17	6.50	1.93	4.74	2.65	0.20	2.41	1.06
	bush	0.19	0.43	1.41	4.23	1.28	3.35	1.72	0.13	1.57	0.69
grassland	prairie	0.10	0.14	0.51	1.34	0.44	0.98	0.62	0.05	0.56	0.25
	shrubs	0.38	0.56	1.97	5.21	1.72	3.82	2.40	0.18	2.18	0.96
wetland	wetland	0.51	0.50	1.90	3.60	3.60	24.23	2.31	0.18	7.87	4.73
bare land	bare land	0.00	0.00	0.02	0.00	0.10	0.03	0.02	0.00	0.02	0.01
water area	waterbody	0.80	0.23	0.77	2.29	5.55	102.24	0.93	0.07	2.55	1.89
	glacier and snow	0.00	0.00	0.18	0.54	0.16	7.13	0.00	0.00	0.01	0.09
construction area	construction area	0.00	0.00	0.00	0.00	0.00	0.00	0.00	0.00	0.00	0.00

Appendix C. Specific Distribution of Intersection Barriers

Province/City		Scenario B1	Scenario B2	Scenario C1	Scenario C2
Gansu Province	Dingxi City	Dacaotan Township			
	Longnan City	Awu Township, Jugan Township, Changdao Township, Yanguan Township, Paosha Township			
		Yuhuang Township	Yuhuang Township, Zhongmiao Township	Linjiangpu Township, Jialing Township, Chengguan Township (Hui County), Yuhuang Township	Linjiangpu Township, Chengguan Township (Hui County), Jialing Township, Zhongmiao Township
Henan Province	Nanyang City	Xiping Township, Chongyang Township, Xihuang Township			
		Shangji Township, Danshui Township, Nanhedian Township, Cuizhuang Township	Nanhedian Township, Cuizhuang Township, Danshui Township, Shangji Township,		Huiche Township, Shangji Township
	Sanmenxia City	Shuanghuaishu Township			
		Dongming Township, Fanli Township, Hengjian Township	Dongming Township, Fanli Township		
	Luoyang City	Checun Township			
		Tantou Township, Miaozi Township	Tantou Township		

Province/City		Scenario B1	Scenario B2	Scenario C1	Scenario C2
Hubei Province	Shiyan City	Chengguan Township (Utopia County), Qingqu Township of Wudang Mountain Special Zone			
		Shuiping Township, Shuangtai Township, Wenfeng Township, Hualongyan Township, Guanshan Township, Baisangguan Township, Shangjin Township, Huanglong Township, Bolin Township	Guanshan Township, Yaohuai Township of Wudang Mountain Special Zone, Shangjin Township, Baisangguan Township, Huanglong Township, Bolin Township, Shuangtai Township, Wenfeng Township, Shuiping Township	Bolin Township, Wenfeng Township, Shuiping Township	Tuguanya Township, Qingfeng Township, Yinjifu Township, Xiangkou Township, Baoxia Township, Huanglong Township, Yishui Township, Shuiping Township
	Xiangyang City				Xiaohe Township
Shaanxi Province	Ankang City	Xianhe Township, Chengguan Township (Ziyang County), Chengguan Township (Pingli County), Lvhe Township, Zongxi Township			
		Hongshan Township, Hengkou Township, Jihe Township, Meizi Township, Huangguan Township, Yunwushan Township, Tongmu Township, Shenhe Township	Hengkou Township, Hongshan Township, Jihe Township, Meizi Township, Huangguan Township, Simudi Township, Yunwushan Township, Tongmu Township, Shenhe Township	Tanba Township, Yanba Township, Tongchewan Township, Yunwushan Township, Tongmu Township, Ganxi Township	Goupa Township, Jihe Township, Hengkou Township, Pingliang Township, Zuolong Township, Tongchewan Township
Shaanxi Province	Baoji City	Pingkan Township, Fengzhou Township			
	Hanzhong City	Xingzhou Street Office, Jinshui Township			
		Wuguanyi Township, Matiwan Township, Lesuhe Township, Chadian Township, Xinjiezi Township, Yuandun Township, Xinpu Township, Liangshan Township, Dahekan Township, Tea Township, Moziqiao Township, Jinshui Township, Longting Township, Yangjiahe Township	Yuanjiazhuang Street Office, Wuguanyi Township, Matiwan Township, Lesuhe Township, Xinjiezi Township, Xinpu Township, Qishuba Township, Dahekan Township, Liangshan Township, Guangping Township, Tea Township, Moziqiao Township, Qi's Street Office, Yangjiahe Township	Yuanjiazhuang Street Office, Xuwang Township, Baiquesi Township, Chadian Township, Yuandun Township, Fuchuan Township, Shengshui Township, Xiaonanhai Township, Hanyuan Street Office, Daijiba Township, Huishuguan Town	Yuanjiazhuang Street Office, Yuhuangmiao Township, Lesuhe Township, Chadian Township, Yuandun Township, Qishuba Township, Hongmiao Township, Yankou Township
	Shangluo City	Zhulinguan Township, Gaobadian Township, Yingpan Township, Huilong Township			
		Longjuzhai Street Office, Sehepu Township, Jinshixia Township, Guofenglou Township, Qingyouhe Township, Chengguan Street Office, Qianyou Street Office, Xiaoling Township, Xingping Township	Longjuzhai Street Office, Guofenglou Township, Qingyouhe Township, Chengguan Street Office, Qianyou Street Office, Xiaoling Township, Xingping Township	Guofenglou Township	Dajing Township, Yicun Township, Xingping Township
	Xi'an City	Shijing Township, Wangchuan Township			

Province/City		Scenario B1	Scenario B2	Scenario C1	Scenario C2
Sichuan Province	Aba Prefecture	Tumen Township			
	Bazhong City	Dongyu Township, Lianghekou Township			
		Guanba Township, Xinchang Township	Guanba Township, Xinchang Township		Guanba Township
	Dazhou City	Hekou Township	Hekou Township		Lishu Township
	Deyang City	Banqiao Township	Banqiao Township	Banqiao Township	
	Guangyuan City	Shahe Township, Sanguo Township			
		Gongnong Township, Yaodu Township, Wali Township, Guanyindian Township	Douzhuan Township, Datan Township, Gongnong Township, Daba Township, Muyu Township, Yaodu Township	Gongnong Township, Wali Township, Guanyindian Township, Yaodu Township	Xuanhe Township
	Mianyang City	Longan Township, Gaocun Township	Longan Township	Longan Township	Longan Township
Chongqing	Chongqing	Tucheng Township	Tucheng Township, Jiangkou Township	Jiangkou Township	Tucheng Township
Major highways		Lanzhou-Haikou Highway, Wuhan-Jiujiang Highway, Shiyan–Tianshui Highway, Huhhot–Beihai Highway, Shanghai–Xi'an Highway, Zhengzhou-Yaoshan Highway, Macheng–Ankang Highway, Fuzhou–Yinchuan Highway, Ankang-Langao Highway, Beijing–Kunming Highway, Ankang–Laifeng Highway, Ningshan-Shiquan Highway, Yinchuan–Kunming Highway, Highway Tunnel of Qinling Zhongnan Mountain, Wudu-Guanzigou Highway, Guangyuan-Pingwu Highway, Pingliang-Mianyang Highway			
		Mianchi-Xichuan Highway, Erenhot–Guangzhou Highway, Yunxi-Wuxi Highway, Baoji-Hanzhong Highway, Zuoshui-Shanyang Highway	Mianchi-Xichuan Highway, Erenhot–Guangzhou Highway, Yunxi-Wuxi Highway, Baoji-Hanzhong Highway, Xixiang-Zhenba Highway, Zuoshui-Shanyang Highway,	Liandang-Huixian Highway, Meixian-Fengxiang Highway	Mianchi-Xichuan Highway, Zuoshui-Shanyang Highway, Liandang-Huixian Highway, Meixian-Fengxiang Highway
Major railways		Xiangyang-Chongqing Railway, Baoji-Chengdu Railway, Xi'an-Chengdu High-Speed Railway			
		Haolebaoji-Ji'an Raiway, Yangpingguan-Ankang Railway, Nanjing-Xi'an Railway	Haolebaoji-Ji'an Railway, Yangpingguan-Ankang Railway, Lanzhou-Chongqing Railway, Nanjing-Xi'an Railway, Xi'an-Ankang Railway	Lanzhou-Chongqing Railway, Yangpingguan-Ankang Railway, Xi'an-Ankang Railway	

Appendix D. Specific Distribution of Township Barriers

Province/City		Scenario B1	Scenario B2	Scenario C1	Scenario C2
Gansu Province	Dingxi City	Lujing Township, Shendu Township			
	Gannan Prefecture	Changchuan Township, Dianzi Township, Shimen Township			
	Longnan City	Xiaochuan Township, Chenyuan Township, Lianghekou Township, Shawan Township, Liulin Township, Nianba Township, Lianghe Township, Zhongba Township, Qishan Township, Shiqiao Township, Jugan Township, Sanhe Township, Shibao Township, Changdao Township			
		Paosha Township, Wangba Township, Yongxing Township, Yanguan Township, Huangping Township	Wangba Township, Huangping Township	Paosha Township, Nanyang Township, Ginkgo Tree Township, Yanguan Township, Pipa Township	Nanyang Township, Ginkgo Township, Yanguan Township, Pipa Township,
	Tianshui City	Yan'an Township, Tange Township			
Henan Province	Luoyang City	Luanchuan Township, Shimiao Township			
		Tantou Township, Guxian Township, Old County Township	Tantou Township, Guxian Township, Old County Township		
	Nanyang City	Chongyang Township, Shuanglong Township, Sangping Township, Wuliqiao Township, Jingziguan Township			
		Nanhedian Township, Taishanmiao Township, Liushan Township, Chengjiao Township, Sikushu Township, Huangludian Township, Shimen Township, Chimei Township, Mashankou Township, Yangcheng Township, Danshui Township, Shangji Township, Madeng Township, Laozhuang Township, Gaoqiu Township	Nanhedian Township, Taishanmiao Township, Liushan Township, Sikeshu Township, Huangludian Township, Shimen Township, Chimei Township, Mashankou Township, Yangcheng Township, Danshui Township, Shangji Township, Madeng Township, Laozhuang Township, Gaoqiu Township		Huiche Township, Shangji Township, Madeng Township
	Sanmenxia City	Zhuyangguan Township			
		Shahe Township, Hengjian Township, Dongming Township	Shahe Township, Hengjian Township, Dongming Township		

Province/City		Scenario B1	Scenario B2	Scenario C1	Scenario C2
Hubei Province	Shiyan City	Qingqu Township, Utopia Chengguan Township, Liubei Township, Huanglong Township			
		Wudang Mountain Special Zone, Haoping Township, Hongta Township, Jundian Township, Hualongyan Township, Hejia Township, Tumen Township, Anyang Township, Tanjiawan Township, Bolin Township, Huaguo Street Office, Baofeng Township, Majiadu Township, Qingu Township, Yishui Township, Shuiping Township, Xianhe Township, Jiangjiayan Township	Wudang Mountain Special Zone, Haoping Township, Hongta Township, Jundian Township, Hualongyan Township	Hejia Township, Tumen Township, Shuping Township, Xianhe Township, Jiangjiayan Township	Sanguandian Street Office, Langhe Township, Hongta Township, Jundian Township, Hualongyan Township, Hejia Township, Tumen Township, Hujiaying Township, Leigu Township, Pankou Township, Qingu Township, Yishui Township, Shuiping Township
Shaanxi Province	Ankang City	Yinghu Township, Xianhe Township, Yanba Township, Jihe Township, Dazhuyuan Township, Liushui Township, Pingliang Township, Lvhe Township, Shuhe Township			
		Hongshan Township, Shuanglong Township, Jianchi Township, Shuangru Township, Puxi Township, Laoxian Township, Lianghe Township, Maping Township, Shimen Township, Xianhe Township, Haoping Township, Huangu Township, Hongchun Township, Shuang'an Township, and Dongmu Township.	Hongshan Township, Jianchi Township, Puxi Township, Lianghe Township, Maping Township, Shimen Township, Xianhe Township, Haoping Township, Huangu Township, Hongchun Township, Shuang'an Township	Dahe Township, Maping Township, Shimen Township, Huangu Township, Hongchun Township	Kazi Township, Maoping Township, Jianchi Township, Shuangru Township, Puxi Township, Chihe Township, Lianghe Township, Hongjun Township, Shuanghe Township, Xiaohe Township, Xianhe Township, Gaotan Township
	Hanzhong City	Xingzhou Street Office, Chenjiaba Township, Sidu Township, Shahe Township, Maoping Township, Xiaoyang Township			
		Juyuan Township, Jinquan Township, Xinjiezi Township, Dahekan Township, Liangshan Township, Hujiaying Township, Xiangshui Township, Yangchun Township, Yishui Township, Qi's Street Office, Longting Township, Moziqiao Township, Xinglong Township, Guanyin Township	Juyuan Township, Jinquan Township, Xinjiezi Township, Dahekan Township, Liangshan Township, Hujiaying Township, Xiangshui Township, Yangchun Township, Bashan Township, Yishui Township, Qi's Street Office, Longting Township, Moziqiao Township, Xinglong Township, Guanyin Township	Tianming Township, Laozhuang Township, Pu Township, Qili Street Office, Hanwang Township, Xuwang Township, Xujiaping Township, Hengxianhe Street Office, Fuchuan Township, Shengshui Township, Mujiaba Township, Hujiaying Township, Xiangshui Township, Lianghe Township, Hujiaba Township, Bashan Township, Hanyuan Street Office, Liushu Township, Chengbei Street Office, Xinglong Township, Guanyin Township	Tianming Township, Chenjiaba Township, Hengxianhe Street Office, Fuchuan Township, Lianghe Township, Hujiaba Township, Chengbei Street Office, Yancang Township, Bashan Township, Xinglong Township, Guanyin Township

Province/City		Scenario B1	Scenario B2	Scenario C1	Scenario C2
Shaanxi Province	Shangluo City	Longjuzai Street Office, Shiping Township, Tumen Township, Tiyupu Township, Baiyu Temple Township, Jingcun Township, Gucheng Township, Zhongcun Township, Shilipu Street Office, Yinhua Township, Gaobadian Township, Qingshan Township, Muhuguan Township, Dajing Township			
		Sihao Street Office, Hujiayuan Township, Shima Township, Banqiao Township, Fenghuang Township, Daping Township, Miliang Township	Sihao Street Office, Hujiayuan Township, Shima Township, Banqiao Township, Majie Township, Fenghuang Township, Daping Township, Miliang Township	Sihao Street Office, Hujiayuan Township, Banqiao Township, Fenghuang Township	Maping Township, Yongfeng Township, Shimen Township, Yaoshi Township, Yecun Township
	Xi'an City	Pangguang Township, Caotang Township, Jiaodai Township, Louguan Township, Guangji Township, Mazhao Township, Zhuyu Township, Cuifeng Township			
		Yucan Township		Yucan Township	Yucan Township
Sichuan Province	Aba Prefecture	Shuanghe Township, Jin'an Township			Longba Township, Guangming Township
	Bazhong City	Dongyu Township, Nanjiang Township, Catchfield Township, Lianghekou Township			
				Pinghe Township	Pinghe Township
	Guangyuan City	Qiaozhuang Township			
		Maliu Township, Sandui Township, Hexi Street Office, Dade Township	Qiaodou Township, Sandui Township, Hexi Street Office, Muyu Township, Dade Township	Sandui Township, Hexi Street Office, Dahe Township	Xuanhe Township, Chaotian Township, Zengjia Township, Dahe Township
	Mianyang City	Gaocun Township, Gucheng Township			
			Sangzao Township, Qushan Township, Chenjiaba Township, Yong'an Township, Leigu Township, Guixi Township		Qushan Township, Chenjiaba Township, Leigu Township, Guixi Township
Chongqing	Chongqing city				Fuxing Street Office

Appendix E. Specific Distribution of Stepping Stones

Province/City		Scenario B1	Scenario B2	Scenario C1	Scenario C2
Gansu Province	Dingxi City	QinXu Township			
	Gannan Prefecture	Lexiu Township,			
		Kaerqin Township	Lijie Township, Kaerqin Township	Lijie Township	Lijie Township
	Linxia Prefecture	Lianlu Township			
	Longnan City	Chengguan Township (Kang County), Zhongmiao Township	Nianba Township	Jialing Township, Mayanhe Township, Nianba Township, Zhongmiao Township, Waina Township	Jialing Township, Mayanhe Township, Nianba Township, Waina Township
Henan Province	Luoyang City			Luanchuan Township	Chitudian Township
	Nanyang City			Chongyang Township	Jingziguan Township, Shangji Township
	Sanmenxia City		Xujiawan Township	Xujiawan Township	Xujiawan Township
Hubei Province	Shiyan City	Eping Township			
		Dianzi Township, Nanhuatang Township, Huanglong Township, Loutai Township, Zhuping Township	Dianzi Township, Nanhuatang Township, Huanglong Township, Zhuping Township, Loutai Township	Huanglong Township, Wenfeng Township, Xinzhou Township, Chengguan Township (Utopia County)	Tuguanya Township, Jiahe Township, Yeda Township, Wufeng Township, Xinzhou Township
Shaanxi Province	Ankang City	Jihe Town, Shuanghekou Town, Huangu Town	Jihe Town, Shuanghekou Town, Huangu Town	Yanba Township, Shuhe Township, Ganxi Township, Chengguan Township (Shiquan County)	Yinghu Township, Xihe Township, Shuanghe Township
	Baoji City	Fengzhou Township, Tangyu Township			
	Hanzhong City	Baique Temple Township,			
		Wuhou Town, Jinquan Town	Jinquan Town, Wuhou Town	Chadian Town, Shengshui Town	Chadian Township, Beiba Township, Bailongtang Township, Huayang Township
	Shangluo City	Wangyan Township, Guofenglou Township, Yungai Temple Township	Wangyan Township, Guofenglou Township, Yungai Temple Township	Zhulinguan Township, Dajing Township, Xingping Township, Yungai Temple Township	Zhulin Guan Township, Shilipu Street Office, Dajing Township

Province/City		Scenario B1	Scenario B2	Scenario C1	Scenario C2
Sichuan Province	Aba Prefecture	Prairie Township			
		Zhenjiangguan Township, Muni Township	Fengyi Township, Yanyun Township, Zhenping Township	Qingyun Township, Jiangguan Township, Huanglong Township	Shidaguan Township, Yanyun Township, Jiangguan Township, Shijiaobao Township
	Bazhong City			Lianghekou Township, Tiechang Township	Nanjiang Township, Lianghekou Township
	Dazhou City				Nanba Township
	Guangyuan City	Pujia Township	Datan Township, Jindong Township	Hexi Street Office	Chaotian Township, Qiaozhuang Township
	Mianyang City			Crystal Township	Longan Township
Chongqing	Chongqing City	Fenghuang Township	Fenghuang Township		
Major rivers		Bailong River, Du River, Han River, Jialing River, Danjiang River, Minjiang River			
		Tao River	Tao River, Yiluo River	Yiluo River, Fu River	Tao River, Yiluo River, Nan River, Danjiangkou Reservoir, Fu River

References

1. Ribeiro, L.; Barão, T. Greenways for recreation and maintenance of landscape quality: Five case studies in Portugal. *Landsc. Urban Plan.* **2006**, *76*, 79–97. [CrossRef]
2. Kent, R.L.; Elliott, C.L. Scenic routes linking and protecting natural and cultural landscape features: A greenway skeleton. *Landsc. Urban Plan.* **1995**, *33*, 341–355. [CrossRef]
3. Chatzimentor, A.; Apostolopoulou, E.; Mazaris, A.D. A review of green infrastructure research in Europe: Challenges and opportunities. *Landsc. Urban Plan.* **2020**, *198*, 103775. [CrossRef]
4. John, H.; Marrs, C.; Neubert, M.; Alberico, S.; Bovo, G.; Ciadamidaro, S.; Danzinger, F.; Erlebach, M.; Freudl, D.; Grasso, S.; et al. Green Infrastructure Handbook—Conceptual & Theoretical Background, Terms and Definitions. 2019. Available online: https://www.researchgate.net/publication/354224061_Green_Infrastructure_Handbook_-_Conceptual_Theoretical_Background_Terms_and_Definitions (accessed on 3 October 2024).
5. Peng, J.; Pan, Y.; Liu, Y.; Zhao, H.; Wang, Y. Linking ecological degradation risk to identify ecological security patterns in a rapidly urbanizing landscape. *Habitat Int.* **2018**, *71*, 110–124. [CrossRef]
6. Peng, J.; Yang, Y.; Liu, Y.; Du, Y.; Meersmans, J.; Qiu, S. Linking ecosystem services and circuit theory to identify ecological security patterns. *Sci. Total Environ.* **2018**, *644*, 781–790. [CrossRef] [PubMed]
7. Jiang, H.; Peng, J.; Liu, M.; Dong, J.; Ma, C. Integrating patch stability and network connectivity to optimize ecological security pattern. *Landsc. Ecol.* **2024**, *39*, 54. [CrossRef]
8. Wang, J.; Bai, Y.; Huang, Z.; Ashraf, A.; Ali, M.; Fang, Z.; Lu, X. Identifying ecological security patterns to prioritize conservation and restoration: A case study in Xishuangbanna tropical region, China. *J. Clean. Prod.* **2024**, *444*, 141222. [CrossRef]
9. Ding, M.; Liu, W.; Xiao, L.; Zhong, F.; Lu, N.; Zhang, J.; Zhang, Z.; Xu, X.; Wang, K. Construction and optimization strategy of ecological security pattern in a rapidly urbanizing region: A case study in central-south China. *Ecol. Indic.* **2022**, *136*, 108604. [CrossRef]
10. Wei, H.; Zhu, H.; Chen, J.; Jiao, H.; Li, P.; Xiong, L. Construction and Optimization of Ecological Security Pattern in the Loess Plateau of China Based on the Minimum Cumulative Resistance (MCR) Model. *Remote Sens.* **2022**, *14*, 5906. [CrossRef]
11. Huse, B.; Szabo, S.; Deak, B.; Tothmeresz, B. Mapping an ecological network of green habitat patches and their role in maintaining urban biodiversity in and around Debrecen city (Eastern Hungary). *Land Use Policy* **2016**, *57*, 574–581. [CrossRef]
12. Yu, K. Security patterns and surface model in landscape ecological planning. *Landsc. Urban Plan.* **1996**, *36*, 1–17. [CrossRef]
13. Fu, Y.; Shi, X.; He, J.; Yuan, Y.; Qu, L. Identification and optimization strategy of county ecological security pattern: A case study in the Loess Plateau, China. *Ecol. Indic.* **2020**, *112*, 106030. [CrossRef]
14. Wang, Y.; Pan, J. Building ecological security patterns based on ecosystem services value reconstruction in an arid inland basin: A case study in Ganzhou District, NW China. *J. Clean. Prod.* **2019**, *241*, 118337. [CrossRef]
15. Assessment, M.E. *Ecosystems and Human Well-Being: Synthesis*; Island Press: Washington, DC, USA, 2005.
16. Pietsch, M. Contribution of connectivity metrics to the assessment of biodiversity-Some methodological considerations to improve landscape planning. *Ecol. Indic.* **2018**, *94*, 116–127. [CrossRef]
17. Liquete, C.; Kleeschulte, S.; Dige, G.; Maes, J.; Grizzetti, B.; Olah, B.; Zulian, G. Mapping green infrastructure based on ecosystem services and ecological networks: A Pan-European case study. *Environ. Sci. Policy* **2015**, *54*, 268–280. [CrossRef]
18. Yu, K. Ecological Security Patterns in Landscapes and GIS Application. *Geogr. Inf. Sci.* **1995**, *1*, 88–102. [CrossRef]
19. Ma, J.; Li, L.; Jiao, L.; Zhu, H.; Liu, C.; Li, F.; Li, P. Identifying Ecological Security Patterns Considering the Stability of Ecological Sources in Ecologically Fragile Areas. *Land* **2024**, *13*, 214. [CrossRef]
20. Xu, J.; Fan, F.; Liu, Y.; Dong, J.; Chen, J. Construction of Ecological Security Patterns in Nature Reserves Based on Ecosystem Services and Circuit Theory: A Case Study in Wenchuan, China. *Int. J. Environ. Res. Public Health* **2019**, *16*, 3220. [CrossRef]
21. Jia, Q.; Jiao, L.; Lian, X.; Wang, W. Linking supply-demand balance of ecosystem services to identify ecological security patterns in urban agglomerations. *Sustain. Cities Soc.* **2023**, *92*, 104497. [CrossRef]
22. Suich, H.; Howe, C.; Mace, G. Ecosystem services and poverty alleviation: A review of the empirical links. *Ecosyst. Serv.* **2015**, *12*, 137–147. [CrossRef]
23. Howe, C.; Suich, H.; Vira, B.; Mace, G.M. Creating win-wins from trade-offs? Ecosystem services for human well-being: A meta-analysis of ecosystem service trade-offs and synergies in the real world. *Glob. Environ. Chang.* **2014**, *28*, 263–275. [CrossRef]
24. Kang, J.; Zhang, X.; Zhu, X.; Zhang, B. Ecological security pattern: A new idea for balancing regional development and ecological protection. A case study of the Jiaodong Peninsula, China. *Glob. Ecol. Conserv.* **2021**, *26*, e01472. [CrossRef]
25. Jiayu, C.; Jiefu, X.; Kang, G.; Yiwu, W. Balancing urban expansion with ecological integrity: An ESP framework for rapidly urbanizing small and medium-sized cities, with insights from Suizhou, China. *Ecol. Inform.* **2024**, *80*, 102508. [CrossRef]
26. Li, C.; Wu, Y.; Gao, B.; Zheng, K.; Wu, Y.; Wang, M. Construction of ecological security pattern of national ecological barriers for ecosystem health maintenance. *Ecol. Indic.* **2023**, *146*, 109801. [CrossRef]
27. Zhao, W.; Han, Z.; Yan, X.; Zhong, J. Ecological security pattern construction based on multi-scenario trade-off of ecosystem services: A case study of Wafangdian, Dalian. *J. Nat. Resour.* **2020**, *35*, 546–562.
28. Wu, S.; Zhao, C.; Yang, L.; Huang, D.; Wu, Y.; Xiao, P. Spatial and temporal evolution analysis of ecological security pattern in Hubei Province based on ecosystem service supply and demand analysis. *Ecol. Indic.* **2024**, *162*, 112051. [CrossRef]
29. Cui, X.; Deng, W.; Yang, J.; Huang, W.; de Vries, W.T. Construction and optimization of ecological security patterns based on social equity perspective: A case study in Wuhan, China. *Ecol. Indic.* **2022**, *136*, 108714. [CrossRef]

30. Zhang, L.; Peng, J.; Liu, Y.; Wu, J. Coupling ecosystem services supply and human ecological demand to identify landscape ecological security pattern: A case study in Beijing-Tianjin-Hebei region, China. *Urban Ecosyst.* **2017**, *20*, 701–714. [CrossRef]
31. Jialei, L.; Hongbin, H.; Qinghua, Z.; Liding, C.; Ranhao, S. Dataset of Soil Conservation Capacity Preventing Water Erosion in China (1992–2019) [DS/OL]. V1. Science Data Bank. 2023. Available online: https://cstr.cn/31253.11.sciencedb.07135 (accessed on 6 October 2024).
32. Sun, J.; Sun, Z.; Guo, H.; Jiang, H.; Gao, J.; Wang, J. A Dataset of Built-Up Areas of Chinese Cities in 2020 [DS/OL]. *V1*. Science Data Bank. 2021. Available online: https://cstr.cn/31253.11.sciencedb.j00001.00332 (accessed on 6 October 2024).
33. Li, S.; Xiao, W.; Zhao, Y.; Lv, X. Incorporating ecological risk index in the multi-process MCRE model to optimize the ecological security pattern in a semi-arid area with intensive coal mining: A case study in northern China. *J. Clean. Prod.* **2020**, *247*, 119143. [CrossRef]
34. Jia, Y.; Wang, B.; Zhang, S. Construction of ecological security pattern of the Chinese section of the "Silk Road Economic Belt" based on the minimum cumulative resistance model. *Geojournal* **2023**, *88*, 409–424. [CrossRef]
35. Yang, Y.; Chen, J.; Huang, R.; Feng, Z.; Zhou, G.; You, H.; Han, X. Construction of Ecological Security Pattern Based on the Importance of Ecological Protection-A Case Study of Guangxi, a Karst Region in China. *Int. J. Environ. Res. Public Health* **2022**, *19*, 5699. [CrossRef] [PubMed]
36. Guan, H.; Bai, Y.; Tang, Y.; Zhang, C.; Zou, J. Spatial identification and optimization of ecological network in desert-oasis area of Yellow River Basin, China. *Ecol. Indic.* **2023**, *147*, 109999. [CrossRef]
37. Sun, F.; Zhang, J.; Wang, P.; Wei, G.; Chu, G.; Cao, Y. Construction and evaluation of urban ecological security pattern: A case study of Suzhou city. *Geogr. Res.* **2021**, *40*, 2476–2493.
38. He, J.; Shi, X.; Fu, Y. Optimization of ecological security pattern in the source area of Fenhe River Basin based on ecosystem services. *J. Nat. Resour.* **2020**, *35*, 814–825.
39. Liang, F.; Liu, H.; Liu, S.; Qi, X.; Liu, L. Spatial Restructuring Countermeasures of Landscape Ecological Security Network in Southern Fujian: A Case Study of Jimei District in Xiamen. *Econ. Geogr.* **2018**, *38*, 231–239.
40. Yu, F.; Zhang, B. Spatial Pattern of Natural Protected Areas in Qinling-Daba Mountains. *Nat. Prot. Areas* **2023**, *3*, 34–43.
41. Ministry of Natural Resources of the People's Republic of China. *Blue Book of China's Ecological Protection Red Line*; Ministry of Natural Resources of the People's Republic of China: Beijing, China, 2023.
42. Xie, G.; Zhang, C.; Zhang, L.; Chen, W.; Li, S. Improvement of the Evaluation Method for Ecosystem Service Value Based on Per Unit Area. *J. Nat. Resour.* **2015**, *30*, 1243–1254.
43. Xie, G.; Lu, C.; Leng, Y.; Zheng, D.; Li, S. Ecological assets valuation of the Tibetan Plateau. *J. Nat. Resour.* **2003**, *18*, 189–196.
44. Fu, M.; Luo, J.; Tian, Y.; Zhao, Z.; Li, J. Establishment and fine-tuning of nature reserve networks based on minimum cumulative resistance model: A case study of Mountain Qinling region. *Chin. J. Ecol.* **2018**, *37*, 1135–1143.
45. Liu, H.; Wang, Z.; Zhang, L.; Tang, F.; Wang, G.; Li, M. Construction of an ecological security network in the Fenhe River Basin and its temporal and spatial evolution characteristics. *J. Clean. Prod.* **2023**, *417*, 137961. [CrossRef]
46. Yu, F.; Zhang, B.; Yao, Y.; Wang, J.; Zhang, X.; Liu, J.; Li, J. Identifying Connectivity Conservation Priorities among Protected Areas in Qinling-Daba Mountains, China. *Sustainability* **2022**, *14*, 4377. [CrossRef]
47. Wang, X.; Xie, X.; Wang, Z.; Lin, H.; Liu, Y.; Xie, H.; Liu, X. Construction and Optimization of an Ecological Security Pattern Based on the MCR Model: A Case Study of the Minjiang River Basin in Eastern China. *Int. J. Environ. Res. Public Health* **2022**, *19*, 8370. [CrossRef] [PubMed]
48. Ye, H.; Yang, Z.; Xu, X. Ecological Corridors Analysis Based on MSPA and MCR Model-A Case Study of the Tomur World Natural Heritage Region. *Sustainability* **2020**, *12*, 959. [CrossRef]
49. Song, T.; Li, D.; Zhang, L.; Wang, G.; Gao, Y.; Yang, C.; Feng, Z.; Ma, H. Importance Evaluation of Ecosystem Services and Construction of Ecological Security Pattern in Qinba Mountain Area. *Strateg. Study CAE* **2020**, *22*, 64–72. [CrossRef]
50. Wang, X.; Feng, Z.; Wu, K.; Lin, Q. Ecological conservation and restoration of Life Community Theory based on the construction of ecological security pattern. *Acta Ecol. Sin.* **2019**, *39*, 8725–8732.
51. Yin, H.; Kong, F.; Qi, Y.; Wang, H.; Zhou, Y.; Qin, Z. Developing and optimizing ecological networks in urban agglomeration of Hunan Province, China. *Acta Ecol. Sin.* **2011**, *31*, 2863–2874.
52. Zheng, Q.; Hu, J.; Shen, M. Construction of Ecological Network in Hunan Province Based on MSPA and MCR Models. *J. Nat. Sci. Hunan Norm. Univ.* **2021**, *44*, 1–10.
53. Zhang, Y.; Xu, R.; Li, X.; Zhang, X.; Wang, X.; Wang, S. Construction of ecological corridors and identification of key nodes in the core area of China-Laos transportation corridors. *Acta Ecol. Sin.* **2020**, *40*, 1933–1943.
54. Zhang, Z.; Niu, J.; Cheng, Q.; Wang, Z. Construction of Eco-tourism Corridor and Eco-tourism Area in Xinyang Section of Huaihe River Basin. *J. Xinyang Norm. Univ. (Nat. Sci. Ed.)* **2023**, *36*, 517–522.
55. Cao, S.; Liu, Z.; Li, W.; Xian, J. Balancing ecological conservation with socioeconomic development. *AMBIO* **2021**, *50*, 1117–1122. [CrossRef]

56. Cao, S.; Chen, L.; Zhu, Q. Remembering the Ultimate Goal of Environmental Protection: Including Protection of Impoverished Citizens in China's Environmental Policy. *AMBIO* **2010**, *39*, 439–442. [CrossRef] [PubMed]
57. Zhai, H.; Zhang, Z.; Zhao, X.; Xie, Q.; Cheng, Q.; Hu, Y. Optimization of Green Infrastructure in Xinyang City Based on Network Structure Analysis. *J. Xinyang Norm. Univ. (Nat. Sci. Ed.)* **2021**, *34*, 260–266.

Disclaimer/Publisher's Note: The statements, opinions and data contained in all publications are solely those of the individual author(s) and contributor(s) and not of MDPI and/or the editor(s). MDPI and/or the editor(s) disclaim responsibility for any injury to people or property resulting from any ideas, methods, instructions or products referred to in the content.

land

MDPI

Article

Spatio-Temporal Variations of Soil Conservation Service Supply–Demand Balance in the Qinling Mountains, China

Pengtao Wang [1], Guan Huang [1,*], Le Chen [1], Jing Zhao [1], Xin Fan [2,3], Shang Gao [4], Wenxi Wang [5], Junping Yan [6] and Kaiyu Li [1,*]

[1] School of Tourism & Research Institute of Human Geography, Xi'an International Studies University, Xi'an 710128, China; wnpengtao@xisu.edu.cn (P.W.); 107242018100023@xisu.edu.cn (L.C.); jingzhao@xisu.edu.cn (J.Z.)
[2] School of Geography and Environmental Engineering, Gannan Normal University, Ganzhou 341000, China; 1400074@gannu.edu.cn
[3] Center for Turkmenistan Studies, China University of Geosciences, Wuhan 430074, China
[4] School of Tourism Management, Henan Finance University, Zhengzhou 451464, China; 33200031@hafu.edu.cn
[5] School of Marxism, Northwestern Polytechnical University, Xi'an 710072, China; wangwenxi@mail.nwpu.edu.cn
[6] School of Geography and Tourism, Shaanxi Normal University, Xi'an 710119, China; yanjp@snnu.edu.cn
* Correspondence: hguan703@xisu.edu.cn (G.H.); likaiyu@xisu.edu.cn (K.L.)

Abstract: The ecological conservation of nature reserves has garnered considerable attention and is subject to stringent management in China. However, the majority of these areas have a history of underdeveloped economies and require urgent improvements in the well-being of local communities. Effectively coupling and harmonizing the dynamic relationship between ecosystem services and socio-economic development has emerged as a crucial concern for nature reserves. Therefore, further exploration is needed to achieve a spatio-temporal balance and alignment between the supply and demand of ESs in nature reserves in China. Utilizing multiple datasets, RULSE, and bivariate autocorrelation methods, this study investigated the spatio-temporal evolution of the ecosystem services supply–demand ratio (ESDR) and supply–demand spatial matches for soil conservation services (SCSs) in the Qinling Mountains (QMs) from 2000 to 2020. The results indicated the following: (1) Over the years, the supply of SCSs exhibited a consistently high level, with an upward trend observed in 63.10% of the QMs, while the demand for SCSs is generally low, with a decreasing trend observed in 82.68% of the QMs. (2) The supply and demand of SCSs remained favorable, with a positive ESDR reaching 82.19% of the QMs. From 2000 to 2010, there was a significant decline in ESDR; however, a substantial rebound was observed in the ESDR across the region from 2010 to 2020. (3) Over years, the majority of counties and districts exhibited positive values in ESDR. When examining cities, Weinan, Xi'an, and Ankang demonstrated relatively consistent patterns with higher ESDR values over time. In 2000, the ESDR on the northern slope exhibited lower values than that on the southern slope; however, this situation subsequently underwent a reversal. (4) The spatial distribution of SCS supply and demand was predominantly characterized by matching regions exhibiting either High Supply–High Demand or Low Supply–Low Demand for years. This study suggests that the supply and demand dynamics of SCSs in the Qinling Mountains have been favorable in recent years, with consistent spatial supply–demand matches. These findings can provide valuable insights for similar nature reserves aiming to implement ecological environmental protection and achieve sustainable development. The future research endeavors, however, should strive to expand upon these findings by exploring the supply and demand patterns associated with other ESs across diverse nature reserves, while considering their unique geographical characteristics, in order to promote more rational ecological management strategies.

Keywords: ecosystem services; supply–demand balance; spatial matches; bivariate spatial autocorrelation; Qinling Mountains; Moran's index

1. Introduction

Ecosystem services (ESs) serve as a crucial intermediary between ecosystems and human well-being, encompassing the tangible products and intangible benefits that ecosystems offer to humans, along with the reciprocal impacts of human society's utilization of these ecosystem goods and services [1,2]. This process encompasses the production, distribution, and consumption of ESs, as well as the supply–demand relationship associated with these services [3,4]. The supply of ESs represents the capacity of ecosystems to provide goods and services to human society, while the demand for ecosystem services reflects the amount of ecological products and services that humans desire [5–7] or are actually consumed [4,8,9]. Currently, within the context of global climate extremes, unprecedented anthropogenic activity intensity, escalating risks of biodiversity loss, and the disparity between supply and demand for regional ESs continue to be exacerbated [10–13]. When utilizing ecosystem services within human society, the decline in their supply capacity will exert a significant impact on the stability of regional socio-economic development, while the surge in demand for ESs may also disrupt both the supply capacity of ESs and the stability of ecosystems [14,15]. Therefore, it is crucial to evaluate the supply and demand status of regional ESs, identify spatial balance patterns, and, subsequently, propose effective ecological management measures to foster regional sustainable development [16,17].

After years of continuous development and dedicated efforts, scholars from various countries have conducted extensive and in-depth research on the supply and demand of ESs across various spatial scales, such as continents and transnational regions [4,18], countries [19,20], provinces [21,22], cities, districts and counties [7,23–28], agricultural [29] and watershed regions [30–32]. The primary focus of scholarly research lies in investigating the regulating, supporting, and provisioning of services, with particular emphasis placed on soil conservation services, water yield services, carbon sequestration services, habitat quality, and grain productions [4,6,28,33]. Additionally, some scholars have also examined the evolutionary aspects pertaining to the supply and demand of cultural services [34–36]. In terms of research methodology, during the initial stages of their study, Burkhard et al. employed expert experience and knowledge to construct a comprehensive matrix depicting the supply and demand of ecosystem services across various land use types, garnering significant attention from scholars [8]. Secondly, the unit area value methods proposed by Costanza et al. [1] and the equivalent factors for different land use types developed by Xie et al. [37] are exemplary in assessing ecosystem values. However, there is still a relative scarcity of research on service demands utilizing these methods [3]. Thirdly, models such as the Invest [32,38], ARIES [39], and RUSLE [16] models have gained widespread recognition for their robust support of processes and mechanisms. Moreover, the continuous advancements in remote sensing data and the integration of socio-economic data into raster format in recent years have significantly bolstered the credibility and popularity of model research as a commonly employed methodology [17,40,41].

In terms of research content, the consistent focal point has been on quantifying and mapping ecosystem supply and demand [3,8]. However, a comprehensive understanding of ES supply and demand ultimately requires a quantitative comparison, as well as an evaluation of the spatial matches between supply and demand [28]. The mutual relationship and dynamic changes between the ES supply and demand constitute crucial aspects in regional ecological risk assessment. The spatial and temporal dynamics of the supply–demand relationship in ESs necessitate a rational evaluation and monitoring to effectively prevent ecological risks and degradation resulting from imbalances [17]. Consequently, scholars have proposed various indices, such as the supply:demand ratios (S:D ratios) [42], the supply–demand relationship (SDR) [43], and the ecosystem services supply–demand ratio (ESDR) [44], to quantitatively evaluate the magnitude and extent of imbalances between the supply and demand in both temporal and spatial dimensions. In comparison to evaluation methods such as map overlay [45], these approaches offer enhanced operability, dimensionless analysis, and improved capability in identifying dynamic changes in supply–demand imbalances. For instance, Liang-Jie Wang et al. [33] conducted a quantitative

assessment of the supply and demand of ESs in Zhejiang Province, China from 2000 to 2020 at both pixel and county scales using the supply–demand ratio index.

In conclusion, previous studies have demonstrated that the utilization of models such as Invest and RULSE for assessing supply and demand is a widely embraced approach in ESs, and they are characterized by well-defined mechanisms and accurate research findings. In terms of achieving a supply–demand balance, the ESDR model enables effective quantitative evaluation of ES supply–demand disparities at different temporal and spatial scales, making it one of the most frequently employed assessment methods due to its operational simplicity. However, it is worth noting that previous studies on the ESDR have primarily focused on examining the temporal and spatial scales of supply–demand balance, while overlooking the crucial aspects related to spatial agglomeration and matching characteristics between supply and demand. The spatial autocorrelation method is a crucial approach for examining the spatial clustering characteristics of geographical phenomena. Based on this, the bivariate spatial autocorrelation method can effectively explore the spatial clustering and matching features of ES supply and demand [6]. Thus, the investigation of spatial matches between supply and demand through bivariate spatial autocorrelation methods deserves greater attention in ES studies.

Furthermore, there remains a lack of research concerning the balances between ES supply and demand in nature reserves. Soil conservation services (SCSs) play a crucial role as ecosystem regulation services in mountainous natural reserves. Soil erosion, as influenced by external forces, can be categorized into hydraulic erosion, gravitational erosion, and wind erosion [46–48]. Therefore, SCSs represent the regulatory capacity of ecosystems in controlling soil erosion under the influence of water flow, gravity, wind, and other factors. The Qinling Mountains (QMs), as a nationally significant mountainous nature reserve in China, play a pivotal role as an ecological barrier for the country. The ecological environment quality of the QMs not only profoundly impacts regional sustainable development, but also holds implications for the high-quality economic and social progress of the entire nation [49]. With the growing national attention to ecological conservation, it has become an urgent issue for natural reserves such as the QMs to scientifically assess the relationship between the supply and demand of ESs, while concurrently fostering a harmonious equilibrium between ecological preservation and developmental activities in the region [49,50].

Therefore, selecting the QMs as a case study area, employing the ecological mechanism model and utilizing mathematical and statistical methods such as the ESDR and bivariate autocorrelation, this study can quantitatively analyze the temporal and spatial balances and matches between the supply and demand from 2000 to 2020. Specifically, the objectives of this study were to achieve the following: (1) analyze the spatial patterns and trends of supply and demand for the SCSs within the region through applying the RUSLE model; (2) conduct an analysis on the spatial patterns and trends of the balance between the supply and demand of SCSs at pixel, district, county, and prefecture-level city scales through employing the ESDR index; and (3) investigate the spatial matching status of the supply and demand of SCSs at the regional, district, and county scales using the bivariate spatial autocorrelation method. The findings of this study can serve as valuable scientific references for optimizing ecosystem service management, promoting socio-economic sustainable development, and facilitating other fundamental work within the QMs and similar regions.

2. Materials and Methods

2.1. Study Area

The Qinling Mountains (QMs), in conjunction with the Huaihe River to its east, serve as the north–south demarcation line in China for a multitude of geographical features [50,51], encompassing climate, hydrology, soil composition, biodiversity, etc. Situated at the heart of China, the QMs serve as a vital strategic barrier within central China, providing essential ESs such as water conservation, soil retention, biodiversity preservation, and climate regulation. Revered as China's "Central Water Tower" and "Central National Park", the

QMs play an indispensable role in maintaining regional stability and safeguarding China's ecological environment, thus holding immense strategic significance in the country's construction of ecological civilization [52,53].

The QMs, typically categorized into a broader and narrower sense, primarily denote the Qinling Mountains in Shaanxi Province in the narrower sense [49,54]. This region represents the core area of the QMs, featuring elevations ranging from 156 to 3473 m (Figure 1). The QMs function as the hydrological divide between the two largest river basins in China, namely the Yangtze River and Yellow River. Consequently, the southern slope (SS) and northern slope (NS) are attributed to the Yellow River basin and Yangtze River basin, respectively, each of which are characterized by notable geographical disparities. Moreover, serving as a vital water source and conservation area for the two largest rivers, the QMs region plays a pivotal role in supplying water to significant projects like China's South-to-North Water Diversion [49].

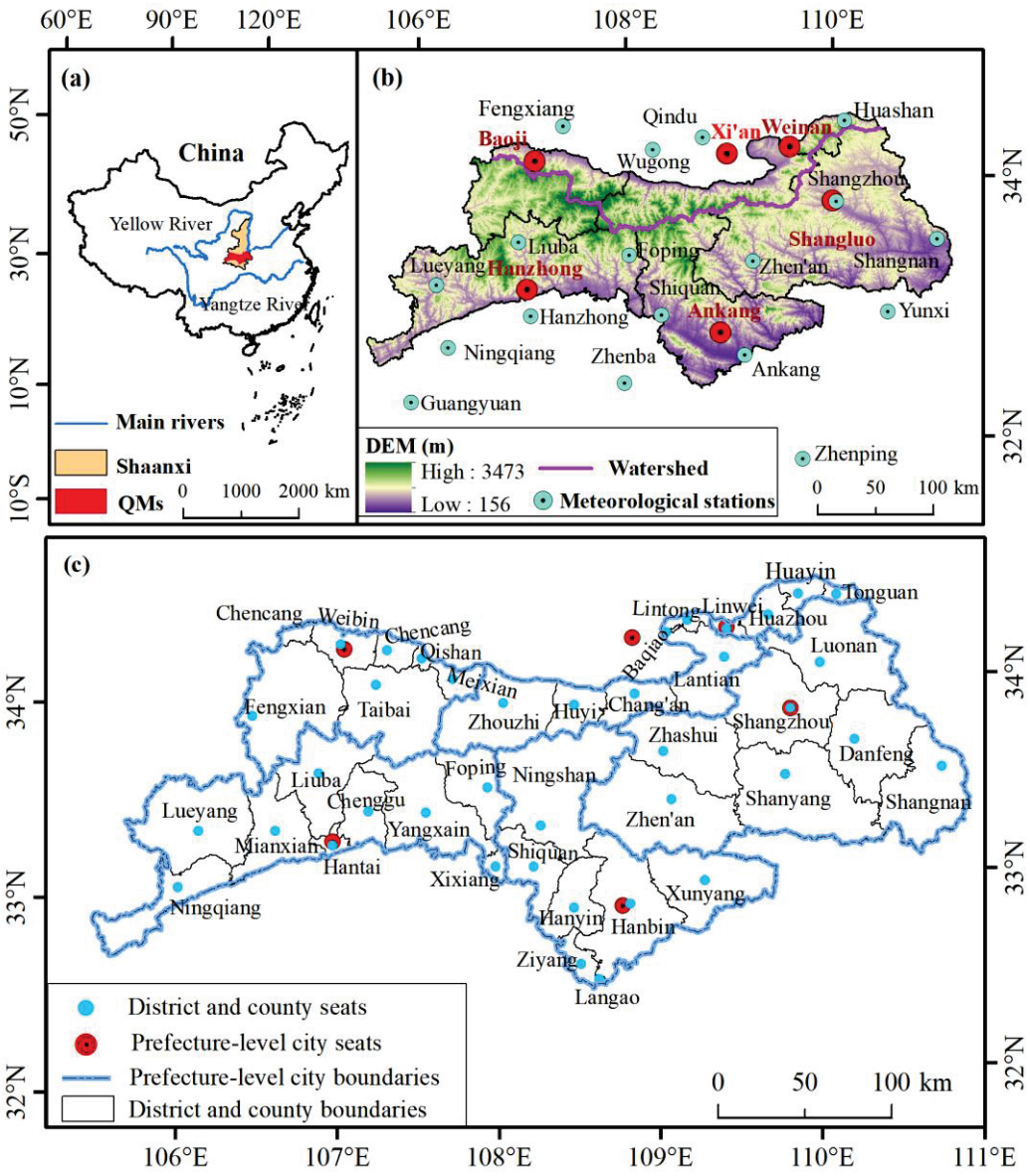

Figure 1. The spatial distribution of the QMs: (**a**) the location in China; (**b**) the elevation and meteorological station; and (**c**) the location and boundaries of administrative districts and counties.

The northern and western regions of the QMs generally exhibit higher elevations. The watershed of the QMs is situated in the central–northern area, with its apex at Mount Taibai,

which is located within Taibai County in the west. Conversely, the eastern and southern parts of this region exhibit a relatively lower topography and higher population density. The region located north of the dividing line is characterized by a temperate climate, whereas the region situated south of the dividing line exhibits a subtropical climate [49]. The distinctive geographical location, intricate terrain features, and diverse climatic conditions create an optimal environment for the proliferation of various communities of plants and animals, rendering Qinling Mountains an ecological haven. Hence, the QMs emerge as one of the most biologically diverse regions globally and serve as a crucial protected area for biodiversity conservation in China. It has gained global recognition as a renowned international repository for genetic resources, serving as a vital ecological hub within China while also standing out as a prominent geographic landmark in the country. Meanwhile, in recent years, the ecological environment quality of Qinling Mountains has witnessed significant improvement owing to the guidance of national policies and rigorous control by local management authorities. As of 2022, the vegetation coverage rate in the Qinling region has soared to an impressive 90.31%, establishing it as the preeminent area in China with unparalleled forest coverage [55].

However, the QMs primarily consist of rocky middle mountains, which are characterized by thin soil layers and steep slopes, thereby rendering the ecological environment highly susceptible. Influenced by global extreme climate patterns, the region experiences concentrated summer precipitation, resulting in frequent occurrences of heavy rain and flooding events [50,56,57]. Meanwhile, the continuous development of regional socio-economy, population growth, urbanization dynamics, and anthropogenic disturbances exert additional influence on the stability of the ecological environment [53]. The combined influence of these factors poses a significant potential risk of landslides, mudslides, and soil erosion in this region.

In terms of administrative divisions, this region encompasses a total area of 58,800 km^2, accounting for 28.59% of the entire Shaanxi Province. In terms of administrative divisions, this region comprises prefecture-level cities, including Xi'an, Weinan, Baoji, Hanzhong, Ankang, and Shangluo, as well as 11 districts and 27 counties [49]. Notably, Xi'an serves as the capital city of Shaanxi Province, while Xunyang and Huayin function as county-level cities. The six cities can be ranked by their involved areas as follows: Weinan < Xi'an < Baoji < Ankang < Hanzhong < Shangluo.

2.2. Research Framework

The specific research process in this study is illustrated in Figure 2.

Firstly, considering the natural environmental characteristics of the QMs region, we selected soil conservation services (SCSs) as a representative ecosystem service type in this area and conducted preliminary work on organizing and processing multi-source data.

Secondly, the Revised Universal Soil Loss Equation (RUSLE) was employed to separate the actual soil erosion from potential soil erosion, enabling the calculation of the supply and demand of the SCSs in the local area. The spatio-temporal evolution characteristics of SCSs were subsequently analyzed. As the parameters required for soil conservation capacity calculation primarily exist in raster data format, the SCSs model initially presents the results of supply and demand calculations in a rasterized form. Considering the inclusion of multiple districts, counties, and cities, as well as the north and south slope divisions within the Qinling region, we employed a partition statistics function of geographic information system software to analyze and present these results through charts, aiming to effectively showcase them at different regional scales.

Thirdly, by utilizing the ecosystem service supply–demand ratio (ESDR), we examined the surplus and deficit status of the supply and demand for SCSs across various research periods and partition scales, as illustrated above.

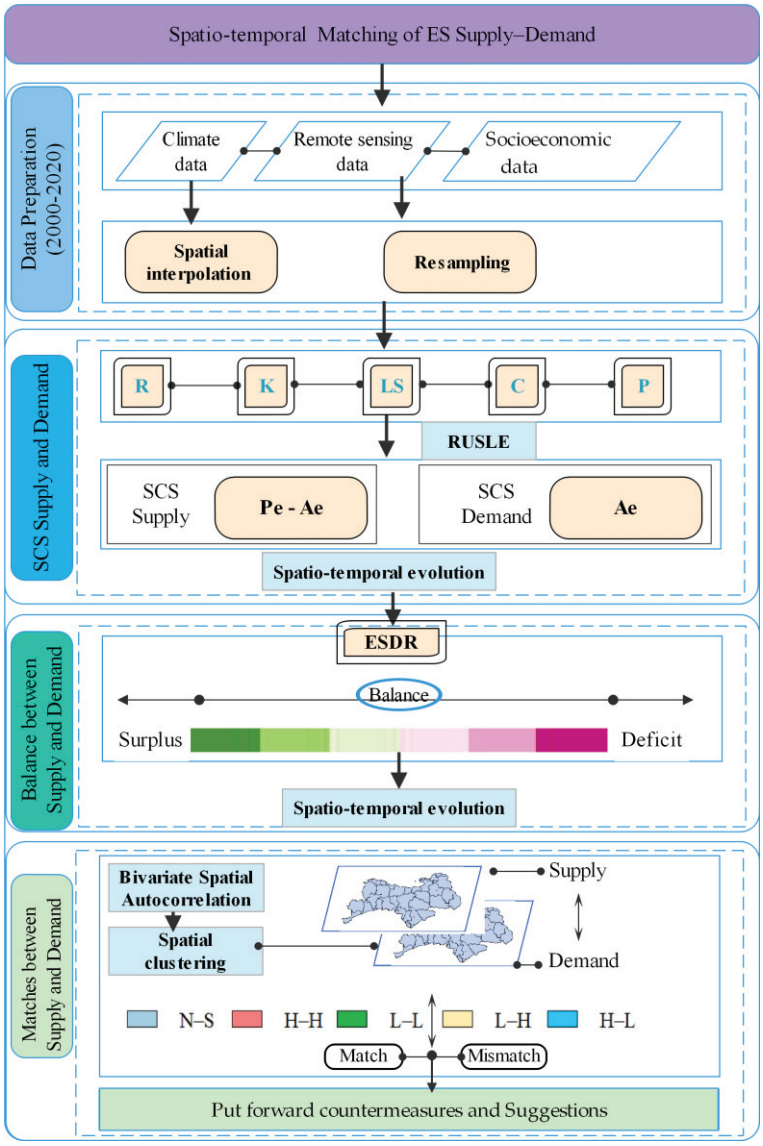

Figure 2. Research framework.

Finally, given that this article primarily presents recommendations for ecological management at the district and county levels, this study evaluated the spatial matching characteristics and trends in SCS supply and demand by utilizing the local Moran's index and global Moran's index at both the county and regional scales on the basis of bivariate spatial autocorrelation. In addition, the research findings of this article were thoroughly discussed and analyzed. Based on the research outcomes, corresponding development recommendations have been formulated to effectively address the local situation.

2.3. Data Sources

The primary data utilized in this study consist of three categories: climatic data, remote sensing data, and socio-economic data.

Specifically, the climate data were obtained from the China Meteorological Data Service Centre established by the China Meteorological Administration with a monthly time resolution for precipitation as the collected climate elements. We carefully selected meteorological stations in the Qinling area and its surrounding regions, meticulously scrutinizing their meteorological data. Ultimately, a total of 18 meteorological stations exhibiting exceptional data continuity were chosen (Figure 1b). The annual data were computed and derived using monthly data obtained from meteorological stations. Subsequently, the

precipitation data were incorporated into the latter erosivity factor of rainfall calculations at both monthly and annual scales. As the meteorological data were site-specific, spatial interpolation methods were employed to transform the calculation results into spatial data in tif format with a resolution of 1 km.

The Digital Elevation Model (DEM) data in this study were derived from the widely accepted Shuttle Radar Topography Mission (SRTM) dataset, which was acquired through collaborative measurements conducted by National Aeronautics and Space Administration (NASA) and National Imagery and Mapping Agency (NIMA) using the SRTM system installed on aircraft, resulting in the generation of the currently prevalent SRTM terrain product data. Currently, this dataset is a widely used and readily available high-resolution DEM product with extensive coverage. To ensure accuracy, we specifically chose the 30 m data and extracted DEM data for the QMs region to facilitate precise calculations of slope lengths and gradients.

The NDVI data were derived from the monthly composite product MODND1M of the Moderate-Resolution Imaging Spectroradiometer (MODIS) with a spatial resolution of 500 m for China. To ensure data quality, the Maximum Value Composite method was employed in this study to convert the monthly data into annual data. The resolution was standardized to 1 km through a resampling tool, and, subsequently, the NDVI time series data for the QMs were acquired using an extraction tool.

The raster data was uniformly resampled to a resolution of 1 km prior to spatial raster calculation, while the vector data remained unchanged. Please refer to Table 1 for the specific characteristics and acquisition methods of the data.

Table 1. Data source information of this study.

Category	Index	Temporal Coverage	Spatial Resolution	Data Sources
Climate data	Precipitation	2000–2020	Meteorological station	China Meteorological Data Service Centre (http://data.cma.cn accessed on 15 December 2021)
Remote sensing data	DEM	2000	30 m	Shuttle Radar Topography Mission (SRTM) dataset (https://srtm.csi.cgiar.org/srtmdata accessed on 18 January 2022)
	MODND1M	2000–2020	500 m	Geospatial Data Cloud site, Computer Network Information Center, Chinese Academy of Sciences. (http://www.gscloud.cn accessed on 18 July 2022) (https://search.earthdata.nasa.gov/search accessed on 10 January 2022)
Socioeconomic data	Administrative seat	2021	Vector data	National geographic information resources directory service system (https://www.webmap.cn/commres.do?method=dataDownload accessed on 26 December 2021)
	Administrative boundary			

2.4. Methods and Processes

2.4.1. Supply and Demand of Ecosystem Services

We conducted a comprehensive quantification on the supply and demand of ecosystem services, specifically focusing on soil conservation services as a quintessential type of ecosystem service in the QMs.

The Universal Soil Loss Equation (USLE), developed by Wischmeier and Smith in 1965 [58], stands as the world's pioneering comprehensive and scientifically rigorous quantitative assessment model for soil erosion, encompassing various influencing factors. In 1997, Renard et al. significantly enhanced the conceptualization and algorithms of these influencing factors, meticulously assessed each factor, accomplished the modification of USLE, and subsequently developed the Revised Universal Soil Loss Equation (RUSLE) model [59]. Over the years, this model has successfully integrated GIS technology with remote sensing data and regional field data, turning it into a universally recognized approach for soil conservation assessment. It has gained global recognition and been extensively applied [48,60,61], and it was rigorously evaluated in the Qinling Mountains and its surrounding regions [38,62,63]. Drawing upon previous research findings and taking into account local conditions, this study quantitatively assesses the supply and demand of soil conservation services by employing the RUSLE model.

1. Quantifying the supply of Soil Conservation Services (SCSs)

The supply of SCSs denotes the actual quantity of locally provided measures for conserving soil and mitigating soil erosion. The quantification formula is as follows:

$$S_{SC} = P_e - A_e = R \times K \times L \times S - R \times K \times L \times S \times C \times P, \quad (1)$$

where S_{SC} denotes the supply of SCSs (unit: t·hm^{-2}·yr^{-1}), and its value is determined by the disparity between the potential erosion (P_e) and the observed amount of soil erosion (actual erosion, A_e). Among them, P_e refers to the theoretical estimation of the soil loss in a given area, assuming the absence of vegetation cover on land and a lack of implementation of any water conservation measures; conversely, A_e represents the actual measured amount of the soil loss in this area with local actual vegetation cover and implementation of soil conservation.

Additionally, the calculation methods for these parameters in the Equation (1) are as follows.

The parameter R denotes the erosivity factor of rainfall for a particular year within the local region (unit: MJ·mm·hm^{-2}·h^{-1}·yr^{-1}), which is determined through the application of the empirical formula developed by Wischmeier and Smith [61].

$$R = \sum_{m=1}^{12} 1.735 \times 10^{\left(1.5 \times \lg \frac{P_m^2}{P_y} - 0.8188\right)}, \quad (2)$$

where P_m denotes the cumulative precipitation for a specific month within a given year, whereas P_y represents the total annual precipitation over the entire year in a given area.

The parameter K represents the erodibility factor of local soil, which remains relatively stable over time (unit: t·ha·h·ha^{-1}·MJ^{-1}·mm^{-1}) and is utilized to assess soil erosion and transport vulnerability under local environmental conditions. The calculation process of this parameter is based on the EPIC model developed by Sharpley and Williams [38].

$$\begin{aligned} K = {} & 0.1317\left\{0.2 + 0.3e^{[-0.0256S_a(1-0.01S_t)]}\right\}\left(\frac{S_t}{C_l+S_t}\right)^{0.3} \times \\ & \left\{1 - \frac{0.25O_r}{C_l + e^{(3.72+2.95O_r)}}\right\}\left\{1 - \frac{0.7(1-0.01S_a)}{(1-0.01S_a) + e^{(-5.51+22.91-0.01S_a)}}\right\}, \end{aligned} \quad (3)$$

where S_a, S_t, C_l, and O_r denote the mass percentages of sand particles, silt particles, clay particles, and organic matter in the local soil, respectively.

The slope length factor, denoted as S_l, and the slope gradient factor, denoted as S_g, are utilized to comprehensively assess the impact of terrain undulations such as slope length

and slope gradient on local soil erosion. The specific calculation formulas are presented below.

$$S_l = \left(\frac{\lambda}{22.13}\right)^n, \begin{cases} n = 0.5 & \theta < 1^\circ \\ n = 0.4 & 1^\circ \le \theta < 3^\circ \\ n = 0.3 & 3^\circ \le \theta < 9^\circ \\ n = 0.2 & 9^\circ \le \theta \end{cases}, \tag{4}$$

$$\lambda = \frac{h}{\sin\left(\frac{\theta \times \pi}{180}\right)}, \tag{5}$$

$$S_g = \left(\frac{\sin\theta}{0.0896}\right)^{0.6}, \tag{6}$$

where λ denotes the length of the slope (unit: m), n represents the slope length index, θ represents the slope steepness, and h represents the height of the slope.

C denotes the vegetation cover factor, which can comprehensively reflect the impact of vegetation cover on local soil erosion and V_c represents the local vegetation coverage status. The presence of vegetation coverage serves as a mitigating factor against soil erosion, whereby areas with abundant vegetation experience reduced rates of soil erosion, while the opposite also holds true.

$$C = \begin{cases} 1 & V_c = 0 \\ 0.6508 - 0.3436\lg V_c & 0 < V_c \le 78.3\% \\ 0 & V_c > 78.3\% \end{cases}. \tag{7}$$

The value of V_c can be derived from the utilization of the NDVI (normalized difference vegetation index) data [64].

$$V_c = \frac{NDVI - NDVI_{min}}{NDVI_{max} - NDVI_{min}}, \tag{8}$$

where $NDVI_{min}$ *and* $NDVI_{max}$ denote the minimum value and maximum value for a particular year within the local region, respectively.

P denotes the soil and water conservation factor, which is determined by the local terrain's slope gradient index α based on the Wener method [65].

$$P = 0.2 + 0.3\alpha. \tag{9}$$

2. Quantifying the demand of Soil Conservation Services (SCSs)

When assessing the demand for SCSs, many scholars have considered the quantification of local actual soil erosion in a local area as an indicator. This is because humans rely on ecosystem services and other related approaches to address existing soil erosion issues. Consequently, within the field of soil conservation, people's desired quantity of SCSs reflects their demand for such interventions [5,6,33]. On this basis, utilizing the A_e value in a RUSLE equation, we can estimate the extent of local demand for SCSs as follows:

$$A_e = R \times K \times L \times S \times C \times P. \tag{10}$$

The calculation methods for each parameter in this formula can be found in the preceding text.

2.4.2. Budgets of SCS Supply and Demand

The current universal indicator for assessing the budgets of the supply and demand of ecosystem services is the ecosystem service supply–demand ratio (ESDR) [6,28]. The calculation principle is outlined as follows:

$$ESDR = 2 \times \frac{S_e - D_e}{S_{max} - D_{max}}, \begin{cases} > 0, & Surplus \\ = 0, & Balance, \\ < 0, & Deficit \end{cases} \quad (11)$$

where S_e represents the supply of soil conservation services at a specific location and year, while D_e denotes the demand for soil conservation services for the specific location in that year. The parameter S_{max} signifies the maximum supply of soil conservation services available within the entire region for that particular year, whereas D_{max} represents the maximum demand for soil conservation services across the entire region during that same year. By integrating this indicator, it becomes possible to quantitatively evaluate and categorize the status of the ecosystem service budgets as demand exceeds supply ($ESDR < 0$, referred to Deficit) and neutral balance ($ESDR = 0$, referred to Balance), and supply exceeds demand ($ESDR > 0$, referred to Surplus) [8], thereby facilitating a more convenient assessment and management of ecosystem services.

2.4.3. Spatial Matching of SCS Supply and Demand

Geographic elements typically exhibit spatial dependence or interrelationships, which can be observed as the clustering or dispersion characteristics of attribute values in space. Therefore, spatial autocorrelation methods construct a spatial weight matrix to quantify the correlation between the value of a geographic feature at a specific location or partition and the values of neighboring areas [66].

The Moran's I is a widely employed approach for analyzing spatial autocorrelation, encompassing both the global index (global Moran's I) and local index (Local Indicators of Spatial Association—LISA) [67]. Among them, the global Moran's index reflects the spatial autocorrelation status of geographic feature values averaged over all pixels or zones in space, while the local Moran's index captures the spatial clustering patterns of geographic feature values at each individual location or zone. The calculation principle is outlined as follows:

$$LISA_i = \frac{(a_i - \overline{a})\sum_j w_{ij}(a_i - \overline{a})}{n\sum_i (a_i - \overline{a})^2}, \quad (12)$$

where a_i denotes the attribute value of a geographic feature on either a pixel or zone i, $\overline{a}$ denotes the average value of the geographic feature across the entire space, n denotes the number of pixels or zones within the space, and w_{ij} denotes the spatial weight (spatial adjacency) between pixel or zone i and j.

The spatial autocorrelation of geographical elements ranges from -1 to 1, with a stronger correlation indicated by the absolute value of the spatial autocorrelation being closer to 1, and the greater the randomness in the spatial distribution is represented by the absolute value being closer to 0 [68]. Specifically, the coexistence of high (low) values in a specific location and its neighboring areas indicates positive spatial autocorrelation within a range from 0 to 1, suggesting that the geographic feature exhibits either high–high clustering or low–low characteristics with surrounding areas. Conversely, if there is a discrepancy between the value at a certain location and its neighboring areas, with one being high and another being low, it signifies negative spatial autocorrelation ranging from -1 to 0, indicating either high–low or low–high clustering between the geographic feature at that location and its surrounding areas [31]. A value of zero signifies a random distribution of this geographic feature in space without any discernible clustering [69].

The LISA formula primarily investigates the spatial autocorrelation of a given geographic element and can be utilized to examine bivariate spatial autocorrelation [70]. In principle, the calculation formulas for both scenarios remain identical; however, in the case

of two variables, the LISA formula can be employed to examine the spatial correspondence between Element A at a specific location and its surrounding Element B. The Moran's index is highly regarded in the field of spatial autocorrelation due to its exceptional convenience, objectivity, and minimal limitations, making it a widely adopted tool for spatial clustering analysis [6]. The bivariate autocorrelation method, based on this, can employ LISA maps to visually depict the spatial matches between ES supply and demand, thereby emerging as an effective approach for investigating ES supply and demand [6,16,71]. Therefore, based on existing research, this study employs GeoDa software to investigate the spatial concordance between ES supply and demand using bivariate spatial autocorrelation at a significance level of 0.1. The spatial patterns of the ecosystem service's supply and demand are classified into five categories: High Supply–High Demand (H-H), Low Supply–Low Demand (L-L), High Supply–Low Demand (H-L), Low Supply–High Demand (L-H), and Not Significant (N-S).

Within the research framework of supply–demand matching, further subdivisions can be made for the aforementioned types of supply–demand agglomeration [16]. The categories of High Supply–High Demand and Low Supply–Low Demand represent regions where there is a relatively balanced alignment between SCS supply and demand, corresponding to an optimal spatial match of H-H and L-L types, respectively. Conversely, the categories of High Supply–Low Demand and Low Supply–High Demand depict regions characterized by a mismatch between supply and demand, namely H-L and L-H type spatial mismatches, respectively.

3. Results

3.1. Spatial Patterns and Trends of SCS Supply and Demand

3.1.1. Spatial Patterns and Trends of Supply from 2000–2020

The supply of SCSs in the QMs exhibited a generally high level, with the maximum value reaching 2718.10 $t \cdot hm^{-2}$ (Figure 3). However, notable disparities existed in the supply levels among the eastern– and central–western regions. The central and western regions were predominantly characterized as high supply areas for SCSs, particularly in Yangxian and Foping, where the SCS supply generally exceeds 1500 $t \cdot hm^{-2}$. The counties and districts of Shangluo City, the eastern counties and districts of Ankang City, as well as areas like Ningshan, Lueyang, and Fengxian in the western region experienced inadequate SCS supply. This inadequacy was primarily characterized by maintaining levels below 500 $t \cdot hm^{-2}$. At the district and county scale, it became increasingly evident that the central region generally exhibited a higher supply of SCSs, while the western and eastern districts and counties demonstrated comparatively lower levels of SCS supply.

Spatially, the proportion of the area exhibiting an increasing supply of SCSs reached 63.10%. The regions experiencing the most rapid growth in SCS supply were primarily situated along the southern and northern peripheries of the QMs, as well as in counties such as Zhen'an and Shanyang within the east. In these areas, the rate of increase for SCS supply generally surpassed 40 $t \cdot hm^{-2} \cdot a^{-1}$. The regions experiencing a decline in SCS supply were primarily situated along the eastern and western peripheries, as well as on both sides of the QMs' watershed. Over the years, the regions experiencing the most rapid decline in SCSs exhibited sporadic distribution across Lueyang and Fengxian within the western region, as well as near the watershed in Yangxian, Foping, Ningshan, and Zhashui. The rate of decline in SCSs generally exceeded 20 $t \cdot hm^{-2} \cdot a^{-1}$. From a county-scale perspective, there had been a gradual decline in SCS supply observed in Shangnan County to the east, as well as in Lueyang and Feng County to the west. Conversely, other counties exhibited an upward trend in SCS supply, with notably higher growth rates primarily observed among counties situated along the northern and southern peripheries of the QMs.

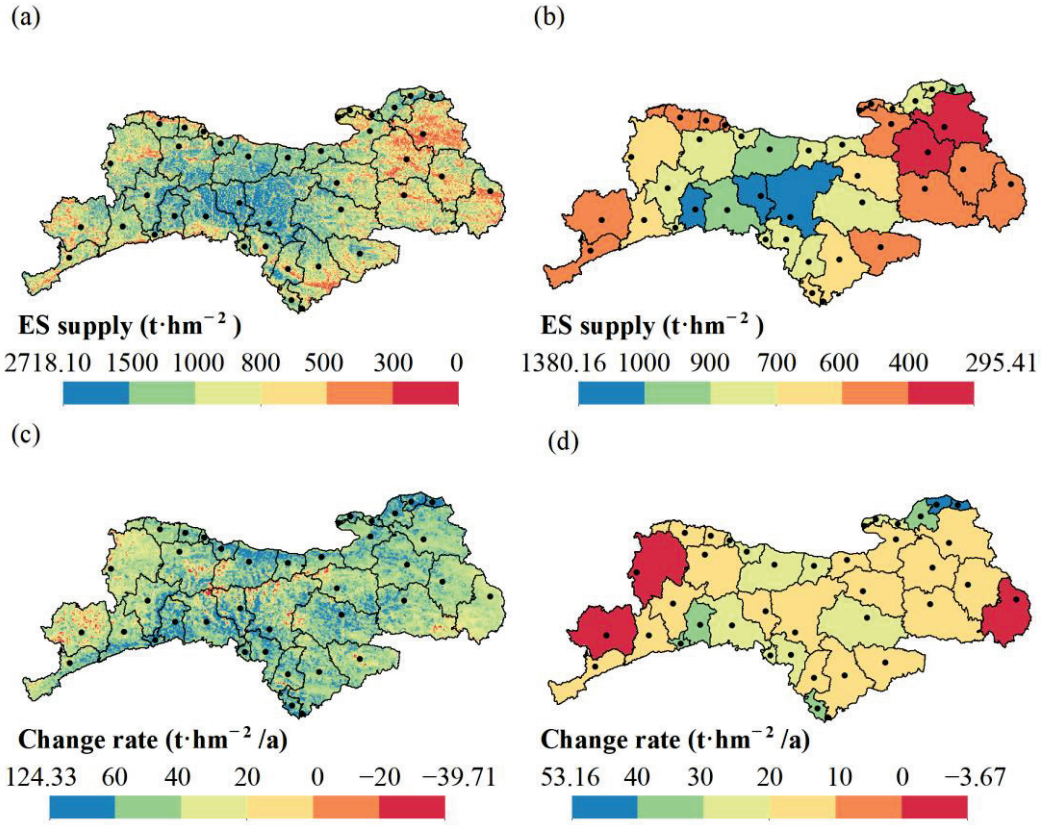

Figure 3. The spatial patterns and trends of the SCS supply at pixel scale (**a**,**c**), district and county scale (**b**,**d**) in the QMs from 2000 to 2020.

3.1.2. Spatial Patterns and Trends of Demand from 2000–2020

There was a significant variation in the SCS demand in the QMs, with values ranging from 0 to 1933.30 t·hm^{-2} (Figure 4). The spatial disparities and trends of SCS demand were categorized into six levels for further analysis. It was generally observed that there was a spatially skewed demand for SCSs. Approximately 67.61% of the total area exhibited a SCS demand of less than 300 t·hm^{-2}. Meanwhile, the regions with a demand below 100 t·hm^{-2} were primarily concentrated in the northern slope of QMs, eastern regions, and in counties including Fengxian, Taibai, Liuba, and Mianxian in the west. These regions inherently possessed relatively lower levels of soil erosion. The areas exhibiting high demand for SCSs were sporadically distributed across Taibai, Lueyang, and Ningqiang in the west; Yangxian, Foping, and Ningshan in the center; as well as districts and counties including Hanbin, Xunyang, Zhashui, Zhen'an, and Shanyang in the east. The SCS demand within these regions generally surpassed 500 t·hm^{-2}. Consequently, these areas experienced substantial soil erosion and faced inherent risks associated with landslides and mudslides. Spatially, the average demand for SCSs in most districts and counties was relatively low, while districts and counties demonstrating higher demand were primarily Ningqiang and Lueyang in the southwest, as well as Zhen'an and Ziyang in the east.

The demand for SCSs in most areas exhibited a consistent downward trend, with the declining regions encompassing 82.68% of the total QMs. The regions exhibiting an upward trend in SCS demand were primarily concentrated in the western and central QMs. The pixels with the highest growth rate of SCS demand were predominantly situated in Yangxian, Foping, Taibai, and Ningshan within the central QMs. The increase rate of demand for these pixels generally exceeded 90 t·hm^{-2}·a^{-1}. In contrast, the areas experiencing a decline in demand for SCSs were widely distributed across the eastern QMS, the northern slope, and the peripheral areas in the southern QMs. Among these regions, districts, and counties, such as Zhen'an, Zhashui, Shanyang, Danfeng, Shangnan, Xunyang,

and Shangzhou, which were located within the eastern QMS, particularly high rates of decline exceeding 30 $t \cdot hm^{-2} \cdot a^{-1}$ had been shown. The growth rate of demand varied significantly across different districts and counties, with the eastern counties exhibiting a gradual decline or increase in demand, while the central and western counties demonstrated a more pronounced upward trend. Based on the spatial distribution analysis of Figure 4, it was evident that regions experiencing a rapid decline in SCS demand coincided with higher average SCS requirements. Consequently, this rapid decline could effectively mitigate the pronounced demand for SCSs in these areas.

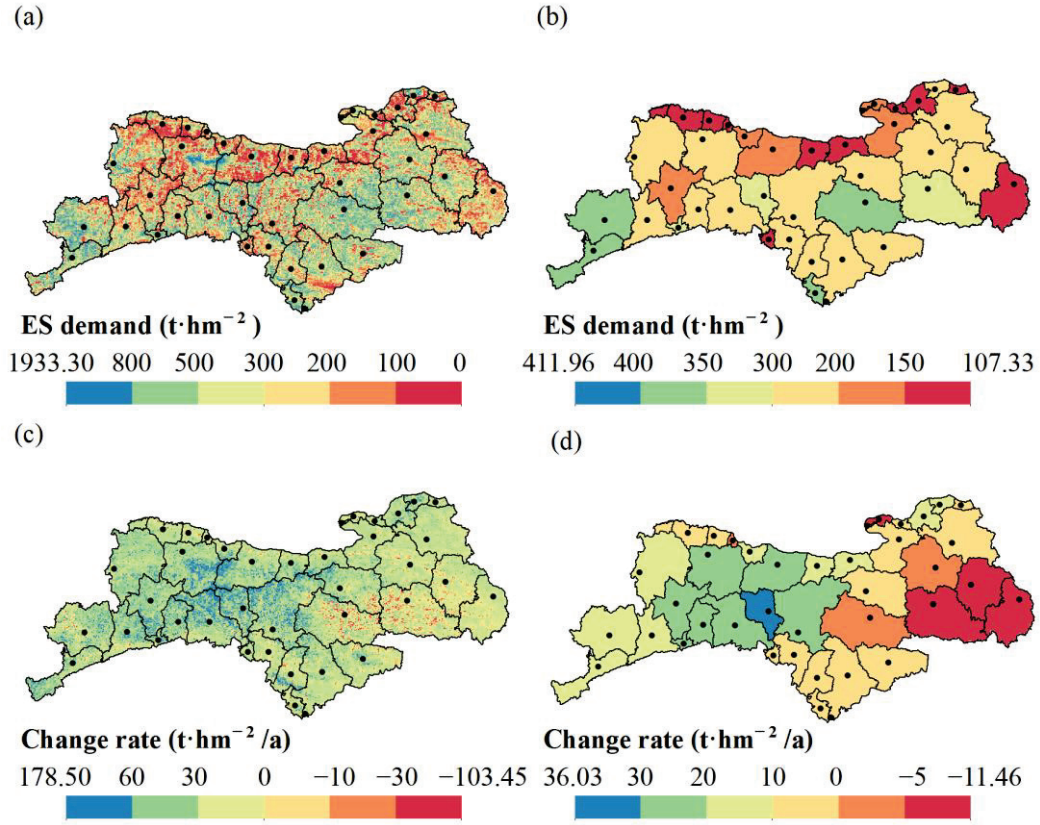

Figure 4. The spatial patterns and trends of the SCS demand at pixel scale (**a**,**c**), district and county scale (**b**,**d**) in the QMs from 2000 to 2020.

3.2. Spatial Patterns and Trends of ESDR from 2000–2020

3.2.1. Temporal Variations from 2000–2020

The spatial distribution maps of the ESDR for the years 2000, 2010, and 2020, respectively, were presented in Figure 5. In 2000, the ESDR exhibited consistently high values throughout the entire region, with an average of 0.19 and a range spanning from −0.79 to 1.17. Spatially, positive ESDR values encompassed a significant proportion (78.39%) of the total area, and these were predominantly characterized by moderate surplus, accounting for 42.35% areas. These surplus areas were widely distributed in the central and western regions. The slight surplus of the ESDR was primarily distributed in the northeastern and southeastern corners of the region, with slight deficits being concentrated in the eastern part, while moderate deficits were predominantly observed in Ningqiang and Lueyang. In 2010, the ESDR variation within the entire region exhibited a relatively narrow range of −0.39 to 0.59, indicating limited fluctuations. Furthermore, there was a significant decline in the overall ESDR value, reaching a minimal level of 0.04. ESDR revealed a prevalence of areas exhibiting slight surplus and slight deficit, accounting for 59.10% and 37.44%, respectively, and these were extensively distributed across the region. Moreover, there was also a notable proportion of areas displaying moderate surplus, primarily concentrated

in the northeastern periphery, Hanbin and Xunyang in the southeast, as well as Foping in the central part. Remarkably, the overall level of the ESDR in the entire region exhibited a general improvement in 2020, with the average ESDR rebounding to 0.14 and an expanded range from −0.88 to 0.82. Furthermore, there had been an increased prominence of spatial disparities in the ESDR. The ESDR revealed a substantial proportion of regions exhibiting a slight deficit, slight surplus, and moderate surplus, respectively. Areas with slight deficit were primarily concentrated in the western region, while areas with slight surplus were predominantly observed in the eastern part. Areas displaying moderate surplus were widely distributed across the entire QMs.

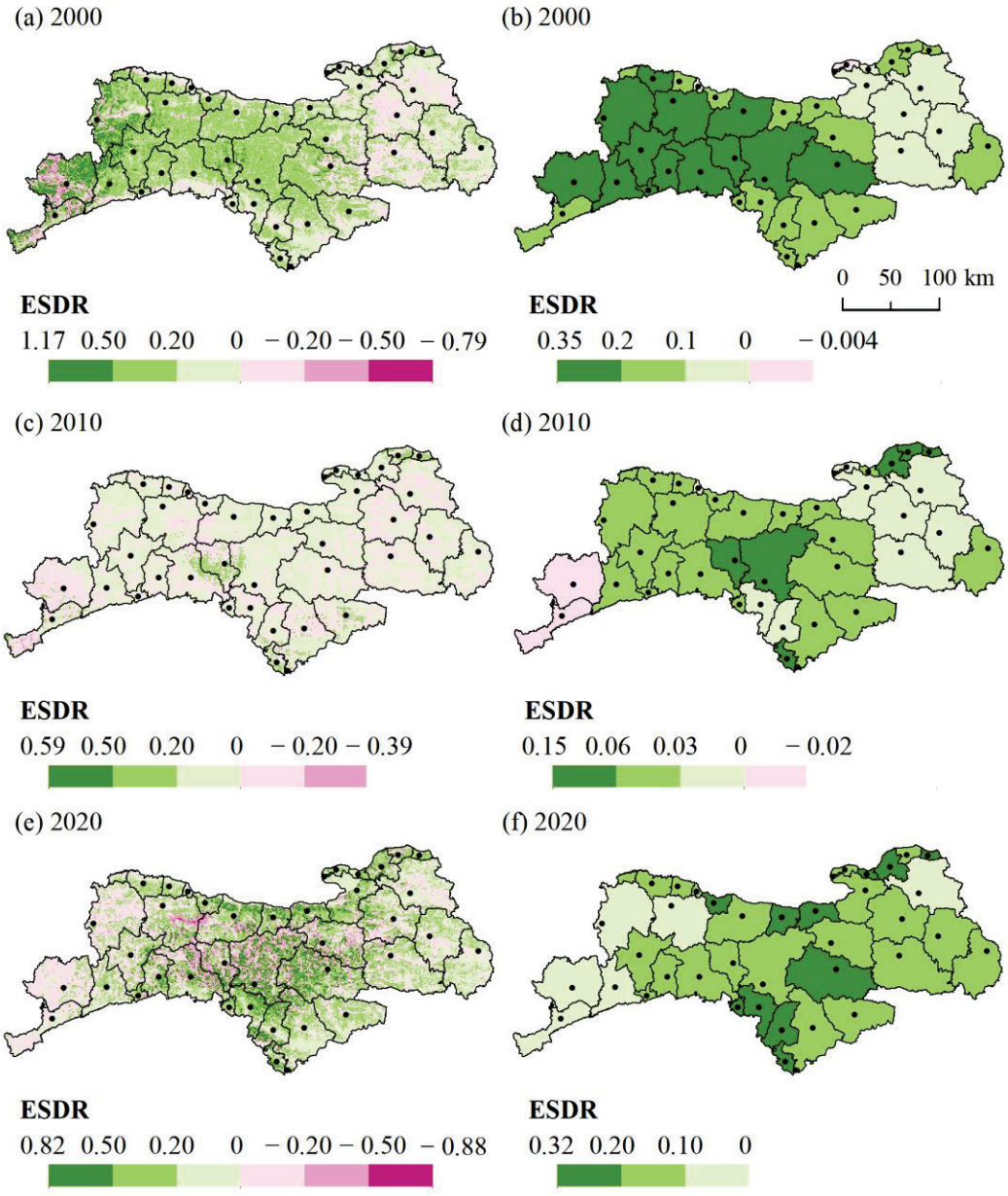

Figure 5. The spatial distribution of the ESDR at pixel scale (**a**,**c**,**e**), district and county scale (**b**,**d**,**f**) in the QMs from 2000 to 2020.

The average values of the ESDR in the entire Qinling region were recorded as 0.19, 0.04, and 0.14 for these respective years. These findings indicated a significant decline in the ESDR from 2000 to 2010; however, there was a partial recovery observed by the year 2020. In combination with the spatial variation at the district and county scales, a larger

number of districts and counties exhibited high surplus across the central and western regions in 2000, while the eastern region predominantly experienced slight-to-moderate surpluses alongside areas with a deficit status. In 2010, the central and western regions predominantly exhibited moderate surpluses, while the eastern region predominantly experienced slight surpluses; however, Ningqiang and Lueyang displayed slight deficits. Surprisingly, a significant spatial redistribution of the ESDR was observed in 2020, with the central and eastern regions predominantly exhibiting high and moderate surpluses, while mild surpluses had shifted to the western region; no counties or districts within the entire area were found to be experiencing an ESDR deficit state.

The partition statistics function in GIS was utilized to analyze and compare the average ESDR values of different cities and regions, thereby unveiling variations at various scales. There had been significant fluctuations in the ESDR levels among prefecture-level cities over the years (Figure 6). In 2000, the ESDR levels were generally high in cities, with Baoji, Hanzhong, and Ankang ranking as the top three cities with ESDR values exceeding 0.2. By 2010, there was a decrease in the ESDR levels across all cities, wherein Weinan, Ankang, and Xi'an emerged as the top three cities with relatively higher ESDR values; however, these values only slightly exceeded 0.05. In 2020, a substantial rebound in the ESDR was observed across all cities, with Weinan, Xi'an, and Ankang remaining at the forefront as the top three cities exhibiting ESDR values exceeding 0.20. Weinan, Xi'an, and Ankang had consistently exhibited a relatively high and stable ESDR over the years, whereas the remaining three cities demonstrated a comparatively lower ESDR. Regarding the scale of north–south slopes, the ESDR was lower on the north slope compared to the south slope in 2000. However, in 2010 and 2020, the ESDR exhibited higher values on the north slope than on the south slope. These findings further underscore substantial spatial and regional variations in the ESDR over the past two decades within QMs.

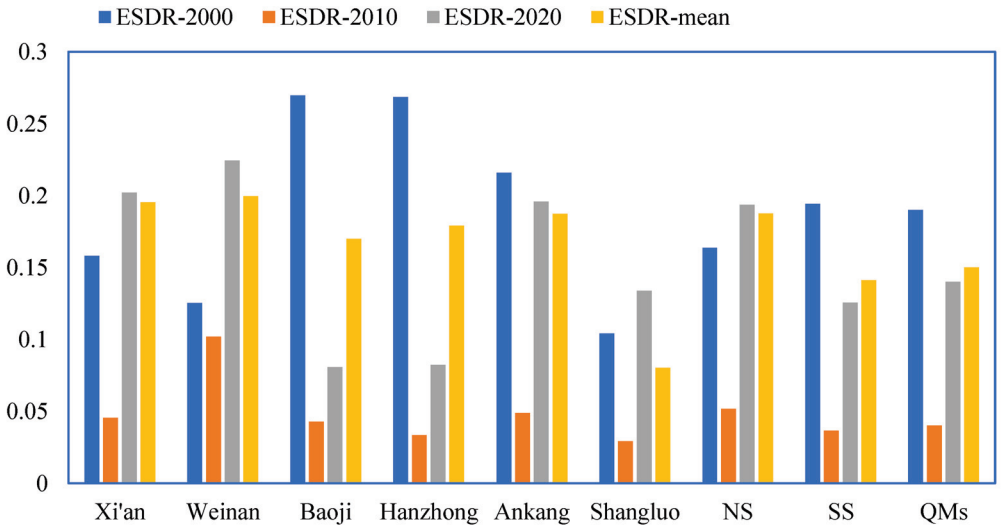

Figure 6. Temporal variations in the mean ESDR across different cities and regions from 2000 to 2020.

3.2.2. Average Spatial Patterns and Trends

From 2000–2020, the soil conservation services in the QMs maintained a spatially favorable supply–demand balance (Figure 7). The proportion of areas exhibiting positive values in the ESDR reached an impressive 82.19% of the total area. The distribution pattern of the ESDR in the entire region exhibited high values in the central part and low values on both the eastern and western sides. Specifically, negative values were predominantly observed in the counties of Shangluo City and the eastern part of Ankang City in the eastern QMs, as well as counties such as Ningshan, Lueyang, and Fengxian in the western QMs. However, these regions generally exhibited an ESDR ranging from −0.2 to 0, indicating a moderate deficit in their supply–demand conditions. The spatial distribution of pixels

exhibiting ESDR values below −0.2 in the specific regions of Lueyang and Taibai appeared to be sporadic. The supply–demand conditions for soil conservation in these areas exhibited a moderate-to-severe imbalance, indicating a significant potential risk for soil erosion. Meanwhile, the pixels exhibiting a positive ESDR were widely distributed across various zones within the QMs. Notably, pixels with a relatively high ESDR primarily concentrated on the northern slope, as well as in the central and western regions. The pixels, which generally had an ESDR exceeding 0.5 and exhibited a favorable supply–demand situation, were primarily concentrated in the central QMs, encompassing Chenggu, Yangxian, and Foping along with their surrounding areas. These territories represented typical regions with a surplus supply over demand of SCSs, indicating relatively lower susceptibility to soil erosion and higher ecological carrying capacity.

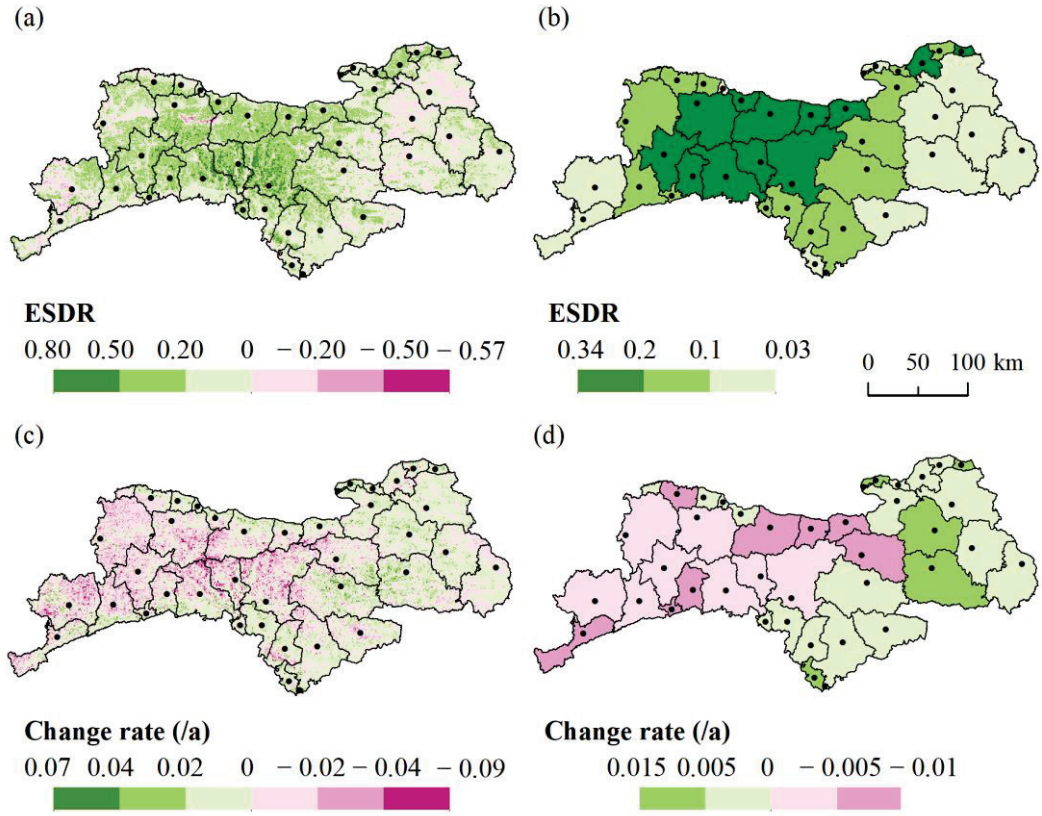

Figure 7. The spatial patterns and trends of the ESDR at pixel scale (**a**,**c**), district and county scale (**b**,**d**) in the QMs from 2000 to 2020.

Subsequently, the partitioning statistics tool in the GIS was employed to assess the spatial distribution of the mean ESDR value across districts and counties. At the district and county level, a relatively favorable supply and demand situation was observed as sporadic negative pixel values were averaged out, resulting in positive values. Consequently, from 2000 to 2020, all the districts and counties within the region exhibited a positive ESDR. The average ESDR values exhibited a range of 0.03 to 0.34 across districts and counties, indicating diverse levels of supply–demand dynamics. Based on the observed disparities in the ESDR, the supply–demand level can be classified as mild oversupply, moderate oversupply, or relatively high oversupply. The county-level analysis revealed a persistent high value of the ESDR in the central region, while lower values were observed on both sides. Notably, the central region exhibited a predominant surplus supply exceeding demand, with the ESDR generally above 0.2. Additionally, there was an expanding moderate level of supply exceeding demand toward both east and west directions, and it was characterized by an ESDR ranging from 0.1 to 0.2. The mild oversupply was primarily concentrated in

Ningqiang and Lueyang, Ziyang and Xunyang, as well as most of the counties in Shangluo City, which is situated on the eastern boundary.

The spatial distribution of the ESDR exhibited an eastward increase and a westward decline, with areas showing upward and downward trends covering approximately half of the entire region, respectively. However, the rate of change in the ESDR across the entire region exhibited a relatively gradual pattern, with fluctuations ranging from −0.09 to 0.07. A substantial decrease in the ESDR was observed in the central and western regions, including Huyi, Ningshan, and Hanyin as their demarcations. In this region, a majority of pixels indicated a decline rate surpassing 0.02. Conversely, an evident upward trend in the ESDR could be observed on the eastern side of this boundary, as well as at the southern and northern peripheries of the QMs, where most of the pixels displayed an increase rate exceeding 0.02.

Compared to the pixel-scale results, the rate of change in the ESDR at the district and county level exhibited a relatively slower pace, ranging from −0.01 to 0.015 only. However, notable regional disparities emerged in the rate of ESDR change. Districts and counties located in the central and western regions generally demonstrated a declining trend in the ESDR, whereas districts and counties in the eastern regions (excluding Zhashui) showed an increasing trend in the ESDR.

Meanwhile, the standardized average values of supply, demand, and ESDR were analyzed to investigate the variation characteristics of the supply–demand relationship across diverse cities and regions from 2000 to 2020 (Figure 8). It could be observed that, over the past two decades, Shangluo and Baoji have been characterized by a low supply and high demand in SCSs, resulting in their relatively lower ESDR. Conversely, Weinan and Xi'an have experienced a high supply and low demand situation, leading to their comparatively higher ESDR. Hanzhong and Ankang fall into the category of high supply and high demand, thereby exhibiting a moderate level of ESDR.

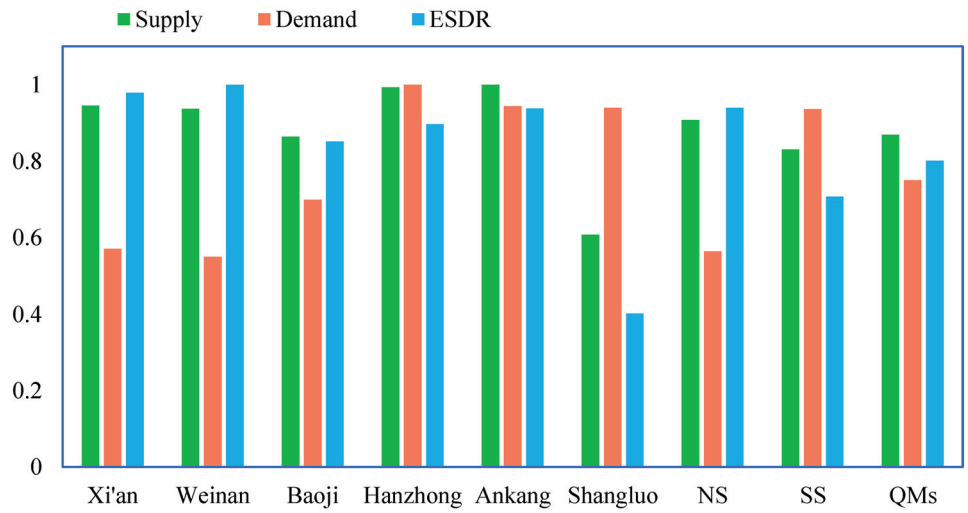

Figure 8. The mean supply, demand, and ESDR across different cities and regions from 2000 to 2020.

3.3. Spatial Matches of the SCS Supply and Demand

3.3.1. Moran Scatterplots of the SCS Supply and Demand

The global Moran's index of the supply–demand conditions in the QMs, obtained through bivariate spatial autocorrelation, effectively captured the overall characteristics of the SCS supply–demand across diverse regions (Figure 9). The global Moran's index exhibited positive values and surpassed the significance level of 0.1 during the years 2000, 2010, and 2020, as well as from 2000 to 2020. This signifies a substantial positive spatial correlation between the supply and demand concerning their distribution across these years, as well as over multiple years on average. In essence, there exists a propensity for the clustering of High–High or Low–Low patterns in the spatial distribution of supply and

demand within the QMs. Simultaneously, the global Moran's index for each year ranged from 0.2 to 0.3, indicating a relatively high level of average spatial clustering of supply and demand during these years, with the most optimal clustering observed in 2010. However, during the period from 2000 to 2020, the global Moran's index for the supply–demand situation was merely 0.045, indicating a decline in the spatial clustering and an increase in the spatial randomness of supply and demand under average circumstances.

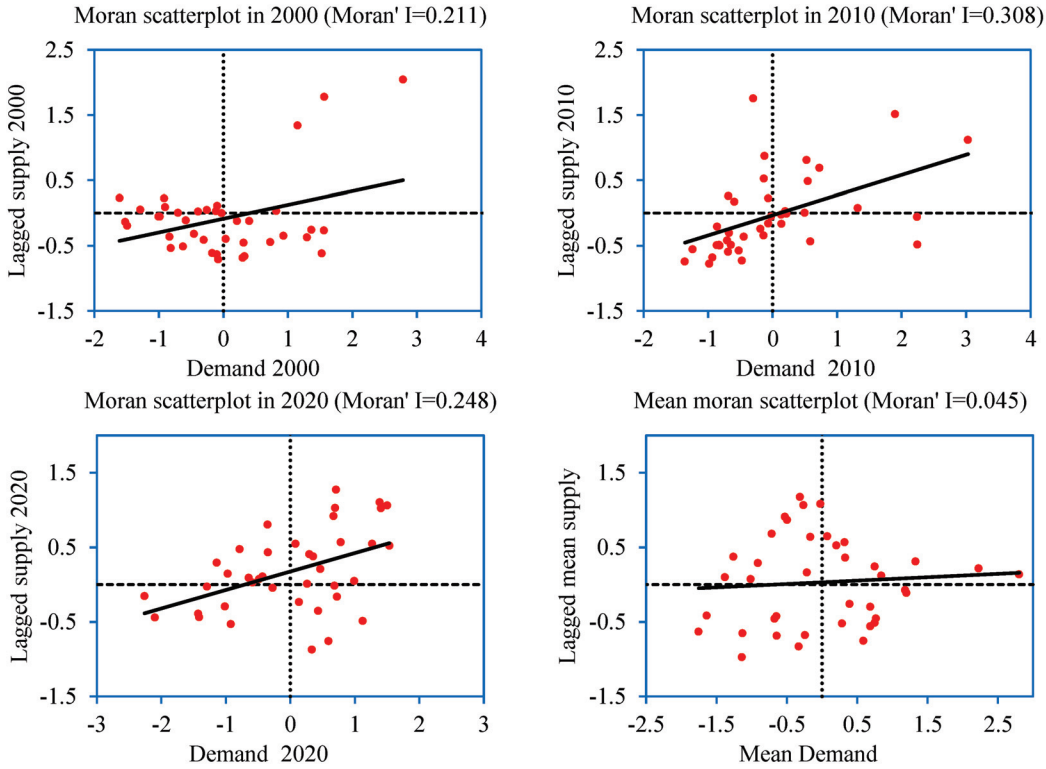

Figure 9. Moran scatterplots of the demand and supply in 2000, 2010, 2020, and during 2000–2020. The red dots represent the Moran scatterplots, while the black line represents the Moran regression line.

Meanwhile, the Moran scatterplots illustrate the spatial distribution patterns of the supply and demand in four quadrants. Specifically, the first and third quadrants depict a positive spatial correlation between the supply and demand in SCSs, representing two clustering types: H-H (High Supply–High Demand) and L-L (Low Supply–Low Demand). Conversely, the second and fourth quadrants indicate a negative spatial correlation between supply and demand in SCSs, representing two dispersion types: H-L (High Supply–Low Demand) and L-H (Low Supply–High Demand). According to the statistics, in 2000, the Moran scatterplots in both the third and fourth quadrants accounted for more than 30% of the total count, indicating that regions characterized by L-L and L-H exhibited a predominant proportion. In 2010, the scatterplots in the third quadrant accounted for nearly half of the total count in 2010, indicating a predominant presence of L-L-type regions. Following closely were H-H-type regions, constituting 20% of the overall distribution. This observation suggests that the entire region is primarily characterized by a positive supply–demand correlation. The year 2020 witnessed a significant prevalence of Moran scatterplots in the first and second quadrants, indicating the dominant spatial presence of regions characterized by H-H and H-L. However, during the period from 2000 to 2020, the average proportion of Moran scatterplots in the second quadrant exceeded 30%, while the proportions for the other three quadrants remained approximately at 23%. This suggests a relatively equitable spatial distribution among these four types.

3.3.2. Spatial Distribution of the Matches of the SCS Supply and Demand

The bivariate spatial autocorrelation analysis function from GeoDa software was utilized to generate Bivariate LISA Cluster Maps, enabling further examination of the spatial matching status between the SCS supply and demand in different periods for each district and county within the QMs region (Figure 10). The software detected spatial matching areas that failed to meet a significance level of 0.1. Consequently, this section focused on analyzing the distribution and variability patterns exhibited by the spatial matches in H-H and L-L, along with significant spatial mismatches in the H-L and L-H observed from 2000 to 2020.

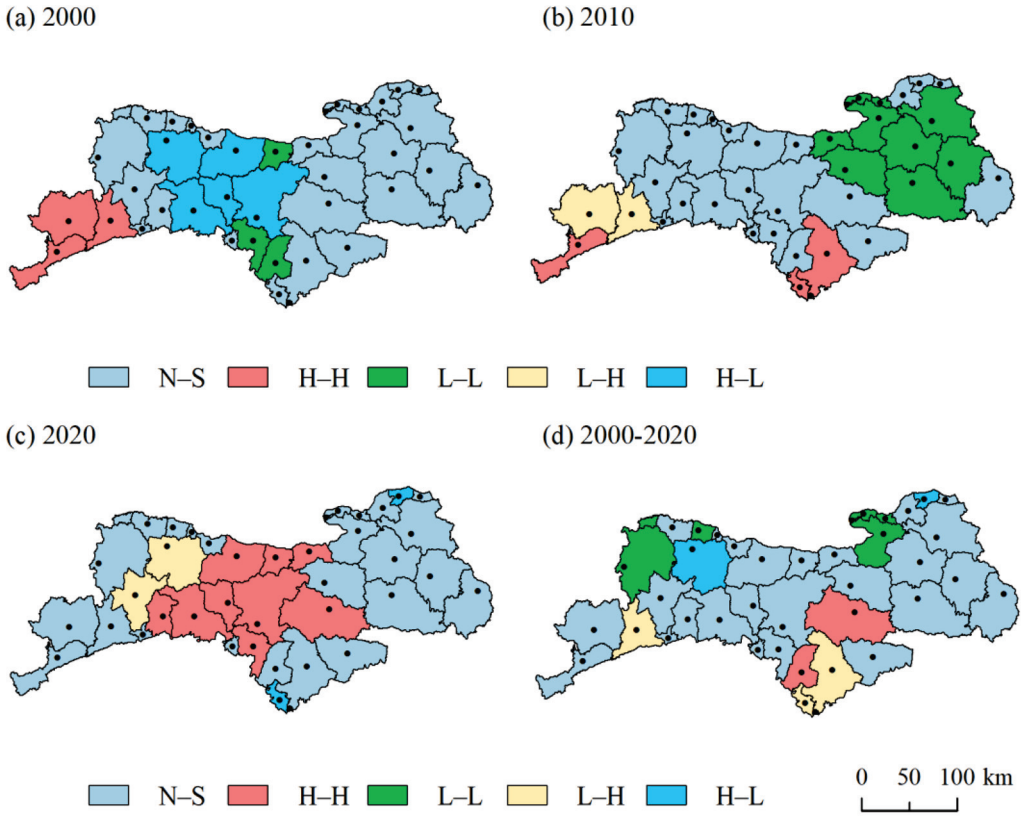

Figure 10. The spatial matches of SCS supply and demand across different districts and counties from 2000 to 2020.

In 2000, a total of 11 districts and counties in the QMS were identified as spatially matched or mismatched areas through significant level tests. These districts and counties were located in the central and western regions, with Zhouzhi, Taibai, Yangxian, Foping, and Ningshan exhibiting the highest proportion of H-L mismatched areas. The remaining districts and counties represented spatially matched regions; Mian County, Ningqiang, and Lueyang in the west demonstrated H-H-matched areas, while Huyi, Hanyin, and Shiquan exhibited L-L-matched areas. The number of districts and counties that passed the significance test significantly increased to 16 in 2010, and they were primarily distributed in the eastern and southern regions of Qinling. Among them, the spatial L-L-matched type accounted for the highest proportion with 10 districts and counties concentrated in the eastern region, belonging to Weinan, Xi'an, and Shangluo. Following this were H-H-matched areas, which were mainly located in Ningqiang in southwestern Qinling, as well as Hanbin, Ziyang, and Langao in southwestern Qinling. Lueyang and Mian County belonged to the L-H-mismatched regions situated in southwestern Qinling. In 2020, the H-H-matched region exhibited the highest spatial proportion, encompassing nine districts and counties predominantly concentrated in the central part of the region. There were only four counties characterized by spatial mismatch: Liuba and Taibai in the west

were classified as L-H-mismatched, and Huayin and Ziyang in the east were classified as H-L-mismatched.

During the period from 2000 to 2020, regions exhibiting spatially matched types accounted for a substantial proportion on average. Specifically, there were five regions characterized by L-L match: Chencang and Fengxian in the southwest, as well as Lin Tong, Lan Tian, and Lin Wei in the southeast. Regions displaying the H-H-matched type were distributed in Hanyin and Zhen'an. Spatial mismatches of the L-H type were observed in Mianxian, Hanbin, Ziyang, and Langao in the south, along with spatial mismatches in H-L being found in Taibai and Huayin in the north.

4. Discussion

4.1. The Spatio-Temporal Disparities and Patterns in the SCS Supply and Demand

As a national-level nature reserve, the QMs possess significant ecosystem services, including soil conservation services. This study revealed that between 2000 and 2020, the majority of areas exhibited a substantially high supply of SCSs with an upward trend and low demand for SCSs in a declining trend. The results indicate a positive trend of improvement in the actual soil erosion condition in the QMs over the years, which is consistent with previous research findings [62,72]. Spatially, most areas exhibit positive values for the ESDR, further confirming relatively less pressure on the SCSs in the region. These findings align with the research conducted by scholars in the Loess Plateau [73], Zhejiang Province [33], and Northeast China [6].

However, spatial characteristics of the ESDR exhibit certain variations at different scales. At the pixel scale, the proportion of positive ESDR regions was 78.39%, 62.44%, and 61.03% in 2000, 2010, and 2020, respectively. Conversely, at the county level, only a few counties displayed negative ESDR values in both 2000 and 2010, whereas all counties exhibited positive values in 2020. Moreover, across all three years, each city demonstrated positive ESDR values. Significant variations in the proportion of positive values were observed across three different scales. During partition statistics, regions exhibiting smaller negative ESDR values or fewer distributions with negative values may have been aggregated as positive within their respective areas. Meanwhile, it was observed that the ESDR on the northern slope exhibited a smaller magnitude compared to the southern slope in 2000, while displaying greater values in subsequent years. These findings imply distinct variations in both spatial distribution patterns and temporal trends of the ESDR across different scales within the QMs. Therefore, employing time and space multi-scale methodologies enables the comprehensive examination of supply and demand dynamics in the SCSs from various perspectives.

Furthermore, the spatial distribution of the ESDR in the QMs region exhibited a distinct pattern characterized by significant increases in the eastern part and decreases in the central and western parts. Approximately half of the area displayed pixels indicating increasing trends while the other half showed decreasing trends. This suggests that there still exists a certain degree of risk in the supply and demand dynamics of the SCSs in the central and western regions, thus deviating from previous research findings on comparing the SCS supply with demand. The EDSR model integrates both supply and demand parameters to enable quantitative evaluation, thereby showcasing its scientific and rational superiority over simplistic supply–demand comparisons. The identified central and western regions are anticipated to encounter substantial supply and demand pressures in the forthcoming years. Hence, local authorities should enhance supervision and implement ecological measures for safeguarding purposes.

From 2000 to 2020, a significant positive spatial correlation was observed between the supply and demand in the region. The prevalence of spatial matching clusters in H-H or L-L was relatively high throughout the entire Qinling region, indicating a consistently favorable spatial matching condition for SCSs over the years. As previously mentioned, this study also indicates that there was a consistently positive ESDR in most areas, suggesting a favorable balance between supply and demand. However, these two phenomena are not

equivalent. A better supply–demand balance denotes a state of surplus between supply and demand, wherein the supply exceeds the demand. The spatial matching reflects the collaborative state of supply and demand, which is only achieved when both supply and demand exhibit high or low values. Hence, it is important to note that regions exhibiting a surplus in supply and demand may not necessarily correspond to spatial matching regions. Therefore, the integration of the ESDR and spatial matching research is imperative to attain a comprehensive comprehension of the supply and demand status of ecosystem services in a given region, thereby furnishing scientific references for the implementation of strategies in regional ecological management.

4.2. Driving Factor Analysis of the SCS Supply and Demand

The supply and demand status of SCSs reflects the capacity of a regional natural ecosystem to provide effective measures for soil erosion control, while also encompassing the societal demand for such services, which is represented by the quantifiable extent of soil erosion in the local area. The processes of soil erosion and soil conservation are intricate, and they are influenced by a myriad of factors encompassing topography and gravity factors; climate (including water, wind, freeze–thaw action, and temperature); the physical and chemical properties of the soil; vegetation cover; land use; and socio-economic development, among others.

According to the different external forces, water is identified as the primary driver of erosion in the QMs region, followed by gravitational and debris flow factors. Wind and freeze–thaw erosions are virtually negligible in this region [63]. Temperature, as another crucial determinant of climate change, exerts its influence on soil erosion processes through its impact on local hydrological circulation and precipitation patterns, vegetation growth, and agricultural activities, among others [74]. The widely employed RUSLE model is specifically designed for investigating water erosion, with due consideration being given to factors such as topography, slope, vegetation.

The QMs region experiences predominant precipitation during the summer flood season, which, in conjunction with the comprehensive influence of the local mountainous environment, designates it as the primary period for soil erosion. Within the RULSE formula, the rainfall erosivity factor (R) is regarded as a pivotal indicator for evaluating the influence of precipitation on soil erosion. In this study, we conducted a Pearson correlation analysis to investigate the relationship between historical precipitation levels and both the supply and demand of SCSs. The results revealed a significant positive correlation between precipitation and both variables, with correlation coefficients of 0.86 and 0.67, respectively. The findings underscore the significant impact of precipitation on the supply and demand dynamics of SCSs. In 2000, the limited supply and demand for SCSs were observed due to relatively low rainfall in the Qinling region. Conversely, in recent years such as 2010 and 2020, which were characterized by abundant rainfall [75], both the supply and demand for SCSs witnessed substantial growth. However, the ESDR was contingent upon the magnitude of the disparity between supply and demand of the SCSs. Consequently, in comparison to 2000 and 2020, the ESDR observed in 2010 exhibited a significantly diminished scale. Nevertheless, this does not imply that there was a reduced amount of precipitation in 2010; rather, it can be attributed to a narrower margin between the supply and demand during that particular year.

Furthermore, vegetation plays a crucial role as a natural protective barrier for soil. Its dense canopy effectively intercepts and redistributes rainwater, while its intricate root system contributes to soil stabilization and enhances its water retention capacity [73]. Consequently, there exists a positive correlation between the extent of vegetation coverage and the provision of soil conservation services. The central and western parts of the Qinling Mountains are predominantly characterized by mid-to-high mountainous terrain with minimal anthropogenic disturbance, thereby fostering the persistence of numerous undisturbed closed forests in this region over an extended period and resulting in commendable vegetation coverage [76]. Under the protective cover of vegetation, these areas also exhibit

significant soil conservation functions, positioning them as high-value regions for SCSs in the Qinling region. Consequently, local soil erosion is relatively minimal, thereby indicating a limited demand for SCS interventions in this area. Accordingly, considering the balance of supply and demand, these regions can be identified as areas characterized by a higher ESDR, indicating a surplus situation due to an abundance in supply but relatively lower demand. On the contrary, the eastern and southern fringe region encompass a medium–low mountainous terrain that exhibits concentrated human population and heightened anthropogenic activities. Consequently, these areas exhibit a relatively higher prevalence of artificial forests, secondary forests, and shrubs with diminished vegetation coverage [76]. The supply of soil conservation services in these regions is relatively inadequate, resulting in a high risk of soil erosion. Consequently, they fall into the category of areas with low supply and high demand for SCSs.

The impact of human factors on SCSs is also significant, encompassing both positive and negative effects. The intricate underlying processes and mechanisms governing this influence are noteworthy. As previously mentioned, anthropogenic activities have the potential to impact SCSs through their influence on vegetation. If humans continue to deforest and exploit wood resources, it will disrupt the natural equilibrium of soil conservation and escalate the potential risk of soil erosion. Notably, recent years have witnessed significant attention toward ecological preservation in the QMs, leading to extensive implementation of diverse ecological initiatives such as afforestation, forest enclosure for regeneration, and aerial seeding. The previous studies have demonstrated a significant enhancement in the vegetation quality, coverage, and ecological environment within the QMs [49,76–78]. Consequently, the local ecosystem is expected to exhibit a positive developmental trajectory while gradually augmenting its capacity for SCSs. Furthermore, changes in land use play a pivotal role as crucial indicators that accurately reflect the extent of human activities. Throughout the course of social and economic production, humans change local land use patterns, thereby inducing changes in vegetation coverage, surface roughness, hydrological characteristics such as infiltration and runoff, ultimately exerting an impact on the soil conservation capacity of the land. The capacity of soil conservation service varies significantly across different land use types, with forest land having the highest capacity, followed by grassland, cultivated land, built-up land, water bodies, and bare land [79]. Zhen et al. conducted a simulation to evaluate the equilibrium between the supply and demand of SCSs in the Chinese Loess Plateau by 2030 [44]. Their findings suggest that transforming cultivated and unused land into ecological areas would enhance precipitation patterns and facilitate vegetation growth, resulting in a substantial surplus of SCS supply and demand. Since 2000, significant changes have occurred in land use within the QMs due to ecological initiatives such as the Grain for Green Project. Notably, there has been a discernible decrease in cultivated land extent, while the areas of other land types have witnessed an increase [80]. In terms of land use conversion, this primarily manifests as a shift from agricultural cultivation toward forested and grassland ecosystems. The cultivated land is primarily concentrated in the low-altitude regions of the eastern and southern QMs, thereby leading to an increased provision of SCSs within these areas. Consequently, this alteration in land use concurrently mitigates the potential risk of local soil erosion, ultimately enhancing the supply–demand ratio of SCSs and aligning with the findings presented in this study. Additionally, it is noteworthy that factors such as topography, soil characteristics, temperature, and landscape patterns also exert discernible influences on the variations of SCSs [73,79], thereby warranting further investigation.

4.3. Management Suggestions

The Qinling region is globally recognized as a biodiversity hotspot and holds paramount significance as one of China's most crucial ecological functional areas. However, owing to the enduring constraints of the mountainous environment, the socio-economic development in this region lags behind. Firstly, for the entire region, the local management authorities should effectively tackle the challenge of balancing ecological and economic

development [49], that is, the local area should strive for moderate economic development, prioritize the well-being of its residents, foster the growth of tertiary industries such as eco-tourism and cultural creativity, gradually limit the expansion of primary and secondary industries, and rigorously safeguard the ecological environment. The ecological background and the ecosystem structure and function will thus steadily improve, leading to a positive development in the supply and demand dynamics for the SCSs.

Furthermore, the regional spatial development direction is synthesized based on land use management and planning [81]. Utilizing frameworks such as " achieving the supply–demand balance of ecosystem services through zoning [28]", ecological management zones can be established in the Qinling Mountains region to formulate diverse development strategies [54,82]. The core protection areas serves as the primary source area for regional ecosystem services, thus resulting in a predominance of High Supply–Low Demand or Low Supply–Low Demand of ESs. The ecosystems in these areas require systematic protection, enabling indigenous residents to engage in sustainable activities that fulfill their basic needs, while prohibiting other forms of construction and industrial operations. The key protected areas primarily encompass national parks, scenic spots, forest parks, etc. The regions under consideration exhibit remarkable biodiversity; however, their ecological environment is highly susceptible to degradation. Consequently, any form of real estate development and the establishment of new hydropower facilities are strictly prohibited in order to ensure ecosystem stability and to gradually enhance local ecosystem services. The general protected areas, which are characterized by a certain population concentration and industrial development, possess delicate ecological environments with a Low Supply–Low Demand of ESs. Therefore, it is urgent for this region to prioritize ecological restoration while simultaneously promoting the growth of ecotourism and the green economy. The peripheral area of the protected zone primarily serves as a hub for population concentration and industrial development, and it is characterized by a low supply but high demand for ESs. The region should adhere to ecological restoration, optimize its industrial structure, promote intensive and environmentally friendly production practices, mitigate the negative impact of socio-economic development on the ecological environment, and progressively enhance the quality of the ecological environment.

Additionally, the local management authorities should enhance spatial planning management and facilitate a coordinated development among the different regions in the Qinling Mountains region [36]. This study revealed that the Qinling region exhibits a relatively higher proportion of areas with supply–demand matches; however, certain areas still fall short of achieving this match. Therefore, we need to continue conducting comprehensive research on the spatial matching and agglomeration of regional ESs, with a focus on identifying the key areas characterized by significant spatial agglomeration in the mismatch between supply and demand. Subsequently, targeted regulations should be implemented throughout the region to gradually achieve coordinated supply and demand at a regional scale.

4.4. Limitations and Prospects

This article utilized the QMs region as a case study to systematically examine the dynamics of spatial balance and matches between the supply and demand of SCSs in protected areas. The research findings demonstrated that, in comparison to other types of areas, protected areas exhibited a superior ecological background. Consequently, the budgets between the supply and demand of ESs were relatively favorable, and they were accompanied by a higher degree of spatial matches. Thus, this represents a commendable endeavor and exploration. However, due to data limitations, this study exclusively examined the dynamics of the ES supply and demand in the QMs from 2000. Future research endeavors should strive to integrate additional data encompassing climate change scenarios and socio-economic scenarios in order to further explore the dynamic changes in the ES supply and demand under future scenarios, as well as to investigate the underlying driving mechanisms of these changes on an extended temporal scale.

Simultaneously, it is important to note that this article solely focuses on the selection of SCSs as a representative ES type. In future studies, it would be beneficial to incorporate additional ES types in order to investigate the balance between supply and demand, as well as the spatial matching characteristics exhibited by various ES types within nature reserves. By considering these distinct spatial matching characteristics, it becomes possible to identify key protected areas and suitable development zones for implementing precise ecosystem management at a regional scale.

5. Conclusions

Taking the Qinling Mountains as a representative case study, this research employed the RUSLE model, bivariate autocorrelation methods, and multi-source data to investigate the spatio-temporal evolution characteristics of supply and demand statuses, the supply–demand index, as well as the matches between supply and demand from 2000 to 2020.

The key conclusions are as follows.

The supply of the SCSs in the QMs demonstrated a consistently high level, with a majority of areas demonstrating an increasing trend. Conversely, the demand for SCSs was predominantly low during this period, with most areas experiencing a decreasing trend. Therefore, based on the comparison of supply and demand, the pressure of SCS supply and demand in the QMs tended to be alleviated.

Over the years, the majority of regions exhibited positive values in the ESDR. However, there was a gradual decline in the SCS demand observed in the central and western QMs, while the eastern QMs predominantly demonstrated a slow upward trend. Consequently, concerning ESDR trends, significant pressure and risks were observed for soil conservation in the central and western QMs.

According to the analysis of the global Moran's index, a significant positive spatial correlation between the supply and demand in the region was observed across various typical years, indicating that the spatial distribution of the SCS supply and demand primarily forms H-H and L-L clusters. The results of the local Moran's index also suggest a higher prevalence of spatial matches in H-H and L-L areas, indicating a robust spatial alignment between the supply and demand in the QMs throughout the years.

In summary, the ecological environment quality of the QMs exhibited a progressive improvement in recent years, and it was characterized by a relatively low pressure on soil conservation services and an optimal spatial alignment between the supply and demand for SCSs. These favorable conditions will facilitate effective ecosystem management by local authorities and contribute significantly to the sustainable development of the region. However, significant disparities in supply and demand dynamics, and the matching status within the region at various temporal and spatial scales, necessitate the implementation of corresponding management measures. To effectively promote the stability and health of ecosystems, it is crucial to conduct supply and demand assessments of ESs across various temporal and spatial scales when implementing ecosystem management in similar nature reserves. This approach holds significant reference value for undertaking ecological management efforts within nature reserve areas.

Author Contributions: Conceptualization, P.W., G.H., and K.L.; methodology, P.W., and L.C.; software, J.Z. and X.F.; validation, L.C., S.G., and P.W.; formal analysis, J.Z.; investigation, P.W. and G.H.; resources, P.W. and K.L.; data curation, P.W. and L.C.; writing—original draft preparation, P.W. and G.H.; writing—review and editing, P.W., G.H., L.C., and W.W.; visualization, P.W. and S.G.; supervision, K.L., S.G., and J.Y.; project administration, J.Y. and K.L.; funding acquisition, K.L., P.W., W.W., and J.Y. All authors have read and agreed to the published version of the manuscript.

Funding: This research was funded by the Scientific Research Project of Shaanxi Provincial Education Department (21JK0306) and the National Natural Science Foundation of China (42001132).

Data Availability Statement: All data and materials are available upon request.

Conflicts of Interest: The authors declare no conflict of interest.

References

1. Costanza, R.; d'Arge, R.; de Groot, R.; Farber, S.; Grasso, M.; Hannon, B.; Limburg, K.; Naeem, S.; Oneill, R.V.; Paruelo, J.; et al. The value of the world's ecosystem services and natural capital. *Nature* **1997**, *387*, 253–260. [CrossRef]
2. Uehara, T.; Hidaka, T.; Tsuge, T.; Sakurai, R.; Cordier, M. An adaptive social-ecological system management matrix for guiding ecosystem service improvements. *Ecosyst. Serv.* **2021**, *50*, 101312. [CrossRef]
3. Wolff, S.; Schulp, C.J.E.; Verburg, P.H. Mapping ecosystem services demand: A review of current research and future perspectives. *Ecol. Indic.* **2015**, *55*, 159–171. [CrossRef]
4. Ala-Hulkko, T.; Kotavaara, O.; Alahuhta, J.; Hjort, J. Mapping supply and demand of a provisioning ecosystem service across Europe. *Ecol. Indic.* **2019**, *103*, 520–529. [CrossRef]
5. Villamagna, A.M.; Angermeier, P.L.; Bennett, E.M. Capacity, pressure, demand, and flow: A conceptual framework for analyzing ecosystem service provision and delivery. *Ecol. Complex.* **2013**, *15*, 114–121. [CrossRef]
6. Xiang, H.; Zhang, J.; Mao, D.; Wang, Z.; Qiu, Z.; Yan, H. Identifying spatial similarities and mismatches between supply and demand of ecosystem services for sustainable Northeast China. *Ecol. Indic.* **2022**, *134*, 108501. [CrossRef]
7. Hanna, D.E.L.; Roux, D.J.; Currie, B.; Bennett, E.M. Identifying pathways to reduce discrepancies between desired and provided ecosystem services. *Ecosyst. Serv.* **2020**, *43*, 101119. [CrossRef]
8. Burkhard, B.; Kroll, F.; Nedkov, S.; Müller, F. Mapping ecosystem service supply, demand and budgets. *Ecol. Indic.* **2012**, *21*, 17–29. [CrossRef]
9. Palacios-Agundez, I.; Onaindia, M.; Barraqueta, P.; Madariaga, I. Provisioning ecosystem services supply and demand: The role of landscape management to reinforce supply and promote synergies with other ecosystem services. *Land Use Policy* **2015**, *47*, 145–155. [CrossRef]
10. Chaplin-Kramer, R.; Sharp, R.P.; Weil, C.; Bennett, E.M.; Pascual, U.; Arkema, K.K.; Brauman, K.A.; Bryant, B.P.; Guerry, A.D.; Haddad, N.M.; et al. Global modeling of nature's contributions to people. *Science* **2019**, *366*, 255–258. [CrossRef]
11. Costanza, R.; de Groot, R.; Sutton, P.; van der Ploeg, S.; Anderson, S.J.; Kubiszewski, I.; Farber, S.; Turner, R.K. Changes in the global value of ecosystem services. *Glob. Environ. Change* **2014**, *26*, 152–158. [CrossRef]
12. Zhang, Z.; Wang, Q.; Feng, Y.; Sun, Y.; Liu, N.; Yan, S. The spatio-temporal evolution of spatial structure and supply-demand relationships of the ecological network in the Yellow River Delta region of China. *J. Clean. Prod.* **2024**, *471*, 143388. [CrossRef]
13. Wang, Z.; Zhang, L.; Li, X.; Li, Y.; Fu, B. Integrating ecosystem service supply and demand into ecological risk assessment: A comprehensive framework and case study. *Landsc. Ecol.* **2021**, *36*, 2977–2995. [CrossRef]
14. Das, M.; Das, A.; Saikh, S. Estimating supply-demand mismatches for optimization of sustainable land use planning in a rapidly growing urban agglomeration (India). *Land Use Policy* **2024**, *139*, 107061. [CrossRef]
15. Chen, W.; Wang, G.; Gu, T.; Fang, C.; Pan, S.; Zeng, J.; Wu, J. Simulating the impact of urban expansion on ecosystem services in Chinese urban agglomerations: A multi-scenario perspective. *Environ. Impact Assess. Rev.* **2023**, *103*, 107275. [CrossRef]
16. Liu, L.; Liu, C.; Wang, C.; Li, P. Supply and demand matching of ecosystem services in loess hilly region: A case study of Lanzhou. *Acta Geol. Sin.* **2019**, *74*, 1921–1937.
17. Wei, H.; Fan, W.; Wang, X.; Lu, N.; Dong, X.; Zhao, Y.; Ya, X.; Zhao, Y. Integrating supply and social demand in ecosystem services assessment: A review. *Ecosyst. Serv.* **2017**, *25*, 15–27. [CrossRef]
18. Schirpke, U.; Vigl, L.E.; Tasser, E.; Tappeiner, U. Analyzing Spatial Congruencies and Mismatches between Supply, Demand and Flow of Ecosystem Services and Sustainable Development. *Sustainability* **2019**, *11*, 2227. [CrossRef]
19. Sun, X.; Tang, H.; Yang, P.; Hu, G.; Liu, Z.; Wu, J. Spatiotemporal patterns and drivers of ecosystem service supply and demand across the conterminous United States: A multiscale analysis. *Sci. Total Environ.* **2020**, *703*, 135005. [CrossRef]
20. Wu, X.; Liu, S.; Zhao, S.; Hou, X.; Xu, J.; Dong, S.; Liu, G. Quantification and driving force analysis of ecosystem services supply, demand and balance in China. *Sci. Total Environ.* **2019**, *652*, 1375–1386. [CrossRef]
21. Wang, Z.; Sun, X.; Shan, R.; Wang, B. Mapping and assessing supply–demand matching of recreational ecosystem services in Shandong province, China. *Ecol. Indic.* **2024**, *160*, 111859. [CrossRef]
22. Xu, Z.; Peng, J.; Dong, J.; Liu, Y.; Liu, Q.; Lyu, D.; Qiao, R.; Zhang, Z. Spatial correlation between the changes of ecosystem service supply and demand: An ecological zoning approach. *Landsc. Urban Plan.* **2022**, *217*, 104258. [CrossRef]
23. Khosravi Mashizi, A.; Sharafatmandrad, M. Investigating tradeoffs between supply, use and demand of ecosystem services and their effective drivers for sustainable environmental management. *J. Environ. Manag.* **2021**, *289*, 112534. [CrossRef] [PubMed]
24. Larondelle, N.; Lauf, S. Balancing demand and supply of multiple urban ecosystem services on different spatial scales. *Ecosyst. Serv.* **2016**, *22*, 18–31. [CrossRef]
25. Peng, L.; Zhang, L.; Li, X.; Wang, Z.; Wang, H.; Jiao, L. Spatial expansion effects on urban ecosystem services supply-demand mismatching in Guanzhong Plain Urban Agglomeration of China. *J. Geogr. Sci.* **2022**, *32*, 806–828. [CrossRef]
26. Xia, Z.; Wang, Y.; Lu, Q.; Shen, Z.; Liu, K.; Wei, X.; Yuan, C.; Gao, Y.; Liu, L. Understanding residents' perspectives on cultural ecosystem service supply, demand and subjective well-being in rapidly urbanizing landscapes: A case study of peri-urban Shanghai. *Landsc. Ecol.* **2024**, *39*, 22. [CrossRef]
27. Xie, Y.; Dai, W.; Xiang, S.; Deng, H.; Wang, Z.; Li, Y.; Wang, Z.; Zhou, M.; Gao, M. Supply and demand of ecosystem services and their interaction with urbanization: The case of Chengdu-Chongqing urban agglomeration. *Urban Clim.* **2024**, *55*, 101978. [CrossRef]

28. Zhao, X.; Xu, Y.; Pu, J.; Tao, J.; Chen, Y.; Huang, P.; Shi, X.; Ran, Y.; Gu, Z. Achieving the supply-demand balance of ecosystem services through zoning regulation based on land use thresholds. *Land Use Policy* **2024**, *139*, 107056. [CrossRef]
29. Kpienbaareh, D.; Bezner Kerr, R.; Nyantakyi-Frimpong, H.; Iverson, A.; Luginaah, I.; Lupafya, E.; Dakishoni, L.; Shumba, L. Ecosystem service demand and supply dynamics under different farming systems: A participatory GIS assessment in Malawi. *Appl. Geogr.* **2024**, *171*, 103372. [CrossRef]
30. Xu, Q.; Yang, R.; Zhuang, D.; Lu, Z. Spatial gradient differences of ecosystem services supply and demand in the Pearl River Delta region. *J. Clean. Prod.* **2021**, *279*, 123849. [CrossRef]
31. Deng, C.; Zhu, D.; Nie, X.; Liu, C.; Zhang, G.; Liu, Y.; Li, Z.; Wang, S.; Ma, Y. Precipitation and urban expansion caused jointly the spatiotemporal dislocation between supply and demand of water provision service. *J. Environ. Manag.* **2021**, *299*, 113660. [CrossRef] [PubMed]
32. Sahle, M.; Saito, O.; Furst, C.; Yeshitela, K. Quantifying and mapping of water-related ecosystem services for enhancing the security of the food-water-energy nexus in tropical data-sparse catchment. *Sci. Total Environ.* **2019**, *646*, 573–586. [CrossRef] [PubMed]
33. Wang, L.-J.; Gong, J.-W.; Ma, S.; Wu, S.; Zhang, X.; Jiang, J. Ecosystem service supply–demand and socioecological drivers at different spatial scales in Zhejiang Province, China. *Ecol. Indic.* **2022**, *140*, 109058. [CrossRef]
34. Inacio, M.; Gomes, E.; Bogdzevic, K.; Kalinauskas, M.; Zhao, W.; Pereira, P. Mapping and assessing coastal recreation cultural ecosystem services supply, flow, and demand in Lithuania. *J. Environ. Manag.* **2022**, *323*, 116175. [CrossRef] [PubMed]
35. Dang, H.; Li, J.; Zhou, Z. Revealing the supply-demand relationship of urban cultural ecosystem services: The combination of open-source spatial model and topic model. *Appl. Geogr.* **2024**, *167*, 103288. [CrossRef]
36. Sun, X.; Liu, H.; Liao, C.; Nong, H.; Yang, P. Understanding recreational ecosystem service supply-demand mismatch and social groups' preferences: Implications for urban–rural planning. *Landsc. Urban Plan.* **2024**, *241*, 104903. [CrossRef]
37. Xie, G.; Zhang, C.; Zhen, L.; Zhang, L. Dynamic changes in the value of China's ecosystem services. *Ecosyst. Serv.* **2017**, *26*, 146–154. [CrossRef]
38. Xu, X.; Yang, G.; Tan, Y.; Liu, J.; Hu, H. Ecosystem services trade-offs and determinants in China's Yangtze River Economic Belt from 2000 to 2015. *Sci. Total Environ.* **2018**, *634*, 1601–1614. [CrossRef]
39. Martinez-Lopez, J.; Bagstad, K.J.; Balbi, S.; Magrach, A.; Voigt, B.; Athanasiadis, I.; Pascual, M.; Willcock, S.; Villa, F. Towards globally customizable ecosystem service models. *Sci. Total Environ.* **2019**, *650*, 2325–2336. [CrossRef]
40. Chen, W.; Gu, T.; Xiang, J.; Luo, T.; Zeng, J. Assessing the conservation effectiveness of national nature reserves in China. *Appl. Geogr.* **2023**, *161*, 103125. [CrossRef]
41. Depellegrin, D.; Martí Llambrich, C.; Roy, S.; Anbleyth-Evans, J.; Bongiorni, L.; Menegon, S. Risk-based analysis of recreational ecosystem services supply and demand in beach areas of the Adriatic Sea. *Ocean Coast. Manag.* **2023**, *243*, 106725. [CrossRef]
42. Boithias, L.; Acuna, V.; Vergonos, L.; Ziv, G.; Marce, R.; Sabater, S. Assessment of the water supply:demand ratios in a Mediterranean basin under different global change scenarios and mitigation alternatives. *Sci. Total Environ.* **2014**, *470–471*, 567–577. [CrossRef] [PubMed]
43. Li, J.; Fang, Z.; Zhang, J.; Huang, Q.; He, C. Mapping basin-scale supply-demand dynamics of flood regulation service—A case study in the Baiyangdian Lake Basin, China. *Ecol. Indic.* **2022**, *139*, 108902. [CrossRef]
44. Jian, Z.; Sun, Y.; Wang, F.; Zhou, C.; Pan, F.; Meng, W.; Sui, M. Soil conservation ecosystem service supply-demand and multi scenario simulation in the Loess Plateau, China. *Glob. Ecol. Conserv.* **2024**, *49*, e02796. [CrossRef]
45. Serna-Chavez, H.M.; Schulp, C.J.E.; van Bodegom, P.M.; Bouten, W.; Verburg, P.H.; Davidson, M.D. A quantitative framework for assessing spatial flows of ecosystem services. *Ecol. Indic.* **2014**, *39*, 24–33. [CrossRef]
46. Xu, X.Z.; Liu, Z.Y.; Xiao, P.Q.; Guo, W.Z.; Zhang, H.W.; Zhao, C.; Yan, Q. Gravity erosion on the steep loess slope: Behavior, trigger and sensitivity. *Catena* **2015**, *135*, 231–239. [CrossRef]
47. Zambrano-Cruzatty, L.; Yerro, A.; Charbonneau, B.R.; Stark, N. A soil mechanics model to determine the onset of wind erosion. *Coast. Eng.* **2024**, *191*, 104523. [CrossRef]
48. Das, S.; Jain, M.K.; Gupta, V. An assessment of anticipated future changes in water erosion dynamics under climate and land use change scenarios in South Asia. *J. Hydrol.* **2024**, *637*, 131341. [CrossRef]
49. Wang, P.; Chen, Y.; Liu, K.; Li, X.; Zhang, L.; Chen, L.; Shao, T.; Li, P.; Yang, G.; Wang, H.; et al. Coupling Coordination Relationship and Driving Force Analysis between Gross Ecosystem Product and Regional Economic System in the Qinling Mountains, China. *Land* **2024**, *13*, 234. [CrossRef]
50. Li, S.; Wang, C.; Yan, J.; Liu, X. Variability of the event-based extreme precipitation in the south and north Qinling Mountains. *Acta Geol. Sin.* **2020**, *75*, 989–1007.
51. Zhao, T.; Bai, H.; Yuan, Y.; Deng, C.; Qi, G.; Zhai, D. Spatio-temporal differentiation of climate warming (1959–2016) in the middle Qinling Mountains of China. *J. Geogr. Sci.* **2020**, *30*, 657–668. [CrossRef]
52. Chen, Y. Significance and strategies on the ecological civilization construction at Qinling Mountains. *J. Earth Environ.* **2019**, *10*, 1–11.
53. Li, J.; Fu, B.; Sun, J.; Hong, Z.; Zhang, B.; Wang, X.; Bai, H.; Wang, F.; Zhao, Z.; Cao, X. Ecological civilization construction at Qinling Mountains in the New Era. *J. Nat. Resour.* **2021**, *36*, 2449–2463. [CrossRef]

54. Yu, F.; Li, C.; Yuan, Z.; Luo, Y.; Yin, Q.; Wang, Q.; Hao, Z. How do mountain ecosystem services respond to changes in vegetation and climate? An evidence from the Qinling Mountains, China. *Ecol. Indic.* **2023**, *154*, 110922. [CrossRef]
55. Shaanxi Qinling Ecological Environment Protection Commission Office; Shaanxi Meteorological Bureau. Eco-Climate Bulletin of Qinling Mountains. 2022. Available online: http://qinling.shaanxi.gov.cn/article/7951.html (accessed on 31 August 2024).
56. Ma, X.; Bai, H.; Deng, C.; Wu, T. Sensitivity of Vegetation on Alpine and Subalpine Timberline in Qinling Mountains to Temperature Change. *Forests* **2019**, *10*, 1105. [CrossRef]
57. Wang, P.; Zhang, L.; Li, Y.; Jiao, L.; Wang, H.; Yan, J.; Lü, Y.; Fu, B. Spatio-temporal variations of the flood mitigation service of ecosystem under different climate scenarios in the Upper Reaches of Hanjiang River Basin, China. *J. Geogr. Sci.* **2018**, *28*, 1385–1398. [CrossRef]
58. Wischmeier, W.H.; Smith, D.D. *Predicting Rainfall-Erosion Losses from Cropland East of the Rocky Mountains, Guide for Selection of Practices for Soil and Water Conservation*; U.S. Department of Agriculture, Agriculture Research Service Agriculture Handbook NO. 282: Washington, DC, USA, 1965. Available online: https://onlinelibrary.wiley.com/action/showCitFormats?doi=10.1002/ldr.5258 (accessed on 31 August 2024).
59. Renard, K.G.; Foster, G.R.; Weesies, G.A.; McCool, D.K.; Yoder, D.C. *Predicting Soil Erosion by Water: A Guide to Conservation Planning with the Revised Universal Soil Loss Equation (RUSLE)*; U.S. Department of Agriculture, Agricultural Research Service Agriculture Handbook NO. 703: Washington, DC, USA, 1997.
60. Nieto, C.E.; Martínez-Graña, A.M.; Merchán, L. Soil Erosion Risk Analysis in the Ría de Arosa (Pontevedra, Spain) Using the RUSLE and GIS Techniques. *Forests* **2024**, *15*, 1481. [CrossRef]
61. David Raj, A.; Kumar, S.; Sooryamol, K.R.; Kalambukattu, J.G.; Kumara, S. Soil redistribution rates along the forested and cultivated steep hillslope in the mid-Himalayas using fallout—137Cs and RUSLE model. *Land Degrad. Dev.* **2024**, *1-19*, 1–19. [CrossRef]
62. Wang, L.; Zhao, T.; Zhu, W.; Zhu, L. The spatiotemporal characteristics of soil erosion in the Qinling-Daba Mountains based on RUSLE model. *J. Soil Water Conserv.* **2024**, *38*, 113–121. [CrossRef]
63. Li, T.; Liu, K.; Hu, S.; Bao, Y. Soil erosion and ecological benefits evaluation of Qinling Mountains based on the Invest model. *Resour. Environ. Yangtze Basin* **2014**, *23*, 1242–1250.
64. Pan, J.; Wei, S.; Li, Z. Spatiotemporal pattern of trade-offs and synergistic relationships among multiple ecosystem services in an arid inland river basin in NW China. *Ecol. Indic.* **2020**, *114*, 106345. [CrossRef]
65. Lufafa, A.; Tenywa, M.M.; Isabirye, M.; Majaliwa, M.J.G.; Woomer, P.L. Prediction of soil erosion in a Lake Victoria basin catchment using a GIS-based Universal Soil Loss model. *Agric. Syst.* **2003**, *76*, 883–894. [CrossRef]
66. Lanorte, A.; Nolè, G.; Cillis, G. Application of Getis-Ord Correlation Index (Gi) for Burned Area Detection Improvement in Mediterranean Ecosystems (Southern Italy and Sardinia) Using Sentinel-2 Data. *Remote Sens.* **2024**, *16*, 2943. [CrossRef]
67. Anselin, L. Local Indicators of Spatial Association—LISA. *Geogr. Anal.* **1995**, *27*, 93–115. [CrossRef]
68. Zhou, X.; Ji, G.; Wang, F.; Ji, X.; Hou, C. Analysis of the Environmental Benefits and Driving Forces of the Development of the "Production–Living–Ecological Space" Pattern Based on the ERI-ESV Geodetector. *Land* **2024**, *13*, 1059. [CrossRef]
69. Zhang, X.; Lu, C.; Ning, Y.; Wang, J. Spatiotemporal Coupling Effect of Regional Economic Development and De-Carbonisation of Energy Use in China: Empirical Analysis Based on Panel and Spatial Durbin Models. *Sustainability* **2022**, *14*, 10104. [CrossRef]
70. Zhang, L.; Hou, Q.; Duan, Y.; Liu, W. Spatial Correlation between Water Resources and Rural Settlements in the Yanhe Watershed Based on Bivariate Spatial Autocorrelation Methods. *Land* **2023**, *12*, 1719. [CrossRef]
71. You, C.; Qu, H.; Feng, C.-C.; Guo, L. Evaluating the match between natural ecosystem service supply and cultural ecosystem service demand: Perspectives on spatiotemporal heterogeneity. *Environ. Impact Assess. Rev.* **2024**, *108*, 107592. [CrossRef]
72. Lin, J.; Lin, Y.; Zhao, H.; He, H. Soil Erosion Processes and Geographical Differentiation in Shaanxi during 1980–2015. *Sustainability* **2022**, *14*, 10512. [CrossRef]
73. Wang, X.; Yang, Q.; Su, K.; Zhang, H.; Lu, D.; Xiang, H.; Zhou, L. Analysis on supply and demand balance of soil conservation service and its driving factors on the Loess Plateau. *Acta Ecol. Sin.* **2023**, *43*, 2722–2733.
74. Woo, D.K. Enhanced crop yields as a potential mitigator of soil organic carbon losses under elevated temperature in erosional and depositional landscape. *Sci. Total Environ.* **2024**, *951*, 175400. [CrossRef] [PubMed]
75. Li, Y.; He, Y.; Liu, W.; Jia, L.; Zhang, Y. Evaluation and Prediction of Water Yield Services in Shaanxi Province, China. *Forests* **2023**, *14*, 229. [CrossRef]
76. Wang, S.; Gao, M.; Li, Z.; Ma, J.; Peng, J. How Do Driving Factors Affect Vegetation Coverage Change in the Shaanxi Region of the Qinling Mountains? *Remote Sens.* **2023**, *16*, 160. [CrossRef]
77. Cheng, D.; Qi, G.; Song, J.; Zhang, Y.; Bai, H.; Gao, X. Quantitative Assessment of the Contributions of Climate Change and Human Activities to Vegetation Variation in the Qinling Mountains. *Front. Earth Sci.* **2021**, *9*, 782287. [CrossRef]
78. Liu, J.; Xie, T.; Lyu, D.; Cui, L.; Liu, Q. Analyzing the Spatiotemporal Dynamics and Driving Forces of Ecological Environment Quality in the Qinling Mountains, China. *Sustainability* **2024**, *16*, 3251. [CrossRef]
79. Chen, J.; Chen, Y.; Wang, K.; Zhang, H.; Tian, H.; Cao, J. Impacts of land use, rainfall, and temperature on soil conservation in the Loess Plateau of China. *Catena* **2024**, *239*, 107883. [CrossRef]
80. Cui, G.; Zhang, Y.; Chao, Y.; Zhao, Y.; Pan, B. Land use change and eco-environmental effects in Qinling Mountains in recent 40 years. *Res. Soil Water Conserv.* **2023**, *30*, 319–326. [CrossRef]

81. Chen, W.; Gu, T.; Xiang, J.; Luo, T.; Zeng, J.; Yuan, Y. Ecological restoration zoning of territorial space in China: An ecosystem health perspective. *J. Environ. Manag.* **2024**, *364*, 121371. [CrossRef]
82. Xiong, X.; Meng, M. Regionalization and optimization strategy of ecological management in Xinjiang, China based on supply-demand relationship and spatial flow of ecosystems. *Chin. J. Appl. Ecol.* **2023**, *34*, 2237–2248.

Disclaimer/Publisher's Note: The statements, opinions and data contained in all publications are solely those of the individual author(s) and contributor(s) and not of MDPI and/or the editor(s). MDPI and/or the editor(s) disclaim responsibility for any injury to people or property resulting from any ideas, methods, instructions or products referred to in the content.

land

MDPI

Article

Ecosystem Services' Response to Land Use Intensity: A Case Study of the Hilly and Gully Region in China's Loess Plateau

Zhongqian Zhang [1,2], Huanli Pan [3], Yaqun Liu [1,*] and Shuangqing Sheng [4,*]

[1] Key Laboratory of Regional Sustainable Development Modeling, Institute of Geographic Sciences and Natural Resources Research, Chinese Academy of Sciences, Beijing 100101, China; zzhang958-c@my.cityu.edu.hk
[2] Department of Architecture and Civil Engineering, City University of Hong Kong, Hong Kong 518057, China
[3] School of Civil Engineering and Architecture, Southwest University of Science and Technology, Mianyang 621010, China; hlpan039-a@mails.swust.edu.cn
[4] College of Land Science and Technology, China Agricultural University, Beijing 100193, China
* Correspondence: liuyaqun@igsnrr.ac.cn (Y.L.); shengsq@cau.edu.cn (S.S.)

Abstract: The hilly and gully region of the Loess Plateau represents one of China's most ecologically vulnerable landscapes, characterized by severe soil erosion, intensive land use, and pronounced disturbances to the structure and functionality of ecosystem services. Taking Zichang City as a case study, this research integrates grid-scale analysis with the InVEST-PLUS model and bivariate spatial autocorrelation techniques to examine the spatiotemporal dynamics and inter-relations of four critical ecosystem services—carbon storage, water yield, biodiversity, and soil retention—under varying land use intensity scenarios from 1990 to 2035. The findings indicate that (1) between 1990 and 2020, land use intensity in Zichang City steadily declined, exhibiting a spatial distribution pattern typified by central-area clustering and gradual peripheral transitions. (2) Across three development scenarios, the spatial distribution of the four ecosystem services aligned with the patterns observed in 2020, with central areas showing pronounced fluctuations, whereas peripheral regions experienced relatively minor changes. Specifically, from 1990 to 2020, the proportion of low-carbon storage areas increased by 2.89%, and high water yield areas expanded by 9.45%, while the shares of low habitat quality and low soil retention areas decreased by 5.59% and 6.25%, respectively. (3) A significant spatial autocorrelation was observed between land use intensity and the four ecosystem services, with widespread cold and hot spots reflecting dynamic spatial clustering patterns. These results offer valuable insights for optimizing land use strategies, improving ecosystem service performance, and advancing ecological conservation and sustainable development initiatives.

Keywords: land use intensity changes; ecosystem service functions; multi-scenario simulation; hilly and gully region of the Loess Plateau; Zichang City

1. Introduction

With the rapid progression of socioeconomic development, the tensions between humanity and the environment have escalated, resulting in significant degradation of the Earth's ecological systems and posing a profound threat to the sustainable development of both people and nature [1]. In light of these challenges, the United Nations has articulated the Sustainable Development Goals (SDGs), which offer a definitive framework for reconciling human-environment relationships and preserving the Earth's natural ecosystems. Notably, Goal 15 underscores the imperative to protect, restore, and promote the sustainable use of terrestrial ecosystems, implement sustainable forest management, adopt effective measures to combat desertification, halt and reverse land degradation, and mitigate biodiversity loss [2]. Realizing these objectives will not only safeguard and restore the health and stability of ecosystems but also sustain the critical services they provide, which are essential for human well-being. Furthermore, ensuring the availability of ecosystem services contributes to alleviating the conflicts between humanity and the

environment, thereby providing robust ecological support for economic development [3]. Consequently, grounded in the principle of coexistence between humanity and nature, it is crucial to harmonize human-environment relationships and enhance sustainable resource management practices to ensure the long-term utilization of resources and the stability of ecosystems, thereby establishing a durable environmental foundation for global sustainable development [4].

Land use changes are primarily driven by the interplay of varying land use demands and types, encompassing key dimensions such as land use categories, intensity, and their spatiotemporal dynamics [5]. Existing research on the relationship between land use changes and ecosystem services has largely concentrated on the effects of alterations in land use structure and quantity [6]. Nonetheless, land use transformation processes also entail shifts in structural composition, functional attributes, and efficiency [7]. A quantitative examination of these processes and their intensities is crucial for comprehensively evaluating their impacts on ecosystem services [8].

Land use intensity quantifies the concentration of human activities per unit area, while ecosystem services encompass the diverse functions and benefits provided by the natural environment, such as food production, water purification, and climate regulation [9]. The interplay between these two elements is vital for achieving environmental sustainability and promoting human well-being. Land use intensity is intricately linked to the sustainable management of natural resources and the overall health of ecosystems [10]. As land use intensity escalates, ecosystem services increasingly confront the risk of degradation, evidenced by challenges such as diminished biodiversity, declining soil quality, and water scarcity [11]. Conversely, moderate land use intensity can generate positive ecological outcomes [12]. For example, the adoption of sustainable agricultural practices can enhance soil organic matter content, thereby increasing crop yields and bolstering the overall functional services of ecosystems. Thus, a comprehensive examination of the dynamic relationship between land use intensity and ecosystem services not only contributes to a deeper understanding of ecosystem operational mechanisms but also provides a robust scientific foundation for effective land management and policy development [13].

The profound impacts of changes in land use intensity on the structure and functionality of ecosystem services have garnered increasing attention [14–16]. Such changes, however, are not solely reflected in historical and current trends but are also crucial under various future development scenarios. The PLUS model, renowned for its high precision and patch-scale analytical capabilities, has been extensively employed for future scenario simulations across multiple scales, including national, provincial, municipal, and watershed levels [17]. Despite these advancements, the interaction mechanisms and response dynamics between land use intensity and ecosystem services remain insufficiently elucidated. Existing research primarily emphasizes simple correlation or sensitivity analyses, with limited exploration of the spatial relationships between land use intensity and ecosystem services through quantitative methods. Spatial autocorrelation models provide a powerful tool for revealing these spatial interactions, enabling the quantification of distribution characteristics and interdependencies in spatial datasets while uncovering latent linkages or similarities among adjacent regions. These models thus offer critical insights for comprehensive assessments [18,19]. In this context, the present study integrates the PLUS-InVEST model with the bivariate Moran's index to systematically quantify the spatiotemporal response relationships between land use intensity and ecosystem service functions from historical, current, and future perspectives.

China has actively engaged with the Sustainable Development Goals by enacting a comprehensive array of policy measures focused on the conservation of land resources and advancing the principle that "lucid waters and lush mountains are invaluable assets" [20]. By protecting natural ecosystems and ensuring the sustainability of ecological resources, humanity can achieve enduring and stable well-being. These policies not only facilitate the restoration and maintenance of ecosystem functions but also lay a robust foundation for fostering harmonious coexistence between humanity and nature [21].

Zichang City, situated within the hilly and gully region of the Loess Plateau, exhibits an ecologically sensitive structure and function, rendering its ecosystems highly susceptible to anthropogenic influences. The region is confronted with severe soil erosion and substantial biodiversity threats [22]. As land use intensity escalates, the degradation of local ecosystem services is likely to intensify, necessitating a deeper understanding of the underlying response mechanisms to preserve ecological equilibrium and restore functional integrity. Moreover, located in an arid to semi-arid zone with complex topography and diverse soil types, the alteration of land use patterns exerts far-reaching effects on soil and water conservation, agricultural productivity, and biodiversity. Investigating the region's distinct characteristics offers valuable guidance for the optimization of land management practices.

With economic development and population growth, Zichang City is confronted with escalating resource pressures and environmental challenges, necessitating the formulation of sustainable land use policies through scientific research to achieve a balance between economic development and ecological conservation, enhance the quality of life for local residents, and promote regional sustainable development. Consequently, investigating the responsiveness of land use intensity in Zichang City to ecosystem services not only holds academic significance but also provides a foundation for addressing pressing ecological and economic issues. In light of this, the objectives of this study are as follows: (1) to analyze the temporal and spatial characteristics of land use intensity in Zichang City; (2) to quantify and map changes in ecosystem services; (3) to elucidate the spatial relationships between land use intensity and ecosystem services.

2. Overview of the Study Area and Data Sources

2.1. Overview of the Study Area

Zichang City (109°11′58″ E−110°01′22″ E, 36°59′30″ N−37°30′00″ N), a county-level city under the administration of Yan'an, Shaanxi Province, lies in the central Loess Plateau, to the north of the revolutionary site of Yan'an. It borders Hengshan District of Yulin City to the north, Zizhou and Qingjian counties to the east, Yanchuan County and Baota District to the south, and Ansai District of Yan'an and Jingbian County of Yulin City to the west, covering a total area of 2,405 square kilometers (Figure 1). The region is dominated by the hilly and gully terrain characteristic of the Loess Plateau, with ridges and valleys accounting for approximately 94.6% of its area. Elevations range from 916 to 1,557 m above sea level. Zichang City experiences a warm, temperate, semi-arid continental monsoon climate characterized by relatively low temperatures and significant seasonal temperature variations. The city has an average annual temperature of 9.1 °C, an average annual precipitation of 514.7 mm, and a frost-free period of 175 days. The Qingjian, Wuding, and Yan rivers form the major water systems in the area. By the end of 2023, Zichang had a permanent population of 215,000 and a gross regional product of CNY 15.74 billion [23].

Zichang City is endowed with rich natural resources, including substantial deposits of coal, oil, and natural gas. Over time, amidst population growth and rapid economic development, the region has undergone significant transformations in land use patterns and intensity, resulting in escalating pressure on the human-environment relationship and posing considerable challenges to the ecological environment. Since 1999, China has implemented ecological conservation initiatives, such as the Grain-to-Green Program, which have led to notable improvements in the region's ecological conditions. Therefore, within the context of substantial fluctuations in land use intensity, exploring the spatiotemporal dynamics of land use intensity and its responsive mechanisms with respect to ecosystem service functions is essential for advancing regional ecological sustainability.

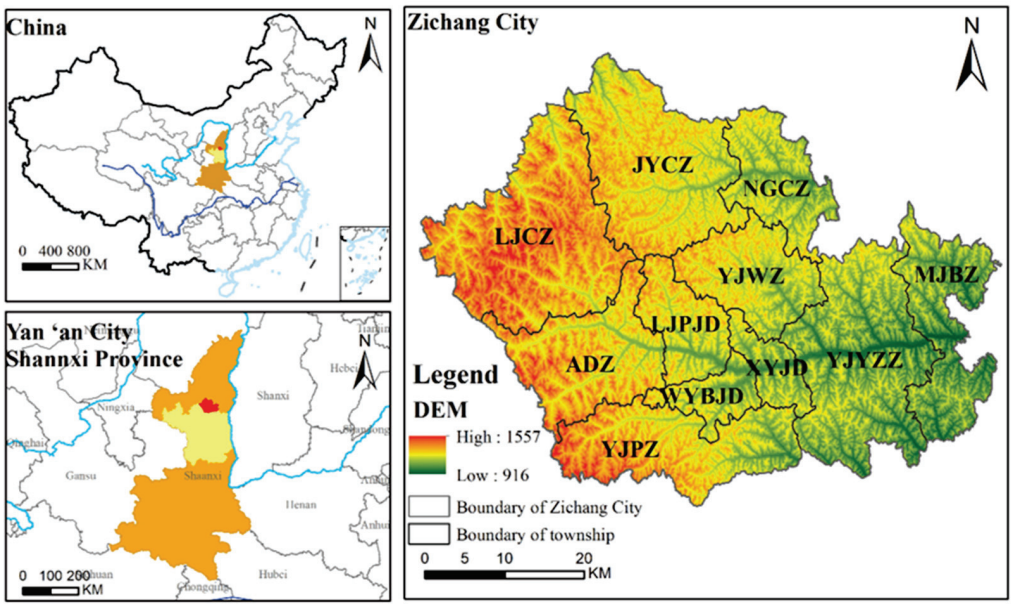

Figure 1. Location of Zichang City, Shaanxi Province, China. Note: LJCZ refers to Lijiacha Town, JYCZ to Jianyucha Town, NGCZ to Nangoucha Town, ADZ to Anding Town, LJP to Luanjiaping Town, YJW to Yujiawan Town, YJP to Yujiaoping Town, WYB to Wayao Fortress Town, XYJD to Xiuyan Subdistrict, YJYZZ to Yangjiayuanze Town, and MJBZ to Majiabian Town.

2.2. Data Sources

The data utilized in this study encompass land use and land cover data, topographic information, soil characteristics, and meteorological variables. The land use data were obtained from remote sensing imagery provided by the Resource and Environmental Science Data Center, Chinese Academy of Sciences (http://www.resdc.cn, accessed on 1 June 2024), with a spatial resolution of 30 m [24]. The digital elevation model (DEM) data were sourced from the ASTER Global Digital Elevation Model (ASTER GDEM), available through the Geospatial Data Cloud (http://www.gscloud.cn/#page1/1, accessed on 1 June 2024), also with a resolution of 30 m [25]. Soil data were acquired from the World Soil Database (http://westdc.westgis.ac.cn/data/611f7d50-b419-4d14-b4dd-4a944b141175, accessed on 1 June 2024), encompassing soil types such as sand, silt, and clay, along with organic carbon content, at a resolution of 1 km [26]. Additionally, the meteorological data, including precipitation and potential evapotranspiration, were provided by the Resource and Environmental Science Data Center, Chinese Academy of Sciences (http://www.resdc.cn, accessed on 1 June 2024) [24]. A comprehensive description of these data is presented in Table 1.

Table 1. Data category, type, source, and resolution.

Category	Data Type	Source	Resolution
Land use and cover	Remote sensing image	Resource Science Data Center, Chinese Academy of Sciences [24]	30 m
Terrain data	DEM	ASTER Global Digital Elevation Model (ASTER GDEM) [25]	30 m
Soil data	Soil attribute data	World Soil Database [26]	1 km
Meteorological data	Precipitation and potential evapotranspiration	Resource Science Data Center, Chinese Academy of Sciences [24]	—

3. Methods

3.1. Research Framework

This study harnesses remote sensing data and GIS technology to gather multidimensional datasets pertinent to land use, climate, and ecosystem services, thereby quantifying land use intensity (LUI) and evaluating carbon storage, water yield, habitat quality, and soil conservation capacity. By employing spatial statistical techniques and regression analysis, the research elucidates the intricate inter-relationships between LUI and ecosystem services. Furthermore, based on the available data, the study will develop various scenarios for 2035, encompassing natural, economic, and ecological protection frameworks, thus providing empirical support for regional sustainable management. The technical pathway for this research is delineated in Figure 2.

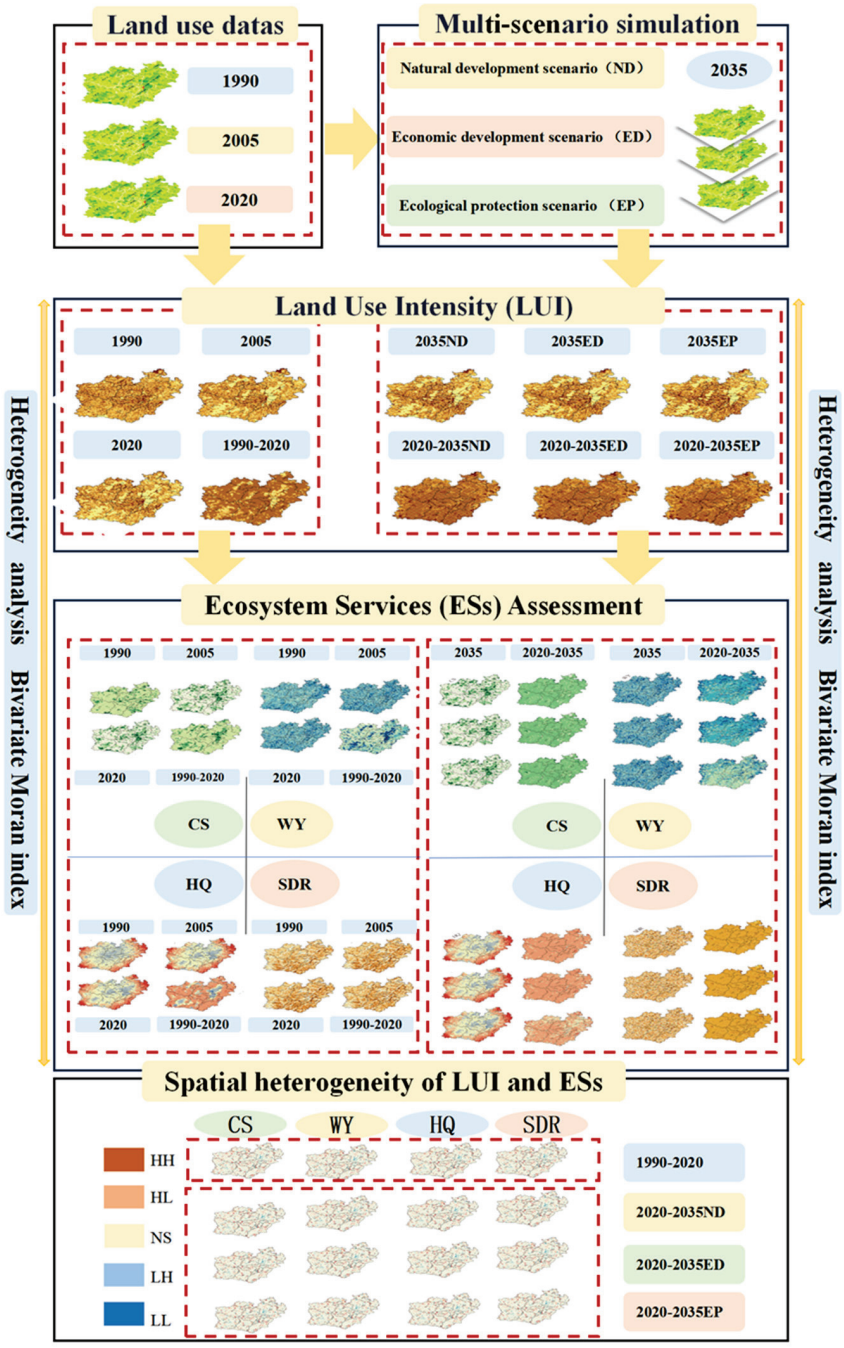

Figure 2. Technical route.

3.2. Grid Effect

A spatial quantification sampling approach was employed for Zichang City through a grid-based methodology to obtain land use data for each sampling unit [27]. Prior to the grid construction for data processing, the selection of a 300 m × 300 m grid was based on a comprehensive assessment of factors such as the resolution of land use data, regional extent, and ecological characteristics. First, the 300 m × 300 m grid efficiently balances spatial resolution with computational efficiency and storage requirements, mitigating the data volume expansion and computational burden associated with finer grids (e.g., 100 m × 100 m). Second, given the complex land use structure and prominent topographic features of Zichang City, this grid size effectively captures spatial variations in land use intensity while minimizing noise interference that could arise from excessively fine grids without sacrificing critical detail. Finally, this grid size has been widely applied in similar studies conducted in regions such as the Loess Plateau, adhering to established norms in the literature and facilitating result comparisons and validation. Thus, the 300 m × 300 m grid is deemed optimal for providing precise and efficient data support for land use and ecosystem service analyses.

3.3. Land Use Intensity

The land use intensity model employed in this study is designed to quantify the extent of human-induced disturbances to land use patterns [28]. Drawing from prior studies [29,30], land use intensity is categorized into four levels based on the distinctive characteristics of each land use type: other land use (corresponding to unused land), forest, grassland, water use (corresponding to forests, grasslands, and water bodies), agricultural land use (corresponding to arable land), and built-up land use (corresponding to urban areas, settlements, industrial zones, and transportation infrastructure). The intensity index for each category is assigned sequential values of 1, 2, 3, and 4. Given the potential coexistence of multiple land use types within a region, a composite land use intensity index is employed to reflect the overall intensity of land use activities. Based on this, the calculation expression for land use intensity is formulated as follows:

$$L_{LUI} = \sum_{i=1}^{n} A_i \times \frac{C_i}{C} \times 100\% \quad (1)$$

In Equation (1), L_{LUI} represents the comprehensive land use intensity index for Zichang City; A_i denotes the graded index of land use intensity for the i level within Zichang City; C_i stands for the area of land use at the i level within Zichang City; C is the total area of land use within Zichang City; and n signifies the number of grades for land use intensity.

3.4. Ecosystem Service Assessment

Ecosystem service assessment represents a pivotal approach to understanding the contributions of ecosystems to human well-being, encompassing both the direct and indirect benefits provided by natural systems [31]. Zichang City, situated on the Loess Plateau, is marked by its complex topography, diverse land use patterns, and fragile ecological conditions, particularly in terms of soil erosion, carbon storage, and biodiversity conservation, all of which hold substantial ecological value. In this study, drawing from prior research and considering the regional context, land use intensity, along with four critical ecosystem service functions—carbon storage, water yield, habitat quality, and soil retention—are selected as the primary indicators for quantifying ecosystem service functions and values. These indicators were chosen for their comprehensive ability to reflect the primary functions and services of the Zichang ecosystem and their close alignment with the region's distinctive environmental characteristics [32,33].

3.4.1. Carbon Fixation Service

The evaluation of carbon sequestration services was conducted using the carbon storage module within the InVEST model for quantification [34]. This model employs land use and land cover types as assessment units, facilitating the calculation of regional carbon stock by multiplying the carbon densities of aboveground biomass, belowground biomass, soil organic carbon, and dead organic matter for each land cover type by their respective areas.

$$C_{total} = C_{above} + C_{\text{below}} + C_{\text{dead}} + C_{\text{soil}} \quad (2)$$

In Equation (2), C_{total}, C_{above}, C_{below}, C_{dead}, and C_{soil}, respectively, represent total carbon (t), aboveground biomass (t), root biomass (t), carbon in dead organic matter (t), and soil organic carbon storage (t).

Acknowledging that dead organic matter carbon represents a relatively minor fraction of the carbon pool and presents challenges in data acquisition, this study has opted not to incorporate it into the analysis. By utilizing a modified carbon density formula, adjustments were made to the national carbon density data, thereby facilitating the estimation of carbon densities associated with various land use types within Zichang City.

$$C_{SP} = 3.3968 \times MAP + 3996.1 \left(R^2 = 0.11\right) \quad (3)$$

$$C_{BP} = 6.798 \times e^{0.0054 \times MAP} \left(R^2 = 0.70\right) \quad (4)$$

$$C_{BT} = 28 \times MAT + 398 \left(R^2 = 0.47, P < 0.1\right) \quad (5)$$

$$K_{BP} = \frac{C'_{BP}}{C''_{BP}} \quad (6)$$

$$K_{BT} = \frac{C'_{BT}}{C''_{BT}} \quad (7)$$

$$K_B = K_{BP} \times K_{BT} \quad (8)$$

$$K_s = \frac{C'_{SP}}{C''_{SP}} \quad (9)$$

In the equation, C_{SP} represents the soil carbon density (t·hm^{-2}) derived from annual precipitation; C_{BP} and C_{BT} represent the biomass carbon density (t·hm^{-2}) derived from annual precipitation and annual mean temperature, respectively; MAP stands for mean annual precipitation (mm); MAT stands for mean annual temperature (°C); K_{BP} and K_{BT} are the correction coefficients for precipitation and temperature factors in biomass carbon density; C' and C'' are the carbon density data for Zichang City and China, respectively; K_B and K_S are the correction coefficients for biomass carbon density and soil carbon density, respectively.

3.4.2. Water Production Service

The water yield module of the InVEST model is predicated on the principles of water balance and is grounded in the hypothesis of water-thermal coupling equilibrium, utilizing annual average precipitation data for quantification [35]. The water yield *Y(x)* is defined as the difference between rainfall and actual evapotranspiration within a grid cell, encompassing surface runoff, soil moisture, canopy interception, and the water retention capacity of litter. Accordingly, this study employs the water yield module of the InVEST model to calculate the water yield in Zichang City. The calculation formula is presented as follows:

$$Y(x) = \left(1 - \frac{AET(x)}{P(x)}\right) \times P(x) \quad (10)$$

$$\frac{AET(x)}{P(x)} = 1 - \frac{PET(x)}{P(x)} - \left[1 - \left(\frac{PET(x)}{P(x)}\right)^{\omega(x)}\right]^{1/\omega(x)} \tag{11}$$

$$PET(x) = K_c(l_x) \times ET_0(x) \tag{12}$$

$$\omega(x) = Z\frac{AWC(x)}{P(x)} + 1.25 \tag{13}$$

In the equation, $Y(x)$ represents the annual water yield (mm) for the grid cell x; $AET(x)$ represents the annual actual evapotranspiration (mm) for the grid cell x; $P(x)$ represents the annual precipitation (mm) for the grid cell x; $PET(x)$ represents the potential evapotranspiration (mm); $\omega(x)$ represents a non-physical parameter related to natural climate and soil properties; $ET_0(x)$ represents the crop (vegetation) evapotranspiration coefficient for a specific land use type in the grid cell x; $AWC(x)$ represents the available water capacity (mm) for plants; Z is an empirical constant that can be obtained based on calculations related to annual precipitation events.

3.4.3. Biodiversity Services

Habitat quality is closely tied to both regional structure and ecological functionality, with its level determined by the availability of resources necessary for the survival, reproduction, and growth of species within a given region. It is generally recognized that higher habitat quality is associated with greater biodiversity. In this study, the habitat quality module of the InVEST model was utilized to evaluate habitat quality, integrating land cover data with biodiversity threat factors to generate raster datasets [36]. The stressors were initially selected and assigned weights to represent the extent of their disturbance on different habitat types. The intensity of these stressors decreases with distance, necessitating the definition of a maximum effective range. Moreover, the response of various habitat types to these stressors differs significantly. The calculation formula is outlined as follows:

$$Q_{xj} = H_j\left(1 - \frac{D_{xj}^z}{D_{xj}^z + \mathrm{k}^2}\right) \tag{14}$$

$$D_{xj} = \sum_{r=1}^{R}\sum_{y=1}^{Y_r}\left(\omega_r / \sum_{r=1}^{R}\omega_r\right) r_y i_{rxy} \beta_x S_{jr} \tag{15}$$

$$i_{rxy} = 1 - \left(d_{xy}/d_{r\max}\right) \tag{16}$$

In the equation, Q_{xj} represents the habitat quality of grid x in habitat type j; D_{xj} represents the degree of disturbance to grid x in habitat type j; k is the half-saturation constant, typically set to Q_{xj}, which is half of the maximum value obtained after a trial run; H_j represents the habitat suitability for habitat type j; R represents the stressor factor; y represents the number of grids in the raster layer for stressor factor r; Y_r represents the total number of grids occupied by stressor factors; ω_r represents the weight of stressor factor r, with values ranging from [0, 1]; r_y represents the value of stressor factor r for grid y (0 or 1); i_{rxy} represents the degree of disturbance caused by stressor factor r of grid y to habitat grid x; β_x represents the accessibility level of grid x, with values ranging from [0, 1], where 1 indicates extreme ease of access; S_{jr} represents the sensitivity of habitat type j to stressor factor r; d_{xy} represents the straight-line distance between grid x and grid y; and $d_{r\max}$ represents the maximum impact distance of stressor factor r.

3.4.4. Soil Conservation Services

This study utilized the sediment delivery ratio module of the InVEST model to evaluate soil erosion and soil retention in Zichang City [37]. This module thoroughly incorporates the sediment interception capacity of the land surface and acknowledges the dual functions of vegetation in both mitigating soil erosion and trapping sediments. As a result, it yields an

estimate of the soil retention capacity (SD) within the study area. The calculation formula is presented as follows:

$$USLE = R \times K \times S \times L \times P \times C \quad (17)$$

$$RKLS = R \times K \times L \times S \quad (18)$$

$$SD = RKLS - USLE \quad (19)$$

In the equation, $USLE$ represents the actual soil erosion amount (t); $RKLS$ represents the potential soil erosion amount (t); R is the rainfall erosivity factor (MJ·mm·hm^{-2}·h^{-1}); K is the soil erodibility factor (t·hm·h·MJ^{-1}·hm^{-2}·mm^{-1}); L and S are slope length and slope steepness factors, respectively; P is the engineering measure factor; and C is the vegetation cover and management factor.

3.5. Ecosystem Service Volume Classification

This study employed the natural breaks classification method, which not only effectively reflects the distribution characteristics of the data but also avoids the smoothing effect associated with fixed breakpoints [38]. By analyzing four ecosystem services—carbon storage (CS), water yield (WY), habitat quality (HQ), and soil retention capacity (SDR)—in Zichang City for the years 1990, 2005, and 2020, as well as during the period from 1990 to 2020, we classified ecosystem service values into five density levels using ArcGIS 10.8. These levels—low, medium-low, medium, high-medium, and high—capture the spatial and temporal dynamics of ecosystem services at the township scale across Zichang City.

3.6. Multi-Scenario Simulation of Land Use

3.6.1. PLUS Model and Accuracy Verification

The PLUS model, developed from the cellular automata framework, is specifically designed to simulate changes across multiple land use types [39]. This model integrates a land expansion strategy analysis module with a cellular automata model that operates on multi-class random patch seeds. The land expansion strategy analysis module extracts expansion data for different land categories over two periods, while the cellular automata model, combined with random seed generation and a decreasing threshold mechanism, facilitates the simulation of spatial-temporal patch dynamics. Before conducting formal simulations, the land use map of Zichang City in 2015 was utilized as a benchmark to validate the accuracy of the PLUS model and to predict land use patterns for 2020. The predicted results were compared to the actual land use map of Zichang City in 2020. High similarity between the two maps indicates good model performance, while low similarity suggests otherwise. To assess the degree of similarity, the Kappa coefficient was applied to quantify the spatial distribution consistency between the images.

3.6.2. Multi-Scenario Settings

In light of the complexities inherent in addressing multifaceted policy and societal changes through a singular future development scenario, this study employs the PLUS model to delineate three distinct scenarios. By analyzing land use transitions in Zichang City from 2015 to 2020 and incorporating the relevant development plans and policies from both Yan'an City and Shaanxi Province, the PLUS model was utilized to refine the transition probabilities, intensities, and directions between various land use categories, thereby constructing three future development pathways for Zichang City.

(1) Natural development scenario: By serving as the reference scenario for the others, this scenario operates under the assumption of no interference from local policies or planning frameworks. It forecasts land use demands in 2035 based solely on the land use transition probabilities observed in Zichang City between 2015 and 2020, as projected by the PLUS model [40].
(2) Economic development scenario: This scenario posits a framework of unconstrained urban expansion. Derived from the land use transition matrix for 2010–2015, the

following adjustments were made: a 60% increase in the transition probability from farmland to construction land, a 50% increase from grassland to construction land, and a 30% increase from unused land to construction land, while other transition probabilities remained unchanged [41].

(3) Ecological protection scenario: In accordance with the directives outlined in the "Shaanxi Provincial Territorial Spatial Plan (2021–2035)" and the "Zichang City Territorial Spatial Plan (2021–2035)", this scenario places paramount importance on ecological redlines and protective frameworks. Water systems and natural reserves within the study area collectively delineate restricted zones. Specific adjustments to land use transitions include the following: a 50% reduction in the probability of grassland and forest land converting to construction land; a 30% increase in the probability of farmland transitioning to forest land, and a 60% increase of it transitioning to grassland; a 50% decrease in the probability of farmland transitioning to construction land; an 80% reduction in the likelihood of forest land shifting to farmland, an 80% reduction in the likelihood of it shifting to grassland, and a 90% reduction in the likelihood of it shifting to construction land; a 20% increase in the probability of grassland transitioning to farmland and an 80% decrease in its probability of transitioning to construction land; a 20% increase in the probability of unused land transitioning to both farmland and forest land, and a 50% increase in the probability of it transitioning to grassland, with other transition probabilities remaining largely unchanged [42].

3.7. Bivariate Moran Index

Spatial autocorrelation is a critical method used to examine whether the attribute values of a given factor are significantly correlated with the attribute values at neighboring spatial points. It typically involves tests of both global and local spatial autocorrelation [43]. By building on this, the study extends the analysis to bivariate global and local spatial autocorrelation to uncover the spatial distributional relationships between different factors, specifically land use intensity and ecosystem service quantities. The formula is provided as follows:

$$I = \frac{N\sum_{i}^{N}\sum_{j\neq 1}^{N} W_{ij} z_i^e z_j^u}{(N-1)\sum_{i}^{N}\sum_{j\neq 1}^{N} W_{ij}} \tag{20}$$

$$I'_{eu} = z^e \sum_{j=1}^{N} W_{ij} z_{ij}^u \tag{21}$$

In the equation, I_{eu} and I'_{eu} represent the bivariate global Moran's I and local Moran's I indices, respectively; z_i^e is the land use intensity of the i unit; z_j^u is the ecosystem service energy in the neighboring area of j; W_{ij} is the spatial weight matrix; and N is the number of grid cells for the evaluation in the city of Zichang. The Moran's I index ranges from $[-1, 1]$. A positive index indicates a positive correlation between regions; a negative index indicates a negative correlation between regions; and an index of 0 indicates no spatial correlation.

4. Results

4.1. Spatial and Temporal Distribution of Land Use Intensity

Between 1990 and 2020, the land use intensity in Zichang City exhibited a continuous decreasing trend, characterized by a distribution pattern that is concentrated in the central areas while exhibiting a gentler slope towards the peripheries. Overall, the land use intensity predominantly reflects low intensity (average proportion: 22.83%), moderate intensity (average proportion: 29.78%), and high intensity (average proportion: 25.37%) (Figure 3). Specifically, in 1990, the area designated as low intensity was relatively small (proportion: 4.69%) and displayed a dispersed distribution, primarily manifested as patchy clusters in the western and southeastern regions. In contrast, the area classified as high intensity was more concentrated (proportion: 10.39%), primarily located in the northern part of MJBZ, as well as in the WYBJD and LJPJD regions. By 2005, the low-intensity area had gradually expanded (proportion: 16.85%) and become more centralized, with

predominant distribution in the central region of LJCZ, southern XYJD, and western YJYZZ. Meanwhile, the moderate-intensity (proportion: 24.22%) and high-intensity (proportion: 7.10%) areas exhibited an interleaved distribution, primarily concentrated in LJPJD, WYBJD, YJPZ, and the northern part of MJBZ. By 2020, the low-intensity area further extended (proportion: 20.17%), forming a continuous region; conversely, the moderate- (proportion: 27.22%), high- (proportion: 23.07%), and very high-intensity (proportion: 6.83%) areas gradually diminished, particularly the high- and very high-intensity areas, which were notably concentrated in the LJPJD and WYBJD regions.

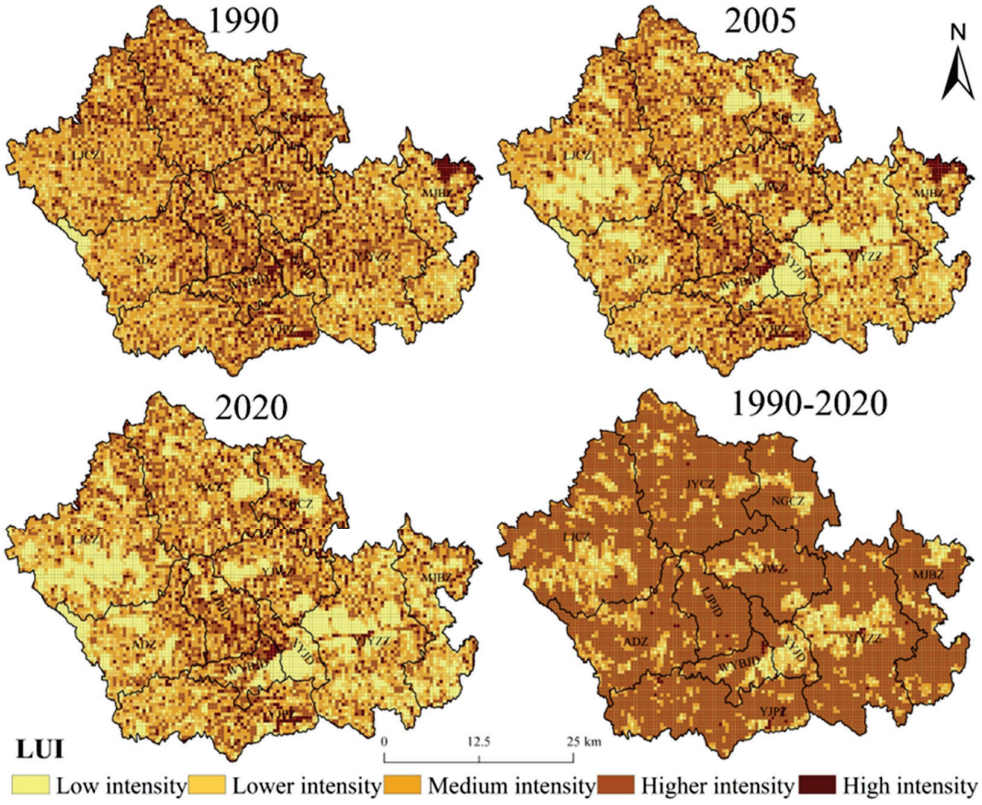

Figure 3. Spatial distribution of land use intensity in Zichang City from 1990 to 2020.

Between 1990 and 2020, the overall changes in land use intensity revealed distinct spatial characteristics, predominantly characterized by the expansion of low-intensity areas and a corresponding decline in other intensity categories (low, moderate, and high) (Figure 3). Notably, low-intensity areas have continued to expand (proportion: 15.48%) and are relatively concentrated, primarily located in regions such as LJCZ, XYJD, YJYZZ, YJWZ, MJBZ, NGCZ, and JYCZ. The variation within the low-intensity category is minimal (proportion: −0.46%), primarily interacting with adjacent low-intensity regions. Conversely, moderate-intensity (proportion: −5.67%) and high-intensity (proportion: −5.77%) areas have experienced substantial reductions, with significant concentrations observed in the central regions of WYBJD, XYJD, and YJYZZ within the study area. The decrease in high-intensity areas is relatively modest (proportion: −3.57%) and is predominantly situated in the WYBJD and YJPZ regions. Furthermore, land use intensity in other towns has exhibited relative stability.

4.2. Temporal and Spatial Changes of Ecosystem Services

Between 1990 and 2020, the four categories of ecosystem services in Zichang City—carbon storage, water yield, habitat quality, and soil retention—exhibited significant spatial differentiation characteristics (Figure 4). Specifically, carbon storage displayed a pronounced patchy distribution, predominantly characterized by low carbon storage areas (average proportion: 61.69%), while high carbon storage regions constituted a relatively

small proportion (average proportion: 5.75%). Water yield was primarily concentrated in the southeastern region, with moderate water yield areas prevailing (average proportion: 30.35%), whereas low water yield areas represented the smallest fraction (average proportion: 2.67%). The spatial distribution of habitat quality was marked by lower values in the central region and higher values in the peripheral areas, where moderate habitat quality dominated (average proportion: 44.83%), and low habitat quality was exceedingly rare (average proportion: 0.08%). Soil retention services exhibited a distribution pattern of higher values in the southwest and lower values in the northeast, predominantly characterized by low soil retention (average proportion: 35.39%), with high soil retention areas comprising the smallest proportion (average proportion: 3.13%).

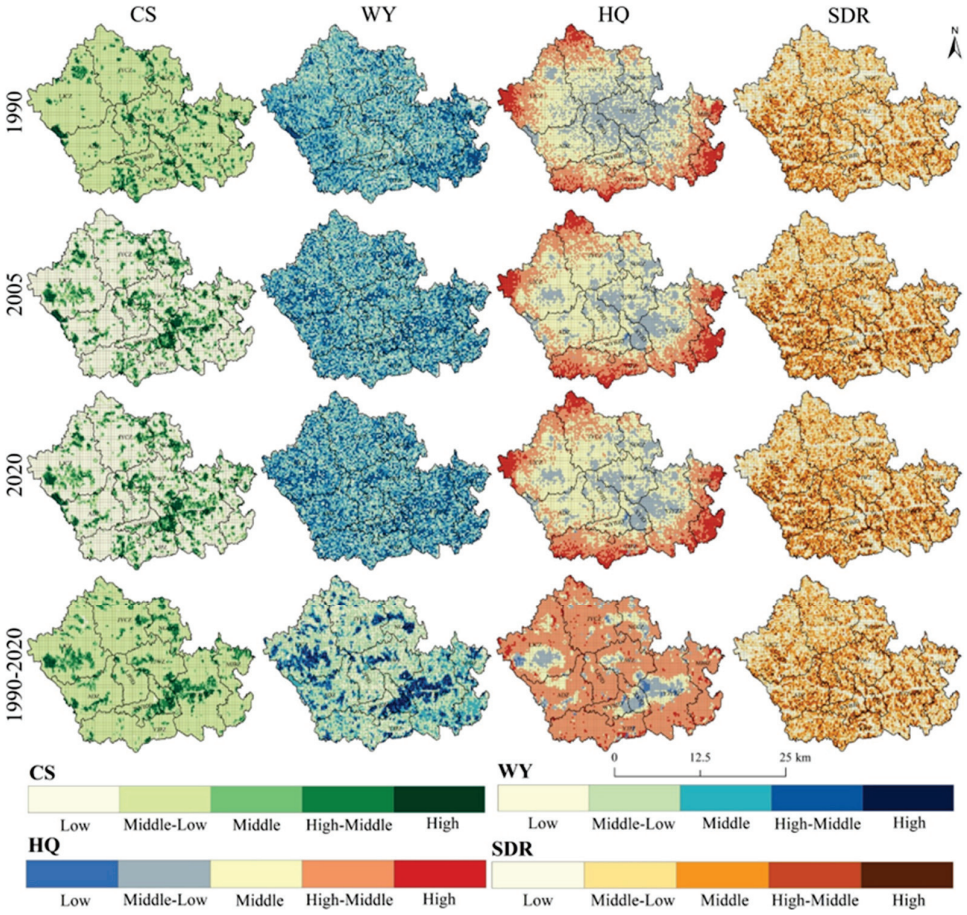

Figure 4. Spatial distribution and changes of ecosystem services in Zichang City from 1990 to 2020.

Between 1990 and 2020, the trend in carbon storage exhibited an increase in low carbon storage, while other categories of carbon storage witnessed a decline (Figure 4). Medium carbon storage (average proportion: 11.50%), higher carbon storage (average proportion: 9.06%), and high carbon storage (average proportion: 5.75%) were predominantly concentrated in the convergence zones of XYJD, YJYZZ, and YJWZ, characterized by relatively large areas. Additional high carbon storage regions were dispersed across the western part of LJCZ, the central area of NGCZ, and the central region of YJPZ. Regarding water production, medium water yield (average proportion: 30.35%), higher water yield (average proportion: 24.93%), and lower water yield (average proportion: 23.49%) emerged as the primary distribution types, with high water yield (average proportion: 18.56%) predominantly concentrated in the convergence areas of XYJD, YJYZZ, and YJWZ, as well as in MJBZ and LJCZ, while low water yield exhibited a patchy distribution. Habitat quality was primarily characterized by medium habitat quality (average proportion: 44.83%), followed by higher habitat quality (average proportion: 26.60%) and lower habitat quality (average

proportion: 18.60%), with low habitat quality (average proportion: 0.08%) being the least prevalent, primarily concentrated in WYBJD and also distributed across XYJD, YJYZZ, YJWZ, NGCZ, and LJCZ. Soil conservation services were predominantly represented by low soil conservation (average proportion: 35.39%), followed by medium soil conservation (average proportion: 26.20%) and low soil conservation (average proportion: 22.45%), while high soil conservation (average proportion: 3.13%) was the least represented, mainly concentrated in the regions of LJCZ, ADZ, and YJPZ, with low soil conservation predominantly distributed in the northern part of LJCZ, JYCZ, NGCZ, and MJBZ.

Between 1990 and 2020, the dynamics of ecosystem services demonstrated a distinct spatial pattern characterized by pronounced fluctuations in the central regions, contrasted by more gradual changes in the peripheral areas (Figure 4). Specifically, low carbon storage exhibited a significant increase, with a proportional rise of 2.89%, predominantly concentrated in the northern sector of LJCZ, the central area of JYCZ, and the southern portions of MJBZ and YJPZ. Conversely, carbon storage in other categories experienced a decline, particularly evident in the convergence zones of XYJD, YJYZZ, and YJWZ. In terms of water production, high water yield registered a notable increase, marked by a proportional rise of 9.45%, primarily situated at the boundary between LJCZ and JYCZ. In contrast, yields in other categories diminished in the convergence zones of XYJD and YJYZZ, as well as in the central region of LJCZ. Regarding habitat quality, lower habitat quality underwent a significant reduction of 5.59%, primarily concentrated at the intersections of XYJD and YJYZZ, along with the central area of LJCZ. Notably, habitat quality in adjacent regions exhibited signs of improvement. For soil conservation, the proportions of both low and moderate soil conservation declined by 4.39% and 1.86%, respectively, with these reductions primarily observed in the northern section of LJCZ, the central region of NGCZ, and MJBZ. In contrast, increases in other categories of soil conservation were noted in the ADZ and YJPZ regions.

4.3. Spatial and Temporal Distribution of Land Use Intensity in Multiple Scenarios

The simulated land use results for Zichang City in 2020 were compared with actual land use conditions, yielding a Kappa coefficient approaching 0.90. This indicates a high level of simulation accuracy, which is sufficient to support the modeling and forecasting of land use changes under multiple scenarios in Zichang City. Furthermore, the model can also be employed to calculate land use intensity and ecosystem service quantities in Zichang City under various future scenarios.

By 2035, land use intensity in Zichang City is projected to exhibit similar spatial consistency across three scenarios, characterized by a central area of moderate intensity and more gradual distributions towards the periphery (Figure 5). In the natural development, ecological conservation, and economic development scenarios, land use intensity is predominantly classified as moderate intensity (average proportion: 26.68%), higher intensity (average proportion: 22.98%), lower intensity (average proportion: 22.88%), and low intensity (average proportion: 17.98%), with high-intensity areas comprising a relatively small proportion (average proportion: 9.10%).

Compared to 2020, under the natural development scenario, low-intensity and high-intensity areas decreased by 2.64% and 0.10%, respectively, while moderate-intensity, lower-intensity, and higher-intensity areas increased by 0.36%, 0.18%, and 1.81%, respectively (Figure 5). Notably, the increase in moderate intensity predominantly occurred in the eastern and northern fringes of the study area, whereas high-intensity areas were concentrated in the western, southern, and northeastern edges. In the ecological protection scenario, high-intensity areas experienced a substantial increase (3.07%), whereas all other intensity categories witnessed a decline. High-intensity land use was primarily distributed along the eastern and western peripheries, with moderate intensity showing a decrease in the central region (−1.68%). Conversely, in the economic development scenario, both low-intensity and moderate-intensity areas exhibited reductions, with the most significant decline occurring in low-intensity areas (−2.78%). In contrast, lower-intensity, higher-

intensity, and high-intensity areas all expanded, with high-intensity areas experiencing a notable increase (1.94%), particularly concentrated in the western and eastern fringes of the study area, while changes in the central region remained relatively minor.

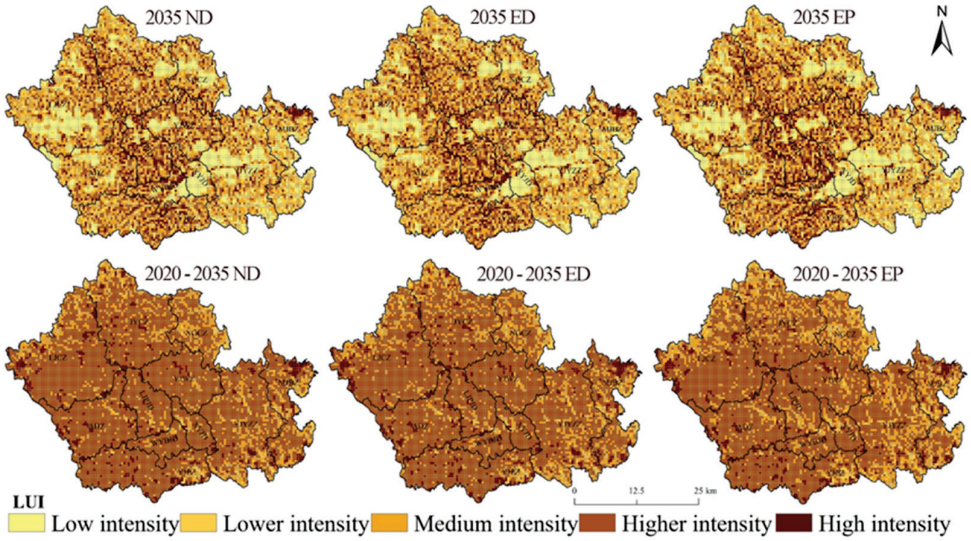

Figure 5. Spatial distribution of land use intensity in Zichang City under different scenarios.

4.4. Spatial and Temporal Distribution of Multi-Scenario Ecosystem Services

By 2035, the spatial distribution characteristics of the four ecosystem service functions across the three development scenarios will largely remain consistent with those observed in 2020 (Figure 6). Carbon storage will exhibit a pattern characterized by high-value clustering and low-value dispersion, with elevated areas primarily concentrated at the intersections of WYBJD, XYJD, YJYZZ, and YJWZ. Water production will demonstrate a trend of higher values in the southeast and lower values in the northwest, with the primary high-value zones located in WYBJD, XYJD, YJYZZ, and MJBZ, resulting in an overall banded distribution. Habitat quality will reflect a pattern of lower values in the center and higher values surrounding it, with the low-value areas gradually expanding outward, encroaching upon adjacent moderate- and low-value regions. Soil conservation will display a distribution characterized by higher values in the southwest and lower values in the northeast, with high-value areas predominantly concentrated at the convergence of XYJD and WYBJD.

During the period from 2020 to 2035, the overall trends in carbon storage across the three development scenarios indicated a reduction in low-value areas, accompanied by increases in other categories (Figure 6). In the 2020-ND scenario, low-value carbon storage decreased by −2.10%, primarily concentrated in the northern region of MJBZ and the eastern and central areas of YJPZ. Conversely, moderate carbon storage saw an increase of 0.85%, exhibiting a general rise across various townships. High-value carbon storage also increased by 0.43%, predominantly found in the eastern parts of NGCZ, MJBZ, and the northeastern region of LJCZ. The spatial distribution characteristics for the 2020-EP and 2020-CB scenarios were largely consistent with those of the 2020-ND scenario, reflecting patchy changes in the aggregation of different categories. Specifically, in the 2020-EP scenario, low-value carbon storage decreased by −2.89%, while moderate- and high-value categories increased by 1.03% and 0.60%, respectively. In contrast, the 2020-CB scenario recorded a reduction in low-value carbon storage of −2.15%, alongside increases of 0.92% in moderate- and 0.43% in high-value categories.

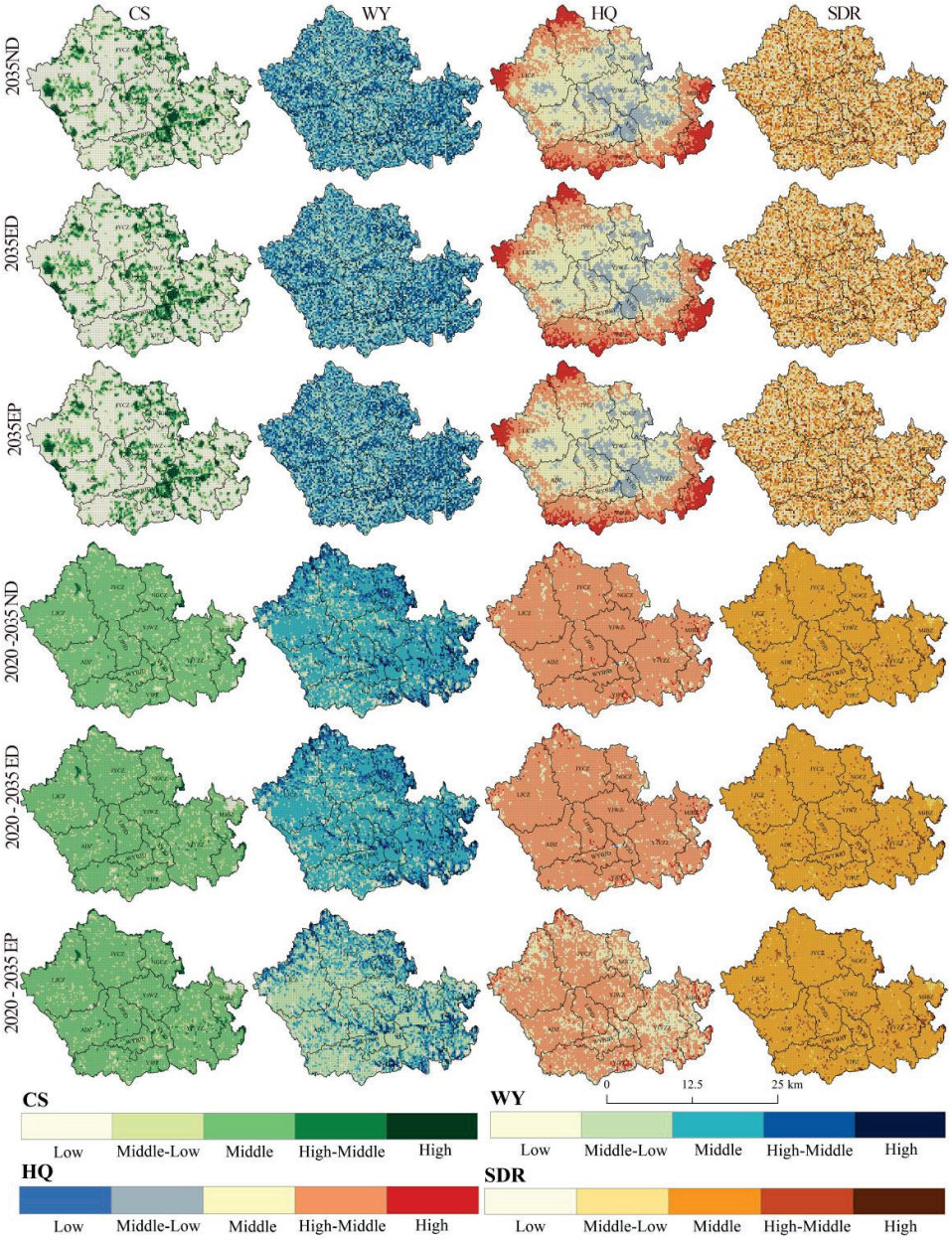

Figure 6. Spatial distribution and changes of ecosystem services in Zichang City (2020–2035) under different scenarios.

Between 2020 and 2035, the water yield across the three development scenarios demonstrated a notable trend characterized by a decline in both low- and moderate-value categories, juxtaposed with a significant increase in high-value categories (Figure 6). In the 2020-ND scenario, low-value water yield (proportion: −0.57%) and moderate-low-value water yield (proportion: −1.96%) exhibited a predominantly patchy distribution, concentrating primarily in the northern region of MJBZ and other township areas. In stark contrast, high-value water yield (proportion: 3.12%) registered a significant increase, predominantly located in the southern part of YJYZZ, as well as in the eastern regions of MJBZ, NGCZ, JYCZ, and the northern section of LJCZ. The spatial distribution characteristics of the 2020-CB scenario mirrored those observed in the 2020-ND scenario. In the 2020-EP scenario, low-value (proportion: −1.13%) and moderate-low-value (proportion: −4.34%) water yields experienced reductions in the regions of LJCZ, JYCZ, YJWZ, ADZ, and YJPZ. Conversely, both high-value (proportion: 2.05%) and very high-value (proportion: 5.16%)

water yields exhibited significant increases along the margins of YJYZZ, MJBZ, NGCZ, JYCZ, and LJCZ.

During the period from 2020 to 2035, habitat quality across the three development scenarios exhibited a trend characterized by decreases in low and moderate categories, accompanied by increases in higher categories (Figure 6). In the 2020-ND scenario, low habitat quality (proportion: −1.68%) predominantly decreased in a patchy distribution across the eastern parts of XYJD and YJYZZ, as well as in the eastern region of NGCZ. Moderate habitat quality (proportion: −0.23%) also diminished in the areas of YJYZZ, MJBZ, XYJD, and LJCZ, while high habitat quality (proportion: 0.54%) experienced sporadic increases in the regions of JYCZ, MJBZ, and YJPZ. The spatial distribution characteristics of the 2020-CB scenario were largely consistent with those observed in the 2020-ND scenario. In the 2020-EP scenario, low habitat quality (proportion: −1.85%) and moderate habitat quality (proportion: −0.73%) exhibited reductions in a contiguous manner across LJCZ, JYCZ, NGCZ, MJBZ, YJYZZ, and XYJD. Conversely, higher habitat quality (proportion: 1.61%) and very high habitat quality (proportion: 0.90%) significantly increased in the southern regions of YJPZ, the eastern parts of MJBZ, and the northern area of JYCZ.

During the period from 2020 to 2035, the trends in soil conservation across the three development scenarios exhibited a pattern characterized by a reduction in both high and very high categories, while other categories showed an increase (Figure 6). In the 2020-ND scenario, the proportions of high and very high categories both decreased by 0.05%, primarily distributed in LJCZ, WYBJD, XYJD, YJPZ, and YJYZZ, displaying a patchy and sporadic decline. The moderate category remained unchanged (proportion: 0.00%), while other categories experienced slight increases, with more dispersed distributions. The spatial distribution characteristics of the 2020-EP and 2020-CB scenarios closely mirrored those of the 2020-ND scenario, predominantly characterized by patchy changes in aggregated areas across all categories, with minimal variation in the moderate category. In the 2020-EP scenario, the reduction in the higher category was recorded at −0.09%.

4.5. Spatial Heterogeneity of Ecosystem Services in Relation to Land Use Intensity

During the period from 1990 to 2020, the spatial clustering distribution of land use intensity and four ecosystem service functions exhibited significant spatial heterogeneity. Under three future development scenarios, the spatial clustering distribution of land use intensity and these four ecosystem service functions closely aligned with the patterns observed from 1990 to 2020.

Specifically, the relationship between land use intensity and carbon storage during the 1990–2020 period demonstrated a non-significant distribution characteristic (proportion: 89.86%). Negative impacts were predominantly concentrated in the western and southeastern regions, while positive influences were observed in the central and southern areas (Figure 7). Notably, high-high (HH) (proportion: 3.70%) and high-low (HL) (proportion: 3.87%) clusters were primarily located in the YJPZ and JYCZ regions, with sparse distribution in MJBZ. Low-high (LH) (proportion: 1.39%) exhibited sporadic aggregation in areas such as LJCZ, JYCZ, and NGCZ, while low-low (LL) (proportion: 1.17%) was concentrated in the central part of LJCZ and the southwestern area of YJYZZ. By the 2020–2035 period, the spatial clustering characteristics under the three scenarios remained largely consistent, displaying a reduction in HH and HL regions, while LH and LL regions increased. In the 2020-EP scenario, the positive impacts in the southeastern area were particularly pronounced, whereas the 2020-CB scenario showed enhanced positive influences in the central and western regions.

During the period from 1990 to 2020, the relationship between land use intensity and water yield was characterized by a predominantly non-significant distribution (proportion: 90.10%), with negative impacts concentrated in the southeastern and western regions, while positive influences were more dispersed (Figure 7). Specifically, high-high (HH) (proportion: 3.91%) and high-low (HL) (proportion: 3.87%) clusters were primarily identified in the LJPZ, WYBJD, and XYJD areas, whereas low-low (LL) (proportion: 1.01%) was predominantly

concentrated in the central regions of YJWZ and WYBJD. By the period of 2020 to 2035, all three development scenarios revealed a reduction in the aggregation of HH and HL, alongside an increase in the clustering of low-high (LH) and LL categories. In the 2020-ND and 2020-CB scenarios, the HH clusters were mainly distributed in the southern areas of LJCZ, southern JYCZ, and the eastern region of ADZ, while HL and LH exhibited a scattered distribution. Notably, in the 2020-EP scenario, the decrease in HH was particularly pronounced (proportion: 0.92%), with weaker positive impacts observed in the central region and significant negative influences in the northern areas.

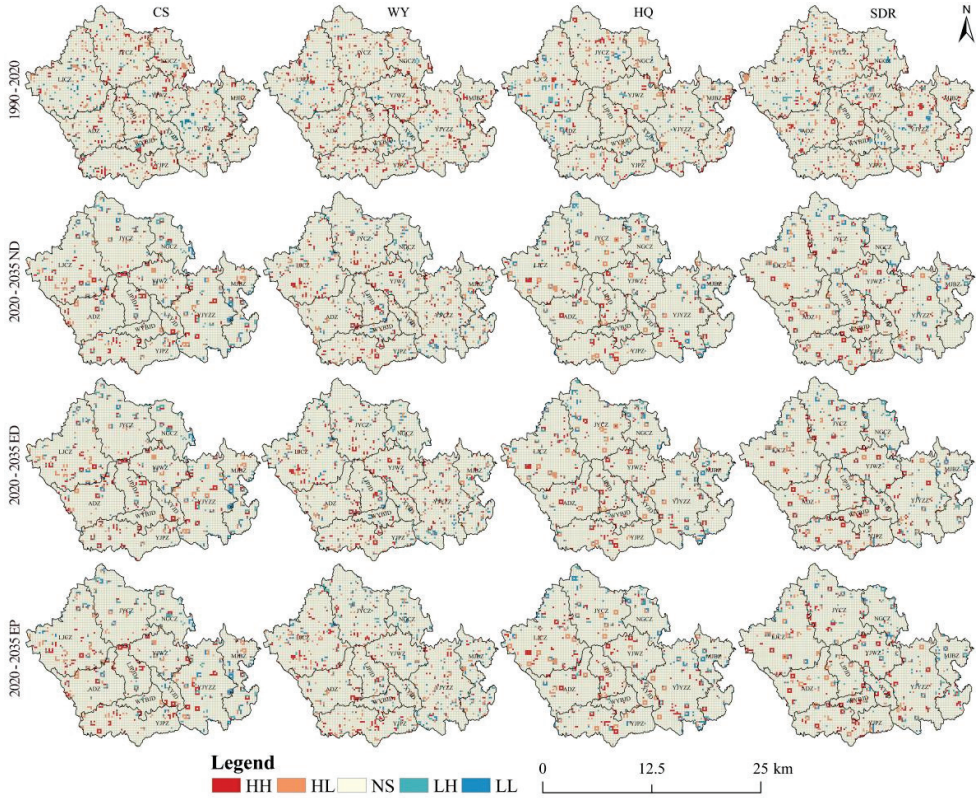

Figure 7. Local spatial autocorrelation distribution of land use intensity (LUI) and ecosystem services in Zichang City from 1990 to 2035.

During the period from 1990 to 2020, the relationship between land use intensity (LUI) and habitat quality primarily exhibited an insignificant distribution pattern (proportion: 90.42%) (Figure 7). In this timeframe, negative impacts were concentrated in the western and southeastern regions, whereas positive effects were relatively sporadic. Specifically, the HH type (proportion: 3.13%) was predominantly located in the eastern part of LJCZ, the northern section of JYCZ, and the northeastern area of YJWZ. The LH type (proportion: 1.55%) and LL type (proportion: 1.20%) were dispersed across other townships, with the smallest area of LH observed in the XYJD region and a similarly limited extent of LL in the NGCZ and LJPJZ areas. In the scenarios projected for 2020–2035, both HH and HL clustering areas exhibited a decrease, while the clustering areas of LH and LL showed an increase, particularly highlighting a more concentrated aggregation of the HH type. This shift is characterized by a reduction in the northern and eastern parts of the study area and an increase in the southern regions. The spatial clustering distribution characteristics across the three scenarios were fundamentally consistent. Notably, in the 2020-EP scenario, the clustering of the HH type demonstrated a significant enhancement (proportion: 3.10%), with marked positive impacts in the central and southern regions. Conversely, in the 2020-ND scenario, the clustering of the LL type (proportion: 1.56%) was more pronounced, accompanied by relatively strong negative impacts in the northern area.

During the period from 1990 to 2020, the relationship between land use intensity (LUI) and soil conservation exhibited a predominantly insignificant distribution (proportion: 89.97%) (Figure 7). Negative impacts were primarily concentrated in the central and southeastern regions, while positive effects were dispersed sporadically. Specifically, high-high (HH) types (proportion: 3.90%) were mainly found in the ADZ, YJYZZ, LJCZ, and JYCZ regions. Low-high (LH) types (proportion: 3.79%) and low-low (LL) types (proportion: 1.10%) also displayed a scattered distribution, whereas high-low (HL) types were characterized by patchy clustering in the western part of LJCZ. LL types (proportion: 1.23%) were primarily concentrated in YJYZZ, with less pronounced distributions in other townships. In the three development scenarios for 2020–2035, both HL and LH clustering areas significantly decreased, while HH types exhibited a gradual aggregation from north to south, maintaining similar spatial clustering characteristics across all three scenarios. Notably, in the 2020-EP scenario, the clustering distribution of HH types in JYCZ was significantly higher than that in the 2020-ND scenario, whereas their performance in NGCZ was relatively weaker.

5. Discussion

5.1. Mechanisms by Which Changes in Land Use Intensity Influence Ecosystem Services

Changes in land use intensity during the process of land use transformation are often accompanied by increased ecological pressures, which, in turn, significantly influence ecosystem service functions [44]. This study, integrating the PLUS-InVEST model and utilizing the bivariate Moran's I index, explores the response dynamics between land use intensity and four ecosystem service functions across three developmental scenarios from 1990 to 2035.

The results indicate that the implementation of the Grain-to-Green Program in Zichang City since 1999 has resulted in extensive cropland conversion to forestland and grassland, exerting a direct influence on ecosystem structure and functionality [45]. However, the fragile ecological environment and severe soil erosion in Zichang City have contributed to ecosystem instability [46]. Despite these challenges, the significant reduction in cropland has led to a sustained decline in land use intensity, particularly in central areas, with more fragmented changes in peripheral regions. Dynamic fluctuations in high-intensity land use have adversely affected ecosystem services, including water yield, soil retention, and biodiversity. This finding aligns with patterns of intensified soil erosion and ecosystem degradation due to overexploitation in the Loess Plateau [47].

Under the three future development scenarios, overall land use changes from 2020 to 2035 remain limited, reflecting the dominance of cropland, forestland, and grassland in the study area. Variations are primarily localized at the intersections of WYBJD, XYJD, YJYZZ, LJPJD, and YJWZ, with minor fluctuations observed. Small-scale transitions among cropland, forestland, and grassland, combined with climatic, topographical, and soil constraints characteristic of semi-arid regions, have contributed to the slow pace of ecosystem restoration. As a result, anticipated improvements in ecosystem services are expected to be modest, a conclusion consistent with the region's historical data.

Land use intensity modifies a range of ecological processes, including the structure and composition of ecosystems, thereby influencing ecosystem service functions. As socioeconomic development progresses, the interplay between natural resources and human well-being becomes increasingly complex [48]. Rising land use intensity exacerbates trade-offs among ecosystem services, and exceeding critical intensity thresholds results in a decline in service capacity [49]. The spatial autocorrelation analysis reveals significant spatial dependencies between land use intensity and ecosystem services, with hot spots and cold spots widely distributed and exhibiting dynamic clustering patterns. In the hilly regions of the Loess Plateau, the dual pressures of climate change and land use transformation demonstrate that unsustainable agricultural practices not only amplify land use intensity but also diminish ecosystem service capacity. These observations align with the declining land use intensity trend associated with cropland reduction [50]. The implemen-

tation of large-scale ecological programs has contributed to a decrease in land use intensity. Under future development scenarios, high-value ecosystem service areas are projected to expand, particularly at the intersections of WYBJD, XYJD, YJYZZ, and YJWZ, mitigating the negative impacts of land use intensity on ecosystem services and progressively enhancing ecological conditions. These findings corroborate studies emphasizing the role of adjusted agricultural land use intensity in improving water yield functions [51].

In conclusion, the remarkable restoration of ecosystem services following the implementation of the Grain-to-Green Program in Zichang City highlights the critical importance of regional governance policies in ecosystem management. Current land use management strategies primarily focus on changes in land use types, with insufficient attention given to the role of land use intensity in ecosystem restoration and regulation. This study underscores the dynamic impacts of land use intensity on multiple ecosystem service functions before and after the implementation of ecological programs and evaluates these dynamics under future policy scenarios. Future research should prioritize localized analyses of land use intensity changes, particularly their critical role in ecological restoration processes.

5.2. Policy Implications

The hilly and ravine region of the Loess Plateau represents one of China's most ecologically vulnerable areas, profoundly affected by soil erosion and experiencing long-term impacts on its ecosystem service functions due to land use intensity [52]. Zichang City, as a quintessential representative of this region, has witnessed a gradual degradation of ecosystem services concomitant with increasing land development and utilization intensity. Historically, the expansion of urban areas and high-intensity land use activities, such as mining, have significantly exacerbated soil erosion, resulting in a pronounced decline in ecosystem services associated with water conservation, soil retention, and biodiversity. Under the pressures of slope farmland development and overgrazing, soil erosion has intensified, leading to severe land degradation and a continual deterioration of the ecological environment within the region.

Since 1999, the implementation of ecological restoration policies—including the conversion of farmland to forest and grassland, as well as the protection of forested mountains—has facilitated substantial improvements in Zichang City's ecological environment. Nevertheless, in recent years, the Chinese government has introduced the "Three Red Lines" for territorial spatial planning: ecological protection red lines, permanent basic farmland red lines, and urban development boundaries. These demarcations serve as non-negotiable limits for adjusting economic structures, planning industrial development, and promoting urbanization, aiming to enforce stringent environmental protection, farmland preservation, and land conservation measures, thereby establishing a robust foundation for sustainable development. This paradigm shift reflects a gradual transition away from a reliance solely on measures such as the conversion of farmland to forest to bolster ecosystem services. When looking ahead, it is imperative to investigate strategies for optimizing land use structure within the framework of spatial planning, harmonizing human-environment interactions, and achieving a dynamic equilibrium in land use to effectively enhance the benefits of ecosystem services.

(1) Zoning classification management and land use optimization. In ecologically sensitive areas and regions with high risks of soil erosion, it is essential to optimize land use structures by enhancing land planning and usage controls, as well as ensuring a rational allocation of forest and grassland proportions. Strict limitations should be imposed on the non-agricultural and non-grain conversion of arable land while promoting the intensive use of urban construction land to ensure the sustainability of land use [53].

(2) Strengthening the enforcement of ecological protection red lines. Based on the "Three Red Lines" policy in territorial spatial planning, it is vital to establish the priority of ecological protection red lines in land management, ensuring the reasonable control of land use intensity. In ecologically vulnerable areas and key ecosystem service zones,

measures such as stringent development controls and ecological restoration should be implemented to enhance regional ecological resilience [54].

(3) Promoting ecological compensation mechanisms. It is important to reinforce ecological compensation mechanisms, incentivizing farmers and land users to participate in ecological protection through fiscal subsidies and ecological compensation measures, thereby ensuring the long-term benefits of ecological restoration [55].

(4) Advancing sustainable agriculture and low-intensity development models. Encouraging the adoption of low-intensity land use practices, such as conservation tillage and precision agriculture, can help achieve a balance between agricultural production and ecological protection. Supporting the development of ecological agriculture and small-scale ecotourism can provide alternative economic benefits to local communities, reducing reliance on land resources [56].

(5) Enhancing monitoring and early warning of land use intensity. Establishing a dynamic monitoring system that utilizes remote sensing and geographic information systems (GIS) to periodically assess the impacts of changes in land use intensity on ecosystem services is crucial. Early warning information should be issued for high-risk areas, providing timely evidence for policy adjustments.

(6) Implementing territorial spatial planning tailored to local conditions. Considering the natural characteristics and socioeconomic conditions of the hilly and ravine region of the Loess Plateau, land use policies that align with local realities should be developed. This approach aims to maintain regional economic development while ensuring the sustainable provision of ecosystem services [54].

5.3. Limitations and Future Perspectives

This study is not without its limitations. Firstly, the temporal and spatial dynamics of four ecosystem services in Zichang City were evaluated using the InVEST model coupled with spatial exploratory analysis methods. Due to challenges in data acquisition, most model parameters were adapted from previous studies conducted in similar regions rather than derived from site-specific measurements. This reliance may introduce a degree of uncertainty into the assessment results, though the overall trends are unlikely to be significantly affected. Secondly, although the United Nations identifies a wide array of ecosystem services, the four key services selected in this study may not comprehensively reflect the ecological conditions of the study area. Future research should prioritize field surveys to obtain region-specific model parameters, thereby enhancing the accuracy of the evaluation. Moreover, expanding the scope of ecosystem service assessments could provide a more holistic understanding of ecological functions.

Furthermore, this study predominantly investigates the spatiotemporal disturbances of ecosystem services resulting from land use intensity changes without fully accounting for other contributing factors. Variations in land use intensity are inherently driven by the interplay between natural and socioeconomic forces. As such, future spatial relationship models should integrate geographic and socioeconomic variables to deliver a more robust and comprehensive framework, thus offering scientifically sound guidance for territorial spatial planning.

6. Conclusions

Between 1990 and 2020, Zichang City exhibited a consistent downward trend in land use intensity, with a distinct pattern characterized by higher intensity in central regions and lower intensity in the periphery. The distribution of varying intensity levels demonstrated notable spatial clustering throughout different phases of this period. Simultaneously, ecosystem services—including carbon storage, water yield, habitat quality, and soil retention—displayed clear spatial differentiation. Regions with low carbon storage and reduced water yield were relatively concentrated, whereas areas characterized by high carbon storage and elevated water yield were comparatively rare.

By 2035, under three potential scenarios—natural development, ecological protection, and economic growth—the spatial distribution characteristics of ecosystem service functions are expected to maintain a high degree of consistency with those observed in 2020. Specifically, regions with high carbon storage and high water yield are projected to further consolidate, while the spatial distribution of habitat quality and soil retention services may be influenced by fluctuations in land use intensity. Furthermore, during this period, the spatial clustering of land use intensity in relation to the four ecosystem service functions exhibited significant spatial heterogeneity. Across the three anticipated development scenarios, the spatial clustering of land use intensity aligns closely with the distributions recorded from 1990 to 2020. Consequently, it is imperative that future development planning emphasizes the prudent regulation of land use intensity to foster the protection and restoration of ecosystem services, thereby facilitating sustainable regional development.

Author Contributions: Conceptualization, Z.Z. and S.S.; Methodology, Z.Z. and Y.L.; Software, Z.Z., H.P. and S.S.; Validation, Z.Z., H.P. and Y.L.; Formal analysis, Z.Z. and Y.L.; Investigation, S.S. and Y.L.; Resources, Z.Z. and S.S.; Data curation, H.P.; Writing original draft preparation, Z.Z. and S.S.; Writing review and editing, S.S. and Y.L.; Visualization, Z.Z. and H.P.; Supervision, Y.L.; Project administration, Y.L.; Funding acquisition, Y.L. and Z.Z. All authors have read and agreed to the published version of the manuscript.

Funding: This research was supported by the National Natural Science Foundation of China (Grant No. 42201289) and the Open Collaboration Fund of State Key Laboratory of Black Soils Conservation and Utilization (Grant No. 2023HTDGZ-KF-09).

Data Availability Statement: The majority of the datasets used in this study are publicly available and can be accessed through public repositories. All used data repositories are cited either in the main text. Land use data were derived from the Remote Sensing Image Database maintained by the Resource and Environment Science Data Center of the Chinese Academy of Sciences (http://www.resdc.cn, accessed on 1 June 2024), with a spatial resolution of 30 m. The digital elevation model (DEM) utilized in this study was the ASTER Global Digital Elevation Model (ASTER GDEM), supplied by the Geospatial Data Cloud (http://www.gscloud.cn/#page1/1, accessed on 1 June 2024), also with a resolution of 30 m. Soil data were acquired from the World Soil Database (http://westdc.westgis.ac.cn/data/611f7d50-b419-4d14-b4dd-4a944b141175, accessed on 1 June 2024), which includes characteristics such as sand, silt, and clay fractions, as well as organic carbon content, with a resolution of 1 km. Furthermore, meteorological data, encompassing precipitation and potential evapotranspiration, were obtained from the Resource and Environment Science Data Center of the Chinese Academy of Sciences (http://www.resdc.cn, accessed on 1 June 2024).

Conflicts of Interest: The authors declare no conflict of interest.

References

1. Jones, H.P.; Jones, P.C.; Barbier, E.B.; Blackburn, R.C.; Benayas, J.M.R.; Holl, K.D.; McCrackin, M.; Meli, P.; Montoya, D.; Mateos, D.M. Restoration and repair of Earth's damaged ecosystems. *Proc. R. Soc. B-Biol. Sci.* **2018**, *285*, 20172577. [CrossRef] [PubMed]
2. United Nations, Department of Economic and Social Affairs. Available online: https://www.un.org/zh/node/21032 (accessed on 1 August 2024).
3. Zamboni, N.S.; Filho, E.M.N.; Carvalho, A.R. Unfolding differences in the distribution of coastal marine ecosystem services values among developed and developing countries. *Ecol. Econ.* **2021**, *189*, 107151. [CrossRef]
4. Li, F.; Altermatt, F.; Yang, J.; An, S.; Li, A.; Zhang, X. Human activities' fingerprint on multitrophic biodiversity and ecosystem functions across a major river catchment in China. *Glob. Change Biol.* **2020**, *26*, 6867–6879. [CrossRef] [PubMed]
5. Wang, Q.; Bai, X. Spatiotemporal characteristics and driving mechanisms of land-use transitions and landscape patterns in response to ecological restoration projects: A case study of mountainous areas in Guizhou, Southwest China. *Ecol. Inform.* **2024**, *82*, 102748. [CrossRef]
6. Hasan, S.S.; Zhen, L.; Miah, M.G.; Ahamed, T.; Samie, A. Impact of land use change on ecosystem services: A review. *Environ. Dev.* **2020**, *34*, 100527. [CrossRef]
7. Stefanidis, S.; Proutsos, N.; Alexandridis, V.; Mallinis, G. Ecosystem Services Supply from Peri-Urban Watersheds in Greece: Soil Conservation and Water Retention. *Land* **2024**, *13*, 765. [CrossRef]
8. Millennium Ecosystem Assessment. *Ecosystems and Human Well-Being: Synthesis*; Island Press: Washington, DC, USA, 2005.
9. Foley, J.A.; DeFries, R.; Asner, G.P.; Barford, C.; Bonan, G.; Carpenter, S.R.; Chapin, F.S.; Coe, M.T.; Daily, G.C.; Gibbs, H.K.; et al. Global Consequences of Land Use. *Science* **2005**, *309*, 570–574. [CrossRef]

10. Felipe-Lucia, M.R.; Soliveres, S.; Penone, C.; Fischer, M.; Ammer, C.; Boch, S.; Boeddinghaus, R.S.; Bonkowski, M.; Buscot, F.; Fiore-Donno, A.M.; et al. Land-use intensity alters networks between biodiversity, ecosystem functions, and services. *Proc. Natl. Acad. Sci. USA* **2020**, *117*, 28140–28149. [CrossRef]
11. Chen, B.; Jing, X.; Liu, S.; Jiang, J.; Wang, Y. Intermediate human activities maximize dryland ecosystem services in the long-term land-use change: Evidence from the Sangong River watershed, northwest China. *J. Environ. Manag.* **2022**, *319*, 115708. [CrossRef]
12. Kremen, C.; Miles, A. Ecosystem Services in Biologically Diversified versus Conventional Farming Systems: Benefits, Externalities, and Trade-Offs. *Ecol. Soc.* **2012**, *17*, 40. [CrossRef]
13. Olaiya, A. Transforming Our World: The 2030 Agenda for Sustainable Development: International. *Civ. Eng. = Siviele Ingenieurswese* **2015**, *24*, 26–30.
14. Degefu, M.A.; Argaw, M.; Feyisa, G.L.; Degefa, S. Dynamics of urban landscape nexus spatial dependence of ecosystem services in rapid agglomerate cities of Ethiopia. *Sci. Total Environ.* **2021**, *798*, 149192. [CrossRef] [PubMed]
15. Le Noe, J.; Erb, K.-H.; Matej, S.; Magerl, A.; Bhan, M.; Gingrich, S. Socio-ecological drivers of long-term ecosystem carbon stock trend: An assessment with the LUCCA model of the French case. *Anthropocene* **2021**, *33*, 100275. [CrossRef]
16. Dahan, K.S.; Kasei, R.A.; Husseini, R. Land use land cover (LULC) degradation intensity analysis of Guinea savannah and mosaic Forest savannah zones in Ghana. *All Earth* **2023**, *35*, 302–328. [CrossRef]
17. Wang, Z.; Guo, M.; Zhang, D.; Chen, R.; Xi, C.; Yang, H. Coupling the Calibrated GlobalLand30 Data and Modified PLUS Model for Multi-Scenario Land Use Simulation and Landscape Ecological Risk Assessment. *Remote Sens.* **2023**, *15*, 5186. [CrossRef]
18. Moindjie, I.-A.; Pinsard, C.; Accatino, F.; Chakir, R. Interactions between ecosystem services and land use in France: A spatial statistical analysis. *Front. Environ. Sci.* **2022**, *10*, 954655. [CrossRef]
19. Shi, L.; Halik, U.; Mamat, Z.; Aishan, T.; Abliz, A.; Welp, M. Spatiotemporal investigation of the interactive coercing relationship between urbanization and ecosystem services in arid northwestern China. *Land Degrad. Dev.* **2021**, *32*, 4105–4120. [CrossRef]
20. Ministry of Ecology and Environment of the People's Republic of China. Available online: https://www.mee.gov.cn/xxgk2018/xxgk/xxgk15/202101/t20210115_817536_wh.html (accessed on 20 August 2024).
21. Jorge-Garcia, D.; Estruch-Guitart, V.; Aragones-Beltran, P. How geographical factors and decision-makers' perceptions influence the prioritization of ecosystem services: Analysis in the Spanish rice field areas in RAMSAR Mediterranean wetlands. *Sci. Total Environ.* **2023**, *869*, 161823. [CrossRef]
22. Zhang, Z.; Liu, Y.; Sheng, S.; Liu, X.; Xue, Q. Evolving Urban Expansion Patterns and Multi-Scenario Simulation Analysis from a Composite Perspective of "Social–Economic–Ecological": A Case Study of the Hilly and Gully Regions of Northern Loess Plateau in Shaanxi Province. *Sustainability* **2024**, *16*, 2753. [CrossRef]
23. Zichang Municipal People's Government. Available online: http://www.zichang.gov.cn/ (accessed on 20 August 2024).
24. Resource and Environmental Science Data Platform. Available online: http://www.resdc.cn (accessed on 20 August 2024).
25. Geospatial Data Cloud. Available online: https://www.gscloud.cn/sources/index?pid=1&rootid=1 (accessed on 20 August 2024).
26. A Big Earth Data Platform for Three Poles. Available online: https://poles.tpdc.ac.cn/zh-hans/data/611f7d50-b419-4d14-b4dd-4a944b141175/ (accessed on 20 August 2024).
27. Schmidt, H.; Rast, S.; Bao, J.; Cassim, A.; Fang, S.-W.; la Cuesta, D.J.-d.; Keil, P.; Kluft, L.; Kroll, C.; Lang, T.; et al. Effects of vertical grid spacing on the climate simulated in the ICON-Sapphire global storm-resolving model. *Geosci. Model Dev.* **2024**, *17*, 1563–1584. [CrossRef]
28. Fahad, S.; Li, W.; Lashari, A.H.; Islam, A.; Khattak, L.H.; Rasool, U. Evaluation of land use and land cover Spatio-temporal change during rapid Urban sprawl from Lahore, Pakistan. *Urban Clim.* **2021**, *39*, 100931. [CrossRef]
29. Feng, X.; Li, Y.; Wang, X.; Yang, J.; Yu, E.; Wang, S.; Wu, N.; Xiao, F. Impacts of land use transitions on ecosystem services: A research framework coupled with structure, function, and dynamics. *Sci. Total Environ.* **2023**, *901*, 166366. [CrossRef] [PubMed]
30. Zhang, Y.; Zhao, X.; Gong, J.; Luo, F.; Pan, Y. Effectiveness and driving mechanism of ecological restoration efforts in China from 2009 to 2019. *Sci. Total Environ.* **2024**, *901*, 166366. [CrossRef]
31. Martini, F.; Conroy, K.; King, E.; Farrell, C.A.; Kelly-Quinn, M.; Obst, C.; Buckley, Y.M.; Stout, J.C. A capacity index to connect ecosystem condition to ecosystem services accounts. *Ecol. Indic.* **2024**, *167*, 112731. [CrossRef]
32. Jiang, C.; Zhang, H.; Zhang, Z. Spatially explicit assessment of ecosystem services in China's Loess Plateau: Patterns, interactions, drivers, and implications. *Glob. Planet. Change* **2018**, *161*, 41–52. [CrossRef]
33. Zhao, T.; Pan, J. Ecosystem service trade-offs and spatial non-stationary responses to influencing factors in the Loess hilly-gully region: Lanzhou City, China. *Sci. Total Environ.* **2022**, *846*, 157422. [CrossRef]
34. Kohestani, N.; Rastgar, S.; Heydari, G.; Jouibary, S.S.; Amirnejad, H. Spatiotemporal modeling of the value of carbon sequestration under changing land use/land cover using InVEST model: A case study of Nour-rud Watershed, Northern Iran. *Environ. Dev. Sustain.* **2024**, *26*, 14477–14505. [CrossRef]
35. Liu, X.; Liu, Y.S.; Wang, Y.; Liu, Z.J. Evaluating potential impacts of land use changes on water supply-demand under multiple development scenarios in dryland region. *J. Hydrol.* **2022**, *610*, 127811. [CrossRef]
36. Aznarez, C.; Svenning, J.-C.; Taveira, G.; Baro, F.; Pascual, U. Wildness and habitat quality drive spatial patterns of urban biodiversity. *Landsc. Urban Plan.* **2022**, *228*, 104570. [CrossRef]
37. Tamire, C.; Elias, E.; Argaw, M. Spatiotemporal dynamics of soil loss and sediment export in Upper Bilate River Catchment (UBRC), Central Rift Valley of Ethiopia. *Heliyon* **2022**, *8*, e11220. [CrossRef]

38. Nasr, M.; Orwin, J.F. A geospatial approach to identifying and mapping areas of relative environmental pressure on ecosystem integrity. *J. Environ. Manag.* **2024**, *370*, 122445. [CrossRef] [PubMed]
39. Mutale, B.; Qiang, F. Modeling future land use and land cover under different scenarios using patch-generating land use simulation model. A case study of Ndola district. *Front. Environ. Sci.* **2024**, *12*, 1362666. [CrossRef]
40. Bacau, S.; Domingo, D.; Palka, G.; Pellissier, L.; Kienast, F. Integrating strategic planning intentions into land-change simulations: Designing and assessing scenarios for Bucharest. *Sustain. Cities Soc.* **2022**, *76*, 103446. [CrossRef]
41. Peng, K.; Jiang, W.; Ling, Z.; Hou, P.; Deng, Y. Evaluating the potential impacts of land use changes on ecosystem service value under multiple scenarios in support of SDG reporting: A case study of the Wuhan urban agglomeration. *J. Clean. Prod.* **2021**, *307*, 127321. [CrossRef]
42. Tang, H.; Halike, A.; Yao, K.; Wei, Q.; Yao, L.; Tuheti, B.; Luo, J.; Duan, Y. Ecosystem service valuation and multi-scenario simulation in the Ebinur Lake Basin using a coupled GMOP-PLUS model. *Sci. Rep.* **2024**, *14*, 5071. [CrossRef]
43. Ahmadi-Mirghaed, F.; Rahmani, M.; Molla-Aghajanzadeh, S. Quantification of water yield concerning land use and climate scenarios in the Tajan watershed, North of Iran. *Int. J. Environ. Sci. Technol.* **2024**. [CrossRef]
44. Borrelli, P.; Robinson, D.A.; Fleischer, L.R.; Lugato, E.; Ballabio, C.; Alewell, C.; Meusburger, K.; Modugno, S.; Schütt, B.; Ferro, V. An assessment of the global impact of 21st century land use change on soil erosion. *Nat. Commun.* **2017**, *8*, 2013. [CrossRef]
45. Chen, W.; Zeng, J.; Li, N. Change in land-use structure due to urbanisation in China. *J. Clean. Prod.* **2021**, *321*, 128986. [CrossRef]
46. Oliver, T.H.; Isaac, N.J.B.; August, T.A.; Woodcock, B.A.; Roy, D.B.; Bullock, J.M. Declining resilience of ecosystem functions under biodiversity loss. *Nat. Commun.* **2015**, *6*, 10122. [CrossRef]
47. Bai, Y.; Liu, Y.; Li, Y.; Wang, Y.; Yuan, X. Land consolidation and eco-environmental sustainability in Loess Plateau: A study of Baota district, Shaanxi province, China. *J. Geogr. Sci.* **2022**, *32*, 1724–1744. [CrossRef]
48. Schirpke, U.; Tscholl, S.; Tasser, E. Spatio-temporal changes in ecosystem service values: Effects of land-use changes from past to future (1860–2100). *J. Environ. Manag.* **2020**, *272*, 111068. [CrossRef] [PubMed]
49. Bennett, E.M.; Peterson, G.D.; Gordon, L.J. Understanding relationships among multiple ecosystem services. *Ecol. Lett.* **2009**, *12*, 1394–1404. [CrossRef] [PubMed]
50. Xu, Y.; Tang, H.; Wang, B.; Chen, J. Effects of land-use intensity on ecosystem services and human well-being: A case study in Huailai County, China. *Environ. Earth Sci.* **2016**, *75*, 416. [CrossRef]
51. Zheng, H.; Peng, J.; Qiu, S.; Xu, Z.; Zhou, F.; Xia, P.; Adalibieke, W. Distinguishing the impacts of land use change in intensity and type on ecosystem services trade-offs. *J. Environ. Manag.* **2022**, *316*, 115206. [CrossRef] [PubMed]
52. Liu, Y.; Huang, X.; Liu, Y. Detection of long-term land use and ecosystem services dynamics in the Loess Hilly-Gully region based on artificial intelligence and multiple models. *J. Clean. Prod.* **2024**, *447*, 141560. [CrossRef]
53. Rahman, M.M.; Szabo, G. Multi-objective urban land use optimization using spatial data: A systematic review. *Sustain. Cities Soc.* **2021**, *74*, 103214. [CrossRef]
54. Liu, Y.; Zhou, Y. Territory spatial planning and national governance system in China. *Land Use Policy* **2021**, *102*, 105288. [CrossRef]
55. Li, Y.; Zhang, X.; Cao, Z.; Liu, Z.; Lu, Z.; Liu, Y. Towards the progress of ecological restoration and economic development in China's Loess Plateau and strategy for more sustainable development. *Sci. Total Environ.* **2021**, *756*, 143676.
56. Qu, L.; Liu, Y.; Li, Y.; Wang, J.; Yang, F.; Wang, Y. Sustainable use of gully agricultural land and water resources for sustainable development goals: A case study in the Loess Plat. *Land Degrad. Dev.* **2023**, *34*, 4935–4949. [CrossRef]

Disclaimer/Publisher's Note: The statements, opinions and data contained in all publications are solely those of the individual author(s) and contributor(s) and not of MDPI and/or the editor(s). MDPI and/or the editor(s) disclaim responsibility for any injury to people or property resulting from any ideas, methods, instructions or products referred to in the content.

land

MDPI

Article

Identifying the Key Protection Areas of Alpine Marsh Wetlands in the Qinghai Qilian Mountains, China: An Ecosystem Patterns–Characteristics–Functions Combined Method

Lei Wang [1,2], Xufeng Mao [2,3,*], Hongyan Yu [4], Baowei Zhao [4], Wenjia Tang [5], Hongyan Li [6], Xianying Wang [4] and Nan Zhou [2]

[1] School of Civil and Architectural Engineering, Nanchang Institute of Technology, Nanchang 330099, China; 18234145683@163.com
[2] Key Laboratory of Tibetan Plateau Land Surface Processes and Ecological Conservation (Ministry of Education), Qinghai Province Key Laboratory of Physical Geography and Environmental Process, College of Geographical Science, Qinghai Normal University, Xining 810008, China; 18329028970@163.com
[3] Academy of Plateau Science and Sustainability, People's Government of Qinghai Province and Beijing Normal University, Xining 810016, China
[4] Management and Service Center of the Qilian Mountain National Park, Xining 810008, China; yuhy502@yeah.net (H.Y.); qlsdsjzx@163.com (B.Z.); 17797437142@163.com (X.W.)
[5] State Key Laboratory for Environmental Protection Monitoring and Assessment of the Qinghai—Xining Plateau, Xining 810007, China; qhtsy@126.com
[6] Qinghai Institute of Quality and Standards, Xining 810001, China; lhy_lovehb@126.com
* Correspondence: maoxufeng@yeah.net

Abstract: The alpine marsh wetlands in the Qilian Mountains of Qinghai (QMQ) are under constant threat from the effects of climate change and human activities. Identifying the key ecological protection areas (KEPAs) of marsh wetlands is the prerequisite for formulating protection strategies and executing spatial planning programs. The current study developed a novel method to identify the KEPAs of marsh wetlands by following the ecosystem pattern–characteristics–functions (EPCFs) combined method and the ecological source–ecological corridor–ecological node research paradigm. More specifically, an evaluation system for ecological resistance was constructed by integrating the drivers of EPCFs in the marsh wetlands. Additionally, the marsh wetland degradation disturbances were analyzed through the drivers of EPCFs incorporated with a field survey. The findings indicated the following: (1) The marsh wetlands had a total water yield of approximately 3.96×10^8 m^3. The soil conservation rate and habitat quality per unit area were calculated to be 52.92 $t \cdot hm^{-2} \cdot a^{-1}$ and 0.992, respectively, with higher values observed on the southern bank and lower values on the northern bank of the river in the QMQ. (2) The KEPAs for the marsh wetlands covered a total extent of 996.53 km^2 in the QMQ, encompassing 40 ecological sources, 39 ecological corridors, and 40 ecological nodes, predominantly located in the river source regions. (3) The KEPAs were restructured into an ecological framework comprising two ecological axes, four ecological belts, four ecological cores, and multiple nodes in the QMQ. In response to the factors contributing to the degradation of marsh wetlands, adaptive measures including prioritizing natural restoration, modifying grazing strategies, executing ecological restoration projects as a minimum, and designating protected areas have been recommended. This research could contribute to enhancing the efficiency of regional territorial planning and offer a theoretical foundation for improving the ecological protection framework of regional marsh wetlands.

Keywords: ecological conservation; ecosystem service functions; ecological resistance surface; alpine marsh wetlands; wetland eco-engineering

1. Introduction

The alpine marsh wetland is a crucial and distinctive natural ecosystem located in the Qinghai–Tibetan Plateau, which has evolved to adapt to the high-altitude climate. As a

kind of typical wetland, marsh wetlands usually develop in areas with excessively moist soil, where marsh plants grow, where peat accumulates, or with gleyic characteristics. This ecosystem plays a vital role in regulating river and stream water sources, sequestering carbon, preserving biodiversity, and ensuring the sustainability of alpine animal husbandry in the plateau [1–4]. Unfortunately, the degradation of the marsh wetlands and their continual reduction in size have been observed in recent years due to the impacts of climate change and human activities [4–8]. Moreover, the fragile natural ecosystem in the Qilian Mountains, coupled with its limited ability to self-repair, accentuates the importance of addressing these issues promptly. The deterioration of the marsh wetlands is predicted to alter the regional landscape, significantly diminish its biodiversity, and reduce its ecosystem services, ultimately disrupting the ecological balance of the region [9–12]. Therefore, there is a critical need to enhance the structure and functionality of the ecosystem by designating protected areas for the marsh wetlands, implementing eco-friendly restoration techniques, and executing sustainable development initiatives [13,14].

In light of the growing significance of wetland ecological conservation and sustainable development, these topics have emerged as pivotal areas of global research. Several associated concepts, including wetland eco-engineering, wetland ecological security patterns, and wetland nature reserves, have recently garnered substantial attention [15,16]. The process of identifying or delineating ecological conservation areas typically adheres to fundamental principles such as holistic regional assessment, comprehensive procedural evaluation, and the inclusion of all elements. An index system has been developed by integrating regional characteristics and follows the ecological source–ecological corridor–ecological node research paradigm [17–21]. This methodology encompasses tasks such as identifying ecological sources, constructing ecological resistance surfaces, and extracting ecological corridors along with ecological nodes. The ecological source areas form the foundation of establishing the key ecological protection areas (KEPAs) [22]. Past research has frequently utilized indicators such as the importance of ecosystem services, ecological sensitivity, and landscape connectivity to evaluate ecological processes or functions [23–25]. These methods have primarily identified key areas providing ecosystem functions as ecological sources [26]. Nevertheless, relatively few studies have concentrated on the integrated application of various assessment models, with a predominant focus on evaluations encompassing all ecosystem types within a region [27–29]. There have been comparatively fewer research efforts dedicated to the conservation of marsh wetland ecosystems [30–33].

Ecological corridors serve as crucial pathways that facilitate species' migration and the flow of ecological processes. These corridors act as linear connectors linking various ecological sources [34], offering a solution to the fragmentation of ecological resources [35]. The extraction of ecological corridors often employs methods such as the minimum cumulative resistance (MCR) model [14], circuit theory [36], and the minimum cost distance model [37]. In particular, the MCR model, which is grounded in source–sink theory, is both adaptable and operationally effective for spatial expansion. This model has seen extensive application in creating ecological safety networks, including in areas like the Loess Plateau [38], the Ebinur Lake Basin [39], and the Poyang Lake urban agglomeration [40].

The simulation of ecological resistance surfaces is essential for identifying ecological corridors and facilitating the evaluation of migration difficulty in ecological flows. Presently, there are three main categories for modeling ecological resistance surfaces: expert experience methods, revised estimation methods, and indicator evaluation methods [41]. Expert empirical methods tend to be highly subjective [42]. Accuracy in adjusting factors such as terrain relief, population density, and night light in revised estimation methods can be challenging to maintain [43]. Furthermore, a universal assessment system for indicator evaluation methods has yet to be established [20]. The marsh wetland ecosystem is intricate, with its landscape configuration, structural traits, ecological roles, and various ecological processes being interlinked, underscoring the system's comprehensive nature. Previous research has predominantly focused on wetlands' ecological conservation and restoration from biodiversity, landscape connectivity, and ecological restoration resistance

standpoints [44–46]. Nonetheless, the interconnection between different elements of the wetland ecosystem is often overlooked. Several reference concepts and standard methods have been suggested for pinpointing key areas in territorial ecological protection. Consequently, further research is required to incorporate EPCF factors into the simulation of ecological resistance surfaces, ensuring alignment with the regional characteristics of marsh wetlands.

The Qilian Mountains in Qinghai (QMQ) hold significant importance as a water conservation region within the Yellow River Basin. Recognized as a critical biodiversity conservation area in China [47], it plays a vital role in the construction of ecological civilization and the protection of ecological security in the country. Nevertheless, the marsh wetlands in this region have been subjected to the dual challenges of natural environmental changes and anthropogenic activities over the past few decades. Climate change has led to glacier melting and increased precipitation, significantly affecting the marsh wetland ecosystem. Concurrently, human activities such as overgrazing and mining have impacted the wetlands' vegetation, soil, and permafrost hydrology, resulting in detrimental effects, including the proliferation of rodents (*Ochotona curzoniae* and *Myospalax baileyi*) and poisonous plants (*Stellera chamaejasme* and *Achnatherum inebrians*), which further exacerbate marsh wetlands' degradation [48,49]. This degradation causes several issues, including reduced vegetation coverage, declining soil nutrients, the disruption of ecological structure, and the potential loss of ecosystem function. Given that the QMQ is a key area for marsh wetland distribution, there is an urgent need to advance the ecological protection and restoration efforts of these wetlands.

Primarily, the goal of this research was the following: (1) To establish a system for assessing the ecological resistance and recognizing the KEPAs of marsh wetlands in the QMQ. (2) To assess the degradation and disruption factors impacting the marsh wetlands, and to offer adaptive reference strategies for safeguarding and restoring the ecological balance of these wetlands.

2. Materials and Methods

2.1. Study Area

The Qilian Mountains lie to the northeast of the Qinghai–Tibetan Plateau and cover an area of 34,200 km^2 in Qinghai (Figure 1). The climate in the Qilian Mountains is characterized as a continental alpine semi-humid mountain climate, displaying clear horizontal and vertical zonal differences. The mean yearly temperature ranges from −11.5 to 6.5 °C, while the annual precipitation varies between 141 and 640 mm, and the area receives approximately about 2100 h of sunshine per year. The terrain exhibits pronounced undulation on both the north and south sides, with landform types changing considerably from east to west. Major soil types in the region include felt soils, cold calcic soils, alpine frozen soils, and marshy soils. The area has a densely distributed river network, incorporating the Heihe River Basin (HH), the Datong River Basin (DT), the Tuole River Basin (TL), and the Shule River Basin (SL). The region's surface water resources total 6.02 billion m^3. The region's marsh wetlands are abundant, occupying 2778.24 km^2 in 2020. Hydrology, vegetation, and water-saturated soil are recognized as the three fundamental components of marsh wetlands. The alpine marshes are mainly found in the depressions, floodplains, and foothill discharge zones of the eastern Qilian Mountains, where the drainage is impeded and the soil permeability is poor. The vegetation of the alpine marsh wetlands is dominated by marsh meadows, with typical dominant species including *Carex capillifolia* (Decne.) S. R. Zhang, *Carex tibetikobresia* S. R. Zhang, *Carex alatauensis* S. R. Zhang, and *Blysmus sinocompressus* Tang and F. T. Wang. They often exhibit distinctive frost heave geomorphic features.

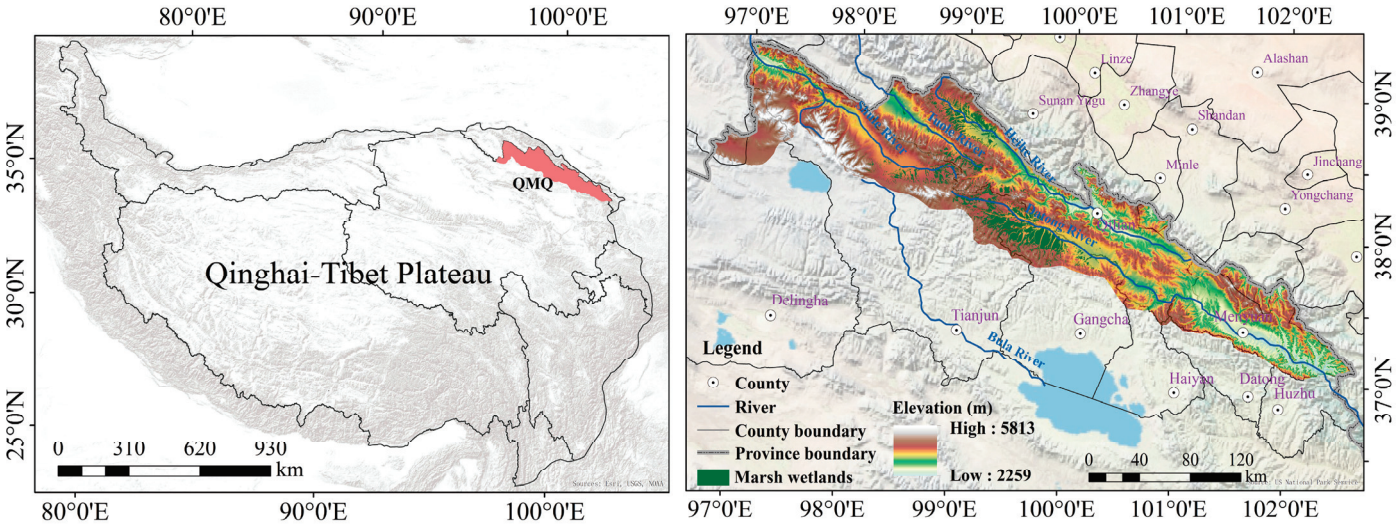

Figure 1. Overview of the study area.

2.2. Data Sources

Table 1 illustrates detailed information regarding the data utilized in this study. For all factors, the WGS84 coordinate system was implemented, and the year chosen was 2020. To facilitate modeling, the factors were resampled to raster cells with a spatial resolution of 30 m.

Table 1. Description of the data used in this study.

Variable Categories	Name (Abbreviation)	Resolution	Data Sources
Meteorological/ Hydrological	Monthly precipitation (PRE)	1 km	National Meteorological Information Center (http://data.cma.cn, accessed on 5 June 2024)
	Average monthly temperature (TEM)	1 km	National Meteorological Information Center (http://data.cma.cn, accessed on 5 June 2024)
	Annual evapotranspiration (EVP)	1 km	MOD 16A2 (https://ladsweb.modaps.eosdis.nasa.gov, accessed on 5 June 2024)
	Annual maximum temperature (AMNT)	1 km	National Earth System Science Data Center (http://www.geodata.cn, accessed on 5 June 2024)
Vegetation	Normalized difference vegetation index (NDVI)	30 m	Landsat 8 OLI (http://lpdaac.usgs.gov, accessed on 5 June 2024)
	Gross primary productivity (GPP)	500 m	MOD 17A3HGF (https://ladsweb.modaps.eosdis.nasa.gov, accessed on 5 June 2024)
Soil	Soil texture (clay/silt/sand)	1 km	Chinese Academy of Sciences (http://www.issas.ac.cn, accessed on 14 July 2024)
	Soil bulk density (BD)	1 km	HWSD (Harmonized World Soil Database)
	Soil organic carbon (SOC)	1 km	HWSD (Harmonized World Soil Database)
	Soil water capacity index (SWCI)	500 m	MOD09A1 V6 (https://ladsweb.modaps.eosdis.nasa.gov, accessed on 14 July 2024)
	Soil type (ST)	1 km	Chinese Academy of Sciences (http://www.issas.ac.cn, accessed on 14 July 2024)
Topographic	Digital elevation model (DEM)	30 m	SRTM (Shuttle Radar Topography Mission)
	Slope (SLOPE)	30 m	SRTM (Shuttle Radar Topography Mission)
	Topographic wetness index (TWI)	90 m	SAGA-GIS [50]
Human activity	Geomorphic type (POP)	1 km	Resource and Environmental Science Data Platform (http://www.resdc.cn, accessed on 14 June 2024)
	Human footprint index (HF)	1 km	National Tibetan Plateau/Third Pole Environment Data Center (https://data.tpdc.ac.cn, accessed on 14 July 2024)

2.3. Methods

Figure 2 illustrates the technical methodology for this research, which was primarily segmented into four main components: (1) Identifying ecological sources. Initially, using the spatial configuration of the marsh wetlands from the year 2020, the ecosystem service functions were evaluated employing the InVEST model as well as the Revised Universal Soil Loss Equation (RUSLE) model. Following this, the significance of comprehensive ecosystem service functions was categorized using a method that superseded equal

weighting. (2) The extraction of ecological corridors. Subsequently, an ecological resistance evaluation framework was established by integrating the drivers of the marsh wetlands' EPCFs. The ecological resistance surface was generated through the MCR model, and ecological corridors were delineated using the minimum cost distance model. (3) Constructing the KEPAs of the marsh wetlands. The points of intersection between the ecological sources and corridors were designated as ecological nodes, thereby forming the KEPAs for the marsh wetlands. (4) In the final phase, an analysis of the ecological disturbance factors contributing to the degradation of the marsh wetlands was conducted, followed by recommendations and strategies for adaptive management.

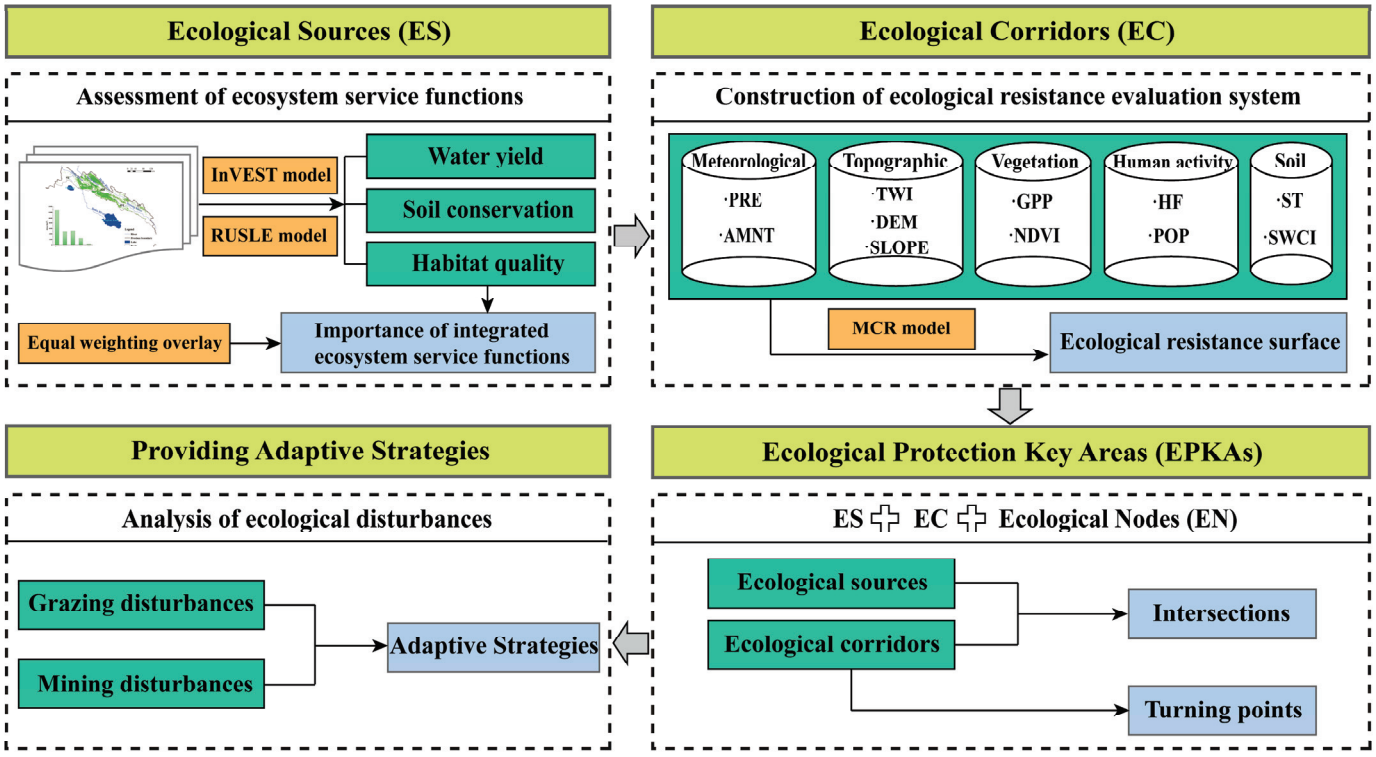

Figure 2. The research framework. Note: PRE, annual precipitation; AMNT, annual minimum temperature; TWI, topographic wetness index; DEM, digital elevation model; SLOPE, topographic slope; GPP, gross primary productivity; NDVI, normalized difference vegetation index; HF, human footprint index; POP, population density; ST, soil type; SWCI, soil water capacity index.

2.3.1. Identification of Ecological Sources

Ecological patches, as crucial components of the regional ecological system, have a key role in enhancing ecological processes, ensuring ecological stability, and improving ecosystem services [51]. Our study focused on two main criteria for identifying ecological patches: the combined ecosystem service capabilities of the marsh wetlands and the overall patch size.

(1) Evaluation of ecosystem service functions

Ecosystem service functions encompassed water yield, soil conservation, and habitat quality. For the assessment of water yield from marsh wetlands in the QMQ region, we employed the Water Yield module from the InVEST model. This module operates on the foundation of Budyko's coupled hydro-thermal equilibrium hypothesis, as articulated by Zhang et al., to estimate total annual water yield [52]. Regarding soil conservation, we utilized the RUSLE model, which calculates soil conservation by deducting the actual soil erosion amount from the potential soil loss. Habitat quality was assessed using the InVEST model's Habitat Quality module, which assigns habitat quality scores between 0 and 1 based on land use and threat source data; higher scores denote superior habitat

quality. We constructed habitat quality parameters by simultaneously considering various threat source data including urban areas, construction zones, agricultural fields, roads, and unused land. Table 2 provides detailed evaluation methods.

Table 2. Evaluation methods of ecosystem service functions.

Ecosystem Service Functions	Models	Formulas	Parameters
Water Yield	The Water Yield module of the InVEST model	$Y_{ij} = (1 - \frac{AET_{ij}}{P_i}) \times P_i$	Y_{ij} is the annual water yield of the study area (mm); AET_{ij} is the annual average actual evaporation of each raster i on a land use type j (mm); P_i is the average annual precipitation (mm).
Soil Conservation	The Revised Universal Soil Loss Equation (RUSLE)	$SC_i = R_i \times K_i \times LS_i \times (1 - C_i \times P_i)$	SC_i is the actual soil conservation ($t \cdot hm^{-2}$); R_i *is* rainfall erosivity factor ($MJ \cdot mm \cdot hm^{-2} \cdot h^{-1} \cdot a^{-1}$); K_i is the soil erodibility factor ($t \cdot hm^2 \cdot h \cdot hm^{-2} \cdot MJ^{-1} \cdot mm^{-1}$); LS_i is the slope length and slope factor; C_i is the vegetation cover management factor; P_i is the factor of water and soil conservation measures.
Habitat Quality	The Habitat Quality module of the InVEST model	$Q_{ij} = H_j \left[1 - \frac{D_{ij}^z}{D_{ij}^z + k^z}\right]$	Q_{ij} is the habitat quality of each raster i; H_j is the habitat suitability of a land use type j; D_{ij} is the habitat degradation degree of each raster i; k is the semi-saturation constant 0.5.

(2) Significance of integrated ecosystem services

Using model assessment, we acquired a raster map depicting the function of ecosystem services within the marsh wetlands. The map was processed with the Raster Calculator in ArcGIS 10.8 software to normalize the data, and we calculated cumulative service values by ranking each function from highest to lowest. We designated the values that represented 50% and 80% of the cumulative ecosystem service functions as key thresholds for classification. Ultimately, we categorized the ecosystem service functions into three levels and allocated scores to each level (Table 3).

Table 3. Grading of ecosystem service assessments.

Importance Levels	Cumulative Service Value Ratio	Grading Criteria	Integrated Ecosystem Service Scores
Generally important	20%	2	0~6
Important	30%	3	7~9
Extremely important	50%	5	10~15

(3) Extraction of ecological sources

In order to prevent the singular nature of the ecosystem service roles and the fragmentation of the marsh wetland landscapes, we combined the three ecosystem service functions with equal weight to derive and identify their highly significant levels. Subsequently, the spatial distribution pattern of the marsh wetlands was overlaid to extract patches exceeding an area of 10 km^2. Ultimately, the ecological sources of the marsh wetlands in the QMQ were determined.

2.3.2. Identification of Ecological Corridors

Ecological networks are systems of nature reserves and their interconnections, which make fragmented natural systems coherent and thus support more biodiversity than non-

connected forms, including core areas, buffers, and corridors [53–55]. Ecological resistance inhibits the flow of materials, energy, and information among various ecological elements, processes, or functions from the ecological source via the ecological corridor [56]. Ecological corridors serve as vital pathways for the migration and diffusion of species or ecological flows, facilitating connections between the linear components of ecological sources [34,57]. To identify ecological corridors, it is essential to construct a surface representing ecological resistance.

(1) Construction of ecological resistance surface

Given the intricacies of the geographical landscape and the pronounced zonal variations in the marshes in the QMQ, we thoroughly examined the factors driving the formation and distribution of marsh wetlands [58], the changes characteristic of degraded marsh wetlands [59], and the factors influencing ecosystem service functions [60]. To this end, we developed an evaluation system for ecological resistance (Table 4). Subsequently, the ecological resistance evaluation indices were normalized in both positive and negative manners, and the significance of the indicators was established by integrating expert scoring with the analysis hierarchical process (AHP). In conclusion, we computed the comprehensive ecological resistance surface based on the superposition of the weights. Tables A1–A6 show the consistency tests and resistance factor weights.

Table 4. The evaluation system for the ecological resistance of the marsh wetlands.

Resistance Categories	Resistance Factors	Weights	Direction
Meteorological/Hydrological	PRE	0.299	−
	AMNT	0.043	+
Topographic	TWI	0.139	−
	DEM	0.262	+
	SLOPE	0.049	+
Vegetation	GPP	0.076	−
	NDVI	0.038	−
Human Activity	HF	0.039	+
	POP	0.019	+
Soil	ST	0.012	+
	SWCI	0.025	−

Note: PRE, annual precipitation; AMNT, annual minimum temperature; TWI, topographic wetness index; DEM, digital elevation model; SLOPE, topographic slope; GPP, gross primary productivity; NDVI, normalized difference vegetation index; HF, human footprint index; POP, population density; ST, soil type; SWCI, soil water capacity index.

(2) Extraction of ecological corridors

Utilizing the MCR model [61,62], input data included ecological sources and ecological resistance surfaces. The Cost Connectivity tool within ArcGIS 10.8 software was employed to determine the potential ecological corridors representing the least costly pathways. Subsequently, these corridors were filtered based on their significance. The algorithm of the model is detailed as follows:

$$M = f_{min} \sum_{j=n}^{i=m} \left(D_{ij} R_i \right) \quad (1)$$

where M represents the minimum cumulative resistance value; f_{min} denotes the unspecified function that indicates the positive relationship between the minimum cumulative resistance and ecological processes; D signifies the spatial distance from the ecological source j to the landscape i; and R_{ij} is the resistance coefficient of the landscape i to the ecological process.

2.3.3. Identification of Key Areas for Ecological Protection

Ecological nodes typically represent point landscape features that play a crucial role in preserving the ecosystem services of a given region [63]. The junctions or pivotal locations where ecological corridors meet ecological sources are considered ecological nodes. To conclude, the findings related to ecological sources, corridors, and nodes were utilized as EPCAs for marsh wetlands in the QMQ.

3. Results

3.1. Evaluation of Ecosystem Service Functions and Ecological Sources of Marsh Wetlands

Figure 3 illustrates that the total water yield reached 3.96×10^8 m^3 in the QMQ, with higher yields observed in the upstream regions of the DT and HH, while lower yields were found in the downstream regions of the SL and TL. This distribution demonstrates a pattern of greater values on the southern bank compared to the northern bank of the river, mirroring the rainfall distribution characteristics in the area [64]. The soil conservation per unit area in the marsh wetlands was recorded as 52.92 $t \cdot hm^{-2} \cdot a^{-1}$, with its spatial distribution pattern aligning with that of the water yield. The regions of high value were primarily located on the southern riverbank, attributable to the presence of dense drainage systems, ample precipitation, extensive vegetation cover, and gradual slope variations that facilitate soil retention. The average habitat quality per unit area within the marsh wetlands was measured as 0.992, exhibiting no notable spatial variation.

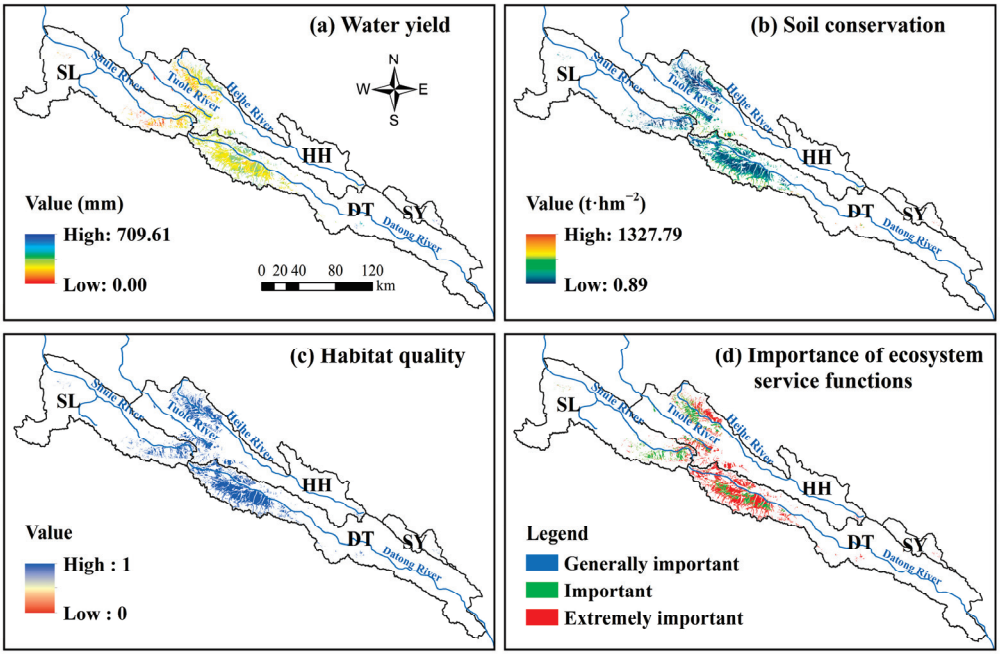

Figure 3. Spatial distribution and importance of ecosystem service functions in QMQ.

Table 5 illustrates that the overall ecosystem service function of marsh wetlands in the QMQ was favorable, with approximately 70% of the region classified as at an extremely important level, 30% categorized as important, and the smallest portion as generally important. The DT exhibited the most extensive areas rated as extremely important (1272.41 km^2), followed by the HH, which made up around 61.87% of the entire marsh wetlands' area in the QMQ.

Table 5. Proportion of area within various classifications of integrated service function of marsh wetlands.

Level	QMQ	DT	HH	SL	SY
Generally important	0.01	0.00	0.01	0.04	0.00
Important	30.50	20.02	38.13	65.30	0.00
Extremely important	69.49	79.98	61.87	34.67	100.00
Areas (km^2)	2778.24	1590.91	893.11	290.74	3.49

Note: QMQ refers to the Qilian Mountains of Qinghai; DT represents the Datong River Basin; HH denotes the Heihe River Basin; SL is the Shule River Basin; and SY signifies the Shiyang River Basin.

According to the principle of integrated ecosystem service functions, which are of critical significance, and considering only patches exceeding 10 km^2, a total of 40 ecological sources were identified (Figure 4). These sources collectively span an area of 996.53 km^2, representing 35.87% of the overall marsh wetland area in the QMQ. Notably, the largest ecological sources are found in the DT, encompassing 729.97 km^2, which constitutes 73.25% of the total ecological sources within the QMQ. The spatial distribution of these ecological sources includes Muli Town, Jiermeng Town, Quanji Town, and Yikewulan Town, situated in the upper DT region, along with Yanglong Town, in the upper HH region, and Suli Town, located in the lower SL region. Due to the availability of ample water resources, a low human population density, and minimal disturbances to the marsh wetlands, these specific areas are recognized as vital ecological sources for the marsh wetlands in the QMQ.

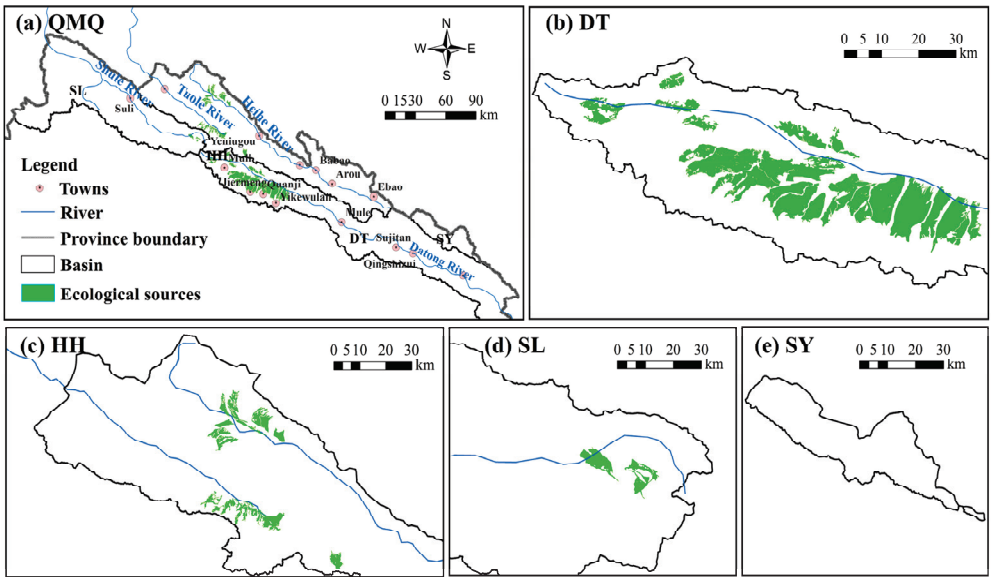

Figure 4. Spatial distributions of marsh wetlands' ecological sources in QMQ.

3.2. Spatial Patterns of Ecological Resistance Surface and Ecological Corridors

Figure 5 illustrates the spatial distribution of ecological resistance surfaces and ecological corridors within the marsh wetlands. The values for the ecological resistance ranged from 0 to 0.68 (Figure 5a). In the QMQ, the development areas of the marsh wetlands correspond to the regions of low ecological resistance, facilitating the migration and dispersal of organisms. Additionally, regions sustaining crucial ecosystem services were also identified as areas exhibiting high ecological security. The high ecological resistance areas are predominantly located in the northwestern region of the SL and HH, where the presence of significant mountain ranges (the Tuole and Shule Mountains) can considerably hinder biological flow transmission. As depicted in Figure 5b, a total of 39 ecological corridors were identified in the QMQ, collectively extending over 505.85 km^2, including 14 ecological corridors spanning 266.13 km^2 that were derived from the DT. These ecological corridors

play a vital role in linking ecological sources characterized by distinct spatial distributions, with notably long corridors crossing the basin.

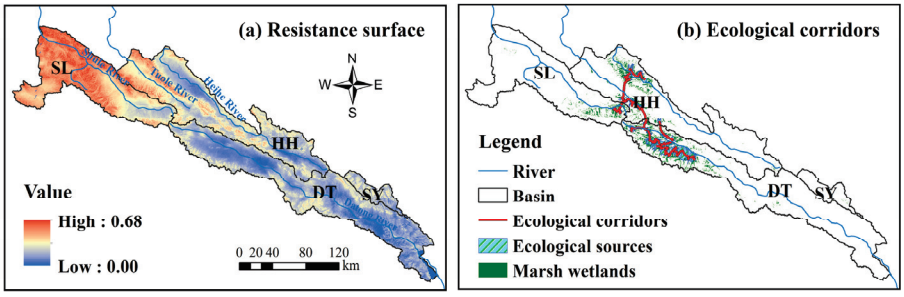

Figure 5. Ecological resistance surface and corridors of marsh wetlands in QMQ.

3.3. Identification of Key Ecological Protection Areas of Marsh Wetlands

Figure 6 illustrates the KEPAs of marsh wetlands in the QMQ. Besides the previously identified ecological sources and corridors, a total of 40 ecological nodes were extracted, which collectively form the KEPAs of the marsh wetlands in the QMQ. These ecological nodes are primarily concentrated in the upper reaches of the DT, enhancing the migration of wetland organisms and significantly supporting the expansion of the marsh wetlands' sources as well as the connectivity of corridors within the QMQ. The biological connections among ecological sources rely on these nodes. For nodes that are spatially separated, they are also the most probable stopover points for organisms during their migration. Thus, protecting these nodes and enhancing the ecological connectivity of the marsh wetlands should be prioritized.

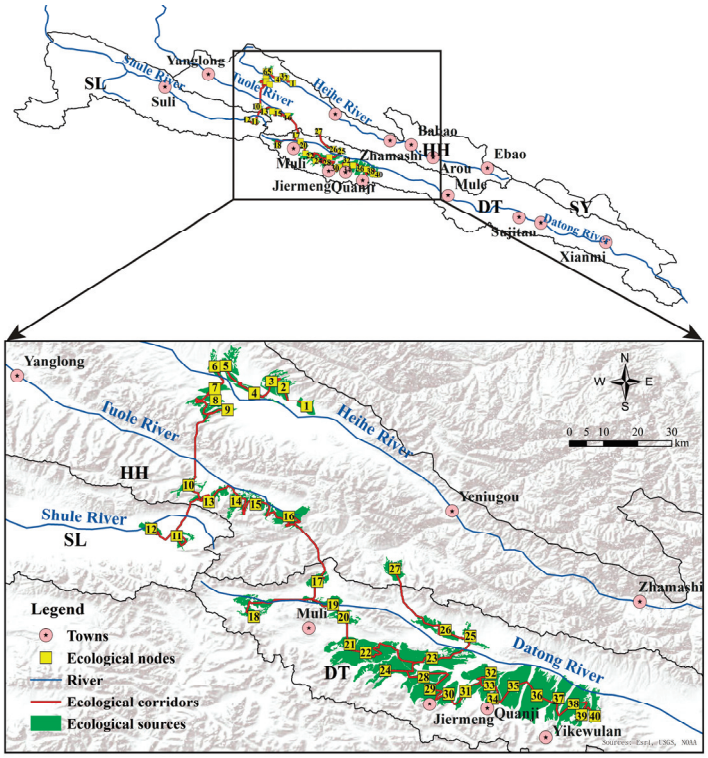

Figure 6. Key ecological protection areas of marsh wetlands in QMQ.

4. Discussion

4.1. Advantages of Constructing Ecological Resistance Surfaces in Marsh Wetlands

Ecological resistance surfaces reflect how the spatial heterogeneity of landscapes influences the movement of ecological flows [39]. Some researchers have directly applied values to these resistance surfaces according to land use type [42], which makes it difficult to reflect differences within the same type of ecosystem and introduces significant subjectivity. Additionally, certain studies have incorporated spatial factors to adjust the ecological resistance associated with land use types, including characteristics such as topographic relief, slope, and vegetation cover [43]. Some studies have identified urban ecological security patterns by considering the type of land use, the normalized difference vegetation index (NDVI), distance from residential area, distance from water source, elevation, slope, and the degree of soil erosion to construct ecological resistance surfaces [65]. However, this approach poses challenges in adequately ensuring the modification degree of the influencing factors on the ecological resistance of various land use types.

Informed by the concept of EPCFs related to marsh wetlands, we constructed an ecological resistance evaluation system (Figure 7). The system considers the driving forces of the formation and distribution of these wetlands, the alterations in the characteristics of the degraded marsh wetlands, and the factors of the ecosystem service functions. This section on evaluation indicators was guided by several criteria: (1) Research conducted by Wang et al. (2024) indicated that meteorological conditions and topography are critical determinants in the formation and distribution of marsh wetlands in the QMQ, with vegetation and soil acting as secondary factors [58]. Additionally, the cumulative impact of anthropogenic activities on marsh formation and distribution surpasses that of soil factors. (2) Findings from Wang et al. (2022) showed that the wetlands' water yield is predominantly influenced by the PRE, while their soil conservation is primarily dictated by the NDVI; furthermore, the habitat quality has faced increasing disturbances from the HF, particularly from the POP [60]. (3) A field survey and experimental analysis revealed (Figure A1) that the marsh wetlands are undergoing severe aridification and an inverse successional trajectory driven by hydrological conditions [66], resulting in diminished soil nutrients and the reduced dominance of wetland plant species. In conclusion, we selected 11 indicators representing the EPCFs of the marsh wetlands, categorized into five groups: meteorology, topography, vegetation, soil, and human activities. According to the impact degree, the weights of these indicators were assigned via expert evaluation and AHP methods, leading to the establishment of the ecological resistance evaluation system for the marsh wetlands. Thus, the system enables an objective and scientific approach to analyzing the ecological resistance surfaces constructed by this method.

4.2. Importance of Identifying Key Ecological Protection Areas of Marsh Wetlands

Identifying KEPAs is of significant importance for the scientific management and effective restoration of regional marsh wetlands [67]. The QMQ serves as a representative area for marsh wetland distribution. However, the natural environmental conditions are characterized as "high, cold, and dry" in the QMQ, resulting in a simpler structure and function of marsh wetlands in this habitat. When exposed to external disturbances, their limited ability for self-regulation and recovery often results in alterations to landscape patterns, which can severely impact hydrological conditions, soil properties, and plant communities, ultimately diminishing ecosystem functions. Utilizing the research framework of ecological sources, corridors, and nodes, we identified the KEPAs of marsh wetlands within the QMQ, considering the drivers of the EPCFs of these wetlands. The KEPAs play a significant role in sustaining the stability of ecological processes and providing beneficial ecosystem services in the QMQ.

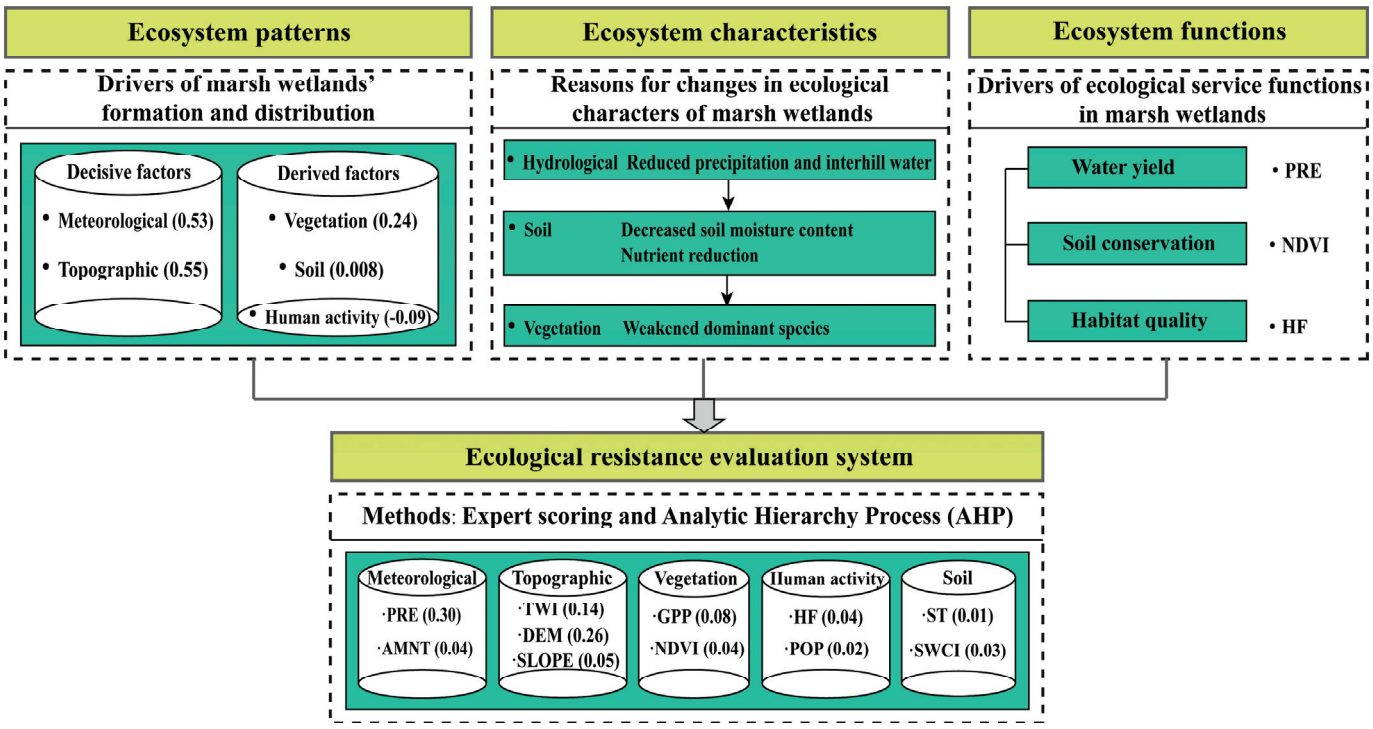

Figure 7. Rationale for constructing ecological resistance evaluation system for marsh wetlands. Note: PRE, annual precipitation; AMNT, annual minimum temperature; TWI, topographic wetness index; DEM, digital elevation model; SLOPE, topographic slope; GPP, gross primary productivity; NDVI, normalized difference vegetation index; HF, human footprint index; POP, population density; ST, soil type; SWCI, soil water capacity index.

Based on the aforementioned Section 3.3, we optimized the KEPAs of the marsh wetlands. Figure 8 shows the optimized ecological framework within the QMQ's marsh wetlands. This framework encompasses two ecological axes, four ecological belts, four ecological cores, and various ecological nodes, collectively forming a well-structured spatial layout system. The four ecological cores comprise the upper reaches of the HH, the lower reaches of the TL, the lower reaches of the SL, and the upper reaches of the DT. This extended ecological axis links the four townships of Muli, Jiermeng, Quanji, and Yikewulan, located within the DT, establishing a relatively smooth ecological network channel. These findings contribute to optimizing the regional spatial territory, sustaining a robust ecological security pattern, and offering theoretical guidance for enhancing the ecological protection system of the marsh wetlands.

4.3. Adaptive Strategies

Regarding management strategies, most of the current programs are put forward based on familiarity with the area, but they lack solid theoretical backing [23,68]. This research proposes adaptive management strategies that integrate the specific environmental features of the region, which can address the limitations of subjective management plans and enhance the precision of the protection strategies. According to observation from field surveys and remote sensing images (Figure A1), the marsh wetlands at the origins of the HH and SL are experiencing slight degradation. This is primarily due to the prolonged use of these areas as summer pastures, leading to meadow status at the edges of the marsh wetland patches as well as the obvious nibbling of plants and noticeable grazing of vegetation. Overall, the marsh wetlands in the DT remain undegraded; however, the wetlands in Muli have decreased in size due to coal mining and excavation activities, which have reduced the marshes' areas, contributed to the drying of nearby wetlands, and destroyed the wetlands' water conveyance system. According to the World Conservation

Union–Conservation Measures Partnership (IUCN-CMP) classification of direct threats to biodiversity (version 1.1), marsh wetlands are threatened by agriculture, aquaculture, energy production, and mining [69]. In response to the disturbance of grazing and mineral extraction (Figure 9), it is essential to formulate measures tailored to local conditions, as this approach is an effective means to prevent marsh wetland degradation.

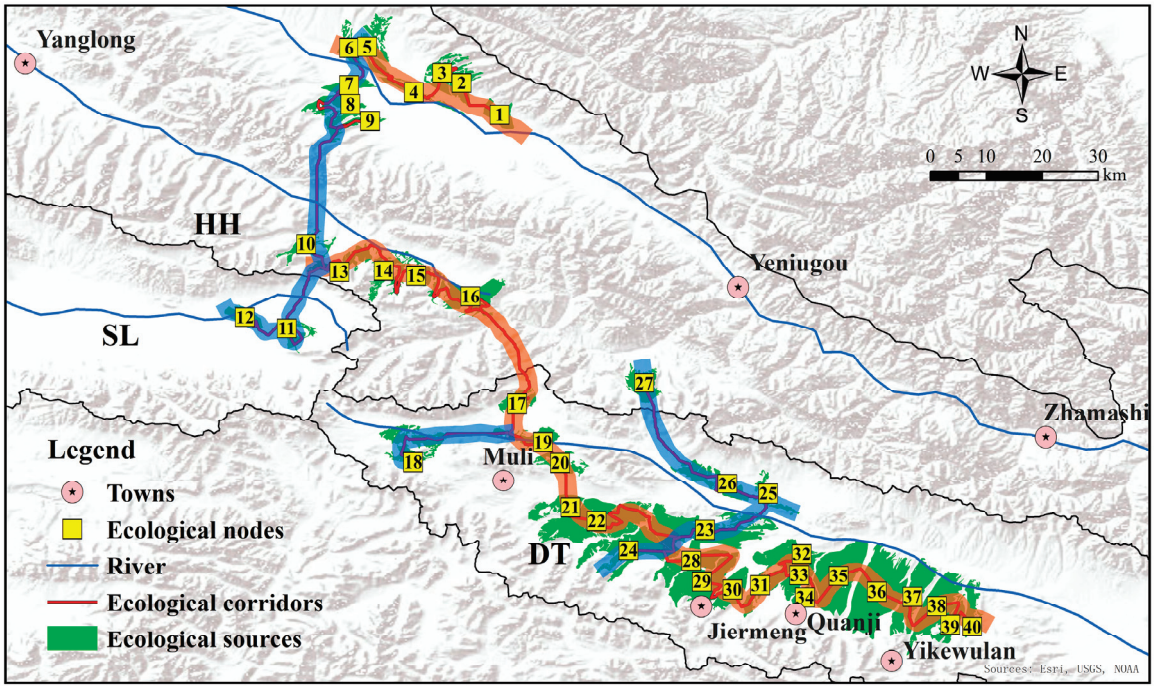

Figure 8. Ecological framework of marsh wetlands in QMQ.

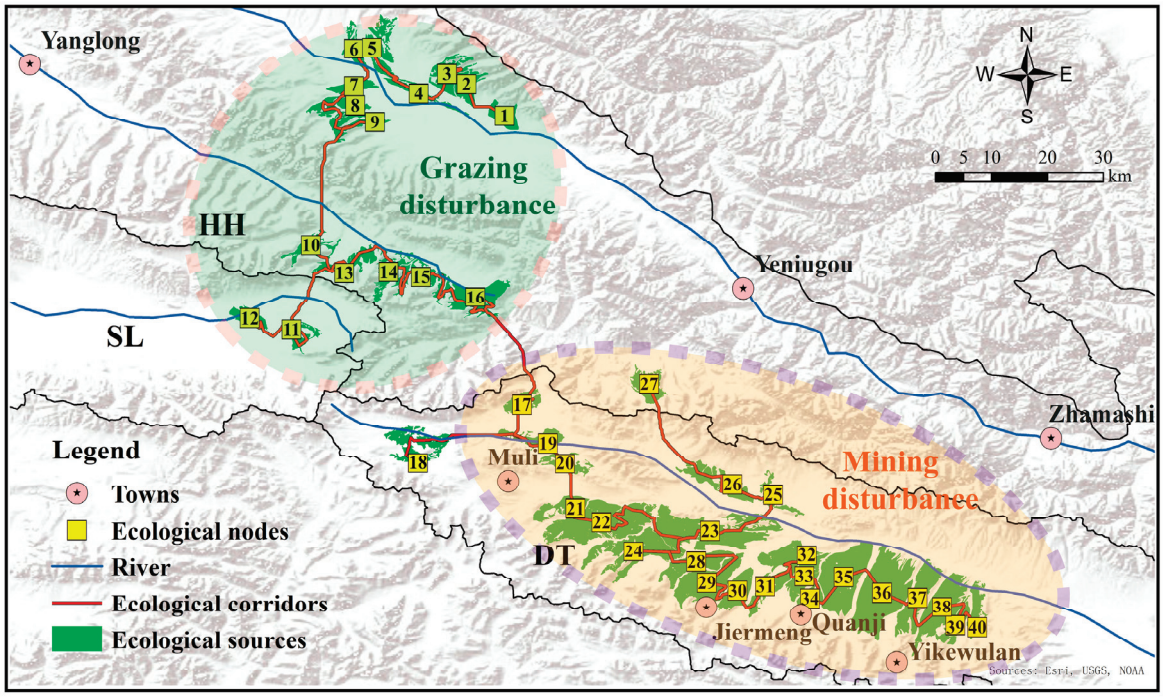

Figure 9. Ecological disturbance factors of marsh wetlands.

Considering the adaptive strategies for grazing disturbances in the marsh wetlands, prioritizing natural restoration, modifying grazing techniques, and strictly regulating the livestock capacity of the wetland pastures are proposed. Grazing should be organized based on grass availability, and conflicts between livestock and grass should be effectively mitigated by altering the grazing system and methods. This aims to harmonize human activities with biodiversity. Concurrently, it is important to limit tourism development initiatives, reinforce fencing, adopt rotational grazing or seasonal livestock management, and create artificial grasslands to alleviate stress on the natural grasslands. Regarding the adaptive strategies for mining disturbances in the marsh wetlands, carrying out ecological restoration projects at mines is recommended to enhance the ecological environmental conditions and improve both the quality and functions of the wetland ecosystem. This could be achieved through vegetation restoration, soil rehabilitation, and landform modification. Additionally, it is suggested that the DT's marsh wetlands should be designated as part of the Qilian Mountains National Park (Qinghai) (Figure 10), with a ban on their development and use. Community members can directly participate in the conservation of biodiversity in the marsh wetlands, such as monitoring species and recording ecological changes. At the same time, it is also possible to teach residents wetland protection knowledge and skills through organizing lectures, exhibitions, practical activities, etc., to improve their environmental awareness and participation. In addition, the introduction of social capital can provide financial support, technical assistance, and management experience for wetland protection. This comprehensive protection model emphasizes multi-party participation, collaboration, and joint efforts to promote the development of wetland conservation.

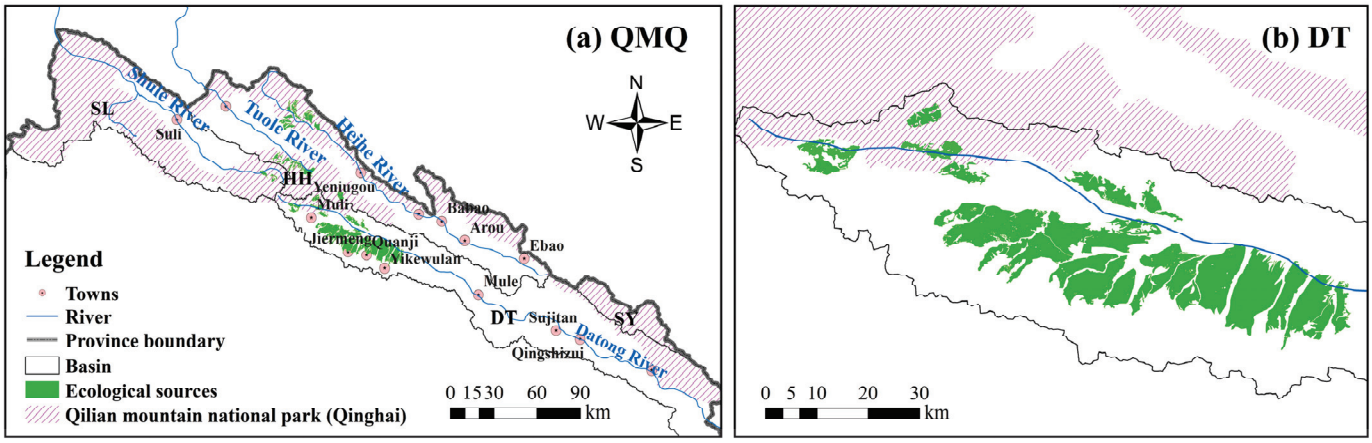

Figure 10. Reference for the delineation of the marsh wetland conservation area.

4.4. Limitations

Firstly, this study focused on modeling only three ecosystem service functions—water yield, soil conservation, and habitat quality—while neglecting carbon storage, windbreak, sand fixation, and biodiversity, resulting in an incomplete evaluation of wetland ecosystem service functions. Additionally, the contiguity of the spatial structure of the marsh wetlands, is the basis for promoting the connectivity of ecological processes and functions, such as species migration, gene exchange, energy flow, and material cycling [70,71]. This research failed to establish a distance threshold for wetland ecological sources. Connectivity between ecological sources is absent when the distance between these sources exceeds that of biological diffusion or migration. Lastly, the impact of the width of ecological corridors and the quantity of ecological nodes on ecosystem functions warrants further exploration.

5. Conclusions

Based on the research paradigm of ecological sources, corridors, and nodes, the KEPAs of marsh wetlands were identified and adaptive strategies for marsh wetland degradation were proposed, combined with the drivers of EPCFs, which are valuable for implementing ecological protection projects and delineating ecological security patterns. The conclusions are as follows:

(1) The water conservation, soil conservation, and habitat quality functions of the marsh wetlands in the QMQ in 2020 were simulated using the InVEST and RUSLE models. The overall ecosystem service function was good, with nearly 70% of the area at the extremely important level.

(2) The KEPAs of marsh wetlands in the QMQ included 40 ecological sources with a total area of 996.53 km^2, 39 ecological corridors, and 40 ecological nodes, which are spatially concentrated in the upper reaches of the DT and the HH. Based on the identification results of the KEPAs, the ecological network system of "two ecological axes, four ecological belts, four ecological cores, and multiple nodes" was proposed.

(3) The internal ecological interference of the KEPAs for wetland ecological protection in the marsh wetlands was highlighted by constructing the ecological resistance evaluation system. In response to the two types (grazing and mineral mining) of interference in the degraded marsh wetlands, it is proposed that natural restoration should be the main approach for marsh wetlands in the source areas of the HH and SL. Grazing strategies should be adjusted to effectively alleviate the conflict between livestock and grass and coordinate the relationship between human activities and biodiversity. In addition, the implementation of mining ecological restoration projects and regulatory measures, such as the delineation of protected areas in the source areas of the DT, have improved the ecological environment and enhanced the quality and function of the regional ecosystem.

Author Contributions: Methodology, Data curation, Writing—original draft, L.W.; Conceptualization, Funding acquisition, Writing—review and editing, X.M.; Supervision, Validation, Writing—review and editing H.Y.; Supervision, Writing—review and editing, B.Z.; Supervision and Validation, Software, W.T. and H.L.; Supervision and Validation, X.W. and N.Z. All authors have read and agreed to the published version of the manuscript.

Funding: This research was supported by the National Natural Science Foundation of China (Project No. 52070108) and the Natural Science Foundation of Qinghai Province (No. 2024–ZJ–9).

Institutional Review Board Statement: Not applicable.

Informed Consent Statement: Not applicable.

Data Availability Statement: Data will be made available on request.

Acknowledgments: All authors gratefully acknowledge the editors and anonymous reviewers for their constructive comments on our manuscript.

Conflicts of Interest: The authors declare that they have no known competing financial interests or personal relationships that could have appeared to influence the work reported in this paper.

Appendix A

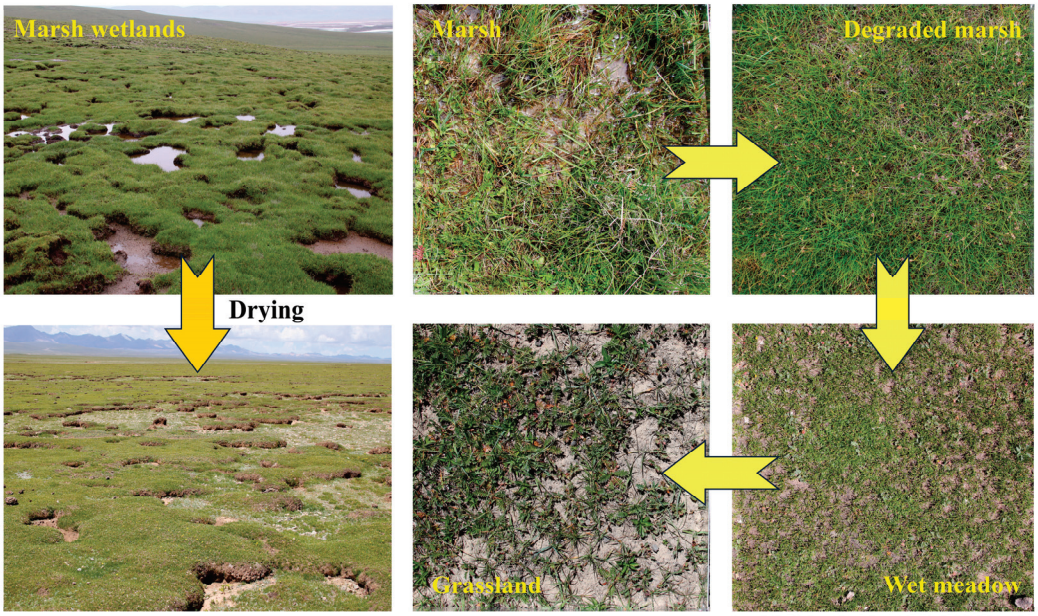

Figure A1. Degradation and aridification of marsh wetlands in QMQ.

Table A1. Consistency tests and indicator weights for marsh wetlands.

Marsh Wetlands	Meteorological/ Hydrological	Vegetation	Human activity	Soil	Topographic	Weight
Meteorological/ Hydrological	1.0000	5.0000	6.0000	8.0000	0.5000	0.3413
Vegetation	0.2000	1.0000	3.0000	4.0000	0.2000	0.1139
Human Activity	0.1667	0.3333	1.0000	2.0000	0.1667	0.0579
Soil	0.1250	0.2500	0.5000	1.0000	0.1250	0.0371
Topographic	2.0000	5.0000	6.0000	8.0000	1.0000	0.4498

Note: Consistency ratio, 0.0480; λ_{max}, 5.2152.

Table A2. Consistency tests and indicator weights for topographic elements.

Topographic	TWI	DEM	SLOPE	Weight
TWI	1.0000	0.5000	3.0000	0.3090
DEM	2.0000	1.0000	5.0000	0.5816
SLOPE	0.3333	0.2000	1.0000	0.1095

Note: Consistency ratio, 0.0036; λ_{max}, 3.0037; TWI, topographic wetness index; DEM, digital elevation model; SLOPE, topographic slope.

Table A3. Consistency tests and indicator weights for meteorological/hydrological elements.

Meteorological/Hydrological	PRE	AMNT	Weight
PRE	1.0000	7.0000	0.8750
AMNT	0.1429	1.0000	0.1250

Note: Consistency ratio, 0.0000; λ_{max}, 2.0000; PRE, annual precipitation; AMNT, annual minimum temperature.

Table A4. Consistency tests and indicator weights for vegetation elements.

Vegetation	GPP	NDVI	Weight
GPP	1.0000	2.0000	0.6667
NDVI	0.5000	1.0000	0.3333

Note: Consistency ratio, 0.0000; λ_{max}, 2.0000; GPP, gross primary productivity; NDVI, normalized difference vegetation index.

Table A5. Consistency tests and indicator weights for human activity elements.

Human Activity	POP	HF	Weight
POP	1.0000	0.5000	0.3333
HF	2.0000	1.0000	0.6667

Note: Consistency ratio, 0.0000; λ_{max}, 2.0000; POP, population density; HF, human footprint index.

Table A6. Consistency tests and indicator weights for soil elements.

Soil	ST	SWCI	Weight
ST	1.0000	0.5000	0.3333
SWCI	2.0000	1.0000	0.6667

Note: Consistency ratio, 0.0000; λ_{max}, 2.0000; ST, soil type; SWCI, soil water capacity index.

References

1. Mitsch, W.J.; Bernal, B.; Nahlik, A.M.; Mander, Ü.; Zhang, L.; Anderson, C.J.; Jørgensen, S.E.; Brix, H. Wetlands, carbon, and climate change. *Landsc. Ecol.* **2013**, *28*, 583–597. [CrossRef]
2. Aung, T.D.W.; Kyi, S.W.; Suzue, K.; Theint, S.M.; Tsujita, K.; Yu, T.T.; Merriman, J.C.; Peh, K.S.H. Rapid ecosystem service assessment of a protected wetland in Myanmar, and implications for policy development and management. *Ecosyst. Serv.* **2021**, *50*, 101336. [CrossRef]
3. Spieles, D.J. Wetland construction, restoration, and integration: A comparative review. *Land* **2022**, *11*, 554. [CrossRef]
4. Mitsch, W.J.; Mander, Ü. Wetlands and carbon revisited. *Ecol. Eng.* **2018**, *114*, 1–6. [CrossRef]
5. Nie, Y.; Li, A. Assessment of alpine wetland dynamics from 1976–2006 in the vicinity of Mount Everest. *Wetlands* **2011**, *31*, 875–884. [CrossRef]
6. Asselen, S.V.; Verburg, P.H.; Vermaat, J.E.; Janse, J.H. Drivers of wetland conversion: A global meta-analysis. *PLoS ONE* **2013**, *8*, e81292. [CrossRef]
7. Creed, I.F.; Lane, C.R.; Serran, J.N.; Alexander, L.C.; Basu, N.B.; Calhoun, A.J.K.; Christensen, J.R.; Cohen, M.J.; Craft, C.; D'Amico, E.; et al. Enhancing protection for vulnerable waters. *Nat. Geosci.* **2017**, *10*, 809–815. [CrossRef]
8. Fluet-Chouinard, E.; Stocker, B.D.; Zhang, Z.; Malhotra, A.; Melton, J.R.; Poulter, B.; Kaplan, J.; Goldewijk, K.K.; Siebert, S.; Minayeva, T.; et al. Extensive global wetland loss over the past three centuries. *Nature* **2023**, *614*, 281–286. [CrossRef]
9. Qin, Y.; Lei, H.; Yang, D.; Gao, B.; Wang, Y.; Cong, Z.; Fan, W. Long-term change in the depth of seasonally frozen ground and its ecohydrological impacts in the Qilian Mountains, northeastern Tibetan Plateau. *J. Hydrol.* **2016**, *542*, 204–221. [CrossRef]
10. Zhang, J.; Zhu, H.; Zhang, P.; Song, Y.; Zhang, Y.; Li, Y.; Rong, T.; Liu, Z.; Yang, D.; Lou, Y. Construction of GI network based on MSPA and PLUS model in the main urban area of Zhengzhou: A case study. *Front. Environ. Sci.* **2022**, *10*, 878656. [CrossRef]
11. Li, H.; Gao, W.; Liu, Y.; Yuan, F.; Wu, M.; Meng, L. Attributing the impacts of ecological engineering and climate change on carbon uptake in Northeastern China. *Landsc. Ecol.* **2023**, *38*, 3945–3960. [CrossRef]
12. Wu, P.; Zhang, H.; Cui, L.; Wickings, K.; Fu, S.; Wang, C. Impacts of alpine wetland degradation on the composition, diversity and trophic structure of soil nematodes on the Qinghai-Tibetan Plateau. *Sci. Rep.* **2017**, *7*, 837. [CrossRef] [PubMed]
13. Dunlop, T.; Glamore, W.; Felder, S. Restoring estuarine ecosystems using nature-based solutions: Towards an integrated eco-engineering design guideline. *Sci. Total Environ.* **2023**, *873*, 162362. [CrossRef] [PubMed]
14. Li, C.; Su, K.; Liang, X.; Jiang, X.; Wang, J.; You, Y.; Wang, L.; Chang, S.; Wei, C.; Zhang, Y.; et al. Identification of priority areas to provide insights for ecological protection planning: A case study in Hechi, China. *Ecol. Indic.* **2023**, *154*, 110738. [CrossRef]
15. Luo, J.; Fu, H. Construct the future wetland ecological security pattern with multi-scenario simulation. *Ecol. Indic.* **2023**, *153*, 110473. [CrossRef]
16. Chen, L.; Ma, Y. Ecological Risk Identification and Ecological Security Pattern Construction of Productive Wetland Landscape. *Water Resour. Manage* **2023**, *37*, 4709–4731. [CrossRef]
17. Zhai, T.; Wang, J.; Fang, Y.; Qin, Y.; Huang, L.; Chen, Y. Assessing ecological risks caused by human activities in rapid urbanization coastal areas: Towards an integrated approach to determining key areas of terrestrial-oceanic ecosystems reservation and restoration. *Sci. Total Environ.* **2020**, *708*, 135153. [CrossRef]
18. Liu, Y.; Liu, S.; Wang, F.; Liu, H.; Li, M.; Sun, Y.; Wang, Q.; Yu, L. Identification of key priority areas under different ecological restoration scenarios on the Qinghai-Tibet Plateau. *J. Environ. Manage* **2022**, *323*, 116174. [CrossRef]

19. Yu, K. Security patterns and surface model in landscape ecological planning. *Landsc. Urban Plann.* **1996**, *36*, 1–17. [CrossRef]
20. Fu, Y.; Shi, X.; He, J.; Yuan, Y.; Qu, L. Identification and optimization strategy of county ecological security pattern: A case study in the Loess Plateau, China. *Ecol. Indic.* **2020**, *112*, 106030. [CrossRef]
21. Han, W.; Xia, S.; Zhou, W.; Shen, Y.; Su, X.; Liu, G. Constructing ecological security pattern based on ecological corridor identification in Lhasa River Basin. *Acta Ecol. Sin.* **2023**, *43*, 8948–8957.
22. Wang, S.; Song, Q.; Zhao, J.; Lu, Z.; Zhang, H. Identification of key areas and early-warning points for ecological protection and restoration in the yellow river source area based on ecological security pattern. *Land* **2023**, *12*, 1643. [CrossRef]
23. Peng, J.; Li, B.; Dong, J.; Liu, Y.; Lv, D.; Du, Y.; Luo, M.; Wu, J. Basic logic of territorial ecological restoration. *China Land Sci.* **2020**, *34*, 18–26.
24. Li, X.; Yu, X.; Wu, K.; Feng, Z.; Liu, Y.; Li, X. Land-use zoning management to protecting the Regional Key Ecosystem Services: A case study in the city belt along the Chaobai River, China. *Sci. Total Environ.* **2021**, *762*, 143167. [CrossRef] [PubMed]
25. Ma, B.; Zeng, W.; Xie, Y.; Wang, Z.; Hu, G.; Li, Q.; Gao, R.; Zhou, Y.; Zhang, T. Boundary delineation and grading functional zoning of Sanjiangyuan National Park based on biodiversity importance evaluations. *Sci. Total Environ.* **2022**, *825*, 154068. [CrossRef]
26. Dong, J.; Peng, J.; Xu, Z.; Liu, Y.; Wang, X.; Li, B. Integrating regional and interregional approaches to identify ecological security patterns. *Landsc. Ecol.* **2021**, *36*, 2151–2164. [CrossRef]
27. Du, J.; Gong, Y.; Xi, X.; Liu, C.; Qian, C.; Ye, B. The study on the spatiotemporal changes in tradeoffs and synergies of ecosystem services and response to land use/land cover changes in the region around Taihu Lake. *Heliyon* **2024**, *10*, e33375. [CrossRef]
28. Zhou, J.; Wang, Z.; He, Y.; Liu, P.; Xu, J.; Lu, C.; Lei, G.; Wen, L. Evaluating the Effects of Wetland Restoration on Ecosystem Services Using InVEST and Geostatistics: A Case Study of Dongting Lake in China. *Remote Sens.* **2024**, *16*, 4062. [CrossRef]
29. Gao, X.; Huang, X.; Chang, S.; Dang, Q.; Wen, R.; Lo, K.; Li, J.; Yan, A. Long-term improvements in water conservation functions at Qilian Mountain National Park, northwest China. *J. Mt. Sci.* **2023**, *20*, 2885–2897. [CrossRef]
30. Yang, R.; Mu, Z.; Gao, R.; Huang, M.; Zhao, S. Interactions between ecosystem services and their causal relationships with driving factors: A case study of the Tarim River Basin, China. *Ecol. Indic.* **2024**, *169*, 112810. [CrossRef]
31. Wang, M.; Wang, X.; Shi, W. Exploring the response of trade-offs and synergies among ecosystem services to future land use changes in the hilly red soil region of Southern China. *J. Environ. Manage* **2024**, *372*, 123283. [CrossRef] [PubMed]
32. Wei, X.; Wu, X.; Wang, D.; Wu, T.; Li, R.; Hu, G.; Zou, D.; Bai, K.; Liu, Y.; Yan, X.; et al. Spatiotemporal changes and management measure to enhance ecosystem services in the Mongolian Plateau. *Environ. Dev.* **2024**, *52*, 101103. [CrossRef]
33. Zhang, X.; Li, S.; Yu, H. Analysis on the ecosystem service protection effect of national nature reserve in Qinghai-Tibetan Plateau from weight perspective. *Ecol. Indic.* **2022**, *142*, 109225. [CrossRef]
34. Xiang, A.; Zhao, X.; Huang, P.; Yi, Q.; Pu, J.; Shi, X.; Chu, B. Diagnosis and restoration of priority area of territorial ecological restoration in Plateau Lake Watershed. *Acta Ecol. Sin.* **2023**, *43*, 6143–6153.
35. Gao, M.; Hu, Y.; Bai, Y. Construction of ecological security pattern in national land space from the perspective of the community of life in mountain, water, forest, field, lake and grass: A case study in Guangxi Hechi, China. *Ecol. Indic.* **2022**, *139*, 108867. [CrossRef]
36. Peng, J.; Yang, Y.; Liu, Y.; Hu, Y.; Du, Y.; Meersmans, J.; Qiu, S. Linking ecosystem services and circuit theory to identify ecological security patterns. *Sci. Total Environ.* **2018**, *644*, 781–790. [CrossRef]
37. Lu, X.; Wang, J.; Li, X.; Feng, Y. Ecological network construction of county land consolidation and rehabilitation based on least cost distance model. *Bull. Soil Water Conserv.* **2017**, *37*, 143–149, 346.
38. Wei, H.; Zhu, H.; Chen, J.; Jiao, H.; Li, P.; Xiong, L. Construction and optimization of ecological security pattern in the loess plateau of China based on the minimum cumulative resistance (MCR) model. *Remote Sens.* **2022**, *14*, 5906. [CrossRef]
39. Wei, Q.; Halike, A.; Yao, K.; Chen, L.; Balati, M. Construction and optimization of ecological security pattern in Ebinur Lake Basin based on MSPA-MCR models. *Ecol. Indic.* **2022**, *138*, 108857. [CrossRef]
40. Dai, L.; Liu, Y.; Luo, X. Integrating the MCR and DOI models to construct an ecological security network for the urban agglomeration around Poyang Lake, China. *Sci. Total Environ.* **2021**, *754*, 141868. [CrossRef]
41. Zhou, G.; Huan, Y.; Wang, L.; Lan, Y.; Liang, T.; Shi, B.; Zhang, Q. Linking ecosystem services and circuit theory to identify priority conservation and restoration areas from an ecological network perspective. *Sci. Total Environ.* **2023**, *873*, 162261. [CrossRef] [PubMed]
42. Wang, C.; Yu, C.; Chen, T.; Feng, Z.; Wu, K. Can the establishment of ecological security patterns improve ecological protection~ An example of Nanchang, China. *Sci. Total Environ.* **2020**, *740*, 140051. [CrossRef] [PubMed]
43. Zhang, L.; Peng, J.; Liu, Y.; Wu, J. Coupling ecosystem services supply and human ecological demand to identify landscape ecological security pattern: A case study in Beijing-Tianjin-Hebei region, China. *Urban Ecosyst.* **2017**, *20*, 701–714. [CrossRef]
44. Qu, Y.; Sun, G.; Luo, C.; Zeng, X.; Zhang, H.; Murray, N.J.; Xu, N. Identifying restoration priorities for wetlands based on historical distributions of biodiversity features and restoration suitability. *J. Environ. Manage* **2019**, *231*, 1222–1231. [CrossRef]
45. Domisch, S.; Kakouei, K.; Martínez-López, J.; Bagstad, K.J.; Magrach, A.; Balbi, S.; Villa, F.; Funk, A.; Hein, T.; Borgwardt, F.; et al. Social equity shapes zone-selection: Balancing aquatic biodiversity conservation and ecosystem services delivery in the transboundary Danube River Basin. *Sci. Total Environ.* **2019**, *656*, 797–807. [CrossRef]
46. Langhans, S.D.; Hermoso, V.; Linke, S.; Bunn, S.E.; Possingham, H.P. Cost-effective river rehabilitation planning: Optimizing for morphological benefits at large spatial scales. *J. Environ. Manage* **2014**, *132*, 296–303. [CrossRef]
47. Tang, Z.; Ma, Y.; Liu, Z. Development strategy of ecotourism resources in Qinghai Lake area. *Resour. Dev. Mark.* **2010**, *26*, 934–936.

48. Yang, L.; Song, M.; Wang, Y.; Wang, H.; Zhou, R. Changes of plant community diversity and soil ecological stoichiometry in alpine meadow under the disturbance of plateau pika Ochotona curzoniae and plateau zokor Myospalax baileyi. *J. Plan Protect.* **2024**, *51*, 1056–1067.
49. Nie, H.; Gao, J. Research progress on the ecological impact and spreading mechanism of weeds on degraded grassland. *Chin. J. Grassl.* **2022**, *44*, 101–113.
50. Conrad, O.; Bechtel, B.; Bock, M.; Dietrich, H.; Fischer, E.; Gerlitz, L.; Wehberg, J.; Wichmann, V.; Böhner, J. System for automated geoscientific analyses (SAGA) v. 2.1. 4. *Geosci. Model Dev.* **2015**, *8*, 1991–2007. [CrossRef]
51. Teng, M.; Wu, C.; Zhou, Z.; Lord, E.; Zheng, Z. Multipurpose greenway planning for changing cities: A framework integrating priorities and a least-cost path model. *Landsc. Urban Plann.* **2011**, *103*, 1–14. [CrossRef]
52. Zhang, L.; Hickel, K.; Dawes, W.R.; Chiew, F.H.S.; Briggs, P.R. A rational function approach for estimating mean annual evapotranspiration. *Water Resour. Res.* **2004**, *40*, 89–97. [CrossRef]
53. Gonzalez, A.; Thompson, P.; Loreau, M. Spatial ecological networks: Planning for sustainability in the long-term. *Curr. Opin. Environ. Sustain.* **2017**, *29*, 187–197. [CrossRef] [PubMed]
54. Boitani, L.; Falcucci, A.; Maiorano, L.; Rondinini, C. Ecological networks as conceptual frameworks or operational tools in conservation. *Conserv. Biol.* **2007**, *21*, 1414–1422. [CrossRef] [PubMed]
55. Gippoliti, S.; Battisti, C. More cool than tool: Equivoques, conceptual traps and weaknesses of ecological networks in environmental planning and conservation. *Land Use Policy* **2017**, *68*, 686–691. [CrossRef]
56. Su, Y.; Zhang, H.; Chen, X.; Huang, G.; Ye, Y.; Wu, Q.; Huang, N.; Kuang, Y. The ecological security patterns and construction land expansion simulation in Gaoming. *Acta Ecol. Sin.* **2013**, *33*, 1524–1534.
57. Battisti, C.; Gallitelli, L.; Scalici, M.; Angelici, F.M. Habitat fragmentation, connectivity conservation and related key-concepts: Temporal trends in their recurrences on web of science (1960–2020). *Land* **2022**, *11*, 230. [CrossRef]
58. Wang, L.; Mao, X.; Wei, X.; Yu, H.; Tang, W.; Zhang, L.; Wu, Y.; Zhang, J.; Gou, L. Exploring the driving forces of potential marsh wetlands formation and distribution in the Qilian Mountains of Qinghai, China. *Ecol. Indic.* **2024**, *158*, 111516. [CrossRef]
59. Lin, C.; Li, X.; Zhang, J.; Sun, H.; Zhang, J.; Han, H.; Wang, Q.; Ma, C.; Li, C.; Zhang, Y.; et al. Effects of degradation succession of alpine wetland on soil organic carbon and total nitrogen in the Yellow River source zone, west China. *J. Mt. Sci.* **2021**, *18*, 694–705. [CrossRef]
60. Wang, L.; Mao, X.; Song, X.; Wei, X.; Yu, H.; Xie, S.; Zhang, L.; Tang, W. How Rising Water Levels Altered Ecosystem Provisioning Services of the Area around Qinghai Lake from 2000 to 2020: An InVEST-RF-GTWR Combined Method. *Land* **2022**, *11*, 1570. [CrossRef]
61. Kong, F.; Yin, H.; Nakagoshi, N.; Zong, Y. Urban green space network development for biodiversity conservation: Identification based on graph theory and gravity modeling. *Landsc. Urban Plann.* **2010**, *95*, 16–27. [CrossRef]
62. Zhang, Y.; Jiang, Z.; Li, Y.; Yang, Z.; Wang, X.; Li, X. Construction and optimization of an urban ecological security pattern based on habitat quality assessment and the minimum cumulative resistance model in Shenzhen City, China. *Forests* **2021**, *12*, 847. [CrossRef]
63. Fang, C.; Kuang, H.; Jia, Q.; Chen, X.; Zhu, Z.; Ye, Q. Evaluation of ecological security pattern in Wuhan City based on the importance of ecosystem services and ecological sensitivity. *J. Environ. Eng. Technol.* **2022**, *12*, 1446–1454.
64. Wei, X.; Eboy, O.V.; Cao, G.; Xu, L. Spatio-temporal variation of water conservation and its impact factors on the southern slope of Qilian Mountains. *Reg. Sustain.* **2023**, *4*, 54–67. [CrossRef]
65. Huang, L.; Tang, Y.; Song, Y.; Liu, J.; Shen, H.; Du, Y. Identifying and optimizing the ecological security pattern of the Beijing-Tianjin-Hebei urban agglomeration from 2000 to 2030. *Land* **2024**, *13*, 1115. [CrossRef]
66. Ma, M.; Zhou, X.; Du, G. Soil seed bank dynamics in alpine wetland succession on the Tibetan Plateau. *Plant Soil.* **2011**, *346*, 19–28. [CrossRef]
67. Song, T.; Li, D.; Zhang, L.; Wang, G.; Gao, Y.; Yang, C.; Feng, C.; Ma, H. Importance evaluation of ecosystem services and construction of ecological security pattern in Qinba Mountain area. *Strateg. Study Chin. Acad. Eng.* **2020**, *22*, 64–72. [CrossRef]
68. Song, W.; Han, Z.; Liu, L. Systematic diagnosis of ecological problems and comprehensive zoning of ecological conservation and restoration for an integrated ecosystem of mountains-rivers-forests-farmlands-lakes-grasslands in Shaanxi Province. *Acta Ecol. Sin.* **2019**, *39*, 8975–8989.
69. Salafsky, N.; Salzer, D.; Stattersfield, A.J.; Hilton-Taylor, C.; Neugarten, R.; Butchart, S.H.M.; Collen, B.; Cox, N.; Master, L.L.; O'connor, S.; et al. A standard lexicon for biodiversity conservation: Unified classifications of threats and actions. *Conserv. Biol.* **2008**, *22*, 897–911. [CrossRef]
70. Bennett, A.F. *Linkages in the Landscape: The Role of Corridors and Connectivity in Wildlife Conservation (No. 1)*; Iucn: Gland, Switzerland, 2003.
71. Lindenmayer, D.; Bowd, E. Critical ecological roles, structural attributes and conservation of old growth forest: Lessons from a case study of Australian mountain ash forests. *Front. For. Glob. Chang.* **2022**, *5*, 878570. [CrossRef]

Disclaimer/Publisher's Note: The statements, opinions and data contained in all publications are solely those of the individual author(s) and contributor(s) and not of MDPI and/or the editor(s). MDPI and/or the editor(s) disclaim responsibility for any injury to people or property resulting from any ideas, methods, instructions or products referred to in the content.

land

MDPI

Article

The Relationship Between Carbon Emissions and Ecosystem Services in Guangdong Province, China: The Perspective of Ecological Function Zones

Yanqing Lang [1], Heng Chao [2,*] and Jingyu Xiao [3]

[1] School of Environment and Energy, Peking University Shenzhen Graduate School, Shenzhen 518055, China; langyq@pku.edu.cn
[2] School of Urban Planning and Design, Peking University Shenzhen Graduate School, Shenzhen 518055, China
[3] Shenzhen New Land Tool Planning & Architectural Design Co., Ltd., Shenzhen 518172, China
* Correspondence: chaoheng@pkusz.edu.cn

Abstract: Ecosystem carbon sinks can offset part of the carbon emissions from human activities, playing a significant role in the carbon neutrality process. Clarifying the relationship between carbon emissions and ecosystem services is crucial for achieving the dual goals of carbon neutrality and ecological environmental protection. Effective ecosystem management is a prerequisite for controlling carbon emissions, as well as for ecosystem conservation and restoration, making a significant contribution to emission reduction and the enhancement of ecosystem services. Therefore, this study takes Guangdong Province as an example, starting with ecological functional zones—units that can enhance the effectiveness of ecosystem management—combining multi-source data and localized methods to develop annual carbon emissions (CEs) and ecosystem service value (ESV) data from 2000 to 2020, and reveals the spatiotemporal relationships between CEs and the ESV. The results showed the following from 2000 to 2020: (1) The net CEs increased from 203.73 to 482.80 million tons, representing an increase of 279.07 million tons, or 136.98%. The metropolitan residential security zone (MRSZ) was the dominant carbon source area, accounting for more than 60% of the total net CEs. (2) The total ESV gradually decreased from CNY 596.95 to 504.56 billion, representing a decline of CNY 92.39 billion, or 15.48%. The WCZ had the highest ESV, accounting for more than 50% of the total in all periods. (3) Temporally, the net CEs were negatively correlated with the total ESV in the study area, especially in the MRSZ, while a positive correlation was observed in the agricultural products provision zone (APZ). Spatially, the main clusters were Low–Low and High–Low clusters, primarily distributed in the APZ and MRSZ. This study explores and reveals the spatiotemporal relationship between CEs and the ESV, providing valuable references for related research in Guangdong Province and other regional comparative studies.

Keywords: carbon emissions; carbon absorption; ecosystem services; ecological functional zones

1. Introduction

Carbon emissions from human activities have resulted in global warming, with emissions since industrialization significantly exceeding historical levels [1–3]. Currently, global temperatures are 1.1 °C higher than pre-industrial levels, with approximately 1.07 °C of this increase attributed to human activities; this human-induced warming is projected to reach 1.5 °C by 2030–2035 [4–6]. Ecosystems such as forests, grasslands, and wetlands play a crucial role as carbon sinks in mitigating carbon emissions and climate warming. On one hand, ecosystems exhibit a degree of adaptability to carbon emissions; as carbon dioxide concentrations rise, the carbon sink capacity of vegetation may strengthen, helping to offset a portion of human emissions and delay warming while reducing mitigation costs [7,8]. On the other hand, scientific ecosystem management and conservation measures, such as nature-based solutions, can enhance carbon sequestration and emissions reduction, thereby

increasing the net carbon sink capacity of ecosystems [9–11]. A significant correlation between carbon emissions and ecosystems exists [12]; research by the Nature Conservancy suggests that nature-based solutions could contribute approximately 30% of the emission reduction potential necessary to achieve the goals of the Paris Agreement, with more than a 66% likelihood of keeping global warming below 2 °C [13].

However, climate extremes resulting from human activities pose a significant threat to the sustainability of ecosystems, further impacting the services that humans derive from them [14,15]. Global warming has triggered changes in phenology and species distribution, resulting in issues such as biological invasions, biodiversity loss, and an increased frequency of ecological disasters. Research indicates that 47% of localized extinctions among 976 studied species are linked to climate warming [16]. In Asia, approximately 70% of studied species are projected to be negatively impacted by climate change, with around 30% facing a high risk of extinction [17]. These changes disrupt ecosystems' structure and function, weakening their stability and resilience and leading to increased fragility and degradation. Furthermore, ecosystem degradation reduces the capacity of ecosystems to provide essential services. Studies suggest that climate change is causing a global redistribution of terrestrial ecosystems, with an estimated 9% loss in ecosystem services by 2100, which will severely diminish the benefits humans receive from ecosystems and pose direct threats to regional and global ecological security [18,19]. Meanwhile, increasing carbon emissions driven by rising human demands and temperatures exacerbate the ongoing degradation of ecosystem services, creating a vicious cycle of intensified human activity, persistent climate change, and ecosystem degradation, thereby posing significant challenges for both human society and ecosystems in adapting to climate change [20,21]. Therefore, quantifying and identifying the spatiotemporal trends of carbon emissions, while clarifying their relationship with ecosystem services, are essential for the synergistic development of emissions reduction and ecosystem service enhancement, thereby supporting sustainable ecosystem development and ensuring continued human benefits, ultimately contributing to carbon neutrality goals.

Well-managed ecosystems play a crucial role in helping human societies mitigate and adapt to current climate disasters and future climate change by providing a range of ecosystem services [22–24]. Ecological functional zones (EFZs), which are delineated based on characteristics such as ecosystem features, service patterns, and the spatial heterogeneity of natural conditions, are units that can enhance the effectiveness of ecosystem management. Implementing governance and management practices within these zones strengthens the overall capacity for ecosystem governance, management, and service delivery [25,26]. Guangdong Province serves as a vital ecological barrier in southern China, maintaining a vegetation coverage of over 0.7 from 2000 to 2020 [27–29]. It is a significant provider of ecosystem services, including water conservation, biodiversity, and the provision of agricultural and forestry products, playing an important role in sustaining human production and livelihoods in the region [30–32]. At the same time, Guangdong is China's leading industrial province, with carbon emissions in 2019 accounting for approximately 5.32% of the national total, making it one of the top five provinces for carbon emissions in China. In recent years, Guangdong has actively responded to the national "carbon neutrality" goals by promoting energy conservation and carbon reduction in the industrial sector, as well as establishing carbon sink forests [33]. While numerous studies on carbon emissions and ecosystem services in Guangdong Province have emerged [34,35], there is a notable lack of research on the relationship between carbon emissions and ecosystem services from the perspective of ecological functional zones.

In light of this, this study focused on Guangdong Province and adopted an ecological functional zone perspective. Utilizing a localized carbon emission valuation methodology, combined with multi-source spatiotemporal data and a spatialization method, the study developed an annual spatiotemporal carbon emission dataset and analyzed the spatiotemporal characteristics of carbon emissions across different ecological functional zones. By employing the ecosystem service value as a representation of ecosystem services, the study

explored the spatiotemporal relationship between carbon emissions and ecosystem services in various ecological functional zones, aiming to provide insights for emission reduction and the enhancement of ecosystem services. The study had the following objectives: (1) to quantify and identify the spatiotemporal evolution characteristics of carbon emissions in each ecological functional zone over the past 20 years; (2) to assess the value of ecosystem services and reveal their dynamic changes; and (3) to uncover the spatiotemporal relationship between carbon emissions and the value of ecosystem services, analyzing the impact of carbon emissions on ecosystem services.

2. Materials and Methods

2.1. Study Area

Guangdong Province is situated in southern China, with a total land area of 179,800 km^2, bordered by Fujian to the east, Jiangxi and Guangxi to the west, Hunan to the north, Hong Kong and Macao to the south, and Hainan Province to the southwest. The terrain varies from high in the north to low in the south, featuring a diverse range of landforms, including plains and plateaus in the south and mountains and hills in the north. The Nanling Mountains in the north and the southern coastal zone play a crucial role in China's ecological security strategy, known as the "two screens and three belts". The province's ecological environment is relatively fragile, susceptible to soil erosion caused by typhoons and heavy rains in hilly areas. The forest structure is simplistic, rendering the ecosystem fragile and vulnerable [36]. Guangdong Province is classified into different ecological function zones under "National Ecological Functional Zoning" [32], including the water conservation zone (WCZ), soil conservation zone (SCZ), agricultural products provision zone (APZ), forest product provision zone (FPZ), and metropolitan residential security zone (MRSZ) (Figure 1).

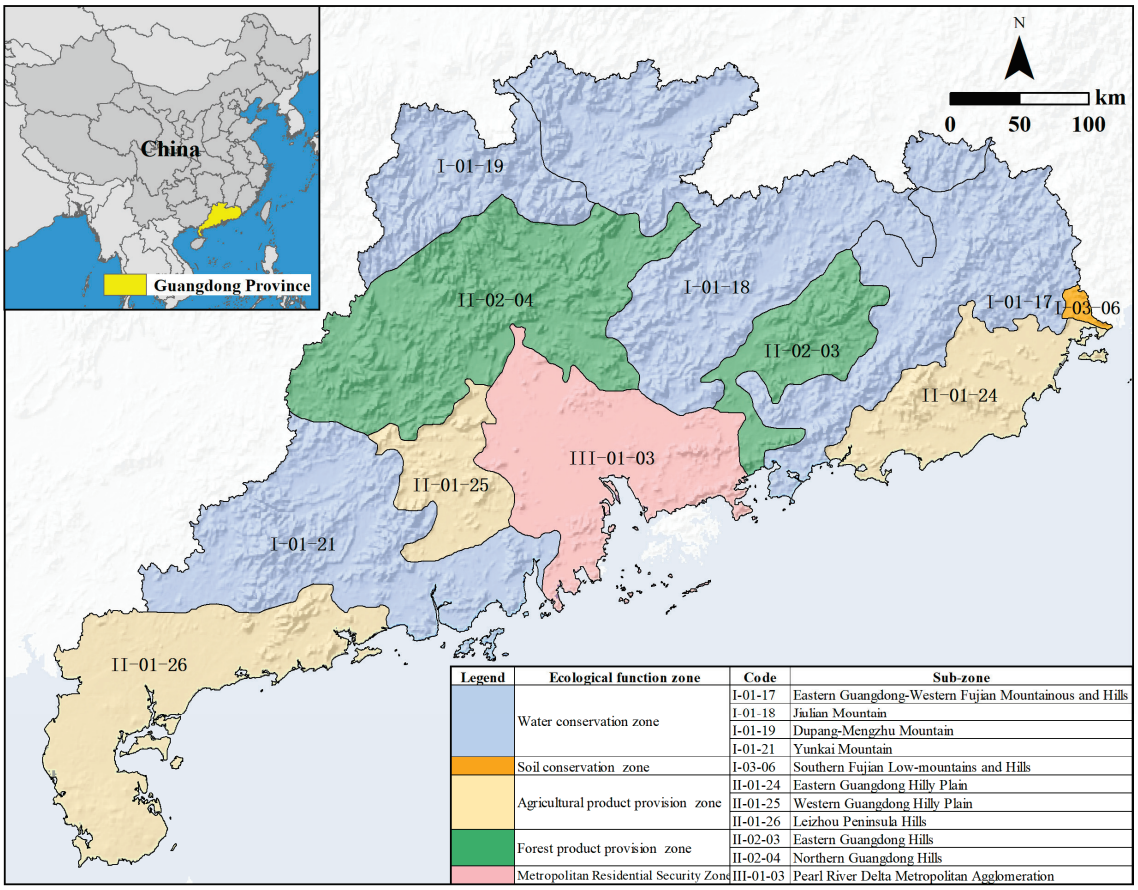

Figure 1. Study area.

2.2. Data Sources

The data used included:

(1) Land use data. The data from 2000 to 2019 were sourced from the China Annual Land Cover Dataset (CLCD) spanning from 1985 to 2019. This dataset is based on 335,709 land satellite images from Google Earth Engine. It was downloaded from Zenodo (https://zenodo.org/record/4417810, accessed on 10 January 2024) and has a spatial resolution of 30 m [37]. Data for the year 2020 were obtained from the Chinese Academy of Sciences Resource and Environmental Science Data Center (http://www.resdc.cn/, accessed on 10 January 2024), derived from LANDSAT TM/ETM+ remote sensing imagery and generated through the human–computer interactive interpretation of land use change remote sensing information, with a spatial resolution of 30 m [38,39]. This study classified the land use types from both datasets into arable land, forest land, grassland, water areas, construction land, and idle land.

(2) Nighttime light data. The dataset comprised DMPS/OLS annual products with a spatial resolution of 1 km for the period 2000–2013 and VIIRS/DNB annual products with a spatial resolution of 500 m for the years 2014–2020. All data were sourced from NOAA's National Geophysical Data Center (NGDC) (https://ngdc.noaa.gov/eog/dmsp/downloadV4composites.html, accessed on 12 January 2024).To match the land use data granularity, this study resampled the data to 30 m [40].

(3) Net ecosystem productivity (NEP) data. The data were derived from the global daily NEP simulation data product spanning from 1981 to 2019, downloaded from the National Ecosystem Science Data Center (http://nesdc.org.cn/, accessed on 14 January 2024) with a spatial resolution of 8 km. The NEP characterizes the flux of carbon exchange between terrestrial ecosystems and the atmosphere under undisturbed conditions, and it can be used to represent the carbon source–sink status of terrestrial ecosystems [41]. This data product was generated by simulating mechanistic ecological models, such as the BEPS model, driven by vegetation parameters (such as the leaf area index, clumping index, and land cover), remote sensing data, meteorological data, and the atmospheric CO_2 concentration [11]. In this study, through data computation and resampling, annual NEP data for the study area from 2000 to 2020 with a spatial resolution of 30 m were obtained.

(4) Statistical data. The data included information used for carbon emission accounting and revised ecosystem service values from 2000 to 2020. The main sources were the China Energy Statistical Yearbook, China Agricultural Statistical Yearbook, China Agricultural Products Price Survey Yearbook, Guangdong Statistical Yearbook, and Guangdong Rural Statistical Yearbook, the municipal statistical yearbooks of various cities in Guangdong Province, Environmental Status Bulletins, Solid Waste Pollution Prevention Information Announcements, and Environmental Statistical Yearbooks, with the data downloaded from CNKI (https://data.cnki.net/yearBook?type=type&code=A, accessed on 15 January 2024).

2.3. Research Design

This study combined remote sensing and multi-source statistical data to assess carbon emissions and ecosystem service values, while exploring the spatiotemporal relationship between carbon emissions and ecosystem services. First, by integrating land use data, energy statistics, NEP data, and localized carbon emission accounting methods, the study evaluated carbon emissions and spatialized the carbon emission data using nighttime light data, thereby analyzing the annual spatiotemporal trends in carbon emissions.

Second, ecosystem services were represented by the ecosystem service value. By integrating land use data with revised ecosystem service value coefficients, the study assessed the ecosystem services value and used the coefficient of variation to evaluate the spatial differences in the ecosystem service value across different ecological functional zones.

Last, based on Pearson correlation coefficients and bivariate Moran's I, the study explored the temporal and spatial relationships between carbon emissions and the ecosystem service value. The specific process is illustrated in Figure 2.

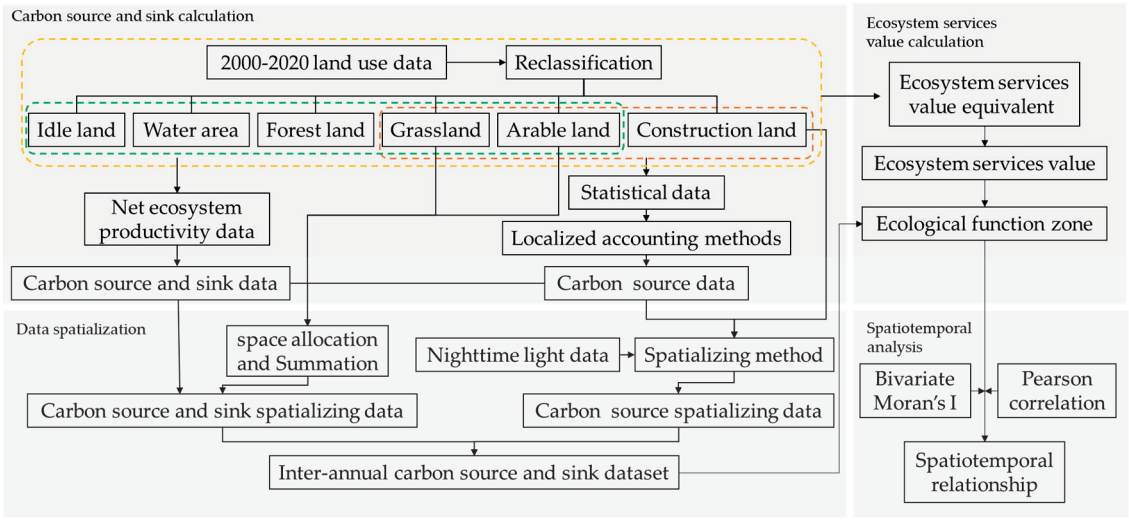

Figure 2. Illustration of the research design. Source: drawn by the author.

2.4. Methodology

2.4.1. The Assessment of Carbon Emissions

The assessment of carbon emission data was primarily based on land use data, NEP data, and energy consumption data. The carbon emissions and absorption for different land types were calculated individually: construction land mainly acts as a carbon source, and its carbon emissions were calculated based on energy consumption data using the methodology outlined in the Guidelines for the Compilation of Greenhouse Gas Inventories at the City, County, and District Levels of Guangdong Province [42]. The guidelines categorize carbon emission activities into five main processes: energy activities, industrial processes, agricultural processes, land use change and forestry, and waste treatment. Construction land involves three main processes: energy activities, industrial processes, and waste treatment. The specific calculation formula is as follows:

$$CE = A{*}EF \tag{1}$$

where CE is the carbon emissions, unit: kg; A is the energy consumption, unit: TJ; and EF is the emission factor, unit: kg/TJ. Specific accounting items and emission factors were referenced from the above-mentioned guideline.

Arable land and grassland primarily exhibit carbon absorption and emissions resulting from the carbon sink function and respiration of vegetation, as well as carbon emissions from human agricultural activities. The carbon absorption and emissions of vegetation were calculated based on NEP data.

The carbon emissions from human agricultural activities were calculated using the formulas for agricultural processes outlined in the Guidelines for the Compilation of Greenhouse Gas Inventories at the City, County, and District Levels of Guangdong Province. For arable land, the primary source of carbon emissions is paddy field emissions, while for grassland, the main sources are enteric fermentation and the management of manure from livestock.

Forest land, water areas, and idle land primarily exhibit carbon absorption resulting from their own carbon sink function and respiration, which was calculated based on NEP data. The difference between carbon emissions and carbon absorption represents the net carbon emissions.

2.4.2. The Spatialization of Carbon Emissions

Using land use data and nighttime light data to spatialize carbon absorption and emissions, this analysis was conducted for each land use type as follows.

For construction land, carbon absorption was not considered. Previous studies have established a linear relationship between nighttime light data and urban carbon emissions [43]. Therefore, carbon emission data were spatialized by fitting a linear relationship between nighttime light data and carbon emissions. The total carbon emissions calculated for each city within the study area were allocated spatially to obtain the carbon emission data for construction land.

For grassland and arable land, the annual number of grassland and arable land grids in each city was first counted. These data, combined with earlier calculations of carbon emissions from agricultural activities, allowed for the computation of carbon emissions per grid for arable land cultivation and grassland livestock management in each city. The calculated emissions were then assigned to the corresponding annual grassland and arable land grid data. Finally, the difference between the NEP values and the per-grid emission data for the arable land and grassland was calculated to derive the spatiotemporal distribution data of the annual net carbon emissions for these land types. The specific calculation formula is as follows:

$$CE_{ij} = NEP_{ij} + CE_a \tag{2}$$

where CE_{ij} is the carbon emissions of grid j of the i-th land use type, unit: kg; NEP_{ij} is the NEP of grid j of the i-th land use type, unit: kg; and CE_a is the average CE per grid, unit: kg.

For forest land, water areas, and idle land, carbon absorption and emissions were directly represented using NEP spatiotemporal distribution data. The specific calculation formula is as follows:

$$CE_{ij} = NEP_{ij} \tag{3}$$

where CE_{ij} is the carbon emission of grid j of the i-th land use type, unit: kg; NEP_{ij} is the NEP of grid j of the i-th land use type, unit: kg.

The spatiotemporal carbon emission data for each land use type were aggregated annually to produce the overall spatiotemporal distribution data of the carbon emissions for the study area from 2000 to 2020. Values less than 0 indicate a carbon sink, representing the absorption of atmospheric carbon, while values greater than 0 indicate a carbon source, representing emissions into the atmosphere. A value of 0 signifies no net carbon emissions.

2.4.3. The Assessment of the Ecosystem Service Value

Based on the research findings of Costanza et al. (1997), Xie et al. (2003) conducted a survey of multiple experts in the field of ecology in China to construct an ecosystem service value equivalency table for the country (Table 1) [44–46]. Building on this framework, the economic value generated by food production per unit area of Guangdong was calculated. The specific calculation method is as follows:

$$Ea = \frac{1}{7}\sum_{i=1}^{n}\frac{m_i p_i q_i}{M} \tag{4}$$

where Ea represents the economic value generated by food production per unit area (CNY/hectare). i denotes the type of crop, p_i is the national average price of crop i in a given year (CNY/ton), q_i is the yield per unit area of crop i (tons/hectare), m_i is the planting area of crop i (hectares), and M is the total planting area of all crops (hectares).

Combining the Ea calculation results with the ecosystem service value equivalent (Table 1), the adjusted ecosystem service value coefficients (Table 2) were calculated using land use data and these adjusted ecosystem service value coefficients, and the ecosystem service values were then computed. Specifically,

$$VC_i = ESVE_i \times Ea_i \tag{5}$$

$$ESV_i = \sum_{i=1}^{n} A_i \times VC_i \quad (6)$$

$$ESV = \sum_{i=1}^{n} ESV_i \quad (7)$$

where VC_i is the ecosystem service value coefficient for the i-th land use type, CNY/hectares, $ESVE_i$ is the ecosystem service value equivalent of the i-th land use type, dimensionless, and Ea_i is the Ea of the i-th land use type. ESV_i represents the ecosystem service value of the i-th land use type, CNY, A_i denotes the area of the i-th land use type, hectares, and ESV is the total ecosystem service value, CNY.

Table 1. The ecosystem service value equivalent per hectare.

	Provisioning Services	Regulating Services	Supporting Services	Cultural Services
Arable land	0.05	2.99	0.85	0.08
Forest land	1.13	13.02	4.62	0.93
Grassland	0.77	7.79	2.92	0.59
Water area	6.46	72.09	6.96	3.31
Construction land	0.00	0.00	0.00	0.00
Idle land	0.03	0.44	0.15	0.03

Note: The ecosystem service value equivalent is a dimensionless factor. According to the definition by Xie et al. (2003), one standard unit of the ecosystem service value equivalent factor refers to the annual economic value of the natural grain yield produced by 1 hectare of farmland with the national average yield [45].

Table 2. The ecosystem service value coefficient of Guangdong Province (CNY/hectare).

	Provisioning Services	Regulating Services	Supporting Services	Cultural Services
Arable land	73.96	4905.77	1388.74	123.26
Forest land	1861.23	21,402.13	7584.63	1524.32
Grassland	1260.00	12,797.18	4798.94	969.65
Water area	10,616.84	118,478.00	11,430.36	5439.90
Construction land	0.00	0.00	0.00	0.00
Idle land	49.30	723.13	246.52	49.30

Furthermore, the coefficient of variation was used to illustrate the spatial variability of ecosystem service values in different EFZs. The coefficient of variation reflects the degree of dispersion of a set of data around its mean. A higher coefficient of variation indicates a greater disparity in ecosystem service values within the study area. The calculation formula is as follows:

$$\mathrm{CV} = \frac{1}{\mathrm{ESV}_{p0}} \sqrt{\frac{\sum_{i=1}^{n} \left(\mathrm{ESV}_{pi} - \mathrm{ESV}_{p0}\right)^2}{n}} \quad (8)$$

where n is the number of EFZs, ESV_{pi} is the per-unit area ecosystem service value of the i-th EFZ, and ESV_{p0} is the average per-unit area ecosystem service value for the entire province.

2.4.4. The Analysis of the Spatiotemporal Relationship

(1) Pearson correlation

The Pearson correlation coefficient was used to analyze the temporal correlation between the net carbon emissions and ecosystem services value. The specific formula is as follows:

$$r_{xy} = \frac{\sum_{i=1}^{n} (x_i - \overline{x})(y_i - \overline{y})}{\sqrt{\sum_{i=1}^{n} (x_i - \overline{x})^2 \sum_{i=1}^{n} (y_i - \overline{y})^2}} \quad (9)$$

where r_{xy} represents the correlation between the net carbon emissions and ecosystem services value. When $r_{xy} > 0$, it indicates a positive correlation between the two variables; when $r_{xy} < 0$, it signifies a negative correlation. The larger the absolute value of r_{xy}, the stronger the correlation. When $r_{xy} = 0$, it implies no correlation between the variables. Here, x_i represents the time series data of the net carbon emissions, x represents the average value of the net carbon emissions, y_i represents the time series data of the ecosystem service values, and y represents the average value of the ecosystem service values. Additionally, a *t*-test was used for significance testing.

(2) Bivariate Moran's I

The bivariate Moran's I index was utilized to assess the spatial correlation between the net carbon emissions and ecosystem services with the following calculation formula:

$$I_{xy} = \frac{n}{\sum\sum w_{ij}} \cdot \frac{\sum\sum w_{ij}(x_i - \overline{x})(y_j - \overline{y})}{\sqrt{\sum(x_i - \overline{x})^2}\sqrt{\sum(y_j - \overline{y})^2}} \quad (10)$$

where I_{xy} represents the bivariate Moran's I index, n is the grid number of spatial units in the study area, x_i is the attribute value of variable x for neighboring region i and y_j is the attribute value of variable y for neighboring region j, and $\overline{x}$ and y are the mean attribute values of x and in the sample, respectively. w_{ij} is the spatial connectivity matrix between regions i and j.

The values of bivariate Moran′s I range from -1 to 1, where $I_{xy} > 0$ indicates a positive spatial correlation between the two variables, with higher values signifying a stronger positive correlation. Conversely, $I_{xy} < 0$ indicates a negative spatial correlation, with lower values indicating a more pronounced negative correlation. $I_{xy} = 0$ signifies a spatially random distribution.

The bivariate Local Indicators of Spatial Association (LISA) cluster map can illustrate the spatial association between two variables at a certain significance level. The clustering results can be categorized into four types: High–High (H-H), Low–Low (L-L), High–Low (H-L), and Low–High (L-H). H-H clustering indicates that both variables have high values, while L-L clustering indicates that both variables have low values. H-L clustering indicates that one variable has a high value while the other has a low value, whereas L-H clustering indicates that one variable has a low value while the other has a high value. H-H and L-L clustering suggest a positive correlation between the two variables, while H-L and L-H clustering indicate a negative correlation.

3. Results

3.1. Carbon Emissions in Ecological Function Zones

3.1.1. Changes in Carbon Emissions and Absorption

From 2000 to 2020, carbon emissions consistently exceeded carbon absorption in the study area. The total carbon emissions increased from 210.78 million tons to 503.96 million tons, representing an increase of 293.17 million tons, or 139.09%. In contrast, the total carbon absorption rose from 7.05 million tons to 21.15 million tons, marking an increase of 14.10 million tons, or 200%. The WCZ functioned as the primary carbon sink, contributing over 58% of total absorption during each period. The FPZ followed with approximately 24%, while the APZ contributed 13%. Both the SCZ and MRSZ accounted for less than 5%. In contrast, the MRSZ was the leading carbon source, responsible for around 60% of total emissions across all periods. The APZ followed with emissions comprising 20–30% of the total, while the WCZ and FPZ contributed approximately 10% and 5%, respectively. The SCZ represented the smallest share, with less than 1%.

There was a general trend of increasing carbon emissions and absorption across all ecological function zones over time (Figure 3). However, the rate of the increase in carbon emissions far exceeded that of carbon absorption, leading to a continuous rise in net carbon emissions. The MRSZ experienced the largest increase in carbon emissions at 164.31 million tons, followed by the APZ at 83.19 million tons, the WCZ at 29.25 million tons, the FPZ

at 16.26 million tons, and the SCZ at 0.17 million tons. In contrast, the WCZ recorded the largest increase in carbon absorption at 7.87 million tons, followed by the APZ at 1.89 million tons, the FPZ at 3.58 million tons, the SCZ at 0.06 million tons, and the MRSZ at 0.71 million tons.

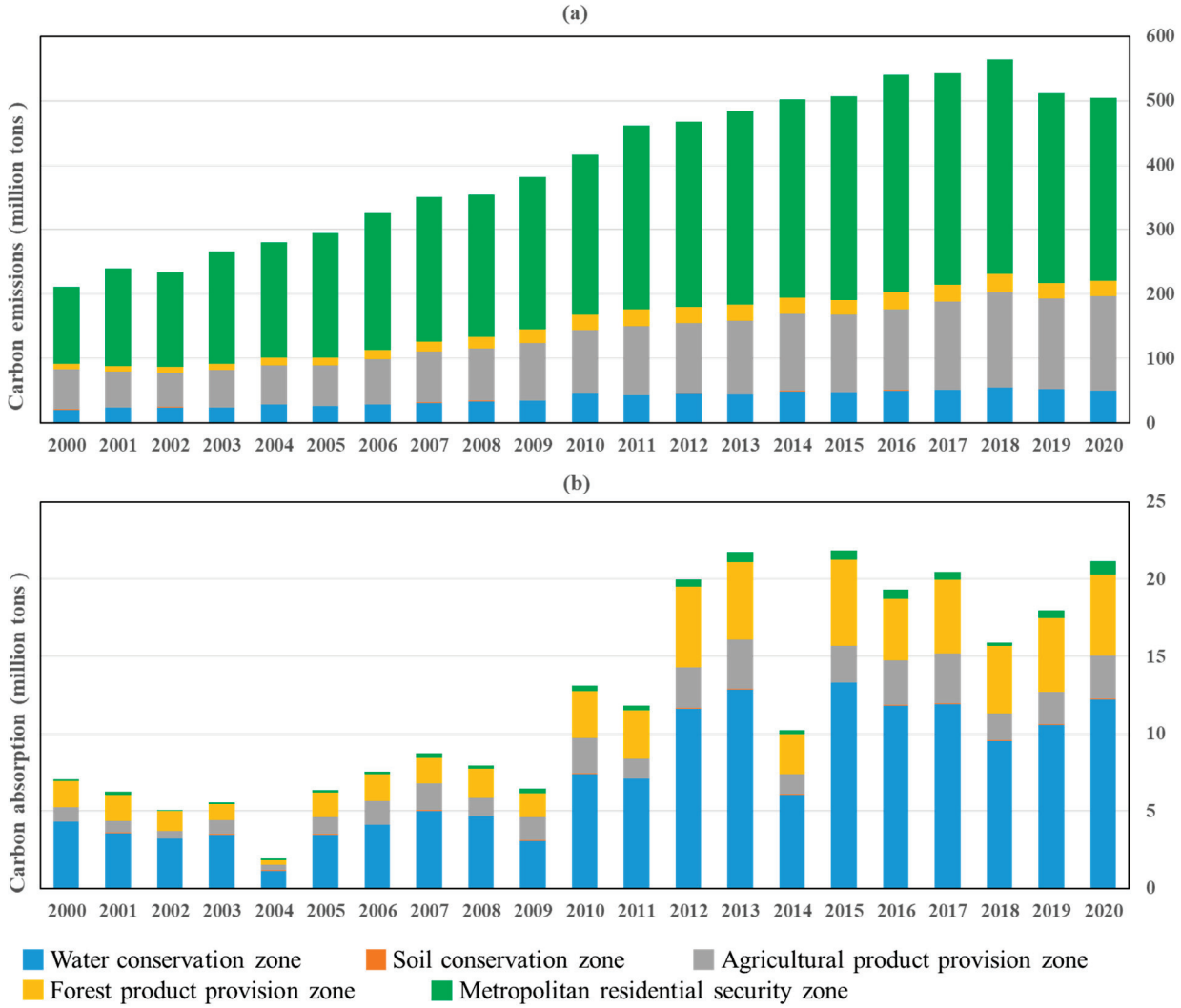

Figure 3. Carbon emissions (**a**) and carbon absorption (**b**) from 2000 to 2020 in each ecological function zone.

Ultimately, net carbon emissions increased from 203.73 million tons in 2000 to 482.80 million tons in 2020, representing an increase of 279.07 million tons, or 136.98%. The increments in the net carbon emissions for each ecological function zone were as follows: 163.61 million tons in the MRSZ, 81.30 million tons in the APZ, 21.38 million tons in the WCZ, 12.68 million tons in the FPZ, and 0.11 million tons in the SCZ.

3.1.2. Carbon Emission and Absorption Density

The MRSZ exhibited the highest carbon emission density, averaging 24.42 kg/m^2 over multiple years. The APZ, FPZ, and SCZ had multi-year averages of 9.69 kg/m^2, 7.03 kg/m^2, and 8.25 kg/m^2, respectively. In contrast, the WCZ had the lowest carbon emission density, with an average of 5.29 kg/m^2. All ecological functional zones demonstrated a gradual increase in the carbon emission density over time (Figure 4a).

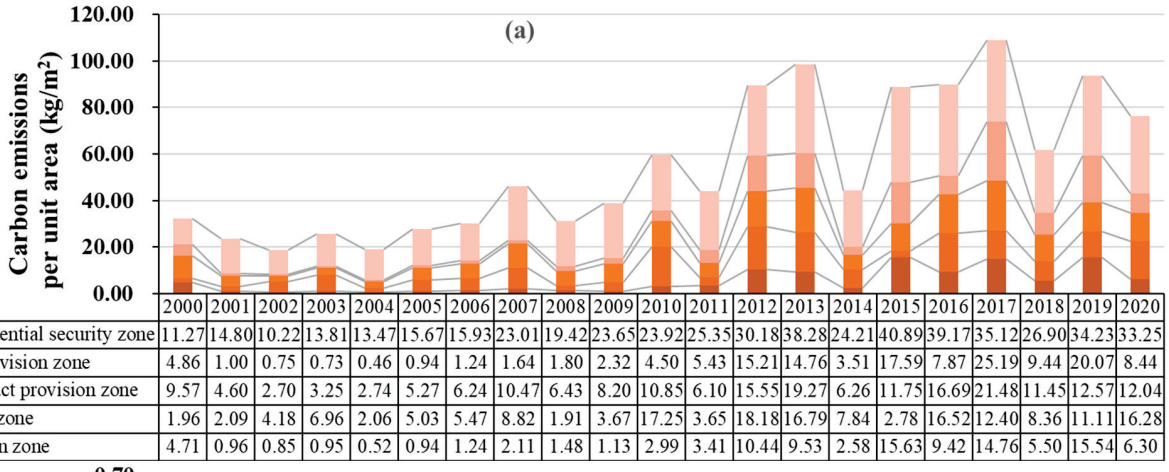

	2000	2001	2002	2003	2004	2005	2006	2007	2008	2009	2010	2011	2012	2013	2014	2015	2016	2017	2018	2019	2020
Metropolitan residential security zone	11.27	14.80	10.22	13.81	13.47	15.67	15.93	23.01	19.42	23.65	23.92	25.35	30.18	38.28	24.21	40.89	39.17	35.12	26.90	34.23	33.25
Forest product provision zone	4.86	1.00	0.75	0.73	0.46	0.94	1.24	1.64	1.80	2.32	4.50	5.43	15.21	14.76	3.51	17.59	7.87	25.19	9.44	20.07	8.44
Agricultural product provision zone	9.57	4.60	2.70	3.25	2.74	5.27	6.24	10.47	6.43	8.20	10.85	6.10	15.55	19.27	6.26	11.75	16.69	21.48	11.45	12.57	12.04
Soil conservation zone	1.96	2.09	4.18	6.96	2.06	5.03	5.47	8.82	1.91	3.67	17.25	3.65	18.18	16.79	7.84	2.78	16.52	12.40	8.36	11.11	16.28
Water conservation zone	4.71	0.96	0.85	0.95	0.52	0.94	1.24	2.11	1.48	1.13	2.99	3.41	10.44	9.53	2.58	15.63	9.42	14.76	5.50	15.54	6.30

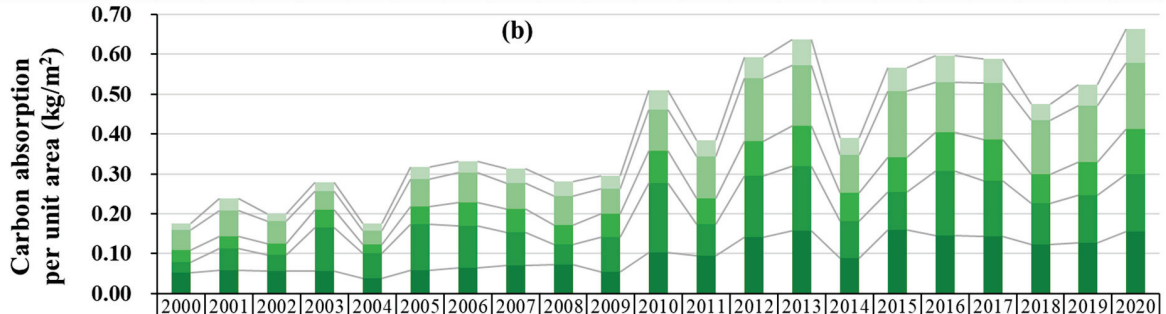

	2000	2001	2002	2003	2004	2005	2006	2007	2008	2009	2010	2011	2012	2013	2014	2015	2016	2017	2018	2019	2020
Metropolitan residential security zone	0.02	0.03	0.02	0.02	0.02	0.03	0.03	0.04	0.04	0.03	0.05	0.04	0.05	0.06	0.04	0.06	0.07	0.06	0.04	0.05	0.09
Forest product provision zone	0.05	0.06	0.06	0.05	0.03	0.07	0.07	0.06	0.07	0.06	0.10	0.10	0.16	0.15	0.09	0.17	0.13	0.14	0.14	0.14	0.16
Agricultural product provision zone	0.03	0.03	0.03	0.05	0.02	0.04	0.06	0.06	0.05	0.06	0.08	0.07	0.09	0.10	0.07	0.09	0.10	0.10	0.07	0.08	0.11
Soil conservation zone	0.03	0.05	0.04	0.11	0.06	0.12	0.10	0.08	0.05	0.09	0.17	0.08	0.15	0.16	0.09	0.10	0.16	0.14	0.10	0.12	0.14
Water conservation zone	0.05	0.06	0.06	0.06	0.04	0.06	0.06	0.07	0.07	0.06	0.10	0.10	0.14	0.16	0.09	0.16	0.15	0.14	0.12	0.13	0.16

Figure 4. Per-unit area carbon emissions (**a**) and carbon absorption (**b**) from 2000 to 2020 in each ecological function zone.

The carbon absorption density in the WCZ, FPZ, and SCZ was comparable, with each exhibiting a multi-year average of 0.01 kg/m^2. The APZ followed with an average of 0.07 kg/m^2, while the MRSZ had the lowest carbon absorption density, averaging 0.04 kg/m^2. Notably, all ecological functional zones demonstrated a gradual increase in the carbon absorption density over time (Figure 4b).

3.2. Ecosystem Service Value Changes in Ecological Function Zones

3.2.1. Changes in the Total Value of Ecosystem Services

In 2000, the total value of ecosystem services in Guangdong Province was CNY 596.96 billion. The values of provisioning services, regulating services, supporting services, and cultural services were CNY 28.25, 391.04, 144.88, and 32.79 billion, respectively (Figure 5). The WCZ had the highest ecosystem service value (ESV) at CNY 257.30 billion, followed by the FPZ with an ESV of CNY 202.74 billion. The APZ and MRSZ had ESVs of CNY 80.41 and 55.40 billion, respectively, while the SCZ had the lowest ESV at CNY 1.11 billion. Regulating services constituted approximately 70% of each zone's ESV, followed by supporting services at around 20%, with provisioning and cultural services each making up about 5%.

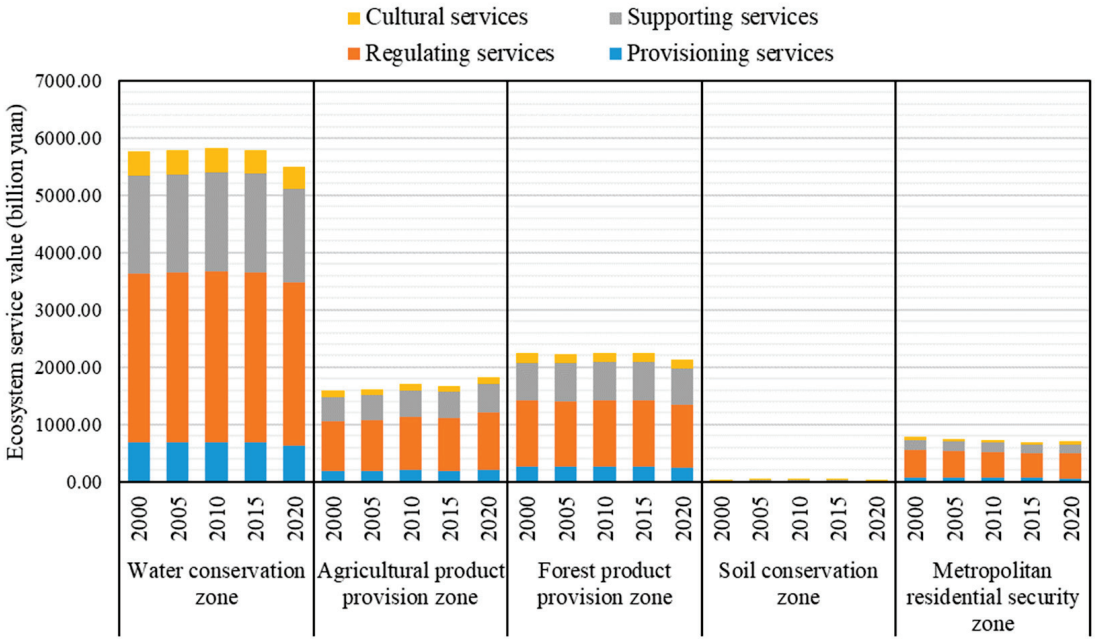

Figure 5. Ecosystem services value from 2000 to 2020 in each ecological function zone.

From 2000 to 2020, the total ESV decreased by CNY 92.39 billion, representing a decline of 15.48%. The values of regulating services, supporting services, and cultural services fell by CNY 38.08, 44.81, and 10.87 billion, respectively, while provisioning services increased by CNY 1.36 billion. The ESV declined in all EFZs except for the APZ, which experienced a notable increase of CNY 20.42 billion. The FPZ saw the largest decrease, losing CNY 105.12 billion, while the WCZ, SCZ, and MRSZ experienced smaller reductions of CNY 3.37, 0.06, and 4.27 billion, respectively.

In terms of the annual average ESV per unit area, the FPZ had the highest value at 2.99 million CNY/km^2, followed by the WCZ, MRSZ, and SCZ with values of 2.99, 2.87, and 2.64 million CNY/km^2, respectively. The APZ had the lowest value at 2.32 million CNY/km^2.

3.2.2. Spatial Changes in Ecosystem Service Value

From the perspective of the coefficient of variation, the spatial differences in the ESV among the EFZs have gradually expanded (Figure 6). From 2000 to 2020, the coefficient of variation exhibited a general upward trend, indicating an increasing degree of spatial variation. Specifically, within the study area, the coefficient of variation first increased, then decreased, showing fluctuations from 2000 to 2008. Starting in 2008, it continued to rise until it experienced a slight decline in 2020.

3.3. The Relationship Between Carbon Emissions and the Ecosystem Service Value

3.3.1. Quantitative Relationship

Based on the results of the Pearson correlation coefficients, the net carbon emissions in Guangdong Province were negatively correlated with the total ecosystem service value, exhibiting a correlation coefficient of −0.4161 ($p = 0.06 < 0.1$). Additionally, the net carbon emissions displayed varying degrees of correlation with different ecosystem service values: they showed a positive correlation with the provisioning services value, while exhibiting negative correlations with the other three service values. However, these correlations were not statistically significant (Table 3).

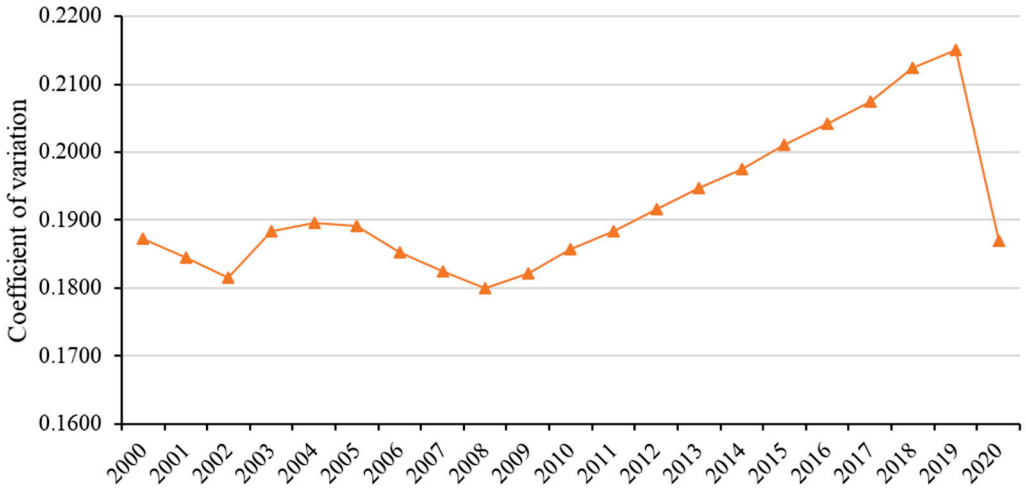

Figure 6. Coefficient of variation in ecosystem services value from 2000 to 2020.

Table 3. Pearson correlation coefficients between net carbon emissions and ecosystem service values.

	Net Carbon Emissions					
	Guangdong Province	**Water Conservation Zone**	**Agricultural Products Provision Zone**	**Forest Product Provision Zone**	**Soil Conservation Zone**	**Metropolitan Residential Security Zone**
Total ecosystem services value	−0.4161 *	0.0390	0.5297 ***	−0.3784 *	0.3376	−0.8565 ***
Provisioning services value	0.0342	0.1509	0.5955 ***	0.6245 *	0.3566	−0.8133 ***
Regulating services value	−0.4504	0.0623	0.5497 ***	−0.3741 *	0.3428	−0.8561 ***
Supporting services value	−0.3716	−0.0381	0.7244 ***	−0.3837 *	0.3142	−0.8906 ***
Cultural services value	−0.3780	0.0525	0.6534 ***	−0.3829 *	0.3387	−0.8259 ***

Note: *** and *, respectively, indicate significance at the 1% and 10% levels.

The relationship between the net carbon emissions and total ecosystem service values varied across different EFZs (Table 3).

Specifically, in the APZ, there was a significant positive correlation between the net carbon emissions and total ecosystem service value (R = 0.5297; $p < 0.01$), indicating that as the net carbon emissions increase, the total ecosystem service value also increases. Moreover, net carbon emissions in the APZ exhibited significant positive correlations with all four ecosystem services. The strongest correlation was with the supporting service value (R = 0.7244), followed by the cultural service value (R = −0.6534). The correlation coefficients for the provisioning service value and regulation service value were below 0.6.

In the MRSZ, the net carbon emissions showed a significant negative correlation with the total ecosystem service value (R = −0.8565; $p < 0.01$), suggesting that higher carbon emissions are associated with declines in ecosystem services. Moreover, net carbon emissions in the MRSZ were significantly negatively correlated with the four ecosystem service values, with the absolute correlation coefficients all exceeding 0.8.

Additionally, in the FPZ, there was a significant negative correlation between the net carbon emissions and the total ecosystem service value (R = −0.3784; $p < 0.1$). However, the relationship between the net carbon emissions and individual ecosystem service values in the FPZ was more complex. The net carbon emissions exhibited a positive correlation with the provisioning service value but negative correlations with the other three service values. Notably, the positive correlations were stronger than the negative ones.

In both the WCZ and SCZ, there was no significant correlation between the net carbon emissions and the total ecosystem service value. Among the correlations between the net carbon emissions and individual ecosystem service values, only in the WCZ was there a non-significant negative correlation with the supporting service value, while all other correlations in both zones were non-significant positive correlations.

3.3.2. Spatial Relationship

The spatial relationship between the net carbon emissions and total ecosystem service value was complex, often showing a random distribution, with consistent clustering primarily observed in the APZ and MRSZ (Figure 7).

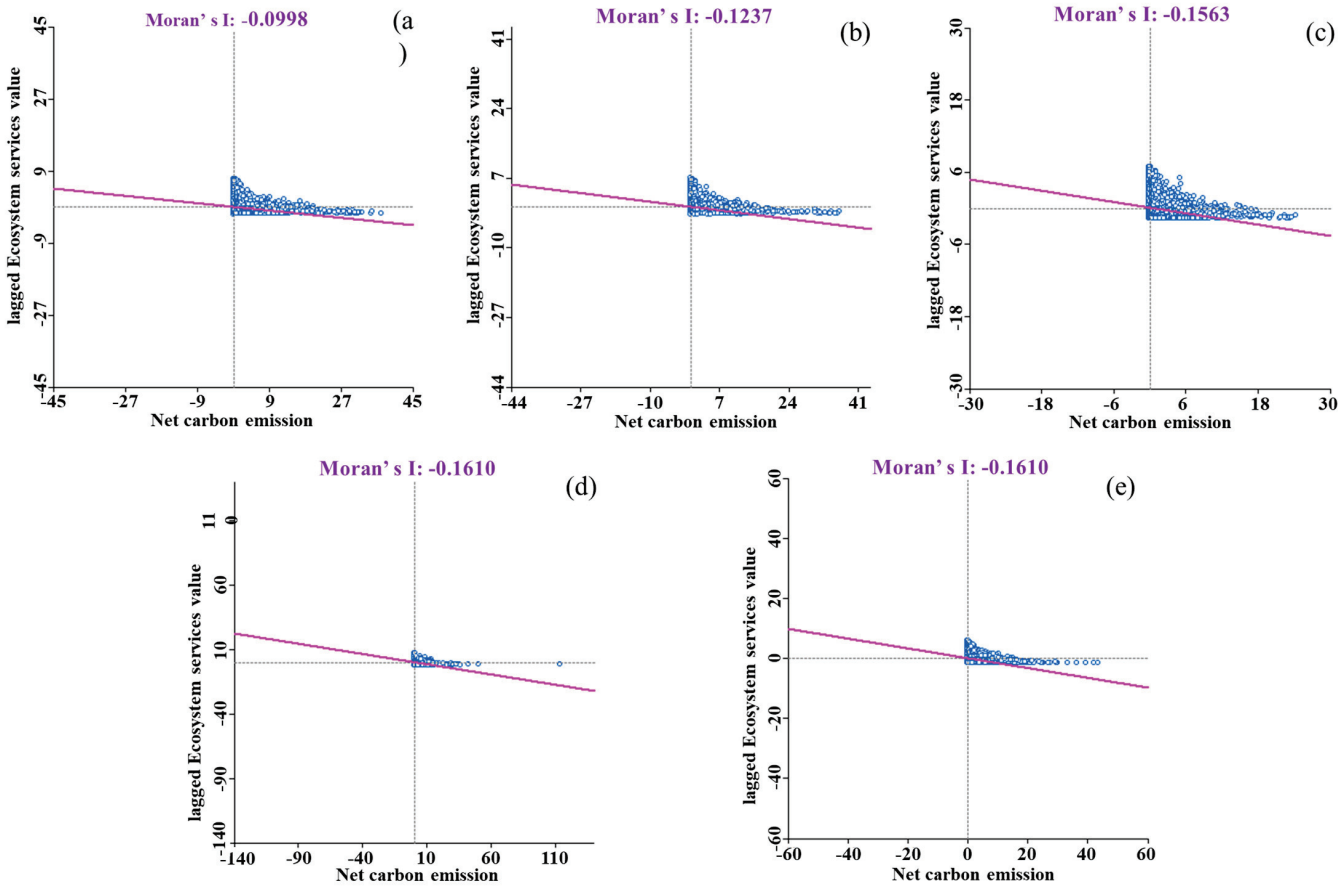

Figure 7. Bivariate Moran's I in 2000 (**a**), 2005 (**b**), 2010 (**c**), 2015 (**d**), and 2020 (**e**).

Specifically, according to the results of bivariate Moran's I from 2000 to 2020, a spatial negative correlation existed between the net carbon emissions and total ecosystem service value in Guangdong Province ($p < 0.01$, $Z < -1.96$). The degree of this negative correlation initially increased and then declined over time. The bivariate Moran's I values for each period approached zero, reflecting the random spatial distribution of the net carbon emissions and the total ecosystem service value.

The spatial clustering patterns for each period further confirm this randomness. From 2000 to 2020, the spatial relationship between the net carbon emissions and the total ecosystem service values was not significant in most areas, indicating that the spatial complexity cannot be captured by a simple linear relationship. The proportion of non-significant areas increased from 72% in 2000 to 74.56% in 2020. These non-significant clusters were predominantly found in the WCZ, APZ, and FPZ, which accounted for more than 40%, 8%, and 16% of the total area, respectively, across all periods (Figure 8).

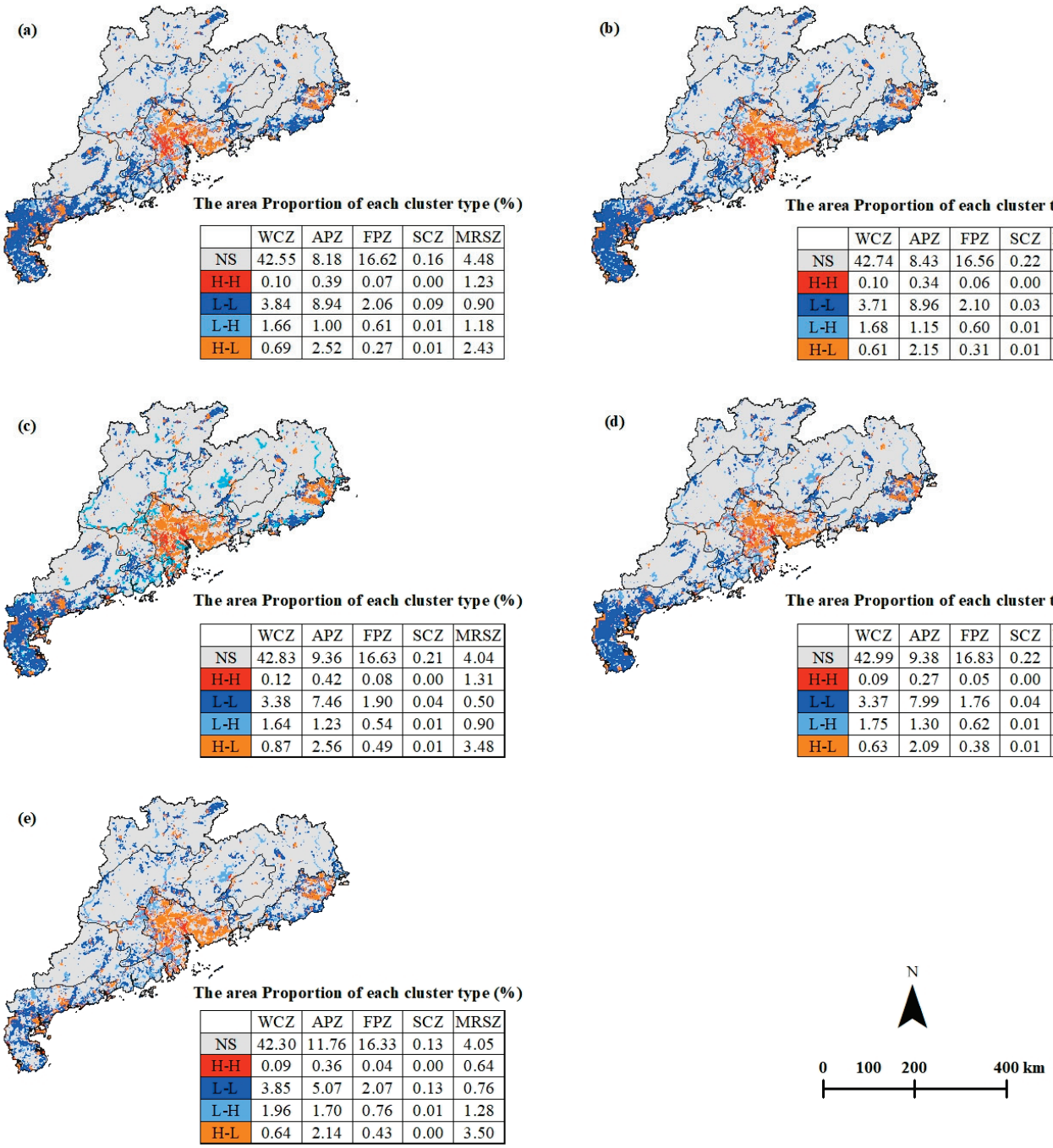

	WCZ	APZ	FPZ	SCZ	MRSZ
NS	42.55	8.18	16.62	0.16	4.48
H-H	0.10	0.39	0.07	0.00	1.23
L-L	3.84	8.94	2.06	0.09	0.90
L-H	1.66	1.00	0.61	0.01	1.18
H-L	0.69	2.52	0.27	0.01	2.43

	WCZ	APZ	FPZ	SCZ	MRSZ
NS	42.74	8.43	16.56	0.22	4.22
H-H	0.10	0.34	0.06	0.00	1.24
L-L	3.71	8.96	2.10	0.03	0.73
L-H	1.68	1.15	0.60	0.01	1.08
H-L	0.61	2.15	0.31	0.01	2.97

	WCZ	APZ	FPZ	SCZ	MRSZ
NS	42.83	9.36	16.63	0.21	4.04
H-H	0.12	0.42	0.08	0.00	1.31
L-L	3.38	7.46	1.90	0.04	0.50
L-H	1.64	1.23	0.54	0.01	0.90
H-L	0.87	2.56	0.49	0.01	3.48

	WCZ	APZ	FPZ	SCZ	MRSZ
NS	42.99	9.38	16.83	0.22	3.99
H-H	0.09	0.27	0.05	0.00	0.80
L-L	3.37	7.99	1.76	0.04	0.75
L-H	1.75	1.30	0.62	0.01	1.09
H-L	0.63	2.09	0.38	0.01	3.60

	WCZ	APZ	FPZ	SCZ	MRSZ
NS	42.30	11.76	16.33	0.13	4.05
H-H	0.09	0.36	0.04	0.00	0.64
L-L	3.85	5.07	2.07	0.13	0.76
L-H	1.96	1.70	0.76	0.01	1.28
H-L	0.64	2.14	0.43	0.00	3.50

Figure 8. Spatial clustering of net carbon emissions and ecological service value in 2000 (**a**), 2005 (**b**), 2010 (**c**), 2015 (**d**) and 2020 (**e**). WCZ, APZ, FPZ, SCZ, MRSZ refer to water conservation zone, soil conservation zone, agricultural products provision zone, forest product provision zone, and metropolitan residential security zone, respectively. NS, H-H, L-L, L-H, and H-L indicate different types of spatial clustering: NS denotes not significant, H-H represents High–High clustering, L-L indicates Low–Low clustering, L-H refers to Low–High clustering, and H-L denotes High–Low clustering. In these clustering types, *L* signifies low net carbon emissions or a low ecosystem service value, while *H* represents high net carbon emissions or a high ecosystem service value.

Approximately 30% of the study area exhibited clustered patterns, predominantly of the L-L type, where low net carbon emissions and low ecosystem service values co-occurred. The proportion of L-L clusters remained above 11% throughout the study period,

gradually declining from 15.83% in 2000 to 11.88% in 2020, with more than half of these clusters consistently located in the APZ.

The next most common clustering type was H-L, characterized by high net carbon emissions and low ecosystem service values. The proportion of H-L clusters increased over time, rising from 5.93% in 2000 to 6.72% in 2020. These clusters were mainly found in the APZ and MRSZ, with both zones accounting for over 2% of the total area during each period.

The L-H clustering type, where low net carbon emissions and high ecosystem service values clustered together, accounted for more than 4% of the total area in each period, increasing from 4.46% in 2000 to 5.17% in 2020. These clusters were mainly distributed across the WCZ, APZ, and MRSZ, with each zone accounting for more than 1% of the total area.

The H-H clustering type, where high net carbon emissions and high ecosystem service values clustered, never exceeded 2% of the total area in any period and showed a decreasing trend from 1.79% in 2000 to 1.13% in 2020. These clusters were primarily located in the MRSZ.

4. Discussion

4.1. Results Validation

In calculating carbon emissions, this study adopted a localized method to assess the carbon emissions. The results were validated using data from the Carbon Emission Accounts and Datasets (CEADs, www.ceads.net.cn, accessed on 14 March 2024), revealing an error margin of less than 6% for the period from 2014 to 2018, which is acceptable. Additionally, the results of this study were compared with those of Zhu et al. (2015) and Huang et al. (2023). The former used a land use-based approach, while the latter applied the Guidelines for Preparing Provincial Greenhouse Gas Inventories issued by the National Development and Reform Commission in 2011 [34,47]. The carbon emission estimates from this study fell between the two, showing the same temporal trends, further demonstrating the reliability of this study's assessment results. For the calculation of the ecosystem service value (ESV), this study's ESV estimates were compared with the results of Ye et al. (2021) for Guangdong Province in 2020 [35]. The error margin was found to be below 4% with consistent trends, which indicates the validity of this study's evaluation results.

Regarding the relationship between carbon emissions and the ecosystem service value, no prior studies have addressed the relationship between carbon emissions and the ESV in ecological functional zones in Guangdong Province. Zhang et al. (2023), in their study on the Guanzhong urban agglomeration, found a significant negative correlation between carbon emissions and the ecosystem service value [12]. Drawing a parallel between their findings on urban agglomerations and the results for the metropolitan residential security zone (MRSZ) in this study, a similar significant negative correlation was observed. In human-aggregated regions, although the degree of correlation varied, a consistent negative correlation existed, further corroborating the validity of this study's findings.

In conclusion, the evaluation results of this study are valid. The findings provide a clear and accurate explanation of carbon emissions, the ecosystem service value, and their relationship in Guangdong Province. The results offer valuable data references for related studies within Guangdong Province and for comparative research in other regions.

4.2. The Exploration of Carbon Emission Reduction and Sink Enhancement

Enhancing ecosystems' carbon sink capacity and reducing emissions from human activities are key strategies for achieving the dual carbon goals [48,49]. Guangdong Province has made notable progress in this regard. During the 13th Five-Year Plan, the province's forest coverage increased from 56.92% to 58.66%, and the forest stock volume grew from 502 to 584 million cubic meters, resulting in a forest carbon sink storage capacity of 310 million tons. For the 14th Five-Year Plan, Guangdong aims to further enhance its carbon sink capacity by improving forest quality and promoting ecological restoration. By 2025, the province

plans to establish 333,000 hectares of high-quality water source conservation forests and 63,000 hectares of coastal protective forests through forest optimization and structural adjustments [50]. It is important to note that vegetation's carbon sink capacity is influenced by factors such as the species, climate, and area [16]. Identifying the emission thresholds for optimizing vegetation's carbon sink potential and addressing carbon sink saturation are key challenges in balancing emission reduction efforts with increased carbon absorption.

This study found that carbon absorption by ecosystems was much lower than carbon emissions, making it impossible to achieve carbon neutrality through ecosystems alone in the short term. In 2022, Guangdong's Carbon Peak Implementation Plan proposed adjustments in industrial, energy, and transportation structures to meet the dual carbon goals [51]. However, the study reveals significant spatial disparities in carbon emissions across the province, while the province's current "dual carbon" strategies exhibit a lack of regional differentiation and specificity, relying on largely uniform approaches [52]. Previous studies have categorized Guangdong's 21 cities into different carbon emission types based on the GDP and carbon emissions, proposing corresponding reduction priorities [53,54]. However, such classifications fail to account for regional natural environmental characteristics and overlook the ecological functions of different areas.

This study also highlights significant differences in CEs, the ESV, and their relationships across ecological functional zones. To achieve the dual goals of carbon neutrality and ecological environmental protection, targeted emission reduction and carbon sink enhancement measures are needed for each ecological zone. In the APZ and MRSZ, where CEs and the ESV were strongly correlated, strategies should balance ecological conservation with emission reduction. In the APZ, improving agricultural land ecology and transitioning energy use will enhance carbon sequestration. In the MRSZ, reducing high carbon emissions through structural adjustments in energy, industry, and transportation, alongside creating ecological landscapes, can support green development. For other regions with more variable relationships between CEs and the ESV, energy structure adjustments remain necessary. In the WCZ, ecological protection and restoration should focus on enhancing both water conservation and carbon sequestration. In the FPZ, expanding the forest area and improving biodiversity can strengthen carbon sequestration. In the SCZ, afforestation, engineering projects, and sustainable farming practices should enhance both soil conservation and the carbon sink capacity.

4.3. Limitations and Prospects

This study, based on extensive data collection and processing, investigated the relationship between carbon emissions and ecosystem services from the perspective of ecological functional zones. It analyzed the impact of carbon emissions on ecosystem services, as well as effective ways to reduce emissions, increase carbon absorption, and enhance ecosystem service values. However, the study did not further analyze the mechanisms linking carbon emissions and ecosystem services. Future research can delve deeper into the following areas: (1) Mechanisms influencing the relationship between regional carbon emissions and ecosystem services: this involves developing an indicator system to identify the factors affecting the relationship between carbon emissions and ecosystem services, thereby uncovering the mechanisms underlying this relationship. (2) Synergy between carbon neutrality and ecosystem services: Build a synergistic model for reducing emissions, increasing carbon absorption, and enhancing ecosystem services based on this study. Analyze the critical thresholds for these synergies under the dual pressures of human activity and extreme climate events, providing valuable results for the coordinated development of carbon neutrality and ecosystem services.

5. Conclusions

This study developed localized time series data on carbon emissions and ecosystem service values using multi-source data and diverse methodologies. It explored the temporal and spatial relationships between carbon emissions and ecosystem service values from the

perspective of ecological function zones. The findings reveal the following trends from 2000 to 2020:

(1) Both carbon emissions and absorption have gradually increased over time, with the increment in carbon emissions far exceeding that of carbon absorption. The total carbon emissions rose from 210.78 million tons to 503.96 million tons, an increase of 293.17 million tons, while carbon absorption increased from 7.05 million tons to 21.15 million tons, an increase of 14.10 million tons. The WCZ was the dominant carbon sink area, while the MRSZ was the dominant carbon source area.

(2) The total value of ecosystem services decreased from CNY 596.95 billion to CNY 504.56 billion, representing a decline of CNY 92.39 billion. The WCZ had the highest ESV, consistently accounting for more than 50% of the total. The FPZ, APZ, and MRSZ accounted for approximately 30%, 16%, and over 9% of the total ESV, respectively, while the SCZ accounted for the smallest proportion, less than 1%.

(3) There was a negative correlation between the net carbon emissions and the total ecosystem service values, both temporally and spatially. Specifically, the net carbon emissions in the MRSZ and APZ exhibited significant correlations with the total ecosystem service values over time, with the former showing a negative correlation and the latter a positive correlation. Spatially, the distribution of the net carbon emissions and ecosystem service values was predominantly random, with clustering patterns primarily reflecting L-L and H-L clustering types, mainly found in the APZ and MRSZ.

This research elucidates the temporal and spatial evolution trends of carbon emissions and ecosystem services in different ecological functional zones. These findings provide a scientific reference for subsequent efforts in emission reduction, carbon absorption, and habitat protection in the study area.

Author Contributions: Conceptualization, Y.L. and H.C.; methodology, Y.L. and H.C.; software, Y.L.; validation, H.C. and J.X.; formal analysis, Y.L.; investigation, Y.L.; resources, J.X.; data curation, H.C.; writing—original draft preparation, Y.L.; writing—review and editing, H.C. and J.X.; visualization, Y.L.; supervision, H.C.; project administration, J.X.; funding acquisition, Y.L. and H.C. All authors have read and agreed to the published version of the manuscript.

Funding: This research was funded by the National Natural Science Foundation of China, grant numbers 42301322 and 42071204.

Data Availability Statement: Data will be made available on request.

Conflicts of Interest: Author Jingyu Xiao was employed by the company Shenzhen New Land Tool Planning & Architectural Design Co., Ltd. The remaining authors declare that the research was conducted in the absence of any commercial or financial relationships that could be construed as a potential conflict of interest.

References

1. Kilkis, S.; Krajacic, G.; Duic, N.; Rosen, M.A.; Al-Nimr, M.d.A. Advances in integration of energy, water and environment systems towards climate neutrality for sustainable development. *Energy Convers. Manag.* **2020**, *225*, 113410. [CrossRef]
2. Hegerl, G.; Zwiers, F. Use of models in detection and attribution of climate change. *Wiley Interdiscip. Rev.-Clim. Change* **2011**, *2*, 570–591. [CrossRef]
3. Yue, X.-L.; Gao, Q.-X. Contributions of natural systems and human activity to greenhouse gas emissions. *Adv. Clim. Change Res.* **2018**, *9*, 243–252. [CrossRef]
4. IPCC. *Climate Change 2021: The Physical Science Basis. Contribution of Working Group I to the Sixth Assessment Report of the Intergovernmental Panel on Climate Change*; Cambridge University Press: Cambridge, UK; New York, NY, USA, 2021.
5. IPCC. *Climate Change 2023: Synthesis Report. Contribution of Working Groups I, II and III to the Sixth Assessment Report of the Intergovernmental Panel on Climate Change*; IPCC: Geneva, Switzerland, 2023.
6. WMO. *State of the Global Climate 2023*; WMO: Geneva, Switzerland, 2023.
7. Piao, S.; He, Y.; Wang, X.; Chen, F. Estimation of China's terrestrial ecosystem carbon sink: Methods, progress and prospects. *Sci. China-Earth Sci.* **2022**, *65*, 641–651. [CrossRef]
8. Liu, Y.; Piao, S.; Gasser, T.; Ciais, P.; Yang, H.; Wang, H.; Keenan, T.F.; Huang, M.; Wan, S.; Song, J.; et al. Field-experiment constraints on the enhancement of the terrestrial carbon sink by CO_2 fertilization. *Nat. Geosci.* **2019**, *12*, 809–814. [CrossRef]

9. Yu, Z.; Ciais, P.; Piao, S.; Houghton, R.A.; Lu, C.; Tian, H.; Agathokleous, E.; Kattel, G.R.; Sitch, S.; Goll, D.; et al. Forest expansion dominates China's land carbon sink since 1980. *Nat. Commun.* **2022**, *13*, 5374. [CrossRef]
10. Sha, Z.; Bai, Y.; Li, R.; Lan, H.; Zhang, X.; Li, J.; Liu, X.; Chang, S.; Xie, Y. The global carbon sink potential of terrestrial vegetation can be increased substantially by optimal land management. *Commun. Earth Environ.* **2022**, *3*, 8. [CrossRef]
11. Chen, J.M.; Ju, W.; Ciais, P.; Viovy, N.; Liu, R.; Liu, Y.; Lu, X. Vegetation structural change since 1981 significantly enhanced the terrestrial carbon sink. *Nat. Commun.* **2019**, *10*, 4259. [CrossRef] [PubMed]
12. Zhang, R.; Yu, K.; Luo, P.; Chaplot, V. Spatio-Temporal Relationship between Land Use Carbon Emissions and Ecosystem Service Value in Guanzhong, China. *Land* **2024**, *13*, 118. [CrossRef]
13. Griscom, B.W.; Adams, J.; Ellis, P.W.; Houghton, R.A.; Lomax, G.; Miteva, D.A.; Schlesinger, W.H.; Shoch, D.; Siikamaki, J.V.; Smith, P.; et al. Natural climate solutions. *Proc. Natl. Acad. Sci. USA* **2017**, *114*, 11645–11650. [CrossRef] [PubMed]
14. Jones, J.A.; Driscoll, C.T. Long-Term Ecological Research on Ecosystem Responses to Climate Change. *Bioscience* **2022**, *72*, 814–826. [CrossRef] [PubMed]
15. Malhi, Y.; Franklin, J.; Seddon, N.; Solan, M.; Turner, M.G.; Field, C.B.; Knowlton, N. Climate change and ecosystems: Threats, opportunities and solutions. *Philos. Trans. R. Soc. B-Biol. Sci.* **2020**, *375*, 20190104. [CrossRef] [PubMed]
16. Wiens, J.J. Climate-Related Local Extinctions Are Already Widespread among Plant and Animal Species. *PLoS Biol.* **2016**, *14*, e2001104. [CrossRef] [PubMed]
17. IPCC. *Climate Change 2022: Impacts, Adaptation and Vulnerability*; IPCC: Geneva, Switzerland, 2022.
18. Bastien-Olvera, B.A.; Conte, M.N.; Dong, X.; Briceno, T.; Batker, D.; Emmerling, J.; Tavoni, M.; Granella, F.; Moore, F.C. Unequal climate impacts on global values of natural capital. *Nature* **2024**, *625*, 722–727. [CrossRef] [PubMed]
19. Weiskopf, S.R.; Rubenstein, M.A.; Crozier, L.G.; Gaichas, S.; Griffis, R.; Halofsky, J.E.; Hyde, K.J.W.; Morelli, T.L.; Morisette, J.T.; Munoz, R.C.; et al. Climate change effects on biodiversity, ecosystems, ecosystem services, and natural resource management in the United States. *Sci. Total Environ.* **2020**, *733*, 137782. [CrossRef] [PubMed]
20. Pfenning-Butterworth, A.; Buckley, L.B.; Drake, J.M.; Farner, J.E.; Farrell, M.J.; Gehman, A.-L.M.; Mordecai, E.A.; Stephens, P.R.; Gittleman, J.L.; Davies, T.J. Interconnecting global threats: Climate change, biodiversity loss, and infectious diseases. *Lancet Planet. Health* **2024**, *8*, e270–e283. [CrossRef]
21. Robinson, A.; Lehmann, J.; Barriopedro, D.; Rahmstorf, S.; Coumou, D. Increasing heat and rainfall extremes now far outside the historical climate. *npj Clim. Atmos. Sci.* **2021**, *4*, 45. [CrossRef]
22. Bustamante, M.M.C.; Silva, J.S.; Scariot, A.; Sampaio, A.B.; Mascia, D.L.; Garcia, E.; Sano, E.; Fernandes, G.W.; Durigan, G.; Roitman, I.; et al. Ecological restoration as a strategy for mitigating and adapting to climate change: Lessons and challenges from Brazil. *Mitig. Adapt. Strateg. Glob. Change* **2019**, *24*, 1249–1270. [CrossRef]
23. Scarano, F.R. Ecosystem-based adaptation to climate change: Concept, scalability and a role for conservation science. *Perspect. Ecol. Conserv.* **2017**, *15*, 65–73. [CrossRef]
24. Pramova, E.; Locatelli, B.; Brockhaus, M.; Fohlmeister, S. Ecosystem services in the National Adaptation Programmes of Action. *Clim. Policy* **2012**, *12*, 393–409. [CrossRef]
25. Deng, Z.-Y.; Cao, J.-S. Incorporating ecosystem services into functional zoning and adaptive management of natural protected areas as case study of the Shennongjia region in China. *Sci. Rep.* **2023**, *13*, 18870. [CrossRef]
26. Li, H.-R.; Ma, S.; Zhang, M.; Yin, Y.-K.; Wang, L.-J.; Jiang, J. Determinants of ecological functional zones in the Qinghai-Tibet Plateau ecological shelter at different scales in 2000 and 2015: From the perspective of ecosystem service bundles. *Ecol. Indic.* **2023**, *154*, 110743. [CrossRef]
27. Feng, X.; Zeng, Z.; He, M. A 20-year vegetation cover change and its response to climate factors in the Guangdong-Hong Kong-Macao Greater Bay Area under the background of climate change. *Front. Ecol. Evol.* **2023**, *10*, 1080734. [CrossRef]
28. Jin, Y.; Zhang, H.; Yan, Y.; Cong, P. A Semi-Parametric Geographically Weighted Regression Approach to Exploring Driving Factors of Fractional Vegetation Cover: A Case Study of Guangdong. *Sustainability* **2020**, *12*, 7512. [CrossRef]
29. Wang, S.; Zhang, L.; Lin, W.; Huang, Q.; Song, Y.; Ye, M. Study on vegetation coverage and land-use change of Guangdong Province based on MODIS-NDVI. *Acta Ecol. Sin.* **2022**, *42*, 2149–2163.
30. Zhang, Q.; Sun, X.; Ma, J.; Xu, S. Scale effects on the relationships of water-related ecosystem services in Guangdong Province, China. *J. Hydrol.-Reg. Stud.* **2022**, *44*, 101278. [CrossRef]
31. Wang, W.; Wu, T.; Li, Y.; Xie, S.; Han, B.; Zheng, H.; Ouyang, Z. Urbanization Impacts on Natural Habitat and Ecosystem Services in the Guangdong-Hong Kong-Macao "Megacity". *Sustainability* **2020**, *12*, 6675. [CrossRef]
32. Ministry of Ecology and Environment of the People's Republic of China. National Ecological Function Zoning. Ministry of Ecology and Environment of the People's Republic of China: China 2015. Available online: https://www.mee.gov.cn/gkml/hbb/bgg/201511/t20151126_317777.htm (accessed on 20 January 2024).
33. Guan, Y.; Shan, Y.; Huang, Q.; Chen, H.; Wang, D.; Hubacek, K. Assessment to China's Recent Emission Pattern Shifts. *Earths Future* **2021**, *9*, e2021EF002241. [CrossRef]
34. Huang, X.; Wang, Y.; Liang, W.; Wang, Z.; Zhou, X.; Yan, Q. Spatial–Temporal Evolution and Driving Factors of the Low–Carbon Transition of Farmland Use in Coastal Areas of Guangdong Province. *Land* **2023**, *12*, 1007. [CrossRef]
35. Ye, Y.; Zhang, J.; Wang, T.; Bai, H.; Wang, X.; Zhao, W. Changes in Land-Use and Ecosystem Service Value in Guangdong Province, Southern China, from 1990 to 2018. *Land* **2021**, *10*, 426. [CrossRef]

36. Gai, M.; Wang, X.; Qi, C. Spatiotemporal Evolution and Influencing Factors of Ecological Civilization Construction in China. *Complexity* **2020**, *2020*, 8829144. [CrossRef]
37. Yang, J.; Huang, X. The 30 m annual land cover dataset and its dynamics in China from 1990 to 2019. *Earth Syst. Sci. Data* **2021**, *13*, 3907–3925. [CrossRef]
38. Liu, J.; Liu, M.; Deng, X.; Zhuang, D.; Zhang, Z.; Luo, D. The land use and land cover change database and its relative studies in China. *J. Geogr. Sci.* **2002**, *12*, 275–282.
39. Kuang, W.; Liu, J.; Dong, J.; Chi, W.; Zhang, C. The rapid and massive urban and industrial land expansions in China between 1990 and 2010: A CLUD-based analysis of their trajectories, patterns, and drivers. *Landsc. Urban Plan.* **2016**, *145*, 21–33. [CrossRef]
40. Baugh, K.; Hsu, F.C.; Elvidge, C.D.; Zhizhin, M. Nighttime Lights Compositing Using the VIIRS Day-Night Band: Preliminary Results. *Proc. Asia-Pac. Adv. Netw.* **2013**, *35*, 70–86. [CrossRef]
41. Zhang, C.L.; Huang, N.; Wang, L.; Song, W.J.; Zhang, Y.L.; Niu, Z. Spatial and Temporal Pattern of Net Ecosystem Productivity in China and Its Response to Climate Change in the Past 40 Years. *Int. J. Environ. Res. Public Health* **2023**, *20*, 92. [CrossRef] [PubMed]
42. Department of Ecology and Environment of Guangdong Province. *Compilation of Greenhouse Gas Inventories at the City, County, and District Levels of Guangdong Province*; Department of Ecology and Environment of Guangdong Province: Guangdong, China, 2020. Available online: https://gdee.gd.gov.cn/shbtwj/content/post_3019513.html (accessed on 15 January 2024).
43. Chen, J.; Gao, M.; Cheng, S.; Liu, X.; Hou, W.; Song, M.; Li, D.; Fan, W. China's city-level carbon emissions during 1992–2017 based on the inter-calibration of nighttime light data. *Sci. Rep.* **2021**, *11*, 3323. [CrossRef] [PubMed]
44. Costanza, R.; dArge, R.; deGroot, R.; Farber, S.; Grasso, M.; Hannon, B.; Limburg, K.; Naeem, S.; Oneill, R.V.; Paruelo, J.; et al. The value of the world's ecosystem services and natural capital. *Nature* **1997**, *387*, 253–260. [CrossRef]
45. Xie, G.D.; Lu, C.X.; Leng, Y.F.; Zheng, D.; Li, S.C. Ecological assets valuation of the Tibetan Plateau. *J. Nat. Resour.* **2003**, *18*, 189–196.
46. Xie, G.; Zhen, L.; Lu, C.; Xiao, J.; Chen, C. Expert Knowledge Based Valuation Method of Ecosystem Services in China. *J. Nat. Resour.* **2008**, *23*, 911–919.
47. Zhu, J.; Li, X.; Huang, H.; Yin, X.; Yao, J.; Liu, T.; Wu, J.; Chen, Z. Spatiotemporal Evolution of Carbon Emissions According to Major Function-Oriented Zones: A Case Study of Guangdong Province, China. *Int. J. Environ. Res. Public Health* **2023**, *20*, 2075. [CrossRef]
48. Liu, M.X.; Dong, X.B.; Wang, X.C.; Zhao, B.Y.; Fan, W.G.; Wei, H.J.; Zhang, P.; Liu, R.R. Evaluating the future terrestrial ecosystem contributions to carbon neutrality in Qinghai-Tibet Plateau. *J. Clean. Prod.* **2022**, *374*, 133914. [CrossRef]
49. Xu, G.Y.; Schwarz, P.; Shi, X.J.; Duma, N. Scenario Paths of Developing Forest Carbon Sinks for China to Achieve Carbon Neutrality. *Land* **2023**, *12*, 1325. [CrossRef]
50. Forestry Administration of Guangdong Province. 14th Five-Year Plan for Forestry Protection and Development of Guangdong. Forestry Administration of Guangdong Province:Guangdong, China, 2021. Available online: http://lyj.gd.gov.cn/notification/content/post_3515131.html (accessed on 10 December 2024).
51. The People's Government of Guangdong Province. Guangdong's Carbon Peak Implementation Plan. The People's Government of Guangdong Province: Guangdong, China, 2023. Available online: https://www.gd.gov.cn/zwgk/wjk/qbwj/yf/content/post_4091117.html (accessed on 10 December 2024).
52. Zhang, Y.; Bai, Y. Regional Differentiated Paths for Realizing "Double Carbon" Targets. *Reform* **2021**, *11*, 1–18.
53. Li, Y. Trend characteristics, regional differences, and emission reduction strategies of carbon emissions in Guangdong Province under the "dual carbon" target. *Acad. Search Truth Real.* **2024**, *5*, 110–120.
54. Ke, Y.; Gao, Y.; Yuan, M.; Liu, W.; Liu, F. Data-driven Analysis on the Spatio-temporal Characteristics and Influencing Factors of Carbon Emissions in Guangdong Province. *Environ. Sci.* **2024**, 1–13. [CrossRef]

Disclaimer/Publisher's Note: The statements, opinions and data contained in all publications are solely those of the individual author(s) and contributor(s) and not of MDPI and/or the editor(s). MDPI and/or the editor(s) disclaim responsibility for any injury to people or property resulting from any ideas, methods, instructions or products referred to in the content.

land

MDPI

Article

From Policy to Practice: Assessing Carbon Storage in Fujian Province Using Patch-Generating Land Use Simulation and Integrated Valuation of Ecosystem Services and Tradeoffs Models

Qin Nie, Wang Man *, Zongmei Li and Xuewen Wu

College of Computer and Information Engineering, Xiamen University of Technology, Xiamen 361024, China; nieqinhongyi@163.com (Q.N.)

* Correspondence: manwang@xmut.edu.cn; Tel.: +86-158-8029-3579

Abstract: Simulating and predicting carbon storage under different development scenarios is crucial for formulating effective carbon management strategies and achieving carbon neutrality goals. However, studies that focus on specific regions and incorporate local policy context require further investigation. Taking Fujian Province as a case study, this research developed four policy-driven scenarios—natural development, farmland protection, urban development, and ecological protection—based on local policy frameworks. Using the PLUS (Patch-generating Land Use Simulation) and InVEST (Integrated Valuation of Ecosystem Services and Tradeoffs) models, the study simulated and predicted the carbon storage dynamics under each scenario. The results show that carbon storage declined from 1995 to 2020, mainly due to the conversion of forests and agricultural land into construction areas. The ecological protection scenario demonstrated the highest potential for carbon storage recovery, projecting an increase to 2.02 billion tons by 2030, driven by afforestation and conservation initiatives. Conversely, the urban development scenario posed the greatest risks, leading to substantial losses. Key conservation areas, including 12 priority districts, were identified in the western and northwestern regions, while coastal urban areas, comprising 31 vulnerable districts, face significant carbon storage losses. These findings emphasize the need for balanced land use policies that prioritize both urban development and ecological protection to achieve sustainable carbon management.

Keywords: carbon storage; land use/cover change; FLUS model; local policy

1. Introduction

The growing urgency to mitigate climate change has elevated the importance of understanding carbon storage dynamics across varying spatial and temporal scales. Globally, the transition toward carbon neutrality has become a central policy focus, with the Paris Agreement setting targets for reducing greenhouse gas emissions and enhancing carbon sinks [1]. Ecosystem carbon storage plays a critical role in achieving these objectives [2,3], with forests, wetlands, and grasslands identified as critical carbon sinks. In contrast, urbanization and land use changes are major drivers of carbon storage loss [4,5]. Against this backdrop, accurately simulating and predicting carbon storage under various policy scenarios has become a pivotal tool for formulating evidence-based strategies to balance economic growth with ecological preservation [6]. China, as one of the world's largest emitters of

carbon dioxide, has committed to peaking carbon emissions by 2030 and achieving carbon neutrality by 2060. This "dual carbon" goal underscores the country's efforts to transition toward sustainable development, with a strong emphasis on integrating ecological conservation into regional planning frameworks [7]. These efforts align with the broader global push for carbon neutrality but also highlight the unique challenges and opportunities in balancing development and conservation in a rapidly growing economy [8].

The factors influencing carbon storage are inherently complex, with a range of drivers altering land cover types and, consequently, affecting the distribution of carbon storage. As a result, land use change serves as a primary driver of the spatiotemporal variability in carbon storage. Given this, future land use simulation forms a critical foundation for predicting carbon storage dynamics. Both climate change and socio-economic development play significant roles in driving land use/cover change (LUCC). This has led to the widespread use of SSP-RCP (shared socio-economic pathway–representative concentration pathway) scenarios [9] to model land use demand. For example, Li et al. [10] utilized these scenarios to predict changes in land use demand in Central Asia. However, such approaches are more effective at macro scales (e.g., national or global levels), with limited applicability at smaller, localized scales. In contrast, system dynamics (SD) models offer greater effectiveness in simulating land use demand changes at the urban level across multiple scenarios [11]. Models such as Logistic-CA [12], ANN-CA [13], CLUE-S [14], CLUMondo [15], and FLUS [16] have been widely applied in this context. Nevertheless, these models tend to be less adept at identifying the specific factors driving LUCC and lack the capacity to simulate the dynamic, spatiotemporal evolution of multiple land use patches, particularly for natural land cover types. The recently developed PLUS (Patch-generating Land Use Simulation) model [17], which integrates the random forest (RF) algorithm [18], offers a more sophisticated method for evaluating the growth potential of various land use types. This, in turn, allows for more accurate simulations of land use spatial distribution and its associated impact on carbon storage.

Recent years have witnessed an increasing number of studies focusing on the simulation and prediction of future carbon storage under various development scenarios [19–29]. The scenarios employed are primarily derived from extensive scientific research and data analysis related to socio-economic development pathways, environmental protection policies, land use/cover change, and carbon emission management policies. For instance, socio-economic development pathways combined with future climate change data are used to predict changes in carbon storage under different climate conditions. This approach helps assess the long-term impact of climate change on carbon storage. Moreover, environmental protection policies, such as afforestation, forest conservation, and wetland restoration, can significantly enhance carbon storage [25]. In parallel, land use policies, encompassing agricultural policies, urban planning, and land management strategies directly affect carbon storage levels [21,26]. Additionally, carbon emission management policies, including carbon taxes, carbon trading, and the promotion of low-carbon technologies, exert a significant indirect influence on carbon storage [27,28]. Despite significant progress in the simulation and prediction of carbon storage, the development scenarios currently employed are often characterized by their broad, macro-level applicability, which may not be sufficiently tailored to specific study areas. There is a need for greater consideration of localized development scenarios that integrate local development plans and context-dependent variables. Therefore, studies that focus on specific regions and incorporate local policy contexts warrant further investigation.

Setting up different scenarios based on varying local policies is a more scientific approach to exploring future carbon storage, providing valuable information for future

urban planning. Although some regions have developed detailed ecological protection and land use plans, these policies are often inadequately represented in the models, reflecting an insufficient consideration of the regional policy context. This gap highlights the need for more context-specific research. Furthermore, the application of future planning policies, such as urban expansion plans and ecological restoration projects, in models can lead to more accurate predictions of future carbon storage changes. By integrating these planning policies into the models, researchers can better anticipate the effects of policy decisions on carbon storage, thereby providing more precise and actionable insights for urban and regional planning. Fujian Province, located on the southeastern coast of China, boasts rich forest resources and diverse ecosystems, making it a crucial ecological barrier and carbon sink region in China. However, with rapid economic development and accelerating urbanization, Fujian Province faces ecological and environmental challenges brought about by land use changes. In recent years, with the release of the "Fujian Provincial Territorial Spatial Planning (2021–2035)" and the "Fujian Provincial Ecological Restoration Plan (2021–2035)", there has been a pressing need to conduct policy-driven carbon storage simulations in this region, characterized by its unique ecological environment and economic background. Such simulations aim to scientifically evaluate and predict the impact of different policy scenarios on carbon storage.

Therefore, this study aims to establish multiple policy-driven scenarios based on Fujian Province's regional policy documents and employ a combination of the Markov model, PLUS model, and InVEST (Integrated Valuation of Ecosystem Services and Tradeoffs) model to simulate and predict land use changes and carbon storage variations under different scenarios. The study seeks to quantify the impact of various policy measures on carbon storage and propose policy recommendations for optimizing land use and ecological protection. The specific research objectives are as follows: (1) to characterize the spatiotemporal evolution of carbon storage in Fujian Province over a long time series; (2) to simulate and predict the spatiotemporal changes in carbon storage under different future scenarios driven by regional policies; (3) to identify regional differences in carbon storage and key protection areas under various future scenarios.

2. Materials and Methods

2.1. Study Area

Fujian Province is located on the southeastern coast of China, between latitudes 23°33′ N and 28°20′ N and longitudes 115°50′ E and 120°40′ E. The province features a diverse topography, with 80% of its land area covered by mountains and hills. This varied landscape is further enriched by a subtropical monsoon climate, characterized by average annual temperatures ranging from 17 °C to 21 °C and annual precipitation between 1400 mm and 2000 mm, which supports rich forest resources and diverse ecosystems. Designated as an ecological civilization pilot zone, Fujian emphasizes its commitment to sustainable development and ecological conservation. However, the province has also experienced rapid economic development and urbanization, leading to significant land use changes and environmental pressures. This unique combination of natural richness and developmental challenges makes Fujian an ideal case study for evaluating and predicting the impact of regional policies on carbon storage. The insights gained from this study will aid in optimizing land use planning and promoting sustainable development both locally and in similar regions globally.

2.2. Data

Land use and land cover classification data for the years 1995, 2000, 2005, 2010, 2015, and 2020 were obtained from the China Multi-Period Land Use Remote Sensing Monitoring Dataset (CNLUCC), developed by Xu Xinliang's team at the Data Center for Resource and Environmental Sciences (RESDC), Chinese Academy of Sciences (https://www.resdc.cn/, accessed on 10 February 2023). The CNLUCC is primarily based on Landsat remote sensing imagery, and it was constructed through manual visual interpretation to create a national-scale multi-temporal land use/land cover database for China. This dataset, with a spatial resolution of 30 × 30 m, was initially categorized into 25 land cover types. For the purposes of this study, these were reclassified into six main categories: cultivated land, forest land, grassland, water bodies, construction land, and unused land. The datasets are reported to have an overall accuracy greater than 90% [30].

Meteorological data, including annual precipitation and average temperature, were sourced from the Annual Spatial Interpolation Dataset of Meteorological Elements in China, also prepared by Xu Xinliang's team at RESDC (https://www.resdc.cn/, accessed on 10 February 2023). Topographic data, such as elevation, slope, and aspect, were derived from the GDEMV3 series (https://www.gscloud.cn/home, accessed on 10 February 2023). Information on administrative boundaries, roads, and rivers was extracted from the National Geographic Information Resources Directory Service System (https://www.webmap.cn/main.do?method=index, accessed on 15 February 2023). Economic indicators, such as GDP and population data, were gathered from the Statistical Yearbook of the Fujian Provincial Bureau of Statistics (https://tjj.fujian.gov.cn/, accessed on 15 February 2023). The datasets used in this study have been rigorously verified and validated through extensive scholarly research [31].

2.3. Scenario Settings Based on Local Policies

The historical land use transfer matrix from 2010 to 2020, in conjunction with the "Fujian Provincial Territorial Spatial Planning (2021–2035)" and the "Fujian Provincial Ecological Restoration Plan (2021–2035)", serves as the foundation for this analysis. These local policies, which outline the key strategic directions for land use and ecological protection in Fujian, are used as the guiding principles and constraints for scenario development. Based on these policy documents, four scenarios are established to predict the spatial pattern of land use in Fujian Province by 2030: natural development scenario (ND), farmland protection scenario (FP), urban development scenario (UD), ecological protection scenario (EP) (Table 1).

The development of these scenarios is deeply rooted in the regional policy documents of Fujian Province. Each scenario is designed to reflect the goals and directives of the Fujian Provincial Territorial Spatial Planning (2021–2035) and the Fujian Provincial Ecological Restoration Plan (2021–2035). The policy-driven factors were incorporated into the PLUS model to simulate land use changes. For example, the FP scenario was specifically developed to reflect the "farmland red line" policy, which restricts the conversion of agricultural land to construction land. This is achieved by reducing the probability of farmland being converted by 60%, ensuring that farmland preservation is prioritized. The UD scenario reflects Fujian's policy to promote urbanization and industrial growth, which is modeled by increasing the likelihood of land use conversion from farmland, forest, and grassland to construction land. The increased urbanization is in line with the strategic directions laid out in the Fujian Provincial Territorial Spatial Planning. The EP scenario was modeled to enhance ecological protection, which is a core goal of the Fujian Provincial Ecological Restoration Plan. This scenario simulates a 30% reduction in the probability of farmland

and forest land being converted to construction land, in line with the policy's commitment to ecological restoration.

Each scenario was carefully tailored to reflect local policies, ensuring that the simulated outcomes are both realistic and representative of the policy goals set for 2030. The use of the PLUS model allows us to incorporate these policy constraints into a spatial simulation, ensuring that the predicted land use changes are not only scientifically grounded but also aligned with the policy vision of Fujian Province.

Table 1. Scenario settings for predicting carbon storage.

Scenario	Policy Background	Setup Method	Characteristics
ND	Projected land use areas in Fujian Province for 2030, based on transfer probability matrices from 2010 and 2020.	This scenario is developed using the PLUS model with a 10-year step, where the 2030 land use areas are estimated based on the historical land use transfer matrix. Conversion to construction land is prohibited due to difficulty in transition.	Land use changes driven by natural growth and market forces, without additional policy interventions or ecological restoration measures. This scenario serves as a baseline reflecting natural trends in land use.
FP	In compliance with the "Fujian Provincial Territorial Spatial Planning (2021–2035)", this scenario strictly protects the farmland red line, rigorously controls and minimizes the occupation of farmland, and implements the "occupation and compensation" policy to ensure the preservation of farmland area.	This scenario reduces the probability of farmland converting to construction land by 60%, in accordance with the stringent farmland protection policies, while keeping the other land use changes aligned with the natural development scenario.	Prioritizes farmland conservation to maintain food security and limit the expansion of construction land. The policies directly influence land use change by enforcing the strict protection of farmland.
UD	Reflecting the directives of the "Fujian Provincial Territorial Spatial Planning (2021–2035)", this scenario strengthens urban areas through population concentration and industrial development, facilitating moderate urban expansion.	Based on the policy's urbanization goals, the scenario increases the probability of converting farmland, forest land, and grassland into construction land by 20%, and reduces the probability of construction land converting to other land types (except farmland) by 30%. This models urban growth according to policy priorities.	Aims to support urbanization and industrialization in Fujian, with a focus on urban land use expansion, while reducing the conversion of construction land to other uses.
EP	Guided by the "Fujian Provincial Ecological Restoration Plan (2021–2035)", this scenario focuses on ecological restoration and environmental protection.	The probability of farmland and forest land converting to construction land is reduced by 30%, while the conversion of construction land to forest land is increased by 10%, reflecting ecological restoration policies. Additionally, the conversion of grassland and water bodies is limited by 20%.	Prioritizes ecological protection by reducing construction land expansion and restoring forests and grasslands. Policy-driven actions, such as afforestation and ecosystem restoration, are modeled to enhance environmental quality.

2.4. PLUS Model

To simulate future land use changes, the PLUS model integrates a rule-mining framework based on LEAS and a cellular automata (CA) module that utilizes multi-type random patch seeds (CARS). In this study, the LEAS module is first used to extract land expansion data for the study area from 2010 to 2020. Following this, the random forest algorithm is employed to determine the development probabilities for various land types and to assess the contributions of driving factors to land expansion. Specifically, from the natural, social, and economic dimensions, ten driving factors—elevation, slope, aspect, annual precipitation, average annual temperature, distance to rivers, distance to highways, distance to railways, population density, and GDP—are employed to compute the occurrence

probabilities of six land use types. These probabilities are then incorporated into the CARS module, which combines random seed generation with a threshold decline mechanism. By utilizing neighborhood weights and a cost matrix as constraints, the CARS module effectively simulates future land use, ensuring a realistic and dynamic representation of spatial changes. For this study, we set neighborhood weights of cultivated land, forest land, grassland, water, construction land, and unused land as 0.01, 0.08, 0.48, 0.52, 1, and 0.4, respectively. The cost matrix in different simulation scenarios is shown in Table 2. Assuming the CARS model's accuracy is robust, different development scenarios are then established to forecast the future land use pattern in Fujian Province for the year 2030 using 2020 as the baseline.

Table 2. Cost matrix of land use transfer in different simulation scenarios in Fujian Province.

Scenario Settings	Land Use Type	L1	L2	L3	L4	L5	L6
ND	L1	1	1	1	1	1	1
	L2	1	1	1	1	1	1
	L3	1	1	1	1	1	1
	L4	1	1	1	1	1	1
	L5	0	0	0	0	1	0
	L6	1	1	1	1	1	1
FP	L1	1	0	0	0	0	0
	L2	1	1	1	0	0	0
	L3	1	1	1	1	1	0
	L4	1	0	0	1	0	0
	L5	0	0	0	0	1	0
	L6	1	1	1	1	1	1
UD	L1	1	0	0	0	1	0
	L2	1	1	1	1	1	0
	L3	1	0	1	0	1	0
	L4	1	1	1	1	1	0
	L5	1	0	0	0	1	0
	L6	1	1	1	1	1	1
EP	L1	1	1	1	1	1	1
	L2	0	1	0	0	0	0
	L3	0	1	1	1	0	0
	L4	0	0	0	1	0	0
	L5	0	0	0	0	1	0
	L6	1	1	1	1	1	1

"0" indicates that conversion is not allowed, while "1" indicates that conversion is permitted. L1, L2, L3, L4, L5, and L6 indicate cultivated land, forest land, grassland, water, construction land, and unused land, respectively.

To evaluate the simulation performance and accuracy of the PLUS model for predicting future land use, this study utilized land use data from Fujian Province for the years 2000 and 2010. By employing the PLUS model, we simulated the land use of Fujian Province for the year 2020. The simulated results were then compared with the actual land use data for 2020. The comparison revealed a model accuracy of 0.948 and a kappa coefficient of 0.908, demonstrating that the PLUS model possesses high accuracy in predicting future land use in Fujian Province, thus confirming the reliability of the simulation results.

2.5. InVEST Model Carbon Module

This study employs the carbon module of the InVEST model to compute the spatiotemporal distribution of carbon storage in Fujian Province across different years. Carbon storage in terrestrial ecosystems is typically classified into four primary sinks: aboveground biomass, belowground biomass, soil, and dead organic matter. The total carbon storage

in the study area is the sum of these four components. The carbon storage for each type is calculated by multiplying the area of each land use type by the corresponding average carbon density for each sink.

Carbon density data are mainly sourced from the existing literature pertaining to the study area or nearby regions, with a preference for field-collected data. Earlier research has established a significant positive correlation between vegetation and soil carbon density changes with annual precipitation, and a weaker correlation with average annual temperature. This study uses national and Fujian Province annual precipitation to calculate the correction coefficient between actual and simulated carbon density. The correction coefficient formula is as follows:

$$Kvp = \frac{6.789e^{0.0054MAP1}}{6.789e^{0.0054MAP2}} \quad (1)$$

$$Ksp = \frac{3.3968MAP1 + 3996.1}{3.3968MAP2 + 3996.1} \quad (2)$$

Kvp and Ksp represent the correction coefficient of vegetation biomass and soil carbon density precipitation factor; MAP1 and MAP2 denote the annual precipitation of Fujian Province and the whole country, respectively.

Root–shoot ratios for different land use types are obtained from relative references, among which, crop 0.19, forest 0.17–0.36, shrub 0.91, desert 5.5, and grassland 5.2. Using these ratios, the carbon density of aboveground and belowground parts for each land use type can be determined. The carbon density of dead organic matter is estimated to be 10–15% of the aboveground carbon density. Table 3 provides a detailed summary of the carbon density data for the study area.

Table 3. Carbon density of different land use types in the study area (t/hm^2).

Types	Above Ground	Below Ground	Soil	Dead Mass
cultivated land	9.78	0.19	35.8	0.98
Forest land	39.1	9.77	159.38	3.91
Grassland	3.22	16.73	138.77	0.32
Water	0.06	0.3	0.66	0.27
Construction land	11.39	2.28	17.68	0
Unused land	15.42	3.08	2.12	0

3. Results

3.1. Spatiotemporal Dynamics of Carbon Storage from 1995 to 2020

3.1.1. Dynamics of Land Use

From 1995 to 2020, the predominant land use types in Fujian Province were forest land, cultivated land, and grassland, collectively accounting for over 90% of the province's terrestrial area. Forest land, in particular, constituted the largest share, covering approximately 62% of the total land area. Cultivated land followed, consistently occupying more than 16% of the province's land area throughout the study period. Grassland maintained a steady presence, comprising around 15% of the land area. In terms of spatial distribution (Figure 1), forest land was predominantly situated in the western and central mountainous and hilly regions of Fujian Province. Conversely, grassland exhibited a scattered, spot-like distribution across the entire province. Cultivated land was primarily arranged in a strip-like pattern along the southeastern coastal areas, with occasional patches in the northwestern regions. Additionally, construction land was largely concentrated in the southeastern coastal urban agglomerations, reflecting the region's urbanization trends.

This spatial analysis underscores the significant geographical variations and land use dynamics within Fujian Province over the 25-year period.

Land use changes in Fujian Province during the study period of 1995–2020 have been characterized by a continuous decrease in the areas of cultivated land and forest land, alongside a consistent increase in construction land (Table 4). Specifically, the forest land area decreased from 76,721.98 km^2 in 1995 to 75,711.29 km^2 in 2020, with the most significant reduction occurring between 2005 and 2010, amounting to a decrease of 419.32 km^2. Similarly, the cultivated land area decreased from 22,494.69 km^2 in 1995 to 20,596 km^2 in 2020, with the largest reduction recorded between 2000 and 2005. Subsequently, the rate of reduction in cultivated land area gradually diminished: 398.08 km^2 between 2005 and 2010, 356.83 km^2 between 2010 and 2015, and 207.99 km^2 between 2015 and 2020. Despite these reductions, the proportion of cultivated land remained stable at over 16% of the province's total land area throughout the study period. In contrast, the grassland area exhibited minor fluctuations around 18,600 km^2, maintaining a steady proportion of approximately 15% of the province's total land area. Meanwhile, construction land experienced significant expansion, increasing from 2371.54 km^2 in 1995 to 5423.09 km^2 in 2020, which represents a growth rate of 1.29%. The most substantial increase in construction land occurred between 2000 and 2005, with an expansion of 1200.19 km^2. The growth rate of construction land then gradually declined in each subsequent five-year period, with increases of 770.78 km^2, 514.72 km^2, and 494.96 km^2, respectively. These findings underscore the dynamic nature of land use in Fujian Province over the past quarter-century, highlighting the significant reductions in forest and cultivated lands and the concomitant increase in construction land. This trend reflects broader socio-economic developments and urbanization processes within the region.

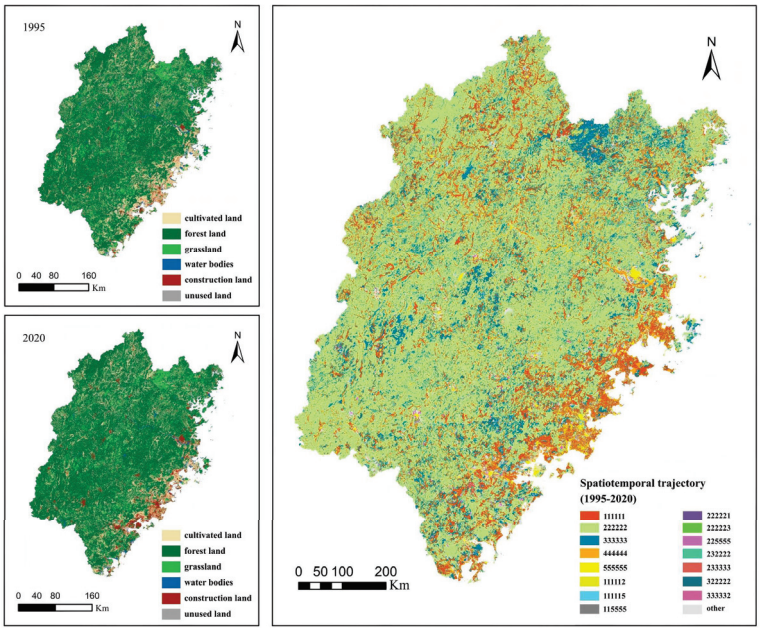

Figure 1. Land use distribution in Fujian from 1995 to 2020. Note: 1~6 indicates cultivated land, forest land, grassland, water, construction land, and unused land, respectively.

Table 4. Land use area change (C/km^2) and dynamic degree (K/%) during 1995–2020.

Land Use Types	1995–2000		2000–2005		2005–2010		2010–2015		2015–2020		1995–2020	
	C	K	C	K	C	K	C	K	C	K	C	K
Cultivated land	−148.85	−0.13	−786.94	−0.70	−398.08	−0.37	−356.83	−0.34	−207.99	−0.20	−1898.68	−1.69
Forest land	−286.18	−0.07	−78.22	−0.02	−419.32	−0.11	−57.73	−0.02	−169.24	−0.04	−1010.70	−0.26
Grassland	316.39	0.34	−635.49	−0.67	108.20	0.12	−41.36	−0.04	−11.93	−0.01	−264.19	−0.28
Water	31.82	0.41	96.29	1.23	214.34	2.57	−61.03	−0.65	−48.88	−0.54	232.54	3.02
Construction land	70.90	0.60	1200.19	9.83	770.78	4.23	514.72	2.33	494.96	2.01	3051.56	5.1
Unused land	14.13	3.79	11.76	2.65	2.05	0.41	−0.51	−0.10	3.43	0.67	30.87	8.28

The Land Use Dynamic Degree Index has been employed to reflect the intensity of changes in a specific land use type over a given period. The formula is as follows:

$$K = \frac{U_b - U_a}{U_a} \times \frac{1}{T} \times 100\% \quad (3)$$

where U_a and U_b represent the area of a specific land use type at time points a and b, respectively. T is the study period (in years). K indicates the dynamic degree of a specific land use type over a certain period.

Over the period from 1995 to 2020, the dynamic degree of land use for forest land in Fujian Province was the smallest, at −0.26, followed closely by grassland and cultivated land, with dynamic degrees of −0.28 and −1.69, respectively. The relatively minor fluctuations in these land types are attributed to their substantial base areas. In stark contrast, the dynamic degree of construction land use has consistently been the highest throughout the years. Notably, between 2000 and 2005, the dynamic degree of construction land use surged to 9.83%. This significant increase underscores the substantial expansion of construction land, which predominantly encroached upon the areas previously designated as cultivated land and forest land. These trends illustrate the aggressive urbanization and development strategies that have been implemented in Fujian Province, leading to a marked shift in land use patterns over the 25-year period.

3.1.2. Dynamics of Carbon Storage

The carbon storage in Fujian Province has exhibited a consistent downward trend, decreasing at an average rate of 0.01 billion tons per year, from 2.042 billion tons in 1995 to 2.017 billion tons in 2020. Significantly, the decade from 2000 to 2010 marked the most pronounced decline in carbon storage, with an accelerated reduction rate of 0.019 billion tons per year. In contrast, post-2010 data reveals a deceleration in this trend, with the rate of decline attenuating to 0.005 billion tons per year, indicating a more gradual reduction of carbon storage in the latter phase of the study period.

The spatial distribution of carbon storage in Fujian Province exhibited significant regional disparities from 1995 to 2020, as illustrated in Figure 2. Notably, carbon storage in the western and northwestern mountainous areas was substantially higher than that in the eastern and southeastern coastal and urban regions. High-value carbon storage areas were predominantly contiguous in the western part of the province. Jian'ou City, which had the highest carbon storage of 72.5355 million tons, accounted for 3.6% of the total carbon storage in Fujian Province. This was followed by Youxi County, Jianyang District, Changting County, and Pucheng County, all located in densely forested and grassland-rich regions of western Fujian. Conversely, low-value carbon storage areas were concentrated in the southeastern coastal urban agglomerations, including Fuzhou, Putian, and the Xiamen–Zhangzhou–Quanzhou region. Taijiang District had the lowest carbon storage at only 52,000 tons, followed by Gulou District, Huli District, Licheng District, and Siming

District. These districts, situated in the highly urbanized eastern coastal areas, have a high proportion of construction land, which contributes to their lower carbon storage capacities.

The study employed the natural break method to classify the carbon storage levels across the region, categorizing them into three levels: general, higher, and key protection areas (Figure 2). The key protection areas encompassed the largest proportion of carbon storage, accounting for 94.02% of the total. Areas with higher carbon storage represented 4.44%, while those with general carbon storage comprised 1.54%. The higher and general carbon storage areas were primarily located in the eastern and southeastern part of Fujian Province, particularly in districts with extensive construction land such as Huli District, Siming District, Jimei District, Longwen District, Jinjiang City, Licheng District, and Gulou District.

To elucidate the regions where carbon storage changes occurred over the past 25 years, a differential analysis was performed on the spatial distribution maps of carbon storage for the study years, followed by reclassification into three categories: decrease, stable, and increase (Figure 2). The results revealed that most areas within the study region maintained relatively stable carbon storage from 1995 to 2020. Regions with increased carbon storage were sporadically distributed across Fujian Province, while areas with decreased carbon storage were primarily concentrated in Licheng District, Huli District, Jimei District, Longwen District, and Cangshan District. These areas, characterized by relatively weak carbon sequestration capacities and limited forest and grassland vegetation, have undergone significant urban expansion over the past 25 years. The conversion of cultivated land to urban use has led to a discernible reduction in carbon storage.

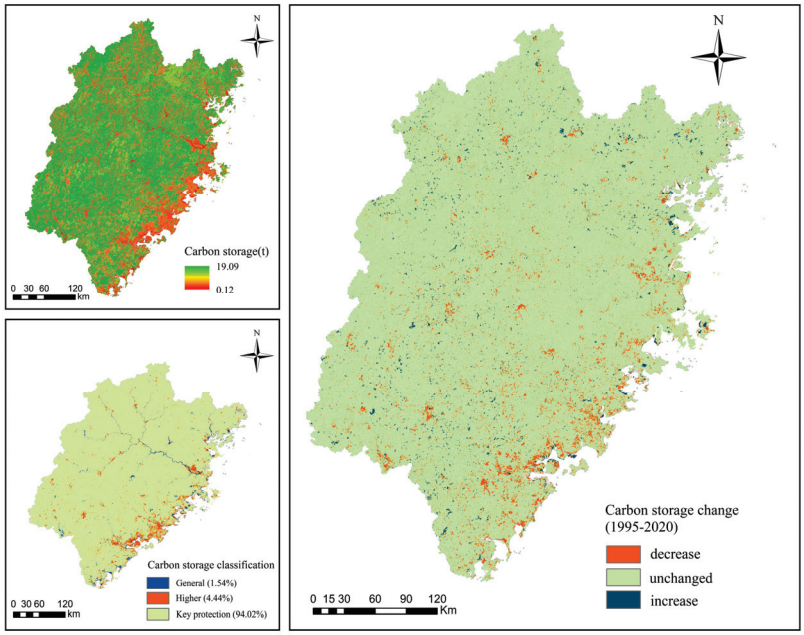

Figure 2. Spatial distribution of carbon storage in Fujian in 2020.

3.2. Land Use Scenario Simulations for 2030

3.2.1. Land Use Changes Under Different Scenarios

Under the four projected scenarios for 2030, land use in Fujian Province will continue to be predominantly forest land, followed by cultivated land and grassland (Figure 3). The western region of Fujian will remain extensively covered with forest land, while the southeastern coastal areas will be primarily occupied by cultivated land, construction land, and other land use types. Despite this general distribution pattern, the characteristics of land

use changes exhibit significant variability under different development scenarios, reflecting the differential impacts of policy interventions, economic drivers, and environmental conditions on land use dynamics.

Under the natural development scenario for 2030, Fujian Province's land use types are primarily characterized by a significant increase in construction land and a decrease in unused land and natural ecological land (such as water bodies, cultivated land, grassland, and forest land). Specifically, construction land is projected to increase by 802.39 km^2, with a dynamic degree of 14.80%, reflecting the rapid pace of urbanization and infrastructure development, making it the most significant change among all the land types (Figure 3). Conversely, unused land is expected to decrease by 31.23 km^2, with a dynamic degree of −29.61%, indicating that previously undeveloped land is being extensively utilized and converted for other purposes. Similarly, water bodies are anticipated to decrease by 110.07 km^2, with a dynamic degree of −6.21%, suggesting significant impacts from climate change and human activities on water resources. Cultivated land is forecasted to decrease by 493.90 km^2, with a dynamic degree of −2.40%, showing that agricultural land is gradually being replaced by other types, mainly construction land. Grassland and forest land are projected to show slight decreases, with dynamic degrees of −0.32% and −0.14%, respectively, indicating more gradual changes. These changes collectively reflect the driving forces of urbanization and industrialization and their significant impacts on agricultural and natural ecological land. Consequently, future land use policies must balance development and conservation to achieve sustainable land use and environmental protection.

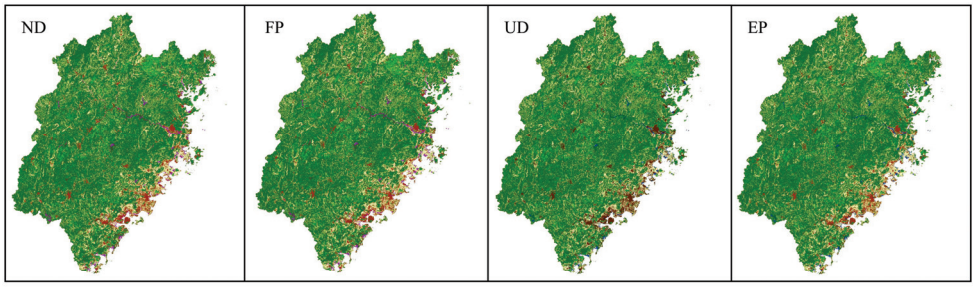

Land use area change (Km²)during 2020-2030

Land use types	ND	FP	UD	NP
cultivated land	-493.9	248.73	-620.05	-561.33
Forest land	-107.38	-216.32	-339.35	420.45
Grassland	-59.82	-55.69	16.08	-84.36
Water	-110.07	-70.9	-126.18	19.53
Construction land	802.39	107	1086.06	213.68
Unused land	-31.23	-12.81	-16.56	-7.97

Land use dynamic degree(%)during 2020-2030

Land use types	ND	FP	UD	NP
cultivated land	-2.4	1.21	-3.01	-2.73
Forest land	-0.14	-0.29	-0.45	0.56
Grassland	-0.32	-0.3	0.09	-0.46
Water	-6.21	-4	-7.12	1.1
Construction land	14.8	1.97	20.03	3.94
Unused land	-29.61	-12.14	-15.7	-7.56

Figure 3. Land use of various forecast scenarios in Fujian Province by 2030.

Under the cultivated land protection scenario for 2030, the land use dynamics in Fujian Province exhibit a pronounced increase in cultivated and construction land, coupled with a decrease in forest land, grassland, water bodies, and unused land. Specifically, cultivated land is projected to increase by 248.73 km^2, with a dynamic degree of 1.21%, underscoring the effectiveness of cultivated land protection policies and marking it as the most significant land use change in this scenario. Construction land is anticipated to see a modest increase of 107.00 km^2, with a dynamic degree of 1.97%, reflecting the ongoing urbanization processes that persist even amid efforts to protect agricultural land. This suggests a nuanced interaction between land protection policies and urban development imperatives. In contrast, water bodies are expected to decline by 70.90 km^2, with a dynamic degree of −4.00%, indicating the potential reallocation of water resources for alternative uses, which may have implications for regional water management strategies. Forest land and grassland are forecasted to decrease by 216.32 km^2 and 55.69 km^2, respectively,

with dynamic degrees of approximately −0.3%. These more gradual reductions point to the secondary effects of prioritizing agricultural land protection, potentially at the expense of other ecological land types. The observed decreases in forest and grassland highlight the complex tradeoffs inherent in land use policy decisions. Overall, the increase in cultivated land is the dominant feature of this scenario, affirming the success of the protection measures. However, the concomitant decrease in other natural ecological land types emphasizes the need for a more balanced approach to land use planning. This scenario elucidates the critical necessity of harmonizing agricultural land conservation with the sustainable management of other land types to ensure a holistic and ecologically sound land use strategy. Future policies must consider these multifaceted impacts to achieve an optimal equilibrium between development and conservation objectives.

Under the urban development scenario projected for 2030, Fujian Province's land use dynamics reveal pronounced transformations, predominantly characterized by a substantial increase in construction land, juxtaposed with a decline in cultivated land, forest land, water bodies, and unused land. By 2030, construction land is expected to encompass 6509.15 km^2, representing 5.33% of the total land area, which marks an increase of 1086.06 km^2 from 2020, with a dynamic degree of 20.03%. This substantial growth reflects the accelerated pace of urbanization and infrastructure development, positioning construction land as the most prominent change within this scenario. However, this rapid urbanization process incurs significant encroachment upon and the conversion of natural ecological land. Cultivated land is projected to decrease by 620.05 km^2, with a dynamic degree of −3.01%, indicating the extensive conversion of agricultural land into construction land. Similarly, forest land is anticipated to decrease by 339.35 km^2, with a dynamic degree of −0.45%, highlighting the pressures exerted by urban expansion on forest resources. Water bodies are expected to decrease by 126.18 km^2, with a dynamic degree of −7.12%, underscoring the substantial loss of water resources as a consequence of urban development. In contrast, grassland exhibits the least significant change, with a slight increase and a dynamic degree of 0.09%, reflecting relatively stable conditions for this land type amidst the broader changes. The dramatic increase in construction land serves as the primary characteristic of this scenario, illustrating the extensive urbanization efforts underway. The concurrent decline in cultivated land, forest land, and water bodies underscores the detrimental impacts of urban expansion on natural ecological areas. This scenario highlights the critical necessity for comprehensive urban planning that not only facilitates growth but also emphasizes the preservation and restoration of natural ecosystems. Achieving a balance between urban development and ecological conservation will be imperative to ensure sustainable land use and the maintenance of environmental integrity in the context of rapid urbanization.

Under the ecological protection scenario, land use dynamics in Fujian Province for 2030 exhibit significant changes, primarily characterized by an increase in forest land, construction land, and water bodies, alongside a decrease in cultivated land, grassland, and unused land. Forest land is projected to increase by 420.45 km^2, with a dynamic degree of 0.56%, reflecting the effectiveness of ecological protection measures in promoting forest recovery and increasing vegetation cover. Construction land is anticipated to grow by 213.68 km^2, with a dynamic degree of 3.94%. Although this increase is relatively modest compared to the other scenarios, it indicates that urbanization processes are continuing under ecological protection policies but are somewhat controlled. Concurrently, cultivated land is expected to decrease by 561.33 km^2, with a dynamic degree of −2.73%, a substantial reduction suggesting that some agricultural land is being converted to forest land or other ecological protection areas, highlighting the impact of ecological protection

measures on agricultural land use. Grassland shows the mildest change, with a dynamic degree of −0.46%, indicating a relatively stable condition. Overall, the increase in forest land, construction land, and water bodies under this scenario underscores the positive impact of ecological protection measures. However, the notable decrease in cultivated land and the minor reduction in grassland suggest a tradeoff between agricultural land use and ecological conservation. This scenario emphasizes the necessity of rational land use planning to achieve a balance between ecological environment protection and economic development. Sustainable policies must integrate ecological conservation goals with urban and agricultural land use to ensure harmonious and sustainable development.

3.2.2. Land Use Changes Across Different Scenarios

The land use in Fujian Province exhibits significant changes under different scenarios, reflecting the impact of local policies on land use and the ecological environment. These changes provide crucial insights for future land use policy formulation, emphasizing the necessity of balancing development and conservation to achieve sustainable land use and ecological protection.

Cultivated land shows a marked decrease in both the natural development scenario and the urban development scenario, with reductions of 493.90 km^2 (dynamic degree −2.40%) and 620.05 km^2 (dynamic degree −3.01%), respectively. These declines reflect the encroachment of urban expansion on agricultural land, underscoring the impact of urbanization on reducing agricultural areas. In the ecological protection scenario, cultivated land decreases by 561.33 km^2 (dynamic degree −2.73%), indicating that some agricultural land is being converted into construction or ecological protection areas. This trend emphasizes the prioritization of ecological protection measures. Conversely, under the cultivated land protection scenario, cultivated land increases by 248.73 km^2 (dynamic degree 1.21%), showcasing the effectiveness of protection policies in expanding agricultural land and preventing its conversion to other uses. Similarly, forest land exhibits a decreasing trend in both the natural development and urban development scenarios, with reductions of 107.38 km^2 (dynamic degree −0.14%) and 339.35 km^2 (dynamic degree −0.45%), respectively. These reductions highlight the significant pressure that urban expansion exerts on forest resources, reflecting the challenges of maintaining forest areas amidst urban growth. However, in the cultivated land protection scenario, forest land decreases by 216.32 km^2 (dynamic degree −0.29%), indicating a more moderate decline compared to the other scenarios. In stark contrast, under the ecological protection scenario, forest land increases significantly by 420.45 km^2 (dynamic degree 0.56%), demonstrating the effectiveness of ecological protection measures in promoting forest recovery and increased vegetation cover. Grassland experiences slight increases or decreases across all the development scenarios, with relatively stable changes.

However, construction land increases significantly across all the scenarios. In the natural development scenario, construction land increases by 802.39 km^2, with a dynamic degree of 14.80%, reflecting the rapid pace of urbanization and infrastructure development. In the cultivated land protection scenario, construction land increases by 107.00 km^2, with a dynamic degree of 1.97%. Although the increase is smaller, it still indicates ongoing urbanization alongside efforts to protect agricultural land. In the urban development scenario, construction land sees the most substantial increase, rising by 1086.06 km^2 with a dynamic degree of 20.03%, highlighting the intense demand for land resources driven by rapid urban expansion. Finally, in the ecological protection scenario, construction land increases by 213.68 km^2, with a dynamic degree of 3.94%. Although the increase is more

moderate, it suggests that urbanization continues, albeit under a more controlled and balanced approach within the context of ecological protection.

Under different scenarios, water bodies and unused land in Fujian Province consistently show a decreasing trend, although water bodies slightly increase under the ecological protection scenario. This trend is particularly pronounced in the natural development and urban development scenarios, where the changes in water bodies and unused land are most dramatic. In the natural development scenario, the dynamic degree for water bodies is −6.21%, and for unused land, it is −29.61%. These significant reductions reflect the impacts of climate change and human activities, such as water resource exploitation, river diversion, and pollution, on water resources and unused land.

3.3. Carbon Storage Scenario Simulations for 2030

3.3.1. Carbon Storage Projections Under Different Scenarios

The simulation results of the total carbon storage in Fujian Province under the four projected development scenarios reveal that by 2030, the overall carbon storage in the region is expected to follow this order: ecological protection scenario (2.02 billion tons) > natural development scenario (2.014 billion tons) > cultivated land protection scenario (2.013 billion tons) > urban development scenario (2.01 billion tons). This hierarchy underscores the differential impacts of various land use strategies on the province's carbon sequestration capabilities.

In the natural development scenario, the total carbon storage is anticipated to reach 2.014 billion tons, representing a reduction of 0.03 billion tons relative to 2020. This decline is primarily attributable to the significant expansion of construction land, which occurs at the expense of unused land, water bodies, cultivated land, grassland, and forest land. The encroachment of construction land, characterized by a lower carbon density, into areas previously dominated by higher carbon density land types will lead to a net decrease in the overall carbon storage by 2030.

Conversely, under the ecological protection scenario, carbon storage is projected to increase to 2.02 billion tons, an increment of 0.05 billion tons compared to 2020. This positive outcome is primarily attributed to the implementation of ecological protection measures, such as afforestation, reforestation, and soil conservation. Consequently, there has been a notable expansion of both forest land and construction land, while cultivated land, grassland, and unused land have contracted. The conversion of cultivated land to forest land, characterized by higher carbon density, coupled with the more controlled expansion of construction land—possessing lower carbon sequestration potential—underscores the success of Fujian Province's afforestation efforts and the strategic conversion of farmland to forest in enhancing carbon storage.

In contrast, the cultivated land protection scenario forecasts a carbon storage of 2.013 billion tons, reflecting a reduction of 0.04 billion tons from 2020 levels. The magnitude of carbon storage loss in this scenario surpasses that observed in the natural development scenario. This is due to the significant increase in both cultivated land and construction land under the influence of cultivated land protection policies, accompanied by a concurrent reduction in forest land, grassland, water bodies, and unused land. While the expansion of construction land is less pronounced than in the natural development scenario, the more substantial reduction in forest land suggests that the primary driver of carbon storage loss is the conversion of high-carbon-density forest land to lower-carbon-density cultivated land.

Finally, the urban development scenario predicts a total carbon storage of 2.01 billion tons, the lowest across all the scenarios, marking a decrease of 0.07 billion tons compared to 2020. This significant decline in carbon storage is predominantly a consequence of the

extensive increase in construction land, which comes at the expense of cultivated land, forest land, water bodies, and unused land. The accelerated urbanization process exerts severe pressure on natural ecological land, leading to its erosion and conversion. This scenario emphasizes the critical need for sustainable urban planning strategies that can mitigate the adverse impacts of rapid urbanization on carbon storage.

3.3.2. Regional Differences of Carbon Storage Under Future Scenarios

The spatial distribution of carbon storage in 2030 under various development scenarios exhibits pronounced regional disparities (Figure 4). Notably, carbon storage is consistently higher in the western and northwestern mountainous regions than in the eastern and southeastern coastal urban areas. This pattern remains consistent across all the scenarios, where areas rich in forests and grasslands in the west and northwest exhibit high carbon storage, while areas dominated by construction land and farmland in coastal and urban regions show significantly lower storage levels.

A differential analysis of carbon storage between 2020 and 2030, followed by a reclassification into three categories—decrease, stability, and increase—reveals that most regions exhibit stable carbon storage across all the scenarios. However, regions experiencing an increase in carbon storage are sporadically distributed across Fujian Province, lacking significant spatial clustering. Conversely, areas with a decrease in carbon storage are closely correlated with the expansion of construction land, predominantly in economically developed coastal urban areas such as Fuzhou, Putian, Xiamen, Zhangzhou, and Quanzhou. The decrease in carbon storage is most pronounced under the urban development scenario, while it is comparatively mitigated under the ecological protection scenario. These findings underscore the influence of urbanization and land use changes on carbon storage patterns, highlighting the critical need for targeted conservation strategies. While urban development poses substantial risks to carbon storage, particularly in coastal regions, ecological protection measures can play a pivotal role in preserving and enhancing carbon sequestration capacities in vulnerable areas.

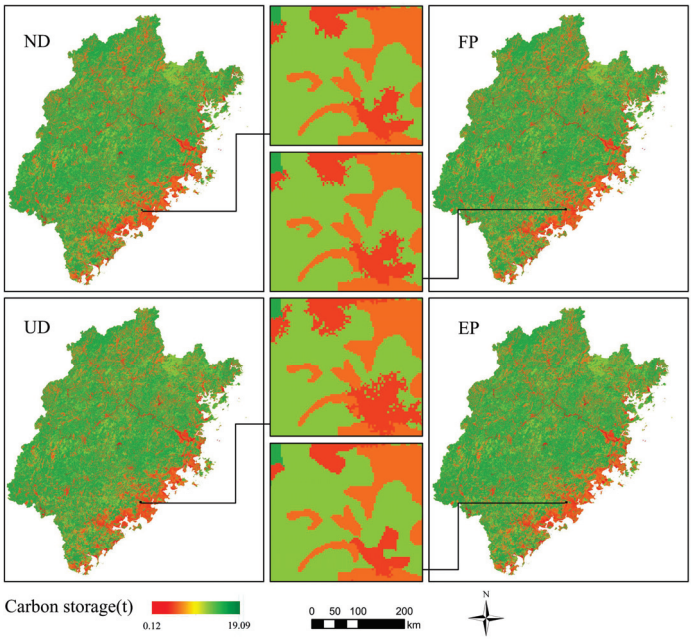

Figure 4. Spatial pattern of carbon storage under various scenarios in Fujian Province in 2030.

3.3.3. Key Protection Areas and Vulnerable Regions Under Future Scenarios

To further refine the identification of key protection areas and vulnerable regions in the spatial distribution of carbon storage under various future scenarios, the study first applied a hotspot analysis to the projected carbon storage distribution in 2030. This analysis targeted the hotspot regions identified within each scenario, with the subsequent statistical evaluation of carbon storage at the district and county levels. This process allowed for the identification of critical areas for protection and zones at risk. As shown in Figure 5, the consistency of the results across all four scenarios—highlighting 12 districts/counties as key protection areas and 31 as vulnerable regions—underscores the importance of targeted conservation efforts.

The key conservation areas are situated in Longyan City in the eastern part of Fujian Province, Sanming City in the west and northwest, and Nanping City in the northern region of the study area. Specifically, these 12 areas include Qingliu County, Changting County, Liancheng County, Wuping County, Shanghang County, and Xinluo District in the eastern region; Youxi County and Datian County in the central region; and Wuyishan City, Jianyang District, Jian'ou City, and Jianping District in the northern region. These regions are distinguished by dense forest cover and favorable ecological conditions, resulting in significant carbon storage and the formation of high-value carbon clusters, thereby prioritizing them for conservation and carbon management initiatives. Notably, Jian'ou City is projected to have the highest carbon storage among all the districts by 2030. Under the natural development scenario, carbon storage is expected to increase by 277,000 tons compared to 2020, primarily driven by a 17.7 km^2 expansion of high-carbon-density forest areas. Conversely, under the cultivated land protection scenario, carbon storage is anticipated to decrease by 389,200 tons due to the expansion of cultivated land, which has lower carbon density. Similarly, the urban development scenario predicts a reduction of 366,800 tons, reflecting the impact of accelerated urbanization and forest loss. Under the ecological protection scenario, however, Jian'ou's carbon storage is projected to reach 72.784 million tons, reflecting an increase of 248,500 tons from 2020, highlighting the benefits of conservation-focused land use policies.

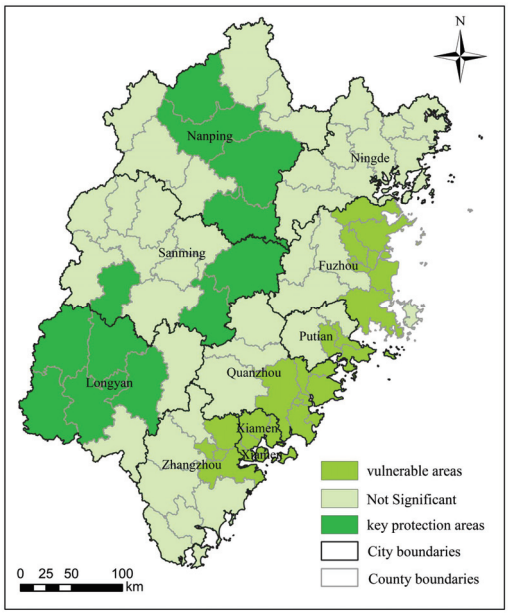

Figure 5. Key protection areas and vulnerable regions in the spatial distribution of carbon storage.

The vulnerable areas of carbon storage are predominantly concentrated in the coastal regions of Fuzhou City in the east, Putian City in the central region, and the Xiamen–Zhangzhou–Quanzhou metropolitan area in the south of Fujian Province, encompassing 31 districts and counties. These regions are characterized by high levels of urbanization and extensive construction land use, resulting in lower carbon storage capacities. The spatial clustering of low carbon storage values in these areas underscores their significance in regional carbon management and conservation strategies. Notably, Taijiang District exhibits the lowest carbon storage among all the districts, with a total of 53,700 tons. Under the cultivated land protection scenario, there is a slight decrease compared to the natural development scenario, primarily due to the district's minimal cultivated land area (0.0072 km^2), which limits the impact of protection policies. Conversely, the urban development scenario predicts a modest increase in carbon storage by 1900 tons, attributed to land use conversion from water bodies to construction land. Districts with carbon storage below 300,000 tons, such as Gulou, Huli, and Licheng, display higher carbon storage under the cultivated land protection scenario than under natural development, indicating that such policies can effectively slow urban expansion and enhance carbon sequestration in southeastern Fujian cities. However, the urban development scenario predicts a decline in carbon storage compared to 2020 levels, underscoring the heightened ecological pressure from urbanization. In contrast, the ecological protection scenario projects higher carbon storage than the natural development scenario, illustrating that conservation measures can effectively mitigate soil erosion and enhance carbon sequestration.

4. Discussion

4.1. From Policy to Practice to Assess Future Carbon Storage

In the context of carbon storage research, modeling and predicting future carbon dynamics based on local policy frameworks offer a more targeted and scientifically rigorous approach. This method aligns with the unique characteristics of the region, generating insights that are highly relevant and practical for urban planning and policy-making. Since the 18th National Congress of the Communist Party of China, the nation has increasingly focused on ecological conservation and sustainable development under the strategic guidance of the ecological civilization framework. This shift has been formalized through policies such as the "National Major Projects Plan for the Protection and Restoration of Important Ecosystems (2021–2035)" and the "National Territorial Spatial Plan Outline (2021–2035)," which integrates multiple planning frameworks into a cohesive strategy. These policies represent China's comprehensive and sustainable development model, referred to as the "Chinese solution," for managing and utilizing national territorial spaces.

In alignment with these national strategies, provincial-level spatial plans and ecological restoration initiatives have been systematically developed, including the "Fujian Provincial Territorial Spatial Plan (2021–2035)" and the "Fujian Provincial Ecological Restoration Plan (2021–2035)." These plans represent the region-specific implementations of national policies and emphasize the importance of integrating regional policy contexts into carbon storage models. Such integration enhances the precision of future carbon storage predictions, providing actionable insights for urban and regional planning that align development trajectories with sustainable ecological objectives.

This study establishes four distinct policy-driven scenarios—natural development, farmland protection, urban development, and ecological protection—based on the historical land use transition matrix of Fujian Province. These scenarios are specifically aligned with Fujian's regional policies, ensuring the seamless integration between policy directives and model projections. The findings reveal that among the four scenarios evaluated,

the ecological protection scenario is the most effective in enhancing carbon stocks, with a projected increase to 2.02 billion tons by 2030, followed by the natural development scenario (2.014 billion tons), the cultivated land protection scenario (2.013 billion tons), and the urban development scenario (2.01 billion tons). This hierarchy underscores the varying impacts of different land use strategies on the province's carbon sequestration potential. The ecological protection scenario underscores the critical importance of ecological protection and restoration policies, emphasizing measures such as forest conservation, ecological agriculture, and the control of urban sprawl. These actions, when combined with the region's economic development needs, highlight the necessity of rational land use planning to maintain ecosystem health and stability. In contrast, the urban development scenario results in the most significant reduction in carbon stocks, with a decrease of 0.007 billion tons compared to 2020, highlighting the environmental risks associated with unchecked urban expansion.

By quantifying the changes in carbon storage from policy implementation to practical outcomes, this research provides a critical assessment of the future effectiveness of policy measures. The findings offer valuable scientific data to support government efforts in policy formulation and adjustment. Moreover, the results serve as a guide for ecological restoration and land use planning in Fujian Province, with the potential to enhance ecosystem services and promote sustainable regional development. Therefore, this study holds significant theoretical and practical implications.

4.2. Refining Regional Analysis: Identifying Regional Differences and Key Areas in Future Carbon Storage

This study provides a refined analysis of carbon storage distribution in Fujian Province, revealing significant regional disparities in future carbon storage under the four simulated scenarios. The analysis identifies a clear spatial pattern, with higher carbon storage projected in the western and northwestern mountainous regions and lower storage in the eastern and southeastern coastal areas. Importantly, the identification of key protection areas and vulnerable regions remains consistent across all the scenarios.

Twelve districts and counties in Longyan, Sanming, and Nanping have been identified as key conservation areas due to their dense forest cover and favorable ecological conditions, which play a crucial role in carbon storage. Recognized as high-value carbon aggregation zones, these areas have been prioritized for conservation and carbon management initiatives. Fujian Province has actively implemented a range of measures in these regions aimed at protecting the ecological environment and enhancing carbon storage, thereby strengthening efforts to safeguard ecological integrity and promote carbon sequestration. For instance, Sanming has initiated pilot projects focused on forestry carbon sequestration, enabling carbon trading through forest management projects. In Meicun Village, Jiangshan Town, Xinluo District, Longyan, a carbon sink forest base has been established, planting broadleaf tree species to enhance the forest's carbon sequestration capacity. Additionally, the introduction of the first national forestry carbon sink index insurance provides risk protection and ensures the restoration of carbon sequestration capacity following environmental disturbances. Meanwhile, Nanping has accelerated the development of a comprehensive green, low-carbon, and circular economy, focusing on optimizing industrial, energy, and transportation structures to reduce carbon emission intensity. In key ecological function areas such as Wuyi Mountain National Park, ecological protection and restoration projects have been implemented to improve ecosystem quality and stability.

Conversely, 31 districts and counties in Fujian's coastal areas, particularly in highly urbanized regions such as Fuzhou, Putian, and the Xiamen–Zhangzhou–Quanzhou metropolitan area, have been identified as vulnerable zones with relatively low carbon storage capacity due to extensive urban development. In response, Fujian Province has undertaken proactive measures to enhance carbon storage in these vulnerable areas, driving a comprehensive green transformation of its economy and society. As a major coastal province, Fujian boasts abundant marine carbon sink resources, including ecosystems such as mangroves, seagrass beds, and salt marshes, which are characterized by their high carbon sequestration potential and long-term carbon storage capacity. Fujian Province is actively advancing research on marine carbon sinks and exploring carbon trading pilot projects through policy support and scientific initiatives, contributing to broader strategies aimed at achieving carbon peaking and carbon neutrality. Furthermore, Fujian supports the accelerated development of a zero-carbon demonstration zone on Meizhou Island in Putian, promoting green and low-carbon transformation through various measures, including green building initiatives, eco-friendly landscaping, and the utilization of renewable energy. These efforts have already yielded significant carbon reduction outcomes.

4.3. The Chinese Experience: Balancing Ecological Protection and Urban Development

This study highlights a critical trend: under the ecological protection scenario, carbon storage in Fujian Province is projected to increase significantly between 2020 and 2030, while under the urban development scenario, carbon storage is expected to decline the most. Urbanization brings opportunities for economic development but also presents ecological challenges, particularly in balancing growth with environmental sustainability. This finding aligns with research conducted both domestically and internationally. For example, He et al. [32] predicted carbon storage changes in Guilin, noting that carbon storage was highest under the ecological protection scenario and lowest under the economic priority scenario. This underscores a critical question: how can ecological protection be balanced with urban expansion? This issue is pivotal for enhancing ecosystem carbon storage and achieving sustainable development goals.

Fujian Province, as China's first national ecological civilization pilot zone and a vital ecological barrier in the southern region, faces unique challenges in balancing ecological protection with urban development. China has adopted a multi-dimensional approach to this challenge, successfully exploring a sustainable development path through policy guidance, technological innovation, and social participation.

Firstly, China has made ecological civilization a central component of its national development strategy, encapsulated in the concept that "lucid waters and lush mountains are invaluable assets." This philosophy emphasizes that economic development must be integrated with ecological protection, driving green development. This approach has been deeply embedded into urban planning, land use, and economic policies, providing clear guidance for balancing ecosystem carbon sinks with urban expansion. For instance, the "Fujian Provincial Territorial Spatial Planning (2021–2035)" and the "Fujian Provincial Ecological Restoration Plan (2021–2035)" were developed under this guiding philosophy.

Secondly, China has implemented a strict "ecological red line" policy, designating key ecological areas where any form of development is prohibited. This policy ensures the protection of critical ecosystems, such as forests, wetlands, and grasslands, allowing these areas to maintain their carbon sink functions despite urban expansion. Additionally, many Chinese cities are committed to green urban development by promoting green buildings, expanding public transportation, increasing urban green spaces, and implementing low-carbon energy projects. These efforts have successfully mitigated the negative impacts of

urban expansion on ecosystems while enhancing the carbon sequestration capacity within cities. For example, increasing urban parks and green spaces has not only improved carbon sink capabilities but also effectively reduced carbon emissions.

Moreover, China has undertaken large-scale ecological restoration projects, such as the Grain for Green Project (returning farmland to forests) and desertification control initiatives, to restore vast degraded ecosystems. In Fujian Province, for instance, four ecological protection and restoration zones have been delineated based on the ecological security framework of "Two Screens, One Belt, Six Rivers, Two Streams", with 59 key ecological restoration areas identified. The "Fujian Provincial Ecological Restoration Plan (2021–2035)" aims to increase the province's forest coverage rate to over 65.37% by 2035. These restoration projects have not only improved the quality of the ecological environment but also provided green buffer zones for urban expansion.

Finally, in advancing new urbanization, China has emphasized the construction of smart cities, using technological innovation to optimize urban planning and management. Smart city technologies, including the Internet of Things (IoT), big data, and artificial intelligence (AI), enable better management of urban ecosystems and carbon emissions, supporting the balance between carbon sinks and urban development. Fujian's smart city initiatives, centered on "Digital Fujian," focus on leveraging IoT, big data, and AI to enhance urban management efficiency and improve residents' quality of life. The province is also advancing the construction of a "digital ecology" demonstration, enhancing the "One Map" for ecological monitoring, conducting satellite remote sensing applications, and automating sound environment quality monitoring. Additionally, Fujian is accelerating the development of an integrated natural resources information platform and the "Smart Forestry 123" project, constructing a comprehensive "sky–earth" integrated sensing and application system.

These strategies illustrate how China has successfully balanced ecological protection with urban development, offering valuable lessons for sustainable development. Fujian Province's experience, as detailed in this study, highlights the importance of aligning regional strategies with national priorities to achieve sustainable growth and carbon neutrality.

4.4. Uncertainty, Limitations, and Prospects

Although this study has produced valuable findings, it also has certain limitations. One key limitation concerns the carbon density data used, which primarily derives from the existing literature for the study area and nearby regions, with a preference for field-collected data. Additionally, the study utilizes national and Fujian Province annual precipitation data to calculate a correction coefficient between the actual and simulated carbon densities. While the corrected carbon density values closely align with the actual data for the study area, environmental changes and human activities continue to influence carbon density, introducing a degree of uncertainty into the estimated carbon storage. To improve the reliability of carbon storage estimates in future studies, it is essential to validate carbon density values with dynamic, region-specific field data. This would provide a more robust foundation for accurate carbon storage assessments.

Secondly, the InVEST model, used to estimate carbon storage, relies on land use types, which overlooks several critical factors influencing carbon sequestration, such as photosynthesis rates and soil microbial activity. Additionally, the model does not account for variations in carbon sequestration capacity due to differences in internal land use structure and vegetation age. As a result, this leads to errors in the spatial distribution of carbon storage, ultimately affecting the accuracy of the results. On the other hand, the PLUS model assumes fixed transition rules based on historical land conversion patterns

when simulating future land use changes. However, these transition rules may evolve as a region develops, and future development plans, along with related policy documents, may not be directly incorporated into the model's constraint rules. To address these limitations, future research could consider estimating carbon storage based on surface cover materials. Additionally, more advanced cellular automata (CA) models, such as the landscape-driven patch-based CA, could be employed to better capture the dynamics of land use changes and carbon sequestration processes.

Finally, despite considering different scenarios, the simulation results for future land use still show a degree of uncertainty. The factors influencing carbon storage are multifaceted, and this study has made simplifications by selecting only 10 driving factors. However, the actual determinants of land use change are often more intricate, and both the quantity and nature of these factors may vary over time. Additionally, the feasibility of policy implementation within a given region, as well as the interactions between different policy measures, play a significant role in influencing carbon storage outcomes. Furthermore, the potential impact of future policy shifts, technological advancements, and market dynamics on carbon sequestration must be accounted for. Future research should, thus, delve deeper into the evolving trends in carbon storage, identify the key factors that influence these trends, and examine the implications under different policy scenarios. Moreover, the feasibility and challenges of policy implementation, as well as the synergies and tradeoffs between policies, should be investigated to provide more comprehensive and actionable policy recommendations. In parallel, the integration of technological progress, market dynamics, and potential future policy changes into carbon storage models is crucial to enhance the robustness of projections for future carbon sequestration.

5. Conclusions

This study integrates the "Fujian Provincial Territorial Spatial Planning (2021–2035)" and the "Fujian Provincial Ecological Restoration Plan (2021–2035)" to analyze the impacts of policy-driven land use changes on carbon storage in Fujian Province. The findings indicate the following:

(1) Spatiotemporal Evolution of Carbon Storage

The spatiotemporal evolution of carbon storage in Fujian Province shows a significant decline from 1995 to 2020, primarily due to the conversion of forests and agricultural lands into construction areas. The FLUS and InVEST models highlight the negative impact of urban expansion on carbon storage.

(2) Carbon Storage Under Different Future Scenarios

The simulations of future scenarios reveal that the ecological protection scenario achieves the highest carbon storage by 2030. This outcome underscores the benefits of afforestation and conservation efforts. In contrast, the urban development scenario results in the lowest carbon storage, emphasizing the risks associated with unchecked urban growth and the importance of sustainable land use policies.

(3) Regional Differences in Carbon Storage and Key Protection Areas

The western and northwestern areas are prioritized as conservation zones, with 12 districts deemed critical for protection. Conversely, the eastern coastal urban regions, comprising 31 vulnerable districts, face the greatest risks to their carbon storage potential. These findings highlight the need for targeted conservation efforts in these regions to balance ecological protection with economic development.

Author Contributions: Conceptualization, Q.N. and W.M.; methodology, X.W. and Z.L.; software, Z.L.; validation, Z.L.; writing—original draft preparation, Q.N.; writing—review and editing, Q.N.

and W.M.; visualization, X.W.; supervision, Q.N. and W.M.; funding acquisition, W.M. All authors have read and agreed to the published version of the manuscript.

Funding: This research was funded by The Guiding Project of Fujian Province Science and Technology Program (No. 2021H0026), the Xiamen City Open Competition for Leadership Project (No. 3502Z20231038) and the Natural Science Foundation of Fujian Province (No. 2024J011194).

Data Availability Statement: Data will be made available upon request.

Conflicts of Interest: The authors declare no conflicts of interest.

References

1. IPCC. *Global Warming of 1.5 °C. An IPCC Special Report on the Impacts of Global Warming of 1.5 °C Above Pre-Industrial Levels and Related Global Greenhouse Gas Emission Pathways*; Intergovernmental Panel on Climate Change: Geneva, Switzerland, 2018.
2. Foley, J.A.; DeFries, R.; Asner, G.P.; Barford, C.; Bonan, G.; Carpenter, S.R.; Chapin, F.S.; Coe, M.T.; Daily, G.C.; Gibbs, H.K.; et al. Global consequences of land use. *Science* **2005**, *309*, 570–574. [CrossRef] [PubMed]
3. Smith, P.; Bustamante, M.; Ahammad, H.; Clark, H.; Dong, H.; Elsiddig, E.A.; Haberl, H.; Harper, R.; House, J.; Jafari, M.; et al. Agriculture, Forestry and Other Land Use (AFOLU). In *Climate Change 2014: Mitigation of Climate Change. Contribution of Working Group III to the Fifth Assessment Report of the Intergovernmental Panel on Climate Change*; Cambridge University Press: Cambridge, UK, 2014.
4. Turner, B.L.; Lambin, E.F.; Reenberg, A. The emergence of land change science for global environmental change and sustainability. *Proc. Natl. Acad. Sci. USA* **2007**, *104*, 20666–20671. [CrossRef] [PubMed]
5. Seto, K.C.; Güneralp, B.; Hutyra, L.R. Global forecasts of urban expansion to 2030 and direct impacts on biodiversity and carbon pools. *Proc. Natl. Acad. Sci. USA* **2012**, *109*, 16083–16088. [CrossRef] [PubMed]
6. Griscom, B.W.; Adams, J.; Ellis, P.W.; Houghton, R.A.; Lomax, G.; Miteva, D.A.; Schlesinger, W.H.; Shoch, D.; Siikamäki, J.V.; Smith, P.; et al. Natural climate solutions. *Proc. Natl. Acad. Sci. USA* **2017**, *114*, 11645–11650. [CrossRef]
7. Zhang, X.; Liu, Y.; Chen, W.; Li, J. China's energy transitions for carbon neutrality: Challenges and opportunities. *Sustain. Energy Transit.* **2022**, *3*, 123–145. [CrossRef]
8. Liu, Z.; Deng, Z.; He, G.; Wang, H.; Zhang, X.; Lin, J.; Qi, Y.; Liang, X. Challenges and opportunities for carbon neutrality in China. *Nat. Rev. Earth Environ.* **2022**, *3*, 141–155. [CrossRef]
9. Gao, F.; Xin, X.; Song, J.; Li, X.; Zhang, L.; Zhang, Y.; Liu, J. Simulation of LUCC Dynamics and Estimation of Carbon Stock under Different SSP-RCP Scenarios in Heilongjiang Province. *Land* **2023**, *12*, 1665. [CrossRef]
10. Li, J.; Chen, X.; Kurban, A.; Van de Voorde, T.; De Maeyer, P.; Zhang, C. Coupled SSPs-RCPs scenarios to project the future dynamic variations of water-soil-carbonbiodiversity services in Central Asia. *Ecol. Ind.* **2021**, *129*, 107936. [CrossRef]
11. Tan, J.; Li, A.; Lei, G.; Xie, X. A SD-MaxEnt-CA model for simulating the landscape dynamic of natural ecosystem by considering socio-economic and natural impacts. *Ecol. Model.* **2019**, *410*, 108783. [CrossRef]
12. Chen, Y.; Li, X.; Liu, X.; Ai, B. Modeling urban land-use dynamics in a fast developing city using the modified logistic cellular automaton with a patch-based simulation strategy. *Int. J. Geogr. Inf. Sci.* **2014**, *28*, 234–255. [CrossRef]
13. Lin, J.; Chen, Q. Analyzing and Simulating the Influence of a Water Conveyance Project on Land Use Conditions in the Tarim River Region. *Land* **2023**, *12*, 2073. [CrossRef]
14. Luo, G.; Yin, C.; Chen, X.; Xu, W.; Lu, L. Combining system dynamic model and CLUE-S model to improve land use scenario analyses at regional scale: A case study of Sangong watershed in Xinjiang, China. *Ecol. Complex.* **2010**, *7*, 198–207. [CrossRef]
15. Zhu, W.; Gao, Y.; Zhang, H.; Liu, L. Optimization of the land use pattern in Horqin Sandy Land by using the CLUMondo model and Bayesian belief network. *Sci. Total Environ.* **2020**, *739*, 139929. [CrossRef] [PubMed]
16. Ding, Q.; Chen, Y.; Bu, L.; Ye, Y. Multi-scenario analysis of habitat quality in the yellow river delta by coupling FLUS with InVEST model. *Int. J. Environ. Res. Public Health* **2021**, *18*, 2389. [CrossRef] [PubMed]
17. Liang, X.; Guan, Q.; Clarke, K.C.; Liu, S.; Wang, B.; Yao, Y. Understanding the drivers of sustainable land expansion using a patch-generating land use simulation (PLUS) model: A case study in Wuhan, China. *Comput. Environ. Urban Syst.* **2021**, *85*, 101569. [CrossRef]
18. Zhai, H.; Lv, C.; Liu, W.; Yang, C.; Fan, D.; Wang, Z.; Guan, Q. Understanding spatio-temporal patterns of land use/land cover change under urbanization in Wuhan, China, 2000–2019. *Remote Sens.* **2021**, *13*, 3331. [CrossRef]
19. Zhang, G.; Shi, P.; Jiang, L.; Hu, X.; Zhong, H.; Chen, Y. Carbon Emission Risk and Governance. *Int. J. Disaster Risk Sci.* **2021**, *13*, 249–260.
20. Wu, X.; Zhang, Y.; Liu, H.; Zhao, Z.; Zhou, X.; Li, Y. Land Use Optimization in Ningbo City with a Coupled GA and PLUS Model. *J. Clean. Prod.* **2023**, *375*, 134004.

21. Wen, D.; He, N.P. Spatial Patterns and Control Mechanisms of Carbon Storage in Forest Ecosystem: Evidence from the North-South Transect of Eastern China. *Ecol. Indic.* **2016**, *61*, 960–967. [CrossRef]
22. Sun, J.; Zhang, Y.; Qin, W.; Chai, G. Estimation and Simulation of Forest Carbon Stock in Northeast China Forestry Based on Future Climate Change and LUCC. *Remote Sens.* **2022**, *14*, 3653. [CrossRef]
23. Sun, X.; Wang, S.; Xue, J.; Dong, L. Assessment and Simulation of Ecosystem Carbon Storage in Rapidly Urbanizing Areas Based on Land Use Cover: A Case Study of the Southern Jiangsu Urban Agglomeration, China. *Front. Environ. Sci.* **2022**, *10*, 647. [CrossRef]
24. Ke, N.; Lu, X.; Zhang, X.; Kuang, B.; Zhang, Y. Urban Land Use Carbon Emission Intensity in China under the "Double Carbon" Targets: Spatiotemporal Patterns and Evolution Trend. *Environ. Sci. Pollut. Res.* **2023**, *30*, 18213–18226. [CrossRef] [PubMed]
25. Li, L.; Fu, W.; Luo, M. Spatial and Temporal Variation and Prediction of Ecosystem Carbon Stocks in Yunnan Province Based on Land Use Change. *Int. J. Environ. Res. Public Health* **2022**, *19*, 16059. [CrossRef]
26. Xu, D.; Yu, C.; Lin, W.; Yao, J.; Zhou, W. Spatiotemporal Evolution and Prediction of Land Use and Carbon Stock in Shanghai. *Land* **2024**, *13*, 267. [CrossRef]
27. Petrokofsky, G.; Kanamaru, H.; Achard, F.; Goetz, S.J.; Joosten, H.; Holmgren, P.; Lehtonen, A.; Menton, M.C.S.; Pullin, A.S.; Wattenbach, M. Comparison of Methods for Measuring and Assessing Carbon Stocks and Carbon Stock Changes in Terrestrial Carbon Pools. How do the accuracy and precision of current methods compare? A systematic review protocol. *Environ. Evid.* **2012**, *1*, 6. [CrossRef]
28. Pan, H.; Wu, C. Bayesian Optimization + XGBoost Based Life Cycle Carbon Emission Prediction for Residential Buildings-An Example from Chengdu, China. *Build. Simul.* **2023**, *16*, 1451–1466. [CrossRef]
29. Nandal, A.; Yadav, S.S.; Rao, A.S.; Meena, R.S.; Lal, R. Advance Methodological Approaches for Carbon Stock Estimation in Forest Ecosystems. *Environ. Monit. Assess.* **2023**, *195*, 315. [CrossRef]
30. Xu, X.; Liu, J.; Zhang, S.; Li, R.; Yan, C.; Wu, S. *China's Multi-Period Land Use Land Cover Remote Sensing Monitoring Data Set (CNLUCC)*; Resource and Environment Data Cloud Platform: Beijing, China, 2018.
31. Wang, H.; Cai, L.; Wen, X.; Fan, D.; Wang, Y. Land Cover Change and Multiple Remotely Sensed Datasets Consistency in China. *Ecosyst. Health Sustain.* **2022**, *8*, 2040385. [CrossRef]
32. He, Y.; Ma, J.; Zhang, C.; Yang, H. Spatio-Temporal Evolution and Prediction of Carbon Storage in Guilin Based on FLUS and InVEST Models. *Remote Sens.* **2023**, *15*, 1445. [CrossRef]

Disclaimer/Publisher's Note: The statements, opinions and data contained in all publications are solely those of the individual author(s) and contributor(s) and not of MDPI and/or the editor(s). MDPI and/or the editor(s) disclaim responsibility for any injury to people or property resulting from any ideas, methods, instructions or products referred to in the content.

land

MDPI

Article

Regional Differences in the Impact of Land Use Pattern on Total Phosphorus Concentration in the Yangtze River Basin

Fuliang Deng [1], Wenhui Liu [1], Wei Liu [1], Yanxue Xu [2,3,*], Yuanzhuo Sun [1], Chen Zhang [1], Mei Sun [1] and Ying Yuan [1]

[1] School of Computer and Information Engineering, Xiamen University of Technology, Xiamen 361024, China; fldeng8266@xmut.edu.cn (F.D.); 2322081026@stu.xmut.edu.cn (W.L.); devilweil@xmut.edu.cn (W.L.); 2422071039@stu.xmut.edu.cn (Y.S.); 2422071056@stu.xmut.edu.cn (C.Z.); sunm@xmut.edu.cn (M.S.); yuanying@xmut.edu.cn (Y.Y.)
[2] United Center for Eco-Environment in Yangtze River Economic Belt, Chinese Academy of Environmental Planning, Beijing 100041, China
[3] Department of Hydraulic Engineering, Tsinghua University, Beijing 100084, China
* Correspondence: xuyx@caep.org.cn

Abstract: Accurately assessing the impact of land use patterns on total phosphorus (TP) concentration in surface water is crucial for protecting the water environment of the Yangtze River Basin (YRB). However, due to the heterogeneity of land use patterns, the regional differences in the intensity and direction of their impacts on TP concentrations in the YRB remain insufficiently understood. This study utilizes water quality monitoring data from state-controlled sections in 2021 and employs spatial autocorrelation analysis, geographic detectors, and Pearson correlation models to identify the impacts of land use on TP concentrations at multiple scales across the YRB. The results indicate that TP concentrations at 98.8% of the monitoring stations in the YRB exceed the Class III standard, with high concentrations of TP concentrated in the Pudu River Basin, Chengdu Plain, Jianghan Plain, and Yangtze River Delta regions. At the YRB scale, the spatial pattern of built-up land, cropland, and industrial and mining land significantly increases TP concentrations, while the pattern of forest and grassland areas exert mitigating effects. At the sub-basin scale, the impact of land use patterns on TP concentrations varies regionally. Specifically, TP concentrations in the Pudu River Basin are primarily attributed to the spatial pattern of industrial and mining land, in the Chengdu Plain to the spatial pattern of cropland and industrial and mining land, and in the Jianghan Plain to the spatial pattern of cropland, built-up land, and industrial and mining land. These results provided decision support for TP concentration control strategies and effective mitigation measures.

Keywords: land use type; total phosphorus concentration; GeoDetector; regional differences; Yangtze River Basin

1. Introduction

Phosphorus, a critical nutrient for algal growth in aquatic ecosystems, is the primary driver of water eutrophication [1]. Eutrophication significantly alters the ecological balance of aquatic systems and poses serious risks to ecosystem security [2]. Land use practices serve as a direct reflection of human activity impacts on the environment, shaping agricultural management, farming practices, and other phosphorus discharge pathways, which significantly influence the input and output of total phosphorus (TP) concentration in water bodies [3–5]. Regional disparities in land use practices create complex, non-linear relationships between land use and TP concentrations [6,7], complicating TP source traceability

and hindering the effective management of aquatic ecosystems. Therefore, understanding watershed land use impacts on TP concentrations is critical for identifying TP sources and protecting aquatic ecosystems effectively.

The Yangtze River, the largest river in China, contributes to around 20% of the nation's wetland area, 35% of its total water resources, and sustains over 40% of its population and GDP [8,9]. Since 2016, TP concentration has been recognized as a key pollutant in the Yangtze River Basin (YRB) aquatic environment [10,11]. Accurately assessing the impact of land use on TP concentrations in the basin has become a key research priority. An increasing body of evidence indicates that land use patterns within a watershed significantly affect water quality [12–14]. Numerous studies have examined the relationship between land use and TP concentrations across different scales, including control units, sub-basins, and the entire basin [15–17]. However, the conclusions of these studies also exhibit discrepancies to some extent. For example, Li et al. [12] identified cropland as the primary source of TP concentrations in the upper Yangtze River, whereas Wang et al. [14] found that both built-up lands and croplands are the major sources in the Gan River Basin. Similarly, Zhang et al. [18] demonstrated that built-up lands is the primary contributor to TP concentrations in the Dianchi Basin of the Jinsha River system. These discrepancies highlight that multi-scale, systematic studies are essential for understanding the mechanisms and regional differences of land use impacts on TP concentrations in the YRB. However, current research often focuses on specific river segments or individual sub-watersheds [19–21].

In addition, the land use types examined in previous studies typically encompass broad categories, including cropland, built-up land, grassland, and forest. However, the influence of industrial and mining land on TP concentrations must not be underestimated. For instance, Guan et al. [22] observed a significant correlation between industrial and mining land and TP concentrations, while Cao et al. [23] identified that sub-basins dominated by industrial and mining land tend to have the worst water quality. The YRB is a major region for phosphate mining, phosphorus chemical industries, and phosphogypsum disposal sites, especially in the upper and middle reaches [10]. However, the extent and regional variations of the impact of industrial and mining land on TP concentrations remain unclear.

This study aimed to investigate the impact of land use on TP concentrations in the YRB at multiple scales, along with regional variations of this influence. Specifically, the study aims are as follows: (1) to analyze the spatial distribution characteristics of TP concentrations across the entire YRB and its secondary water resource divisions, and identify the spatial hot and cold zones of total TP concentrations; (2) to examine the spatial distribution of different land use types at three scales (the entire basin, hot and cold zones of TP concentrations, and secondary water resource divisions); (3) to explore the impact of land use on TP concentrations at the above three scales and identify regional differences in the dominant factors influencing TP concentrations. The results provide decision support for regional management and the control of TP concentrations in the YRB.

2. Materials and Methods

2.1. Study Area

The YRB is a key strategic economic region in China, comprising 16 provinces and municipalities, including Qinghai, Zhejiang, and Shanghai, etc. The Yangtze River's main stem is divided into three sections: the upstream, extending from Yichang to the river's upper reaches, with a catchment area of approximately 100×10^4 km^2; the midstream, from Yichang to Hukou, covering around 68×10^4 km^2; and the downstream, from Hukou onwards, with a catchment area of about 12×10^4 km^2 [24] (Figure 1). The YRB spans China's eastern, central, and western economic zones, linking the north and south, and

plays a pivotal role in national economic development. The upper and middle reaches of the YRB are rich in the country's phosphate mineral resources and are the regions most impacted by the "three phosphorus" issue. In recent years, TP has emerged as the primary pollutant in the YRB, posing a significant barrier to water quality improvement in the region [25].

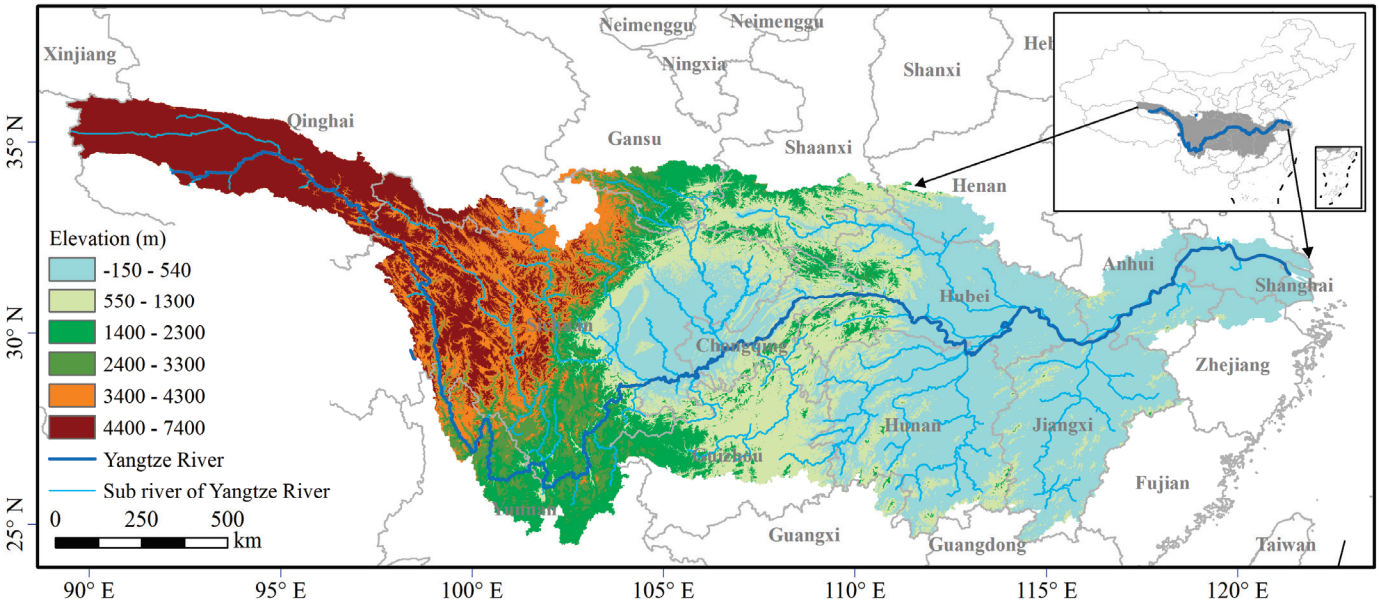

Figure 1. Overview of the Yangtze River Basin.

2.2. Data Source

2.2.1. State-Controlled Sections and Water Resource Allocation

TP concentration monitoring data were obtained from the China National Environmental Monitoring Center (https://www.cnemc.cn, accessed on 20 August 2024). The monitoring parameters encompass water temperature, pH, dissolved oxygen, conductivity, turbidity, permanganate index, ammonia nitrogen, TP, and total nitrogen. In accordance with the "Surface Water Environmental Quality Assessment Method (Trial)" issued by the Ministry of Environmental Protection in 2011, the annual TP concentration indicator for the 2021 monitoring data was derived using the arithmetic mean of TP concentrations. During the 14th Five-Year Plan, the Ministry of Ecology and Environment set up 3641 state-controlled sections (monitoring stations) nationwide [26]. These stations monitor the main streams and major tributaries of key national river basins, vital water bodies at provincial and municipal boundaries, cities at or above the prefecture level, and significant river and lake water functional zones across the country. Specifically, the YRB includes 1252 state-controlled sections and 12 secondary water resource divisions.

2.2.2. Land Use Type Data

This study utilizes land use type data from the WorldCover dataset released by the European Space Agency (ESA) in 2021, which has a resolution of 10 m. The WorldCover v200 product provides a global land cover map for 2021, generated from Sentinel-1 and Sentinel-2 data (https://viewer.esa-worldcover.org/worldcover/, accessed on 20 August 2024). It includes 11 land cover classes aligned with the UN-FAO Land Cover Classification System, developed within the ESA WorldCover project. Based on existing research and the land use types in the YRB, six land use types were selected as potential determinants of phosphorus concentrations: forest, grassland, cropland, built-up land, bareland, and wetland.

Industrial and mining land use data were obtained from the National Land Use/Cover Change Dataset, provided by the Institute of Remote Sensing and Digital Earth, Chinese Academy of Sciences (https://www.resdc.cn, accessed on 20 August 2024). This dataset represents a secondary classification within land use/cover change data, encompassing areas designated for industrial and mining activities, including factories, large industrial zones, oil fields, salt fields, quarries, transportation infrastructure, airports, and specialized land uses. To assess the distribution of industrial and mining land, this study employed 2022 Point of Interest (POI) data (https://lbs.amap.com/, accessed on 20 August 2024), filtering records based on keywords such as "phosphorus", "chemicals", "phosphate", "fertilizer", and "mining". A total of 19,609 POI records corresponding to industrial and mining land were retrieved. Since the POI data are point-based, a 3000 m buffer was applied to extract areas within transportation infrastructure related to industrial and mining land use, thereby delineating the land use areas corresponding to industrial and mining activities.

2.3. Methods

This study is comprised of two primary components: the first involves employing hotspot analysis to investigate the spatial aggregation characteristics of TP concentrations, and the second focuses on constructing a land use impact index to identify the mechanisms by which land use influences TP concentrations across multiple scales. The technical approach is illustrated in Figure 2.

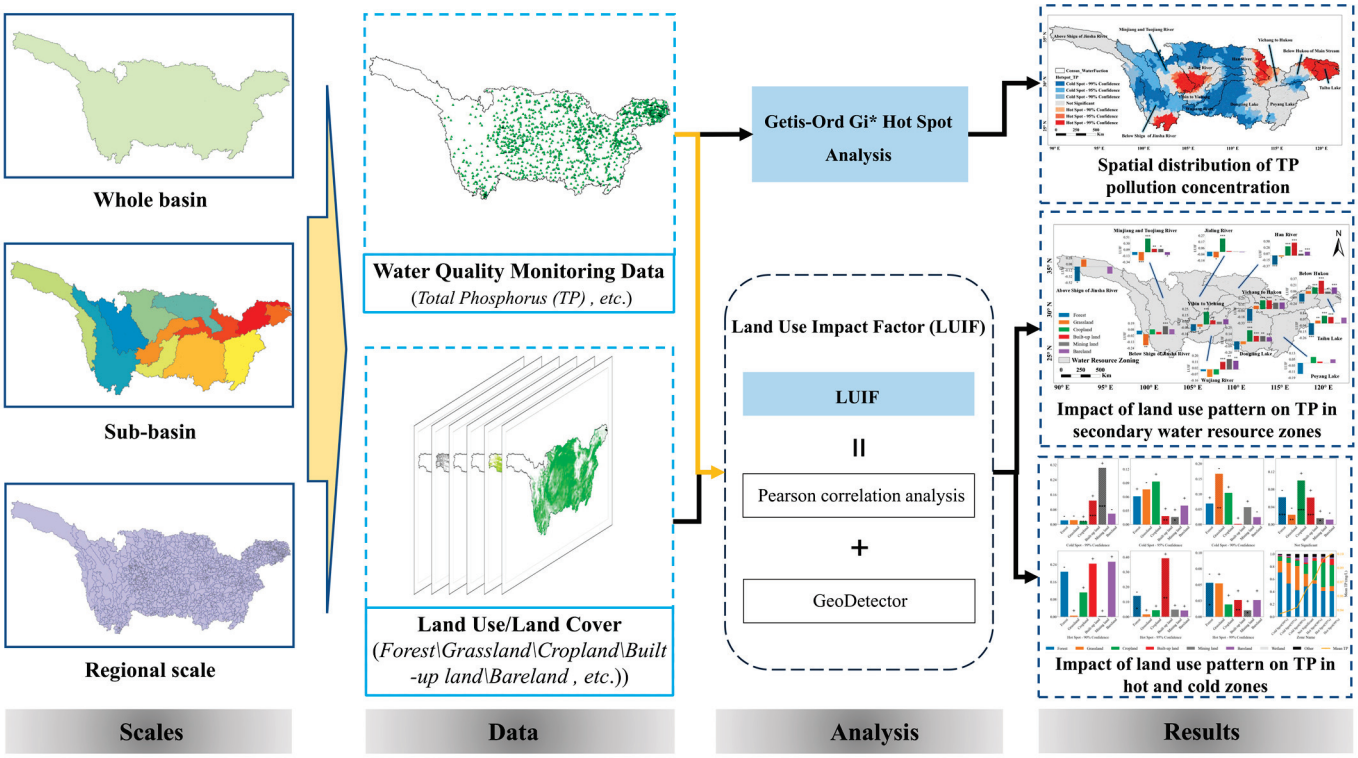

Figure 2. Technical Scheme.

2.3.1. Getis-Ord Gi* Hot Spot Analysis

Getis-Ord Gi* is a spatial clustering method, used to reveal the spatial distribution patterns of statistically significant hot and cold spots [27]. Specifically, it identifies regions of high (hot spots) and low (cold spots) concentrations of TP concentrations in the YRB. The specific calculation formula of Getis-Ord Gi* is as follows:

$$G_i^*(d) = \sum_{j=1}^{n} w_{ij}(d)X_j - \overline{X}\sum_{j=1}^{n} w(d)_{ij} / S\sqrt{\left[n\sum_{j=1}^{n} w(d)_{ij}^2 - \left(\sum_{j=1}^{n} w(d)_{ij}\right)^2\right] / n - 1} \quad (1)$$

where i is the central section, j is the adjacent section within the distance d from the central section i, X_j is the TP concentration of section j, $w(d)_{ij}$ is the spatial weight between section i and section j, and n is the total number of sections within the distance d. Moreover:

$$\overline{X} = \sum_{j=1}^{n} X_j / n \quad (2)$$

$$S = \sqrt{\left(\sum_{j=1}^{n} X_j^2 / n\right) - \left(\overline{X}\right)^2} \quad (3)$$

where $G_i^*(d)$ is the Z-score and no further calculations are required.

2.3.2. Land Use Impact Factor (LUIF)

To quantify the strength and direction of the impact of land use type on TP concentration and to comprehensively evaluate the impact of land use type on TP concentration, we proposed an innovative index, Land Use Impact Factor (LUIF). LUIF combines the q-value (interpretability) of GeoDetector and Pearson correlation (directionality) as follows:

$$LUIF = \begin{cases} q, & if\ corr \geq 0 \\ -q, & if\ corr < 0 \end{cases} \quad (4)$$

where q is the GeoDetector statistic, which characterizes the influence of land use type on TP concentration, and *corr* is the Pearson correlation coefficient.

Pearson correlation analysis is a statistical method used to measure the strength and direction of a linear relationship between two continuous variables. It has a value between -1 and 1, where 1 indicates a perfect positive correlation, -1 indicates a complete negative correlation, and 0 indicates no correlation. The Pearson correlation calculation is based on the covariance and standard deviation of the two variables, which are calculated as follows:

$$corr = \frac{\sum_{i=1}^{n}(x_i - \overline{x})(y_i - \overline{y})}{\sqrt{\sum_{i=1}^{n}(x_i - \overline{x})^2 \sum_{i=1}^{n}(y_i - \overline{y})^2}} \quad (5)$$

where x_i and y_i are the observed values of the two variables, $\overline{x}$ and $\overline{y}$ are the mean values of the two variables.

GeoDetector is a statistical method proposed by Wang Jinfeng in 2017 to detect spatial heterogeneity and reveal the driving factors behind it [28]. The q statistic of GeoDetector can be used to measure spatial heterogeneity, detect explanatory factors, and analyze the interaction between variables. The specific formula for calculating the q value is as follows:

$$q = 1 - \frac{\sum_{h=1}^{L} N_h \sigma_h^2}{N\sigma^2} = 1 - \frac{SSW}{SST} \quad (6)$$

$$SSW = \sum_{h=1}^{L} N_h \sigma_h^2 \quad (7)$$

$$SST = N\sigma^2 \quad (8)$$

where $h = 1, \cdots, L$ is the strata of the variable Y or factor X, i.e., classification or partitioning; N_h and N are the number of units in layer h and the whole area, respectively; σ_h^2 and σ^2 are the variances of the Y values for layer h and the whole area, respectively. The q value ranges from [0, 1], and the larger the value, the more obvious is the spatial heterogeneity of Y. If the stratification is generated by the independent variable X, a higher q value indicates

that the independent variable X is more explanatory to the dependent variable Y, and vice versa. In the extreme case, a q value of 1 indicates that factor X fully controls the spatial distribution of Y; a q value of 0 indicates that factor X has no relationship to Y; and a q value indicates that X explains $100 \times q\%$ of Y.

Interactive detectors are an important part of the GeoDetector method, which can study the effects of any two land use types on the TP concentration, and the following five situations may occur when the two factors are interacted (Table 1).

Table 1. The type of interaction between two independent variables on the dependent variable.

Judgment Basis	Interaction
$q(X1 \cap X2) < min[q(X1), q(X2)]$	Nonlinear weakening
$min[q(X1), q(X2)] < q(X1 \cap X2) < max[q(X1), q(X2)]$	Single-factor nonlinear weakening
$q(X1 \cap X2) > max[q(X1), q(X2)]$	Two-factor enhancement
$q(X1 \cap X2) = q(X1) + q(X2)$	Independence
$q(X1 \cap X2) > q(X1) + q(X2)$	Nonlinear enhancement

3. Results

3.1. Spatial Distribution Pattern of TP Concentration in the YRB

3.1.1. Spatial Distribution Characteristics of TP Concentration

The spatial distribution of TP concentration in the YRB shows a fragmented pattern, with areas of high TP concentration predominantly located in low-elevation plains, such as the Chengdu Plain, Jianghan Plain, and the Yangtze River Delta (Figure 3). TP concentrations in the middle reaches of the Yangtze River are significantly lower than those in both the upper and lower reaches. Among the 12 secondary water resource divisions, areas such as the downstream of the Jinsha River, the mainstream from Yibin to Yichang, the Han River, the mainstream from Yichang to Hukou, and the Dongting Lake water system exhibit more frequent extreme TP concentration values, marking them as high-risk zones for TP concentration (Figure A1). According to the water quality classification standards issued by the Ministry of Ecology and Environment, TP concentration in the YRB ranges from Class I to Class V. Notably, 98.8% of state-controlled sections report TP concentration above the Class III standard, indicating that the overall water quality in the basin is predominantly classified as good or better. However, certain areas in the basin exhibit TP concentrations that exceed the standard. The highest recorded TP concentration is at the Muguodian Village section in Wuding County, Chuxiong Yi Autonomous Prefecture, Yunnan Province, where the TP concentration is 0.45 mg/L, corresponding to the Class V standard, indicating poor water quality.

3.1.2. Analysis of Hotspot Areas for TP Concentration

TP concentration in the YRB displays distinct spatial clustering, predominantly concentrated in low-lying plains, including the Chengdu Plain in the Sichuan Basin, the Pu River Basin in Yunnan, the Jianghan Plain, the Central Anhui Plain, and the Yangtze River Delta (Figure 4). TP concentration in hotspot areas ranges from 0.02 mg/L to 0.45 mg/L, which are classified below the Class II water quality standard. In contrast, TP concentration in cold spot areas remains consistently below 0.3 mg/L, all surpassing the Class III water quality standard. In non-hotspot regions, TP concentrations range from 0.005 mg/L to 0.25 mg/L, with pollution levels meeting or surpassing the Class IV standard.

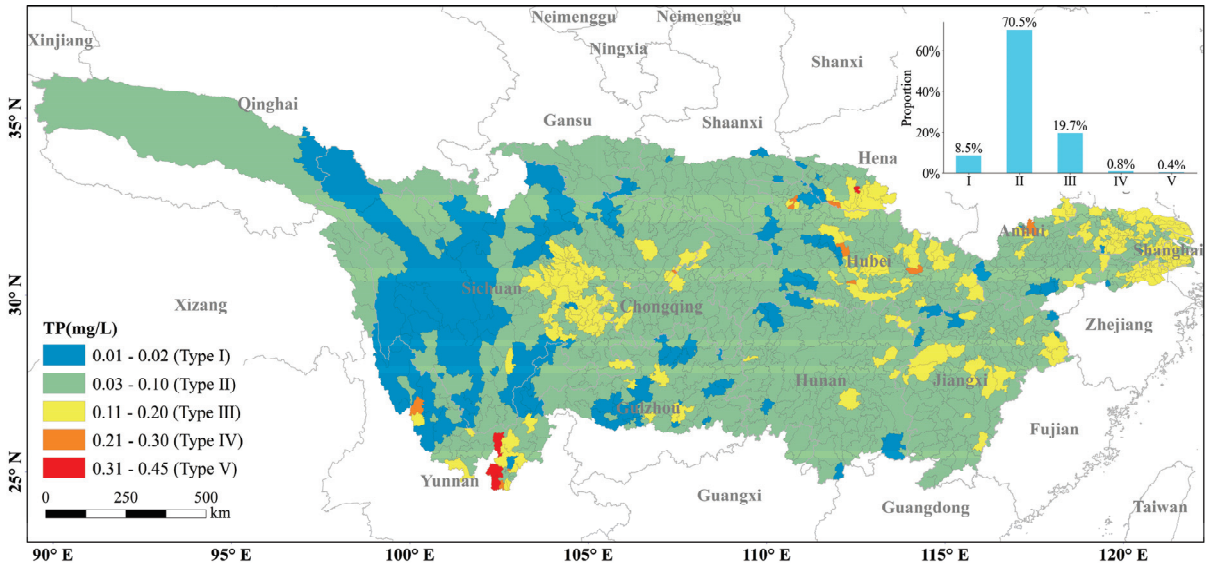

Figure 3. Spatial distribution map of TP concentration in the Yangtze River Basin based on national control cross-sections.

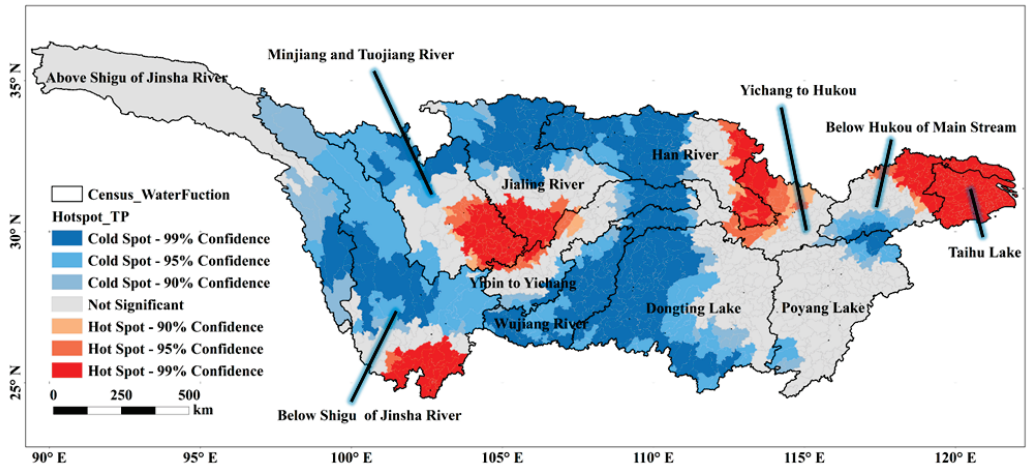

Figure 4. Hotspot analysis and secondary water resource zoning-based TP concentration hot and cold zoning map in the Yangtze River Basin.

3.2. Spatial Distribution Characteristics of Land Use Patterns in the YRB

The land use in the YRB is predominantly composed of forests, grasslands, and croplands (Figure 5). The distribution of land use types is as follows: forests (53.5%), grasslands (22.1%), croplands (14.5%), built-up lands (2.9%), barelands (3.2%), and wetlands (0.2%). Forests are predominantly located in the middle reaches of the YRB, forming a concentric pattern around the Chengdu Plain. Grasslands are mainly found in the upper reaches of the basin, while croplands are concentrated in the middle and lower reaches, including the Sichuan Basin. Built-up lands, which occupy a significant proportion, are mainly located in the downstream sections of the basin and around the Chengdu Plain. Barelands are primarily located in the upper and lower reaches, with limited presence in the middle reaches. Wetlands are predominantly distributed in the lower reaches, especially within the Poyang Lake and Dongting Lake water system.

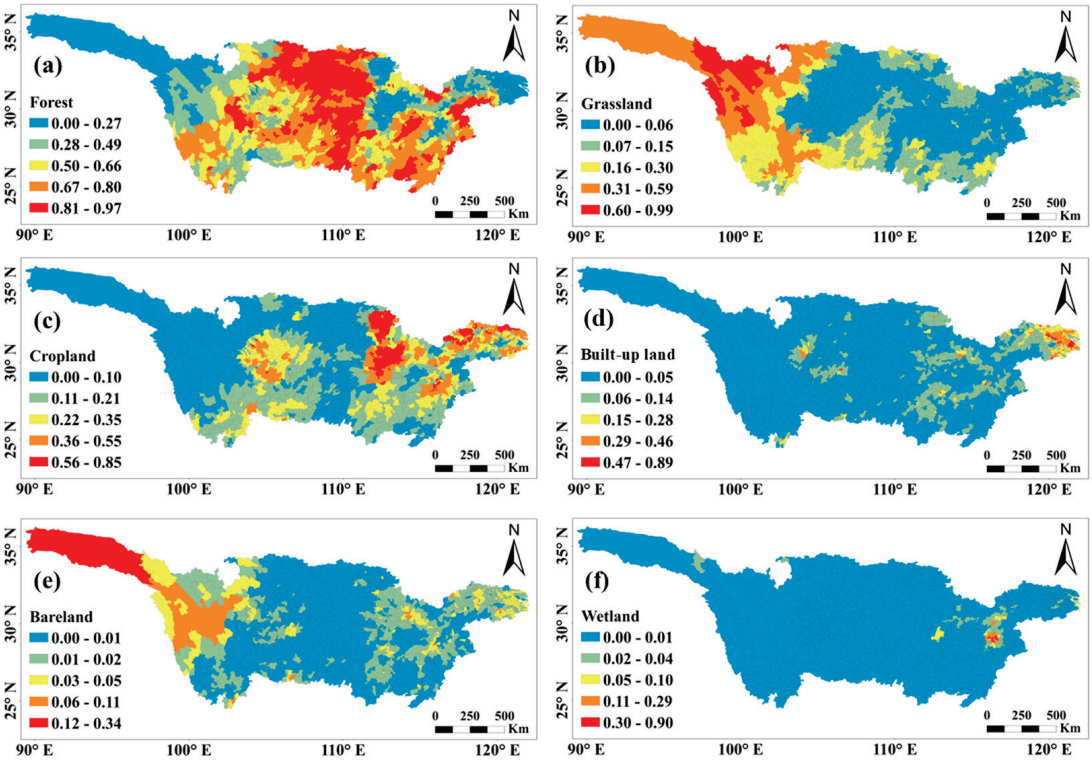

Figure 5. Spatial distribution map of the 6 main land use types in the Yangtze River Basin: (**a**) forest; (**b**) grassland; (**c**) cropland; (**d**) built-up land; (**e**) bareland; (**f**) wetland.

3.3. Effects of Land Use Types on TP Concentration at Different Scales

3.3.1. Impact of Land Use Patterns on TP Concentrations at the Whole Basin Scale

Land use types in the YRB, including built-up lands, croplands, forests, grasslands, industrial and mining lands, and barelands, show significant correlations with TP concentration (Table 2). The top three land use types influencing TP concentration in the basin are built-up lands (q = 0.19, $corr$ = 0.43, $p < 0.001$), croplands (q = 0.18, $corr$ = 0.40, $p < 0.001$), and forests (q = 0.16, $corr$ = −0.38, $p < 0.001$). Built-up lands, croplands, industrial and mining lands, and barelands significantly increase TP concentration, whereas forests and grasslands significantly reduce them. Wetlands have a negative effect on TP concentrations; however, the p-value exceeds 0.05, indicating statistical insignificance. Due to the limited distribution of wetlands in the YRB and the absence of a significant correlation, wetlands are excluded from the analysis of the impact of land use types on TP concentration in subsequent analyses of secondary water resource divisions and hotspot/coldspot areas.

Table 2. Land use impact factor of land use type and TP concentration across the Yangtze River Basin in 2021.

Land Use Type	*q* Value	Pearson Correlation (*corr*)	Direction
Built-up land	0.19 ***	0.43 ***	+
Cropland	0.18 ***	0.40 ***	+
Forest	0.16 ***	−0.38 ***	-
Bareland	0.10 ***	0.24 ***	+
Industrial and mining land	0.06 ***	0.24 ***	+
Grassland	0.05 ***	−0.16 ***	-
Wetland	0.00	−0.02	-

Note: "***" indicates a significance level of $p < 0.001$, "+" indicates a positive correlation, "-" indicates a negative correlation.

The interaction between any two land use types leads to either bilinear or nonlinear increases in explanatory power (Figure 6). Notably, the interaction between built-up lands and croplands demonstrates the highest explanatory power, reaching 0.30. The TP concentration increases under the influence of any two land use types, with a notable strengthening in the explanatory power of the interaction factor. This further validates the impact of combined land use types on TP concentration.

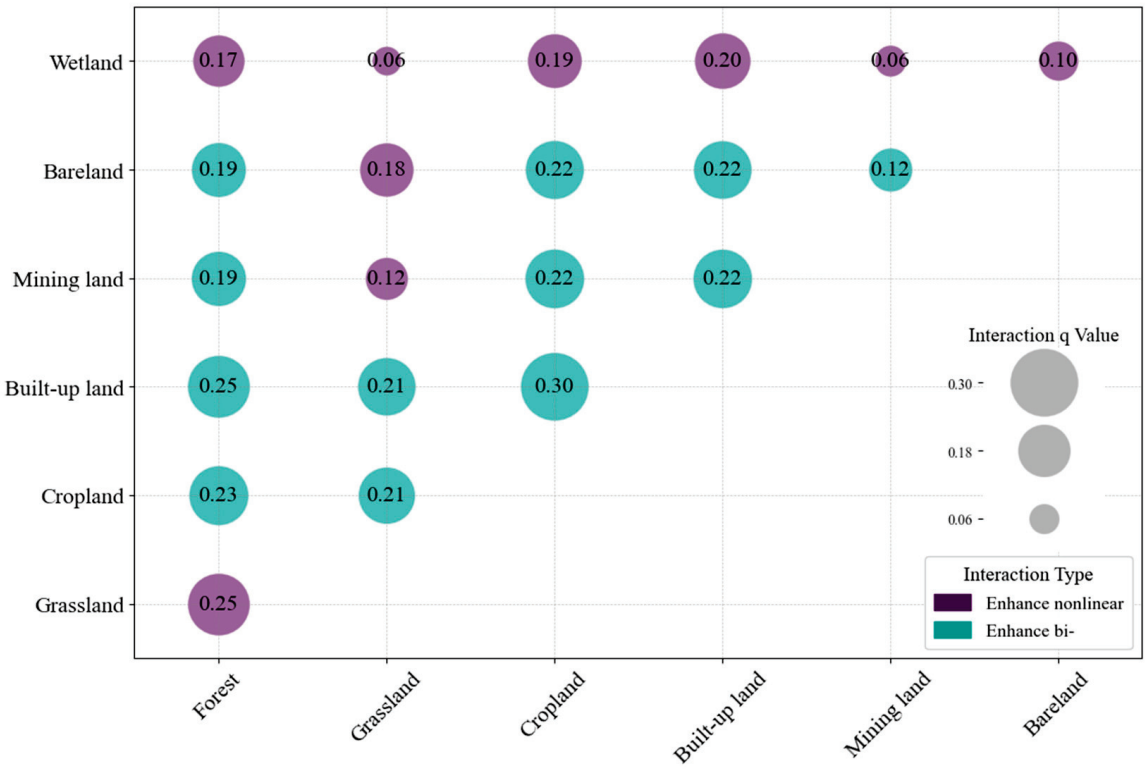

Figure 6. Interaction *q* value of different land use types and TP concentration in the Yangtze River Basin. Mining land refers to industrial and mining land.

3.3.2. Impact of Land Use Patterns on TP Concentrations at the Sub-Basin Scale

The impact of land use patterns on TP concentrations varies across the sub-basins of the YRB. Figure 7 illustrates that TP concentration in the above Shigu of the Jinsha River primarily originates from grasslands. In contrast, TP concentration in the below Shigu of the Jinsha River primarily originates from industrial and mining lands. In the Minjiang and Tuojiang Rivers, TP concentration is predominantly derived from croplands, built-up lands, and industrial and mining lands, with croplands exerting the most significant impact on TP concentrations in these regions. In the Jialing River, TP concentration is primarily derived from croplands. Along the mainstream from Yibin to Yichang, TP concentration is driven primarily by croplands, built-up lands, and barelands, with croplands having the most significant impact on TP concentrations. In the Wujiang River, TP concentration originates mainly from built-up lands, industrial and mining lands, and barelands, with industrial and mining lands exerting the greatest impact on TP concentrations in this area. In the Han River, TP concentration is primarily derived from croplands, built-up lands, industrial and mining lands, and barelands, with built-up lands having the greatest impact on TP concentrations in this region. Along the mainstream from Yichang to Hukou, TP concentration is driven by grasslands, croplands, built-up lands, industrial and mining lands, and barelands, with croplands exerting the greatest impact on TP concentrations. In the Dongting Lake water system, TP concentration primarily originates from croplands, built-up lands, industrial and mining lands, and barelands, with croplands exerting the

greatest impact on TP concentrations. Below Hukou of the mainstream, TP concentration originates from grasslands, croplands, built-up lands, industrial and mining lands, and barelands, with built-up lands exerting the greatest impact on TP concentrations. In the Taihu Lake water system, TP concentration is primarily derived from grasslands, croplands, and built-up lands, with croplands having the greatest impact on TP concentrations.

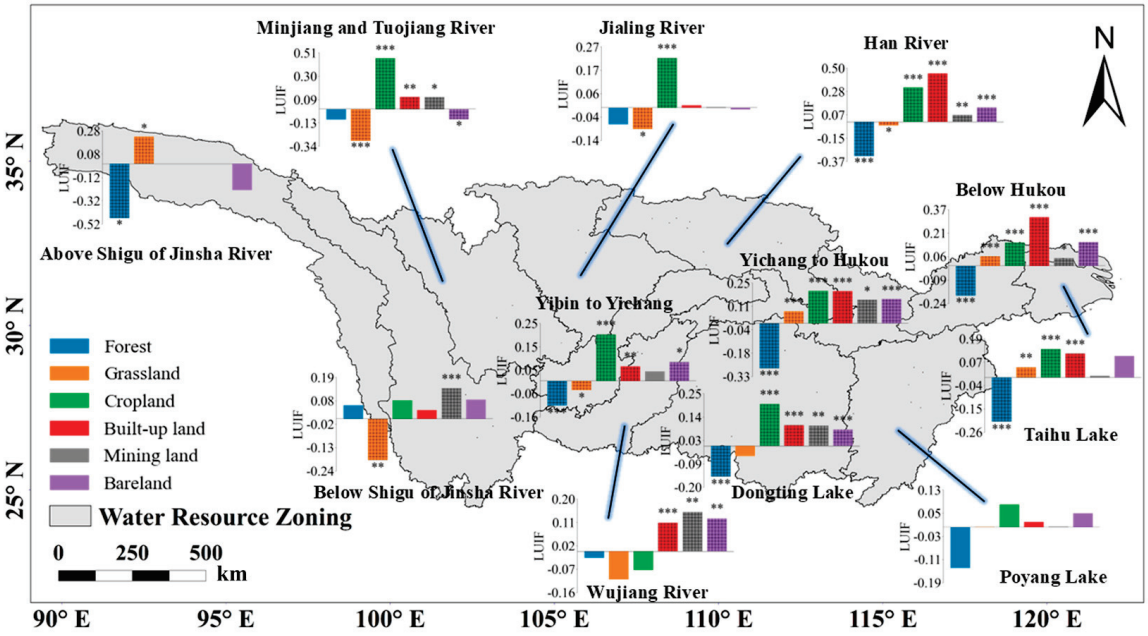

Figure 7. Histogram of land use impact factor (LUIF) of secondary water resources in the Yangtze River Basin. Mining land refers to industrial and mining land. "***" indicates a significance level of $p < 0.001$, "**" indicates a significance level of $p < 0.01$, and "*" indicates a significance level of $p < 0.05$.

3.3.3. Impact of Land Use Patterns on TP Concentrations at the Regional Scale

Significant differences in the impact of land use patterns on TP concentrations exist across different hotspot zones (Figure 8a–g). In the three high-value hotspot areas, forests play a mitigating role, with TP concentration primarily originating from built-up lands and industrial and mining lands. In the three low-value coldspot areas, grasslands exert a mitigating effect, with TP concentration primarily stemming from built-up lands, croplands, and industrial and mining lands. In non-hotspot areas, both forests and grasslands provide a mitigating effect, with TP concentration primarily emanating from built-up lands, croplands, and industrial and mining lands. According to Figure 8h, TP concentration hotspots are predominantly located in areas with a higher proportion of croplands and built-up lands, while coldspot areas are more prevalent in regions dominated by forests and grasslands. From coldspot low-value areas to hotspot high-value areas, the proportion of forests decreases progressively (area proportion from 70.4% to 40.7%), while the proportion of croplands increases (area proportion from 7.2% to 33.7%), along with a rise in the proportion of built-up lands (area proportion from 1.2% to 10.2%).

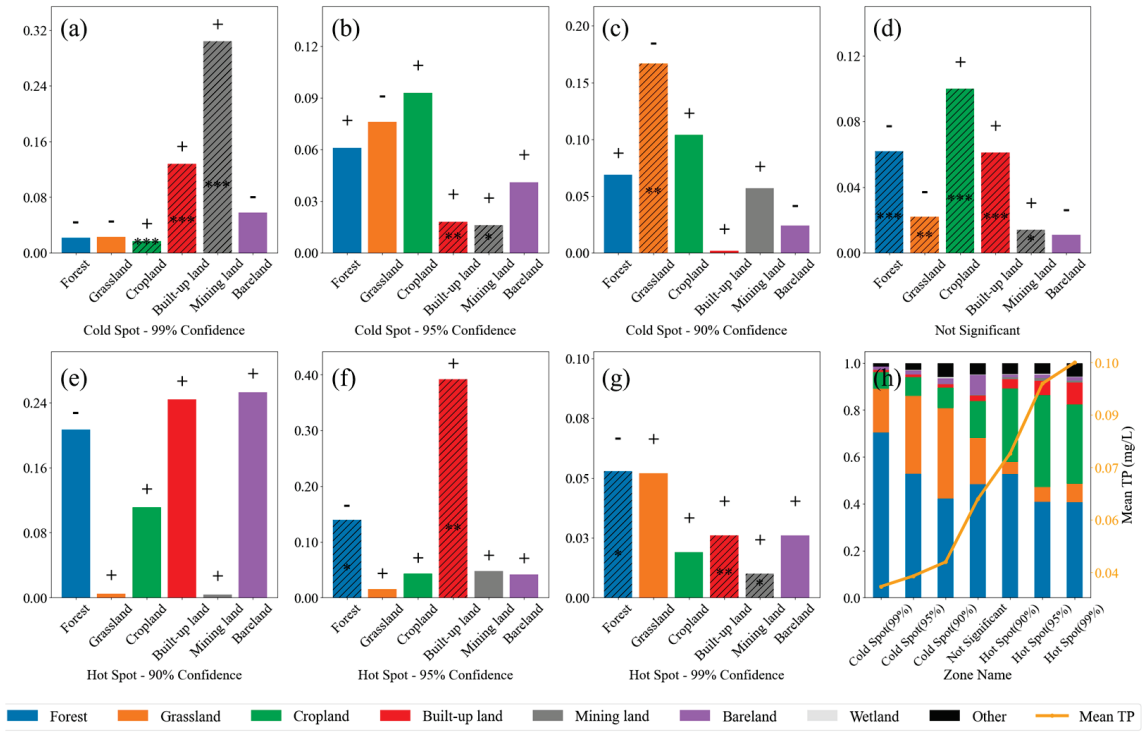

Figure 8. Histogram of land use impact factor (LUIF) of land use type in hot and cold zones in the Yangtze River Basin (**a**–**g**). Accumulation histogram of land use area proportion and TP concentration curve of the hot and cold zones in the Yangtze River Basin (**h**). "***" indicates a significance level of $p < 0.001$, "**" indicates a significance level of $p < 0.01$, and "*" indicates a significance level of $p < 0.05$. "+" indicates a positive value of LUIF, and "-" indicates a negative value of LUIF.

4. Discussion

4.1. Significant Spatial Clustering of TP Concentration in the YRB

This study reveals the spatial clustering of TP pollution in the YRB using hotspot analysis. Hotspot regions of TP concentration include the Pudu River Basin, Chengdu Plain, Jianghan Plain, and the Yangtze River Delta. In comparison to the studies by Ji et al. [29] and Chen et al. [30], this study also identifies the Chengdu and Hanjiang Plains as hotspots for TP concentration. This distribution corresponds to areas rich in China's renowned phosphate mineral deposits, such as the Jinhua-Qingping mines in Sichuan, Dianchi mines in Yunnan, Yichang mines in Hubei, and Fuquan mines in Guizhou [10,31,32]. These areas, rich in phosphate resources, experience elevated TP concentrations due to intensive mining activities and high-load emissions from phosphate chemical industries, which significantly contribute to persistent pollution levels.

In August 2019, the Ministry of Ecology and Environment published a rectification report, revealing that 276 out of 692 "three phosphorus" enterprises (phosphate mines, storage, and chemical industries) were found to have ecological and environmental issues (Figure 9). Upstream of the four primary hotspots for elevated TP concentrations, a dense cluster of "three phosphorus" enterprises requiring rectification is observed. TP concentrations from these enterprises accumulate through tributaries, eventually flowing into the main rivers, forming high-value hotspot areas along the river. Research by Yan et al. [33] also highlights significant spatial variations in phosphorus loads entering the river from "three phosphorus" enterprises in the YRB. Sub-basins such as the downstream of the Jinsha River, Wujiang River, Minjiang and Tuojiang Rivers, and Han River contribute 32.8% to the TP flux in the Yangtze River, marking them as key sources of phosphorus in the basin. In addition, in the 12 secondary water resource zones within the basin, TP concentration in

the below Shigu of the Jinsha River and Wujiang River is primarily attributed to industrial and mining lands. Industrial and mining lands are also key contributors to TP concentration in the Minjiang and Tuojiang Rivers, Han River, the stretch from Yichang to Hukou, the Dongting Lake water system, and downstream of Hukou. Furthermore, in the high-value areas identified through hotspot analysis, TP concentration primarily originates from built-up lands and industrial and mining lands, emphasizing that the major sources of TP concentration in these hotspots are mining activities and high-load emissions from phosphate mining and chemical industries.

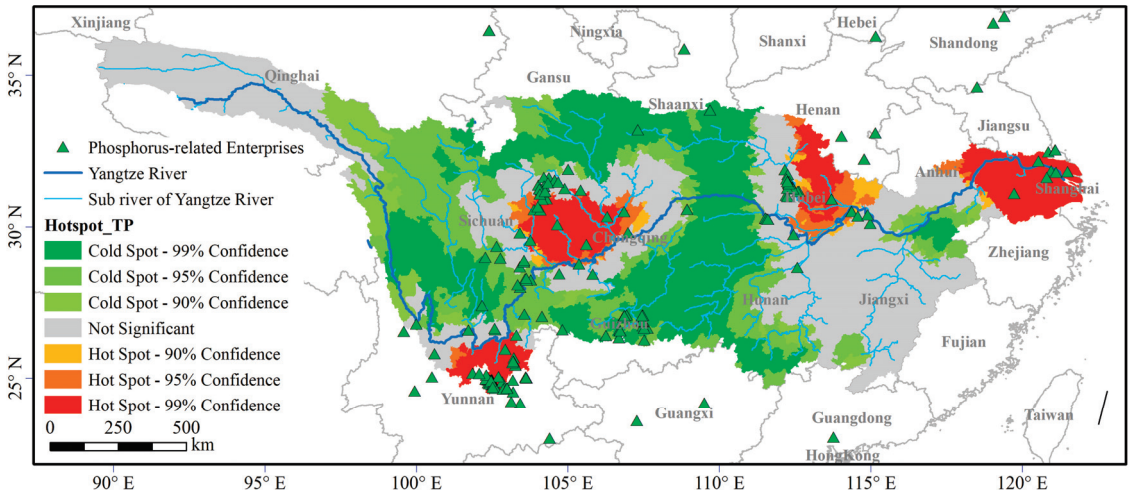

Figure 9. Distribution map of enterprises that need to be rectified in the self-examination of "three phosphorus" in the Yangtze River Basin in 2019.

4.2. Regional Differences in the Impact of Land Use Patterns on TP Concentration in the YRB

At the basin-wide scale, the primary sources of TP concentration are ranked as follows: built-up land, cropland, industrial and mining land, and bareland. However, the main sources of TP concentration vary significantly across the sub-basins. Specifically, TP concentration in seven sub-basins are primarily driven by cropland, while in two sub-basins, built-up land is the predominant source, and in two others, industrial and mining land are the major contributors. (Figure 10). These findings align with the general trend observed by Zou et al. [34], which indicates that 83% of TP concentrations in China originate from agricultural non-point source pollution. However, discrepancies between the basin-wide results and those at the sub-basin scale may be related to the scale-dependent nature of land use impacts on water quality [19].

In this study, the sources of TP pollution in the sub-basins of the Yangtze River exhibit considerable complexity, with four predominant types of pollution sources identified: industrial and mining land type, cropland type, cropland-dominant type, and built-up land-dominant type. In the below Shigu of the Jinsha River, TP concentration primarily originates from industrial and mining land. This is primarily due to the region's status as a major phosphate mining area in the Dianchi region, where the proven P_2O_5 reserves amount to 8.94×10^8 tons. The extraction and processing of phosphate ores have caused significant vegetation degradation, contributing to persistently high TP concentrations in this sub-basin [18,32,35]. Therefore, the focus for TP concentration control in this region should be directed towards the management of mining areas and regulation of phosphorus emissions.

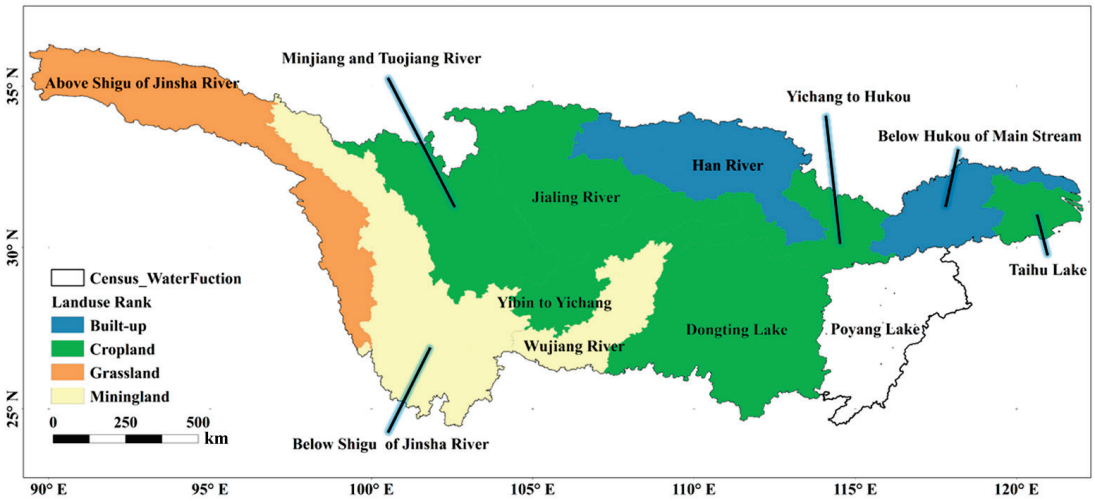

Figure 10. The distribution map of the dominant land use types for TP concentration sources in the 12 sub-basins of the Yangtze River.

In the Jialing River, TP concentration arises predominantly from cropland, a finding consistent with the results of Wu et al. [36], which indicates that cropland contributes the most to TP concentration in the Jialing River. Consequently, TP control efforts in this sub-basin should prioritize preventing soil erosion and implementing ecological fertilization techniques to reduce pollution in croplands.

The sources of TP concentration in the Minjiang and Tuojiang Rivers, the Dongting Lake water system, the mainstream from Yibin to Hukou, and the Taihu Lake water system are characterized as cropland-dominant type. Within these regions, the influence of built-up land and industrial and mining land is also substantial, further exacerbating TP concentration levels. Notable examples include the phosphate mines in the Jinhe-Qingping area of Sichuan and the dense concentration of phosphorus chemical industries along the Yichang section of the Yangtze River [37,38]. In these cropland-dominant sub-basins, TP concentration control should focus on large-scale agricultural management practices, including optimizing fertilizer use and promoting conservation tillage.

In the Han River and the downstream section below Hukou, the primary source of TP concentration is built-up land, although cropland and industrial and mining land also significantly influence the TP concentrations in these areas, such as phosphorus enterprises are concentrated below the Danjiangkou section of the Han River [24]. For sub-basins dominated by built-up land, the control of TP concentration should focus on the management of domestic sewage discharge and waste treatment.

In the Wujiang River, TP concentration is predominantly from industrial and mining land, with substantial contributions from built-up land and bareland. The basin contains strategically significant national-level phosphate mines, such as the Kaiyang and Wengfu mines, which have been in continuous development, contributing notably to TP concentration due to mining activities and the associated phosphate chemical industries [39]. Therefore, TP concentration control in these sub-basins should focus on the regulation of mining areas, emissions from phosphate production, and the management of domestic wastewater and solid waste disposal.

The land use types in the Poyang Lake watershed did not pass the significance test, and the main factors driving TP pollution have yet to be identified. However, studies by Sun et al. [40] and Wang et al. [41] indicated that the TP concentration in Poyang Lake is primarily influenced by five rivers: Xiu River, Gan River, Fu River, Xin River, and Rao River. The pollution load from these rivers, along with hydrological changes, are key factors influencing the TP concentration in the lake's waters. Therefore, the control and mitigation

of TP concentration in the Poyang Lake watershed should focus on the management of these five rivers. In conclusion, effective TP concentration management in the YRB requires a tailored approach, with zonal management and systematic governance based on regional characteristics.

4.3. Limitations and Future Works

Although this study has made significant progress in examining the impact of land use on TP pollution, several limitations need to be addressed in future research. First, the water quality data used in this study consist solely of national monitoring data from 2021, which limits the ability to analyze the spatiotemporal variations and trends of TP concentration in the YRB. Second, the land use types considered in this study, except for industrial and mining land, are based on the primary classification of land use, which may obscure spatial heterogeneity within these types. For example, the influence of different crop types within cropland on TP concentration can vary significantly. In this study, TP concentration in many sub-basins primarily originates from croplands, representing agricultural non-point source pollution. Future research could explore the impact of different farming practices on TP concentration.

5. Conclusions

This study provides a systematic analysis of the impact of land use on TP concentration at various scales, including both watershed and sub-watershed levels. In 2021, 98.8% of the state-controlled sections in the YRB were classified with TP concentration as "good" or better. TP concentration showed clear spatial clustering, with notable pollution detected in the Pudu River Basin, Chengdu Plain, Jianghan Plain, and the Yangtze River Delta. At the basin-wide scale, built-up land and cropland were identified as the most significant land use types influencing TP concentration levels. A significant regional variation exists in the sources of TP concentration within the YRB, with over half of the sub-basins identifying cropland as the primary source of pollution. Notably, phosphorus concentrations in hotspot regions, including the Pudu River Basin, Chengdu Plain, and Jianghan Plain, are strongly correlated with the distribution of industrial and mining lands. Therefore, TP concentration management in the YRB should implement targeted strategies that address the specific sources of pollution in individual sub-basins.

Author Contributions: Methodology, F.D. and Y.X.; Investigation, F.D. and Y.Y.; Data curation, W.L. (Wenhui Liu) and W.L. (Wei Liu); Writing—original draft, F.D., W.L. (Wenhui Liu), W.L. (Wei Liu), Y.X., Y.S., C.Z., M.S. and Y.Y.; Writing—review & editing, F.D., Y.X., W.L. (Wenhui Liu), W.L. (Wei Liu) and Y.S.; Visualization, W.L. (Wei Liu) and M.S. All authors have read and agreed to the published version of the manuscript.

Funding: This research was funded by the Xiamen Natural Science Foundation Project (3502Z202372044) and the Xiamen Natural Science Foundation Project (3502Z202471079).

Data Availability Statement: The raw data supporting the conclusions of this article will be made available by the authors on request.

Conflicts of Interest: The authors declare no conflict of interest.

Appendix A

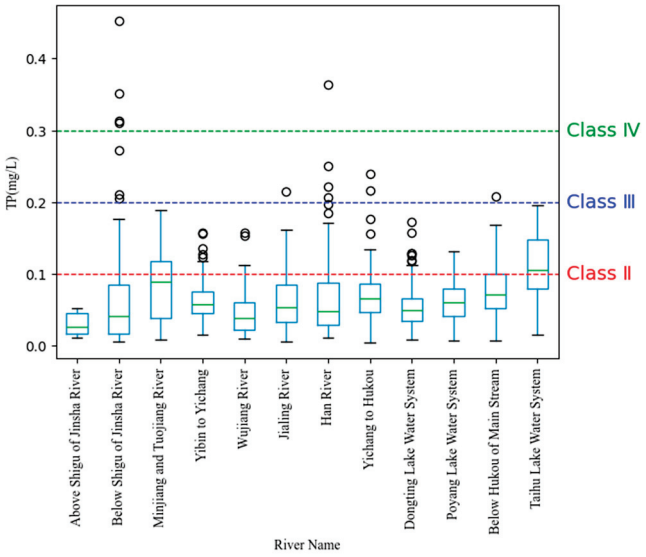

Figure A1. Box plot of TP concentration in 2021 for secondary water resources in the Yangtze River Basin.

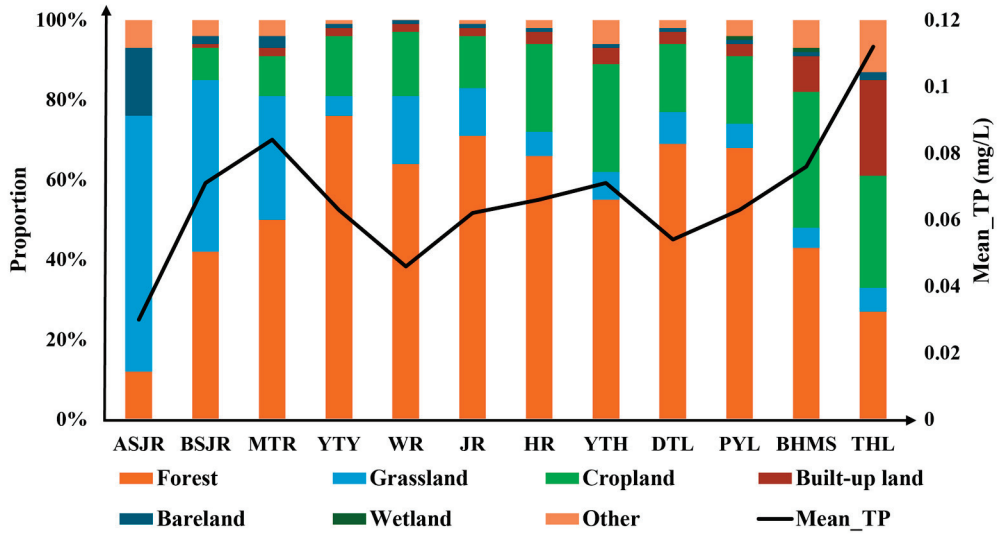

Figure A2. Accumulation histogram of land use area proportion and TP concentration curve of secondary water resources in the Yangtze River Basin. ASJR is the above Shigu of the Jinsha River; BSJR is the below Shigu of the Jinsha River; MTR is the Minjiang and Tuojiang Rivers; YTY is the mainstream from Yibin to Yichang; WR is the Wujiang River; JR is the Jialing River; HR is the Han River; YTH is the mainstream from Yichang to Hukou; DTL is the Dongting Lake Water System; PYL is the Poyang Lake Water System; BHMS is the Below Hukou of Main Stream; THL is the Taihu Lake Water System.

References

1. Qin, Y.W.; Ma, Y.Q.; Wang, L.J.; Zheng, B.; Ren, C.; Tong, H.; Wang, H. Pollution of the total phosphorus in the Yangtze River Basin: Distribution characteristics, source and control strategy. *Res. Environ. Sci.* **2018**, *31*, 9–14.
2. Yao, J.Z.; Fan, X.J.; Yang, X.; Huang, Y.B. Current situation, causes and control measures of water bloom in the key tributaries of the Three Gorges Reservoir. *Chin. J. Environ. Eng.* **2022**, *16*, 2041–2048.
3. Song, J.W.; Zhang, X.X.; Jiang, D.Y.; Zhao, C.H.Z.; Li, P.F. Impact of Land Use Types at Different Scales on Surface Water Environment Quality and Its Driving Mechanism. *Environ. Sci.* **2022**, *43*, 3016–3026. [CrossRef]
4. Zhang, J.; Li, S.Y.; Jiang, C.S. Effects of land use on water quality in a River Basin (Daning) of the Three Gorges Reservoir Area, China: Watershed versus riparian zone. *Ecol. Indic.* **2020**, *113*, 106226. [CrossRef]

5. Xu, S.; Li, S.L.; Zhong, J.; Li, C. Spatial scale effects of the variable relationships between landscape pattern and water quality: Example from an agricultural karst river basin, Southwestern China. *Agric. Ecosyst. Environ.* **2020**, *300*, 106999. [CrossRef]
6. Xu, E.Q. Research progress in the impact of land use on water nutrients. *Chin. J. Eco-Agric.* **2019**, *27*, 1880–1891. [CrossRef]
7. Wen, J.W.; Wang, P.; Huang, G.X.; Zahng, H.; Nie, M.H.; Ding, M.J.; She, Y.Y. Influence of Land Use Structure and Spatial Pattern on Water Quality of Small and Medium-sized Rivers in Poyang Lake Basin. *Environ. Sci.* **2023**, *44*, 6728–6743. [CrossRef]
8. Xu, Y.X.; Wu, X.; Lu, R.; Yang, W.J.; Zhao, Y. Total Phosphorus Pollution, Countermeasures and Suggestions of the Yangtze River Economic Belt. *Environ. Conform. Assess.* **2018**, *10*, 70–74. [CrossRef]
9. Liu, L.S.; Huang, G.X.; Wang, F.; Chu, Z.S.; Li, H.S. Problems, Situation and Countermeasures of Water Eco-Environment Security in the Yangtze River Basin. *Res. Environ. Sci.* **2020**, *33*, 1081–1090.
10. Chen, F.; Li, X.H.; Wang, W.J.; Peng, L.; Qian, B. and spatial variation characteristics of total phosphorus in Yangtze River Basin from 2018 to 2022. *Express Water Resour. Hydropower Inf.* **2023**, *44*, 91–97.
11. Yin, W.; Wang, C.; Zhang, H. Consideration on total phosphorus problem in Yangtze River Basin. *Yangtze River* **2022**, *53*, 44–52. [CrossRef]
12. Li, Q.; Yang, Z.H.; Yin, W.; Yu, M.H.; Bai, F.P.; Yue, Y.; Ren, Y.F. Tracing the sources and transport of the total phosphorus in the upper Yangtze River. *Ecol. Inf.* **2023**, *77*, 102230. [CrossRef]
13. Yi, F.; Chen, M.; He, X.F.; Yu, C.H.; An, R.D. Effect of spatial scale on water quality in watershed land use analysis. *China Environ. Sci.* **2023**, *43*, 4280–4291. [CrossRef]
14. Wang, P.; Qi, S.H.; Chen, B. Influence of land use on river water quality in the Ganjiang basin. *Acta Ecol. Sin.* **2015**, *35*, 4326–4337. [CrossRef]
15. Chen, Y.P.; Yue, A.R.; Wei, Y.L.; Yang, C.J. Source Apportionment of Ammonia Nitrogen and Total Phosphorus of Minjiang Bridge Control Unit. *Sichuan Environ.* **2018**, *37*, 44–50. [CrossRef]
16. Fang, N.; Liu, L.L.; You, Q.H.; Tian, N.; Wu, Y.P.; Yang, W.J. Effects of Land Use Types at Different Spatial Scales on Water Quality in Poyang Lake Wetland. *Environ. Sci.* **2019**, *40*, 5348–5357. [CrossRef]
17. Wang, J.; Liu, A.A.; Zhang, J.W.; Chen, Q.S.; Yang, H.W. Effect of Integrated Landscape Characteristics Around Chaohu Lake on River Water Quality Based on Watershed Units. *Environ. Sci.* **2024**, *45*, 3214–3224. [CrossRef]
18. Zhang, H.S.; Jiao, Y.M.; Xu, Q.E.; Zhang, Z.N.; Tao, Y. Research review on land use change in Dianchi Lake Basin and its impact on water quality. *Yangtze River* **2023**, *54*, 65–73. [CrossRef]
19. Ding, J.; Jiang, Y.; Liu, Q.; Hou, Z.J.; Liao, J.Y.; Fu, L.; Peng, Q.Z. Influences of the land use pattern on water quality in low-order streams of the Dongjiang River basin, China: A multi-scale analysis. *Sci. Total Env.* **2016**, *551–552*, 205–216. [CrossRef]
20. Wang, Y.B.; Junaid, M.; Deng, J.Y.; Tang, Q.P.; Luo, L.; Xie, Z.Y.; Pei, D.S. Effects of land-use patterns on seasonal water quality at multiple spatial scales in the Jialing River, Chongqing, China. *Catena Giess.* **2024**, *234*, 107646. [CrossRef]
21. Guan, W.H.; Luo, G.H.; Wang, P.F.; Lou, B.F.; Qiu, G.S. Variation of TP flux in Jialing River and spatial source apportionment. *China Environ. Sci.* **2024**, *44*, 1448–1456. [CrossRef]
22. Guan, B.H.; Li, J.; Zeng, A.B.; Deng, J.S.; Zhang, J. Impacts of Urban Land Use on Water Quality in Hangzhou. *Resour. Sci.* **2008**, *30*, 857–863. [CrossRef]
23. Cao, X.F.; Sun, J.H.; Huang, Y. The impact of landscape pattern on water quality in Lake Dianchi watershed. *Ecol. Environ. Sci.* **2012**, *21*, 364–369. [CrossRef]
24. Yang, W.; Li, R.Q. Characteristics and Causes of the Total Phosphorus Pollution in the Yangtze River and Han River. *China Rural. Water Hydropower* **2021**, *1*, 42–47. [CrossRef]
25. Chen, S.R.; He, L.; Zhang, F.Y.; Ma, G.W.; Lin, L.Y. Characteristics of Surface Water Quality of the Yangtze River Basin during 2016–2019. *Res. Environ. Sci.* **2020**, *33*, 1100–1108.
26. Deng, F.L.; Lin, T.; Zhao, Y.; Yuan, Y. Zoning and Analysis of Control Units for Water Pollution Control in the Yangtze River Basin, China. *Sustainability* **2017**, *9*, 1374. [CrossRef]
27. Wang, J.Y.; Xie, D.T.; Wang, S.; Yan, J.Z. Research on spatial distribution of rural tourism in mountainous and hilly areas base Don POI extraction—A case study of Chongqing city. *Chin. J. Agric. Resour. Reg. Plan.* **2020**, *41*, 257–267.
28. Wang, J.; Xu, C. Geographical Detector: Principles and Prospects. *Acta Geogr. Sin.* **2017**, *72*, 116–134.
29. Ji, X.Y.; Peng, D. Characteristics of Total Phosphorus Concentration in the Yangtze River Basin in the Thirteenth Five-Year Plan Period. *J. Chang. River Sci. Res. Inst.* **2022**, *39*, 1–9. [CrossRef]
30. Chen, S.R.; He, L.H.; Lin, L.Y.; Fang, D.K.; Zhang, F.Y. Change Trends of Surface Water Quality in the Mainstream of the Yangtze River during the Past Four Decades. *Res. Environ. Sci.* **2020**, *33*, 1119–1128. [CrossRef]
31. Li, Z.M. Introduction to China's Chemical Mineral Geology. *Ind. Miner. Process.* **2002**, *5*, 33–34.
32. Shi, Y.; Qin, Y.W.; Ma, Y.Q.; Zhao, Y.M.; Wen, Q.; Cao, W.; Qiao, F. Pollution Status and Control Strategy of 'Three Phosphorus' Pollution in the Upper Reaches of Yangtze River Basin, China. *Res. Environ. Sci.* **2020**, *33*, 2283–2289.

33. Yan, W.J.; Li, Q.Q.; Wang, F.; Wang, J.N.; Yu, Q.B.; Song, Y.H.; Wang, D.S. Basin-scale phosphorus and "three-P" loads into the river network and their contributions to the riverine P fluxes at key stations of the Changjiang River: Model and scenario analysis. *Acta Sci. Circumstantiae* **2022**, *42*, 149–159. [CrossRef]
34. Zou, L.L.; Liu, Y.S.; Wang, Y.S.; Hu, X.D. Assessment and analysis of agricultural non-point source pollution loads in China: 1978–2017. *J. Env. Manag.* **2020**, *263*, 110400. [CrossRef] [PubMed]
35. Jiang, W.; Li, J.; Chen, Y.H. Current Situation and Analysis of Water Quality of the Jinsha River(Yunnan Section) Basin. *Environ. Sci. Surv.* **2023**, *6*, 78–82. [CrossRef]
36. Wu, L.; Long, T.Y.; Wang, Y.X.; Lu, Q.Q. Prediction of non-point source nitrogen and phosphorus pollution load in Jialing River watershed based on distributed hydrological model. *Trans. Csae* **2011**, *27*, 55–60. [CrossRef]
37. Zhao, L. Analysis of water quality changes in Yichang section of the Changjiang River Basin under the background of Great Protection of the Changjiang River. *Environ. Prot. Technol.* **2023**, *29*, 41–46+64. [CrossRef]
38. Cheng, M.; Tang, M.; Liang, G.L. Research on the transformation of one kilometer industrial space along the Yangtze River in Yichang under the background of Yangtze River protection. *Contemp. Econ.* **2019**, *4*, 24–28. [CrossRef]
39. Sun, J.; Wang, Z.F. Water quality and main pollutants in the Sinan section of the Wujiang river in Guizhou Province. *Inn. Mong. Environ. Sci.* **2020**, *32*, 24–25. [CrossRef]
40. Sun, J.W.; Wang, J.; Yang, Y.L.; Chen, J.; Zhou, Q.; Zhong, W.J. Temporal and spatial characteristics and abnormal changes of nitrogen and phosphorus in Poyang lake and the impact pathways. *Jiangxi Hydraul. Sci. Technol.* **2024**, *50*, 199–205. [CrossRef]
41. Wang, Y.D.; Jia, J.J.; Lu, Y.; Tian, L.L.; Gao, Y. Nitrogen and phosphorus budget and eutrophication impacts in Poyang Lake from 2010 to 2019. *Acta Sci. Circumstantiae* **2024**, *44*, 151–160.

Disclaimer/Publisher's Note: The statements, opinions and data contained in all publications are solely those of the individual author(s) and contributor(s) and not of MDPI and/or the editor(s). MDPI and/or the editor(s) disclaim responsibility for any injury to people or property resulting from any ideas, methods, instructions or products referred to in the content.

land

MDPI

Article

Ecological Compensation and Comprehensive Zoning of Cultivated Land Based on Ecosystem Service Value and Extended Three-Dimensional Ecological Footprint Model: A Case Study of Shandong Province

Jia Xiang [1,*] and Junjun Niu [2]

[1] School of Law, Hohai University, Nanjing 211100, China
[2] School of Public Administration, Hohai University, Nanjing 211100, China; niujunjun@hhu.edu.cn
* Correspondence: jiaxiang@hhu.edu.cn

Abstract: At present, with the rapid development of urbanization and industrialization, the contradiction between development and cultivated land protection is exacerbated. Scientifically quantifying ecosystem service value and constructing an ecological compensation mechanism of cultivated land are significant paths for cultivated land protection. This study originates from an extended three-dimensional ecological footprint model, introduces a carbon footprint accounting path, and thoroughly evaluates the sustainable use of farmland ecology. It aimed to accurately calculate the ecosystem service value of farmland, formulate ecological compensation standards, establish an ecological compensation model to measure the total amount of ecological compensation for cultivated land, and delineate the "five-zone map" of ecological compensation for farmland. (1) There is a partial spatial heterotopia phenomenon between ecological consumption and ecological services. (2) In 2022, the ecosystem service value of cultivated land in Shandong Province is high, reaching CNY 78.479 billion. Overall, exported the ecological service value of cultivated land to the outside world. Qingdao, Yantai, and Weihai are farmland ecological compensation zones, with a compensation amount of CNY 71 million. (3) The priority compensation zones are Qingdao and Yantai on the Shandong Peninsula. The priority compensated zones are mainly located in the northern region of Shandong. Exploring ecological compensation for cultivated land ecology at the spatial and temporal scale has important value for ecological protection and security of cultivated land.

Keywords: ecosystem service value; three-dimensional ecological footprint model; cultivated land; ecological compensation; ecological surplus deficit; comprehensive zoning

1. Introduction

As a carrier of food production and an important ecological resource, cultivated land is the lifeline for ensuring food security and a red line affecting ecological security. Farmland is a seminatural, semiartificial, and multifunctional ecosystem that relies on natural elements like water, light, temperature, and soil, as well as artificial inputs such as seeds, machinery, and irrigation [1]. It utilizes interactions between organisms and the environment, as well as between organisms, to produce agricultural products, providing rich and diverse ecosystem services and ensuring regional ecological security. At the same time, it is also the ecosystem with the highest degree of human dependence. In addition to production functions, it also provides multiple ecological services like water

and soil conservation, climate regulation, biological diversity maintenance, nutrient cycling, and waste treatment for humans [2]. Nevertheless, as a result of the speedy progress of industrialization and urbanization, a large amount of cultivated land has been converted for use in construction. Meanwhile, driven by economic interests, farmers have overused chemical fertilizers and pesticides in farming production. Moreover, many unreasonable practices, such as high-load development and predatory management, have brought about acute issues in cultivated land, like non-agriculturalization, quality degradation, and ecological environment deterioration of cultivated land [3]. As the pressure to provide ecological protection for arable land continues to increase, contradictions between arable land resource endowment, ecological preservation, and economic growth are becoming increasingly outstanding, affecting the ecological safety and sustainable utilization of cultivated land.

China has proposed various policies for farmland protection, adhered to the strictest farmland protection system and red line, comprehensively delineated permanent basic farmland, vigorously implemented rural land consolidation practices, and promoted the "three in one" protection for farmland quantity, quality, and ecology [4]. The current farmland ecological protection policy overly relies upon rigid administrative constraints and ignores the importance of economic incentives [5]. Constructing an ecological compensation (EC) mechanism for farmland is essential in protecting the ecosystem's ecological value and service function. One crucial element of the ecological civilization system is the compensation mechanism for ecological conservation. On 10 April 2024, China announced the "Regulations on Ecological Protection Compensation", which for the first time established the connotation and basic institutional rules for ecological protection compensation, with clarified classification compensation in eight major fields. Evaluating ecosystem service value (ESV) provides an important basis for ecological compensation and ecological protection. Quantifying and compensating for ESV of farmland promotes resource utilization in surplus farmland areas, thereby enhancing agricultural productivity. On the other hand, it can help alleviate the conflict between "promoting growth" and "protecting farmland" in areas with limited farmland.

Shandong Province is one of the few regions in China that is both an economically strong province and a major agricultural contributor. It is a base for high-quality commodity grain, a major grain producer, and a national key EC pilot area. Shandong Province has a wide range of cultivated land types and planting areas, with abundant natural endowments of cultivated land. Its comprehensive agricultural production capacity ranks among the top in the country, and the degree of agricultural intensification is high. It shoulders a significant responsibility for the country's economic development and food security. In recent years, due to the excessive development of arable land resources and the degradation of these areas and the surrounding environment caused by land use change, resource stability has been disrupted, and the ecological service functions and sustainable utilization of arable land in the region have been severely restricted. In Shandong Province, farmland protection achievements are directly related to national food security and the dynamic balance of the ecosystem. There is, therefore, strong motivation for selecting Shandong as a demonstrative research area for investigating farmland EC and zoning. As a microcosm of the whole country, there is heterogeneity within Shandong's ecological status, as well as the level of protection of arable land within the area. By applying the experiences and innovation of the province's arable land EC system, Shandong can provide a reference for establishing a diversified and market-oriented mechanism on the national scale. Taking the reduction in regional differences and ecological protection as the driving force, gradually expanding the coverage of market-oriented and diversified compensation, and promoting the realization

of a unified plan for national farmland protection and EC have strong applicability and practical guidance significance.

The ecological footprint (EF) model, an ecosystem assessment method based on social–economic metabolism, accounts for natural resource consumption. From an ecological perspective, it studies how humans consume and utilize natural resources and affect the ecosystem [6]. The two-dimensional EF model focuses on resource consumption and flow, but lacks a consideration of resource stock [7]. Considering the traditional two-dimensional ecological footprint mold, Niccolucci et al. divided resource supply into two categories: flow and stock. They introduced two new indicators, footprint breadth and depth, to characterize resource flow occupancy and resource stock overdraft, respectively. They also extended the two-dimensional plane analysis of the traditional EF model to three-dimensional spatiotemporal analysis, endowing the burden with a time dimension [8]. The pioneering three-dimensional EF model only visualizes a two-dimensional analysis of ecological surplus status and cannot account for the three-dimensional expression of the deficit status [9]. Jin Xiangmu further expanded the concept and the scope of its application, established a three-dimensional EF model, expanded the footprint depth from ecological deficit to surplus scenarios, and unified ecological profit and loss status representation, incorporating it into a unified framework and achieving natural resource consumption unity in accounting for resource flow and stock occupancy [10]. Researchers have evaluated whether there is horizontal overloading, as well as the degree of vertical overloading; this reflects the intra- and intergenerational distribution of natural resource consumption [11]. Researchers typically combine the ecological footprint with the equivalent factor approach in order to obtain the amount of EC farmland as calculated via the ESV. However, the carbon emissions generated in farmland production are often ignored [12]. An EF incorporating carbon footprints is more closely aligned with the concept of low-carbon agriculture, in that it takes the negative ecological impacts of farmland production into account, as well as the real ecological footprint of farmland [13].

An ecosystem service is one from which humans, directly or indirectly, obtain goods and services through various functions [14], comprising supply, climate regulation, culture, and sustainable services. The natural attributes of an ecosystem are reflected in various ecological effects, while the socio-economic attributes are reflected in ESV. An ecosystem service meets the two attribute conditions of scarcity and utility. The ESV theory focuses on ecosystem service functions in terms of natural resources and attempts to quantify service function value, which is an important means of measuring EC [15]. Scholars are currently gradually diversifying their research on ESV, expanding it to specific ecosystem fields such as rivers, lakes, farmland, forests, and deserts [16]. In recent years, as the ecological environment continues to deteriorate, the ESV of cultivated land has been given special attention, including carbon, biodiversity, and hydrological services and landscape beautification. Research on the value of ecosystem services in cultivated land in China focuses on two aspects: one is evaluating the value itself, and the other is exploring the impact of human activities and land use change on the ESV of cultivated land. The calculation methods for ESV include the opportunity cost method [17], conditional value method [18], and shadow engineering approach [19]. Some scholars have established an evaluation indicator system for ecological service functions in order to assess the ESV. Some scholars have also evaluated the sustainability of farmland ecosystem services through organic cultivation [20]. In addition to positive ESV, some scholars have also studied the negative values resulting from pesticide, fertilizer, and plastic film use and greenhouse gas emissions. Applying the functional value and equivalent factor approach to calculate positive and negative ecological farmland values across several provinces [21] makes their quantification more comprehensive. Taking cost–benefit, opportunity loss, and externality

spillovers into account, the negative externalities of farmland protection are calculated, which also provides a new idea for measuring and computing ESV of farmland [22]. Scholars have also explored the impact of change in land use policies on the ESV of cultivated land [23]. Changes in land use are closely related to ESV, in that changes in types, patterns, and intensities affect, to varying degrees, the ecosystem services they carry [24]. Calculating ESV can help in quantifying regional ecosystem service levels, reflecting the relationship between regional land use and ecosystems. By comparing and analyzing the spatiotemporal changes in land use and ESV, this study explores the impact of land use changes on the overall ESV of the region [25]. The cellular automata Markov model (CA Markov) was used to simulate land use change under different scenarios and predict ESV spatial distribution and aggregation patterns [26,27].

Due to the positive externality of farmland, there appears to be a certain loss of interest in ecological consumption and service subjects in the farming production and protection processes. In terms of farmland, EC is compensation for lost benefits in a process of redistributing the farmland ESV among different entities [28]. The theory of EC originates from the theory of ESV. Currently, land compensation in China is mainly based on the farmland annual output value and ignores its ecological value [22]. Farmland protection compensation focuses on compensating for ecological value [29]. Compensation for the ecological benefits of farmland stems from its ESV. Providing corresponding subsidies to farmers according to the quality of their farmland ensures the ecological and environmental value of natural resources [30]. Quantitative EC for farmland is a research focus for scholars, focusing on commonly used methods such as the energy value, ecological footprint, ecosystem service function value, and survey methods [31]. Farmland ESV can be measured by using the opportunity cost approach [32], employing the conditional value evaluation method, or conducting experiments [33] to investigate farmland compensation and payment willingness [34]. Using the energy method to construct a "pressure state response" model for arable land, researchers can establish a functional relationship between ecological security and land finance, calculate a regional farmland ecological security score, and finally obtain the arable land ecological transfer payment amount [35]. Research on EC for farmland protection primarily centers on the delineation of EC responsibilities, measuring compensation standards, and selecting compensation methods. From the perspective of ecological supply–demand equilibrium [36], food security [37], and virtual farmland [38], it is necessary to identify the areas responsible for EC in farmland protection and determine the interest of EC stakeholders. In light of ESV quantification, ecological overload coefficients, adjustment coefficients for administrative and financial rights, and farmland quality coefficients are introduced to design EC standards and quotas for farmland [39]. It is important that scholars conduct in-depth research on government subsidies and market operations, vertical and horizontal fiscal transfers, and cash and technology subsidies, exploring more efficient farmland EC methods [40]. The implementation of EC policies or systems helps to stimulate enthusiasm for regional farmland ecological protection and implement responsibility. Combining agricultural location theory with spatial polarization theory, and taking into account the inherent spatial connections and practical needs of cultivated land quality, Shandong's cultivated land is divided into four protection areas: the core protection area, comprehensive reconstruction area, key improvement area, and priority enhancement area. Large-scale, ecological, and factory agriculture, as well as other cultivated land protection models and plans, have been proposed [41]. Others have evaluated and analyzed the ecological balance of black soil farmland in northeast China from a spatiotemporal perspective, introducing a dynamic balance model and understanding the relationship between EC and farmland protection as one that is dynamic and interrelated, providing a new path for the sustainable utilization and protection of farmland [42].

Although there have been studies scientifically quantifying the value of ecosystem services and exploring mechanisms of EC for cultivated land, these emerged relatively late; as such, the methods for determining the amount of EC for cultivated land are still relatively traditional. They fail to explore the impact of food production processes on cultivated land ecology from multiple dimensions and thus have certain limitations. In an attempt at further quantification, this study takes the value of farmland ecosystem services as a springboard and constructs an EC model. This study's contribution mainly includes the following three aspects. (1) Firstly, it applies the improved three-dimensional EF model to the study of regional farmland EC, taking into account both spatial and temporal dimensions, introducing the perspectives of resource flow and stock, and comprehensively analyzing farmland ecological status. This model is more advantageous in evaluating natural resource consumption and quantifying EC value. Based on this, the measured EC value and standards are more scientifically feasible in compensation transfer payments. (2) The second contribution lies in its taking into account the negative impact of utilizing arable land in agricultural production. Based on the carbon cycle, the carbon footprint method is introduced to account for carbon emissions and sinks, making up for the shortcomings of the original model that ignores any negative ecological value. (3) Thirdly, based on zoning thinking, the total amount of and priorities regarding EC for cultivated land are overlapped and analyzed. Taking into account the regional natural resource endowment and socio-economic differences, a five-zone map of EC for cultivated land is delineated, providing a spatial screening basis for promoting regional EC in a classified and orderly manner. In the context of ecological civilization construction, the sustainable utilization and protection of farmland ecosystems, as well as the compensation mechanism for farmland protection, are highly significant, promoting the realization of the "three in one" farmland protection goal in the new era.

2. Research Area and Data

2.1. Research Area

Shandong Province, an important farmland protection and major grain-producing area, is located on the eastern coast of China at the lower reaches of the Yellow River (Figure 1). The province's entire land area is 15.89 million hectares, of which 6.4149 million are cultivated land, and the per capita area of farmland is 0.06 hectares. Shandong Province has a well-developed water system, with plains as the main terrain. The central mountainous areas protrude, while there are low-lying and flat areas in the south- and northwest. The eastern part has gentle undulations, forming a terrain with mountains and hills as the skeleton and plains and basins crisscrossing each other. The natural landscape of the province consists of three mountains, one body of water, and six fields. The average annual figures for precipitation, temperature, and sunshine are 874.12 mm, 14.58 °C, and 2320 h, respectively, thus meeting the conditions of two crops per year. Its unique geographical, climatic, and resource conditions endow Shandong Province with inherent agricultural development advantages. Farmland is mainly used for planting grain and economic crops, including rice, wheat, corn, sorghum, millet, potatoes, and soybeans, while economic crops include cotton, oilseed, vegetables, fruits, etc. Shandong Province has a total of 16 prefecture-level cities; by the end of 2022, the permanent population was 101.6279 million, with a gross domestic product of CNY 8743.51 billion and a primary industry output value of CNY 629.862 billion. Its added agricultural value has consistently ranked first among all provinces in China, with a total grain output of 55.438 million tons. The planting area and yield of grain have consistently ranked among the top three in the country, making it the province with the highest cultivated land rate. As a primary province in China for both agriculture and the economy, Shandong has been designated a cultivated

land retention area of 94.911 million mu, a permanent basic farmland protection area of 84.122 million mu, and an ecological protection red line area of 2.06 million hectares. The ecological protection of farmland significantly affects national ecological and food security.

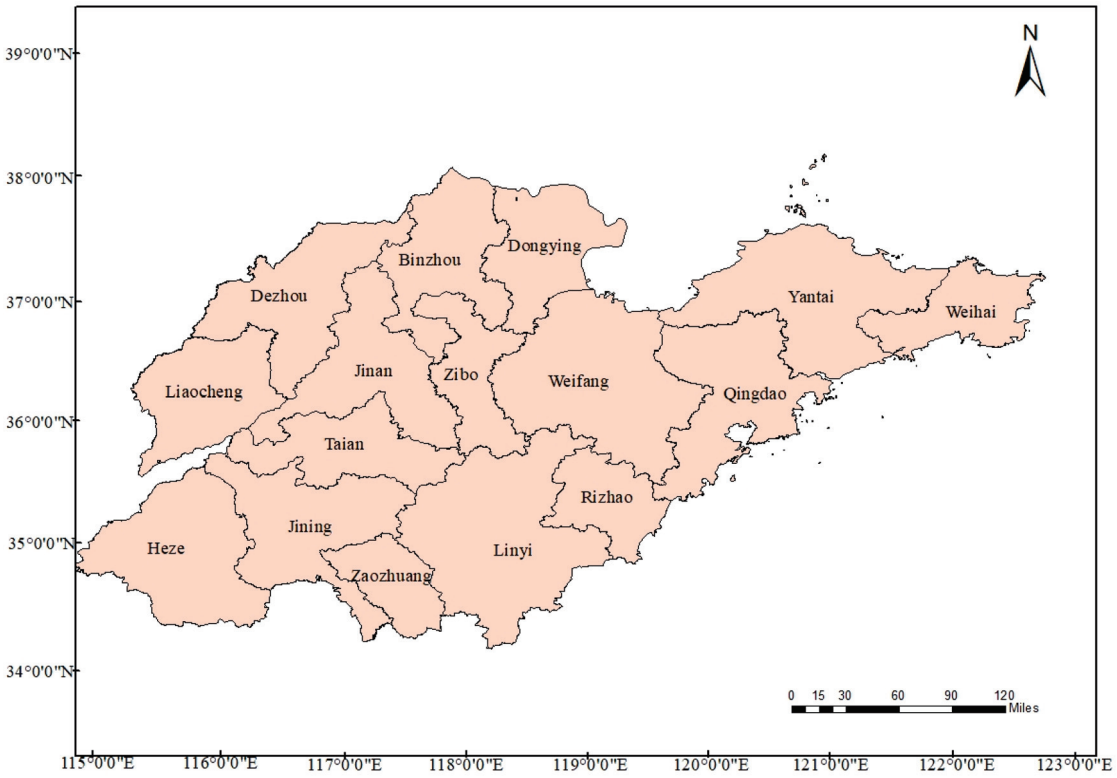

Figure 1. Research area.

2.2. Data Sources

Sources of data used in this research include: (1) overview data, population data, crop yield, sowing area, GDP of each city, cultivated land area data, pesticide and fertilizer application data of various cities in Shandong Province are all derived from Shandong Provincial Statistical Yearbook 2023. (2) National crop yield data and GDP are derived from China Statistical Yearbook 2023. (3) Unit area yield and Engel's coefficient data of grain crops of each city in Shandong Province are sourced from 2023 Statistical Yearbook data of each city.

3. Research Method

3.1. Cultivated Land Ecological Footprint Measurement Model

The EF of cultivated land reflects the pressure exerted by human production and consumption on cultivated land. When tracking human ecological occupation of arable land resources, ecological footprint accounting is classified into biological resource footprint accounting and carbon footprint accounting.

3.1.1. Bioresource Footprint Accounting of Cultivated Land

The bioresource footprint (BF) of cultivated land refers to the ecologically productive cultivated land area that provides and maintains the resources required for production and consumption by a specific population in a region [43]. The quantitative model for the footprint of arable land biological resources is:

$$EF_{br} = N \times ef_{br} = N \times \sum_{i=1}^{n}(aa_i) = N \times \sum_{i=1}^{n} \frac{C_i}{P_i} \times r \quad (1)$$

EF_{br} is the BF of farmland in the region (hm^2), N is the number of permanent residents in the area, ef is per capita BF of farmland in the area (hm^2/person), i is the crop type produced or consumed in the region, aa_i is per capita area of biologically productive cultivated land that was transformed from the i-th crop in the region (hm^2/person), C_i is per capita annual consumption of the i-th crop (kg/person); P_i is average annual yield of the i-th crop nationwide; r is the equilibrium factor of farmland, which was calculated by Liu and is 1.49 in the case of Shandong Province.

3.1.2. Carbon Footprint Accounting for Cultivated Land

When calculating the EF of arable land, it is also essential that consider the carbon footprint (CF) of farmland caused by the "by-products" that damage farmland ecology.

Carbon Emission Calculation

The primary sources of carbon emissions during the arable land cultivation process include chemical fertilizers, pesticides, agricultural plastic films, diesel combustion, agricultural irrigation, as well as mechanization. The estimation formula for carbon emissions is [44]:

$$E = E_f + E_p + E_m + E_e + E_i + E_t \quad (2)$$

E is total carbon emissions from farmland in the study area (t), E_f is chemical fertilizers' contribution to carbon emissions; E_p is the carbon emissions caused by pesticides; E_m represents agricultural plastic films' contribution to carbon emissions; E_e is carbon emissions caused by diesel fuel; E_i is agricultural irrigation's contribution to carbon emissions; E_t is carbon emissions from agricultural mechanization. The calculation formula for each item is as follows:

$$E_f = G_f \times A \quad (3)$$

$$E_p = G_p \times B \quad (4)$$

$$E_m = G_m \times C \quad (5)$$

$$E_e = G_e \times D \quad (6)$$

$$E_i = A_i \times G \quad (7)$$

$$E_t = (A_t \times D) + (W_e \times F) \quad (8)$$

G_f is chemical fertilizer usage (kg), G_p is pesticide usage (kg), G_m is agricultural plastic film usage (kg), G_e is agricultural diesel usage, A_i represents irrigation area (hm^2), W_e is the total power of agricultural machinery (kw), A_t is the planting area of crops (hm^2). A. B, C, D, F, and G express carbon emission coefficients of chemical fertilizers, pesticides, agricultural plastic films, agricultural diesel, agricultural irrigation, and agricultural mechanization, respectively. Referring to authoritative research [45], the following coefficients are determined: A = 0.89 kg/kg, B = 4.934 kg/kg, C = 5.18 kg/kg, D = 0.5927 kg/kg, G = 266.48 kg/hm^2, D = 16.47 kg/hm^2, F = 018 kg/kw.

Carbon Absorption Calculation

To quantitatively calculate the carbon absorption of different crops, it is necessary to combine indicators such as crop yield, economic coefficient, root to shoot ratio carbon content, and water coefficient. The calculation formula is as follows:

$$C_t = \sum_{i=1}^{n} C_i \times Y_i \times (1 - V_i) \times (1 + R_i)/H_i \quad (9)$$

C_t is the carbon storage (t) of the regional farmland ecosystem, that is, carbon absorption, C_i is the carbon content (%), Y_i indicates the i-th crop's yield (t), V_i indicates the i-th crop's water coefficient (%), R_i indicates the i-th crop's root to shoot ratio coefficient, H_i indicates the i-th crop's economic coefficient, n indicates the crop types' species number, with n = 9 in this study. The H, C, R, and V of primary crops in China are shown in Appendix A.

Carbon Footprint Accounting

The carbon footprint (CF) refers to the productive land area that needs to absorb carbon emissions, that is, the ecological footprint of carbon emissions:

$$CF = \frac{E}{NEP}, NEP = \frac{C_t}{S} \tag{10}$$

CF indicates the CF of farmland in the region (10,000 hm^2), E indicates total carbon emissions from farmland use, NEP indicates the carbon sequestration capacity of crops, C_t indicates all crops' carbon absorption throughout the whole growth phase in the farmland ecosystem, S indicates farmland area (hm^2).

3.1.3. Accounting for Total Ecological Footprint of Cultivated Land

The total EF of cultivated land refers to the combined total of the biological resource footprint of cultivated land and carbon footprint of cultivated land:

$$EF = EF_{br} + CF \tag{11}$$

3.2. Ecological Carrying Capacity Accounting

The ecological carrying capacity (ECC) of farmland is the maximum ecological service capacity that the farmland ecosystem can continuously provide to humans. Corresponding to the EF of arable land on the demand side, the ECC of arable land describes the ecological service area that the arable land ecosystem can provide on the supply side; it characterizes the degree of satisfaction of regional arable land against human actual consumption. The following is the computation model:

$$EC = N \times ec = N \times a \times r \times y \tag{12}$$

EC indicates total ECC of farmland in the region (hm^2), N indicates the number of permanent residents in the region, ec indicates per capita ECC of farmland (hm^2/person), a indicates per capita biological productive land area of farmland (hm^2/person), r indicates farmland's equilibrium factor, and y indicates cultivated land's yield factor. The farmland's yield factor computed by Liu et al. is 1.13 in Shandong Province.

3.3. Expanded 3D Ecological Footprint Model

Niccolucci et al. pioneered a three-dimensional EF model, originating from a two-dimensional model, and achieved vertical expansion in this field. The concept of natural resource stock has been introduced, with two indicators: footprint breadth (EF_{size}) and footprint depth (EF_{depth}).

3.3.1. Footprint Breadth

Footprint breadth characterizes degree to which human production and consumption occupy natural resource flow, and it has spatial attributes. It is divided into two scenarios: surplus and deficit:

If $EC - EF > 0$, it is in an ecological surplus state, then: EF_{size} = EF.

If $EC - EF < 0$, it is in an ecological deficit state, then: $EF_{size} = EC$.

3.3.2. Footprint Depth

Footprint depth characterizes the degree to which resource consumption occupies natural resource stock, which is the ratio of regional EF to ecological carrying capacity. It falls into two categories: ecological surplus that consumes flow resources and ecological deficit that consumes stock resources, or ecological productive land in a region that takes most of a year to produce the natural resource flow consumed by humans [8]. The expanded three-dimensional EF model is shown in Appendix B, and the ecological footprint depth of cultivated land is:

$$EF_{depth} = \frac{EF}{EC} \tag{13}$$

3.4. Measurement Model for Ecosystem Service Value of Cultivated Land

3.4.1. Equivalent Factor of Ecosystem Service Value of Farmland

The equivalence factor of the ESV of farmland is the economic value of the annual food production service as a function of the farmland's per unit area. A 1/7 market value of average grain output is used as the economic value of the per unit ESV equivalence factor. Its formula is as follows:

$$E_a = \frac{1}{7} \times \frac{C_i}{A_i} \tag{14}$$

E_a is the economic value of the cultivated land ecosystem service's unit equivalence factor (yuan/hm^2), C_i represents the economic output of grain in the region for the current year (yuan), A_i represents the regional grain-planting area (hm^2), and 1/7 represents that, without human input, the unit area ESV is 1/7 the grain production value that the existing cultivated land can provide.

3.4.2. Equivalent Correction of Farmland Ecosystem Service Value

There is heterogeneity in the natural geographical environment of various zones. Consequently, it may be necessary to adjust the equivalence of ESV for farmland based on natural conditions of farmland in each region:

$$f' = f \times \frac{p}{\overline{p}} \tag{15}$$

f indicates the equivalence of the unit area ESV of the farmland ecosystem calculated by Xie Gaodi, with an equivalent value of 5.91. p is the crop's per unit production in the regional farmland ecosystem for the current year (t/hm^2), while $\overline{p}$ is the crop's per unit production of the countrywide farmland ecosystem for the same year (t/hm^2).

3.4.3. Economic Adjustment Coefficient of Farmland Ecosystem

The ESV of farmland calculated in the previous step is only a theoretical value, which only reflects cultivated land's value under natural conditions. It does not take into account social and economic development factors, making it impossible to distinguish differences in different stages and regions of economic development. There is a significant positive correlation between residents' income level and their ability to pay for public goods. The formula for the adjustment coefficient of the resident payment level is:

$$P_i = \frac{A_i}{N_i} \tag{16}$$

P_i is the adjustment coefficient for the payment level of residents in region i, and A_i and N_i are the per capita GDP of the region and countrywide, respectively.

We introduced a social development stage coefficient that represents the relative level of people's willingness to pay and adjusted the development stage coefficient through the Pearl growth curve and Engel coefficient. The formula is:

$$W_i = \frac{1}{1 + e^{-t}} \tag{17}$$

$$t = \frac{1}{E_n} - 3 \tag{18}$$

W_i is the adjustment coefficient for the willingness to pay of regional residents, while E_n is the Engel coefficient of the region. In theory, the lower the Engel coefficient in economically developed regions, the higher residents' willingness to pay, the higher the ecological payment amount they can afford. The overall economic adjustment coefficient of the cultivated land ecosystem is calculated by combining the coefficient of residents' payment level, the coefficient of social development stage, and the coefficient of willingness to pay:

$$a_i = P_i \times W_i \tag{19}$$

3.4.4. Ecosystem Service Value of Cultivated Land

The measurement model for the ESV of farmland by means of the above equivalence factor correction and economic adjustment coefficients is as follows:

$$ESV = E_a \times f' \times a_i \tag{20}$$

$$ESV_t = ESV \times A_i \tag{21}$$

3.5. Cultivated Land Ecological Compensation Measurement Model

3.5.1. Accounting of Total Ecological Compensation for Cultivated Land

Taking the ecological deficit and surplus of farmland as the area and the quantified EC of farmland as compensation amount unit area, and adjusting the regional actual compensation capacity, a farmland EC model is established as follows:

$$V = ET \times ESV \times R_i \tag{22}$$

$$R_i = \frac{e^{E_n} \times GDP_i}{(e^{E_n} + 1) \times GDP} \tag{23}$$

V indicates the total amount of EC for farmland (yuan/year), ET indicates the three-dimensional ecological surplus and deficit of farmland (ER/ED), R_i indicates the regional EC coefficient for cultivated land, En indicates the comprehensive Engel coefficient for regional urban and rural areas, GDP_i is the regional annual gross domestic product, and GDP is the province's gross domestic product.

3.5.2. Priority of Ecological Compensation for Cultivated Land

In terms of economic progress, disparities exist between the output and beneficiary areas from cultivated land. To balance the efficiency and fairness of EC for farmland, a fair EC priority approach is proposed to define the urgency of EC for farmland in various regions [46], expressed as:

$$ECPS = \frac{ESV}{GDP_{ua}} \tag{24}$$

ECPS represents the priority of EC for farmland in region i, while GDP_{ua} represents the regional annual GDP unit area (yuan/hm^2). The higher the priority of the EC for

farmland in a region, the more urgent the need for compensation. Conversely, a lower priority indicates that the urgency of EC for farmland in a region is relatively mild.

4. Results Analysis

4.1. Ecological Footprint Analysis of Cultivated Land in Shandong Province

The primary uses of farmland are to cultivate food crops, including cereal crops, potato crops, and legumes, and economic crops, including fiber crops, oil crops, sugar crops, medicinal crops, vegetables, fruits, etc. Comprehensively considering Shandong Province's agricultural production status, nine crops were chosen for this study—including rice, wheat, corn, beans, and potatoes, as well as cotton, oil crops, vegetables, and fruits—as indicators to measure the ecological status of farmland. Using an EF measurement model, the 2022 biological resource footprint, carbon footprint, and total EF of farmland, as well as per capita EF, in each city of Shandong Province were obtained, as shown in Table 1. The total farmland biological resource footprint in Shandong Province in 2022 was 6.8358 million hectares, with Linyi having the largest footprint of 90.78 $\times$ 10^4 hectares and Dongying having the smallest at 15.89 $\times$ 10^4 hectares. The per capita farmland biological resource footprint in the province is 0.07 $\times$ 10^4 hectares per person. Excluding Weihai, the per capita biomass footprint of farmland in the other 15 cities is below 0.10 $\times$ 10^4 hm^2. Regarding the crop-planting structure, crops' rates of contribution to the biological resource footprint of cultivated land are as follows, in descending order: wheat, oil, beans, vegetables, rice, fruits, melons, corn, cotton, and potatoes. Among them, wheat has a contribution rate of 49%, oilseeds have a contribution rate of 20.1%, and legumes have a contribution rate of 10.4%. The average annual contribution rate of these three crops to the biological resource footprint of cultivated land is as high as 79.5% (Figure 2). This is because Shandong Province, as the main grain-producing area in China, is positioned to supply major grain crops such as wheat and corn. The scale of wheat and bean planting is large, meeting the policy requirements of "treating rice and wheat as essential varieties to ensure basic self-sufficiency of grains". In addition, strict land use management and control systems are implemented, restricting the conversion of agricultural land for construction purposes. The high yields of economic crops, mainly based on oil crops, excessive population, and rapid urbanization, have also increased food consumption.

Table 1. Biological resource footprint and carbon footprint of farmland in Shandong Province.

	Footprint of Cultivated Land Biological Resource (10^4 hm^2)	Per Capita Cultivated Land Biological Resource Footprint (hm^2)	Total Carbon Emission (10^4 t)	Total Carbon Absorption (10^4 t)	Carbon Footprint of Cultivated Land (10^4 hm^2)
Jinan	53.45	0.06	36.36	439.54	2.84
Qingdao	69.34	0.07	51.32	501.46	4.40
Zibo	24.18	0.05	16.47	204.27	1.27
Zaozhuang	23.88	0.06	27.84	290.42	1.93
Dongying	15.89	0.07	16.43	200.01	1.79
Yantai	57.91	0.08	55.20	314.39	6.19
Weifang	55.86	0.06	97.46	700.77	8.28
Jining	53.81	0.06	59.23	719.38	4.13
Taian	36.02	0.07	32.43	402.33	2.28
Weihai	27.92	0.10	29.91	130.88	3.74
Rizhao	25.66	0.09	19.91	147.45	2.44
Linyi	90.78	0.08	65.52	694.37	5.93
Dezhou	31.27	0.06	54.38	1060.70	3.25
Liaocheng	31.26	0.05	61.97	827.59	3.88

Table 1. *Cont.*

	Footprint of Cultivated Land Biological Resource (10^4 hm^2)	Per Capita Cultivated Land Biological Resource Footprint (hm^2)	Total Carbon Emission (10^4 t)	Total Carbon Absorption (10^4 t)	Carbon Footprint of Cultivated Land (10^4 hm^2)
Binzhou	24.10	0.06	33.92	514.01	2.54
Heze	62.25	0.07	73.63	1180.71	5.81
Province	683.58	0.07	731.96	8328.27	60.70

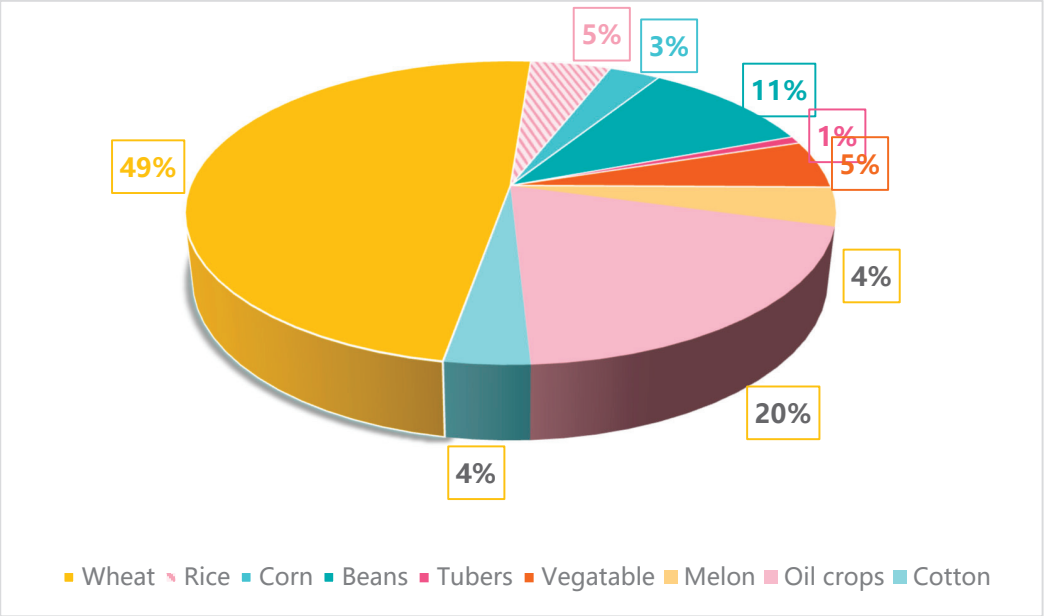

Figure 2. Contribution rates of crops to the biological resource footprint of cultivated land.

In 2022, carbon emissions from the farmland ecosystem in Shandong Province were 7.3196 million tons, of which 3.2226 million tons were caused by fertilizer application, representing 44% of overall carbon emission (Figure 3). In 2022, the average fertilizer application intensity in various cities in Shandong Province was 493.92 kg/hm^2, far higher than the safety warning line of 225 kg/hm^2. In 2022, the total carbon absorption of farmland ecosystems in Shandong Province was 83.2827 million tons, with the value of wheat being as high as 47.37%, and corn accounting for 35.81% of the total carbon absorption. These two food crops account for 83.18% of the total carbon absorption of farmland ecosystems (Figure 4). Compared to other cities, Yantai, Weifang, Linyi, and Heze all have carbon footprints above 50,000 hm^2, which is relatively high.

In 2022, the total EF of farmland in Shandong Province was 7.4428 million hectares, and the per capita EF of cultivated land was 0.07 hectares (Table 2). Compared to other cities, the EF of cultivated land in Heze, Linyi, and Qingdao is comparatively large. Compared to other crops, the EF contribution rate of corn- and vegetable-growing areas is relatively high. Only Weihai has a per capita EF of farmland that is consistently over 0.1 hm^2. The per capita EF of farmland in Zibo is only 0.05 hm^2, moreover, the ratio at which all kinds of crops contribute to the EF of farmland is relatively small. In accordance with the EF of farmland in each region, Shandong Province is divided into five regions (Figure 5). The main body of total EF and per capita EF of farmland in each city of Shandong Province indicates low-value areas. In terms of the spatial pattern aspect, there is an obvious spatial difference between the total EF and per capita EF of farmland in various cities in Shandong Province, highlighting a pattern that is low in the northwest and high in the southeast.

Overall, in terms of the biological resource and carbon footprints of cultivated land, the trends in the change are roughly the same, indicating a strong correlation between the two.

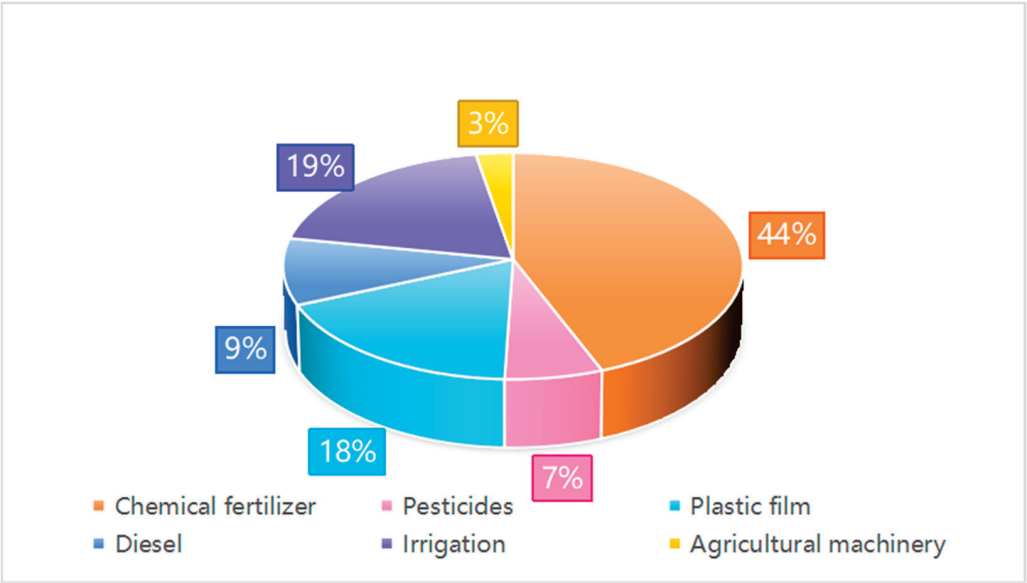

Figure 3. The proportions of carbon emissions from farmland.

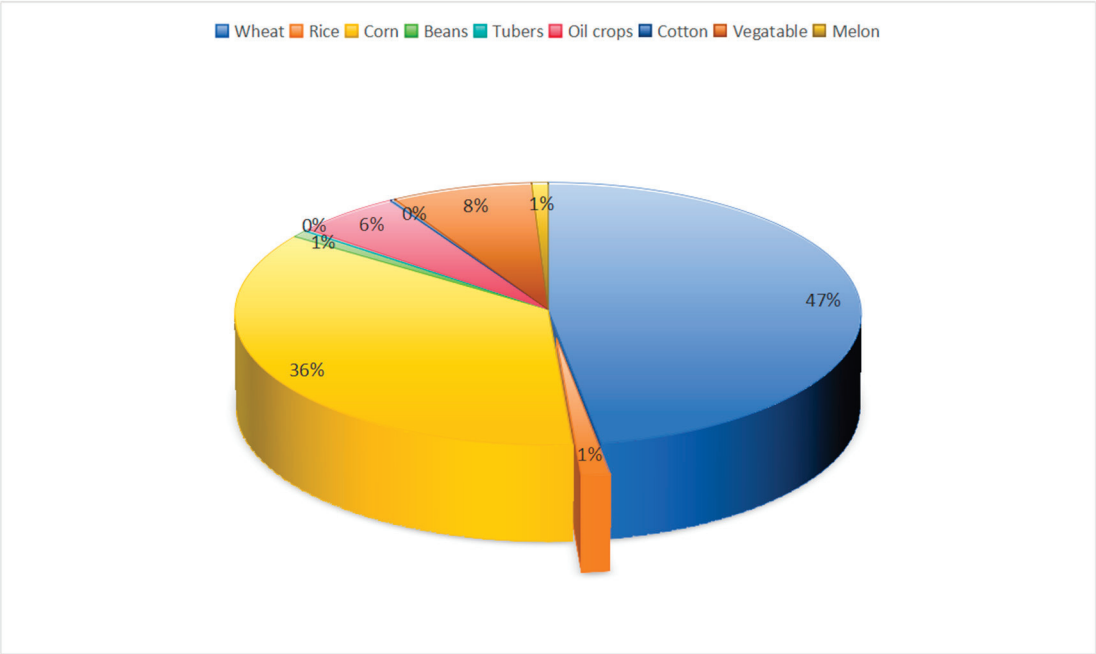

Figure 4. The proportions of carbon absorption on farmland.

Table 2. EF and ECC of farmland in various cities of Shandong Province in 2022.

	Total EF of Cultivated Land (10^4 hm^2)	Per Capita EF of Cultivated Land (hm^2)	Total ECC of Cultivated Land (10^4 hm^2)	Per Capita ECC of Cultivated Land (hm^2)
Jinan	56.28	0.06	57.73	0.06
Qingdao	73.74	0.07	72.4	0.07
Zibo	25.46	0.05	26.58	0.06
Zaozhuang	25.81	0.07	33.9	0.09
Dongying	17.67	0.08	36.61	0.17
Yantai	64.1	0.09	59.36	0.08
Weifang	64.13	0.07	100.22	0.11

Table 2. *Cont.*

	Total EF of Cultivated Land (10^4 hm^2)	Per Capita EF of Cultivated Land (hm^2)	Total ECC of Cultivated Land (10^4 hm^2)	Per Capita ECC of Cultivated Land (hm^2)
Jining	57.94	0.07	84.52	0.10
Taian	38.3	0.07	47.64	0.09
Weihai	31.66	0.11	27.59	0.09
Rizhao	28.1	0.09	30.38	0.10
Linyi	96.71	0.09	105.76	0.10
Dezhou	34.52	0.06	106.83	0.19
Liaocheng	35.15	0.06	87.3	0.15
Binzhou	26.64	0.07	64.92	0.17
Heze	68.05	0.08	156.78	0.18
Province	744.26	0.07	1098.52	0.11

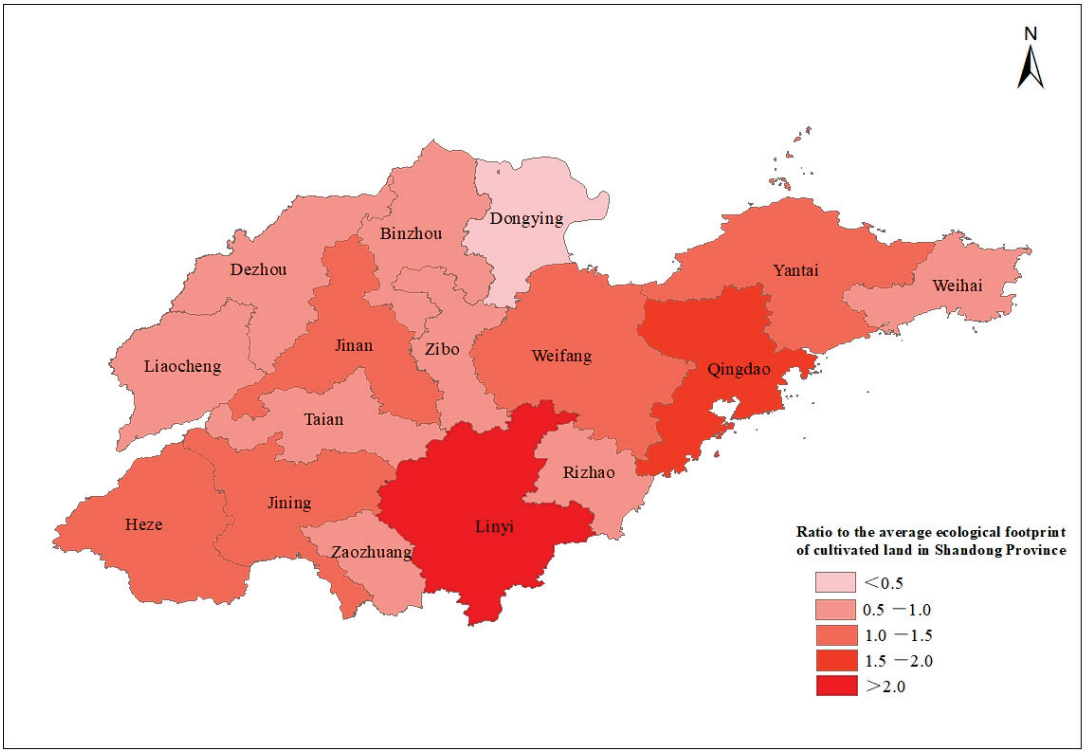

Figure 5. Total ecological footprint of farmland in each city of Shandong Province.

4.2. Analysis of Ecological Carrying Capacity of Cultivated Land in Shandong Province

Using Formula (12), the ecological carrying capacity of farmland in Shandong Province is calculated (Figure 6). Heze has the largest farmland area and the highest ECC of farmland, at 1.5678 million hectares, with per capita ECC of 0.18 hectares. Dezhou has the highest per capita ECC of farmland, at 0.19 hectares. The ECC of farmland in Zibo is the smallest, at 26.58 × 10^4 hm^2. Under the undulating natural terrain of the southern and east–west wings, the per capita area of biologically productive farmland in Zibo is only 0.03 hm^2. Jinan is adjacent to Mount Taishan in the south and across the Yellow River in the north, situated at the junction where low mountains and hills in the middle and south meet an alluvial plain in the northwest of Shandong Province. Meanwhile, the cultivated land area only accounts for 5.26% of the province (Figure 7), while the population is close to 10 million, resulting in a per capita ECC of farmland of 0.06 hm^2. The high-value areas of ECC are mainly distributed in the northwest plain (Liaocheng, Dezhou, Heze, Weifang), while low-value regions are distributed in central and southern mountainous hills (Zibo, Zaozhuang, Rizhao). The ecological consumption areas of farmland are concentrated in

the Shandong Peninsula and southern region of Shandong Province, while the ecological service regions are primarily centered on the northwest plain and southern regions. There is a phenomenon of "spatial ectopia" between ecological consumption and services, wherein high farmland EF and ECC are relatively concentrated. The Shandong northwest plain is the largest plain in Shandong Province, constituting a section of the North China Plain, and it is also an important agricultural production region in China. Heze, Weifang, Dezhou, and Linyi have large areas of cultivated land, representing 42.75% of total farmland in the province. When the yield of grain and cash crops is high, this produces higher ecological farmland effects.

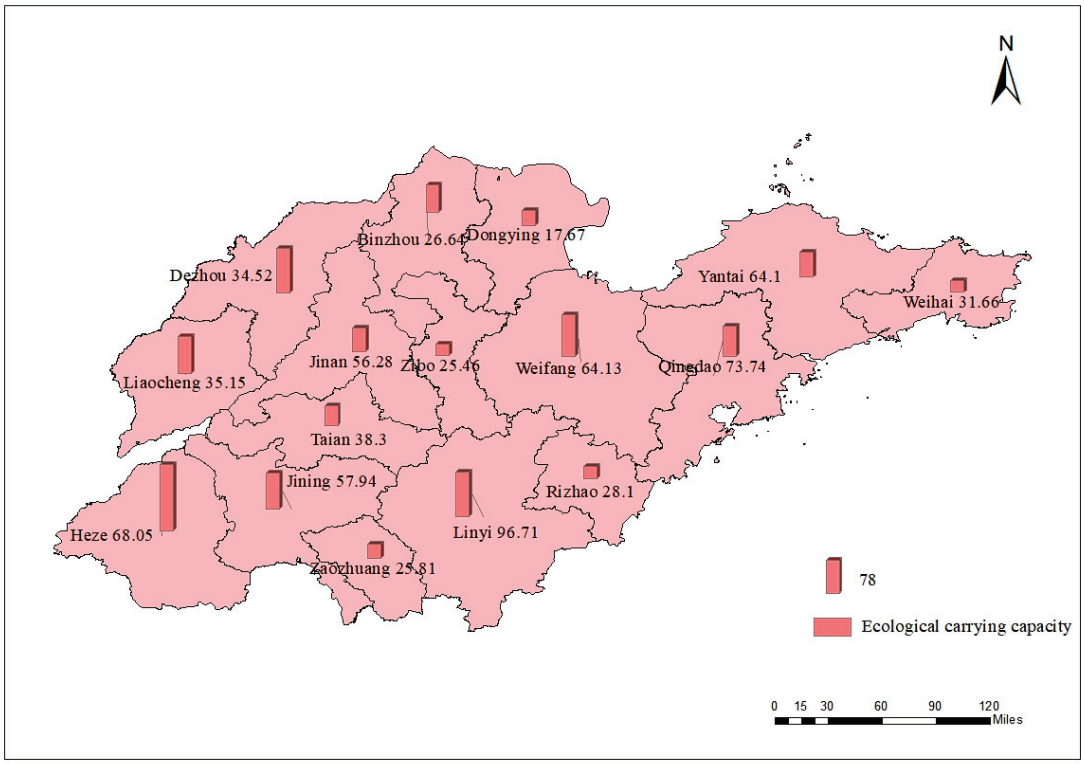

Figure 6. Ecological carrying capacity of farmland in various cities of Shandong Province.

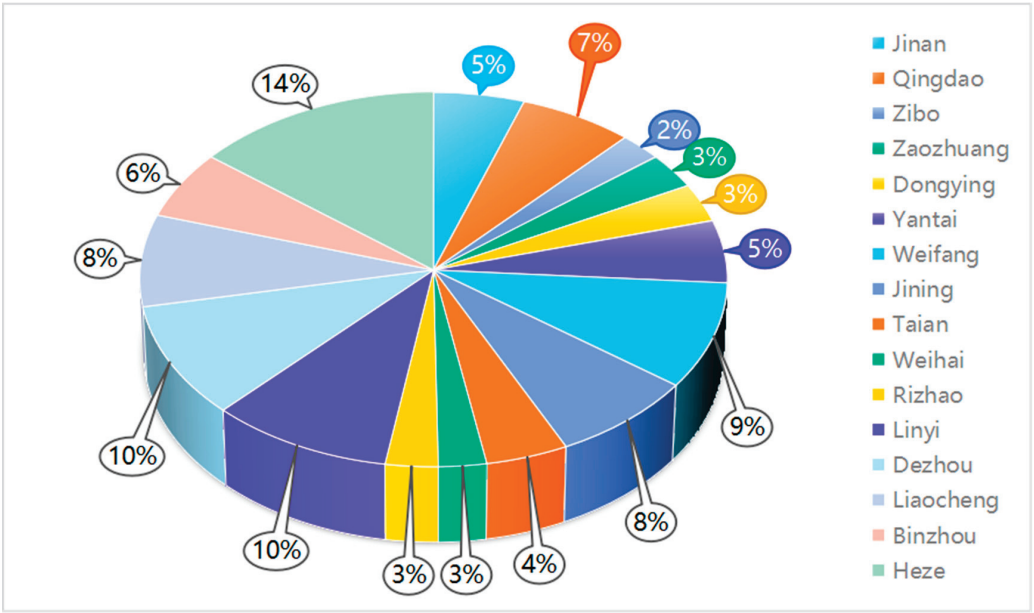

Figure 7. The proportion of farmland area in each city of Shandong Province.

4.3. Analysis of Ecological Surplus and Deficit of Cultivated Land

Under the extended three-dimensional EF model, the EF breadth and depth of farmland can be obtained through examining the regional ecological deficit and surplus situation, which characterizes farmland resource flow occupancy and reflects the degree of adaptation between the EF of cultivated land and the level of ECC (Table 3). The EF depth of farmland in the three regions of Qingdao, Yantai, and Weihai is greater than 1; moreover, farmland resource flow is insufficient to support actual food consumption demand, requiring additional consumption of existing cultivated land resources. Among them, the EF depth of farmland in Weihai City is above 1.15, which means that the amount of resource stock overdrawn in 2022 is equivalent to the natural resource accumulation of ecological production land under the national average yield of 0.15 years; as such, resource consumption puts greater pressure on farmland resource stock. The ecological footprint depth of farmland in 13 regions, including Jinan and Zibo, is less than 1, indicating that regional farmland resource flow can meet their food consumption needs, and there is surplus flow converted into stock without occupying farmland resource stock. Consequently, the ecological carrying status is good.

Table 3. Ecological footprint, surplus, and deficit of farmland in Shandong Province.

	Breadth of EF on Cultivated Land (10^4 hm^2)	**Depth of EF on Cultivated Land**	**Ecological Surplus of Cultivated Land (10^4 hm^2)**	**Ecological Deficit of Cultivated Land (10^4 hm^2)**
Jinan	56.28	0.97	1.45	
Qingdao	72.40	1.02		−1.34
Zibo	25.46	0.96	1.13	
Zaozhuang	25.81	0.76	8.09	
Dongying	17.67	0.48	18.93	
Yantai	59.36	1.08		−4.73
Weifang	64.13	0.64	36.08	
Jining	57.94	0.69	26.57	
Taian	38.30	0.80	9.34	
Weihai	27.59	1.15		−4.08
Rizhao	28.10	0.93	2.28	
Linyi	96.71	0.91	9.06	
Dezhou	34.52	0.32	72.31	
Liaocheng	35.15	0.40	52.15	
Binzhou	26.64	0.41	38.28	
Heze	68.05	0.43	88.73	
Province			364.40	−10.15

From the perspective of farmland ecological deficit and surplus, Qingdao, Yantai, and Weihai are deficit areas, with a total ecological deficit of 101,500 hectares and a population of 20.3186 million people. The other 13 cities are surplus areas, with a total ecological surplus of 3.644 million hectares and a population of 81.3093 million people. Heze has the largest ecological surplus of 88.73 $\times$ 10^4 hectares, while Yantai has the largest ecological deficit of 4.73 $\times$ 10^4 hectares. Heze farmland area ranks first in Shandong, at 1.5–6 times that of other cities, thus it has the highest ECC and ecological surplus. Regions with high per capita farmland ecological surplus are Heze, Dezhou, and Binzhou, all of which are higher than 0.1 hm^2/person. Yantai's terrain is a low mountain and hilly area, with gentle undulations and crisscrossing gullies; this means that per capita farmland area is only 0.05 hm^2, while fertilizer application intensity is as high as 781.82 kg/hm^2, resulting in a high carbon footprint. The EF of arable land is higher than the ECC of farmland. From the perspective of the population and ecological deficit of farmland, the population surplus regions in the province account for about 80%, while farmland area accounts for about 85.49%. The ECC of farmland is good, with no observed imbalance phenomena. In

addition to supplying its own food demand, Shandong Province also has a 70.39% grain production farmland ecosystem that can supply other provinces with deficits. From a spatial distribution perspective, the ecological deficit and surplus of cultivated land in Shandong Province show a clear four-zone distribution (Figures 8 and 9), with Qingdao, Yantai, and Weihai forming ecological deficit zones. Major grain-producing areas, like Heze, Dezhou, and Liaocheng, are ecological surplus advantage areas, with amounts exceeding 50×10^4 hm^2. Binzhou, Weifang, Jining, and Dongying constitute ecological surplus development zones, with ecological surplus amounts exceeding 10×10^4 hm^2. Jinan, Zibo, Zaozhuang, Tai'an, Rizhao, and Linyi are potential ecological surplus zones, with amounts all below 10×10^4 hm^2. Major grain-producing cities in Shandong Province, like Heze, Dezhou, Liaocheng, and Jining along the Yellow River, are mostly ecological surplus regions.

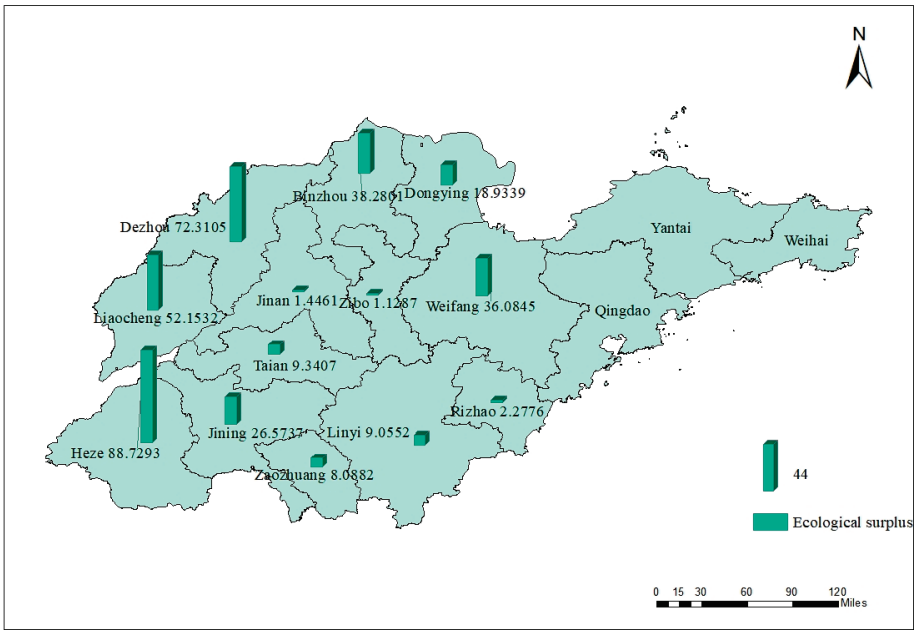

Figure 8. Ecological surplus of cultivated land.

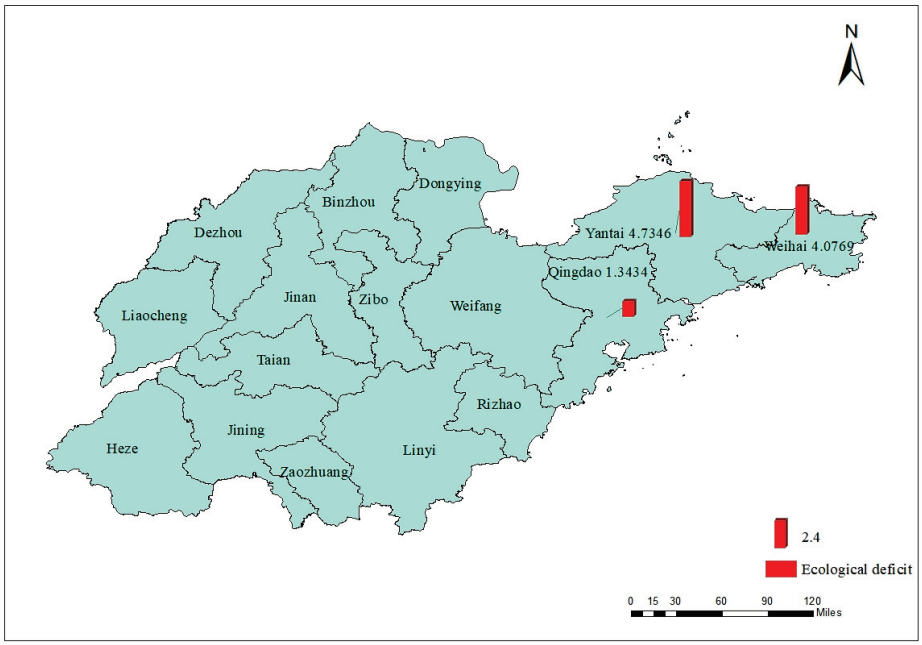

Figure 9. Ecological deficit of cultivated land.

4.4. Ecosystem Service Value and Ecological Compensation for Cultivated Land in Shandong Province

4.4.1. Ecosystem Service Value of Farmland in Shandong

The eastern coastal and central regions of Shandong Province possess a high degree of economic advancement; as such, residents are psychologically resilient and able to pay for the consumption of public goods. After adjusting using economic coefficients, the spatial heterogeneity of the ESV of farmland in Shandong Province in 2022 becomes apparent, forming a spatial differentiation pattern of high value in eastern and central areas and low value in western and southern regions (Figure 10). The total ESV of cultivated land is CNY 78.479 billion, with Dezhou having the highest ESV of CNY 9.534 billion. Due to the fact that Shandong's northwest plain is a major area of grain cultivation, and that several cities in the west like Heze and Dezhou have large grain-planting areas, the total farmland ESV ranks among the top in the province (Figure 11). Meanwhile, the total ESV of farmland in Qingdao and Jinan is comparatively high, indicating that this value is not only influenced by natural resources and ecological endowments, but also closely bound up with the processes of socio-economic growth. In terms of the ESV of farmland, ecological endowment and socio-economic progress are mutually beneficial and synergistic. In regions with lower farmland ESV in Shandong Province, attention should be paid to the coordinated development of farmland ecological protection practices and socio-economic progress.

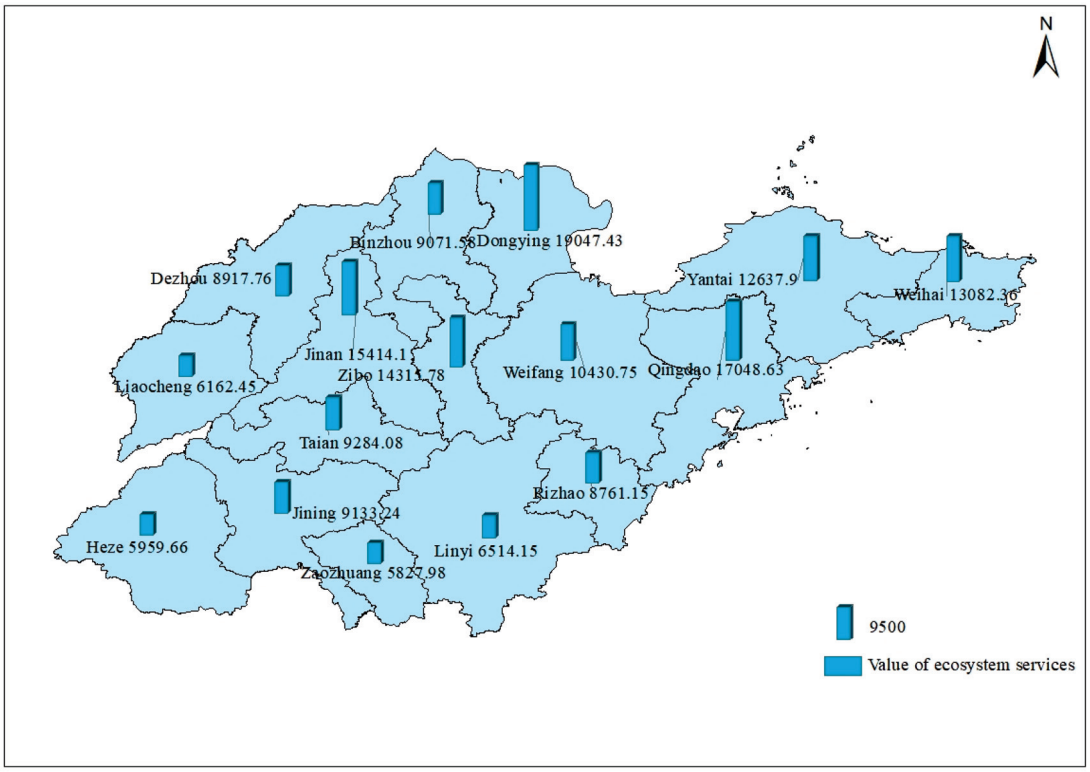

Figure 10. Ecosystem service value for cultivated land.

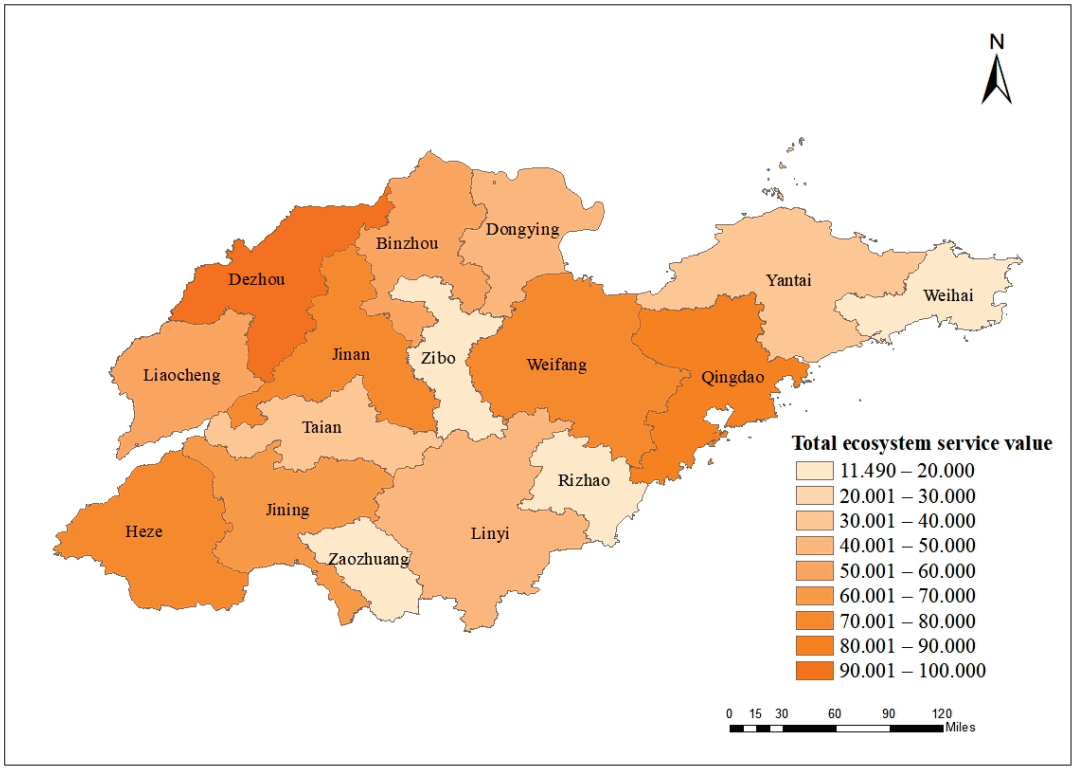

Figure 11. Total ecosystem service value for farmland.

4.4.2. Total Amount of Ecological Compensation for Cultivated Land

Based on the three-dimensional ecological surplus and deficit and ESV of farmland, economic adjustments were made to the arable land EC coefficient. Using the three-dimensional EF of farmland EC measurement model, the total amount of farmland EC in 16 cities of Shandong Province was finally obtained (Table 4). In 2022, the city of Weifang had the highest total EC for arable land. Compared to other cities, the economic value of the equivalent factor of unit ESV in Weifang was relatively high, with an ESV about twice that of Heze and EC being higher. Areas where the ecological supply of arable land is lower than the demand are referred to as arable land ecological deficit areas. Due to the spatial spillover effect of arable land ecosystem services, these deficit areas enjoy various ecological services provided by surplus areas without compensation; as such, they need to be compensated.

Table 4. Ecological compensation for farmland of Shandong Province in 2022.

	Ecological Surplus/ Deficit of Cultivated Land (10^4 hm^2)	Ecosystem Service Value for Cultivated Land (yuan/hm^2)	Total ESV for Cultivated Land (10^8 yuan)	Compensation Coefficient	Total Amount of Ecological Compensation for Cultivated Land (10^8 yuan)
Jinan	1.45	15,414.10	73.05	0.08	0.17
Qingdao	−1.34	17,048.63	82.00	0.10	−0.22
Zibo	1.13	14,315.78	16.25	0.03	0.05
Zaozhuang	8.09	5827.98	16.55	0.01	0.06
Dongying	18.93	19,047.43	48.40	0.02	0.83
Yantai	−4.73	12,637.90	38.19	0.06	−0.37
Weifang	36.08	10,430.75	70.94	0.05	1.77
Jining	26.57	9133.24	65.76	0.03	0.84
Taian	9.34	9284.08	34.42	0.02	0.18
Weihai	−4.08	13,082.36	16.31	0.02	−0.12
Rizhao	2.28	8761.15	11.49	0.02	0.03
Linyi	9.06	6514.15	41.78	0.04	0.22
Dezhou	72.31	8917.76	95.34	0.02	1.54
Liaocheng	52.15	6162.45	50.10	0.02	0.59

Table 4. *Cont.*

	Ecological Surplus/ Deficit of Cultivated Land (10^4 hm^2)	Ecosystem Service Value for Cultivated Land (yuan/hm^2)	Total ESV for Cultivated Land (10^8 yuan)	Compensation Coefficient	Total Amount of Ecological Compensation for Cultivated Land (10^8 yuan)
Binzhou	38.28	9071.58	53.38	0.02	0.67
Heze	88.73	5959.66	70.83	0.03	1.45
Province	354.25	9529.11	784.79		7.68

In accordance with the determination method for EC and payment of regional farmland, Qingdao, Yantai, and Weihai belong to ecological payment regions for farmland, and the total amount of EC to be paid in 2022 is CNY 71 million. Thirteen other cities, including Jinan and Zibo, are designated as ecological acceptance compensation zones for farmland, with a total EC amount of CNY 839 million in 2022 (Figures 12 and 13). Overall, the EC amount for farmland of Shandong Province in 2022 is in an unsustainable state. The total ecological payment amount for farmland in Qingdao, Yantai, and Weihai is significantly different from the total ecological acceptance compensation amount for farmland in the other 13 regions. Relying solely on EC in these three regions would not meet the requirements of ecological acceptance compensation for farmland in the other thirteen regions. It is necessary for the government and other provinces with ecological deficits in cultivated land to coordinate and provide funds for compensation. In 2022, Shandong Province exported the ESV of farmland to the outside world as a whole, receiving CNY 768 million in EC costs for arable land. The overall spatial pattern and footprint depth of the total EC for farmland in Shandong Province in 2022 are strongly correlated. The ecological payment area is situated in the littoral part of Shandong Peninsula, and the EC area is concentrated in major grain-producing regions along the Yellow River in the northwest Shandong plain.

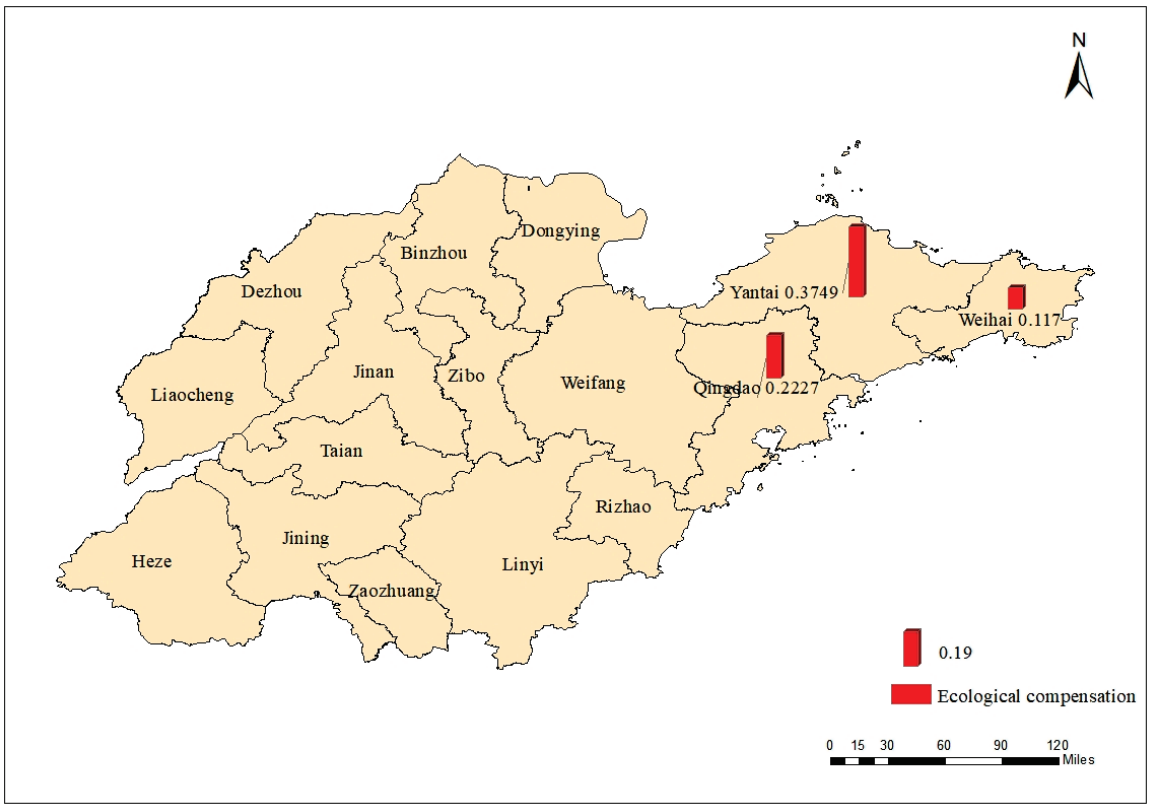

Figure 12. Ecological compensation for cultivated land.

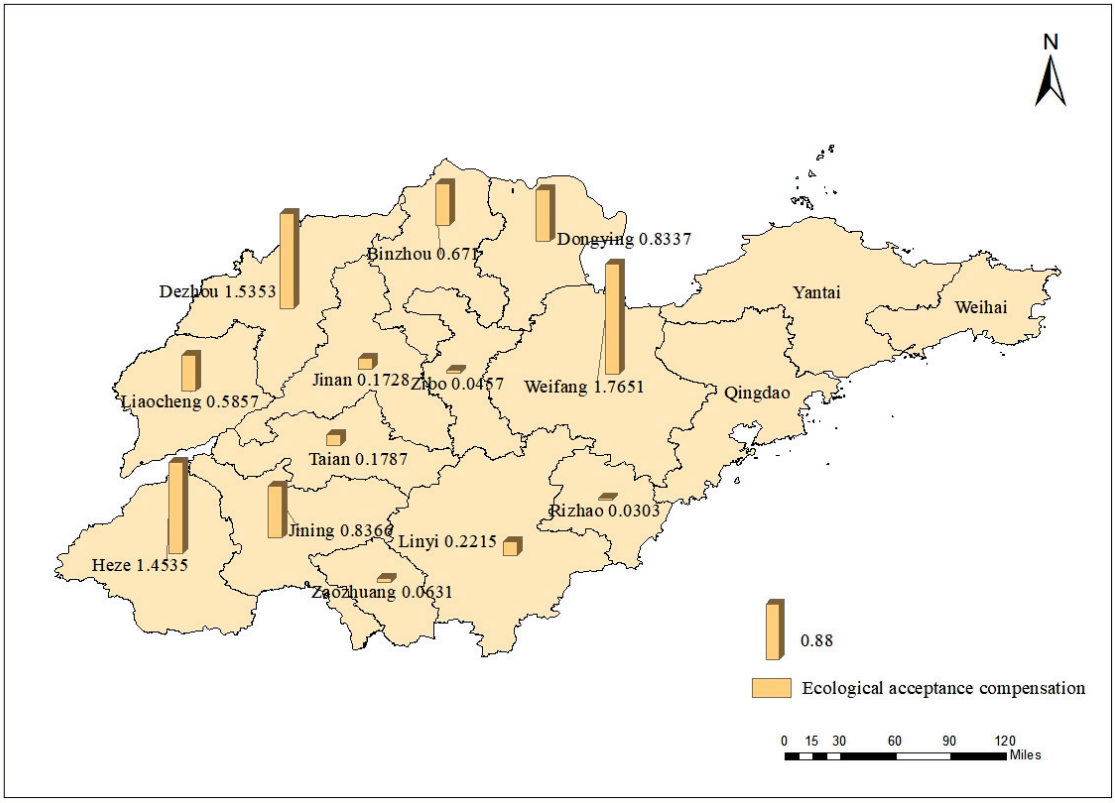

Figure 13. Ecological acceptance compensation for cultivated land.

4.5. Priority and Comprehensive Zoning of Ecological Compensation for Farmland in Shandong Province

4.5.1. Priority Measurement of Ecological Compensation for Cultivated Land

The priority of EC for farmland characterizes the urgency of EC for farmland in various regions. Combined with the regional GDP output value unit area, the priority sequence of EC for farmland in various regions of Shandong Province in 2022 can be obtained (Table 5).

Table 5. Priority of ecological compensation for cultivated land.

	Regional Gross Domestic Product (10^8 yuan)	Compensation Priority
Jinan	12,027.46	1.31
Qingdao	14,920.75	1.29
Zibo	4402.59	1.94
Zaozhuang	2039.04	1.30
Dongying	3620.74	4.34
Yantai	9515.86	1.85
Weifang	7306.45	2.31
Jining	5316.88	1.92
Taian	3198.13	2.25
Weihai	3408.18	2.23
Rizhao	2306.77	2.04
Linyi	5778.52	1.94
Dezhou	3633.07	2.54
Liaocheng	2779.85	1.91
Binzhou	2975.15	2.80
Heze	4205.34	1.72

In 2022, Dongying has the highest priority for EC farmland in Shandong Province, which is three times higher than that of Qingdao. Dezhou and Liaocheng, the values of

which are both above 2.5, belong to the first tier of EC for cultivated land. Compared to other cities, the urgent demand for EC for farmland in these three cities is relatively high. Dongying has a high ESV and quality of farmland, while Dezhou and Liaocheng have a low unit area GDP output value. The compensation priority of Qingdao and Jinan is lower than 1.5, belonging to the areas with lower priority for EC of farmland. The GDP output value ranks among the top two in Shandong Province, and a comparatively developed economic foundation has reduced the urgency of EC for farmland in both cities. With the dual impact of farmland's ecological status and regional economic development, the high priority of EC for farmland in Shandong Province is concentrated in the northern region, and there is a trend of spreading to the northwest plain of Shandong with abundant cultivated land resources. These regions have relatively backward economies, but high grain yields and large sowing areas contribute to the local surplus of arable land ESV, supplying agricultural products to other cities and provinces. As such, priority should be given to compensation to ensure ecological and food security of cultivated land. The Shandong Peninsula, which is an ecological consumption area for arable land, is a place into which materials, population, and resources are flowing, and the urgent need for EC for farmland is comparatively low, so it should preferentially disburse EC for arable land.

4.5.2. Comprehensive Zoning of Priority for Ecological Compensation of Cultivated Land

Before implementing EC for farmland, the key to ensuring a scientific and effective compensation mechanism is to accurately identify the compensation objects in light of the region's real circumstances. The zoning thinking and coordination of regional natural factors and economic and social differences can help in quickly identifying priority compensation areas with high ESV and strong compensation urgency, accurately locating priority compensation areas with serious ecological deficits and stable and superior economic foundations, and providing a spatial basis for the practice of EC mechanisms. Arable land is the main component of land use in various cities in Shandong Province. High-quality arable land is mainly irrigated and is relatively stable and concentrated. The output of both grain and economic crops is relatively consistent. Therefore, zoning and strategizing have high reference value and practical significance. This research integrates measurements of the total amount and priorities of EC for farmland in various cities for spatial overlap. Based on high, medium, and low levels of ecological farmland compensation, in terms of both amount and priority, 16 cities in Shandong province are divided into five comprehensive priority areas: priority compensation zone, compensation potential zone, priority acceptance compensation zone, acceptance compensation potential zone, and ecological balance zone. In EC areas where total quantity of compensation for farmland is negative, those with high to medium compensation amounts and those of low priority belong to the "priority compensation zone". The economic conditions are often superior, but regional cultivated land resources have difficulty in meeting their own ecological consumption needs. Areas with medium to high compensation amounts and priorities, those with low compensation amounts, and those with medium to low priority belong to the "compensation potential zone". Based on the differences in compensation and priorities, compensation measures should be refined and adapted to regional circumstances. In areas where the total compensation amount is positive for EC of farmland, areas with high compensation amounts and high priority belong to the priority acceptance compensation zone. These areas undertake partial ecological services of farmland in ecological deficit regions, and the regional economy is relatively backward. Those areas with a high compensation amount, low priority, low compensation amount, and medium to high priority all belong to the "acceptance compensation potential zone", as a low ESV limits the total compensation amount. The remaining areas are called the "ecological balance zone", and the size of these

areas reflects farmland ecology coordination. The goal of interregional farmland EC is to expand the scope of the ecological balance zone.

Based on the logic and principles of zoning, priority comprehensive spatial zoning was constructed for farmland EC in 16 cities in Shandong Province; from this, a five-zone map of EC was obtained (Figure 14). The population resources in the priority compensation area are concentrated, and the socio-economic development is superior. The impact of EC on local economic development is relatively small, as is the financial pressure. This phenomenon can mainly be seen in cities of Qingdao and Yantai on the Shandong Peninsula; as such, the EC for cultivated land should be preferentially disbursed to balance supply and demand within the region. Due to the limited quantity of farmland, the quality and ecological conditions in potential compensation areas, such as Weihai, need to be improved. Priority compensation areas are mainly located in the northern region, with abundant arable land resource stock that provides ecological services to other regions; this is in comparison to eastern coastal regions, which exhibit a significant disparity in terms of economic development. Therefore, obtaining ecological farmland compensation should preferably be treated as a priority. The acceptance compensation potential zones are mostly concentrated in Shandong's southwestern areas, which is also an area where surplus ecological services are provided. Most areas have high urgency, but because of their low ESV, the total compensation amount is lower than that of the northern region of Shandong. The contradiction between socio-economic development and farmland ecology of ecological balance zones is relatively mild, and the compensation amount and priority are at a low level; these are mainly distributed in the cities of Jinan and Zibo in the central region of Shandong, and the cities of Zaozhuang and Rizhao in the southern region.

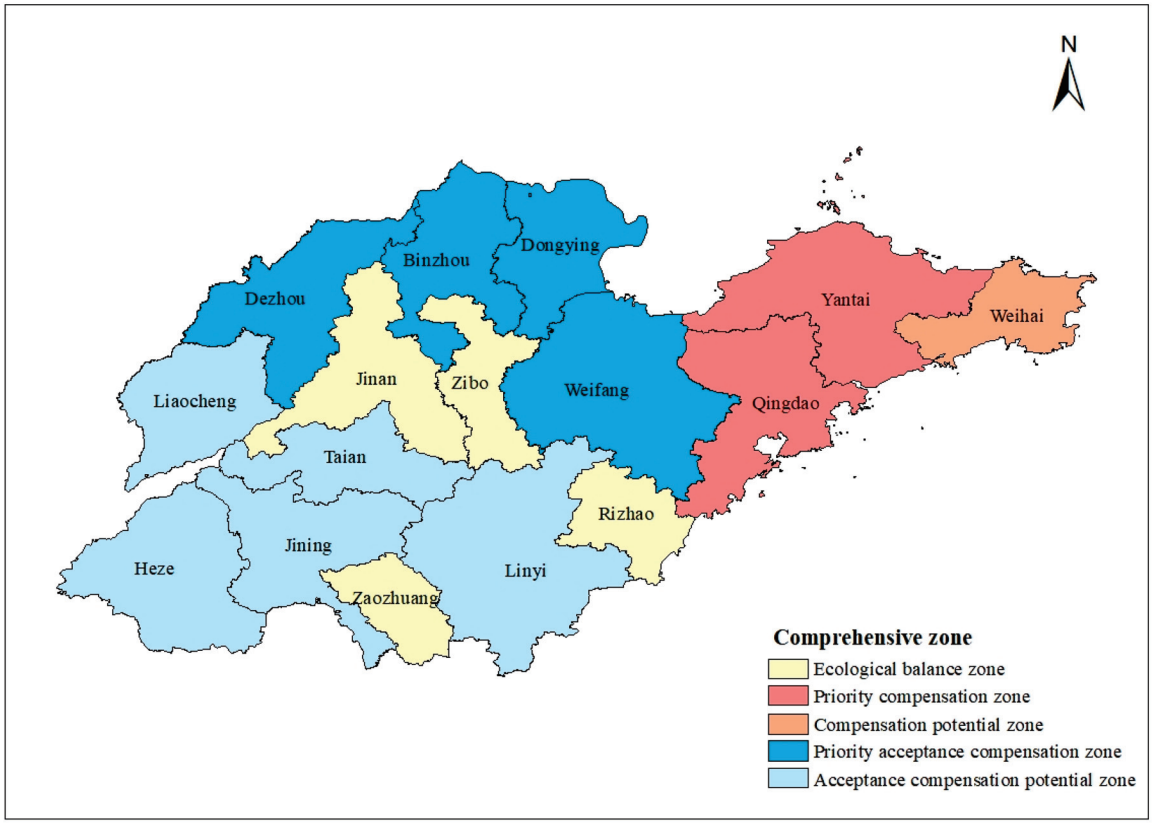

Figure 14. Five-zone map of ecological compensation.

5. Discussion

This study is based on the differences in farmland ecology, socio-economic development, and willingness to pay in 16 cities of Shandong Province. It introduces a carbon footprint and an extended three-dimensional EF model, combined with the ESV of farmland, to measure and analyze the EC of farmland in each city and further refine the comprehensive zoning of compensation priority. This offers a theoretical framework and reference for constructing EC mechanisms, facilitating innovation in farmland ecological protection policies.

Compared to the existing research findings of traditional EF methods, the computing method in this study is more comprehensive and applicable to local farmland's ecological characteristics. In addition to meeting demand for human biological products, arable land also needs to bear the "by-products" caused by ecological damage to arable land. The combination of both biological resource and carbon footprints takes carbon emission from agricultural production as part of the farmland EF, systematically and comprehensively analyzing positive and negative ESVs. The extended three-dimensional EF model characterizes farmland resource stock occupancy with "footprint depth", which can better demonstrate sustainable advancements in the utilization and ecology of regional farmland [47]. The three-dimensional EF model that characterizes the "dual burden" of arable land resources can more accurately evaluate the true ecological footprint status of regional arable land, further refining ecological footprint measurement. By combining the modified equivalence factor method and functional value approach, the farmland ESV in each city was comprehensively and accurately calculated; based on this, farmland EC standards were formulated. By adjusting the economic adjustment coefficient of the farmland ecosystem, this reflects the true farmland ESV and promotes practical operability in formulating EC standards.

The ECC of the northwest Shandong plain is strong, and the endowment of arable land resources is excellent. The arable land ecosystem has a strong sustained support capacity for agricultural production and consumption. In addition to meeting local demand, it also has resource stock to provide ecological services to areas of deficit. Due to population aggregation and high demand for ecological consumption, the pressure on farmland ecological production is high in coastal cities in the Shandong Peninsula, such as Qingdao and Yantai. Arable land currently suffers from an ecological deficit, which occupies a significant amount of farmland resource stock; as such, the amount of EC is high. Due to resource aggregation and the high level of socio-economic development, the financial burden of EC for cultivated land is low. In terms of affordability, farmers have a high acceptance of EC payments. However, due to the limitations of urban development, the "non-grainization" of cultivated land is severe; the year-by-year dwindling of these areas needs to be controlled. The factory agriculture model should be adopted, an agricultural industrial park should be established, modern agricultural technology should be utilized to develop agricultural resources reasonably, and the intensity of agricultural space should be improved to make room for high-quality urban development. Priority should be given to strengthening the protection of high-quality arable land, improving the utilization level and production efficiency and actively driving its radiation out into surrounding areas. It is essential that the internal ecological pressure on arable land is alleviated by conducting agricultural resource trade and importing agricultural products from surrounding areas. In terms of ecological status, as a whole, there is a surplus of farmland in Shandong Province. The farmland's ECC can sufficiently withstand the pressure exerted by agricultural production and consumption. As a major agricultural province and grain-producing area in China, the ecological balance of farmland in Shandong is correlated with the nation's farmland ecosystem as a whole and with food security.

Under a coastal topography, there are relatively few arable land resources. Shandong Peninsula's urban agglomeration is a key area of focus for development and a leading area of the Yellow River Basin that is attracting more people and consuming more arable land and ecological resources. In this case, it is more likely to form an ecological deficit of arable land and deeper ecological footprint. The population agglomeration, increased payment levels, and willingness of residents brought about by socio-economic development will, on the one hand, exacerbate the consumption of farmland resources in ecological payment areas, stimulating more severe conflicts between the people and land. On the other hand, it contributes to enhancing the ESV of farmland in ecologically compensated areas, as well as the total compensation amount raised. The total EC amount of farmland is significantly influenced by natural resources, while the priority of compensation is further influenced by socio-economic factors. The distribution of compensated and compensation zones is consistent with actual natural conditions of cultivated land resources and ecosystems. In areas with superior socio-economic development that rely on ecological services of the surrounding cultivated land, compensation and support should be provided to those areas with relatively backward economies via exporting ecological services. The comprehensive priority zoning of EC for farmland provides direction and inspiration for effectively promoting EC mechanisms, leveraging comparative advantages, mutual support, and coordinated high-quality development in various regions. Ultimately, this unifies the exploration of diversified EC and protection mechanisms for farmland nationwide.

Increased governmental support for agricultural technology, the deepening of agricultural modernization, technological progress, and further improvements in the agricultural production system have all promoted enhanced agricultural production efficiency. With the deepening of the concept of sustainable development and increasing awareness about farmland protection, the rational utilization of land resources has become a focus in policy. In recent years, Shandong Province has steadfastly implemented policies to protect arable land and ensure food and ecological security, achieving good results. The urbanization and industrialization processes in Shandong Province are steadily advancing. In order to improve land use efficiency, the government has promoted a large number of land consolidation and reclamation projects, effectively managing wasteland and farmland and promoting the sustainable use of land resources. More detailed policies have been adopted in land management to balance the needs of urban development and farmland protection. The formulation and strict implementation of the "occupation compensation balance" policy have a positive effect on the protection of farmland quality, thereby promoting the precise implementation of the farmland EC mechanism.

6. Conclusions, Policy Recommendations, and Limitations

6.1. Conclusions

1. Affected by the natural endowment of farmland and socio-economic development, the regional distribution of EF and ECC of farmland in Shandong Province is uneven, and the areas with high EF and high ECC of farmland are relatively concentrated. The ecological consumption regions of farmland are concentrated in Shandong Peninsula and the southern region, while the ecological service regions are mostly located in the northwest Shandong plain and the southern region. There is a phenomenon of "spatial ectopia" between ecological consumption and ecological services, and the northwest plain of Shandong plays a vital part in agricultural production. Fertilizer application intensity in 16 cities in Shandong Province has exceeded 300 kg/hm^2, far surpassing the safety warning line. In the context of the dual carbon target, attention should be paid to carbon emissions in agricultural production processes.

2. The total ecological surplus of farmland in Shandong Province is 3.644 million hectares, and total ecological deficit of farmland is 10.15×10^4 hectares. In terms of spatial distribution, ecological surplus and deficit of farmland show a clear four-zone distribution, with Qingdao, Yantai, and Weihai forming ecological deficit zones. The major grain-producing areas like Heze, Dezhou, and Liaocheng have formed ecological surplus advantage areas; Binzhou, Weifang, Jining, and Dongying have formed ecological surplus development zones, while Jinan, Zibo, Zaozhuang, Tai'an, Rizhao, and Linyi have formed ecological surplus potential zones. In addition to supplying its own food demand, Shandong Province also has a 70.39% of grain production by farmland ecosystem that can supply other provinces with ecological deficit areas of farmland.
3. The EC regions for farmland in Shandong Province are Qingdao, Yantai, and Weihai, with a total compensation amount of CNY 71 million. The other 13 cities are EC areas for farmland, with a total compensation amount of CNY 839 million. In 2022, Shandong Province exported the ESV of farmland to the outside world as a whole. Relying solely on the EC amount of farmland in Qingdao, Yantai, and Weihai to compensate for the other 13 cities is difficult to achieve. Therefore, it is necessary to coordinate with other provinces with ecological deficits in cultivated land and provide EC for the other 13 cities through off-site purchases and transfer payments.
4. According to the spatial zoning model of compensation priority and compensation amount overlap, a "five-zone map" for the EC of farmland is delineated. The priority compensation zones in Shandong Province are Qingdao and Yantai, which have superior economic conditions in the Shandong Peninsula. The priority acceptance compensation zones are mostly in the northern region of Shandong Province, where farmland resources are abundant and the degree of compensation is urgent, followed by the southwestern region of Shandong. The ecological balance zones are distributed in central and southern regions.

6.2. Policy Recommendations

1. Building an overall framework for EC of cultivated land. Overall, it is necessary to establish an ecological protection compensation mechanism led by the government, with orderly social participation and effective market regulation. (1) Based on the principles of "whoever benefits, pays compensation", fairness and efficiency are paramount. Based on the calculation results of the ecological footprint model of cultivated land in each province, and the matching of ecological demand and supply, the compensation areas and subjects are determined, and the responsibilities and obligations of the stakeholders, under the strategies of food and ecological security, are reasonably defined. (2) Clearly defining and differentiating compensation standards and methods. Taking into account multiple factors such as regional farmland protection responsibility, economic and financial rights, regional farmland ecological function awareness, and fiscal payment capacity. Combine the inter provincial farmland EC quota with the intra provincial farmer farmland EC quota to determine the farmland EC standard. It is important to establish specialized farmland EC fund committees at each regional level, using a combination of funds, technology, social security, policies, and other means to actively leverage the economic advantages and resource allocation capabilities of ecological consumption areas. Based on the "five-zone map" of farmland ecological protection compensation, the compensation sequence is reasonably expected to improve the compensation efficiency. (3) It is necessary to innovate diversified fundraising and distribution mechanisms. In terms of fundraising, we will integrate government department budgets, land use fees, farmland cultivation fees, farmland indicator trading incomes, farmland occupa-

tion taxes, land transfer incomes, etc.; actively explore market-oriented farmland ecological products and property rights trading markets; encourage enterprises to participate in EC projects through technological innovation, public welfare donations, and participation in development; and guide social capital to invest in farmland ecological protection and restoration, as well as green financial services. In terms of fund allocation, it is necessary to clarify the proportion of input factors of relevant stakeholders, examine and quantify the cost losses and contributions between different entities, and determine the allocation ratio of compensation funds in the compensated area. It is also important to integrate central and local farmland protection funds; fully consider factors such as farmland area, farmland quality, grain sowing range, grain yield, grain commercialization rate, and farmland protection task indicators; and make overall arrangements for funds. Through inclusive compensation, bonus incentives, permanent farmland protection compensation, and new farmland plan indicator rewards, the compensation funds will be reasonably distributed. Compensation funds should fully cover areas such as basic farmland protection and construction, farmland remediation, soil fertility cultivation, and improvement in farmland quality. The raising and distribution of funds for EC of cultivated land can also draw on the successful experience of watershed EC. (4) It is paramount that effective guarantees and supervision mechanisms are strengthened. On the one hand, it is necessary to accelerate the legislative process of EC; clarify governmental task assessments at all levels; promote a nationwide monitoring network for ecological farmland environments; implement administrative law enforcement inspections and natural resource verification; and establish a long-term accountability mechanism. On the other hand, it is crucial that we improve the feedback mechanism for farmland EC, broaden online and offline feedback channels, introduce third-party supervision institutions, conduct performance evaluations of farmland EC at all stages, and mobilize the enthusiasm of the masses to participate in farmland EC supervision.

2. It is necessary to establish multilevel subject participation and a both vertically and horizontally integrated fiscal transfer method for farmland EC. Building a financial transfer payment network for farmland EC, mediated by central, watershed, and municipal management platforms, will aid in coordinating the compensation difference between the payment and compensated areas and allocating corresponding compensation funds to subjects. At the watershed level, EC for cultivated land is achieved through macro-scale fiscal transfer payments, which are directly managed by the central government and compensated through a first-level vertical fiscal transfer. The corresponding compensation funds are deposited into a special regulatory account. At the municipal level, areas receiving EC for cultivated land within the province coexist with the payment areas. The payment areas will pay the compensation funds to a dedicated account from the watershed management platform. Through the coordination and overall planning of the watershed management platform, the amount compensated to cities will be determined, and corresponding funds will be allocated to achieve horizontal and vertical financial transfer between urban EC and cultivated land. It is important that the effectiveness of the policy tool of fiscal transfer for farmland EC is strengthened, innovating the rigid governmental control mechanism of farmland ecological protection and achieving precise compensation for farmland ecology by regulating the relationship between local farmland protection rights and economic development financial rights, so ensure coordinated and integrated development between regions.
3. It is crucial to develop a differentiated ecological protection strategy for cultivated land and leverage the comparative advantages of different regions. For surplus farm-

land and priority compensation areas, we must fully utilize compensation funds for farmland protection; increase investment in agricultural infrastructure and subsidies for farmland ecological protection; effectively guarantee agricultural product production and supply; and improve the sustainable development capacity of agricultural production and farmland utilization. For areas with compensation potential, it is necessary to focus on strengthening technical support for agricultural production and product supply, as well as for improving the service value of farmland ecosystems. For farmland deficit and EC areas, high-speed economies and societal progress have resulted in serious losses in terms of non-agricultural cultivated land. We should guide the flow of technology, factors, and resources; provide diversified support to compensated areas such as digital agriculture, technological innovation, and advanced production models; and develop ecological agriculture in order to best exploit agricultural ecological resources. In addition, we will enhance regional linkage, build a cross-regional cooperation network, deepen the coordination of farmland ecological protection, take the concept of "three in one" farmland ecological protection as a guide, focus on controlling carbon emissions in agricultural production, reduce the negative value of farmland ecosystem services, fully promote modernized, green agriculture, and promote the development of eco-friendly agriculture, thereby improving the quality of farmland, optimizing farmland ecology, assisting the transformation of farmland ecological protection, forming a virtuous cycle, and ensuring ecological and food security.

6.3. Limitations

This study constructed an EC mechanism and examined comprehensive zoning for cultivated land in Shandong Province. From this, we obtained important conclusions. However, there are still some limitations. Firstly, the study used time series data, focusing on calculating the total amount of EC for cultivated land in Shandong Province and delineating comprehensive zones. It did not explore the dynamic changes in the service value and EC of cultivated land ecosystems from a long-term perspective; we will use this as a key direction for future research. Secondly, the carbon emission factors used in carbon footprint accounting were sourced from authoritative research sources, such as IPCC and Oak Ridge National Laboratory in the United States, the effectiveness and scientific nature of which have been widely applied and validated in numerous studies. However, there are still minor deviations and subsequent impacts. Future research should prioritize the development of more detailed and accurate carbon emission models and improve and update conversion coefficients based on methods such as energy analysis to enhance accuracy. Finally, farmers' willingness to pay is influenced by multiple factors such as consumer prices, consumption patterns in different regions, and the natural environment. Using only the Engel coefficient as an adjustment coefficient to reflect residents' willingness to pay creates a small discrepancy with the actual situation.

Author Contributions: Conceptualization, methodology, data curation, J.X. and J.N.; software, validation, formal analysis, investigation, writing—original draft preparation, visualization, project administration, funding acquisition, J.X.; resources, writing—review and editing, supervision, J.N. All authors have read and agreed to the published version of the manuscript.

Funding: This work was supported by National Social Science Foundation of China (21CKS028).

Data Availability Statement: The data presented in this study are available on request from the corresponding author due to the privacy and continuity of the research.

Conflicts of Interest: The authors declare no conflicts of interest.

Appendix A

Carbon absorption correlation coefficient of main crops.

Crop Type	Economic Coefficient	Root Ratio	Carbon Content	Water Coefficient
Rice	0.49	0.6	41.7	11.9
Wheat	0.36	0.4	47.1	11.7
Corn	0.46	0.16	46.4	12.2
Beans	0.38	0.13	44.5	15
Tubers	0.68	0.18	43.3	77.1
Cotton	0.28	0.12	45	11.5
Oils	0.25	0.04	45	9
Vegetables	0.65	/	45	90
Fruit	0.7	/	45	90

Appendix B

Expanding of three-dimension model.

If $0 \leq EF_{depth} < 1$ (M-point),

$$EF^{M}_{depth} = \frac{EF^{M}}{BC} \tag{A1}$$

$$EF^{M} = BC \times EF^{M}_{depth} \tag{A2}$$

EF^{M}_{depth} represents the ecological footprint at point M. At this time, it is in an ecological surplus state, and there is a surplus in the flow of arable land resources.

$$ER^{M} = BC \times \left(1 - EF^{M}_{depth}\right) \tag{A3}$$

ER^{M} represents the surplus of farmland resource flow after deducting natural resource consumption.

If $EF_{depth} = 1$ (N-point),

$$EF^{N} = BC \tag{A4}$$

EF^{N} represents the ecological footprint at point N, where natural resource flow is equal to the amount consumed, and it is experiencing a critical condition of ecological surplus and ecological deficit.

If $EF_{depth} > 1$ (P-point),

$$EF^{P}_{depth} = \frac{EF^{P}}{BC} \tag{A5}$$

$$EF^{P} = BC \times EF^{P}_{depth} \tag{A6}$$

EF^{P}_{depth} represents the depth of footprints at point P and the ecological footprint at point P. At this time, it is in an ecological deficit state, where natural resource consumption has exhausted natural resource flow and occupied natural resource stock.

$$ED^{P} = BC \times \left(EF^{P}_{depth} - 1\right) \tag{A7}$$

ED^{P} represents the ecological deficit at point P. The expanded 3D model considers the ecological footprint as a cylinder, and uses the volume of the cylinder to represent the surplus of natural resource flow, i.e., the size of ecological surplus. The range of footprint depth values is extended from $EF_{depth} \geq 1$ to $EF_{depth} \geq 0$.

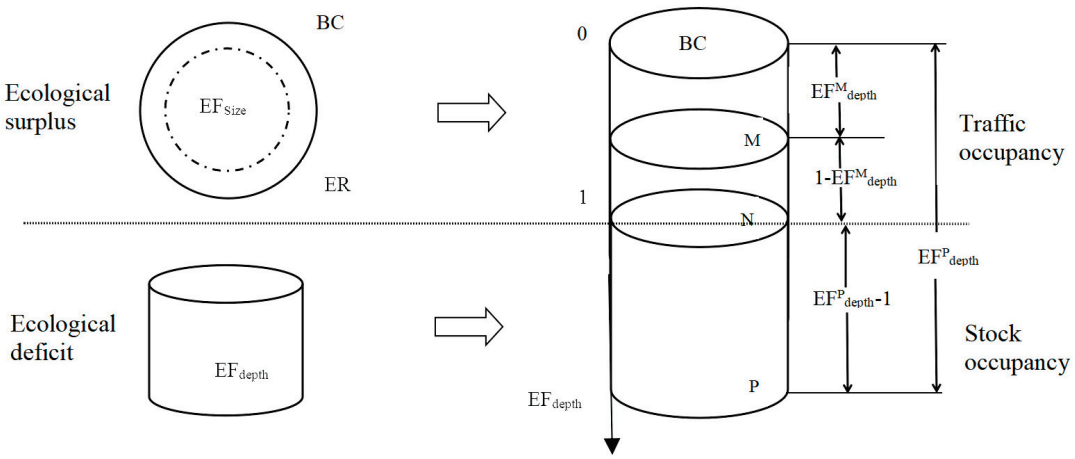

Appendix C

Economic value of equivalent factor of farmland ecosystem service value per unit.

	E_a (yuan/hm^2)
Jinan	2392.9786
Qingdao	2492.0586
Zibo	2720.4357
Zaozhuang	2540.4472
Dongying	2258.9688
Yantai	2362.7420
Weifang	2469.9336
Jining	2725.5987
Taian	2757.4838
Weihai	2289.4133
Rizhao	2573.5557
Linyi	2540.0161
Dezhou	2774.8772
Liaocheng	2719.9250
Binzhou	2477.4584
Heze	2610.6723

Appendix D

Equivalent correction for ecosystem service value of cultivated land.

	f′
Jinan	6.0151
Qingdao	6.3615
Zibo	6.5957
Zaozhuang	6.3576
Dongying	5.6244
Yantai	5.9836
Weifang	6.2670
Jining	6.6813
Taian	6.8329
Weihai	5.8064
Rizhao	6.4776
Linyi	6.3723
Dezhou	7.0711
Liaocheng	6.9294
Binzhou	6.2719
Heze	6.5770

Appendix E

Economic adjustment coefficient of cultivated land ecosystem.

	Adjustment Coefficient of Resident Payment Willingness	Adjustment Coefficient of Resident Payment Level	Economic Adjustment Coefficient
Jinan	0.7154	1.4970	1.0709
Qingdao	0.6362	1.6905	1.0754
Zibo	0.7311	1.0913	0.7978
Zaozhuang	0.5826	0.6194	0.3608
Dongying	0.7813	1.9187	1.4992
Yantai	0.5692	1.5704	0.8939
Weifang	0.7437	0.9061	0.6739
Jining	0.6721	0.7463	0.5015
Taian	0.7154	0.6888	0.4927
Weihai	0.7216	1.3638	0.9841
Rizhao	0.5799	0.9063	0.5255
Linyi	0.6569	0.6126	0.4025
Dezhou	0.5990	0.7587	0.4545
Liaocheng	0.5962	0.5484	0.3270
Binzhou	0.6599	0.8847	0.5838
Heze	0.6159	0.5635	0.3471

Appendix F

GDP per unit area and Engel's coefficient.

	Land Area (km^2)	GDP per Unit Area	Engel's Coefficient	Per Capita GDP
Jinan	10,244	11,740.98	0.255	128,287
Qingdao	11,294.91	13,210.15	0.281	144,870
Zibo	5965	7380.70	0.25	93,526
Zaozhuang	4564	4467.66	0.3	53,081
Dongying	8243	4392.50	0.234	164,430
Yantai	13,930.34	6831.03	0.305	134,581
Weifang	16,167	4519.36	0.246	77,655
Jining	11,187	4752.73	0.269	63,954
Taian	7761	4120.77	0.255	59,029
Weihai	5800	5876.17	0.253	116,871
Rizhao	5371	4294.86	0.301	77,669
Linyi	17,191	3361.36	0.274	52,502
Dezhou	10,358	3507.50	0.294	65,022
Liaocheng	8628	3221.89	0.295	46,995
Binzhou	9172	3243.73	0.273	75,813
Heze	12,155	3459.76	0.288	48,294

Appendix G

Cultivated area.

	Cultivated Area (10^4 hm^2)	Per Capita Cultivated Area	Grain-Planting Area (10^4 hm^2)
Jinan	34.288	0.04	47.3928
Qingdao	43	0.04	48.0987
Zibo	15.789	0.03	11.3492
Zaozhuang	20.135	0.05	28.3893
Dongying	21.742	0.10	25.4089
Yantai	35.257	0.05	30.2205
Weifang	59.523	0.06	68.0069
Jining	50.197	0.06	72.0016
Taian	28.295	0.05	37.0731
Weihai	16.384	0.06	12.4707
Rizhao	18.043	0.06	13.1194
Linyi	62.817	0.06	64.135
Dezhou	63.449	0.11	106.9077
Liaocheng	51.85	0.09	81.3009
Binzhou	38.56	0.10	58.8377
Heze	93.118	0.11	118.8552
Province	652.447	0.06	823.5676

Appendix H

Cultivated area and yield per unit area of grain crops.

	Cultivated Area (hm^2)					Per Unit Area Yield (kg)				
	Wheat	**Rice**	**Corn**	**Bean**	**Tuber**	**Wheat**	**Rice**	**Corn**	**Bean**	**Tuber**
Jinan	219,574	902	235,985	8568	8899	6362	7327	6022	2630	8766
Qingdao	228,468	370	241,262	5774	5113	6195	6810	6789	2735	7693
Zibo	96,593	375	11,315	3019	2190	6826	8102	6765	2554	7595
Zaozhuang	140,238	1816	127,209	10,106	4524	6400	7634	6700	2889	9575
Dongying	108,174	17,573	113,103	14,946	293	6248	5659	5742	1786	8382
Yantai	121,905	128	161,063	8695	10,414	6050	7485	6110	2858	9018
Weifang	329,286	1232	336,386	6871	6294	6401	7392	6417	3097	7944
Jining	347,379	39,156	265,486	50,923	17,072	6707	9385	7142	2758	9285
Taian	167,318	102	172,108	23,142	8061	7002	10,423	7368	2796	9261
Weihai	49,139	598	63,871	4876	6223	5473	7059	6251	2450	8258
Rizhao	52,022	1985	65,204	4619	7364	6427	8786	6666	2735	9575
Linyi	291,533	38,599	246,942	18,904	45,372	6199	9109	6425	2815	8094
Dezhou	542,877	145	513,168	11,922	965	7022	8287	7465	2398	9505
Liaocheng	412,393	3	391,291	8343	979	6887	6958	7296	2648	8276
Binzhou	281,429	767	296,132	9575	474	6687	6603	6186	2997	7995
Heze	615,225	2684	537,898	28,505	4240	6625	8285	6941	2856	7818

Appendix I

Prices of grain crops in Shandong Province in 2022.

	Wheat (yuan/kg)	**Rice**	**Corn**	**Bean**	**Tuber**
Shandong	2.83	2.74	2.55	6.38	2.56

References

1. Xie, G.; Xiao, Y. Research progress on agricultural ecosystem services and its value. *Chin. J. Eco-Agric.* **2013**, *21*, 645–651. [CrossRef]
2. Zhang, Y.; Ma, Y. Analysis of cultivated land ecological compensation efficiency and influencing factors in grain core area. *Areal Res. Dev.* **2022**, *6*, 153–158. [CrossRef]
3. Hu, H.; Yin, Y. Research on the mechanism and implementation path of ecological compensation for cultivated land under the strategy of food Security. *Agric. Econ.* **2023**, *1*, 96–98.
4. Song, M.; Cao, B. Priority of ecological compensation for cultivated land protection in Hubei Province. *Sci. Technol. Manag. Land Resour.* **2020**, *37*, 37–49.
5. Jin, Y.; Zhao, K.; Xiao, G. The economic compensation zoning of the cultivated land protection in Shaanxi province: From the perspective of food and ecological security. *China Land Sci.* **2015**, *29*, 12–19.
6. Wackernagel, M. National natural capital accounting with the ecological footprint concept. *Ecol. Econ.* **1999**, *29*, 375–390. [CrossRef]
7. Xu, Z.; Zhang, Z.; Cheng, G.; Chen, D. Ecological footprint calculation and development capacity analysis of China in 1999. *Chin. J. Appl. Ecol.* **2003**, *2*, 280–285. [CrossRef]
8. Niccolucci, V.; Bastianoni, S.; Tiezzi, E.B.P.; Wackernagel, M.; Marchettini, N. How deep is the footprint? A 3D representation. *Ecol. Model.* **2009**, *220*, 2819–2823. [CrossRef]
9. Niccolucci, V.; Galli, A.; Reed, A.; Neri, E.; Wackernagel, M.; Bastianoni, S. Towards a 3D national ecological footprint geography. *Ecol. Model.* **2011**, *222*, 2939–2944. [CrossRef]
10. Jin, X.; Liu, Q. Analysis of a land carrying capacity index based on an expanded three-dimensional ecological footprint model: A case study of Wenzhou. *Acta Ecol. Sin.* **2017**, *37*, 2982–2993. [CrossRef]
11. Jin, X.; Liu, Q. Evolution of ecological footprint models for natural resources accounting. *J. Nat. Resour.* **2017**, *32*, 163–176. [CrossRef]
12. Cui, N.; Sheng, S. Quantitative research on cultivated land ecological compensation standard based on equity. *Bull. Soil Water Conserv.* **2021**, *41*, 138–143. [CrossRef]
13. Qian, F.; Xu, H. Estimation and analysis of cultivated land ecological compensation in Liaoning province based on three-dimensional ecological footprint model. *Chin. J. Agric. Resour. Reg. Plan.* **2023**, *6*, 97–109.

14. Xie, G.; Zhen, L.; Lu, C.; Xiao, Y. Expert knowledge based valuation method of ecosystem services in China. *J. Nat. Resour.* **2008**, *23*, 911–919.
15. Qiu, J.; Liu, Y.; Yuan, L. Research progress and prospect of the interrelationship between ecosystem services and human well-being in the context of coupled human and natural system. *Prog. Geogr.* **2021**, *40*, 1060–1072. [CrossRef]
16. Wu, Y.; Wang, X.; Wang, S. Spatio-temporal changes and trade-offs of ecosystem service value and their correlation with human activity intensity—a case study of cili county. *Res. Soil Water Conserv.* **2022**, *29*, 311–321. [CrossRef]
17. Wang, H.; Chen, K.; Wang, L. Eco-compensation standard of sloping land conversion program based on opportunity cost method—Taking ecological vulnerable region of northwestern liaoning as an example. *J. Shenyang Univ.* **2020**, *22*, 176–181. [CrossRef]
18. Ahrabous, M.; Allali, K.; Fadlaoui, A. Economic valuation of cultural services at the Todgha Oasis, Morocco. *J. Nat. Conserv.* **2023**, *73*, 126731. [CrossRef]
19. Wu, J.; Wang, M.; Wang, T. Evaluation of ecological service function of liquidambar formosana plantations. *Int. J. Environ. Res. Public Health* **2022**, *19*, 15317. [CrossRef]
20. Liu, L.; Yang, B. Research on ecological compensation of provincial cultivated land in China. *Chin. J. Popul. Resour. Environ.* **2019**, *29*, 52–62.
21. Zhang, J.; Mei, L. Spatial and temporal characteristics of the ecological value of cultivated land and its differentiated compensation mechanisms in the Yangtze River Economic Belt. *Chin. J. Popul. Resour. Environ.* **2022**, *32*, 173–183. [CrossRef]
22. Moura, E.; Sousa, R.; Campos, L. Could more efficient utilization of ecosystem services improve soil quality indicators to allow sustainable intensification of Amazonian family farming? *Ecol. Indic.* **2021**, *127*, 107723. [CrossRef] [PubMed]
23. Bernués, A.; Tello-García, E. Agricultural practices, ecosystem services and sustainability in High Nature Value farmland: Unraveling the perceptions of farmers and nonfarmers. *Land Use Policy* **2016**, *59*, 130–142. [CrossRef]
24. Fang, Z.; Ding, T.; Chen, J.; Xue, S.; Zhou, Q.; Wang, Y.; Wang, Y.; Huang, Z.; Yang, S. Impacts of land use/land cover changes on ecosystem services in ecologically fragile regions. *Sci. Total Environ.* **2022**, *831*, 154967. [CrossRef]
25. Hu, B.; Li, Z.; Wu, H.; Han, H.; Cheng, X.; Kang, F. Coupling strength of human-natural systems mediates the response of ecosystem services to land use change. *J. Environ. Manag.* **2023**, *344*, 118521. [CrossRef]
26. Shi, J.; Shi, P.; Wang, Z.; Wang, L.; Li, Y. Multi-scenario simulation and driving force analysis of ecosystem service value in arid areas based on plus model: A case study of Jiuquan city, China. *Land* **2023**, *12*, 937. [CrossRef]
27. Zhang, M.; Chen, E.; Zhang, C.; Liu, C.; Li, J. Multi-scenario simulation of land use change and ecosystem service value based on the markov–flus model in Ezhou city, China. *Sustainability* **2024**, *16*, 6237. [CrossRef]
28. Yong, X.; Zhang, A. Discussion on the compensation standard of the arable land protection based on food security. *Res. Sci.* **2012**, *34*, 749–757.
29. Sterling, E.; Betley, E.; Sigouin, A. Assessing the evidence for stakeholder engagement in biodiversity conservation. *Biol. Conserv.* **2017**, *209*, 159–171. [CrossRef]
30. Salvati, L.; Ferrara, C.; Corona, P. Indirect validation of the environmental sensitive area index using soil degradation indicators: A country-scale approach. *Ecol. Indic.* **2015**, *57*, 360–365. [CrossRef]
31. Shi, F.; Yang, Q.; Wang, C.; Jiang, J.; Hu, R. Scale of the cultivated land fallow based on the emergy-ecological footprint in Songtao county, Guizhou provice, China. *Acta Ecol. Sin.* **2021**, *41*, 5747–5763. [CrossRef]
32. Dang, Y.; Kong, X.; Wen, L. Provincial eco-compensation zonings and standards of cultivated land in China. *Trans. Chin. Soc. Agric. Eng.* **2022**, *38*, 254–263. [CrossRef]
33. Xie, Y.; Wen, G.; Hu, X. Research on the influence of farmer differentiation and ecological cognition on farmers'willingness to accept for cropland non-point source pollution control. *Resour. Environ. Yangtze Basin* **2021**, *30*, 1992–2001.
34. Luan, R.; Wen, G.; Hu, X. Ecological compensation standard and its influencing factors of agricultural non-point source pollution control based on farmers'willingness to accept compensation. *Chin. J. Ecol.* **2021**, *40*, 2954–2966. [CrossRef]
35. Zhang, Y.; Zhang, A. Study on the fiscal transfer payment of cultivated land ecological compensation based on the perspective of ecological security—Taking Hubei province as an example. *Chin. J. Agric. Resour. Reg. Plan.* **2021**, *42*, 220–232.
36. Zhang, J.; He, S.; Zhang, G. Ecological benefit, spatial spillover and fiscal transfer of farmland in watershed: Evidence from the Yangtze River Economic Belt. *Int. Assoc. Agric. Econ.* **2020**, *41*, 120–132. [CrossRef]
37. Wen, L.; Zhang, B.; Kong, X. Construction and calculation of cultivated land protection compensation framework based on regional coordination in China. *J. China Agric. Univ.* **2021**, *26*, 155–171.
38. Liang, L.; Gao, P.; Liu, L. The "Two Horizon" inter-regional agro-ecological compensation standard and cross-regional financial transfer mechanism: A study based on virtual cultivated land. *Acta Ecol. Sin.* **2019**, *39*, 9281–9294. [CrossRef]
39. Zhang, H.; Fang, B.; Wei, Q. Building quantitative model of ecological value compensation for regional arable land: A case study of Jiangsu province. *China Land Sci.* **2015**, *29*, 63–70. [CrossRef]
40. Yang, F.; Zheng, X. Impact of ecological compensation methods on farmers'green production behaviors from the perspective of value perception. *Chin. Popul. Resour. Environ.* **2021**, *31*, 164–171.

41. Zhang, J.; Hao, J.; Wang, N.; Shi, Y. Protection zoning of cultivated land based on spatial autocorrelation in Shandong province. *Chin. J. Soil Sci.* **2023**, *54*, 757–767. [CrossRef]
42. Wang, L.; Faye, B.; Li, Q.; Li, Y. A spatio-temporal analysis of the ecological compensation for cultivated land in northeast China. *Land* **2023**, *12*, 2179. [CrossRef]
43. Cui, N.; Sheng, S. Quantitative research on ecological compensation for cultivated land in black soil region in northeast China from perspective of food security. *Acta Agric. Zhejian* **2021**, *33*, 1759–1769. [CrossRef]
44. Hang, X.; Zhang, J.; Hu, L. Analysis of carbon footprints in farmland ecosystem of Chongqing city 2006–2015. *J. Hunan Agric. Univ.* **2018**, *44*, 524–531. [CrossRef]
45. Zhang, P.; He, J.; Pang, B. Temporal and spatial differences in carbon footprint in farmland ecosystem: A case study of Henan province, China. *Chin. J. Appl. Ecol.* **2017**, *28*, 3050–3060. [CrossRef]
46. Zhang, J.; Luo, G.; Wang, X.; Zhu, B. Carbon stock estimation and sequestration potential of crops in the upper Yangtze River Basin. *Southwest China J. Agric. Sci.* **2009**, *22*, 402–408. [CrossRef]
47. Wang, N.; Liu, J.; Wu, D. Regional eco-compensation based on ecosystem service assessment: A case study of Shandong province. *Acta Ecol. Sin.* **2010**, *30*, 6646–6653.

Disclaimer/Publisher's Note: The statements, opinions and data contained in all publications are solely those of the individual author(s) and contributor(s) and not of MDPI and/or the editor(s). MDPI and/or the editor(s) disclaim responsibility for any injury to people or property resulting from any ideas, methods, instructions or products referred to in the content.

land

MDPI

Article

Identification of Ecological Functional Areas and Scenario Simulation Analysis of the Wanjiang Urban Belt from a Trade-Off/Synergy Perspective

Yuchun Wang †, Yufeng Ang †, Yingying Zhang, Yunfeng Ruan and Bingyi Wang *

School of Public Administration, Anhui Jianzhu University, Hefei 230601, China; wyc0101@ahjzu.edu.cn (Y.W.); ayf111031@stu.ahjzu.edu.cn (Y.A.); zyy111026@stu.ahjzu.edu.cn (Y.Z.); ruanyunfeng13@mails.ucas.ac.cn (Y.R.)
* Correspondence: wangbingyi@ahjzu.edu.cn
† These authors contributed equally to this work.

Abstract: Identifying ecological functional areas by clarifying the trade-off synergies of multiple ecosystem services to meet the practical needs of coordinating different ecosystem services in a specific region is highly important. Based on InVEST, RUSLE and other models, this study analyzed the tradeoff synergies of five typical ecosystem services in the Wanjiang Urban Belt from 1990 to 2020 using Pearson correlation analysis, and self-organizing map (SOM) carried out ecological functional zoning. The PLUS model was used to simulate the evolution of ecological functional zones in 2030. The results revealed that (1) from 1990 to 2020, water yield (WY), soil reservation (SR), and food production (FP) services in Wanjiang Urban Belt increased, whereas carbon storage (CS) and habitat quality (HQ) services decreased. The value of ecosystem services showed a pattern of "high in the south and low in the north". (2) WY–SR, WY–HQ, HQ–CS, and HQ–SR were synergistic, and the synergistic relationship showed a weakening trend. There were trade-offs in WY–CS, WY–FP, and SR–FP, and the trade-off effects increased with time. (3) The study area was divided into an ecological transition area, an ecological conservation area, an urban development area, an ecological restoration area, an agroecological area, and a water conservation area, and the functions and structures of each cluster significantly differed. (4) Under the natural development scenario, the scales of the ecological transition, ecological conservation, and agroecological areas increased. Under the cropland protection scenario, the urban development and ecological conservation areas began to transform into agroecological areas. Under the urban development scenario, the transfer of areas from ecological conservation, ecological restoration, and agroecological areas to urban development areas increased. In conclusion, the ecosystem services of the Wanjiang Urban Belt are dominated by synergistic effects, but there is a potential risk of shifting to trade-off relationships. In the future, targeted regional ecosystem optimization measures according to the evolution status of each ecological functional zone are urgently needed to provide references for territorial space management and control in this region.

Keywords: ecosystem services; trade-off and synergy; Wanjiang urban belt; ecosystem service bundle; ecological functional areas; scenario simulation

1. Introduction

Ecosystem services (ESs) are the benefits that nature provides and directly or indirectly may facilitate sustainable human well-being. In an ecosystem, the sustainable supply of ESs is the basis for maintaining the smooth operation of socioeconomic systems [1–3]. However,

with continuous population growth and economic development, there has been escalating ecosystem pressure, and the decline or even loss of various services [4,5]. According to the United Nations Millennium Ecosystem Assessment (MA), more than 50% of global ESs are already degraded, and this trend will continue in the future [6,7]. In addition, due to the diversity of ecosystem services, uneven spatial distribution, and selectivity of human use, the relationships between ESs are also dynamic, mainly in the form of trade-offs and synergies [8]. With the deepening of the understanding of the trade-offs and synergistic relationships between ESs, people have begun to identify trade-offs and synergistic areas through the study of trade-offs and synergistic relationships between different services to provide countermeasures and suggestions for ecological construction, protection and restoration, as well as the delineation of nature reserves and the positioning of functional areas [9]. Ecological functional zoning involves analyzing the characteristics and composition of trade-offs and synergies between ESs in time and space, identifying the main ecological functions and dominant ecosystem services, and delineating functional areas in this way. Therefore, comprehensive studies of the relationships among diverse ecosystem service functions, the pattern characteristics of multiple ESs, the functional zoning of the study area and the development of targeted control measures for specific areas are crucial for enhancing human well-being [8,10].

Existing studies on multiple types of ES have focused mainly on hot topics such as trade-offs and synergies, spatial and temporal evolution, and agglomeration characteristics [11–13]; scholars commonly use mathematical analysis methods such as Pearson correlation analysis [14] and Bayesian belief networks [15] to explore the trade-offs and synergies of ESs in a region or reveal the specific spatial distribution characteristics of trade-offs and synergies through spatial analysis methods such as spatial autocorrelation [16] and geographically weighted regression [17], and important research results have been achieved. However, the above approaches tend to overlook the potential spatial correlation patterns of ESs and fail to reveal the interdependence of multiple ESs [18], whereas the ecosystem service bundle (ESB) provides a viable quantitative perspective. ESBs can reflect the interdependence among various ESs and identify the aggregation mode in the ecosystem. Moreover, they enable quantitative analysis of the spatial distribution patterns of diverse services, facilitating identification of dominant services and enabling ecological function zoning [19].

Ecosystem service bundles refer to sets of ESs that repeatedly appear together across space or time [20]. Since this concept was first proposed by Kareiva in 2007 [13], scholars in China and abroad have extensively explored the interactions among ESs from the perspective of ESBs, and the existing results not only focus on the spatial and temporal evolution and structural composition characteristics of ESBs but also explore the driving factors that cause these changes. For example, Wu [21] took the Chongqing Liangjiang New Area as an example and explored the spatial and functional attributes of various types of land use by analyzing its ecosystem service distribution characteristics and cluster patterns. Li [22] studied the combination patterns of different ecosystem services in the Inner Mongolia Autonomous Region from the perspective of ESBs and classified the ecological functional zones in the region. Chang [22] used the urban clusters in northern China as the research object to reveal the complex interactions between ecosystem services and their influencing factors at different scales. The main research methods used were K-means cluster analysis, structural equation modeling (SEM), and self-organizing map analysis (SOM) for service cluster identification. Among these methods, Mouchet [23] and Cord [3] listed SOM as a promising and novel approach for ES bundle analysis because of its advantages of high tolerance of error, robustness, and applicability at different spatial scales. Existing studies have analyzed ESBs in the past or in the current period, ignoring the correlation between

ecological services and the evolution of service clusters under different scenarios in the future. As the time scale changes, the trade-offs/synergies of ESs may increase, decrease, or completely change direction over time [24]. Land is an important carrier of various terrestrial ecosystems, and land use change modeling has become an important basis for scenario analysis of ecosystem services. It has been demonstrated that shifts in land use types can directly change ESs, thus affecting the spatial pattern of ESBs. Integrating future ES outcomes into ESB provides intuitive insights into future ecological patterns, optimizing benefits, enhancing sustainability, and promoting coordinated conservation and management [25–28]. In addition, the traditional ecological function zoning depends on expert integration, the combination of qualitative and quantitative approaches, etc. These methods excessively consider the similarity or dissimilarity of geographical environment elements and their spatial combinations, but ignore the integrity of regional ecology, which is highly subjective and the results are very different [29].

Since 2010, when the Wanjiang Urban Belt adopted the "Industrial Transfer Demonstration Zone", the population and industries in the region have begun to grow, and industrial parks have continued to appear, with increasing intensity of interference in and destruction of the natural environment in the region, resulting in ecological resource risks such as serious degradation of biodiversity, declines in ecological and environmental functions, and oversaturation of the environmental carrying capacity. This not only threatens the health and stability of the ecosystem but is also not conducive to the sustainable development of the region, and the region has become a microcosm for studying the synergistic relationship between the trade-offs between ecological protection, economic development, and human well-being in China's rapidly urbanizing regions [30].

However, the current identification of ESBs has focused mostly on large urban agglomerations [31], and it is mostly seen in the use of ESB to grasp the overall pattern of the study area, relatively few studies on ecosystem services in small- and medium-sized urban zones in the stage of rapid urbanization and development. The region is in urgent need of a new way of ecosystem service clustering and a new perspective on balancing the relationship between economic development and ecological protection. There is a relative lack of localized studies on the quantitative measurement of the relationship between ecosystem services and their spatial distribution patterns in the Wanjiang Urban Belt, and there are not many studies on the delineation of the ecological functional zones in the Wanjiang Urban Belt. Therefore, recognizing the interaction mechanism between various ESs and identifying various types of ecological functional areas are especially crucial for seeking management methods and decision-making suggestions for ecological functional zoning, and analyzing the future spatial and temporal change patterns of ESs and ecological functional zones through simulating different development scenarios will also be an important prerequisite for the region to further realize the coordination between ecological environmental protection and socioeconomic development in the future.

In summary, this study used the Wanjiang Urban Belt as the research object and synthesized various models to reveal the spatial and temporal evolution of five typical ESs in the region from 1990 to 2020. Trade-offs/synergies between the two ESs in each study period were explored through Spearman's correlation analysis. The cluster analysis method (SOM) was used to identify ESBs, delineate ecological functional zones, and propose targeted management measures for ecological functional areas. Finally, the PLUS model was used to simulate the changes in various ESs under different development scenarios in the Wanjiang Urban Belt in 2030 and to predict the spatial distribution patterns of ecological functional areas under different development conditions. The objectives of this study are (1) to analyze the synergistic effects of trade-offs among ecosystem services and their spatial distribution characteristics in the Wanjiang Urban Belt; (2) to clarify the

structure of ecosystem services and the dominant types of services in different regions through ESBs for ecological function zoning in the study area; and (3) to reveal the trend of the evolution of ecosystem services and ecological function zones in the Wanjiang Urban Belt in the future under different scenarios of development. The results of this study not only provide targeted regional development and control measures for the Wanjiang Urban Belt but also have important practical significance for the region's territorial spatial planning and regional sustainable development. The research flowcharts used in this study are shown in (Figure 1).

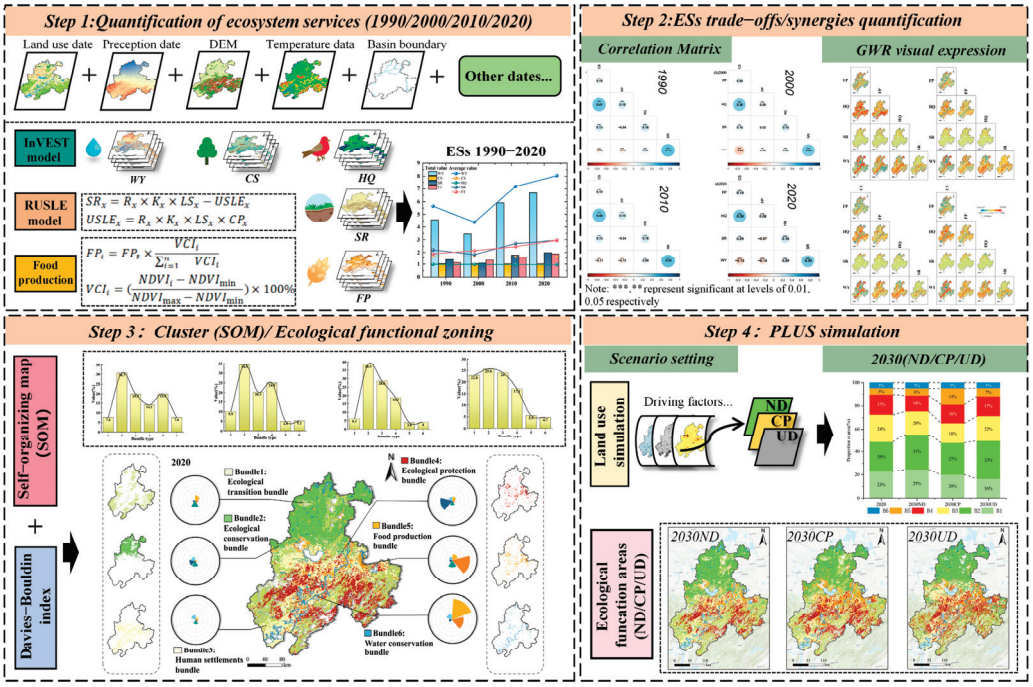

Figure 1. Research flowcharts. Note: ***, ** represent significant at levels of 0.01, 0.05, respectively.

2. Study Area and Data

2.1. Study Area

The Wanjiang Urban Belt (29°32′–33°13′ N, 115°58′–119°39′ E) is located in the Anhui section of the Yangtze River in the interior of East China; it covers an area of approximately 76,000 km^2 and is an important part of the Yangtze River Economic Belt (Figure 2). The Wanjiang Urban Belt includes the entire territories of eight cities, namely, Hefei, Wuhu, Maanshan, Anqing, Chizhou, Chuzhou, Tongling, and Xuancheng, as well as Jin'an District and Shucheng County in Lu'an City, with the topography of the region being higher in the north and south and lower in the northeast; sloping and occasional hills scattered in between; a landscape consisting of hills, plains, and depressions; a climate that is transitional from warm temperate to subtropical, with an average precipitation of approximately 772–1670 mm; and obvious differences in spatial distribution. The region has abundant water resources, boasting numerous rivers and lakes, including Chaohu Lake, one of China's five largest freshwater lakes [32]. The study area serves as an ecological barrier for the middle and lower reaches of the Yangtze River eco-belt and the Yangtze River Delta, and its ecological status is extremely important. As an important strategic region in China's territorial space development, Wanjiang Urban Belt plays a key supporting role in economic development and regional revitalization. The region is also an important base for agricultural production, energy, raw materials, and the processing and manufacturing industry in China [33,34]. In 2020, the gross national product (GDP) of the Wanjiang Urban Belt reached USD 349.81 billion, which was three times greater than that in 2010, with an

average annual growth rate of 14.6%. The study period covers the period before and after the Wanjiang Urban Belt Industrial Transfer Demonstration Zone, which is convenient for comparative analysis to reveal the evolution trend of each ecosystem service.

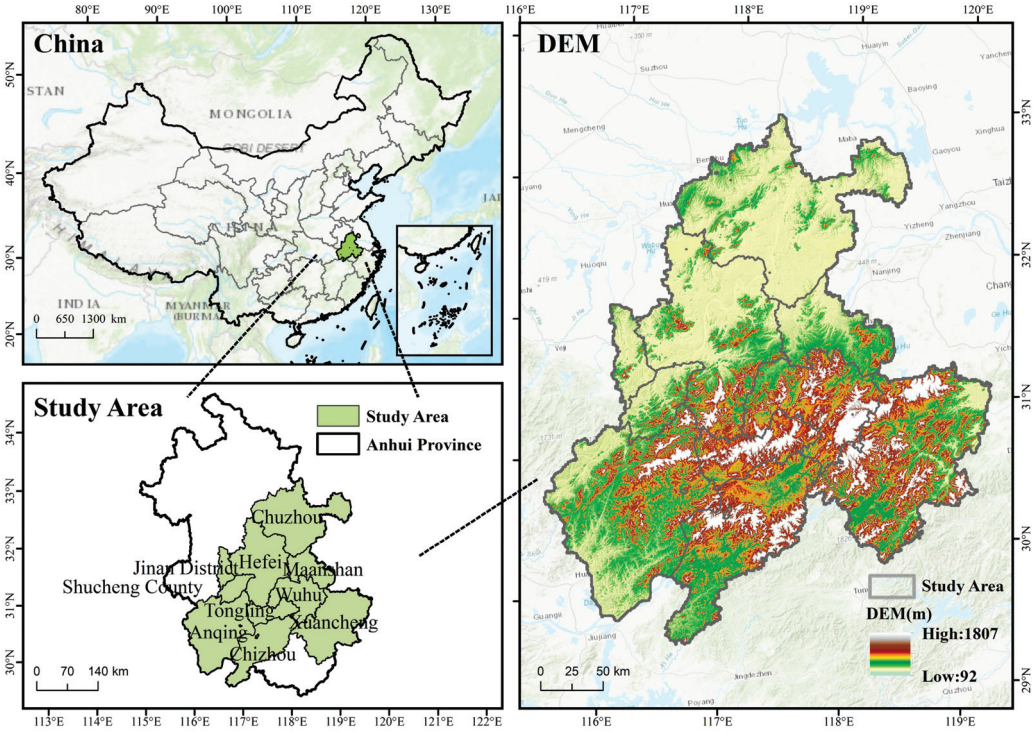

Figure 2. Sketch map of the research area.

2.2. Data Sources and Processing

The data used in this study include land use data, digital elevation data (DEM), normalized difference vegetation index (NDVI), soil data, evapotranspiration data, precipitation data, population density data, total food production data, socioeconomic data, watershed boundary data, and road map data (Table 1). Four years, 1990, 2000, 2010, and 2020, were selected for this study, and all the data were consistently resampled to raster data with a resolution of 100 m.

Table 1. Summary of the primary date.

Date Type	Date Source	Spatial Resolution
Land use date	Resource and Environment Science and Data Center (http://www.resdc.cn/, accessed on 1 September 2024)	30 m
Digital elevation model (DEM)	Geospatial date cloud (http://www.gscloud.cn/, accessed on 1 September 2024)	90 m
Normalized difference vegetation index (NDVI)	Resource and Environment Science and Data Center. (http://www.resdc.cn/, accessed on 15 September 2024)	250 m
Precipitation	National Tibetan Plateau/Third Pole Environment Data Center. (https://doi.org/10.5281/zenodo.3114194, accessed on 20 September 2024)	1 km
Evapotranspiration	National Tibetan Plateau/Third Pole Environment Data Center. (http://loess.geodata.cn, accessed on 22 September 2024)	1 km
Soil data	FAO., International, I. (2019). China soil map based harmonized world soil database (HWSD) (v1.1)	1 km
Food yield	Anhui Statistical Yearbook, Anhui Provincial Bureau of Statistics. (https://tjj.ah.gov.cn/oldfiles/tjj/tjjweb/njlm/njbooks.htm, accessed on 22 September 2024)	
Population density data	Resource and Environment Science and Data Center (http://www.resdc.cn/, accessed on 22 September 2024)	1 km
Socioeconomic data	Resource and Environment Science and Data Center (http://www.resdc.cn/, accessed on 25 September 2024)	1 km
Road map	Open Street Map (https://www.openstreetmap.org/, accessed on 22 September 2024)	1 km
Watershed boundary	It is obtained by hydrologic analysis software in ArcGIS (10.8)	

3. Materials and Methods

3.1. Methodology for the Quantitative Assessment of ESs

The current ecological and socioeconomic status (e.g., soil erosion, insufficient water supply, agricultural production, and resource exploitation) of the Wanjiang Urban Belt should be considered. Based on environmental and socioeconomic data, we used the InVEST model and the Revised Universal Soil Loss Equation (RUSLE) to quantify these five ESs.

3.1.1. Water Yield

In this study, water yield was quantified by the water supply module in the InVEST model. The calculation formula is as follows:

$$Y(x) = \left(1 - \frac{AET(x)}{P(x)}\right) \times P(x) \tag{1}$$

$$\frac{AET(x)}{P(x)} = 1 + \frac{PET(x)}{P(x)} - \left[1 + \left(\frac{AET(x)}{P(x)}\right)^{\omega}\right]^{\frac{1}{\omega}} \tag{2}$$

$$W(x) = Z\frac{AET(x)}{P(x)} + 1.25 \tag{3}$$

where $Y(x)$ is the water yield (mm) of each pixel (x); $P(x)$ is the average annual precipitation (mm); AET(x) is the actual annual evapotranspiration; $PET(x)$ is the annual potential evapotranspiration(mm); $\omega(x)$ is the physical parameters of natural climate and soil properties; $AWC(x)$ is derived from the plant-available water capacity (PAWC), the maximum rooting depth of the soil, and the minimum value of the vegetation root depth; and Z is the Zhang coefficient. Reference was made to Li [35] to set the localization parameter to 7.8.

3.1.2. Carbon Storage

Carbon storage was estimated in this study using the carbon storage module within the InVEST model to quantify the aboveground biomass carbon, belowground biomass carbon, soil carbon, and dead organic carbon represented by different land use types [36].

$$CS = C_{above} + C_{below} + C_{dead} + C_{soil} \tag{4}$$

where C*above*, C*below*, C*dead*, and C*soil* are the aboveground, belowground, dead organic, and soil organic CS, respectively. The carbon density data come from the collection and arrangement of the results in [33] and the reference database in [37].

3.1.3. Habitat Quality

Habitat quality was assessed in this study using the InVEST model to identify the interference of human and natural threat factors on habitat quality under different land use types and the degree of habitat degradation [38].

$$Q_{xj} = H_{xj}\left[1 - \left(\frac{D_{xj}^{z}}{D_{xj}^{z} + K^{z}}\right)\right] \tag{5}$$

Q*xj*: habitat quality index; H*xj* habitat suitability; D*xj*: the degree of habitat degradation; K: saturated system count; and *z*: constant; For the parameters of threat factors and sensitivity of different land use types, refer to Zheng [39] to set the localization parameters.

3.1.4. Soil Reservation

The Revised Universal Soil Loss Equation (RUSLE) was employed to evaluate the ecosystem's ability to mitigate soil erosion caused by rainfall impacts through its own structure and functions [40].

$$SR_x = R_x \times K_x \times LS_x - USLE_x \tag{6}$$

$$USLE_x = R_x \times K_x \times LS_x \times CP_x \tag{7}$$

SR*x*: soil reservation supply of grid cell x; R*x*: rainfall erosivity factor; K*x*: soil erodibility factor; LS*x*: slope length slope factor, no dimension; CP*x*: vegetation cover and soil and water conservation factor, dimensionless; and USLE*x*: the actual amount of soil erosion in management and engineering measures is considered

3.1.5. Food Production

This study assigns actual food production to each grid based on the vegetation condition index (*VCI*) of the cropland to assess FP, a method that can take into account the variability in yields between farmlands.

$$FP_i = FP_t \times \frac{VCI_i}{\sum_{i=1}^{n} VCI_i} \tag{8}$$

$$VCI_i = \left(\frac{NDVI_i - NDVI_{\min}}{NDVI_{\max} - NDVI_{\min}} \right) \times 100\% \tag{9}$$

FP*i* is the grain yield of grid i, FP*t* is the total grain output of grid i, VCI*i* is the vegetation condition index of grid i, NDVI is the normalized vegetation index of the vegetation condition index of grid i, NDVI*max* is the maximum value of the normalized vegetation index, and NDVI*min* is the minimum value of the normalized vegetation index. The total grain production data from 1990 to 2020 were obtained from the Anhui Provincial Statistical Yearbook, and the total grain production data for 2030 were obtained by Matlab linear fitting.

3.2. Correlation Analysis

Based on the 'corrplot' package in R 4.4.2, a correlation analysis of the five ecosystem services was carried out using Pearson's correlation coefficients. The model is shown below:

$$P_{xy} = \frac{n\sum_{i=1}^{n} x_i y_i - \sum_{i=1}^{n} x_i \sum_{i=1}^{n} y_i}{\sqrt{n\sum_{i=1}^{n} x_i^2 - \left(\sum_{i=1}^{n} x_i\right)^2} \sqrt{n\sum_{i=1}^{n} y_i^2 - \left(\sum_{i=1}^{n} y_i\right)^2}} \tag{10}$$

where Pxy is the correlation coefficient, x and y are the two variables, and n is the number of values taken by the variables. When Px, y > 0, and the test of significance is passed (P < 0.01), then it is considered that there is a synergistic relationship between the two, and vice versa for the trade-off relationship.

3.3. Geographically Weighted Regression

To understand the spatial distribution of the TOS between ESs more clearly, we use geographically weighted regression (GWR) to quantify the trade-offs and synergistic relationships among the ESs. One ES is used as the independent variable, and the other ES is used as the dependent variable. Therefore, the two research methods used in this study

to investigate the trade-offs and synergies of ES pairs were complementary. The form of the GWR model is as follows:

$$y_i = \beta_0(\mu_i, \nu_i) + \sum_{k=1}^{p} \beta_k(\mu_i, \nu_i) x_{jk} + \varepsilon_i \quad (11)$$

where (μi, νi) is the spatial location of point i; p is the number of independent variables; yi is the dependent variable; xjk is independent variables; εi is random errors; β0(μi, νi) represents the intercept at point i; and βk(μi, νi) represents the regression coefficient.

3.4. Self-Organizing Map (SOM)

In this study, the SOM was used to identify ESBs at the grid scale in the study area. SOM is an unsupervised learning neural network method that can allocate each grid into ESBs based on their similarities of ES co-occurrence in space. The SOM was implemented using the 'kohonen' package in R 4.4.2 software [41]. The SOM was first applied to construct 2–10 bundles, and then the Davies–Bouldin index was calculated to determine the optimal number of bundles in this study. The Davies–Bouldin index is an internal evaluation metric for assessing the effectiveness of clustering algorithms that measures the tightness within clusters and the separation between clusters [42]. A lower Davies–Bouldin index reflects higher intercluster and lower intracluster variability, providing a better clustering result [43]. The analysis revealed that the Davies–Bouldin index reached its minimum value when six ecosystem service clusters were identified in the study area from 1990 to 2020, indicating an optimal classification into six distinct service cluster types.

3.5. Land Use Multi-Scenario Simulation

The PLUS model integrates the rule detection method based on a land expansion analysis strategy (LEAS) and the cellular automata (CA) model based on a multitype random seed mechanism, and is the latest land use simulation model developed by [44]. Compared with the previously developed FLUS model, the PLUS model better simulates changes at the patch level for multiple land use categories. The rational utilization of land resources plays a key role in balancing the competing forces of economic development and ecological protection, and the dynamics of their quantitative scale and spatial distribution depend on the trade-offs between the two [45]. In the past 30 years, the land use changes in the Wanjiang Urban Belt have mainly manifested as a decrease in arable land and grassland, as well as a rapid increase in construction land area. On the one hand, with the continuous growth of population and economy in the Wanjiang Urban Belt, the demand for construction land continues to increase, which leads to other land types constantly shifting towards construction land to meet the industrial, transportation, and residential land needs of the region, and the phenomenon of severe degradation of arable land. On the other hand, with the gradual transition from traditional agriculture to modern agriculture and the impact of policies such as 'returning farmland to forests' and 'returning farmland to wetlands', some farmland with steep slopes and relatively severe soil erosion has begun to be converted into forest land or other land to meet the needs of improving the ecological environment [34].

3.5.1. Model Validation

The land use types in this study are divided into six types: cropland, forest land, grassland, water, construction land, and unused land; the driving factors affecting the land use changes in the Wanjiang Urban Belt, such as DEM, socioeconomics, and traffic, are selected; and the land use data based on the 2010 land use data use the transfer matrix, the regional weights, and the land use demand to determine land use status under the natural development scenario of the year 2020. In order to assess the reasonableness of the PLUS

model simulation in predicting the area and spatial distribution pattern of different land use types, the Kappa coefficient is introduced in this paper to test the simulation effect.

$$\text{Kappa} = \frac{P_o - P_c}{P_p - P_c} \tag{12}$$

where Po denotes the proportion of correct simulations, Pc denotes the correct proportion of the model under random conditions, and Pp denotes the proportion of correct simulations under ideal classification conditions. The calculated Kappa value is 0.92, which is in line with the accuracy test, and the simulation data in 2020 under the natural development scenario (ND) are closer to the actual land use situation in 2020, with the error of arable land and forest land area being about 1.2%, the error of construction land area being about 4.6%, the remaining four land use types having smaller errors, and the overall spatial distribution pattern being more stable and meeting the requirements of the simulation.

3.5.2. Multi-Scenario Setting

Based on the changing law of land use in the Wanjiang Urban Belt from 1990 to 2020, and with reference to the current urbanization development process, the natural development scenario is set up without setting the mutual transformation among land use types and policy intervention as the constraints, and this scenario is the basis for analyzing the simulated changes in other scenarios in the study area. In reference to the study of [46], long-term stable and unchanged cropland in 1990, 2000, 2010, and 2020 was extracted as the restricted conversion area, cropland protection scenarios were set, and Markov transfer probabilities were corrected to set the probability of conversion of cropland to other land types to decrease by 30% and the probability of conversion of other land types to cropland to increase by 20% so that cropland protection policies were strictly implemented. In the urban development scenario, considering that the Wanjiang Urban Belt is in a period of major strategic opportunities for rapid development, referring to the relevant study of [47], the reservoirs and lakes in the study area were set as restricted conversion zones; the probability of transferring cropland, forestland, and grassland to construction land was increased by 20%; and the probability of transferring construction land to landscape types other than cropland was decreased by 30%.

4. Results

4.1. Characteristics of the Spatial Distribution and Temporal Evolution of ESs

The spatial distribution of the five ESs in the Wanjiang Urban Belt is characterized by heterogeneity (Figure 3), especially the difference between the north and south, which is more prominent. The value of each service is essentially characterized by a gradual decrease from south to north. The areas with high values of ESs were mainly concentrated in the Dabie Mountain area in the western part of the study area and in Anqing and Chizhou in the southern part, whereas the areas with low values were located in the northern part of the study area and in the zones along the Yangtze River and Huaihe River watersheds. During the study period, except for the relatively high WY in Chaohu Lake, the zone along the Yangtze River, and various reservoirs, the remaining areas with increased values were located mainly in the Dabie Mountain Region in the west and in Lu'an, Anqing, and Chizhou in the southern region, whereas the decrease in WY essentially occurred in the northern regions, such as Chuzhou and Xuancheng. CS services were dominated by medium and high values in most areas, except for some scattered zones distributed along the water system, including hilly and mountainous areas in the western and southern parts of the study area, and relatively low values along the Jianghuai Basin and Chaohu Lake areas. The value of HQ services was relatively high in the southeastern and western

regions but relatively low in the Jianghuai watershed and northern region. The SR service was not only affected by vegetation coverage but also closely related to topography. The value of the SR service is relatively high in the Dabie Mountains in the southern part of the study area, whereas the SR quantity is low in the northern plain area. Compared with the other four kinds of services, the value distribution of the FP service is the opposite; that is, it gradually increases from south to north, except for the FP service along the Yangtze River plain, which decreases, and the other areas increase. The areas with low values of this service are distributed in the southern and western parts of the study area, and the areas with high values are located mainly in the northern plain of the study area. In terms of time, there were differences in the evolution of ESs during the study period (Figure 4). From 1990 to 2020, the total WY service of the Wanjiang Urban Belt increased from 4.56×10^{10} m^3 to 6.68×10^{10} m^3, and the average WY increased to 7.98×10^3 mm. Under the influence of rapid urbanization and the continuous interference of human activities, the average values of both HQ and CS showed downward trends, and the total CS decreased by nearly 2% per year. The total amount and average value of SR services increased from 1.38×10^{10} t to 1.97×10^{10} t, and the average SR value increased from 2.61×10^5 t/hm^2. During the study period, the total FP service increased from 1.14×10^7 t to 1.88×10^7 t, and the average FP increased from 2.63×10^2 t/hm^2.

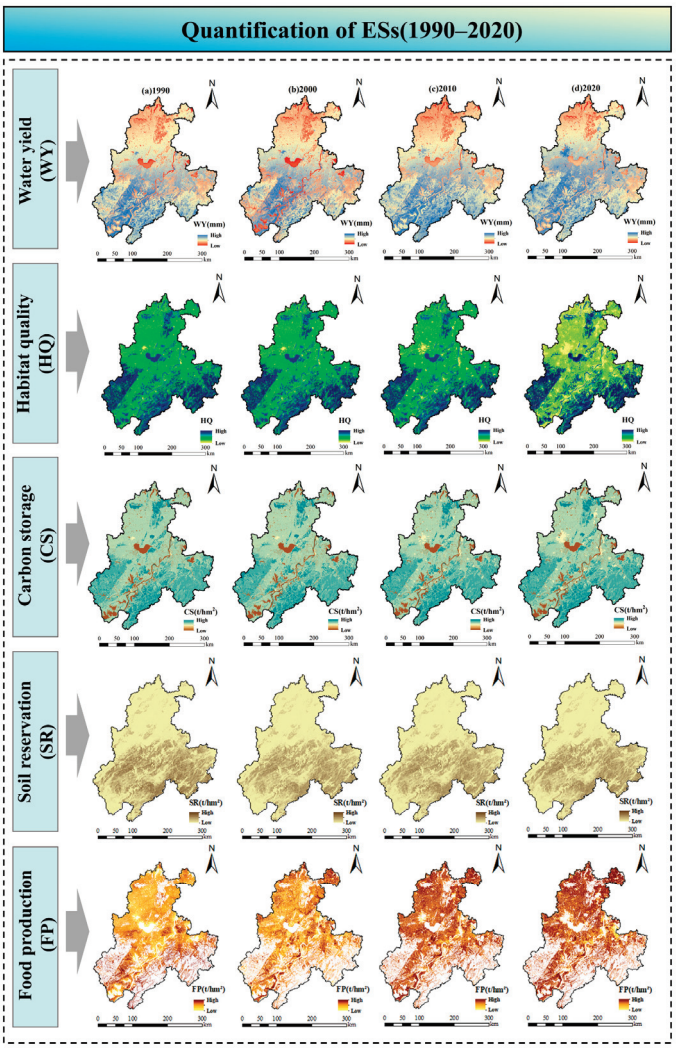

Figure 3. Spatio-temporal distribution and changes in ecosystem services in Wanjiang Urban Belt from 1990 to 2020. (WY: water yield, HQ: habitat quality, CS: carbon storage, SR: soil reservation, FP: food production).

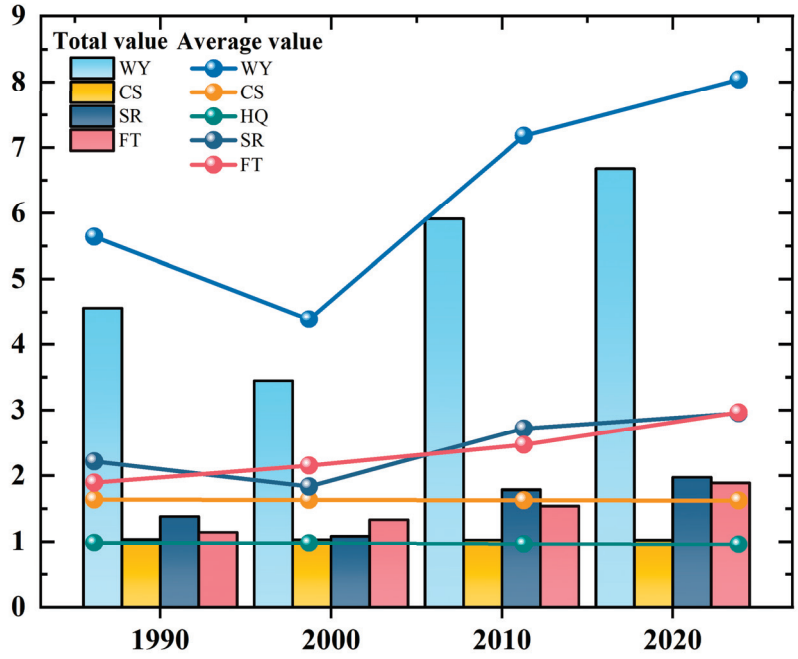

Figure 4. Changes in ecosystem services from 1990 to 2020. (Total value: WY (10^{10} m^3), CS (10^9 t), SR (10^{10} t), FT (10^7 t); average value: WY (10^3 mm), CS (10^5 t/hm^2), SR (10^5 t/hm^2), FT (10^2 t/hm^2)).

4.2. Ecosystem Service Trade-Off/Synergistic Quantification

4.2.1. Correlation Analysis

At the 1 km grid scale, 10 pairs of correlated services were identified among the five ecosystem services in the Wanjiang Urban Belt by Pearson correlation analysis, and most of the services reached the significance level test ($p < 0.05$) (Figure 5). The results revealed that regional ESs were dominated by synergistic relationships and that there were stable and significant synergistic relationships among WY–SR, WY–HQ, CS–HQ and SR–HQ. However, this positive synergistic relationship gradually weakened; compared with that of synergies, the impact of trade-offs on human well-being was more direct and obvious. During the study period, there was a significant trade-off relationship between CS and WY, and this relationship slowly increased annually. The trade-offs in FP–WY and FP–SR also showed an enhanced performance from 2010 to 2020, which is consistent with the degree of change in regional construction land expansion. According to the identification results, the trade-off relationships between the three pairs of services should be regarded as the key issues faced by the region.

4.2.2. Results of Geographically Weighted Regression Analysis

Correlation analyses explore the trade-off/synergistic relationships among ecosystem services in general but cannot capture the spatial heterogeneity of the trade-offs/synergies among ESs [48]. We further revealed the geospatial heterogeneity of trade-offs/synergies between ESs at grid scales using geographically weighted regression. The results show that the tradeoff synergies among the five ecosystem services are significantly different (Figure 6). Specifically, most ESs in the study area are dominated by synergistic relationships, with the synergistic areas located mainly in the western Dabie Mountain area and the southern part of the area; the trade-off relationships are essentially distributed in the river plain in the central part of the study area, where the proportion of built-up land is high, as well as in the northern township area. Among them, FP–HQ, FP–WY, and HQ–CS have stronger trade-offs and the most serious competition between services, with the number of images with trade-offs ranging from 79.8 to 88.7%, which is significantly greater than that in the synergistic region. For the whole study period, trade-off effects occurred mainly in

WY, FP, and HQ, especially in WY–FP, where the area share of the trade-off relationship increased by 22.6%. These findings suggest that these services have been in competition over the past 30 years and that the synergistic development of food security and ecosystems in the Wanjiang Urban Belt still faces many challenges.

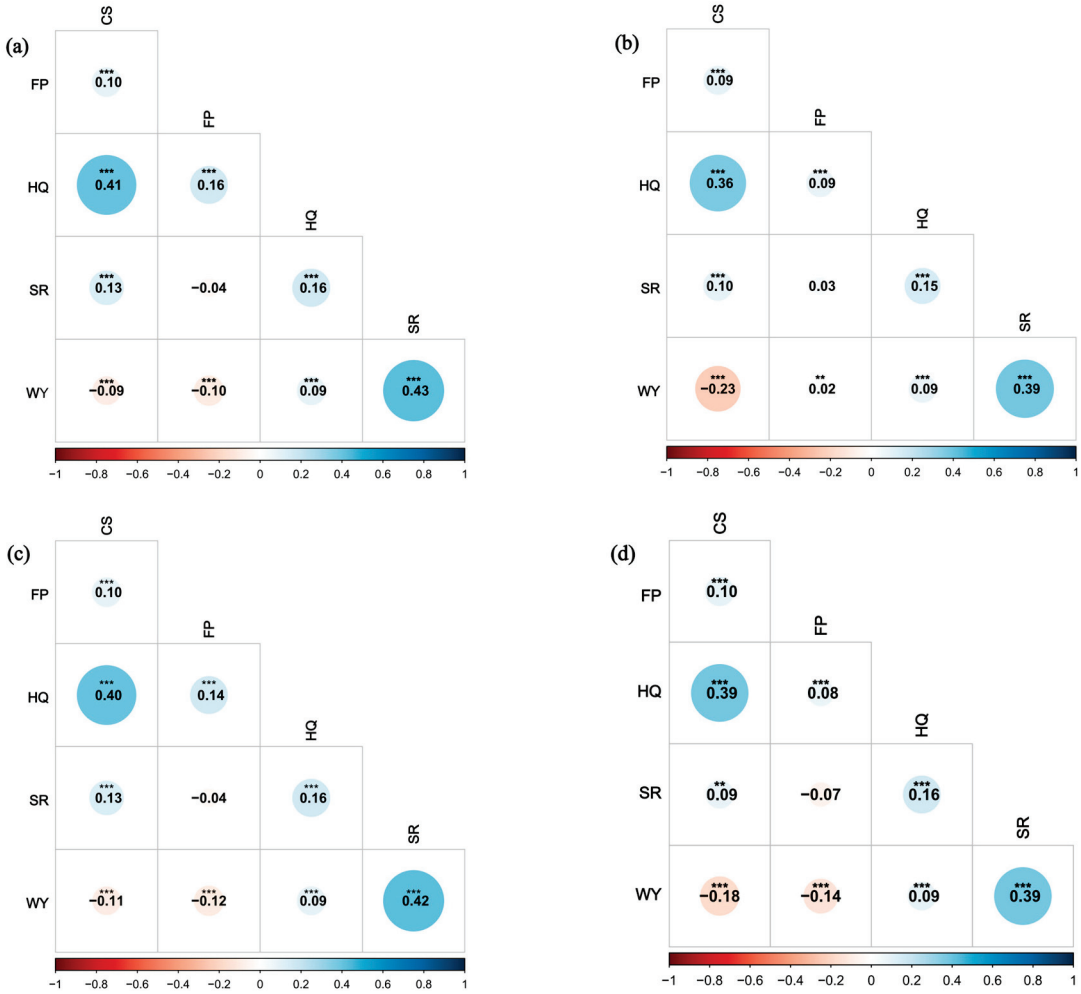

Figure 5. Correlation between ecosystem services. (** $p < 0.01$; *** $p < 0.001$, red signifies a negative correlation. Note: ***, ** represent significant at levels of 0.01, 0.05, respectively. (**a**) represent 1990; (**b**) represent 2000; (**c**) represent 2010; (**d**) represent 2020, while blue signifies a positive correlation, with darker colors indicating stronger correlations).

4.2.3. Identification of Ecosystem Service Clusters and Delineation of Ecological Functional Areas

For regional ecosystems, not all ESs contribute equally; therefore, further identification of ESBs cooccurring at the same spatial and temporal scales across the evaluation units in the study area is needed. Taking the 1 km grid as the sample, a self-organizing mapping neural network was constructed, and 77,508 ecological grids in the Wanjiang Urban Belt were hierarchically clustered. The clustering quality was evaluated using the Davis–Bouldin index, and the number of ESBs was divided into 6 categories. Considering the topographic characteristics of the Wanjiang Urban Belt region and the regional continuity and independence, the study area is categorized into six distinct ESBs. The six service bundles were divided into the B1 ecological transition bundle, the B2 ecological conservation bundle, the B3 human settlement bundle, the B4 ecological protection bundle, the B5 food production bundle, and the B6 water conservation bundle (Figure 7).

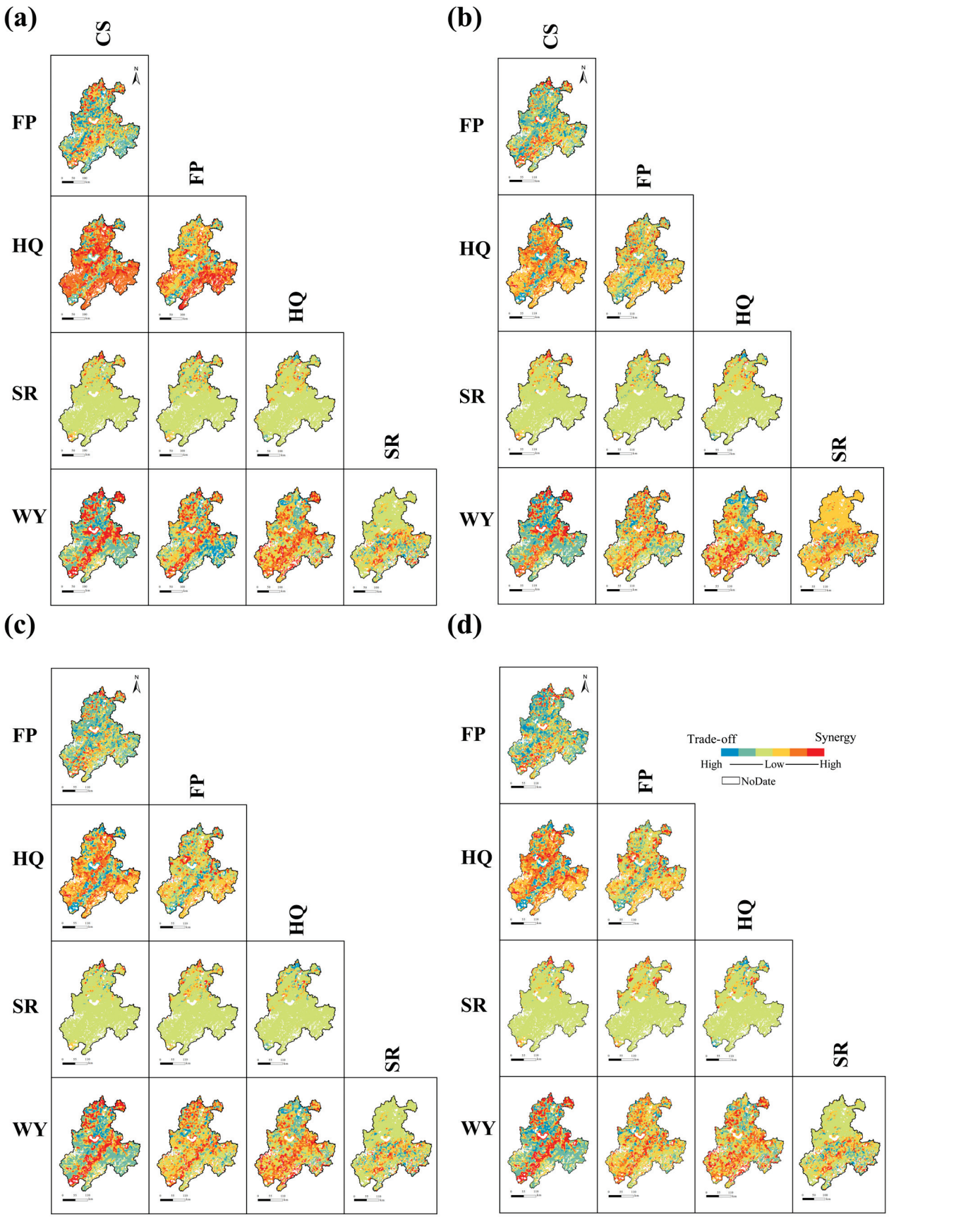

Figure 6. Spatial distribution of ecosystem service pairs' trade-off synergies: (**a**) 1990; (**b**) 2000; (**c**) 2010; (**d**) 2020; In the blue areas, there is a strong synergy, while in the red areas, there are significant trade-offs.

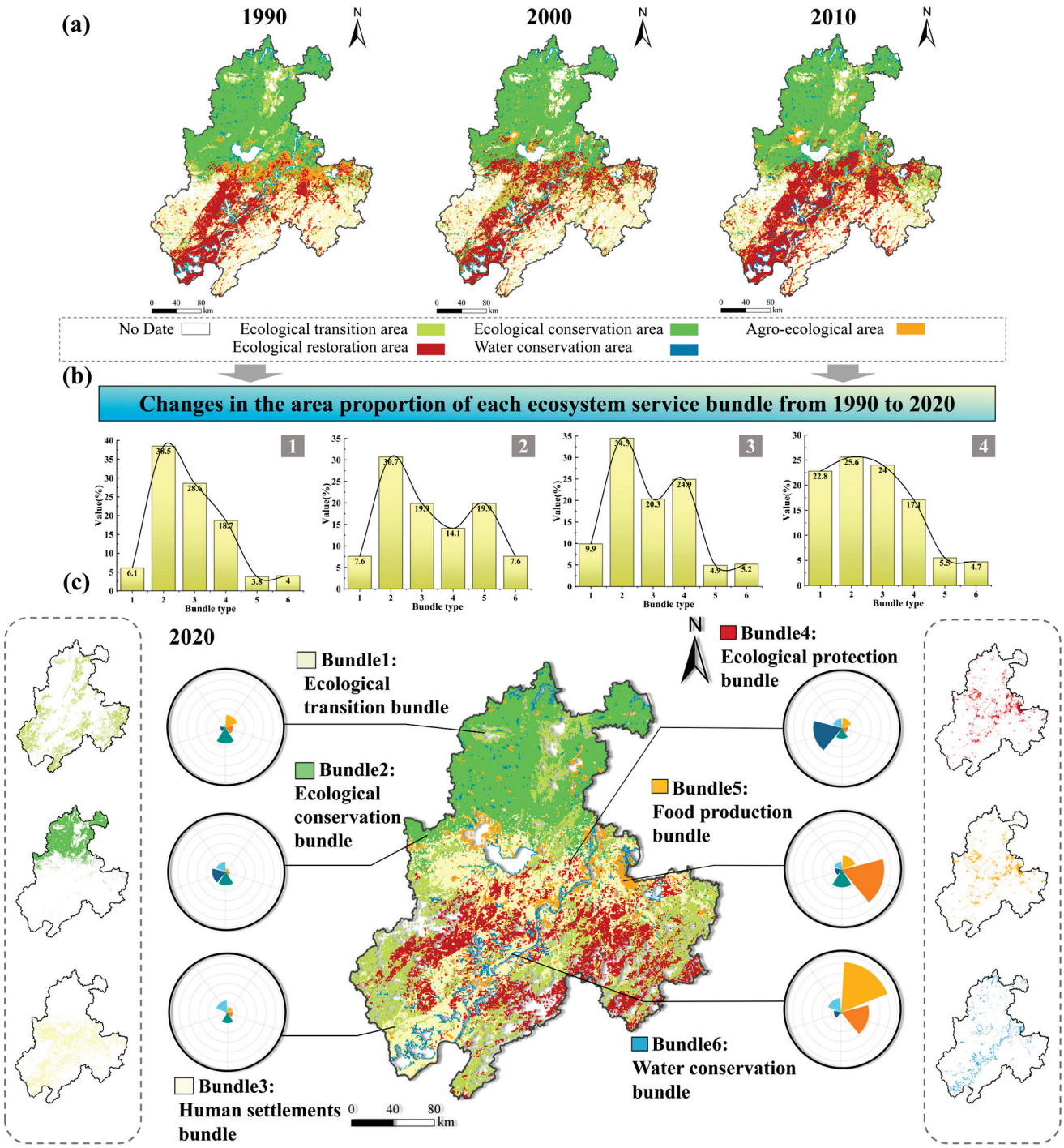

Figure 7. Spatial and temporal distribution and area change in ecosystem service bundles. (**a**) refers to the spatial distribution of ecosystem service bundles from 1990 to 2010; (**b**) 1–4 refer to the change in the proportion of each ecosystem service bundle area from 1990 to 2020; (**c**) refers to the spatial distribution of ecosystem service bundles in 2020, and the wind rose diagram illustrates the composition and proportional significance of ecosystem services within each ecosystem service bundle.

Bundle 1, which provides HQ and CS services, is widely distributed in the central plains of the study area as well as in the hilly, mountainous and wooded areas in the south and covers approximately 22.8% of the study area, remaining stable in the early part of the study period and increasing in the later part of the study period. Bundle 2 has high proportions of WY, SR, and HQ services and is located mainly on the southern

edge of the North China Plain, north of the study area. The spatial distribution pattern of Bundle 2 has been relatively stable over the past 30 years, and its area is the largest among the ESBs, accounting for approximately 25.6% of the study area; Bundle 3, with slightly lower-than-average shares of all three services except WY and HQ, is essentially distributed in the central river plain area, with an area share of 24%; and Bundle 4, with SR services at its core, is mainly distributed along the two sides of the water system in the central plain, the southern mountainous area, and the Taiping Lake area in the southeastern part of the study area. This bundle accounts for approximately 17.4% of the area, and although its size has fluctuated slightly during the evolutionary process, it is still in a relatively stable state of development. Bundle 5 is dominated by HQ and FP services and is distributed in the watershed and part of the northern plains of the study area, with the smallest area of this bundle accounting for approximately 5.5% of the total study area. At the beginning of the study, the area of Bundle 5 was relatively high, but to meet the development needs of the economic construction of the Wanjiang Urban Belt, most of the area gradually shifted to the ecological protection and urban development bundles, and then, the area gradually rebounded due to the influence of policies related to the protection of cropland. Bundle 6 had the most prominent WY capacity among the various ESBs and a relatively high level of FP, mainly in areas along rivers and lakes, with an area share of 4.7%.

4.3. Multiscenario Simulation Analysis of Land Use Change and Ecosystem Services

4.3.1. Multiscenario Simulation Analysis of Land Use in the Wanjiang Urban Belt

Figure 8 illustrates the patterns of spatial and temporal differences and shifts in each land use type under the three scenarios. Under different development scenarios, the magnitude of changes in each land use type in the Wanjiang Urban Belt is small, and the land use changes in the region are characterized by small fluctuations on the premise of total control. In 2020, the regional land use types were mainly cropland, forestland, and construction land, with areas of 38,136.2 km^2, 204,341.2 km^2, and 6530.3 km^2, respectively. Under the natural development scenario, by 2030, all land types in the study area will be transformed into construction land on a large scale, and the area of construction land will increase by 12.7%, whereas the areas of cropland and forestland will decrease. Most of the cropland will be transformed into construction land, indicating that the rapid expansion of urbanization in this scenario has not been effectively restricted. The ecological land in the region is still experiencing a trend of continuous encroachment. Under the cropland protection (CP) scenario, the cropland area increased slightly, the grassland area was protected and restored to a certain extent, and the expansion trend of the core construction land in the study area gradually slowed. Under the urban development (UD) scenario, the scale of construction land in the Wanjiang Urban Belt further expanded, with 944.8 km^2 of cropland and 57.6 km^2 of grassland converted into construction land, making it the scenario with the greatest reduction in cropland. In all three future scenarios, the area of construction land increased, mainly in areas with relatively high human activity, such as Hefei and Wuhu, and in some scattered areas along the Yangtze River line. In general, the transfer of cropland, forestland, and grassland together constitutes the phenomenon of land use conversion. However, because the Wanjiang Urban Belt has entered the process of rapid urbanization, it has chosen to meet the vigorous expansion demand of construction land at the expense of cultivated land, which is bound to affect the sustainable development of the ecological environment in the study area in the future.

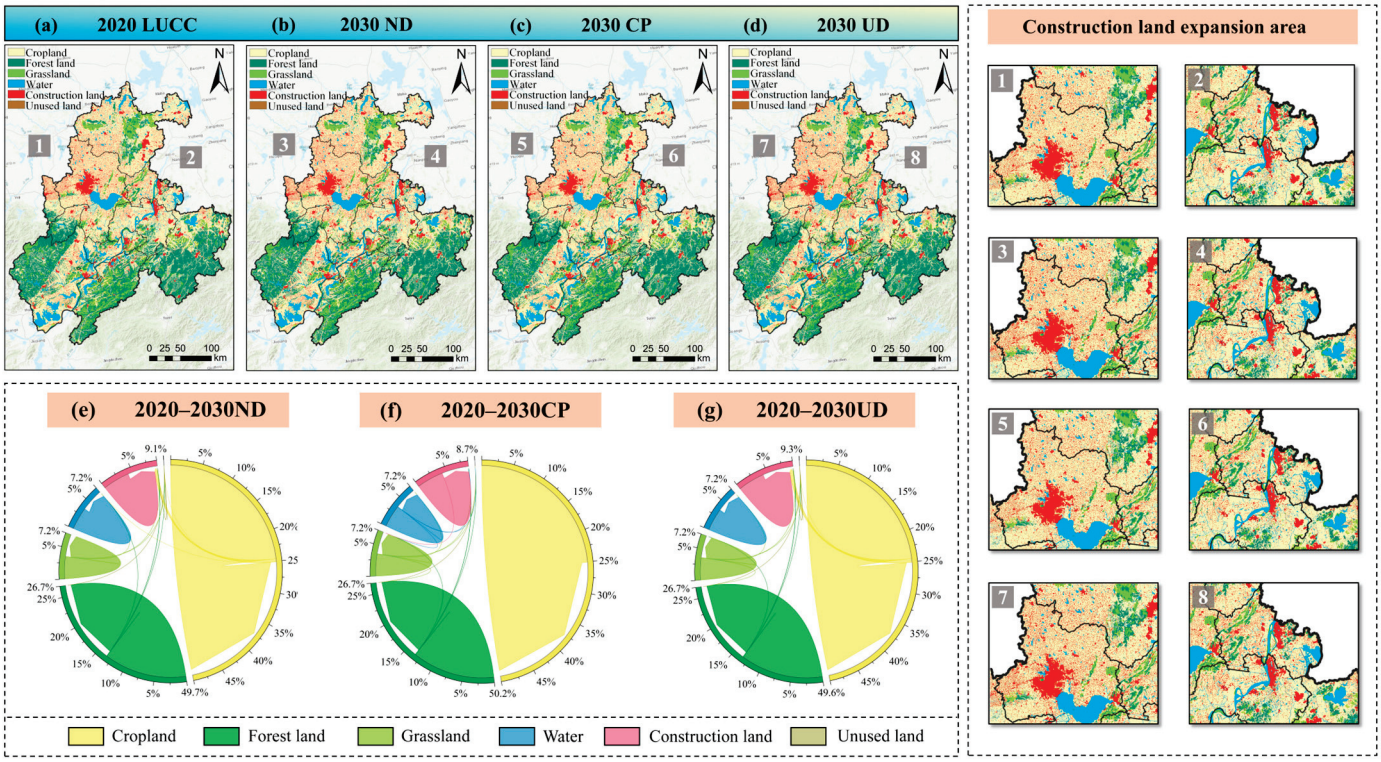

Figure 8. Land use distribution under different scenarios in 2030. (**a**) LUCC for 2020; (**b**) natural development scenario for 2030; (**c**) cropland protection scenario for 2030; (**d**) urban development scenario for 2030; Regions 1–8 refer to areas of major expansion of building land under different development scenarios; (**e**) 2020–2030ND land use transfer status; (**f**) 2020–2030CP land use transfer status; (**g**) 2020–2030UD land use transfer status.

4.3.2. Multiscenario Simulation Analysis of Ecosystem Services and Ecological Functional Areas

In the 2030 natural development scenario, there is a tendency for the total amounts of the three services, except for the WY, SR, and FP services, to decrease (Table 2). The urban development area (B3) and ecological restoration area (B4) shrank by 4.1% and 3.7%, respectively (Figure 9), and the shrunken areas were transformed into mainly ecological transition areas (B1) and ecological conservation areas (B2) (Figure 10a, Region 1). The agroecological area (B5) also showed an increasing trend, and the ecological restoration area still occupied a certain share of the southeastern part of the study area, including Wuhu and Xuancheng (Figure 10a, Region 2). The WY, CS, SR, and FP services all increased in the cropland protection scenario, but the extent of impairment of these two services in this scenario was relatively small compared with those in the other two development scenarios, and the disturbance of the quality of the ecological environment was relatively mild. In the central part of the study area, there was a shift from urban development and ecological conservation areas to agroecological areas along the periphery of Chaohu Lake (Figure 10b, Region 3); the same trend was observed in the plains along the river (Figure 10b, Region 4). In the urban development scenario, HQ and total CS declined significantly, and the total FP increased but remained at a low level compared with those in the other two scenarios. Focusing on Hefei, the ecological conservation area (B2) in the surrounding region has begun to transform into urban development area (Figure 10c, Region 5), and most agroecological and ecological transition areas in the central part of the study area have also begun to transform into this functional area (Figure 10c, Region 6).

Table 2. Assessment and forecast of five ecosystem services in Wanjiang Urban Belt under different scenarios.

Year	Water Yield/(10^{10} m^3)	Carbon Storage/(10^8 t)	Habitat Quality	Soil Retention/(10^9 t)	Food Production/ (10^7 t)
2020 LUCC	6.68	10.25	0.44	19.73	1.89
2030 ND	6.78	10.25	0.42	21.75	2.3
2030 CP	6.69	10.26	0.43	21.77	2.36
2030 UD	6.71	10.23	0.41	21.75	2.29

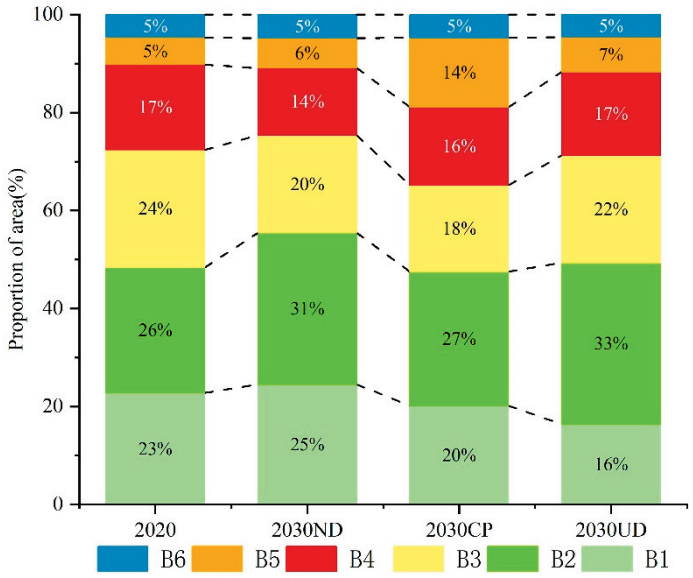

Figure 9. Changes in the proportion of each ecological function area under different development scenarios. (ND: natural development scenario; CP: cropland protection scenario; UD: urban development scenario; B1–B6 means Bundle 1–Bundle 6.)

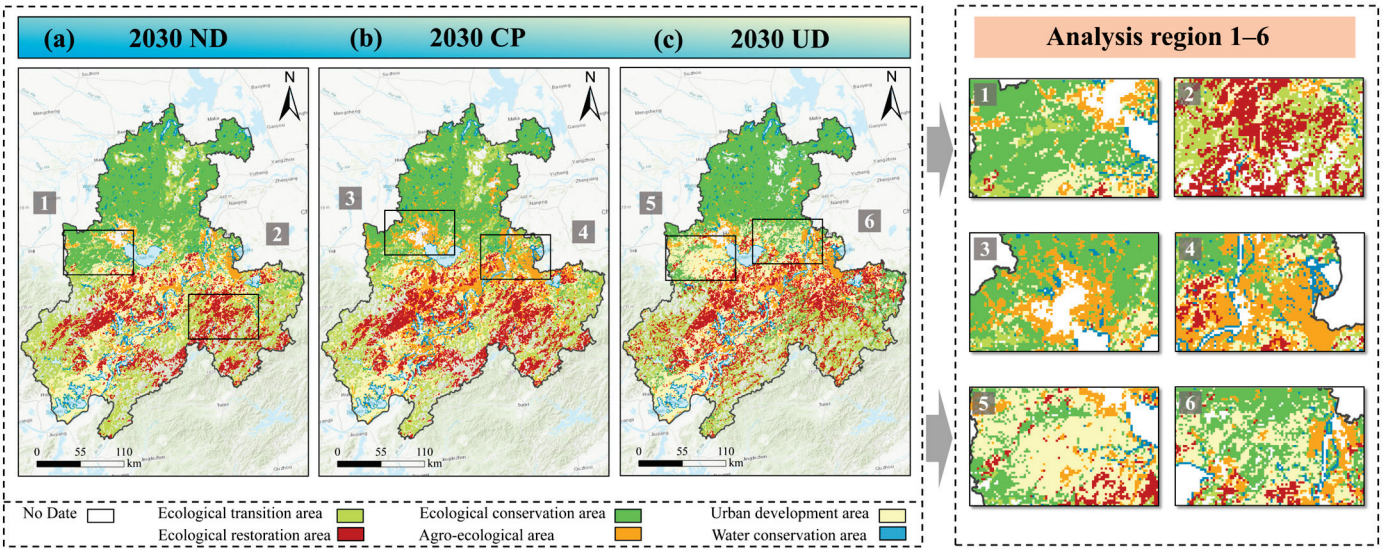

Figure 10. Distribution maps of ecosystem service function areas in Wanjiang Urban Belt under different scenarios in 2030. (ND: natural development scenario; CP: cropland protection scenario; UD: urban development scenario; Region 1, ecological transition area and ecological conservation area expansion zone; Region 2, ecological conservation area stable distribution zone; Region 3–4, agro-ecological area expansion zone; Region 5–6, urban development area expansion zone).

5. Discussion

5.1. Trends in the Spatial and Temporal Evolution of Ecosystem Services

With respect to the spatial distribution of ESs, the WY, CS, and HQ services had similar distribution characteristics, with the areas with increasing values located southeast and southwest of the Wanjiang Urban Belt, and the areas where WY services were impaired mainly concentrated in the northern part of the study area, which was similar to the results of the studies conducted by Li [35] and Sun [33]. On the one hand, the distribution of precipitation in the Wanjiang Urban Belt is less common in the southern and northern regions, and the southern and western regions are dominated by mountainous woodlands, with undulating terrain contributing to the formation of rainwater harvesting and runoff. These areas have diverse tree species and distinct vertical structures of vegetation, which are prone to water-sourcing and nutrient-supporting effects. On the other hand, the land use type in the northern part of the study area is mostly dominated by cropland, the vegetation type is relatively singular, the transpiration of plants is weak, and the soil is compacted, so the rainwater easily forms surface runoff on the surface of the farmland, meaning that it is not easy for precipitation to infiltrate downward when it falls to the ground, which is not conducive to its retention [45,49]. The growth areas of the SR and HQ services are essentially located in the mountainous and forested areas in the eastern and western parts of the study area, which have relatively gentle slopes and are rich in biological species, and the Dabie Mountain Range in the west and the Huangshan Mountain Range in the south provide good ecological substrates for these areas. In addition, the aboveground parts of forested areas, such as the forest canopy, the understory vegetation layer, and the layer of fallen leaves and branches, constitute important links in WY and can reduce the direct scouring effect of rainfall on the soil. Moreover, benefiting from the gradual implementation of policies such as ecological nature reserves and returning farmland to forests and grasslands, the vegetation cover has significantly increased, further increasing the ability of the regional environment to resist external interference [50]. However, the central river plains are areas of intensive human industrial and agricultural production activities, with a relatively high proportion of arable land, and with the development of the regional economy, the rapid expansion of land for construction, and the continued interference of human activities, the biodiversity of this area is under constant threat and the HQ and SR services are gradually declining. The northern plains as well as the plains along the river have high FP services, with the region formed by the Huaihe River crossing the border, featuring cropland all over the area, fertile soil, and little undulation; it is the indispensable core zone of grain and cotton production in the Wanjiang Urban Belt.

From the perspective of temporal change, all ecosystem services in the Wanjiang Urban Belt essentially showed increasing trends from 1990 to 2020; from 1990 to 2000, the study area was frequently hit by drought, and some areas in the southern region were particularly severely affected by the lower depth of water conservation compared to those in the northern region, which were affected by the superimposed effects of decreasing precipitation and greater evapotranspiration, and the regional WY and SR services all significantly decreased. Drought has severely affected the growth of crops and led to a reduction in FP services. Since 2010, the urbanization of the study area has accelerated markedly, with a significant increase in construction land. High-intensity human activities inevitably have negative impacts on the HQ and CS, resulting in declines in HQ and total CS in the study area over the years [51]. With the successive completion and commissioning of a series of major water conservancy projects, such as 'the project of leading water from the Yangtze River to the Huaihe River', the previous downward trend in regional WY services has only begun to gradually reverse since that period, showing a rebound trend. The total amount of regional FP services has always been on an upward trend except during

droughts, yet the area of arable land has not increased over the past 30 years. The increase in total FP is due mainly to the increase in crop yields per unit, but excessive agricultural activities are likely to lead to a decline in soil fertility in the Wanjiang Urban Belt, and soil protection needs adequate attention.

5.2. Ecosystem Service Trade-Off/Synergy Analysis

Pearson correlation analysis and geographically weighted regression were used to explore the trade-offs/synergies and spatial distribution patterns of ESs in the Wanjiang Urban Belt. During the study period, most ESs were synergistic and were distributed mainly in the western and southern mountainous areas, whereas the trade-off relationships were essentially located in the construction land concentration areas, such as the central area along the river and the northern plain. Overall, WY–SR, WY–HQ, HQ–CS, and HQ–SR services in the study area had significant positive synergistic relationships with mutual gain, and the correlation coefficients were relatively stable. The abundant supply of WY services significantly promotes the growth and development of vegetation, which not only enhances the synthesis rate of the photosynthetic effect and the ability to resist the urban heat island effect but also promotes the CS capacity of vegetation. The well-developed root system of vegetation also enhances the SR capacity of the region to a certain extent, and the thick soil layer provides a necessary supportive base for the growth of plants. In addition, considering the high altitude and relatively rugged mountainous conditions that characterize the forested areas of the southern and western mountain zones, along with elevation, topography has a lifting effect on moist airflow, resulting in abundant regional precipitation [52]. A relatively high altitude also leads to relatively low evapotranspiration, and the characteristics of the woodland soil layer, namely, high porosity, low bulk density, and good permeability, prolong the surface circulation process of rainfall. The deep soil layer forms a 'reservoir' and acts as a 'water purifier' for water, which further enhances the capacity of WY and SR in this region [35,53]. Therefore, synergies in the study area are reflected mainly in the above ESs. The WY service, as an important component of ESs, is indispensable in affecting ecological functions such as biomass and the carbon cycle. Although the total amounts of WY and SR are increasing annually, with decreasing forestland and grassland areas annually, the ESs in the region still face the risk of HQ degradation, and the CS capacity decreases. Given the weakening trends of the positive synergistic relationships between the above services, there may be a possible change from synergistic relationships to trade-off relationships, which should be given sufficient attention over time.

Compared with synergies, trade-offs have a more direct and obvious impact on human well-being, and there is a significant trade-off between CS and WY services in the study area. Since 2010, the land use situation in the Wanjiang Urban Belt has changed significantly, and to satisfy the trend of continuous expansion of land for construction, large amounts of forestland, grassland, and other land classes with relatively low economic effects have been encroached upon, whereas vegetation change has been the dominant factor in generating CS change [54]. With a gradual reduction in vegetation cover, the temperature of the soil surface does not decrease, and the evaporation of water increases, which is detrimental to WY, ultimately leading to the emergence of the trade-off effect, which slowly increases from year to year [55]; the trade-off in the FP–WY and FP–SR services has also been increasing since that period. Human activities that increase FP and other supply services are influenced by human demand, which in turn affects the allocation of regional water resources to a certain extent and thus places pressure on the enhancement of regional WY services. At the same time, the gradual lack of natural and seminatural landscapes in the region and the increasing intensity of human activities will lead to trade-offs between FP

and other ESs. In response to the increasing demand for FP, farmers may adopt tillage practices that are not conducive to SR, such as over-tillage and monoculture farming patterns, and excessive reclamation of other land types, resulting in consequent reductions in woodland and grassland areas. These behaviors increase the risk of soil erosion and degradation, weaken the regional SR capacity, and lead to trade-offs in FP–SR services [56]. In addition, the soil types in the western and southern mountainous and hilly areas of the study area are mainly red earth, those in the coastal area of the Huaihe River are fluvo–aquic soils, and those in the northern plain are yellow–cinnamon soils [57–59]. The soil texture and infiltration capacity influence surface runoff, flushing, and water seepage processes, thereby affecting WY and SR functions [60]. In the study area, the soil types in the soil and water loss area are mainly red earth and yellow–cinnamon soils, and the slope is relatively high. With the annual increase in total precipitation in the Wanjiang Urban Belt, these two soil types have gradually failed to meet the regional soil's demand for water conservation capacity under the influence of rainwater erosion, resulting in a decrease in the correlation coefficient of the WY–SR. There is potential for a shift toward trade-off relationships. The trade-offs between WY–FP, WY–CS, and SR–FP, based on the identification results, should be key issues in the restoration of ecosystems in the Wanjiang Urban Belt.

5.3. Analysis of the Characteristics of the Ecosystem Functional Areas

Currently, China is adjusting and building a new territorial spatial pattern of harmonious coexistence between human beings and nature, which requires an overall layout that integrates multiple factors and their interactions [61]. ESBs reflect not only the aggregation of ecosystem services but also the multifunctionality of ecosystems in coupled processes and changing patterns, and introducing ESBs into regional land spatial planning provides a series of new opportunities and insights for ecological environmental governance and socioeconomic development [62–64]. Therefore, in this study, the SOM method was used to identify a variety of ESBs to divide the ecological functional areas in the study area, which will be conducive to optimizing the spatial layout of "mountains, rivers, forests, fields, lakes, grasses and sand" throughout the entire Wanjiang Urban Belt.

The total amounts of WY, SR, and FP services in B1 are low, although the synergistic relationship in CS–HQ is more obvious, which is mainly distributed in the transition zone from B3 to B2 in the central part of the study area; therefore, it is classified as an ecological transition area. In B2, the synergistic effect is observed in WY, SR, and HQ services. This bundle is mainly distributed in the plains of the northern part of the study area where cropland is distributed in patches, and these areas can undertake a certain degree of development and construction activities, with strong antidisturbance ability, but the difficulty of ecological restoration is relatively high; therefore, it is classified as an ecological conservation area. B3, with the exception of WY and HQ services, has a low proportion of services and features densely populated areas, such as urban centers and urban and rural settlements in counties, which are classified as urban development areas because of the need for adequate water supply for their development. In view of the high demand for land use and development in the area, this area is also a key area for ecosystem protection in the Wanjiang Urban Belt in the future. B4 is dominated by SR services, with synergistic effects among the other four services. This bundle is distributed mainly along both sides of the water system, and the area has a high degree of sensitivity to human activities. If the vegetation is damaged, it will cause irreversible damage to the overall ecosystem, which is a key protection area for ecosystem restoration and protection in the Wanjiang Urban Belt, and its development should be strictly controlled and defined as an ecological restoration area. B5 is dominated by FP services, owing to the flat terrain and abundant water supply,

and the region has frequent agricultural activities and is a key zone for maintaining food security in the study area, so it is classified as an agroecological area. B6, which has a relatively strong WY capacity, is located mainly in areas with good ecological environments such as rivers and lakes, and has good hydrothermal and topographical conditions and quicker ecological restoration; therefore, it is classified as a water source and is considered a water conservation area.

Overall, the changes in the ecological functional areas in the Wanjiang Urban Belt have phased characteristics. Since the 1990s, development and construction in the region have gradually increased, and land with relatively low economic benefits has begun to be transferred to meet the needs of construction and development. By 2000, the agroecological functional area had decreased by 14.4%, and the urban development area had expanded by 8.7%. In 2010, the research area entered a stage of rapid urbanization, the scale of construction land further expanded, and large-scale functional area transformation occurred in the region. Most ecological restoration areas and ecological transition areas began to transform into urban development areas, and mountain forest areas and wetlands along rivers and lakes were affected by construction land occupation and landscape fragmentation, resulting in fragmentation of natural habitats. The value of biodiversity has decreased. The ecosystem structure with plantation forests and secondary forests as the main surface vegetation types causes the urban development area to suffer from a serious imbalance between the supply and demand of ESs, and a large amount of replenishment from other functional areas is urgently needed to satisfy normal industrial and agricultural activities, ultimately leading to a serious weakening of the antidisturbance capacity of the regional ecosystems and an obvious degradation of ecosystem services. Ecological restoration areas have appeared in patches in the southern mountainous regions and in the more developed areas along the river, with an expansion area of 6.2%. In the later stage of urbanization, the Wanjiang Urban Belt focused on the protection of cropland and actively promoted the construction of an ecological civilization. From 2010 to 2020, the retreat of industrial land in the region promoted the optimization of the land use structure. Although the urban development area is still expanding, its expansion speed has slowed significantly, and the ecological restoration and urban development areas have gradually transformed into ecological transition areas. The agroecological area in the central plain along the Yangtze River has also increased, which indicates that reasonable human intervention plays an important role in the orderly development of urban land use; however, the ecological restoration area still accounts for approximately 20% of the total area, and regional ecosystem governance and restoration still need to be practiced continuously in the future.

5.4. Evolution of Ecological Functional Areas Under Different Scenarios and Recommendations for Future Development

Under the three different development scenarios, in 2030, the spatial patterns of the various types of ecological functional areas in the Wanjiang Urban Belt remain essentially stable, but the spatial distributions of the functional areas vary significantly. Under the natural development scenario, the development trend of the large-scale expansion of the urban development area has slightly eased, the ecological transition and ecological conservation areas have increased, and the agroecological area has further expanded along the Yangtze River line, indicating that under the guidance of the 'Anhui Provincial Territorial Spatial Plan (2021–2035)', the provincial government's strict control of the disorderly expansion of construction land and the implementation of the cropland protection policy have achieved initial results. With the implementation of current ecological projects, the expansion of plantation forests has led to a gradual reduction in the fragmentation of the regional landscape, and the risk of natural disasters and water and carbon retention effects has increased, thus offsetting the negative effects of anthropogenic activities to some extent [65]. How-

ever, under this scenario, the ecological restoration area still accounts for a considerable proportion of the central and southern parts of the study area. The reason for this is that the expansion of urban development areas is mainly based on the use of grasslands and forests, and at the end of urbanization, although the growth rate of construction land area slows, the native vegetation on the surface of the previously occupied areas shrinks and breaks up severely, and the ecosystem's self-regulation function is seriously weakened, increasing its sensitivity to external disturbances and making it difficult to achieve effective restoration in a short time, thus gradually transforming it into an ecological restoration area. The root systems of trees anchor the soil in place, creating a network of fibers that stabilize the soil structure and prevent soil erosion [66]. Therefore, the future Wanjiang Urban Belt should adhere to the joint construction of forestland, grassland, and water areas; improve the ecological functions of blue and green spaces; protect forestland and grassland with ecological regulation functions; anchor the protection target of cultivated land; promote the restoration of ecological land in the central plain along the river and forest phase protection of the forest belt; and release the SR function of ecological land. Trade-off effects between economic development and ecological protection should be avoided. The ecological transition zone should reasonably control new construction land on the premise of protecting the integrity of ecological land. Among them, the ecological transition zone in the north is in the plains, with low vegetation coverage, and it is recommended to improve the green coverage of the area and connect the natural space inside and outside the town by constructing ecological corridors and green spaces. The ecological transition zone in the center has relatively frequent and sensitive human activities, leading to drastic conversion of arable land and grassland along the central part of the river. It is recommended that the system of returning ploughland to forests and grasslands be further implemented to reduce the fragmentation of natural surfaces such as forests and grasslands, and to improve the soil conservation capacity in order to stabilize the ecosystem service functions of the functional zone.

In the cropland protection scenario, the agroecological area expands from south to north, and the increases in FP are particularly prominent in all three scenarios. Driven by a series of government policies to benefit agriculture and increase food production, farmers' irrational cultivation of arable land is increasing, which is leading to gradual declines in HQ, SR, and the total amount of CS; coupled with the increase in precipitation in the Wanjiang Urban Belt, the erosive force of rainfall is increased, which further weakens the SR capacity of the region so that the original ecological baseline of the ecological conservation area, which has a relatively better base, shrinks. The area of the original ecological base is relatively good, but the phenomenon of shrinking occurs. The above changes indicate that this scenario can help ensure food supply, but although cropland is protected, the protection and improvement of the ecological environment should be emphasized. The ecological conservation area covers nature reserves such as the Yaoluoping National Nature Reserve and the Tiantangzhai National Forest Park, highlighting the biodiversity conservation value of this functional area. In the future, the ecological conservation area should be included within the scope of priority protection, focusing on the maintenance of biodiversity and strengthening the protection and management of nature reserves. At the same time, the management of the natural landscape wetland reserve around Chaohu Lake and Wuhu Lake in the ecological conservation area in the central part of the study area should be strengthened so as to enhance the stability and self-repairing ability of the wetland ecosystem through the protection and restoration of plant and animal species in the wetland. In the northern part of the study area, which is adjacent to the ecological conservation area of the relatively developed industrial and agricultural zones in the Wanjiang urban belt, it is recommended that the red line of ecological protection be strictly abided by, and that the

stability of the ecosystem service function of the area be continuously improved and its ecological conservation function be further utilized, on the premise of ensuring the safety of the existing ecosystems.

In the urban development scenario, the urban development area expands around relatively developed economic core areas such as Hefei and Wuhu, and these core areas have strong radiation-driving effects on neighboring areas. Driven by these core areas, the surrounding ecological functional areas begin to gradually transform into urban development areas. In the future, the eco-agricultural zones along the periphery of the Chaohu Lake basin should strengthen the management of the balance of arable land occupation and compensation, improve the ecological compensation mechanism, and change the rough agricultural production mode; this part of the area, as a core agricultural production zone, should take agricultural intensification measures to reduce the spatial conflict between arable land and other land use modes, so as to ensure the stability of food supply in the area. In addition, the eco-agricultural zones in the central part of the study area and the eastern part bordering the ecological conservation zone should make full use of the long-term feedback mechanism for the mutual conversion of arable land and ecological land such as forest land and grassland; establish a flexible transformation space; reasonably plan the agro-ecological zones, the ecological conservation zones, and the flexible conversion zones; and push forward the integration of the arable land protection and ecological protection policies. In the urban development zones in the urban development and construction zones, the layout of population, towns, and cities should be guided to match the carrying capacity of the region, and land use planning should be integrated with regional development and use, so as to reduce the occupation of arable land, forest land, and other types of land. In addition, there is a need to consider qualitative rather than incremental development to mitigate ecosystem degradation. Therefore, the promotion of high-quality construction of urban green spaces, such as "park cities" and "forest cities", should be implemented to enhance the comprehensive ES benefits of green spaces within cities [67,68]. Given that ecological restoration areas are characterized by high ecological sensitivity and a relatively high degree of restoration difficulty, these functional areas should be subject to strict restrictions on agricultural production or infrastructure construction activities to reduce the destruction of natural vegetation. Considering that high-cover grasslands and woodlands have significant positive effects on regional ecosystem services, the ecological restoration area in the western part of the study area should give full play to the relatively good natural ecological base of the Dabie Mountain area, and focus on improving the integrity and connectivity of the woodland patches, so as to safeguard the diffusion and exchange of biological species in the region and maintain regional ecological security. The ecological restoration area in the central part of the study area is strongly disturbed by human activities, and has formed a land use pattern of interlaced distribution of arable land and forest land. It is recommended that the ratio of arable land, grassland, and construction land be reasonably optimally regulated and determined so as to prevent excessive interference of the natural environment by human activities, slow down the reduction in the area of arable land and grassland caused by large-scale urban construction and other activities, and try to maintain the stability of the ratio of natural land use within the functional area. Water conservation areas are located in the core construction areas of urban agglomerations, and it is crucial to guide urban development effectively to ensure a sustainable water supply and avoid undue pressure on WY. The Wanjiang Urban Belt should continue to adhere to the principle of "jointly focusing on conservation and not engaging in large-scale development", further improving the horizontal ecological compensation mechanism of the entire Yangtze River Basin and encouraging all regions of the Yangtze River Basin to actively participate in ecological protection work to realize the green development of the

region and the sustainable restoration of natural ecosystem functions. At the same time, attention will be paid to core water conservation areas such as Taiping Lake and Fuziling.

6. Limitations and Prospects of the Study

First, in this study, although four different future development scenarios were generated using the PLUS model, the three scenarios are not representative of all the feasible possibilities, and future research should consider government policy interventions as well as lifestyle- and technology-driven changes for scenario setting. Second, the correlation coefficient can be used to determine the numerical relationships of ecosystem service trade-off synergies. GWR can characterize the spatial relationships of ecosystem service trade-off synergies, but it still cannot reflect the internal and action mechanisms of ESs. Therefore, further analysis by other methods is needed in the future. The driving factors affecting the change in trade-off synergies are discussed. Finally, the identification of ESBs is affected by the assessment methods and scales of ecosystem service functions. This study explored the interaction of ecosystem services in small- and medium-sized urban zones at the grid scale, and further analysis should be performed on assessment methods applicable to different types of urban ecosystem services [45] to apply the research results to more targeted measures and suggestions for the management and control of ecosystem services and ecological function zoning.

7. Conclusions

In this study, five typical ecosystem services in the Wanjiang Urban Belt from 1990 to 2020 were evaluated based on a variety of models. The Spearman coefficient and SOM methods were used to explore the synergistic effects of ecosystem service trade-offs and the dynamic evolution characteristics of each ecological functional area in the region. The PLUS model was used to simulate the changes in ESs and ecological functional areas under different scenarios in 2030 to provide feasible references for the identification of ecological functional areas and the formulation of zoning management and control strategies in the Wanjiang Urban Belt. The results are as follows:

(1) From 1990 to 2020, the spatial distribution characteristics of the ESs in the Wanjiang Urban Belt were “high in the south and low in the north”. During the study period, the total WY, SR, and FP services increased, whereas the total HQ and CS services decreased slightly.

(2) The ESs in the Wanjiang Urban Belt are mainly synergistic, and there are synergistic effects in WY–SR, WY–HQ, HQ–CS, and HQ–SR, which are mainly distributed in the western and southern mountainous areas of Anhui Province. These synergistic relationships tend to weaken, and WY–SR may change from synergistic to trade-off. The trade-off effect was reflected in WY–CS, WY–FP, and SR–FP, which were mainly distributed in the central plain along the river and the northern region of the study area, and showed a gradually increasing trend.

(3) The spatial patterns of the ESBs essentially remained stable, but the composition structure and spatial distribution of the various ESBs significantly differed. The central plain and southern mountain areas of the study area are dominated by ecological transition bundles. The ecological conservation bundle occupies the largest area and is widely distributed in the northern area along the Yangtze River line. In the middle of the region along the river, the economic development is relatively mature. The ecological protection bundle is mainly distributed in the central plain, the southern mountainous area, and the southeastern area. Food production bundles are distributed in the watershed of the Jianghuai River and some areas of the northern plain. Water conservation bundles are mainly distributed along the Yangtze River and

Chaohu Lake. The Wanjiang Urban Belt can be divided into six types of ESBs: ecological transition, ecological conservation, urban development, ecological restoration, agroecological, and water conservation areas.

(4) The ecological functional area has the characteristics of phased evolution. From 1990 to 2000, the scale of agroecological areas was seriously reduced by the influence of regional development policies, and the reduced area was transformed into urban development areas. From 2000 to 2010, large-scale transformations occurred in various ecological functional areas, and most of the ecological transition areas in the central and southern parts of the study area were transformed into urban development areas, which also led to the expansion of ecological restoration areas. From 2010 to 2020, with the promotion of national ecological civilization construction, the expansion rate of construction land gradually slowed, and ecological restoration and urban development areas transformed into ecological transition areas.

(5) Under different development scenarios, the evolution status of each ecological functional area is different. In the natural development scenario, owing to the gradual improvements in water and carbon conservation capacity, the ecological transition and ecological conservation areas expanded, and the agroecological area also increased in the plain along the river, whereas the ecological restoration area changed little. Under the cropland protection scenario, the agroecological zone expanded further from south to north, and SR and HQ decreased due to the superimposed effects of reclamation activities and rainwater erosion, which led to a reduction in the ecological conservation area and posed a potential threat to regional food security. In the urban development scenario, with Hefei as the center, the scale of the surrounding urban development area increased significantly, and the CS and HQ decreased substantially, which affected the overall ecological security pattern of the region.

Author Contributions: Conceptualization, Y.W.; Methodology, Y.W. and Y.R.; Software, Y.Z. and B.W.; Validation, Y.R.; Formal analysis, Y.W. and Y.Z.; Investigation, Y.A., Y.Z. and Y.R.; Data curation, Y.A. and Y.R.; Writing—original draft, Y.A. and Y.Z.; Writing—review & editing, Y.W. and Y.A.; Visualization, Y.A.; Supervision, B.W.; Project administration, B.W.; Funding acquisition, Y.W. All authors have read and agreed to the published version of the manuscript.

Funding: This research was funded by Research project of Anhui Social Science Federation, grant number 2022CX093, Open project of Key Laboratory of Jianghuai Cultivated Land Resource Protection and Ecological Restoration of Ministry of Natural Resources, grant number ARPE-2023-KF04 and ARPE-2024-KF06.

Data Availability Statement: The original contributions presented in this study are included in the article. Further inquiries can be directed to the corresponding author.

Conflicts of Interest: The authors declare no conflict of interest.

References

1. Reid, W.V.; Mooney, H.A.; Cropper, A.; Capistrano, D.; Carpenter, S.R.; Chopra, K.; Dasgupta, P.; Dietz, T.; Duraiappah, A.K.; Hassan, R. *Ecosystems and Human Well-Being-Synthesis: A Report of the Millennium Ecosystem Assessment*; Island Press: Washington, DC, USA, 2005.
2. Li, Y.; Li, Y.; Fan, P.; Sun, J.; Liu, Y. Land use and landscape change driven by gully land consolidation project: A case study of a typical watershed in the Loess Plateau. *J. Geogr. Sci.* **2019**, *29*, 719–729. [CrossRef]
3. Cord, A.F.; Bartkowski, B.; Beckmann, M.; Dittrich, A.; Hermans-Neumann, K.; Kaim, A.; Li enhoop, N.; Locher-Krause, K.; Priess, J.; Schröter-Schlaack, C. Towards systematic analyses of ecosystem service trade-offs and synergies: Main concepts, methods and the road ahead. *Ecosyst. Serv.* **2017**, *28*, 264–272. [CrossRef]
4. Balvanera, P.; Pfisterer, A.B.; Buchmann, N.; He, J.S.; Nakashizuka, T.; Raffaelli, D.; Schmid, B. Quantifying the evidence for biodiversity effects on ecosystem functioning and services. *Ecol. Lett.* **2006**, *9*, 1146–1156. [CrossRef] [PubMed]

5. Costanza, R.; De Groot, R.; Braat, L.; Kubiszewski, I.; Fioramonti, L.; Sutton, P.; Farber, S.; Grasso, M. Twenty years of ecosystem services: How far have we come and how far do we still need to go? *Ecosyst. Serv.* **2017**, *28*, 1–16. [CrossRef]
6. Costanza, R.; De Groot, R.; Sutton, P.; Van der Ploeg, S.; Anderson, S.J.; Kubiszewski, I.; Farber, S.; Turner, R.K. Changes in the global value of ecosystem services. *Glob. Environ. Change* **2014**, *26*, 152–158. [CrossRef]
7. Deng, C.; Liu, J.; Nie, X.; Li, Z.; Liu, Y.; Xiao, H.; Hu, X.; Wang, L.; Zhang, Y.; Zhang, G. How trade-offs between ecological construction and urbanization expansion affect ecosystem services. *Ecol. Indic.* **2021**, *122*, 107253. [CrossRef]
8. Wang, Y.-C.; Zhao, J.; Fu, J.-W.; Wang, Y.-Q.; Wen, Y.-Y. Recognition of ecosystem services trade-offs and synergistic comprehensive relations. *Editor. Dep. Res. Soil Water Conserv.* **2023**, *30*, 274–284.
9. Zhu, H.; Zhai, J.; Hou, P.; Wang, Q.; Chen, Y.; Jin, D.; Wang, Y. The protection characteristics of key ecological functional zones from the perspective of ecosystem service trade-off and synergy. *Acta Geogr. Sin.* **2022**, *77*, 1275–1288.
10. Vallet, A.; Locatelli, B.; Levrel, H.; Wunder, S.; Seppelt, R.; Scholes, R.J.; Oszwald, J. Relationships between ecosystem services: Comparing methods for assessing tradeoffs and synergies. *Ecol. Econ.* **2018**, *150*, 96–106. [CrossRef]
11. Li, D.; Wu, S.; Liu, L.; Liang, Z.; Li, S. Evaluating regional water security through a freshwater ecosystem service flow model: A case study in Beijing-Tianjian-Hebei region, China. *Ecol. Indic.* **2017**, *81*, 159–170. [CrossRef]
12. Yang, Y.; Yuan, X.; An, J.; Su, Q.; Chen, B. Drivers of ecosystem services and their trade-offs and synergies in different land use policy zones of Shaanxi Province, China. *J. Clean. Prod.* **2024**, *452*, 142077. [CrossRef]
13. Kareiva, P.; Watts, S.; McDonald, R.; Boucher, T. Domesticated nature: Shaping landscapes and ecosystems for human welfare. *Science* **2007**, *316*, 1866–1869. [CrossRef] [PubMed]
14. Lyu, R.; Clarke, K.C.; Zhang, J.; Feng, J.; Jia, X.; Li, J. Spatial correlations among ecosystem services and their socio-ecological driving factors: A case study in the city belt along the Yellow River in Ningxia, China. *Appl. Geogr.* **2019**, *108*, 64–73. [CrossRef]
15. Yu, H.; Jiang, J.; Gu, X.; Cao, C.; Shen, C. Using dynamic Bayesian belief networks to infer the effects of climate change and human activities on changes in regional ecosystem services. *Ecol. Indic.* **2025**, *170*, 113023. [CrossRef]
16. Li, L.; Tang, H.; Lei, J.; Song, X. Spatial autocorrelation in land use type and ecosystem service value in Hainan Tropical Rain Forest National Park. *Ecol. Indic.* **2022**, *137*, 108727. [CrossRef]
17. Cao, H.; Wu, Z.; Zheng, W. Impact of touristification and landscape pattern on habitat quality in the Longji Rice Terrace Ecosystem, southern China, based on geographically weighted regression models. *Ecol. Indic.* **2024**, *166*, 112259. [CrossRef]
18. Wei, J.-P.; Yang, Y.-C.; Xin-Chang, X.; Liao, L.-P.; Tian, Y.; Zhou, J.-Y. Quantifying ecosystem service trade-offs and synergies in Nanning City based on ecosystem service bundles. *J. Ecol. Rural Environ.* **2022**, *38*, 21–31.
19. Bennett, E.M.; Peterson, G.D.; Gordon, L.J. Understanding relationships among multiple ecosystem services. *Ecol. Lett.* **2009**, *12*, 1394–1404. [CrossRef] [PubMed]
20. Raudsepp-Hearne, C.; Peterson, G.D.; Bennett, E.M. Ecosystem service bundles for analyzing tradeoffs in diverse landscapes. *Proc. Natl. Acad. Sci. USA* **2010**, *107*, 5242–5247. [CrossRef] [PubMed]
21. Wu, J.; Zhong, X.; Peng, J.; Qin, W. Function classification of ecological land in a small area based on ecosystem service bundles: A case study in Liangjiang New Area, China. *Acta Ecol. Sin.* **2015**, *35*, 3808–3816.
22. Li, H.; Peng, J.; Hu, Y.; Wu, W. Ecological function zoning in Inner Mongolia Autonomous Region based on ecosystem service bundles. *Chin. J. Appl. Ecol.* **2017**, *28*, 2657–2666.
23. Mouchet, M.A.; Lamarque, P.; Martín-López, B.; Crouzat, E.; Gos, P.; Byczek, C.; Lavorel, S. An interdisciplinary methodological guide for quantifying associations between ecosystem services. *Glob. Environ. Change* **2014**, *28*, 298–308. [CrossRef]
24. Li, H.; Xu, Q.; Qiu, H.; Du, J.; Xu, Z.; Liu, L.; Zhao, Z.; Zhu, Z.; He, Y. Study on Ecosystem Service Trade-Offs and Synergies in the Guangdong–Hong Kong–Macao Greater Bay Area Based on Ecosystem Service Bundles. *Land* **2024**, *13*, 2086. [CrossRef]
25. Feng, L.; Lei, G. Study on spatial-temporal evolution characteristics and functional zoning of ecosystem services and trade-offs/synergies relationships in Northeastern China. *China Land Sci.* **2023**, *37*, 100–113.
26. Lu, Z.; Li, W.; Yue, R. Investigation of the long-term supply–demand relationships of ecosystem services at multiple scales under SSP–RCP scenarios to promote ecological sustainability in China's largest city cluster. *Sustain. Cities Soc.* **2024**, *104*, 105295. [CrossRef]
27. Renard, D.; Rhemtulla, J.M.; Bennett, E.M. Historical dynamics in ecosystem service bundles. *Proc. Natl. Acad. Sci. USA* **2015**, *112*, 13411–13416. [CrossRef] [PubMed]
28. Zou, Z.; Yuan, X.; Zhang, Z.; Li, X.; Zhou, C. Spatiotemporal Evolution and Influencing Factors of Coupling and Coordination between the Ecosystem Service Value and Economy in the Pearl River Delta Urban Agglomeration of China. *Land* **2024**, *13*, 1670. [CrossRef]
29. Zhao, X.; Shi, X.; Li, Y.; Li, Y.; Huang, P. Spatio-temporal pattern and functional zoning of ecosystem services in the karst mountainous areas of southeastern Yunnan. *Acta Geogr. Sin.* **2022**, *77*, 736–756.
30. Cao, Y.; Chen, C.; Zhang, D.; Liu, M.; Dong, S. Evolution of ecological risk pattern of land use change in Wanjiang City Belt. *Acta Ecol. Sin.* **2019**, *39*, 4773–4781.

31. Huang, Y.; Wu, J. Spatial and temporal driving mechanisms of ecosystem service trade-off/synergy in national key urban agglomerations: A case study of the Yangtze River Delta urban agglomeration in China. *Ecol. Indic.* **2023**, *154*, 110800. [CrossRef]
32. Mei, Z.; Li, C.; Zhao, J.; Li, Z.; Chen, K.; Huang, X.; Zhao, Z. The Temporal and Spatial Evolution Characteristics and Driving Factors of Ecosystem Service Bundles in Anhui Province, China. *Land* **2024**, *13*, 736. [CrossRef]
33. Sun, F.; Fang, F.; Hong, W.; Luo, H.; Yu, J.; Fang, L.; Miao, Y. Evolution analysis and prediction of carbon storage in Anhui Province based on PLUS and InVEST model. *J. Soil Water Conserv.* **2023**, *37*, 151–158.
34. Li, Q.; Wei, J.-f. Spatio-temporal coupling relationship between territory spatial utilization efficiency and high-quality development in Wanjiang City Belt. *J. Nat. Resour.* **2022**, *37*, 2867–2883. [CrossRef]
35. Li, Y.; Ma, X.; Qi, G.; Wu, Y. Studies on water retention function of Anhui Province based on InVEST model of parameter localization. *Resour. Environ. Yangtze Basin* **2022**, *31*, 313–325.
36. Liu, J.; Pei, X.; Zhu, W.; Jiao, J. Scenario modeling of ecosystem service trade-offs and bundles in a semi-arid valley basin. *Sci. Total Environ.* **2023**, *896*, 166413. [CrossRef] [PubMed]
37. Xu, L.; He, N.; Yu, G. A dataset of carbon density in Chinese terrestrial ecosystems (2010s). *China Sci. Data* **2019**, *4*. [CrossRef]
38. Bace, R.; Hofmeister, J.; Vitkova, L.; Brabec, M.; Begovic, K.; Cada, V.; Janda, P.; Kozak, D.; Mikolas, M.; Nagel, T.A. Response of habitat quality to mixed severity disturbance regime in Norway spruce forests. *J. Appl. Ecol.* **2023**, *60*, 1352–1363. [CrossRef]
39. Zheng, Q.; Xu, G.; Liu, Y.; Yang, Q.; Chi, J.; Sun, J.; Zhang, T. Assessment and Driving of Habitat Quality in Anhui Province Based on InVEST and MGWR Models. *Res. Soil Water Conserv.* **2024**, *31*, 373–382.
40. Li, P.; Zha, Y.; Zuo, B.; Zhang, Y. A family of soil water retention models based on sigmoid functions. *Water Resour. Res.* **2023**, *59*, e2022WR033160. [CrossRef]
41. Zhao, T.; Pan, J. Ecosystem service trade-offs and spatial non-stationary responses to influencing factors in the Loess hilly-gully region: Lanzhou City, China. *Sci. Total Environ.* **2022**, *846*, 157422. [CrossRef]
42. Davies, D.L.; Bouldin, D.W. A cluster separation measure. *IEEE Trans. Pattern Anal. Mach. Intell.* **1979**, *PAMI–1*, 224–227. [CrossRef]
43. Shen, J.; Li, S.; Liang, Z.; Liu, L.; Li, D.; Wu, S. Exploring the heterogeneity and nonlinearity of trade-offs and synergies among ecosystem services bundles in the Beijing-Tianjin-Hebei urban agglomeration. *Ecosyst. Serv.* **2020**, *43*, 101103. [CrossRef]
44. Liang, X.; Guan, Q.; Clarke, K.C.; Liu, S.; Wang, B.; Yao, Y. Understanding the drivers of sustainable land expansion using a patch-generating land use simulation (PLUS) model: A case study in Wuhan, China. *Comput. Environ. Urban Syst.* **2021**, *85*, 101569. [CrossRef]
45. Shi, M.; Wu, H.; Jiang, P.; Zheng, K.; Liu, Z.; Dong, T.; He, P.; Fan, X. Food-water-land-ecosystem nexus in typical Chinese dryland under different future scenarios. *Sci. Total Environ.* **2023**, *880*, 163183. [CrossRef] [PubMed]
46. Fang, C.; Cui, X.; Li, G.; Bao, C.; Wang, Z.; Ma, H.; Sun, S.; Liu, H.; Luo, K.; Ren, Y. Modeling regional sustainable development scenarios using the Urbanization and Eco-environment Coupler: Case study of Beijing-Tianjin-Hebei urban agglomeration, China. *Sci. Total Environ.* **2019**, *689*, 820–830. [CrossRef]
47. Chen, L.; Binpin, G.; Yingmei, W.; Kejun, Z.; Yan, W. Dynamic simulation of landscape ecological risk in mountain towns based on PLUS model. *J. Zhejiang AF Univ.* **2022**, *39*, 84–94.
48. Chang, B.; Chen, B.; Chen, W.; Xu, S.; He, X.; Yao, J.; Huang, Y. Analysis of trade-off and synergy of ecosystem services and driving forces in urban agglomerations in Northern China. *Ecol. Indic.* **2024**, *165*, 112210. [CrossRef]
49. Sun, H.; Zhang, X.; Liu, X.; Liu, X.; Shao, L.; Chen, S.; Wang, J.; Dong, X. Impact of different cropping systems and irrigation schedules on evapotranspiration, grain yield and groundwater level in the North China Plain. *Agric. Water Manag.* **2019**, *211*, 202–209. [CrossRef]
50. Guan, Q.; Li, H.; Guan, C.; Chen, J.; Fan, Y. Identification of Ecological Compensation Zones and Compensation Amounts: A Case Study of the Yellow River Delta. *Land* **2024**, *13*, 1582. [CrossRef]
51. Xing, L.; Hu, M.; Wang, Y. Integrating ecosystem services value and uncertainty into regional ecological risk assessment: A case study of Hubei Province, Central China. *Sci. Total Environ.* **2020**, *740*, 140126. [CrossRef]
52. Xia, H.; Yuan, S.; Prishchepov, A.V. Spatial-temporal heterogeneity of ecosystem service interactions and their social-ecological drivers: Implications for spatial planning and management. *Resour. Conserv. Recycl.* **2023**, *189*, 106767. [CrossRef]
53. Liu, J.; Han, X.; Liu, J.; Liang, Z.; He, R. Understanding of critical zone structures and hydrological connectivity: A review. *Adv. Water Sci.* **2019**, *30*, 112–122.
54. Xiang, S.; Wang, Y.; Deng, H.; Yang, C.; Wang, Z.; Gao, M. Response and multi-scenario prediction of carbon storage to land use/cover change in the main urban area of Chongqing, China. *Ecol. Indic.* **2022**, *142*, 109205. [CrossRef]
55. Linan, N.; Quanqin, S.; Meiqi, C.; Xiongyi, Z.; Tingjing, Z. Changes in ecosystem services and their tradeoffs and synergies in the Yangtze River Basin from 2000 to 2020. *Resour. Sci.* **2024**, *46*, 853–866. [CrossRef]
56. Gao, C.; Hu, B.; Wang, Z.; Huang, S.; Zhang, L. Study on spatiotemporal changes of ecosystem service trade-offs/synergies and driving mechanisms in the key zone of mountain-river-sea coupling: A case study of the southwest Guangxi Karst-Beibu Gulf. *Ecol. Indic.* **2024**, *169*, 112892. [CrossRef]

57. Zhao, M.-S.; Qiu, S.-Q.; Wang, S.-H.; Li, D.-C.; Zhang, G.-L. Spatial-temporal change of soil organic carbon in Anhui Province of East China. *Geoderma Reg.* **2021**, *26*, e00415. [CrossRef]
58. Zhu, G.; Tang, Z.; Shangguan, Z.; Peng, C.; Deng, L. Factors affecting the spatial and temporal variations in soil erodibility of China. *J. Geophys. Res. Earth Surf.* **2019**, *124*, 737–749. [CrossRef]
59. Quinn, J.E.; Fergus, C.; Hyland, E.; Vickery, C.; Lacher, I.L.; Akre, T.S. Ecosystem Service and Biodiversity Patterns Observed across Co-Developed Land Use Scenarios in the Piedmont: Lessons Learned for Scale and Framing. *Land* **2024**, *13*, 1340. [CrossRef]
60. Lu, H.; Yan, Y.; Zhu, J.; Jin, T.; Liu, G.; Wu, G.; Stringer, L.C.; Dallimer, M. Spatiotemporal water yield variations and influencing factors in the Lhasa River Basin, Tibetan Plateau. *Water* **2020**, *12*, 1498. [CrossRef]
61. Chang, Y.; Wu, D.; Li, H.; Liu, X.; Wang, Y.; Guo, J. Spatio-temporal variations of ecosystem service bundles in Huaihe River Basin based on SOFM. *Acta Ecol. Sin.* **2024**, *44*, 4544–4557.
62. Chen, S.; Chen, H.; Yang, R.; Ye, Y. Linking social-ecological management and ecosystem service bundles: Lessons from a peri-urban agriculture landscape. *Land Use Policy* **2023**, *131*, 106697. [CrossRef]
63. Chen, Q.; Liu, S.; Pan, Z.; Ning, Y.; Wei, B. Projected LUCC dynamics and ecosystem services in an emerging urban agglomeration under SSP-RCP scenarios and management implications. *Sci. Total Environ.* **2024**, *949*, 175100. [CrossRef]
64. Peng, X.; Dai, X.; Shi, R.; Zheng, Y.; Liu, X.; Xiao, Y.; Li, W.; Zhang, Y.; Wang, J.; Huang, H. Investigating the Effects of Mining on Ecosystem Services in Panzhihua City: A Multi-Scenario Analysis. *Land* **2024**, *13*, 819. [CrossRef]
65. Xi, Y.; Peng, S.; Liu, G.; Ducharne, A.; Ciais, P.; Prigent, C.; Li, X.; Tang, X. Trade-off between tree planting and wetland conservation in China. *Nat. Commun.* **2022**, *13*, 1967. [CrossRef]
66. Keshtkar, M.; Mokhtari, Z.; Sayahnia, R. Impact of land use/land cover change on soil retention service: A case of agricultural-urbanized Landscape in Northern Iran. *J. Landsc. Ecol.* **2022**, *15*, 34–58. [CrossRef]
67. Chang, J.; Qu, Z.; Xu, R.; Pan, K.; Xu, B.; Min, Y.; Ren, Y.; Yang, G.; Ge, Y. Assessing the ecosystem services provided by urban green spaces along urban center-edge gradients. *Sci. Rep.* **2017**, *7*, 11226. [CrossRef] [PubMed]
68. Dong, D.; Zhang, R.; Guo, W.; Gong, D.; Zhao, Z.; Zhou, Y.; Xu, Y. Assessing Spatiotemporal Dynamics of Net Primary Productivity in Shandong Province, China (2001–2020) Using the CASA Model and Google Earth Engine: Trends, Patterns, and Driving Factors. *Remote Sens.* **2025**, *17*, 488. [CrossRef]

Disclaimer/Publisher's Note: The statements, opinions and data contained in all publications are solely those of the individual author(s) and contributor(s) and not of MDPI and/or the editor(s). MDPI and/or the editor(s) disclaim responsibility for any injury to people or property resulting from any ideas, methods, instructions or products referred to in the content.

land

MDPI

Article

Do Small Livestock Producers Adapt to Climate Variability? An Approach to the Case of the Upper Fonce River Páramo in Santander, Colombia

Victoria-Eugenia Guáqueta-Solórzano *, César Enrique Ortiz-Guerrero and Edna Castañeda Salazar

Departamento de Desarrollo Rural y Regional, Facultad de Estudios Ambientales y Rurales, Pontificia Universidad Javeriana, Bogotá 110231, Colombia; c.ortiz@javeriana.edu.co (C.E.O.-G.); edna-castaneda@javeriana.edu.co (E.C.S.)
* Correspondence: vguaqueta@javeriana.edu.co

Abstract: This article presents the changes in the climatic variables of precipitation and temperature, the perceptions of producers regarding these variables, and the strategies and social, economic, and political factors that affect adaptations of small livestock producers in the páramo ecosystem at the upper Rio Fonce region. Data from 33 questionnaires, 12 interviews, and two workshops with key actors and producers were analyzed. A workshop resulted in a traffic light table assessing indicators from Bergamini related to vulnerability and adaptive capacity. Survey results helped identify adaptation strategies, while public policy documents underwent deductive content analysis. The findings revealed that changes in precipitation and temperature affect livestock systems. Farms with silvopastoral systems implement more adaptation strategies than conventional farms, even when not anticipated. Additionally, the ambiguity of the concept of adaptation hinders the development of policies that would enable livestock producers to transition towards more adaptive livestock systems.

Keywords: climate variability; adaptation strategies; strategic ecosystem páramo; livestock; public policies

1. Introduction

Climate variability, exacerbated by the atmospheric emissions of greenhouse gases of anthropogenic origin, is recognized today as a threat whose consequences differentially affect high Andean agro-ecosystems [1]. The Fifth Assessment Report of the Intergovernmental Panel on Climate Change (IPCC) states that the earth's temperature has increased by approximately 0.75 °C since the industrial revolution and is projected to continue to increase if the current development model continues, favoring an increase in temperature by 0.2 °C per decade with direct impacts on ecological and social systems [2]. Likewise, the Colombian Institute of Hydrology, Meteorology and Environmental Studies (IDEAM) has forecast for Colombia an increase in the average annual temperature in 50 years of between 1 °C and 2 °C with direct repercussions on the agricultural sector, classified as the most vulnerable sector [2].

Literature reports different impact analyses of this phenomenon on livestock [3–5]. The main impacts reported are associated with reduced livestock growth, decreased milk production, limited productive performance, and increased animal mortality and birth rates. Producers implement different adaptation strategies in response to the nature of the threat. In the case of high rainfall scenarios, there are practices of physical modification of

the indoor and outdoor environment where the animals remain: at the indoor level, the restoration of paddocks with the introduction of species that generate shade to reduce the exposure of animals to solar radiation and heat stress [6], and at the indoor level, ventilation and construction of spaces to reduce heat [7].

On the other hand, reports indicate that in drought scenarios, producers implement genetic improvement strategies to reduce animal size, knowing that smaller and clear-colored animals are more resistant to heat stress [8]. It also highlights the modification of diets, changes in feeding times, and increased fumigation practices to control pests and diseases in dry times. In addition to the above, public policy promotes rapid adaptation and technological and management changes in production systems with less vulnerability [5]. In this context, vulnerability is expressed in terms of the lack of technological, social, economic, material, and human capital that limits adaptation [9].

At the same time, livestock farming is a climate change and ecosystem loss driver, generating 14.5% of total anthropogenic greenhouse gas (GHG) emissions and reducing water resources and availability, forests, and soils [10,11]. For this reason, silvopastoral livestock farming becomes an adaptation strategy that requires further evaluation [12].

In regions like South America and Colombia, the El Niño-La Niña Southern Oscillation (ENSO) has the most marked effect on climate [2]. According to the National Unit for Risk and Disaster Management (UNGRC) in the period including the years 1990–2024, the ENSO contributed to a decrease in agricultural productivity of 16% and to a loss of glacier mass of 56% and affected more than 75% of the páramo ecosystem. For example, every time an El Niño event occurred, the average reduction was about 5% in agricultural yields and 4.9% in milk production in conventional production systems, while in silvopastoral systems, milk production reduction was 2.2% [13].

The National Federation of Ranchers [14] stipulates a negative variation of −2.2% in livestock inventories from 2010 to 2018 due to Niño and Niña events. This percentage applies to the 23.5 million head of cattle that the country had at that time throughout the national territory, of which 130,000 died of thirst due to an increase in temperature [14]. The situation persists, reporting ever higher figures: between 30 November 2019, and 25 January 2020, 34,925 heads of cattle died in Colombia due to extreme temperatures, and another 742,000 livestock were relocated to different areas. Concern about this impact on livestock is mainly because the livestock subsector currently contributes 1.4% of the national GDP and 21.8% of the agricultural GDP [15] and is an active part of the livelihoods of more of 638,941 families [16]. The role of livestock in climate issues is also important because it represents the activity generating the second highest amount of emissions of greenhouse gases (GHG) with 14% (32 Mt de CO_2) after 33% deforestation, added to pressures on land use and impact on the high Andean and páramo ecosystems [17].

Public policies in Colombia recognize and address this complex situation, although their application is sectoral and has represents an important challenge to solve with regard to emerging tradeoffs from the conservation of affected ecosystems, protection for the growth of the economy, and demands that come from the marginal communities located in the páramos. These aspects are observed first in the national climate change policy—PNCC—that promotes research and actions to identify strategies for adaptation and mitigation of impacts, risk reduction, disaster response, and reconversion of the different bovine production systems [18–21] and second, in Law 1930 of 2018, wherein it is considered urgent to reduce the impacts generated by cattle ranching in the páramo through productive reconversions adapted to current environmental change conditions. Since 2020, the country has been consolidating the climate resilience policy (E2050), which includes a framework to define a route to achieve sustainable socioeconomic development, seeking a more systemic measure. This policy is expected to overcome the predominant

sectoral vision where adaptation to climate events and ecosystems conservation are independently developed and change towards a systemic and territorial policy where economic development based on livestock, a difficult-to-eliminate traditional activity, technologically changes to adapt to these ecosystems and settles with sustainability in strategic ecosystems such as the páramo s, without displacing the communities that have traditionally inhabited these territories.

Given the existing interest at the academic and political levels on this topic, this document offers a balance of the situation that in terms of adaptation is presented in Guantiva La Rusia Páramo for their location in the paramos, the confluence of different protected areas and livelihoods, the latter incorporating livestock as one of their basic components.

The development of the exercise allowed us to identify the hydroclimatological state of the case study and the set of strategies used by producers to respond to the events of climatic variability. It also provided an understanding of the Colombian public policy commitments to promote adaptation strategies in traditional livestock production within its conceptual gaps. The document concludes with a set of public policy recommendations and conclusions.

2. Study Area

2.1. Location

Páramo ecosystems are localized at high latitudes and considered strategic areas for the conservation of ecosystem services and biodiversity. Regulation of water resources, carbon sequestration, and the protection of unique flora species are among their crucial functions, essential for the provisioning of ecosystem services. They contain 10% of Colombia's biodiversity with endemic species of plants, mammals, birds, and amphibians [22]. In addition, these ecosystems have been the livelihood of a sizable number of families who benefit from the water for their consumption and agricultural and livestock activities. The study area is located within the buffer zone of the Guantiva-La Rusia complex, which supplies 87% of the water of the 22 municipalities that border the complex (Figure 1) [23].

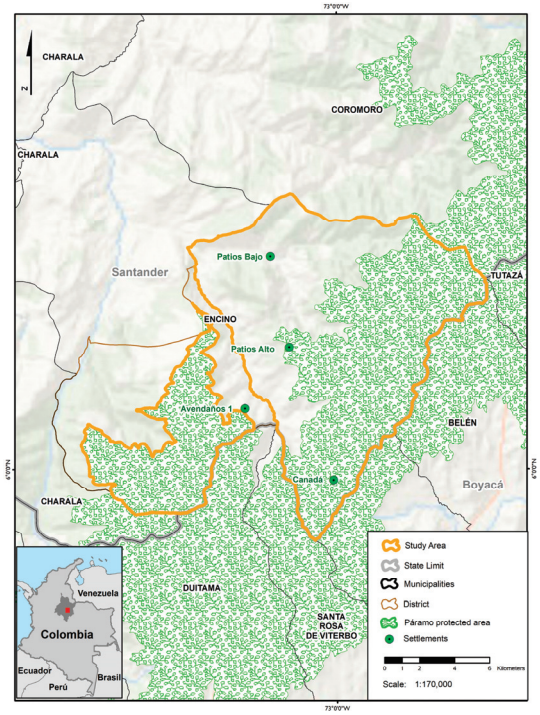

Figure 1. Study area. The green points mark Patios Bajo, Patios Alto, Avendaños 1, and Canada villages of where the research took place. The map of Colombia locates the study area in the country.

2.2. Characteristics of Páramo

In Colombia, paramo ecosystems, water sources, and aquifers are priority areas for conservation. This is because one of the main criteria for determining strategic areas for conservation, planning, and environmental management has been their ecological importance and their role in providing water resources for the population. This last aspect has been a recurrent criterion in the declaration of protected areas [24].

The páramo passes through transition zones from high Andean forests to herbaceous cover as altitude increases and is characterized by its floristic diversity, which includes approximately 128 different species of mosses, and 302 species of vascular flora, mainly of the genus Asteracea [25].

The paramo's climate is cold and humid, with an average annual temperature ranging from 12 °C–18 °C, annual average rainfall of 1000 mm–1500 mm, average relative humidity of 80%, annual average daily solar brightness of 4–5 h, and annual evaporation between 900–1100 mm [26].

The main coverages of the Guantiva-La Rusia páramo are pastures and stubble, followed by forest areas. The paramo holds livestock production, minor species, and some forest plantations [27].

2.3. Socioeconomic Aspects

The major socioeconomic activities are primary production systems based on conventional semi-intensive livestock farming, including pasture monocultures, and silvopastoral, with diversification practices of pastures and tree species in the same area for livestock feeding.

The main source of income is of the traditional type with herds of approximately 1–10 animals per family with a prevalence of smallholdings (3–20 ha), mixed with agricultural activities for self-consumption (home gardens) such as potatoes, corn, peas and carrots, onions, some cold-climate fruit trees, and minor species such as chickens, sheep, and rabbits. Dual-purpose livestock activities constitute the activity of greatest economic importance in the area and in the municipality. Thus, livestock is even more important than agriculture and labor.

3. Methods

This research is exploratory and qualitative in nature [28]. Likewise, it has an inductive nature, based on the case study [29]. To analyze the variables of the climate, we carried out a review and compilation of information on climate variability provided by the Institute of Hydrology, Meteorology and Environmental Studies (IDEAM) on the closest stations. We selected the main pluviometric and climatological categories, and we analyzed a data record of 35 years and the variables of precipitation and temperature.

To assess the adaptive capacity and vulnerability of the system, two workshops with male farmers aged 30 to 60 years, representing both conventional and silvopastoral production systems, were held. During these sessions, we utilized traffic light perception tables. Participants rated various adaptation and vulnerability indicators at the farm level, as proposed by Bergamini [30], on a 1 to 3 scale (where 1 indicates low, 2 indicates medium, and 3 indicates high) (Table 1).

The workshops followed a different logic for each type of production. In the first workshop, 18 producers (men) participated with conventional systems, and in the second, 15 (11 men and 4 women) participated with silvopastoral systems. In these instances, timelines helped to track climate changes and social mapping to identify the spatial development of the adaptation strategies. To corroborate the information from the workshops, visits to ten farms (five under silvopastoral arrangements and five conventional) took place to weigh the results of the workshops and to validate the status of the indicators with the

households. The data obtained from the 33 surveys complemented the indicators and made it possible to understand the perceptions of impact and adaptability of producers.

Table 1. Adaptation and vulnerability variables and indicators.

Variables	Indicators
Landscape	Landscape diversity Slope Proximity to forest and protected areas Live fences and windbreaks Proximity to water sources
Production systems	Diversity of productive systems Practices of conservation of forest and water Drains (Channels and ditches) Use of water technologies Self-consumption of products generated at the farm Farm infrastructure Pasture rotation Variety of breeds Variety of grasses Soil fertility Rainwater harvesting practices Practices to increase soil organic matter Sustainable management of weeds and practices
Local knowledge	Seed selection of grasses resistant to dryness and humidity Use of breeds tolerant to dryness and humidity Water conservation practices Use of climatic indicators Strategies for prevention of drying Strategies for prevention of rain Inherited technologies Possibility of generacional relief
Institutions and social networks	Facilitation of interchange of local cooperation and knowledge Support from institutions to productive systems Participation in organizations
Gender	Women involved in decision-making in the productive systems Women's access to resources and employment opportunities
Infrastructure	Knowledge of management of productive systems Contribution of infrastructure of productive systems (roads, schools and services)

Moreover, 12 interviews were conducted with key stakeholders, including technicians from protected areas, municipal technical assistance units (UMATA), and municipal delegations of the Agrarian Bank directors and representatives of local organizations. The results provided a better understanding of climate and policy impacts on adaptation strategies for climate events (changes in temperature and precipitation).

A content analysis of different normative instruments was also conducted based on Clemence and colleagues' [31] coding proposal. Six laws were reviewed: Law 1972 of 2019; Law 1931 of 2018; Law 1844 of 2017; Law 1776 of 2016 Law 629 of 2000; Law 164 of 1994; and Law 1931 of 2018, as well as a policy, National Adaptation Plan, 2014, and a technical document, Climate Resilience Strategy E2050 of 2021. The exercise allowed for the identification of descriptive codes of the adaptation category that define the concept according to specific analytical approaches. Conceptual trends to elaborate network graphs with word frequencies (codes) in Gephi 0.10 software are available.

The selection of the case study villages responds to the presence of livestock-based livelihoods in the high Andean forests and the buffer zones of the National Natural Park, placed in the biogeographic region of the páramo.

4. Results

4.1. Climate Characteristics

The results show that the most important changes for livestock-based livelihoods are related to changes in precipitation and temperature. The average annual temperature ranges from 12 °C to 16 °C, with an average annual rainfall of 1000 mm a 4000 mm, average relative humidity of 80%, annual average daily solar brightness of 4–5 h, and annual evaporation between 900–1100 mm. The results show a tendency to increase the annual mean precipitation, and the temperature variable increases with respect to the current mean of 0.5 °C–0.75 °C (Figure 2).

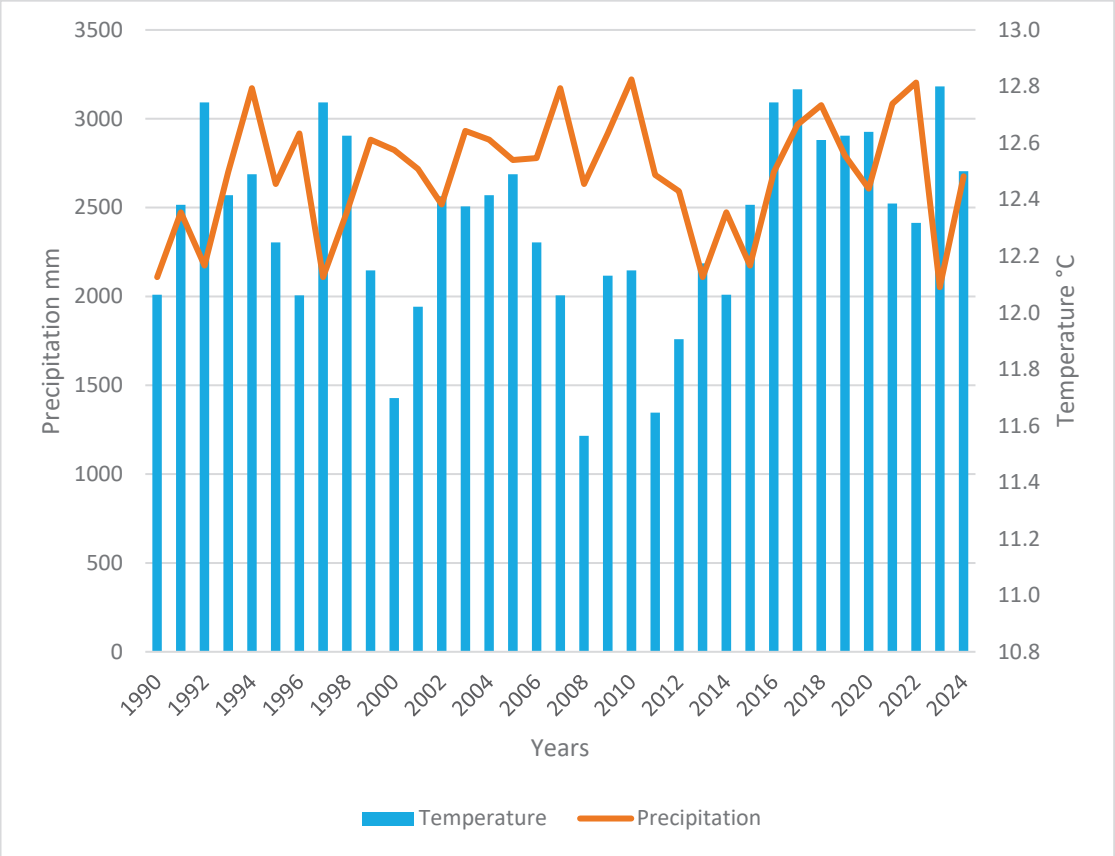

Figure 2. Average annual precipitation and temperature variation from 1990 to 2024 in the study area.

4.2. Perceptions of Producers Regarding Climate Variability Phenomena

The perceptions of livestock producers regarding climate phenomena depend on their productive activity and the type of capital they have available to manage their activities. Farmers who engage in conventional livestock production report receiving monthly incomes ranging from US$290 to US$400 from milk sales, and 80% feel that they have adequate technology, labor, and productive infrastructure (farms, milking machines, barns) to manage their animals. Similarly, 94% suggest that the natural resources on their farms are in a good state of conservation, and, as a result, the soil and water are sufficient to meet the requirements of their animals in terms of food and water. However, 6% mentioned that in the last 10 years, water has reduced, and soil erosion has increased due to animal

trampling on their farms; however, this is not associated with climate variability events, although they identify that the climate is less predictable nowadays.

Access to stable income, the technical support they pay for, and the possibility that more than 80% of producers access productive loans allow them to acquire technologies and invest in improvements to their farms and their family homes. However, part of the income does not address climate threats. In the case of producers who perceive a decrease in water and soil, monetary resources are not allocated to their conservation.

For producers with silvopastoral systems, income ranges between USD 350 and USD 500 per month. Of this income, 70% comes from the sale of milk and 30% from the sale of agricultural products they produce on their farms. Productive diversification in this case is widely used for animal management, since from the harvested corn crops, forages are obtained that are reserved for the months of less rainfall, and from the organic waste of the home and other crops, composting is carried out that serves as a fertilizer for the crops and improves soil conditions in areas of the property with greater erosion.

Ninety-five percent of these producers indicate that they have little dependence on chemical inputs, although they dedicate at least USD 20 per month to purchase inputs for tick control. However, they point out that they implement ecological measures to reduce the presence of these animals, such as planting bitter plants and rotating pastures. In terms of conservation, all respondents say that they implement strategies for reforestation of pastures and streams, fencing water sources to prevent the introduction of animals, and composting organic waste for fertilizer production for family crops and soil improvement. They also mention that some organizations and pasture foundations have contributed knowledge to promote conservation strategies; however, they point out that government entities do not provide any technical or environmental support.

Unlike conventional producers, all producers who develop silvopastoral arrangements claim to have observed changes in the behavior of climatic variables in the last 30 years, particularly associated with the increase in temperature and precipitation. For example, they point out that the years 1994, 2007, 2010, and 2022 were the rainiest, while 1997, 2013, and 2023 were the driest years. They also affirm that it was in these years that production decreased the most, diseases increased, and there were animal deaths. However, they mention that they do not have enough resources to face these problems; even if they receive income from the activity, it is not adequate to cover their livelihoods.

According to producers, two variables directly influenced production: temperature and precipitation. First, the increase in temperature generates weight loss due to heat stress, a decrease in milk production, an increase in pests, a decrease in water sources, a decrease in reproduction, and even the death of animals due to thirst. Second, increased rainfall affects fungal diseases and causes damage to the physical structures of buildings, loss of pasture due to waterlogging, and increased proliferation of bacteria and fungi. In addition, excess rainfall causes a reduction in milk production due to lower availability of pastures, since they rot due to the floods; and the soil deteriorates due to trampling. Similarly, production is affected by the energy expenditure of the animals because of the formation of mud, the occurrence of leg diseases, and the difficult transit to the milking points when the mud hardens. In this sense, two different types of impact on properties with silvopastoral arrangements exists.

- *Impacts on animal comfort*

Temperature is the variable that causes the greatest physiological reactions in cattle. Producers (silvopastoral) who recognize impacts point out that in El Niño years, animals can lose up to 50 kg due to food shortages and energy loss because of temperature regulation. According to the information obtained, although the climatic averages do not exceed 13 °C, during El Niño years, the temperature can increase up to 1 °C, which impacts

animals adapted to colder climates. According to the producers, although technically the Holstein and Norman breeds, predominant in the area, are resistant to the climate, when there are temperature increases, the animals become stressed, and milk production decreases. The stress is because animals, in addition to having very thick skin, have a coat that reduces perspiration. Impacts due to temperature are lower in properties with greater shade and greater presence of tree cover. In silvopastoral systems, more than 20% of the pasture area has trees that provide shade and reduce energy consumption for the animals' thermal regulation.

- *Impacts on the appearance of pests and diseases*

According to producers, during the summer, animals experience increased parasitism caused by ticks, which aggravates nutritional stress due to food deficit. Water scarcity also causes animals to concentrate on small water sources, which results in contamination with eggs or cysts, leading to severe clinical cases of parasitic diseases.

It is striking that producers with conventional systems do not explicitly mention climate impacts on their production. For these producers, reduced production, weakening of pastures, and decline and deterioration of water are associated with anthropogenic dynamics. For example, reduced production is associated with poor animal and pasture genetics; the worsening of pastures is associated with trampling and the limited knowledge that producers must carry out rotations; and the low availability of water is due to pollution and excessive use in other farms where tuber production is developed, where water demand is usually higher.

4.3. Vulnerability and Adaptation Strategies

- *Vulnerability*

The results allow us to point out that the changes in precipitation and temperature gave rise to various manifestations of vulnerability.

First, vulnerability increases due to limited access to diverse sources of income. The most vulnerable producers are those who depend exclusively on the income generated by livestock activity; however, most producers reduce their vulnerability by deriving income from various agricultural and non-agricultural activities. This occurs on properties with silvopastoral arrangements.

Second, the absence of physical capital (e.g., with drainage ditches and signaling) generates risks of landslides, all of which imply greater efforts by producers for almost any type of commerce, and they increase transportation costs. In the rainy season, all these tertiary roads with steep slopes are not passable.

Third, in terms of technological innovation, changes are minimal due to a lack of capital and also because of a limited institutional offer and support for accessing technology. This increases the vulnerability of producers because there is no evidence of cases of continuous technical assistance. Only one silvopastoral production program, led by a national NGO, was identified. Although it has not been assessed, the producers with silvopastoral arrangements considered that it contributed to improving the practices of production.

Finally, in relation to the membership of producers in social organizations, vulnerability increases in both cases due to a lack of stable organizations with the capacity for collective action. However, the existence of producer associations has increased their capacity for milk transformation, negotiation, and commercialization, hence contributing to the permanence of livestock activity and the families settled there. In the field of marketing, the production of conventional and silvopastoral farms aims at the same commercial spaces. No differences are present in terms of the organizational capacity of the activities.

The analysis of the 33 indicators proposed by Bergaminni [30] demonstrated an important level of vulnerability in the Rio Fonce (47.9%) and a low and medium response capacity in most of the indicators (Table 2).

Table 2. List of indicators to estimate adaptative capacities with vulnerability elements.

Indicators	Variables	S1	S2	S3	S4	S5	C6	C7	C8	C9	C10
Landscape	Landscape diversity										
	Slope										
	Proximity to forests and protected areas										
	Live fences and windbreaks										
	Proximity to water sources										
Production systems	Diversity of productive systems										
	Practices of conservation of forest and water										
	Drains (channels and ditches)										
	Use of water technologies										
	Self-consumption of products generated at the farm										
	Farm infrastructure										
	Pasture rotation										
	Variety of breeds										
	Variety of grasses										
	Soil fertility										
	Rainwater harvesting practices										
	Practices to increase soil organic matter										
	Sustanaible management of weeds and practices										
Local knowledge	Seed selection of grasses resistant to dryness and humidity										
	Use of breeds tolerant to dryness and humidity										
	Water conservation practices										
	Use of climatic indicators										
	Strategies for prevention of drying										
	Strategies for prevention of rain										
	Inherited technologies										
	Possibility of generational relief										
Institutions and social networks	Facilitation of interchange of local cooperation and knowledge										
	Support from institutions to productive systems										
	Participation in organizations										
Gender	Women involved in decision-making in the productive systems										
	Women's access to resources and employment opportunities										
Infrastructure	Knowledge of management of productive systems										
	Contribution of infrastructure of productive systems (roads, schools and services)										

In this table, each column corresponds to a farm as a sample to determine vulnerability level; the column with word S corresponds to conventional systems of livestock, and columns with word C correspond to farms with silvopastoral arrangements. Colors represent vulnerability level: red: high vulnerability; yellow: medium vulnerability; green: low vulnerability.

In general terms, the results show limited capacity to respond to climate variability, especially noticeable in the indicators associated with the practices of the production systems and the strategies for the prevention of impacts of rain and drought. Although

silvopastoral systems are present in the territory, the limited climate activities developed on these farms aim at improving production under a conservation model.

However, indicators of landscape, knowledge, institutions and social networks, gender, and infrastructure showed an average response capacity, meaning that in the midst of conditions of vulnerability there is some knowledge associated with climate management and collective work in silvopastoral properties that can lead to actions aimed at improving productivity and responding better in the long term to events of climate variability.

- *Adaptation strategies*

The results show a total of 19 adaptive practices associated with elements of production, associativity, income diversification, and conservation of natural resources for use in livestock activity, given the influence and investment of some environmental projects. Producers implement these practices exclusively on farms with silvopastoral arrangements.

In general terms, more than half of the identified practices (13) are associated with activities to conserve production and indirectly reduce climate impacts. To start with, there have been improvements in cleaning, planting, and pasture rotation, as well as enhancements to watering troughs, the procurement of pasture, animal feed, vitamins, and salts; second, activities have been implemented to prevent and cure diseases through vaccination, deworming, and baths against ticks and flies; and third, there are practices of genetic improvement through artificial insemination. In addition, strategies for reducing production costs and achieving market access were identified. These include forming partnerships with local environmental and territorial organizations focused on soil and water conservation, as well as diversifying income streams through tourism (Table 3).

Table 3. Adaptation strategies common in Upper Rio Fonce region.

Climate Variable	Strategies	Effect
Temperature increase	Planting trees and living fences to create shady spaces	Reduce the impact of heat stress and weight loss of the animal
	Purchase and transport of grass	Maintain a balance in the weight of the animal and quality in the production of milk and meat
	Rent of farms with pastures in higher elevations	
	Increase in the dose of salt and vitamins	Prevent fluid retention and increase nutrients in the diet to improve the quality of meat and milk
	Greater frequency of cattle sales in critical periods of El Niño	Reduce costs generated by the maintenance of animals
	Genetic improvement	Increase productivity and find breeds more resistant to the weather
	Increase in the application of medicines and vitamins	Disease and fungus reduction
	Purchase of concentrates	Improve diet and avoid weight loss
	Periodic baths	Reduce infection by ticks and flies
	Search for activities to diversify income	Improve income and maintain livelihoods
	Technical assistance (private not certified service)	Improvement in knowledge aimed at increasing productivity
Precipitation rise	Purchase and transport of grass	Maintain the diet of the animal in the face of a shortage of pasture generated by waterlogging and trampling
	Construction of trenches and drains	Avoid creation of ponds in paddocks
	Increase in the purchase of vitamins, salt, and molasses	Provision of dietary vitamins, minerals and energy
	Greater frequency of cattle sales in critical periods of La Niña	Avoid financial losses
	Increase in the purchase of supplements and concentrates	Maintain the animal's diet and reduce weight loss
	Construction of water points, avoiding entrance of cattle into the water source	Conserve water sources
	Strengthening of associativity	Continuous sale of milk
	Animal deworming	Prevention against parasites generated by contaminated water

Evidence shows that 80% of the practices recognized as adaptations are unplanned interventions designed to cope with climate variability.

4.4. Policy Analysis: Conceptual Approach and Institutional Information Review

The development of the concept of adaptation represents one of the most important efforts at the level of public policy and international cooperation during the last 30 years [1].

Furthermore, adaptation has generally prevailed, aimed at incremental changes in the economy by reducing risk exposure, control, and vulnerability and improving resilience [1,32,33]. This emphasis has not made it possible to address adaptation as a strategy for promoting effective transformation of production systems based on understanding and assembling them as complex systems in constant coevolution with nature.

Failures for understanding and using the concept in the policy realm and limitations for its application in the producer realm are related to limitations that arise from worldviews and myths about the society–nature relationship, rooted in politics and public institutions. Each myth leads to different assumptions about adaptations and consequently leads to different types of policies and producer activities that are considered the most appropriate. Table 3 classifies the predominant ways of understanding and using the concept, the consequences of planning, and the way they are addressed in Colombian public policies.

Table 3 also shows the emphasis of the Colombian Institutional Framework on defining adaptation as a reactive and disaster preventive capacity, including elements of the following:

(1) Direct adaptation: mitigating potential impacts of vulnerable groups (capacity-building people and systems, social protection measures, insurance to reduce potential adverse effects);
(2) Balanced adaptation: preparation for emergency responses (establishment of alert systems, contingency plans, construction of shelters, stocks of food reserves, medicines, and essential materials);
(3) Balanced adaptation: response to the crisis that includes the humanitarian measures necessary to meet the basic needs of the affected population;
(4) Resilient adaptation: recovery, rehabilitation, and reconstruction with measures that help overcome the emergency, focused on the recovery of livelihoods and the reorganization of basic public services.

The typology offered in Table 4 allows the identification of five central arguments that are used later as an interpretive framework:

1. The concept of adaptation reflects a predominant trend, both from academia and from public institutions, that promotes reactive actions aimed at reducing risk and damage caused by climatic events and to enable the continuity of economic growth [34–36]. Little has been written about the structural factors that determine adaptation, as well as the strategies that human groups develop to face these changes and develop possible forms of adaptation that allow for a transformation of the current situation in the Andes [37,38].

2. This concern has prompted the creation of various definitions and ways of using the concept, although they are mainly focused on aspects relating to risk and disaster response [39–41] that restrict a broader application of the concept within the framework of public policy and in particular in the field of adaptation to high Andean ecosystems where there is little information on the strategies and factors that influence adaptation [42].

3. Although a tendency towards analysis was identified in politics, recognizing the importance of reducing vulnerability was identified, which is mainly attributed to the set of threats that come from biophysical external drivers. This aspect limits an understanding of the set of endogenous elements affecting production systems and livelihoods in the Andes, as well as the combination of the characteristics of actors, individuals, households, and communities, expressed in relation to exposure to a threat derived from their own social, cultural, and economic conditions [32].

4. Recently, there has been a shift in public policy and international cooperation towards the need to improve understanding of human groups' adaptations to climate variability with a focus on resilience [42]. This approach has not been developed in adaptation policies and practice, since it presents an important challenge in the Andes related to the need to understand the impacts of climate phenomena and hence the totality

of relationships, dynamics, and interactions that occur between ecological and social systems and that facilitate adaptation as well as planning as a fundamental aspect of long-term adaptation [43].

5. Finally, it is worth noting that the literature regarding adaptation in páramo ecosystems is still limited. There is a large body of literature relating to the importance of conserving this ecosystem, as well as a reduction of impacts generated by mining and agricultural activities [44–47]; however, not enough studies have been identified to show the adaptation strategies of agricultural producers in these systems, much less how these activities would contribute to sustainable production [42].

6. As illustrated in Table 4, definitions of adaptation and their inclusion in current adaptation policies are diverse and chaotic and follow mental models of nature, deeply rooted in the environmental policy realm. This presents an important challenge for conciliating this diversity of approaches and creates an Andean consensus on the climate question, its regional manifestation, and its sustainment in the social-ecological realities of the Andes.

Table 4. Definitions on adaptation and forms of application identified in the literature and their use in the Colombian Institutional Framework.

Concept	Definition	Characteristics	Type of Planning	Scale and Temporal Level	Colombian Institutional Framework
Direct adaptation	Adjustment of human or natural systems to new or changing environments [1,48].	Reduce risks and control vulnerabilities	Static and reactive. Reaction when shock occurs.	Closed systems. Sectoral interventions on micro and medium-term scales.	Ley 1972 of 2019 Ley 1931 of 2018 Ley 1844 of 2017 Ley 1776 of 2016 Ley 629 of 2000 Ley 164 of 1994
Anarchic adaptation	Minimal system adjustments due to minimal system demands [36].	Maintain the balance of the system	Static and caution. It reacts when a shock occurs.	Closed systems without intervention	It is not directly included in Colombian regulations
Balanced adaptation	Gradual adjustments in daily practices made by human systems [35].	Maintain the essence and integrity of what exists.	Static and reactive. It reacts when a shock occurs.	Open systems.	National Adaptation Plan, 2014
Resilient adaptation	Capacity of a social or ecological system to absorb disturbances, maintaining the basic structure and modes of operation [49].	Manage the transformation of systems by increasing absorption and adaptive capacities.	Dynamic and flexible. Adaptive planning with principles aimed at prevention	Sectoral interventions at micro and short-term scales. Open systems. Inclusive approach that integrates actions at the local, national, regional, and global levels, in the short, medium, and long term.	Law 1931 of 2018 Climate resilience strategy E2050, 2021
Co-evolutionary adaptation	Capacity of complex systems to learn and respond to disturbances under uncertainty scenarios [50,51].	Manage uncertainty	Dynamic and flexible	Open and multi-scale systems	Not directly included in the regulations

Source: Typology elaborated from [34–36,38,49,51].

5. Discussion

This study confirms that livestock production systems under conventional arrangements in the Upper Fonce River are more vulnerable than silvopastoral systems, like Peri and colleagues mention [52] regarding the current state of the silvopastoral systems in Latin America, finding that these systems are more resilient because of their adaptative capacity. This is because traditional producers do not develop adaptation strategies, nor do they recognize the impacts of these phenomena. In the case of silvopastoral systems, results indicate that although limited, farmers develop adaptation innovations to improve pastures, protect water, and maintain production. Likewise, producers recognize the existence of climate variability, its impacts, and the need to continue promoting their systems, as Kargbo and colleagues mention as well [53]. In this case, silvopastoral livestock have better capacities to adapt to páramo ecosystems and utilize tools to conserve natural resources [4,5,54].

Despite the benefits of silvopastoral systems, Ramírez-Gómez and colleagues [54], argue that evaluating different livestock production systems is not enough, and the adoption of practices and technologies that make livestock farming a sustainable activity in sensitive ecosystems such as the páramo is needed. Three strategies are crucial for livestock management in páramo areas: pasture management, water resource management, and animal production management, which coincide with the practices of adaptation to climate change identified in our study. Nevertheless, these adaptation strategies must be complemented by other complex studies to monitor climate and biodiversity. This will allow for making decisions and strategies to guarantee the development of the livelihoods of small livestock producers and farmers and the maintenance of the ecosystem services provided by the páramo [37,55,56].

In terms of public policy, there is a divergence of conceptual definitions that prevents specific adaptation actions from materializing in strategic ecosystems [57]. Currently, politics promotes actions that ignore three aspects: (1) threats and their frequency and intensity; (2) territorial planning and its determinants of land use; and (3) the exogenous and endogenous elements that determine the system's vulnerability and limit adaptation [58–60]. If the concept of adaptation were approached from a multilevel perspective through public policy discussions at the national and regional levels, it would be necessary to move from the linear and static consideration of adaptation as an end and advance in the understanding of the processes and dynamics carried out by producers to co-evolve with nature and adapt in the biogeographic regions of the páramo.

In the Alto Río Fonce, practices identified in silvopastoral systems coincide with official strategies designed for the sustainable development and conservation of the high Andean paramos and forests. These practices are based on previous ideas to reduce environmental impacts, protect water sources and soil, and increase the economic and social choices of inhabitants. However, these are not preventive or anticipatory. In general, response strategies do not align with the definitions of early adaptation suggested by Colombian policies [60].

The final highlighted element is the policy scarcity adaptation of practices in training, communication, and rural non-livestock activities, such as tourism and other economic services. These practices correspond to adaptations that promote good management of the high Andean Forest. However, in this research, given the incipient level of development in the study area, the communities did not prioritize these activities. Practices such as strengthening human capital, communication, and social organization have obvious benefits; however, they do not have a direct impact on the conservation of ecosystems or adaptation to climate change.

6. Conclusions

This research confirms the existence of interannual climate variability phenomena in the analyzed area, as well as intensified changes in these climatic variables in a period not exceeding 50 years. The observed temperature increased by up to 1.3 °C in the study area. These data confirm that climate variability negatively affects livestock production, with direct impacts on milk and meat production due to a decrease in pasture and water, an increase in pests and diseases, and a decline in conditions that ensure animal well-being.

Small livestock producers are increasingly aware of how climate variability affects livestock production, and their main response focuses on maintaining productivity. However, this awareness and response primarily occur on farms that utilize silvopastoral arrangements. In contrast, farmers operating under conventional systems often do not recognize the impacts of climate variability or identify any adaptation strategies.

Overall, production systems are currently at a critical vulnerability level that hampers their ability to effectively respond to climate challenges. This vulnerability arises from many factors, including weak infrastructure, limited household income, lack of technological innovation, and poorly developed organizations and social networks.

Regarding their response capacity, the identified strategies tend to be reactive, aimed at mitigating the effects and risks posed by climate variability on agricultural activities and the sustainability of livelihoods. Unfortunately, these strategies do not involve initiative-taking adaptive actions, which are necessary for effective planning and prevention regarding the examined climate variables.

We conclude that the lack of knowledge regarding the experiences and research related to the adaptation of small livestock production systems to climate variability has hindered the development of effective measures and strategies for managing páramo ecosystems across the country. Therefore, it is essential to allocate resources to science and technology to deepen the analysis of these variables and identify tailored management strategies.

Generating new knowledge is crucial, but it must be approached within a framework that connects science with public policies and the daily practices of high Andean livestock. This approach will facilitate a co-evolutionary process of transformed adaptation, considering not only the necessary social and biophysical conditions but also the capacity of local actors to integrate them.

Author Contributions: Conceptualization, V.-E.G.-S. and C.E.O.-G.; methodology, V.-E.G.-S. and C.E.O.-G.; formal analysis, V.-E.G.-S. and C.E.O.-G.; investigation, V.-E.G.-S. and C.E.O.-G.; resources, Helvetas Foundation.; writing—original draft preparation, V.-E.G.-S.; writing—review and editing, V.-E.G.-S., C.E.O.-G. and E.C.S.; visualization, E.C.S.; project administration, Facultad de Estudios Ambientales y Rurales, Pontificia Universidad Javeriana.; funding acquisition, C.E.O.-G. All authors have read and agreed to the published version of the manuscript.

Funding: This research was funded by the Helvetas Foundation and the Pontificia Universidad Javeriana. grant number: 00020115.

Data Availability Statement: The data presented in this study are available on request from the corresponding author due to privacy reasons.

Acknowledgments: We thank the Pontificia Universidad Javeriana, the producers, and local organizations for providing information and supporting us in the field work.

Conflicts of Interest: The authors declare no conflicts of interest.

References

1. IPCC. *Climate Change 2014: Synthesis Report. Contribution of Working Groups I, II and III to the Fifth Assessment Report of the Intergovernmental Panel on Climate Change*; Core Writing Team, Pachauri, R.K., Meyer, L.A., Eds.; IPCC: Geneva, Switzerland, 2014; p. 151.
2. IDEAM-UNAL. *Variabilidad Climática y Cambio Climático en Colombia*; IDEAM: Bogotá, Colombia, 2018.
3. Cheng, M.; McCarl, B.; Fei, C. Climate Change and Livestock Production: A Literature Review. *Atmosphere* **2022**, *13*, 140. [CrossRef]
4. Thornton, P.K. Livestock Production: Recent Trends, Future Prospects. *Philos. Trans. R. Soc. B Biol. Sci.* **2010**, *365*, 2853–2867. [CrossRef] [PubMed]
5. Rojas-Downing, M.M.; Nejadhashemi, A.P.; Harrigan, T.; Woznicki, S.A. Climate Change and Livestock: Impacts, Adaptation, and Mitigation. *Clim. Risk Manag.* **2017**, *16*, 145–163. [CrossRef]
6. Silanikove, N. Effects of Heat Stress on the Welfare of Extensively Managed Domestic Ruminants. *Livest. Prod. Sci.* **2000**, *67*, 1–18. [CrossRef]
7. Schauberger, G.; Mikovits, C.; Zollitsch, W.; Hörtenhuber, S.J.; Baumgartner, J.; Niebuhr, K.; Piringer, M.; Knauder, W.; Anders, I.; Andre, K.; et al. Global Warming Impact on Confined Livestock in Buildings: Efficacy of Adaptation Measures to Reduce Heat Stress for Growing-Fattening Pigs. *Clim. Change* **2019**, *156*, 567–587. [CrossRef]

8. Singh, S.V.; Naskar, S. Adaptation and Mitigation Strategies for Sustained Livestock Production under Changing Climatic Scenario. *J. Agrometeorol.* **2019**, *21*, 14–26.
9. Berkhout, F.; Dow, K.; Thomas, A. Delayed, Abrupt and Unjust: An Institutionalist Perspective on Limits to Climate Change Adaptation. *Clim. Risk Manag.* **2024**, *44*, 100611. [CrossRef]
10. González-M., R.; Posada, J.M.; Carmona, C.P.; Garzón, F.; Salinas, V.; Idárraga-Piedrahita, Á.; Pizano, C.; Avella, A.; López-Camacho, R.; Norden, N.; et al. Diverging Functional Strategies but High Sensitivity to an Extreme Drought in Tropical Dry Forests. *Ecol. Lett.* **2021**, *24*, 451–463. [CrossRef]
11. Postigo, J.C.; Guáqueta-Solórzano, V.-E.; Castañeda, E.; Ortiz-Guerrero, C.E. Adaptive Responses and Resilience of Small Livestock Producers to Climate Variability in the Cruz Verde-Sumapaz Páramo, Colombia. *Land* **2024**, *13*, 499. [CrossRef]
12. Alves, B.J.R.; Madari, B.E.; Boddey, R.M. Integrated Crop–Livestock–Forestry Systems: Prospects for a Sustainable Agricultural Intensification. *Nutr. Cycl. Agroecosystems* **2017**, *108*, 1–4. [CrossRef]
13. PNGRD. *Una Estrategia de Desarrollo 2015–2025*; Sexto informe de seguimiento y evaluación; Unidad Nacional para la Gestión del Riesgo de Desastres: Bogotá, Colombia, 2019. Available online: https://portal.gestiondelriesgo.gov.co/Documents/PNGRD/PNGRD_Informe6_v1.pdf (accessed on 11 February 2025).
14. FEDEGAN. *Ganadería Colombiana Hoja de Ruta 2018–2022*; FEDEGAN: Bogotá, Colombia, 2018; pp. 17–101. Available online: https://consejoderedaccion.org/webs/CdRLab_Periodismo_de_soluciones_para_cubrir_la_deforestacion/Modulo03/Hoja_de_ruta_Fedegan.pdf (accessed on 20 January 2025).
15. FEDEGAN. *Introducción Balance y Perspectivas del Sector Ganadero Colombiano Mercado de la Leche Producción de Leche*; FEDEGAN: Bogotá, Colombia, 2023.
16. FEDEGAN. *Balance y Perspectivas del Sector Ganadero Colombiano 2024–2025*; FEDEGAN: Bogotá, Colombia, 2024.
17. Instituto de Hidrología, Meteorología y Estudios Ambientales—IDEAM. *Escenarios de Cambio Climático de la Cuarta Comunicación de Colombia*; IDEAM: Bogotá, Colombia, 2021.
18. Ministerio de Ambiente y Desarrollo Sostenible. *Política Nacional de Cambio Climático*; Ministerio de Ambiente y Desarrollo Sostenible: Bogotá, Colombia, 2017.
19. Bernal Morales, R.; Hernández, M. de los Ã. V.; Acoltzi, T.M.; Vázquez, M.H.; Flores, S.O.; López, J.J. Impacto de la variabilidad climática en la agricultura de temporal en el estado de Tlaxcala, México. *Agric. Soc. Desarro.* **2020**, *17*, 713–733. [CrossRef]
20. DNP; BID. *Impactos Económicos del Cambio Climático en Colombia-Síntesis*; DNP: Bogotá, Colombia, 2014.
21. Gonzalez Diez, V.M.; Verner, D.; Corrales, M.E.; Puerta, J.M.; Mendieta Umaña, M.P.; Morales, C.; Suárea, D.; Linares, A.M.; Scholl, L.; Quintanilla, O.; et al. *Climate Change at the IDB: Building Resilience and Reducing Emissions | Publicaciones*; Inter-American Development Bank: Washington, DC, USA, 2014. Available online: https://publications.iadb.org/es/publications/english/viewer/Climate-Change-at-the-IDB-Building-Resilience-and-Reducing-Emissions.pdf (accessed on 30 January 2025).
22. Vergara-Buitrago, P.A. Estrategias implementadas por el Sistema Nacional de Áreas Protegidas de Colombia para conservar los páramo s. *Rev. Cienc. Ambient.* **2020**, *54*, 167–176. [CrossRef]
23. Díaz-Acevedo, C.J.D.; Romero-Alarcon, L.V.; Miranda-Esquivel, D.R. Páramo s Neotropicales como unidades biogeográficas. *Rev. Biol. Trop.* **2020**, *68*, 503–516. [CrossRef]
24. Afanador, J. A Formal Critique of the Value of the Colombian Páramo. *arXiv* **2020**. [CrossRef]
25. Olaya-Angarita, J.A.; Díaz-Pérez, C.N.; Morales-Puentes, M.E. Composición y estructura de la transición bosque-páramo en el corredor Guantiva-La Rusia (Colombia). *Rev. Biol. Trop.* **2019**, *67*, 755–768. [CrossRef]
26. Gutiérrez-Salazar, P.; Medrano-Vizcaíno, P. The effects of climate change on decomposition processes in andean paramo ecosystem–synthesis, a systematic review. *Appl. Ecol. Environ. Res.* **2019**, *17*, 4957–4970. [CrossRef]
27. Osejo, A.; Amador Moncada, J.; Ungar, P.; Hernández-Manrique, O.L. Habitar el Páramo | Biodiversidad 2018. Available online: https://reporte.humboldt.org.co/biodiversidad/2018/cap4/402/ (accessed on 15 March 2025).
28. Babbie, E.R. *The Practice of Social Research*, 13th ed.; Wadsworth Cengage Learning; Cengage AU: Southbank, Australia, 2020.
29. Yin, R. *Case Study Research: Design and Methods. Applied Social Research Methods Series*; SAGE Publishing: Washington, DC, USA, 1994; pp. 19–116.
30. Bergamini, N.; Blasiak, R.; Eyzaguirre, P.B. *Indicators of Resilience in Socio-Ecological Production Landscapes (SEPLs)*; United Nations University Institute of Advanced Studies: Yokohama, Japan, 2013.
31. Clemence, A.; Doise, W.; Lorenzi-Cioldi, F. *The Quantitative Analysis of Social Representations*; Routledge: London, UK, 2014. [CrossRef]
32. Adger, N.; Arnell, N.W.; Tompkins, E.L. Successful Adaptation to Climate Change across Scales. *Glob. Environ. Change* **2005**, *15*, 77–86. [CrossRef]
33. Smit, B.; Wandel, J. Adaptation, Adaptive Capacity and Vulnerability. *Glob. Environ. Change* **2006**, *16*, 282–292. [CrossRef]

34. Lavell, A.; Oppenheimer, M.; Diop, C.; Hess, J.; Lempert, R.; Li, J.; Muir-Wood, R.; Myeong, S.; Moser, S.; Takeuchi, K.; et al. Climate Change: New Dimensions in Disaster Risk, Exposure, Vulnerability, and Resilience. In *Managing the Risks of Extreme Events and Disasters to Advance Climate Change Adaptation*; Field, C.B., Barros, V., Stocker, T.F., Dahe, Q., Eds.; Cambridge University Press: Cambridge, UK, 2012; pp. 25–64. [CrossRef]
35. Settele, J.; Scholes; Betts, R.; Bunn, S.; Leadley, P.; Nepstad, D.; Overpeck, J.T.; Taboada, M.A. Terrestrial and Inland Water Systems. In *Climate Change 2014: Impacts, Adaptation, and Vulnerability. Part A: Global and Sectoral Aspects*; Cambridge University Press: Cambridge, UK, 2014.
36. Walker, B.; Carpenter, S.; Anderies, J.; Abel, N.; Cumming, G.; Janssen, M.; Lebel, L.; Norberg, J.; Peterson, G.; Pritchard, R. Resilience Management in Social-Ecological Systems: A Working Hypothesis for a Participatory Approach. *Conserv. Ecol.* **2002**, *6*, 14. [CrossRef]
37. Ballesteros, J.; Isaza, C. Adaptation Measures to Climate Change as Perceived by Smallholder Farmers in the Andes. *J. Ethnobiol.* **2021**, *41*, 428–446. [CrossRef]
38. Park, S.E.; Marshall, N.A.; Jakku, E.; Dowd, A.M.; Howden, S.M.; Mendham, E.; Fleming, A. Informing Adaptation Responses to Climate Change through Theories of Transformation. *Glob. Environ. Change* **2012**, *22*, 115–126. [CrossRef]
39. ISDR. *Living with Risk: A Global Review of Disaster Reduction Initiatives*; International Strategy for Disaster Reduction, Ed.; United Nations: New York, NY, USA; Geneva, Switzerland, 2004.
40. Mechler, R.; Mochizuki, J.; Hochrainer-Stigler, S. *Disaster Risk Management and Fiscal Policy: Narratives, Tools, and Evidence Associated with Assessing Fiscal Risk and Building Resilience*; World Bank: Washington, DC, USA, 2016. [CrossRef]
41. Thomalla, F.; Downing, T.; Spanger-Siegfried, E.; Han, G.; Rockström, J. Reducing Hazard Vulnerability: Towards a common approach between disaster risk reduction and climate adaptation. *Disasters* **2006**, *30*, 39–48. [CrossRef] [PubMed]
42. UICN. *REDD-Plus: Alcance y Opciones para el Papel de los Bosques en las Estrategias de Mitigación al Cambio Climático*; Unión Internacional para la Conservación de la Naturaleza (UICN): Washington, DC, USA, 2015.
43. Gallopín, G.C. Linkages between Vulnerability, Resilience, and Adaptive Capacity. *Glob. Environ. Change* **2006**, *16*, 293–303. [CrossRef]
44. GTP. *Páramo 21: Investigaciones Biofísicas en el Páramo*; Órgano de difusión del Grupo de Trabajo en Páramo s del Ecuador (GTP): Quito, Ecuador, 2006.
45. Herzog, S.; Martínez, R.; Jørgensen, P.M.; Tiessen, H. *Climate Change and Biodiversity in the Tropical Andes*; Inter-American Institute for Global Change Research (IAI); Scientific Committee on Problems of the Environment: Delft, The Netherlands, 2011.
46. Mena-Vásconez, P.; Medina, G.; Hofstede, R. *Los Páramo s del Ecuador. Particularidades, Problemas y Perspectivas*; USFQ PRESS: Quito, Ecuador, 2023.
47. López, E.I. *El Cambio Climático y la Gestión de Páramo s*; Documento preparado para el Foro Nacional de los Recursos Hídricos; CAMAREN/AVSF, Agrónomos y Veterinarios: Quito, Ecuador, 2012.
48. Tompkins, E.L.; Adger, W.N.; Boyd, E.; Nicholson-Cole, S.; Weatherhead, K.; Arnell, N. Observed Adaptation to Climate Change: UK Evidence of Transition to a Well-Adapting Society. *Glob. Environ. Change* **2010**, *20*, 627–635. [CrossRef]
49. Gunderson, L.H.; Holling, C.S.; Ludwig, D. *Panarchy: Understanding Transformations in Human and Natural Systems*; Island Press: Washington, DC, USA, 2002.
50. Gunderson, L.H.; Holling, C.S.; Light, S.S. (Eds.) *Barriers and Bridges to the Renewal of Ecosystems and Institutions*; Columbia University Press: New York, NY, USA, 1996; pp. 553–587, ISBN 0-231-10102-3.
51. Berkes, F.; Ross, H. Panarchy and Community Resilience: Sustainability Science and Policy Implications. *Environ. Sci. Policy* **2016**, *61*, 185–193. [CrossRef]
52. Peri, P.L.; Chará, J.; Viñoles, C.; Bussoni, A.; Cubbage, F. Current Trends in Silvopastoral Systems. *Agrofor. Syst.* **2024**, *98*, 1945–1953. [CrossRef]
53. Kargbo, A.; Jawo, E.; Amoutchi, A.I.; Ndow, M.; Bojang, A.; Zainabou, D.; Kumah, F.J.A.; Koua, H.K.; Kuye, R. Perceptions and Impacts of Climate Variability on Livestock Farming in The Gambia. *J. Appl. Anim. Res.* **2023**, *51*, 366–374. [CrossRef]
54. Ramírez-Gómez, C.J.; García-Cuervo, A.; Rodriguez-Espinosa, H. The Adoption of Sustainable Practices in Livestock Production Systems in Tropical Andean Páramo s. *Front. Sustain. Food Syst.* **2025**, *8*, 1461713. [CrossRef]
55. Cresso, M.; Clerici, N.; Sanchez, A.; Jaramillo, F. Future Climate Change Renders Unsuitable Conditions for Paramo Ecosystems in Colombia. *Sustainability* **2020**, *12*, 8373. [CrossRef]
56. Valencia, J.B.; Mesa, J.; León, J.G.; Madriñán, S.; Cortés, A.J. Climate Vulnerability Assessment of the Espeletia Complex on Páramo Sky Islands in the Northern Andes. *Front. Ecol. Evol.* **2020**, *8*, 565708. [CrossRef]
57. Chará-Serna, A.M.; Chará, J.; Giraldo, L.P.; Castaño-Quintana, K. Effect of Silvopastoral Systems on Biodiversity and the Provision of Environmental Services in Tropical Agro-Landscapes. In *Silvopastoral Systems of Meso America and Northern South America*; Chará, J., Jose, S., Eds.; Springer International Publishing: Cham, Swizerland, 2023; pp. 85–104. [CrossRef]
58. Birchall, S.J.; Bonnett, N. Climate Change Adaptation Policy and Practice: The Role of Agents, Institutions and Systems. *Cities* **2021**, *108*, 103001. [CrossRef]

59. Suprayitno, D.; Iskandar, S.; Dahurandi, K.; Hendarto, T.; Rumambi, F.J. Public Policy in The Era of Climate Change: Adapting Strategies for Sustainable Futures. *Migr. Lett.* **2024**, *21*, 945–958.
60. Ocampo, K. *Retos Asociados al Uso del Suelo: El Dilema Entre Conservación y Producción en los Bosques Andinos de Robles del Corredor Ecológico Guantiva-La Rusia-Iguaque (Challenges Associated to Land Use: The Trade-Off Between Conservation and Production on the Andean Oak Forests in the Ecological Corridor Guantiva-LaRusia-Iguaque)*; Social Science Research Network: Rochester, NY, USA, 2018. [CrossRef]

Disclaimer/Publisher's Note: The statements, opinions and data contained in all publications are solely those of the individual author(s) and contributor(s) and not of MDPI and/or the editor(s). MDPI and/or the editor(s) disclaim responsibility for any injury to people or property resulting from any ideas, methods, instructions or products referred to in the content.

land

MDPI

Article

A Framework for Multifunctional Green Infrastructure Planning Based on Ecosystem Service Synergy/Trade-Off Analysis: Application in the Qinling–Daba Mountain Area

Mingjie Song [1], Shicheng Li [2,*], Basanta Paudel [3,4] and Fangjie Pan [5]

[1] College of Public Administration, Central China Normal University, Wuhan 430079, China; smingjie@ccnu.edu.cn
[2] Department of Land Resource Management, School of Public Administration, China University of Geosciences, Wuhan 430074, China
[3] Southasia Institute of Advanced Studies, Kathmandu 44600, Nepal; basanta@sias-southasia.org
[4] Nepal Mountain Academy, Tribhuvan University, Kathmandu 44613, Nepal
[5] School of Management, Wuhan Institute of Technology, Wuhan 430205, China; panfangjie@wit.edu.cn
* Correspondence: lisc@cug.edu.cn

Abstract: The multifunctionality of green infrastructure (GI) can be enhanced through intentional planning that promotes synergies among various functions while minimizing trade-offs. Despite its significance, methodologies for implementing this approach remain underexplored. This paper presents an application-oriented framework for GI planning that emphasizes the relationship between GI functional performance and the provision of ecosystem services. By reframing the issues of multifunctional synergies and trade-offs as quantifiable and spatially explicit problems associated with ecosystem services, the framework offers both a conceptual foundation and technical protocols for practical application. This framework was implemented in the Qinling–Daba Mountain Area (QDMB) in China to evaluate its practicality and identify potential challenges. The planned GI system aims to fulfill multiple functions, including biodiversity maintenance, water and soil conservation, eco-farming, and ecotourism development. Additionally, 73 wildlife corridors were established to connect GI elements, thereby enhancing habitat services for biodiversity. Furthermore, the analysis identified 245 townships and 273 sites as strategic areas and points requiring targeted intervention to mitigate potential multifunctional trade-offs. These locations are characterized by their location within protected areas, protected buffer zones, or wildlife corridors, or at the intersection of wildlife corridors with existing transportation infrastructure. The findings validate the framework's practicality and highlight the necessity for additional research into the capacity of GI to support diverse human activities and the approaches to enhance GI elements' connectivity for multifunctionality.

Keywords: nature-based development; ecosystem services; natural and semi-natural assets; mountainous region

1. Introduction

Green infrastructure (GI) has emerged as a widely adopted planning approach to guide spatial development for sustainability since the 1990s [1,2]. Both the World Bank and the Intergovernmental Panel on Climate Change (IPCC) recognize the important role of GI in enhancing urban and rural resilience to climate change [3,4]. The European Union promotes GI as a key strategy to achieve its 2030 biodiversity targets. Many European countries and cities have adopted GI solutions in response to climate change and environmental

degradation, recognizing benefits such as increased resilience to floods and urban heat, improved air and water quality [5]. In the United States, the Environmental Protection Agency (EPA) emphasizes efforts at the federal and state levels to integrate green infrastructure into stormwater management, urban planning, and climate resilience initiatives. The EPA also provides various toolkits to support the planning and implementation of green infrastructure for multiple objectives [6].

The European Commission defines GI as a network of natural and semi-natural areas, features, and green spaces that can be found in urban, rural, terrestrial, freshwater, marine, and coastal environments [5]. This network includes individual GI elements and the corridors that connect them. As a result, the terms "GI system" and "GI network" are often used interchangeably with GI. In addition, related terms such as natural infrastructure, nature-based solutions, nature-based climate solutions, and low-impact development are frequently used in similar contexts [2]. However, these concepts differ in important ways from GI. Unlike approaches that focus on specific asset types, GI encompasses natural, semi-natural (enhanced), and engineered systems, providing a comprehensive framework for integrating diverse asset types (see Figure 1).

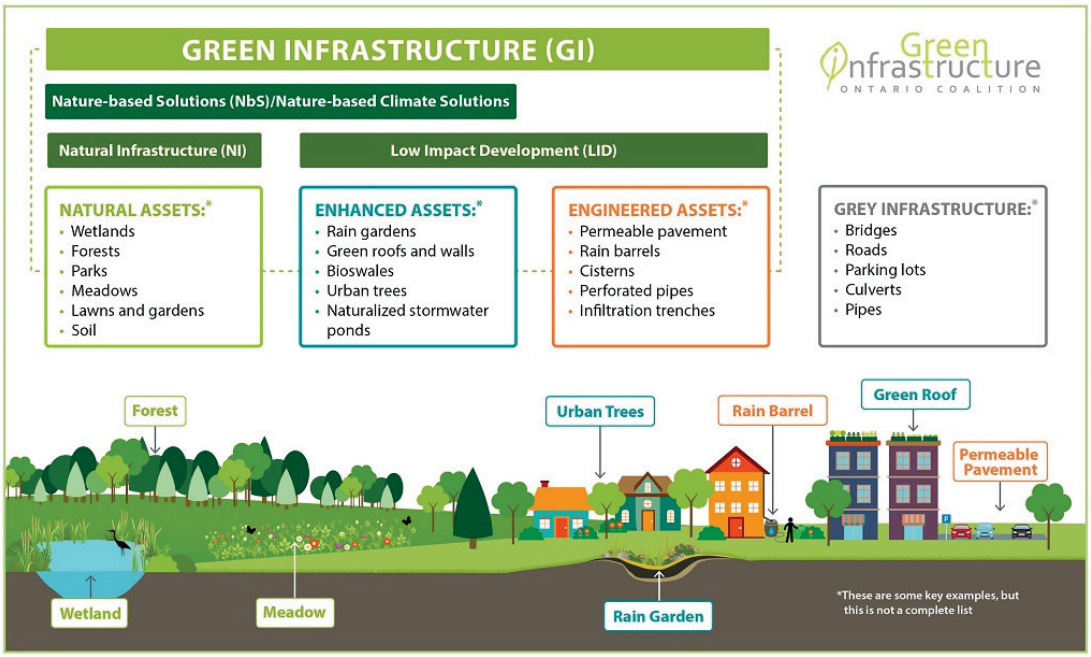

Figure 1. The differences between green infrastructure and other nature-based development approaches. Source: https://greeninfrastructureontario.org/what-is-green-infrastructure/ (accessed on 4 June 2025).

Early GI planning programs primarily emphasized their ecological function in biodiversity conservation; however, the recognition of GI's potential to fulfill multiple functions has gradually increased. These functions encompass biodiversity conservation, the promotion of human health and well-being, climate change mitigation and adaptation, soil and water conservation, food production, and support for the development of a green economy [7–11]. Despite two decades of discussion, the multifunctional potential of GI is often assessed only after GI elements are installed, rather than being adequately considered during the planning, design, and construction phases. Intentional planning and design for the multifunctionality of GI systems remain challenging [8,12–14].

Encouragingly, a growing body of research is dedicated to addressing this issue from various perspectives. For instance, Hansen and Pauleit [13] propose a social–ecological framework for assessing GI multifunctionality, focusing on the relationships between

ecosystem service (ES) supply, demand, and GI function. McPhearson et al. [15] advocate for proactive and systematic approaches to coordinate the various entities responsible for GI planning, design, and construction. Apfelbeck et al. and Karlsson et al. [16,17] emphasize the importance of interdisciplinary design teams and stakeholder involvement in wildlife-inclusive urban design. Cook et al. [8] established an element–objective matrix to discuss the coordination between GI elements and planning objectives for multifunctionality. Based on these studies, promoting multifunctional synergies and minimizing trade-offs is essential for enhancing multifunctionality; however, how to implement this approach remains a focus of ongoing discussion. While these studies often propose conceptual frameworks and approaches, they frequently lack empirical research to validate and test these frameworks or approaches.

Discussions on GI functions and planning in urban areas, particularly in cities and metropolitan regions, have attracted much attention [2,8,18,19]. However, the definition of GI highlights the necessity of studying it across various ecosystems and spatial scales [1,20,21]. The functions of GI at the urban and regional scales differ, which results in different approaches and techniques for its planning. At the urban level, GI primarily aims to improve the quality of the human living environment and enhance climate change resilience. This is achieved through the systematic integration of natural, semi-natural, and constructed elements to create interconnected networks [18,22–24]. For instance, urban GI mitigates the urban heat island effect through vegetation cover and water networks; it reduces flood risk through optimizing surface runoff management [23]; and it enhances human health and well-being through the creation of green space networks [19]. At the regional scale, the core function of GI shifts to maintaining ecological security of the large region and conserving biodiversity for sustainable development. The planning emphasizes spatial pattern optimization of natural/semi-natural elements to support the ecological processes. This involves strategies such as establishing ecological corridor networks across administrative boundaries to facilitate species migration, creating ecological buffers to limit the impact of human activities on natural landscapes, and supporting eco-tourism or eco-farming development to avoid degradation of natural and agricultural ecosystems [1,20,21].

The concept of ecosystem services (ESs) is frequently referenced in GI-related literature [8,13–15,18]. The relationship between ESs and GI is often articulated as follows: ESs are integral to GI, and GI serves as the unit for ES provision [1]. Some studies even equate GI functions with ESs [25]. Integrating GI and ES theories into a unified framework offers several potential benefits: (1) It enhances the understanding of the interrelations between social and ecological systems in GI planning, as ESs serve as a linkage between the two systems [13,15]. (2) It facilitates multifunctional synergy and trade-off analysis, given that many methods and software have been developed for ES assessment and valuation [14,15].

In light of the identified research gap and the benefits of integrating GI and ES research, we propose an application-oriented framework for multifunctional GI planning at the regional level. This framework aims to enhance the multifunctionality of the GI system by leveraging the interrelations between GI function performance and ES delivery. We implemented the framework in the Qinling–Daba Mountain Area to evaluate its effectiveness and discuss its strengths and challenges.

2. Framework Proposal

This section presents the conceptual framework and technical procedures of the proposed approach for GI planning aimed at enhancing its multifunctionality. The conceptual framework illustrates the goal of multifunctional GI planning, the pathway to attain this goal, and the key challenges that need to be addressed along the pathway. The technical

procedure offers a detailed, step-by-step guide to implementing the framework within GI planning processes, ensuring systematic and effective application.

2.1. Conceptual Framework

Both single-function and multifunction-oriented GI planning aim to enhance the ESs provided by natural or semi-natural elements through the design of their spatial configuration. Additionally, multifunction-oriented GI planning seeks to enhance the multifunctionality of the GI system by encouraging synergies among multiple functions and services while reducing trade-offs [8,14].

Regional-level green infrastructure provides ecological, economic, and social benefits through functions such as water source conservation, soil and water retention, flood control and disaster mitigation, windbreak and sand fixation, habitat provision, and support for sustainable development. These functions rely on ESs supplied by natural or semi-natural elements; however, the provisioning of ESs by individual elements is limited in terms of spatial distribution and functional capacity, which challenges the realization of the multi-functionality inherent in GI systems. To address this, multi-functional GI planning involves the systematic integration of natural and semi-natural elements within the region, enhanced by artificial facilities, thereby establishing a multi-functional system [1,20,21]. During the planning process, particular attention should be given to coordinating two key types of ES relationships: (1) synergistic ESs, such as enhanced carbon sequestration through afforestation, which contributes to the multifunctionality of GI by simultaneously addressing climate change and improving air quality; and (2) competitive ESs, such as the trade-off between agricultural production and wildlife habitat preservation, where dominant function planning, prioritizing either intensive cultivation or ecological conservation in specific zones, can help mitigate land–use conflicts (see Figure 2).

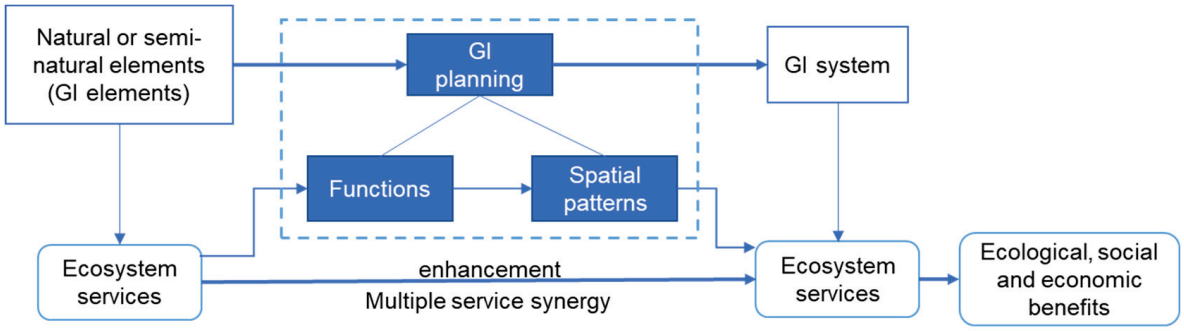

Figure 2. Conceptual framework for green infrastructure planning for multifunctionality.

The focus of Green Infrastructure (GI) system planning is on how to assemble natural and semi-natural elements to enhance ESs and promote multifunctional synergies. Addressing this challenge requires a thorough understanding of the relationship between the ESs provided by these elements and the functions of the GI system. Specifically, two key questions must be answered:

1. How do the ESs provided by natural or semi-natural elements support the functional performance of the GI system?
2. How does the functional performance of the GI system impact the delivery of ESs, particularly in terms of fostering multiple ES synergies or trade-offs?

The first question can be addressed through ES assessments, which aid in identifying GI elements and their potential functions. The second question informs whether a GI element should be planned for multifunctionality.

2.2. Technical Procedure

The technical procedure for multifunctional GI planning is proposed based on the conceptual framework and composed of six steps as follows.

Step 1: Determine the planning functions of the GI system;

Step 2: Analyze the interrelations between the performance of planning functions and the delivery of ESs;

Step 3: Assess and map the ESs relevant to the planning functions of the GI system;

Step 4: Identify GI elements based on the ES assessment and plan their functions in accordance with the principle of promoting synergy among multiple ESs and functions;

Step 5: Analyze the connectivity of GI elements and map the GI network to enhance ES provision;

Step 6: Identify strategic areas or points that are vulnerable to multifunctional trade-offs and propose strategies to mitigate these trade-offs.

The following section will elaborate on the technical procedure using a case study from the Qinling–Daba Mountain Area to evaluate feasibility and identify challenges.

3. Case Study in Qinling–Daba Mountain Area, China

3.1. Study Area and Materials

The Qinling–Daba Mountain Area (QBMA) is located in central China, including parts of Gansu, Shaanxi, Henan, Hubei, Sichuan Province, and Chongqing City, and covers an area of over 300,000 km^2 (Figure 3). It is the transitional area of the warm temperate and subtropical zones, where mountains and hills are the prominent landforms, and basins are only scattered in a few places. Because of the specific climate and terrain features, the QBMA is characterized by ecosystem diversity and biodiversity. It is one of China's NKEFAs that performs critical functions of wildlife conservation, water retention, regulation, and soil conservation. Forests are the dominant ecosystem in the study area, accounting for more than 70 percent of the area.

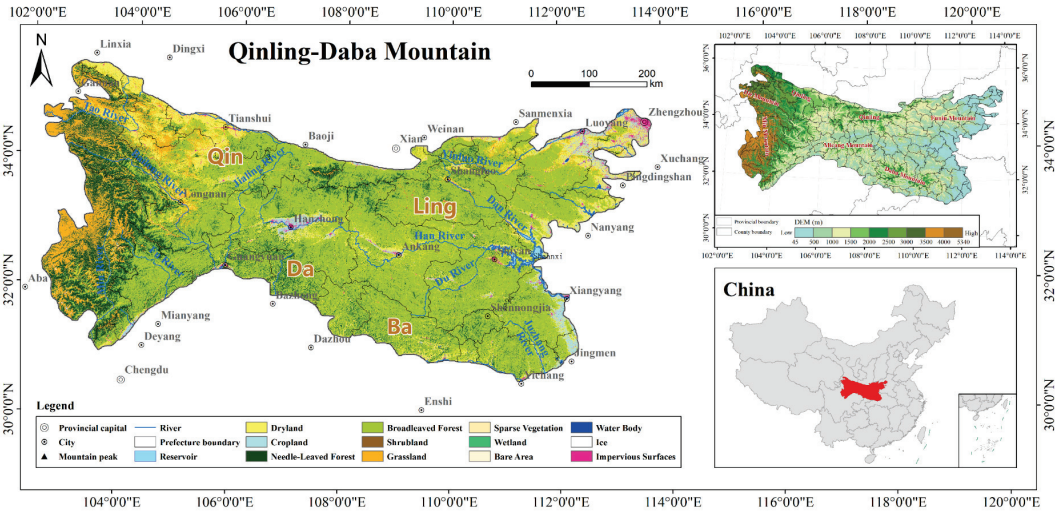

Figure 3. Location, terrain, and ecosystem structure of the Qinling–Daba Mountain Area (QBMA), China.

Except for the above natural features, the QBMA was one of China's 14 contiguous areas of deep poverty. Although people's livelihoods have been greatly improved through China's Poverty Alleviation Project, the area still faces great challenges for ecosystem protection and socioeconomic development. The mountainous terrain limits agricultural

and industrial development, but the area is rich in natural reserves, forest parks, scenic spots, and cultural relics, allowing it to develop ecotourism.

Table 1 summarizes the data used for this study and their sources. All datasets were projected to the same coordinate system (WGS_1984_UTM_Zone_49N) and resampled to 1 km × 1 km resolution for ES valuation and GI planning.

Table 1. Data sources and processing method.

Data	Resolution/ Year	Source	Processing
Digital Elevation Model (DEM)	30 m/2020	NASA https://www.nasa.gov (accessed on 19 May 2024)	Processed with ArcGIS 10.8 to obtain elevation and slope.
Land use and land cover	30 m/2020	CAS Earth Data Sharing and Service Portal https://data.casearth.cn (accessed on 20 May 2024)	Reclassified into 12 ecosystems.
Normalized Difference Vegetation Index (NDVI)	30 m/2020	Resources and Environmental Science Data Center https://www.resdc.cn (accessed on 19 May 2024)	
Net Primary Production (NPP)	500 m/2020	United States Geological Survey (USGS) https://www.usgs.gov (accessed on 19 May 2024)	
Precipitation	1000 m/2020	National Earth System Science Data Centre http://www.geodata.cn (accessed on 22 May 2024)	
Soil retention data	300 m/2020	[26] https://www.scidb.cn/en (accessed on 22 May 2024)	
Built-up areas of Chinese cities	10 m/2020	[27] https://www.scidb.cn/en (accessed on 25 May 2024)	
Rivers and roads	/	Open Street Map, National Geomatics of China https://www.openstreetmap.org https://www.webmap.cn (accessed on 25 May 2024)	
Natural reserves (NRs)	/	Geographic remote sensing ecological network platform http://www.gisrs.cn/index.html (accessed on 1 June 2024)	
Population	1000 m/2019	OakRidge National Laboratory https://landscan.ornl.gov (accessed on 2 June 2024)	
A-level scenic spots	/	Official website of Culture and Tourism Bureau	Converted to points with geographic coordinates in ArcGIS

3.2. Framework Implementation

3.2.1. Planning Function Determination

The planning functions of the GI system vary across different regions and programs. The initial step in multifunctional GI planning is to clarify these functions. In the QBMA, the study identifies the expected functions of the GI system based on environmental and socioeconomic planning developed and published by government agencies.

Firstly, the QBMA is recognized as one of China's National Key Ecological Function Areas (NKEFAs) for biodiversity conservation. Maintaining biodiversity is the primary

function that the GI system is expected to perform in this region. Additionally, QBMA serves as a crucial strategic water source area in China, facing ecological challenges, such as water erosion and soil degradation. Therefore, the GI system is also anticipated to play a vital role in water and soil conservation [28]. Furthermore, QBMA has historically been one of China's spatially contiguous deep poverty areas. Developing the economy and improving people's livelihoods remain priorities for the region. Eco-farming and ecotourism are significant strategies aimed at alleviating poverty while fostering economic development [29,30]. Both strategies leverage the region's mountainous landscapes and ecological resources, effectively combining nature conservation with sustainable development. The success of eco-farming and ecotourism is closely linked to the GI system, particularly its semi-natural components.

Based on the analysis above, the GI system is anticipated to perform four key functions: maintaining biodiversity, conserving water and soil, and supporting the development of eco-farming and ecotourism. The first two functions aim to achieve ecological benefits, while the latter two primarily target social and ecological advantages. The prioritization of these functions can be ranked as follows: biodiversity conservation > water and soil conservation > eco-farming and ecotourism development.

3.2.2. Interrelation Analysis Between GI Function Performance and ES Delivery

A matrix linking the four categories of ESs with the four planning functions of the GI system has been developed. This matrix facilitates the analysis of their relationships from two perspectives: (1) how ESs support the performance of these functions, and (2) how the performance of these functions can give rise to ES synergies or trade-offs. The first perspective assists in identifying GI elements, while the second informs whether a GI element should be planned for multifunctionality (see Figure 4).

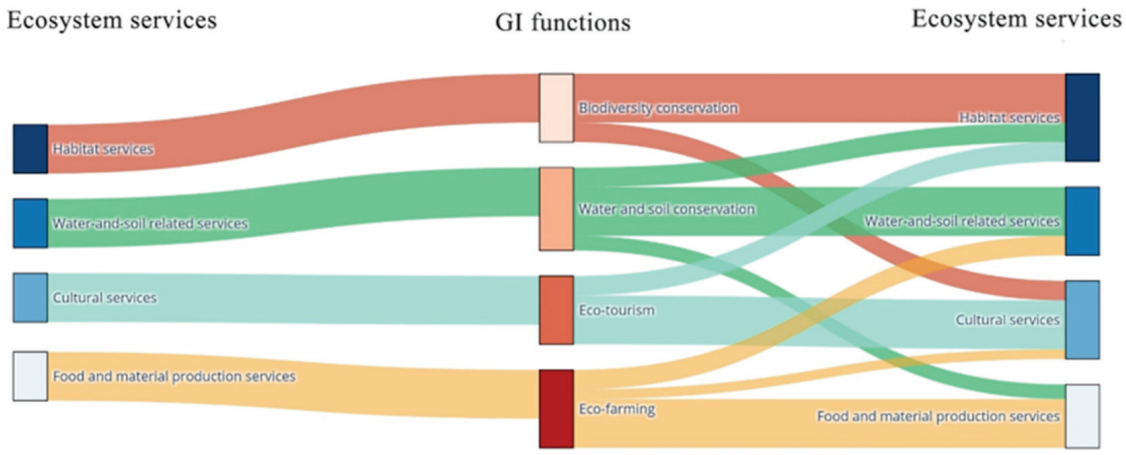

Figure 4. Interrelation between green infrastructure function performance and ecosystem service delivery.

Biodiversity is directly dependent on the habitat services (HES) provided by ecosystems. Sufficient and stable habitats for wild plants and animals form the foundation of biodiversity. By performing the biodiversity conservation function, GI enhances the habitat services of ecosystems. This enhancement, in turn, promotes the cultural services of habitats, particularly in terms of their value for scientific research and education.

The water and soil conservation function relies on water–soil-related ecosystem services (WSES), such as water storage, hydrological regulation, erosion prevention, and soil fertility maintenance. Excessive water erosion threatens wildlife and undermines the production of agricultural and forest products, resulting in the loss of both habitat and food

production services. By conserving water and soil, GI elements can foster synergies among habitat, water–soil-related, and food production services.

Ecotourism involves sustainable and responsible travel to natural areas, aiming to conserve local and surrounding environments, support local communities, and promote cultural heritage. Its development primarily depends on the cultural ecosystem services (CES) provided by ecosystems. Ecotourism educates tourists about the significance of protecting biodiversity and natural habitats, thereby enhancing both HES and CES of ecosystems.

The farming function is fundamentally linked to the food and material production services (FMPES) provided by ecosystems. Although large-scale farming, especially through deforestation, can boost food production, it often harms other ESs. In contrast, eco-farming techniques integrate modern science with a commitment to nature and biodiversity. For instance, terracing, a method used in the mountainous regions of China, helps prevent soil erosion, conserve water, and enhance agricultural yields. This practice also creates unique landscapes that attract agricultural tourism. Therefore, eco-farming has the potential to harmonize WSES, FMPES, and CES.

3.2.3. Ecosystem Service Assessment and Hotspots Analysis

The four categories of ESs (including HES, WSES, FMPES and CES) closely related to the four planning functions of the GI system were assessed and valued using the unit-based ES valuation method. The method and its application in this study are illustrated in detail in Appendix A.1. Then, the Hot Spot Analysis in ArcGIS was employed to identify the clusters of high values (hotspots) for each service by calculating the Getis-Ord Gi* statistic and mapping them in Figure 5 [31].

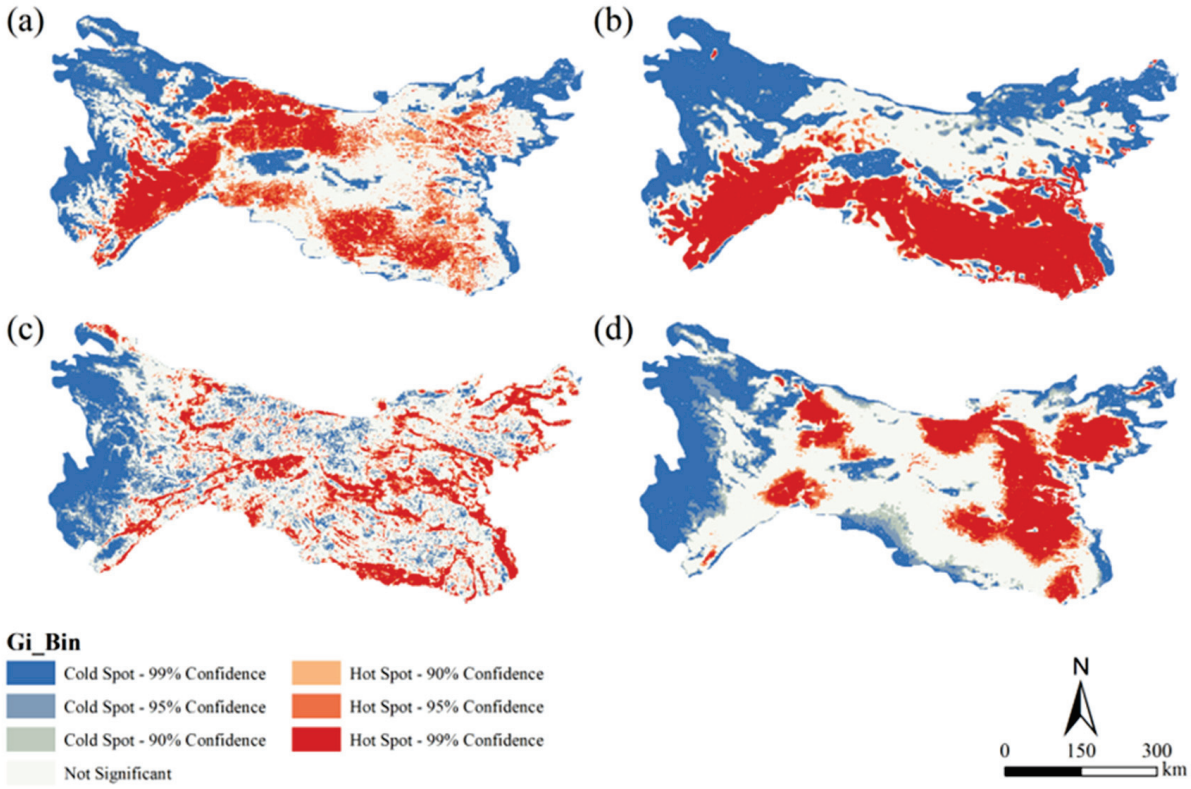

Figure 5. Hotspots of ecosystem services in Qinling–Daba Mountain Area. (**a**) hotspots of habitat service, (**b**) hotspots of water–soil-related services, (**c**) hotspots of food and material provisioning services, and (**d**) hotspots of cultural service.

Hotspots of HES and CES are spatially clustered, while hotspots of WSES also exhibit a clustering trend, albeit to a lesser degree. In contrast, hotspots of FMPES are distributed more sporadically across the landscape. HES and WSES hotspots demonstrate strong synchronization in their distribution, with both types concentrated in areas such as the Micang-Daba-Shennongjia Mountain region, the Qinling Mountains, and the Pu River and Bailong River basins at the junction of Gansu and Sichuan provinces. A notable distinction is that in the Qinling area, only WSES hotspots are distributed. Furthermore, while FMPES and CES hotspots show significant differences in spatial distribution compared to HES and WSES hotspots, there are also overlapping regions.

3.2.4. GI Element Identification and Multifunctional Mapping

Although the multifunctionality of GI has been widely recognized, its ecological functions are still regarded as more important and prioritized over other functions. Two principles were adhered to in the process of GI element identification and their function planning: first, prioritizing the ecological functions of GI; second, pursuing synergies between ecological functions and socioeconomic functions. Specifically, based on the interrelation analysis between GI function performance and ES delivery in Section 3.2.2, GI elements for biodiversity conservation and water and soil conservation were first identified and planned as Protected Areas (PAs) and Protected Buffer Zones (PBZs). Next, GI elements suitable for eco-farming and ecotourism development were identified within PAs or PBZs to encourage synergy among multiple ES/functions. The criteria for identifying GI elements are illustrated in Table 2. Figure 6 maps the spatial distribution of GI elements and their functionalities. The mapping results are analyzed below.

Table 2. Criteria for planning green infrastructure functionality based on ecosystem service assessment.

Criteria	Planning Function
Established natural reserves *	Protected areas (PAs)
Hot spots of habitat services (HES)	Protected areas
Intersections of HES and water-and-soil service (WSES) hotspots	Protected areas
WSES hotspots bot not HES hotspots	Protected buffer zone (PBZs)
Cultural service (CES) hotspots in PAs or PBZs	Ecotourism
Food and material production service (FMPES) hotspots in PAs or PBZs	Eco-farming

* Natural reserves in China are designated areas for the protection of specific ecosystems, wildlife species, and natural resources. They play a crucial role in biodiversity conservation.

First, ecological functions were prioritized. Hotspots of HES and WSES were identified and designated as Protected Areas (PAs) or Protected Buffer Zones (PBZs). The primary function of PAs is to support biodiversity, while they also contribute to water and soil conservation. PBZs were primarily planned for water and soil conservation; they serve as buffers and subsidiary areas for PAs, enhancing the habitat services provided by PAs. Together, PAs and PBZs cover approximately 55% of the study area. They display a spatially clustered pattern, though they are not completely connected.

In addition to ecological functions, the GI system is expected to perform socioeconomic functions to support eco-farming and ecotourism development. In response, we recognized the multifunctional potential of GI elements and identified those suitable for eco-farming and ecotourism within the PAs or PBZs. Approximately 17% of GI elements in the PAs or PBZs are found to be suitable for eco-farming, and these elements are scattered across the study area. In contrast, GI elements suitable for ecotourism development display a clustered pattern, primarily distributed in the North Daba Mountain area, Funiu Mountain

area, Middle Qinling Mountain area, and West Micang Mountain area. These elements account for about 33% of the area of PAs and PBZs. The multifunctionality of GI elements in each type is listed in Table 3.

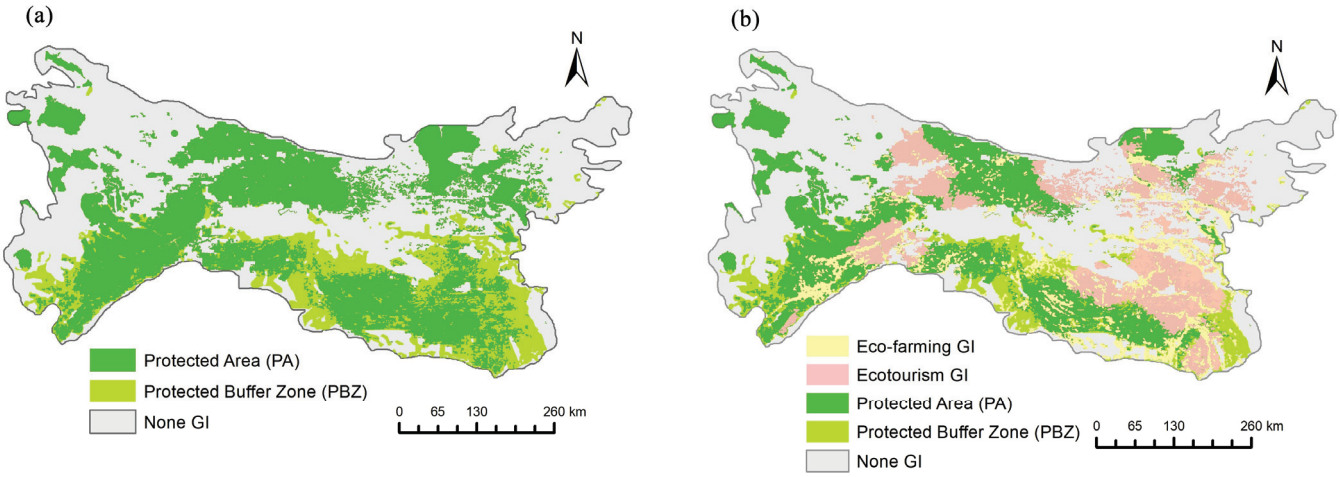

Figure 6. Green infrastructure (GI) elements for ecological functions and multifunctionality: (**a**) GI elements for ecological functions, (**b**) GI elements for multifunctionality.

Table 3. Multifunctionality of GI elements in each category.

Green Infrastructure Type	Multifunctionality
Protected Area	Biodiversity conservation and water and soil conservation
Protected Buffer Zone	Water and soil conservation
Eco-farming GI	Eco-farming development, biodiversity conservation, and water and soil conservation
Ecotourism GI	Ecotourism development, biodiversity conservation, and water and soil conservation

3.2.5. Green Infrastructure Connectivity Analysis and Green Infrastructure Network Mapping

It is widely recognized that the GI system functions as a connected network rather than merely a combination of separate elements. The performance of many ecological functions, such as flood mitigation and biodiversity conservation, requires GI elements to be linked by corridors composed of natural or semi-natural features. In the case study of the QBMA, biodiversity conservation is the primary function that the GI system is expected to perform. Protected Areas (PAs) are combinations of GI elements aimed at biodiversity conservation; however, separated PAs need to be linked to support wild animal migration among them. The habitat services provided by the GI system will be enhanced by constructing such a connected network. We simulate the wildlife corridors linking these PAs using the Minimum Cumulative Resistance (MCR) model. An explanation of the MCR model and its application in this study can be found in Appendix B.

The simulated GI networks are mapped in Figure 7. GI elements are connected by 73 wildlife corridors. The minimum, maximum, and average lengths of the corridors are 30 km, 255 km, and 86 km, respectively.

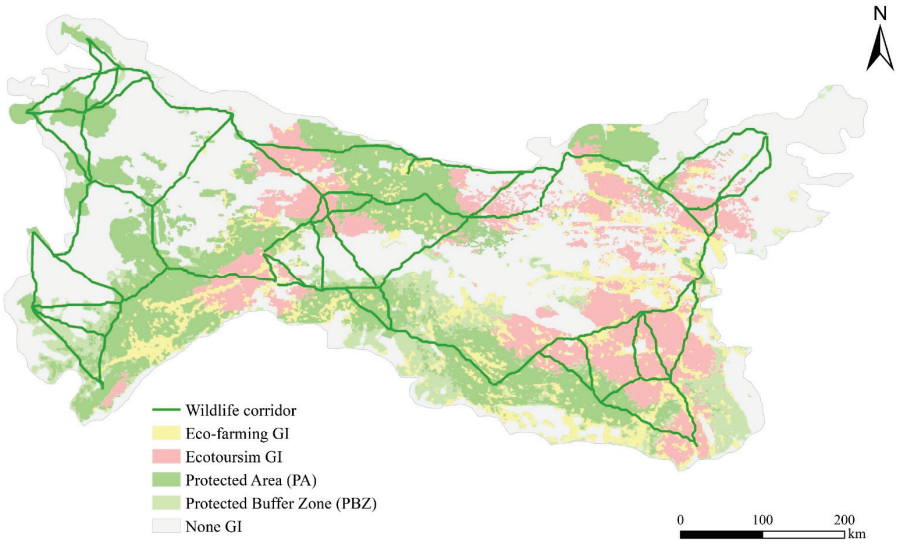

Figure 7. Simulated green infrastructure network in Qinling–Daba Mountain Area, China.

3.2.6. Strategic Areas/Points Identification

The above procedure for identifying GI elements and planning their functions aims to promote multiple ES/function synergies across the entire study area. However, trade-offs among ESs and functions may occur locally. Areas or sites that are susceptible to these trade-offs are strategically important for GI construction and management and are therefore designated as strategic areas or points. In the QBMA, the primary trade-offs are between the ecological functions of biodiversity maintenance and water and soil conservation, and the socioeconomic functions of supporting eco-farming and ecotourism development.

First, population distribution plays a crucial role in these multifunctional trade-offs. Population agglomeration can enhance eco-farming and ecotourism functions by providing human resources, potential markets, and tourists. However, it can also negatively impact HES and compromise WSES, particularly in PAs and PBZs, and on wildlife corridors. Consequently, we identify densely populated townships located within PAs and PBZs, or on wildlife corridors, as strategic areas for GI construction and management. The categories and spatial distributions of these townships are mapped in Figure 8.

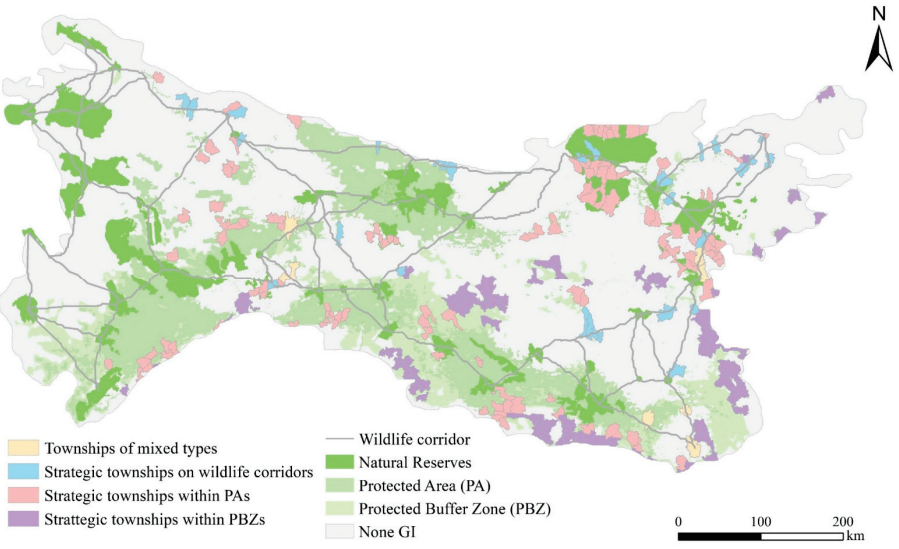

Figure 8. Strategic areas for the green infrastructure construction and management in Qinling–Daba Moutain Area, China.

A total of 245 townships have been recognized as strategic areas, accounting for 10.3% of all townships in the study area. These townships are dispersed throughout the region, with a significant concentration in the Funiu Mountain and Daba Mountain areas. A large percentage of these townships fall within PAs or PBZs, meaning that part or all of the townships have been designated as such. These townships, on one hand, possess green GI that is significant for biodiversity maintenance, as well as water and soil conservation. On the other hand, they are densely populated, and the livelihoods of the residents need to be supported. Leveraging GI to develop eco-farming and ecotourism is a feasible approach to realize the multifunctional value of GI while generating economic and social benefits for local communities. However, the carrying capacity of GI for farming and tourism activities must be assessed. The development of eco-farming and ecotourism should not exceed the carrying capacity of GI to avoid negative impacts on its ecological functions. Furthermore, the number of townships within PBZs is greater than that within PAs, implying that GI in PBZs is more likely to perform multiple functions. Additionally, 40 of these townships were in wildlife corridors. It is necessary to construct wildlife corridors in these townships to minimize human interference on wildlife migration. Meanwhile, local governments should take responsibility for educating the public on the significance and approach to wildlife protection.

Second, the connectivity of GI is closely related to the trade-off between ecological functions and socioeconomic functions. The connectivity of GI elements facilitates the migration of wild animals among different habitats. Meanwhile, in the development of eco-farming and ecotourism, agricultural products need to be transported from GI elements to markets, and tourists must travel between various tourism destinations via human-constructed transportation routes. However, these artificial transportation networks may intersect with wildlife corridors, disrupting the connectivity of the GI network. Consequently, the pursuit of socioeconomic functions can create trade-offs with biodiversity conservation efforts. These intersections can be regarded as strategic points for GI construction and management, as illustrated in Figure 9.

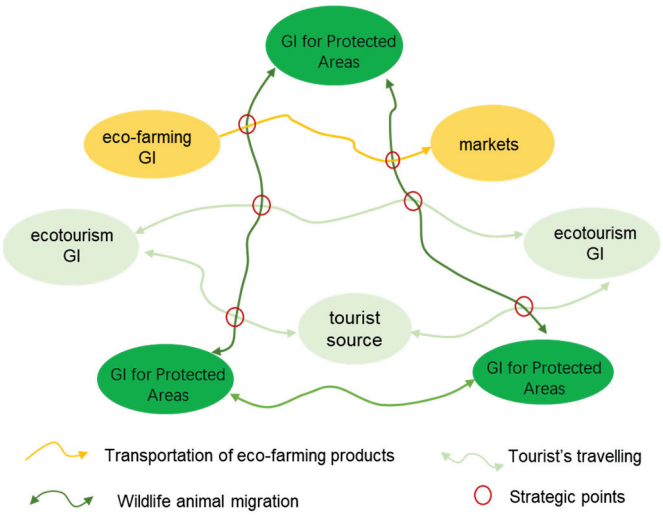

Figure 9. Conceptual map of green infrastructure connectivity and strategic points.

By identifying the intersections of wildlife corridors and major traffic routes in the study area, we have located and mapped the strategic points, as shown in Figure 10. A total of 273 strategic points have been identified for green infrastructure (GI) construction and management.

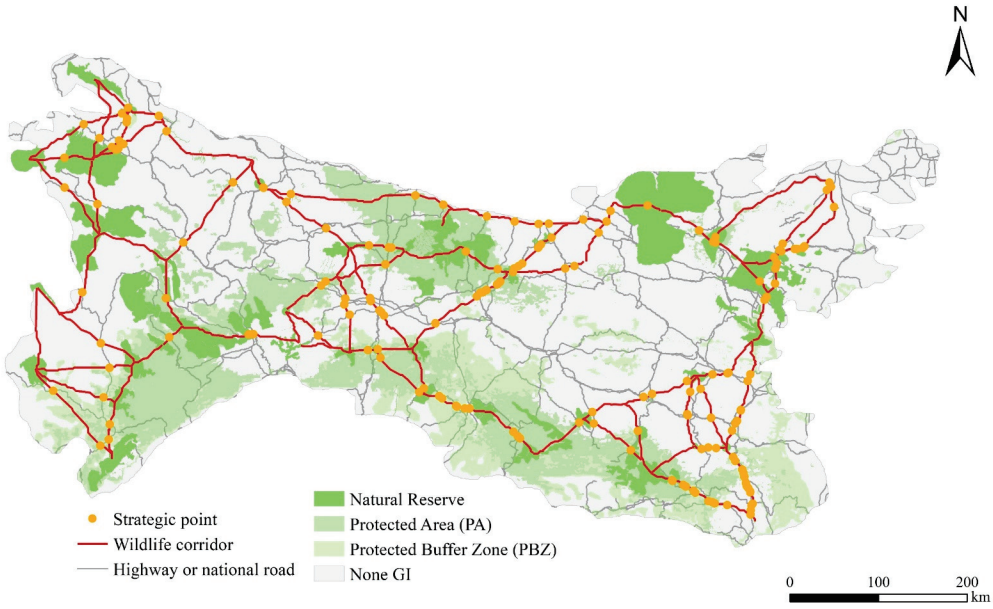

Figure 10. Strategic points for green infrastructure construction and management in Qinling–Daba Mountain Area, China.

In certain road sections, the simulated wildlife corridors are in close proximity to the roads, resulting in a dense concentration of strategic points, particularly in the G421 Baokang and Yuanan sections, the G331 Songxian section, the G210 Ningshan section, and the G347 Xingshan section. In these road sections, it is crucial to establish animal migration corridors alongside the roads. Additionally, installing warning signs to indicate potential animal presence is essential to alert passing vehicles, helping to reduce their speed and minimize the risk of collisions between wildlife and vehicles.

For other dispersed strategic points, field observations should be conducted in the vicinity of the identified locations. In areas where wild animals are frequently sighted, priority should be given to implementing engineering solutions, such as constructing animal passage bridges or culverts. For strategic points where engineering interventions are not feasible, appropriate warning signs should be installed to remind drivers to slow down.

4. Discussion

This study integrates ES evaluation and synergy/trade-off analysis into the planning of GI systems, establishing a planning framework to enhance the multifunctionality of GI at the regional scale. Using the Qinling–Daba Mountain Area (QBMA) as a case study, the practicality of this framework is demonstrated, along with an identification of the challenges encountered during its implementation. This section discusses the study's contributions, limitations, and remaining challenges.

4.1. Contributions

Despite a growing body of literature on urban green infrastructure, the planning and implementation of regional green infrastructure remain comparatively understudied. This research addresses this gap by providing valuable insights into effective strategies and approaches for regional-scale green infrastructure development.

Urban GI often incorporates engineered elements, such as permeable pavement, infiltration trenches, and perforated pipes [22]. However, at the regional level, GI planning usually prioritizes the identification and conservation of existing natural features, supplemented by semi-natural elements [1,20,21]. This approach aims to balance ecological benefits with the costs associated with construction and ongoing maintenance. Regional

GI is often designed and constructed to safeguard regional ecological security and biodiversity. Based on this functional orientation, it exhibits a fundamental alignment with the ecological security patterns extensively investigated by Chinese academia [32–35]. Both approaches emphasize identifying core areas with critical ecological functions and establishing interconnected networks. Building upon this shared functional grounding, this study innovatively incorporates methods for constructing ecological security patterns into regional green infrastructure planning.

This research employs a "core protection, network construction, and cost control" framework to plan the green infrastructure network in the QBMA. Initially, based on ecological security pattern theory, the case study identifies natural and semi-natural elements that provide essential ESs, such as habitat, water and soil management, food and material production, and cultural benefits, through ES assessment and mapping. Subsequently, using principles from landscape ecology, it selects existing natural and semi-natural features, such as rivers and agricultural shelterbelts, to establish cost-effective wildlife migration corridors connecting core protection zones. Finally, it employs the minimum cumulative resistance model to optimize the network structure, minimizing the development costs for wildlife corridors. This configuration model, which emphasizes natural elements supplemented by semi-natural elements, ensures the functionality of the green infrastructure network while controlling construction expenses.

Building upon prior research on ecological security patterns in the QBMA [36], this study conducts a comparative analysis to highlight key distinctions and concordances. Regarding the identification of ecological sources, both studies exhibit a notably similar spatial distribution of protected areas. However, this work innovatively identifies areas characterized by multiple functions. For instance, within protected areas and their buffer zones, eco-farming is suitable for development in 17% of the area and ecotourism in 33%. Concerning ecological corridor simulation, despite a high degree of consistency in the spatial distribution of key wildlife migration routes identified across both studies, this research yields a greater total number and cumulative length of wild corridors. This discrepancy primarily arises from the different criteria used for core GI/ecological source identification. This study incorporates established nature reserves as core green infrastructure elements, whereas prior investigations did not include nature reserves within the criteria for ecological source determination. However, nature reserves, serving as repositories of representative natural ecosystems, habitats for rare and endangered species, and areas of concentrated natural heritage, represent integral elements of the regional GI system [37,38].

4.2. Challenges and Limitations

A central challenge in implementing the proposed framework for multifunctional green infrastructure planning lies in addressing two fundamental questions: (1) How do the ESs provided by natural and semi-natural elements contribute to the functionality of the GI system? (2) How does the functional performance of the GI system foster multiple ES synergies or trade-offs?

In response to the first question, the case study initially identified four key functions expected of the GI system: biodiversity maintenance, water and soil conservation, support for eco-farming, and promotion of ecotourism. It then analyzed the ESs associated with these functions. Finally, it evaluated and mapped the four categories of ESs in the study area and accordingly identified that GI (natural/semi-natural) elements play significant roles in the provision of these ESs.

The second question, concerning the potential for synergies or trade-offs among ESs, presents a more complex challenge. The occurrence of synergies or trade-offs is influenced

not only by the type of function but also by the intensity of its implementation. For instance, in the case study, the development of eco-farming and ecotourism can complement the ecological functions of GI, enhancing services such as habitat provision, water and soil conservation, food production, and cultural benefits. Conversely, if farming and tourism activities exceed the GI's carrying capacity, it may degrade its ecological functions, leading to trade-offs among various ESs. Thus, assessing the carrying capacity of GI concerning different human activities is essential for promoting multifunctional synergies and minimizing trade-offs. This evaluation is challenging as it must consider the variations in human activities, the differences in green infrastructure, and its surrounding natural and socioeconomic environment. A limitation of our case study is that it did not assess the carrying capacity of GI for farming and tourism activities.

Another challenge in planning multifunctional GI is addressing the connectivity of its elements, a topic that has received little attention in current literature. GI is defined as a strategically planned network of natural and semi-natural areas that provide a wide range of ESs benefiting both biodiversity and society, as noted by the International Union for Conservation of Nature (IUCN) and the European Commission (EC) [5]. The connectivity of GI elements varies based on their functions. In single-function-oriented planning, connectivity can be relatively straightforward to simulate. For example, the connectivity for biodiversity conservation can be mapped by simulating the migration routes of large mammals or aquatic species. However, in a multifunctional system, the connectivity of GI elements becomes more complex. Some functions, such as soil conservation and climate regulation, do not require full connectivity among elements. Additionally, functions like ecotourism development necessitate connections with human-made transportation routes, raising questions about whether these routes should be integrated into the GI system. Consequently, determining which elements should be connected and designing their connectivity patterns is a challenging task in multifunctional GI planning. In our case study, this article focused solely on analyzing the connectivity of GI for biodiversity conservation and how transportation routes disrupt this connectivity. This choice was made to prioritize biodiversity conservation as a primary goal of GI planning while also aiming to simplify the network for effective construction and management.

5. Conclusions

This study presents an application-oriented framework for green infrastructure (GI) planning aimed at enhancing multifunctionality. By integrating ES methodologies, the framework examines the relationships between GI function performance and ES delivery. It reframes challenges related to multiple functions and trade-offs as issues concerning the synergies and trade-offs of ESs, allowing for quantitative and spatial analysis. This framework facilitates the planning of GI systems to promote synergies among various functions while identifying strategic locations for GI construction and management to minimize trade-offs.

The framework was applied in the Qinling–Daba Mountain Area of China, where the planned GI system includes protected areas (PAs), priority biodiversity zones (PBZs), eco-farming GI, and ecotourism GI. These elements are designed to support biodiversity conservation, water and soil preservation, and the development of eco-farming and ecotourism. Four categories of ESs—habitat, water–soil-related, food and material provisioning, and cultural services—were assessed and mapped to inform the identification and functional planning of GI elements. Additionally, 73 wildlife corridors were simulated to connect these GI elements, thereby enhancing habitat services for biodiversity. Strategic areas/points for GI development and management were identified, including densely pop-

ulated townships within PAs or PBZs, or on wildlife corridors, as well as at intersections of wildlife corridors and human-made roads.

This case study demonstrates the framework's potential for facilitating multifunctional GI planning. However, it also highlights challenges in its implementation, such as assessing the carrying capacity of GI for various human activities and simulating the connectivity of GI elements to achieve multifunctionality.

Author Contributions: Conceptualization, M.S. and S.L.; methodology, M.S. and S.L.; formal analysis, M.S. and F.P.; writing—original draft preparation, M.S.; writing—review and editing, M.S., S.L. and B.P.; visualization M.S. and F.P.; project administration, S.L.; funding acquisition, M.S., S.L. and F.P. All authors have read and agreed to the published version of the manuscript.

Funding: This research was funded by the Research Project of Humanities and Social Sciences of the Ministry of Education, China (grant number 23YJA630046), the National Natural Science Foundation of China (grant number 42401330, 42001229) and the Foundation of Key Laboratory of Law and Government, Ministry of Natural Resources of China, (grant number CUGFZ-2507).

Data Availability Statement: The data that support the findings of this research will be provided by request.

Conflicts of Interest: The authors declare no conflicts of interest.

Appendix A. Methods for Ecosystem Service Valuation: Unit-Based ES Valuation Method

The planning function of the GI system in the Qinling–Daba Mountain area is closely associated with four categories of ESs: habitat services (HES), water–soil-related services (WSES), food and material production services (FMPES), and cultural services (CES). We utilize the unit-based ES valuation method proposed and developed by [39–41] for the valuation of ESs, while extending it by incorporating spatial adjustment factors for FMPES and CES. This method first evaluates ES values based on the ecosystem types of land units and then adjusts these values according to the biophysical and socioeconomic characteristics of the land units. The valuation process involves establishing an equivalent coefficient table (ECT) and calculating the value of the standard equivalent factor (SEF). The method is illustrated below.

Appendix A.1. The Equivalent Coefficient Table (ECT) and the Standard Equivalent Factor (SEF) for ES Valuation

Based on the research conducted by Costanza et al. [42] and TEEB [43], Xie et al. [39] classify ecosystems into seven categories and 14 subcategories, while ESs are categorized into four categories and 11 subcategories. They developed an equivalent coefficient table (ECT) to represent the relative value of ESs provided by different ecosystems in relation to the standard equivalent factor (SEF). The value of the SEF is proposed to be estimated based on the food supply value of one hectare of farmland, which is suggested to be assessed according to the market price of crops. In this study, we construct an equivalent coefficient table (see Table A1) for the four categories of ESs relevant to our research, based on the ECT proposed by Xie et al. [39–41]. This table indicates the relative values of ESs in comparison to the SEF. For instance, the coefficient for the erosion prevention service provided by broad-leaved forests is 2.65, meaning that the value of this service from one hectare of broad-leaved forest is 2.65 times greater than that of the SEF.

Table A1. Equivalent coefficient table for ecosystem service valuation.

Ecosystem Services / Ecosystems		Food and Raw Material Supply		Water–Soil-Related Services				Habitat Services	Cultural Services
Category	**Subcategory**	**Food Supply**	**Raw Material Supply**	**Water Retention**	**Hydrological Regulation**	**Erosion Prevention**	**Soil Fertility Maintenance**	**Habitat Services**	**Cultural and Recreational Services**
farmland	dry land	0.85	0.40	0.02	0.27	1.03	0.12	0.13	0.06
	paddy field	1.36	0.09	−2.63	2.72	0.01	0.19	0.21	0.09
forest	coniferous forest	0.22	0.52	0.27	3.34	2.06	0.16	1.88	0.82
	broad-leaved forest	0.29	0.66	0.34	4.74	2.65	0.20	2.41	1.06
	Bush	0.19	0.43	0.22	3.35	1.72	0.13	1.57	0.69
grassland	prairie	0.10	0.14	0.08	0.98	0.62	0.05	0.56	0.25
	shrubs	0.38	0.56	0.31	3.82	2.40	0.18	2.18	0.96
wetland	wetland	0.51	0.50	2.59	24.23	2.31	0.18	7.87	4.73
Bare land	bare land	0.00	0.00	0.00	0.03	0.02	0.00	0.02	0.01
water area	waterbody	0.80	0.23	8.29	102.24	0.93	0.07	2.55	1.89
	glacier and snow	0.00	0.00	2.16	7.13	0.00	0.00	0.01	0.09
construction area	construction area	0.00	0.00	0.00	0.00	0.00	0.00	0.00	0.00

Appendix A.2. Spatial Adjustment Factor Designation and Application

The ES value of a unit is influenced not only by its ecosystem type but also by its biophysical and socioeconomic characteristics. Xie et al. [39] proposed several spatial adjustment factors to modify the ES values estimated solely based on ecosystem types. These factors include biomass (net primary productivity), precipitation, and erosion prevention capacity, which integrates soil properties, rainfall, landform, and land cover. For this study, we also incorporate population adjustment factors for food and raw material supply services, as well as scenic spot adjustment factors for cultural services. The adjustment factors are applied to the equivalent coefficient table (ECT) (Table A1) using Formulas (A1) to (A4).

$$F_{ni} = \begin{cases} N_i \times F_{n1} & OR \\ R_i \times F_{n2} & OR \\ S_i \times F_{n3} & OR \\ P_i \times N_i \times F_{n4} & OR \\ C_i \times N_i \times F_{n5} & \end{cases} \quad \text{(A1)}$$

where F_{ni} is the adjusted equivalent coefficient for unit i. N_i, R_i, S_i, P_i, and C_i represent the *NPP* adjustment factor, rainfall adjustment factor, soil erosion prevention adjustment factor, population adjustment factor, and scenic spot adjustment factor, respectively, for unit i. F_{n1} denotes the equivalent coefficient for soil fertility maintenance service, habitat service, or cultural service. F_{n2} refers to the equivalent coefficient for water supply service or hydrological regulation service. F_{n3} indicates the equivalent coefficient for soil prevention service. F_{n4} represents the equivalent coefficient for food or raw material supply service. Finally, F_{n5} refers to the equivalent coefficient for cultural service.

N_i, R_i, and S_i calculations are similar to that of Xie et al. 's research [39], illustrated in Formula (A2).

$$N_i = \frac{NPP_i}{\overline{NPP}}, \quad R_i = \frac{PRE_i}{\overline{PRE}}, \quad S_i = \frac{SC_i}{\overline{SC}} \quad \text{(A2)}$$

where NPP_i, PRE_i, and SC_i are, respectively, the *NPP* (t/ha), annual precipitation (mm/ha), and soil conservation quantity (t/ha) for unit i. $\overline{NPP}$, $\overline{PRE}$, and $\overline{SC}$ are, respectively, the national average values for the above three indicators in China.

The calculation of P_i is informed by the analysis of population distribution in the study area, as outlined in Formula (A3). This indicates that units with higher population densities are assigned greater values for food and raw material provisioning services.

$$P_i = \ln \frac{POP_i}{\overline{POP}} + N \tag{A3}$$

$$N = \left\lceil \left| \min(\ln \frac{POP_i}{\overline{POP}}) \right| \right\rceil$$

where POP_i is the population density of unit i, and $\overline{POP}$ is the average population density in the study area[1].

The calculation of C_i is based on the kernel density analysis of A-level scenic spots in the study area. China has established a standardized quality rating system for scenic spots, categorizing them into the 5A, 4A, 3A, 2A, and A grades. The density of A-level scenic spots reflects both the quantity and quality of tourism resources in the area. Kernel density mapping of A-level scenic spots was conducted for the study area using a cell size of 1 km^2 (see Figure A1). Subsequently, C_i is calculated using Formula (A4).

$$C_i = \frac{SCD_i}{\overline{SCD}} \tag{A4}$$

where SCD_i is the kernel density value of A-level scenic spots for unit i, and $\overline{SCD}$ is the national average value for this indicator. This calculation implies that a unit with a higher density of scenic spots is assigned a greater cultural service value.

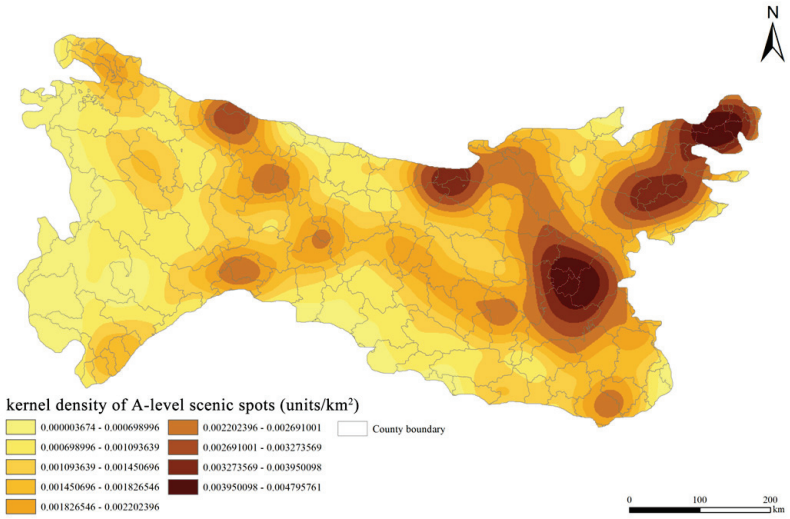

Figure A1. Kernel density map of A-level scenic spots in Qinling–Daba Mountain Area.

Appendix A.3. Ecosystem Service Valuation

When assessing the ES values of China's terrestrial ecosystems, Xie et al. [41] proposed that the value of the SEF should be set at one-seventh of the national average market value of crops produced per hectare of farmland for a specific year. We adopt this method but utilize crop production and market data specific to the Qinling–Daba Mountain Area instead of the national average. Based on statistical data provided by the prefecture-level governments in the study area, the estimated value of the SEF for this study is 1794.3 CNY (approximately 260 USD).

Using the ecosystem map (Figure 1), the ECT (Table A1), the adjusted equivalent coefficients (Formulas (A1)–(A4)), and the SEF value, we estimated the values of the

eight subcategory ESs. The values for HES, WSES, FMPES, and CES were calculated by combining the corresponding subcategory service values and subsequently mapped using ArcGIS (see Figure A2).

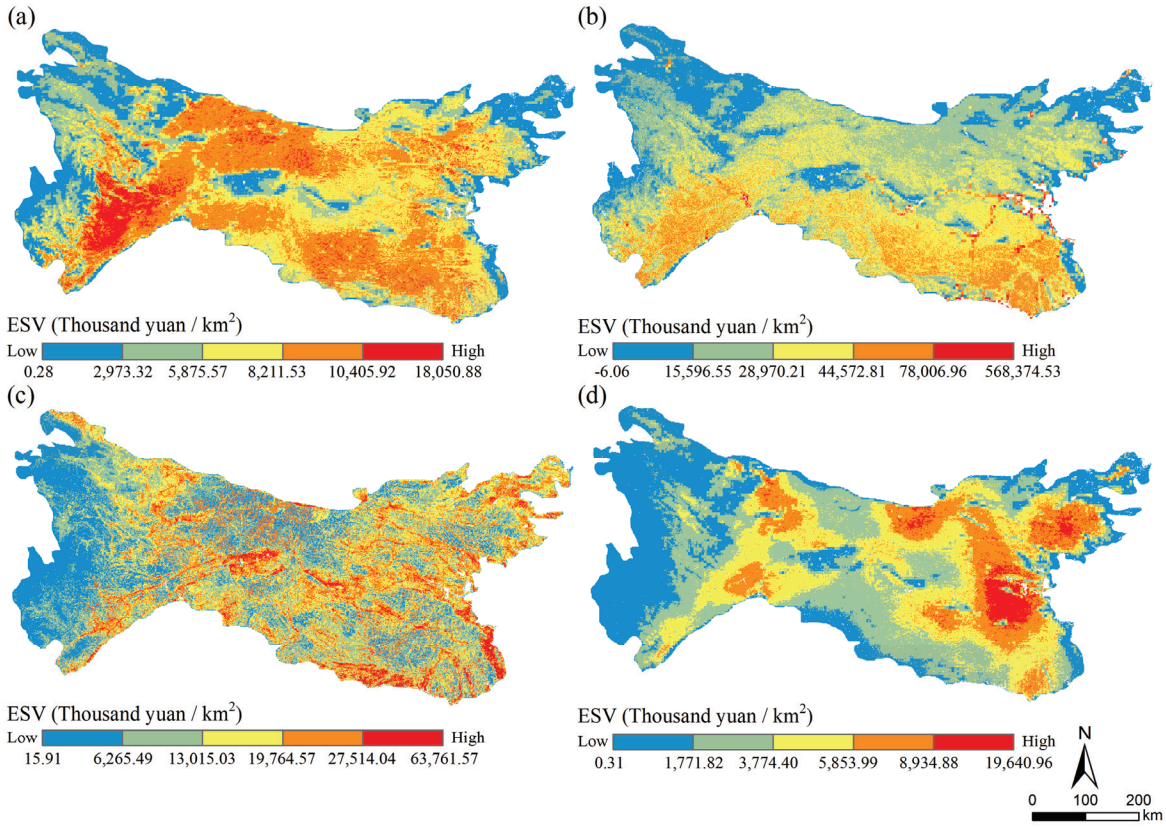

Figure A2. Ecosystem service values (ESV) in Qinling–Daba Mountain Area: (**a**) ESV of habitat services (HES), (**b**) ESV of water-and-soil-related services (WSES), (**c**) ESV of food and material provisioning services (FMPES), (**d**) ESV of cultural services (CES).

Appendix B. Method for Green Infrastructure Connectivity Analysis: Minimum Cumulative Resistance Model

The Minimum Cumulative Resistance (MCR) model was employed for connectivity analysis to identify corridors linking Protected Areas (PAs) based on resistance surfaces and Formula (A5) [44–46]. The resistance surface was generated by evaluating multiple criteria relevant to the resistance of wildlife movement.

$$MCR = f_{\min} \sum_{j=n}^{i=m} (D_{ij} \times R_i) \quad \text{(A5)}$$

where MCR is the minimum cumulative resistance value, D_{ij} is the distance between source j to unit i, R_i is the resistance value of unit i, and f indicates the positive correlation function between MCR and D_{ij} and R_i. Since Natural Reserves (NS) are officially designated areas for wildlife protection in China, we use NRs as sources in the wildlife corridor simulation. The value of R_i was calculated through multi-criteria evaluation. The criteria (resistance factors) and their weighting and valuing schemes are shown in Table A2.

Table A2. Criteria, weighting, and valuing scheme for assessing wildlife movement resistance.

Resistance Factor	Weight	Grading Standard	Resistance Value	Resistance Factor	Weight	Grading Standard	Resistance Value
land cover	0.4	forest, wetland	1	elevation (m)	0.15	<700	10
		grassland, waterbodies	20			700–1000	30
		farmland	50			1000–1500	50
		bare land	70			1500–2000	70
		construction land	90			>2000	90
distance to roads (m)	0.03	<1000	90	Slope (degree)	0.1	0–8°	10
		1000–3000	70			8–15°	30
		3000–5000	50			15–25°	50
		5000–10,000	30			25–35°	70
		>10,000	10			>35°	90
distance to railways (m)	0.03	<1000	90	vegetation cover (%)	0.21	0–20	90
		1000–3000	70			20–40	70
		3000–5000	50			40–60	50
		5000–10,000	30			60–80	30
		>10,000	10			80–100	10
distance to waterbodies (m)	0.05	<1000	10	distance to build-up areas (m)	0.02	<1000	90
		1000–2000	30			1000–3000	70
		2000–5000	50			3000–5000	50
		5000–10,000	70			5000–10,000	30
		>10,000	90			>10,000	10

Notes

[1] Since the population density varies greatly in the study area, the log transformation is applied to control the impacts of a few extremely high values on the results. *N* is used for converting negative values to positive values.

References

1. Liquete, C.; Kleeschulte, S.; Dige, G.; Maes, J.; Grizzetti, B.; Olah, B.; Zulian, G. Mapping Green Infrastructure Based on Ecosystem Services and Ecological Networks: A Pan-European Case Study. *Environ. Sci. Policy* **2015**, *54*, 268–280. [CrossRef]
2. Seiwert, A.; Rößler, S. Understanding the Term Green Infrastructure: Origins, Rationales, Semantic Content and Purposes as Well as Its Relevance for Application in Spatial Planning. *Land Use Policy* **2020**, *97*, 104785. [CrossRef]
3. World Bank Group. *Investing in Urban Resilience: Protecting and Promoting Development in a Changing World*; World Bank Group: Washington, DC, USA, 2016.
4. Intergovernmental Panel on Climate Change. *Climate Change 2022: Mitigation of Climate Change*; Intergovernmental Panel on Climate Change: Geneva, Switzerland, 2022.
5. European Commission. The Multifunctionality of Green Infrastructure. In *Science for Environmental Policy*; European Commission: Brussels, Belgium, 2012; p. 37.
6. United States Environmental Protection Agency. Available online: https://www.epa.gov/green-infrastructure (accessed on 2 June 2024).
7. Bohn, K.; Chu, D. Food-Productive Green Infrastructure: Enabling Agroecological Transitions from an Urban Design Perspective. *Urban Agric. Reg. Food Syst.* **2021**, *6*, e20017. [CrossRef]
8. Cook, L.M.; Good, K.D.; Moretti, M.; Kremer, P.; Wadzuk, B.; Traver, R.; Smith, V. Towards the Intentional Multifunctionality of Urban Green Infrastructure: A Paradox of Choice? *npj Urban Sustain.* **2024**, *4*, 12. [CrossRef]
9. Evans, D.L.; Falagán, N.; Hardman, C.A.; Kourmpetli, S.; Liu, L.; Mead, B.R.; Davies, J.A.C. Ecosystem Service Delivery by Urban Agriculture and Green Infrastructure—A Systematic Review. *Ecosyst. Serv.* **2022**, *54*, 101405. [CrossRef]
10. Lourdes, K.T.; Hamel, P.; Gibbins, C.N.; Sanusi, R.; Azhar, B.; Lechner, A.M. Planning for Green Infrastructure Using Multiple Urban Ecosystem Service Models and Multicriteria Analysis. *Landsc. Urban Plan.* **2022**, *226*, 104500. [CrossRef]
11. Rigo, R.; Houet, T.; Gonthier, C. Disseminating Land Use Land Cover Change Scenarios for Improving the Role of Blue and Green Infrastructure: Evaluation and Perspectives. *Environ. Sci. Policy* **2024**, *160*, 103821. [CrossRef]
12. Connop, S.; Vandergert, P.; Eisenberg, B.; Collier, M.J.; Nash, C.; Clough, J.; Newport, D. Renaturing Cities Using a Regionally-Focused Biodiversity-Led Multifunctional Benefits Approach to Urban Green Infrastructure. *Environ. Sci. Policy* **2016**, *62*, 99–111. [CrossRef]
13. Hansen, R.; Pauleit, S. From Multifunctionality to Multiple Ecosystem Services? A Conceptual Framework for Multifunctionality in Green Infrastructure Planning for Urban Areas. *AMBIO* **2014**, *43*, 516–529. [CrossRef]

14. Korkou, M.; Tarigan, A.K.M.; Hanslin, H.M. The Multifunctionality Concept in Urban Green Infrastructure Planning: A Systematic Literature Review. *Urban For. Urban Green.* **2023**, *85*, 127975. [CrossRef]
15. McPhearson, T.; Cook, E.M.; Berbés-Blázquez, M.; Cheng, C.; Grimm, N.B.; Andersson, E.; Barbosa, O.; Chandler, D.G.; Chang, H.; Chester, M.V.; et al. A Social-Ecological-Technological Systems Framework for Urban Ecosystem Services. *One Earth* **2022**, *5*, 505–518. [CrossRef]
16. Apfelbeck, B.; Snep, R.P.H.; Hauck, T.E.; Ferguson, J.; Holy, M.; Jakoby, C.; Scott MacIvor, J.; Schär, L.; Taylor, M.; Weisser, W.W. Designing Wildlife-Inclusive Cities That Support Human-Animal Co-Existence. *Landsc. Urban Plan.* **2020**, *200*, 103817. [CrossRef]
17. Karlsson, A.; Guillén, L.A.; Brukas, V. Regional Forest Green Infrastructure Planning and Collaborative Governance: A Case Study from Southern Sweden. *Environ. Sci. Policy* **2024**, *160*, 103840. [CrossRef]
18. Serra, V.; Defraia, S.; Ledda, A.; Calia, G.; Corona, F.; De Montis, A.; Mulas, M. Ecological Network, Ecosystem Services, and Green Infrastructure Planning: A Method for the Metropolitan City of Cagliari, Italy. *Netw. Spat. Econ.* **2025**, *25*, 95–120. [CrossRef]
19. Barreira, A.P.; Andraz, J.; Ferreira, V.; Panagopoulos, T. Perceptions and Preferences of Urban Residents for Green Infrastructure to Help Cities Adapt to Climate Change Threats. *Cities* **2023**, *141*, 104478. [CrossRef]
20. Murkin, K.; Shiode, N.; Shiode, S.; Kidd, D. Biodiversity and the Recreational Value of Green Infrastructure in England. *Sustainability* **2023**, *15*, 2915. [CrossRef]
21. Hansen, R.; Mattes, A.; Meier, M.; Kurths, A. Reorienting Urban Green Infrastructure Planning towards Biodiversity—Perspectives and Ongoing Debates from Germany. *Urban For. Urban Green.* **2023**, *90*, 128155. [CrossRef]
22. Ignatieva, M.; Mofrad, F. Understanding Urban Green Spaces Typology's Contribution to Comprehensive Green Infrastructure Planning: A Study of Canberra, the National Capital of Australia. *Land* **2023**, *12*, 950. [CrossRef]
23. Wang, Z.; Li, Z.; Wang, Y.; Zheng, X.; Deng, X. Building Green Infrastructure for Mitigating Urban Flood Risk in Beijing, China. *Urban For. Urban Green.* **2024**, *93*, 128218. [CrossRef]
24. Wang, A.; Wang, J.; Zhang, R.; Cao, S. Mitigating Urban Heat and Air Pollution Considering Green and Transportation Infrastructure. *Transp. Res. Part A Policy Pract.* **2024**, *184*, 104079. [CrossRef]
25. Lovell, S.T.; Taylor, J.R. Supplying Urban Ecosystem Services through Multifunctional Green Infrastructure in the United States. *Landsc. Ecol.* **2013**, *28*, 1447–1463. [CrossRef]
26. Sun, Z.; Sun, J.; Guo, H.; Jiang, H.; Gao, J.; Wang, J. A Dataset of Built-up Areas of Chinese Cities in 2020[DS/OL]. *Sci. Data Bank* **2021**, *7*, 184–198. [CrossRef]
27. Li, J.; He, H.; Zeng, Q.; Chen, L.; Sun, R. Dataset of Soil Conservation Capacity Preventing Water Erosion in China (1992–2019)[DS/OL]. *Sci. Data Bank* **2023**. [CrossRef]
28. National Forestry Administration, PRC. *Planning for Ecosystem Protection and Construction in National Key Ecological Function Areas*; China Forestry Publishing Press: Beijing, China, 2017.
29. National Development and Reform Commission; National Tourism Administration. *National Ecotourism Development Plan (2016–2025)*; National Development and Reform Commission: Beijing, China, 2016.
30. Office of the Leading Group for Poverty Alleviation and Development of the State Council. *Guideline for China's Rural Poverty Alleviation and Development (2011–2020)*; International Poverty Reduction Center in China: Beijing, China, 2011.
31. Getis, A.; Ord, J.K. The Analysis of Spatial Association by Use of Distance Statistics. In *Perspectives on Spatial Data Analysis*; Anselin, L., Rey, S.J., Eds.; Springer: Berlin/Heidelberg, Germany, 2010; pp. 127–145.
32. Yu, K. Security Patterns and Surface Model in Landscape Ecological Planning. *Landsc. Urban Plan.* **1996**, *36*, 1–17. [CrossRef]
33. Jiang, H.; Peng, J.; Xu, D.; Tang, H. Constructing Ecological Security Patterns with Differentiated Management Intensity Based on Multifunctional Landscape Identification and Multi-Criteria Decision-Making. *Glob. Ecol. Conserv.* **2024**, *50*, e02862. [CrossRef]
34. Ding, M.; Liu, W.; Xiao, L.; Zhong, F.; Lu, N.; Zhang, J.; Zhang, Z.; Xu, X.; Wang, K. Construction and Optimization Strategy of Ecological Security Pattern in a Rapidly Urbanizing Region: A Case Study in Central-South China. *Ecol. Indic.* **2022**, *136*, 108604. [CrossRef]
35. Peng, J.; Yang, Y.; Liu, Y.; Hu, Y.; Du, Y.; Meersmans, J.; Qiu, S. Linking Ecosystem Services and Circuit Theory to Identify Ecological Security Patterns. *Sci. Total Environ.* **2018**, *644*, 781–790. [CrossRef]
36. Song, T.; Li, D.; Zhang, L.; Wang, G.; Gao, Y.; Yang, C.; Feng, C.; Ma, H. Importance Evaluation of Ecosystem Services and Construction of Ecological Security Pattern in Qinba Mountain Area. *Strateg. Study Chin. Acad. Eng.* **2020**, *22*, 64–72. [CrossRef]
37. Li, X.; Ma, B.; Lu, C.; Yang, H.; Sun, M. Spatial Pattern and Development of Protected Areas in the North-South Transitional Zone of China. *Chin. Geogr. Sci.* **2021**, *31*, 149–166. [CrossRef]
38. Zhang, Y.; Yin, H.; Zhu, L.; Miao, C. Landscape Fragmentation in Qinling–Daba Mountains Nature Reserves and Its Influencing Factors. *Land* **2021**, *10*, 1124. [CrossRef]
39. Xie, G.; Zhang, C.; Zhen, L.; Zhang, L. Dynamic Changes in the Value of China's Ecosystem Services. *Ecosyst. Serv.* **2017**, *26*, 146–154. [CrossRef]
40. Xie, G.; Zhen, L.; Lu, C.; Xiao, Y.; Chen, C. Expert Knowledge Based Valuation Method of Ecosystem Services in China. *J. Nat. Resour.* **2008**, *23*, 911–919.

41. Xie, G.; Lu, C.; Leng, Y.; Zheng, D.; Li, S. Ecological Assets Valuation of the Tibetan Plateau. *J. Nat. Resour.* **2003**, *18*, 189–196.
42. Costanza, R.; d'Arge, R.; de Groot, R.; Farber, S.; Grasso, M.; Hannon, B.; Limburg, K.; Naeem, S.; O'Neill, R.V.; Paruelo, J.; et al. The Value of the World's Ecosystem Services and Natural Capital. *Nature* **1997**, *387*, 253–260. [CrossRef]
43. TEEB. *The Economics of Ecosystems and Biodiversity: Ecological and Economic Foundations*; Earthscan: London, UK; Washington, DC, USA, 2010.
44. Jiang, H.; Peng, J.; Dong, J.; Zhang, Z.; Xu, Z.; Meersmans, J. Linking Ecological Background and Demand to Identify Ecological Security Patterns across the Guangdong-Hong Kong-Macao Greater Bay Area in China. *Landsc. Ecol.* **2021**, *36*, 2135–2150. [CrossRef]
45. Zhang, Z.; Niu, J.; Cheng, Q.; Wang, Z. Construction of Eco-tourism Corridor and Eco-tourism Area in Xinyang Section of Huaihe River Basin. *Xinyang Norm. Univ. (Nat. Sci. Ed.)* **2023**, *36*, 517–522.
46. Zhai, H.; Zhang, Z.; Zhao, X.; Xie, Q.; Cheng, Q.; Hu, Y. Optimization of Green Infrastructure in Xinyang City Based on Network Structure Analysis. *J. Xinyang Norm. Univ. (Nat. Sci. Ed.)* **2021**, *34*, 260–266.

Disclaimer/Publisher's Note: The statements, opinions and data contained in all publications are solely those of the individual author(s) and contributor(s) and not of MDPI and/or the editor(s). MDPI and/or the editor(s) disclaim responsibility for any injury to people or property resulting from any ideas, methods, instructions or products referred to in the content.

land

MDPI

Article

Spatiotemporal Variation and Influencing Factors of Ecological Quality in the Guangdong-Hong Kong-Macao Greater Bay Area Based on the Unified Remote Sensing Ecological Index over the Past 30 Years

Fangfang Sun [1,†], Chengcheng Dong [1,†], Longlong Zhao [2], Jinsong Chen [2], Li Wang [3], Ruixia Jiang [2,3,*] and Hongzhong Li [2,*]

[1] Shenzhen Academy of Environmental Science, Shenzhen 518001, China; sunffgz@163.com (F.S.); dongcc@pku.edu.cn (C.D.)
[2] Shenzhen Institutes of Advanced Technology, Chinese Academy of Sciences, Shenzhen 518055, China; ll.zhao@siat.ac.cn (L.Z.); js.chen@siat.ac.cn (J.C.)
[3] School of Surveying and Land Information Engineering, Henan Polytechnic University, Jiaozuo 454003, China; wangli29@hpu.edu.cn
* Correspondence: rx.jiang1@siat.ac.cn (R.J.); hz.li@siat.ac.cn (H.L.); Tel.: +86-156-7088-5517 (R.J.); +86-137-2349-2858 (H.L.)
† These authors contributed equally to this work.

Abstract: The Guangdong-Hong Kong-Macao Greater Bay Area (GBA) is one of China's three major urban agglomerations. Over the past thirty years, the region has undergone intensive economic development and urban expansion, resulting in significant changes in its ecological conditions. Due to the region's humid and rainy climate, traditional remote sensing ecological indexes (RSEIs) struggle to ensure consistency in long-term ecological quality assessments. To address this, this study developed a unified RSEI (URSEI) model, incorporating optimized data selection, composite index construction, normalization using invariant regions, and multi-temporal principal component analysis. Using Landsat imagery from 1990 to 2020, this study examined the spatiotemporal evolution of ecological quality in the GBA. Building on this, spatial autocorrelation analysis was applied to explore the distribution characteristics of the URSEI, followed by geodetector analysis to investigate its driving factors, including temperature, precipitation, elevation, slope, land use, population density, GDP, and nighttime light. The results indicate that (1) the URSEI effectively mitigates the impact of cloudy and rainy conditions on data consistency, producing seamless ecological quality maps that accurately reflect the region's ecological evolution; (2) ecological quality showed a "decline-then-improvement" trend during the study period, with the URSEI mean dropping from 0.65 in 1990 to 0.60 in 2000, then rising to 0.63 by 2020. Spatially, ecological quality was higher in the northwest and northeast, and poorer in the central urbanized areas; and (3) in terms of driving mechanisms, nighttime light, GDP, and temperature were the most influential, with the combined effect of "nighttime light + land use" being the primary driver of URSEI spatial heterogeneity. Human-activity-related factors showed the most notable variation in influence over time.

Keywords: ecological quality; URSEI; spatial autocorrelation; influencing factors; geographical detector; Guangdong-Hong Kong-Macao Greater Bay Area (GBA)

1. Introduction

The ecological environment is the foundation of human survival and social development, and its condition and evolution are directly linked to human existence and sustainable development. Over the past half-century, rapid population growth and advancements in science and technology have accelerated the exploitation of natural resources in both scale and intensity. While these activities have brought substantial material wealth to human society, they have also exacerbated ecological imbalances. Issues such as vegetation destruction, climate change, water shortages, land degradation, and biodiversity loss have become increasingly prevalent, posing significant threats to regional ecological security and economic sustainability [1–3]. Accurately understanding and assessing regional ecological conditions, clarifying their changing trends, and identifying driving mechanisms are fundamental to environmental protection. These efforts also serve as a critical basis for formulating environmental policies and resource development plans [4–6].

In recent years, remote sensing technology has become an essential tool for regional ecological quality assessment due to its advantages of fast processing speed, wide coverage, and high timeliness. Many scholars have used remote sensing indices to evaluate ecological conditions, such as monitoring changes in vegetation cover through vegetation indices [7–9], studying urban heat island effects using surface temperature data [10,11], and assessing regional water environments through water indices to extract river information [12]. However, ecological conditions are a complex system influenced by multiple factors, and independent evaluations based on a single indicator can only reflect a specific aspect of the ecosystem, making it difficult to fully and accurately capture the overall ecological quality [13–16]. In response, Professor Xu Hanqiu [17] proposed the Remote Sensing Ecological Index (RSEI) in 2013. This index, entirely based on remote sensing technology, integrates four indicators: greenness, humidity, heat, and dryness, enabling a comprehensive assessment of ecological conditions. It also visually reflects spatial variations in regional ecological quality and has been widely applied in different regions [18–20]. As the application of the RSEI in ecological monitoring has expanded, many scholars have improved the method by refining aspects such as indicator selection [21,22], normalization [23], and indicator synthesis [24,25] to meet the ecological assessment needs of various regions. These improvements have enhanced the applicability of the RSEI in regional ecological monitoring, yielding positive results. Therefore, to more accurately monitor and assess regional ecological quality, developing a more refined regional remote sensing ecological index is essential [26].

The changes in ecological quality are influenced by multiple factors. In addition to natural factors, human activities are considered to be a major driving force behind the decline in ecological quality in some cases [27–30]. However, most studies focus primarily on analyzing the ecological quality of a study area and its spatiotemporal changes, with limited exploration of the specific factors driving these changes [31,32]. In fact, a thorough analysis of driving factors can more precisely reveal the root causes of ecological issues, providing a scientific basis for ecological protection and sustainable development [33]. Common methods for analyzing influencing factors include correlation coefficient methods [34,35], elasticity coefficient methods [36], panel quantile regression [37], and geographically weighted regression [38]. While these methods can effectively assess the impact of multiple factors, they struggle to uncover the interactions between factors and their combined effects on ecological quality changes. To address this limitation, Wang Jinfeng et al. [39] proposed the Geographical Detector Model, a statistical method for detecting spatial heterogeneity and revealing underlying driving factors. This model not only quantitatively analyzes the explanatory power of each driving factor on ecological changes but also detects the interaction effects of driving factors on ecological quality. It has been

widely applied in fields such as land use [40], regional economy [41], meteorology [42], environment [43], and public health [44].

The Guangdong-Hong Kong-Macao Greater Bay Area (GBA) is the fourth largest bay area in the world, following the New York Bay Area, San Francisco Bay Area, and Tokyo Bay Area. It serves as an important spatial platform for the country's development of a world-class city cluster and participation in global competition. Over the past few decades, the rapid economic development and urban expansion in the GBA have disrupted the original ecological system elements, structure, and functions, presenting severe challenges to ecological civilization construction. Timely and accurate acquisition of the spatiotemporal distribution characteristics, evolution trends, and driving mechanisms of ecological quality in the GBA is of great significance for promoting ecological governance and protection of urban environments. Given that the GBA is located in South China, with a consistently cloudy and rainy climate, and experiences dramatic ecological changes, the use of the RSEI for long-term ecological monitoring and assessment is often affected by cloud cover in optical imagery. This impact influences various aspects, such as regional image stitching, indicator extraction, normalization, and consistency of data acquisition across different time phases, ultimately affecting the spatiotemporal comparability of ecological indices and the accuracy of evolution pattern analysis. In previous studies on long-term ecological quality assessment in the GBA, the comparability of time series has been relatively low, making it difficult to accurately reflect the spatiotemporal distribution and evolution patterns of ecological quality [45–48].

To address this issue, based on the RSEI, a Unified Remote Sensing Ecological Index (URSEI) was developed by optimizing data selection, normalizing invariant regional indicators, and integrating multi-temporal principal component analysis. This method is designed for long time series and regions with dramatic ecological changes. Using long-term satellite remote sensing data, this study analyzed the spatiotemporal distribution patterns and evolution trends of ecological environmental quality in the GBA from 1990 to 2020. Spatial autocorrelation analysis was then applied to investigate the spatial clustering of ecological indices in the GBA. Furthermore, the Geographical Detector Model was employed to quantitatively explore the impact mechanisms of natural factors such as topography and climate, and human factors such as land use types and population density, on the spatial differentiation of ecological quality. The findings contribute to a comprehensive understanding of the ecological environment in the GBA and its driving mechanisms, providing a scientific basis for regional ecological protection and governance.

2. Materials and Methods

2.1. Study Area

The GBA is located in the central and southern part of Guangdong Province (21°32′–24°26′ N, 111°20′–115°24′ E), covering an area of approximately 56,000 km^2. It includes nine cities in Guangdong Province: Guangzhou, Shenzhen, Zhuhai, Foshan, Dongguan, Zhongshan, Jiangmen, Huizhou, and Zhaoqing, as well as the two Special Administrative Regions of Hong Kong and Macao (Figure 1). The region has a unique topography, surrounded by hilly and mountainous terrain in the west, north, and east, with a vast plain in the center. The southern part faces the South China Sea, forming a geographical pattern of "mountains on three sides, the sea on one side", with the terrain gradually descending from the northwest and northeast toward the central and southern parts. The GBA has a subtropical humid monsoon climate with abundant rainfall, receiving an annual precipitation of 1900–2000 mm, and a mild climate, with an average annual temperature of 21–23 °C. Thanks to its favorable geographical conditions and strong national policy support, the region has experienced rapid economic development and has become one

of the fastest urbanizing, most open, and economically dynamic regions in China. As of 2024, the GBA's permanent population has reached 86.17 million, with a population density of 1531 people per km^2. For the purposes of the subsequent results and discussion, the locations of the urban core area of cities in the Greater Bay Area are also shown in Figure 1.

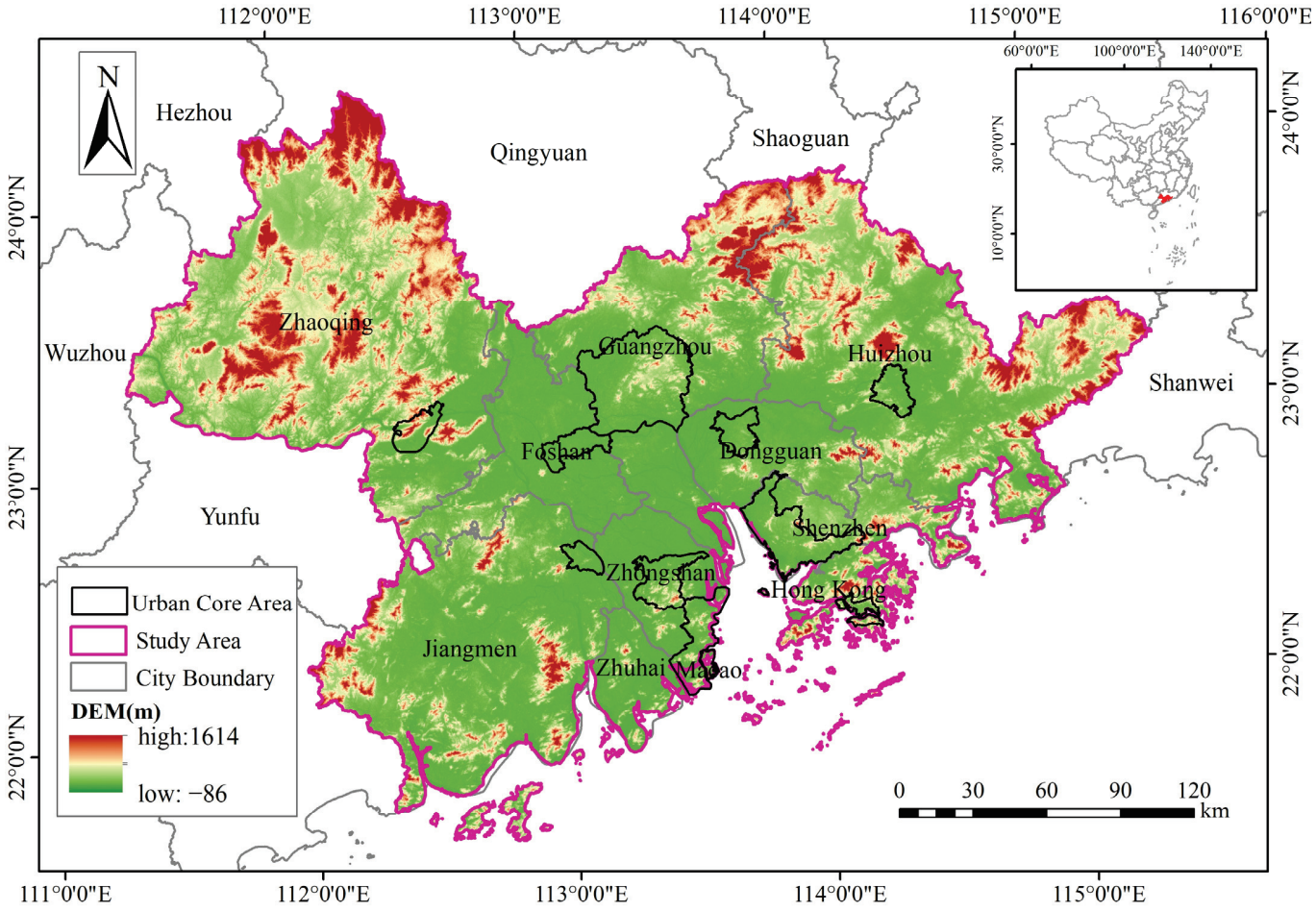

Figure 1. Location of the GBA, China.

2.2. Data Sources and Preprocessing

2.2.1. Remote Sensing Data and Preprocessing

This study utilizes Landsat series remote sensing images provided by NASA (https://images.nasa.gov/, accessed on 10 May 2021) as the primary data source. Landsat-5 TM images were selected for the years 1990, 2000, and 2010, while Landsat-8 OLI images were used for 2020. Given the long acquisition cycle of Landsat data and the frequent cloud cover in the GBA, this study modified the conventional approach of selecting a single cloud-free or minimally clouded image from the target year. Instead, images were selected from the target year and the adjacent years within the vegetation growth period (September, October) and the non-growth period (December, January), ensuring cloud coverage below 30%. Data preprocessing included cloud removal and water masking. Cloud removal was performed using the CFMASK algorithm based on the QA quality assessment band of Landsat images. Additionally, permanent water bodies, including rivers and reservoirs, were masked using the secondary wetland category from the 1990–2020 land cover product of the Greater Bay Area [49] to minimize the impact of surface water on the humidity principal component load.

2.2.2. Impact Factor Data and Preprocessing

The driving factors influencing the distribution and evolution of ecological quality can be categorized into natural and anthropogenic factors. Based on previous studies [50–53] and data availability, this study selects four natural factors—temperature, precipitation, elevation, and slope—and four anthropogenic factors—land use type, population density, GDP, and nighttime light index. The primary data sources and details are listed in Table 1. Since nighttime light and GDP data for 1990 are unavailable, this study substitutes them with data for 1992.

Table 1. Main information and sources of impact factor data.

Data	Time	Resolution	Data Source
Temperature	1990, 2000, 2010, 2020	1 km	http://www.geodata.cn/, accessed on 16 July 2024
Precipitation	1990, 2000, 2010, 2020	1 km	
Population density	1990, 2000, 2010, 2020	1 km	https://www.resdc.cn/, accessed on 16 July 2024
Nighttime lights	1990, 2000, 2010, 2020	1 km	https://dataverse.harvard.edu/, accessed on 16 July 2024
GDP	1990, 2000, 2010, 2020	1 km	https://www.resdc.cn/, accessed on 16 July 2024
Type of land use	1990, 2000, 2010, 2020	30 m	ChinaCover
DEM	——	30 m	https://www.gscloud.cn/, accessed on 16 July 2024

The preprocessing of driving factor data was conducted primarily using ArcGIS 10.2. Due to inconsistencies in spatial extent and projection among different datasets, all data were first clipped and reprojected to align with the study area. Additionally, considering variations in spatial resolution, all datasets were resampled to a uniform resolution of 1 km × 1 km.

Since the geographical detector model used in the subsequent analysis requires categorical variables, the independent variables were reclassified. Land use type data were classified into six categories based on product specifications, while other numerical driving factors were discretized into five categories using the natural breaks method in ArcGIS.

2.3. Constrcution of the URSEI

2.3.1. Indicator Factors

The Remote Sensing Ecological Index (RSEI) model integrates four key indicator factors closely related to human daily life: greenness, humidity, heat, and dryness. Specifically, the Normalized Difference Vegetation Index (NDVI) represents the greenness indicator, the humidity component (WET) derived from tasseled cap transformation represents surface moisture, the average synthesis of the Index-Based Built-up Index (IBI) and the Soil Index (SI) serves as the dryness indicator (NDBSI), and the Land Surface Temperature (LST) represents the heat indicator. These four indicators are entirely derived from remote sensing data, making them easily accessible, with a computational process that requires no manual intervention, ensuring objective and reliable results. The Unified Remote Sensing Ecological Index (URSEI) retains the four indicator factors of RSEI, with the calculation methods for each ecological indicator shown in Table 2.

Table 2. The calculation method of ecological indicators.

Index	Calculation Methods	
NDVI	$NDVI = (B_{nir} - B_{red})/(B_{nir} + B_{red})$	(1)
NDBSI	$SI = \frac{[(B_{swir1}+B_{red})-(B_{nir}+B_{blue})]}{[(B_{swir1}+B_{red})+(B_{nir}+B_{blue})]}$	(2)
	$IBI = \frac{2B_{swir1}/(B_{swir1}+B_{nir})-\left[B_{nir}/(B_{nir}+B_{red})+B_{green}/\left(B_{green}+B_{swir1}\right)\right]}{2B_{swir1}/(B_{swir1}+B_{nir})+\left[B_{nir}/(B_{nir}+B_{red})+B_{green}/\left(B_{green}+B_{swir1}\right)\right]}$	(3)

Table 2. *Cont.*

Index	Calculation Methods	
	$NDBSI = (SI + IBI)/2$	(4)
WET	TM : $WET = 0.0315 \times B_{blue} + 0.2021 \times B_{green} + 0.3012 \times B_{red} + 0.1594 \times B_{nir} - 0.6806 \times B_{swir1} - 0.6109 \times B_{swir2}$	(5)
	OLI : $WET = 0.1511 \times B_{blue} + 0.1973 \times B_{green} + 0.3283 \times B_{red} + 0.3407 \times B_{nir} - 0.7117 \times B_{swir1} - 0.4559 \times B_{swir2}$	(6)
LST	This study selects the land surface temperature (LST) from the Landsat SR product as the LST indicator factor.	(7)

Note: B_{red}, B_{blue}, B_{green}, B_{nir}, B_{swir1}, and B_{swir2} represent the reflectance of the Landsat imagery in the red, blue, green, near-infrared (NIR), shortwave infrared 1(SWIR1), and shortwave infrared 2 (SWIR2) bands, respectively.

2.3.2. Synthesis of Indicator Factors

In this study, multiple images were selected for each monitoring year, necessitating a synthesis process to generate the four indicator factors for each monitoring period. For greenness, humidity, and dryness indicators, a median composite was first applied separately to the vegetation growing season and the non-growing season images, followed by averaging the results from both periods. The median composite effectively reduces the influence of weather conditions, precipitation, and solar altitude angle, minimizing anomalies and ensuring that the indicators accurately reflect the average conditions of each period. This approach prevents extreme observations from skewing the overall assessment. The final averaging process provides a more comprehensive representation of the ecological conditions throughout the year, mitigating potential biases from single-period observations and delivering a more stable and integrated ecological evaluation.

$$I_y = \frac{1}{2}\left(I_y^a + I_y^w\right) \tag{8}$$

$$I_y^a = \text{Median}\left\{I_{y_i}^{d_j}\right\} \tag{9}$$

$$y - 1 \le y_i \le y + 1 \qquad d_j \in \{a\}$$

$$I_y^w = \text{Median}\left\{I_{y_i}^{d_j}\right\} \tag{10}$$

$$y - 1 \le y_i \le y + 1 \qquad d_j \in \{w\}$$

where I represents the indicator factor, y denotes the year, a represents the vegetation growing season, w represents the non-growing season, *Median* denotes the median operator, and $I_{y_i}^{d_j}$ represents the I indicator on date d_j of year y_i.

For the heat indicator, imagery from the autumn vegetation growing season is selected for each monitoring period. The Landsat thermal infrared data from path/row 122/44 at the center of the study area is used as the reference. A random forest regression model is applied to calibrate the thermal infrared data from other path/row numbers using overlapping areas, generating temperature-consistent thermal infrared data aligned with the reference (122/44). A median operator is then used to synthesize the thermal infrared data for the entire GBA. In the random forest regression model, input variables include land cover type, elevation, slope, NDVI, NDWI, WET, IBI, and SI.

2.3.3. Indicator Normalization Based on Invariant Regions

The RSEI model employs range normalization to eliminate dimensional differences among indicators. In existing studies, normalization is typically performed separately for each time period by applying the minimum and maximum values from individual datasets to normalize corresponding indicators. However, this method is susceptible to extreme values, which may introduce biases in the results. Over the past 30 years, the Greater Bay Area has undergone significant urban expansion and ecological changes,

leading to substantial differences in the statistical distribution of ecological indicators. While conventional probability-based normalization methods (such as Z-score or Gaussian normalization) can adjust data distribution, they may reduce time-series consistency, affecting the spatial-temporal comparability of indicators and the accuracy of evolution pattern analysis.

To address the issue of indicator normalization, this study proposes an invariant-region-based normalization method. First, using land cover classification data of the Greater Bay Area from 1990 to 2020 [49], a pixel-by-pixel comparison method was applied to identify areas with unchanged land cover types. To accurately delineate long-term stable land cover regions, three decadal intervals (1990–2000, 2000–2010, and 2010–2020) were established to generate stable land cover layers for each period. Finally, spatial intersection analysis was performed to extract areas where land cover types remained unchanged over the entire 30-year period. The formula is as follows:

$$U = U_1 \cap U_2 \cap U_3 \tag{11}$$

U_1, U_2, and U_3 represent the land cover layers for the periods 1990–2000, 2000–2010, and 2010–2020, where no changes in land cover occurred; U represents the intersection of the three invariant region layers.

Then, based on the invariant layer U, the indicator factors for different monitoring periods are masked. The cumulative probability distribution function method is applied to calculate the 1st and 99th percentiles of the masked indicators, which are used as the minimum and maximum values. Finally, these statistical results are used to normalize the original, non-masked indicator factors, ensuring that their range is constrained between 0 and 1. At the same time, dryness and heat are treated as negative indicators and undergo reverse normalization to ensure that the negative indicators are reasonably reflected in the overall ecological assessment.

2.3.4. Multi-Temporal Fusion Principal Component Analysis

The RSEI model uses principal component analysis (PCA) to construct a composite ecological index for each monitoring period and standardizes the RSEI values to a range of 0–1 using range normalization, effectively reflecting the relative ecological condition of a specific spatial region at a given time. However, in areas with significant ecological changes, the RSEI value only represents the relative condition within a specific period, making it difficult to accurately reflect the long-term ecological evolution trend across different years.

In this study, ecological indicator factors from four monitoring periods are fused using a unified principal component analysis to construct a composite ecological index. First, the normalized indicator factors are used as variables, and they are input into PCA synchronously and with equal weight to ensure that the data are processed under the same standard. Then, the contribution rate of the first principal component (PC1) is assessed. If it exceeds 70%, PC1 can be used to create the composite ecological index. Unlike the traditional RSEI model, this study does not re-normalize the composite ecological index. Instead, it normalizes the feature vector of PC1 and applies it uniformly to all monitoring periods to generate the Unified Remote Sensing Ecological Index (URSEI), ensuring the comparability of ecological quality changes across different time periods. The formula is as follows:

$$[\lambda_1, \lambda_2, \lambda_3, \lambda_4] = \mathrm{PC1}(\mathrm{NDVI}, \mathrm{WET}, \mathrm{NDBSI}, \mathrm{LST}) \tag{12}$$

$$\mathrm{URSEI} = \lambda_1 \mathrm{NDVI} + \lambda_2 \mathrm{WET} + \lambda_3 \mathrm{NDBSI} + \lambda_4 \mathrm{LST} \tag{13}$$

where λ_i is the eigenvector of PC1, satisfying $\sum \lambda_i^2 = 1$.

2.4. Average Correlation

Average correlation $\overline{C}$ is used in this study to test the applicability of URSEI. A value close to 1 indicates a higher degree of comprehensive representation by the model, signifying stronger applicability. The formula is as follows:

$$\overline{C} = \frac{\left(|C_p| + |C_q| + |C_r| + \ |C_g|\right)}{n} \tag{14}$$

where C_p, C_q, C_r, and C_g represent the correlation coefficients of the p, q, r, and g indicators at the same time, and n is the number of indicators.

2.5. Spatial Autocorrelation Analysis

Spatial autocorrelation analysis is used to test whether the attribute values of elements with spatial locations are related to the attribute values at neighboring spatial points. It is an important indicator of the aggregation or dispersion of spatial elements. It includes both global spatial autocorrelation and local spatial autocorrelation [54–57]. By calculating the global Moran's I index, it can be used to analyze the overall spatial correlation and spatial differences in the region during different periods. The formula is as follows:

$$I_g = \frac{n\sum_{i=1}^{n}\sum_{j=1}^{n}\left(X_i - \overline{X}\right)\left(X_j - \overline{X}\right)}{\left(\sum_{i=1}^{n}\sum_{j=1}^{n} W_{ij}\right)\sum_{i=1}^{n}\left(X_i - \overline{X}\right)^2} \tag{15}$$

where n is the number of samples, X_i and X_j are the attribute values of X at spatial locations i and j, $\overline{X}$ is the average value of attribute X_i, and W_{ij} is the spatial weight matrix. The range of Moran's I index is $(-1, 1)$. When $I_g > 0$, it indicates a positive correlation between spatial units; when $I_g < 0$, it indicates a negative correlation between spatial units; when $I_g = 0$, it indicates no correlation, representing a random distribution.

The local Moran's I index can be used to assess the correlation and significance between a region and neighboring regions and to visualize it using the Local Indicators of Spatial Association (LISA). The calculation formula for the local Moran's I is as follows:

$$I_l = \frac{n\left(X_i - \overline{X}\right)\sum_{j=1}^{n} W_{ij}\left(X_j - \overline{X}\right)}{\sum_{i=1}^{n}\left(X_i - \overline{X}\right)^2} \tag{16}$$

where the meanings of the parameters are the same as in the previous Formula (15).

2.6. Geographical Detector

The geographical detector is a statistical model proposed by Wang Jinfen et al. [39] specifically designed to detect spatial differentiation characteristics and their driving mechanisms. In this study, the eight driving factors from Section 2.2.2 are used as independent variables X, with URSEI values as the dependent variable Y. The factor detector, interaction detector, and risk zone detector in the geographical detector are used to systematically explore the impact and interrelationships of various factors on the spatial differentiation of ecological quality.

(1) Factor detection: This is used to analyze the extent to which the selected independent variables X explain the spatial differentiation of the dependent variable Y (URSEI) at different time stages. Its explanatory power is measured by the q-value, as follows:

$$q = 1 - \frac{\sum_{h=1}^{L} N_h \sigma_h^2}{N\sigma^2} \tag{17}$$

where L represents the stratification of the independent variable X, i.e., the number of categories; N_h and N are the number of sampling points in the h-th category of the independent variable X and the total number of sampling points in the region, respectively; σ_h^2 and σ^2 are the variances of the h-th category region for the independent variable X and the variance of Y across the entire region, respectively; and the range of q is from 0 to 1. The larger the q value, the stronger the explanatory power of the independent variable X on the dependent variable Y, and vice versa. The q value indicates that X explains 100 q% of Y.

(2) Interaction detection: This is used to identify the interactions between different influencing factors X_i and assess how the explanatory power of the dependent variable Y changes when two factors (such as X_1 and X_2) act together. The interactions between factors can be divided into five types, and their corresponding q-value ranges are shown in Table 3.

Table 3. Interaction types of the detection factors.

Q-Value Range	The Type of Interaction
q(X1∩X2) < Min[q(X1),q(X2)]	Nonlinear weakening
Min[q(X1),q(X2)] < q(X1∩X2) < Max[q(X1),q(X2)]	Univariate nonlinear weakening
q(X1∩X2) > Max[q(X1),q(X2)]	Bivariate enhancement
q(X1∩X2) = q(X1) + q(X2)	Independence
q(X1∩X2) > q(X1) + q(X2)	Non-linear enhancement

(3) Risk zone detection: This is used to evaluate whether there is a significant difference in the mean of the dependent variable Y between any two sub-regions within the different strata of the independent variable X, and to conduct significance testing using the t-statistic.

$$t_{\overline{y}_{h=1}-\overline{y}_{h=2}} = \frac{\overline{Y}_{h=1} - \overline{Y}_{h=2}}{\left[\frac{Var\left(\overline{Y}_{h=1}\right)}{n_{h=1}} + \frac{Var\left(\overline{Y}_{h=2}\right)}{n_{h=2}}\right]^{1/2}} \quad (18)$$

where $\overline{Y}_h$ is the mean URSEI value in region h, n_h is the sample size within the sub-region, and Var represents variance.

3. Results

3.1. Model Validation

Table 4 presents the principal component analysis results for the four monitoring periods from 1990 to 2020 and the fused data, including the eigenvalue and contribution rate of the first principal component (PC1), as well as the corresponding eigenvectors for each indicator factor in PC1. As shown in Table 4, the contribution rate of PC1 exceeds 75% for each period, and for the fused and unified principal component analysis result, the contribution rate of PC1 reaches 81.6%. This indicates that PC1 integrates the majority of the characteristics of the four indicator factors and can be used to create the comprehensive ecological index. The feature vector of the unified fusion shows that the PC1 weights for NDVI, WET, NDBSI, and LST are 0.612, 0.425, 0.525, and 0.413, respectively. Since the negative indicators NDBSI and LST have been reverse normalized, their eigenvectors are positive values.

The correlation coefficients between each indicator and the average correlation between the URSEI and the individual indicators were calculated. The results are shown in Table 5, where all correlation coefficients pass the significance test at the 99% confidence level. The average correlation between the URSEI and the ecological indicators for the four monitoring periods from 1990 to 2020 is 0.763, 0.733, 0.791, and 0.812, respectively, indicating that the URSEI is a reasonable comprehensive ecological quality assessment

metric. Furthermore, in all four monitoring periods, the average correlation of the URSEI is higher than that of any single ecological indicator, demonstrating that the URSEI is more suitable for evaluating ecological quality than individual indicators.

Table 4. The result of principal component analysis.

Year	PC1		The Eigenvector Corresponding to Each Indicator			
	Eigen Value	Eigen Percent	NDVI	WET	NDBSI	LST
1990	0.134	75.3%	0.551	0.492	0.593	0.327
2000	0.141	75.8%	0.576	0.469	0.544	0.392
2010	0.186	81.0%	0.633	0.402	0.530	0.397
2020	0.194	85.3%	0.557	0.436	0.549	0.446
Convergence and unity	0.146	81.6%	0.612	0.425	0.525	0.413

Table 5. Correlation matrix among the URSEI and four indicators.

Year	Indicator	NDVI	WET	NDBSI	LST	URSEI
1990	NDVI	1	0.419	0.576	0.479	0.853
	WET	0.419	1	0.691	0.612	0.735
	NDBSI	0.576	0.691	1	0.652	0.769
	LST	0.479	0.612	0.652	1	0.693
	$\overline{C}$	0.491	0.574	0.640	0.581	0.763
2000	NDVI	1	0.492	0.608	0.591	0.720
	WET	0.492	1	0.647	0.654	0.648
	NDBSI	0.608	0.647	1	0.665	0.831
	LST	0.591	0.654	0.665	1	0.732
	$\overline{C}$	0.564	0.598	0.640	0.637	0.733
2010	NDVI	1	0.536	0.676	0.635	0.785
	WET	0.536	1	0.793	0.706	0.736
	NDBSI	0.676	0.793	1	0.729	0.858
	LST	0.635	0.706	0.729	1	0.783
	$\overline{C}$	0.616	0.678	0.733	0.690	0.791
2020	NDVI	1	0.587	0.831	0.605	0.822
	WET	0.587	1	0.788	0.753	0.787
	NDBSI	0.831	0.7788	1	0.765	0.864
	LST	0.605	0.753	0.765	1	0.774
	$\overline{C}$	0.674	0.706	0.795	0.708	0.812

3.2. Spatiotemporal Changes in Ecological Quality

To better quantify and visualize the URSEI, this study follows literature [17] and classifies the URSEI values into five levels at intervals of 0.2: [0–0.2), [0.2–0.4), [0.4–0.6), [0.6–0.8), and [0.8–1], representing poor, relatively poor, moderate, good, and excellent ecological quality, respectively. The classification maps of ecological quality in the GBA from 1990 to 2020 are shown in Figure 2.

From 1990 to 2020, the spatial heterogeneity of ecological quality across the GBA was high, with significantly lower ecological quality in urban areas compared to non-urban areas. Over the 30-year period, ecological quality exhibited substantial changes with notable temporal variations. In 1990, areas classified as "poor" in ecological quality were relatively scattered, aligning with the geographic locations of built-up urban areas across the GBA, forming a distinct multi-center distribution pattern. Meanwhile, areas classified as "excellent" were mainly concentrated in the northeastern and northwestern parts of the GBA. By 2000, the extent of areas classified as "poor" had increased significantly compared to 1990, with major expansions occurring in Guangzhou, Dongguan, and Shenzhen along the eastern Pearl River estuary, as well as in Foshan, which is adjacent to Guangzhou. By 2010, the overall ecological quality of the GBA had further deteriorated, with a more pronounced spatial clustering of areas classified as "poor" in the central region. However,

by 2020, the rate of ecological quality decline had slowed, with "poor" ecological quality areas remaining largely unchanged. At the same time, areas classified as "excellent" had significantly expanded in the northwestern and northeastern parts of the GBA.

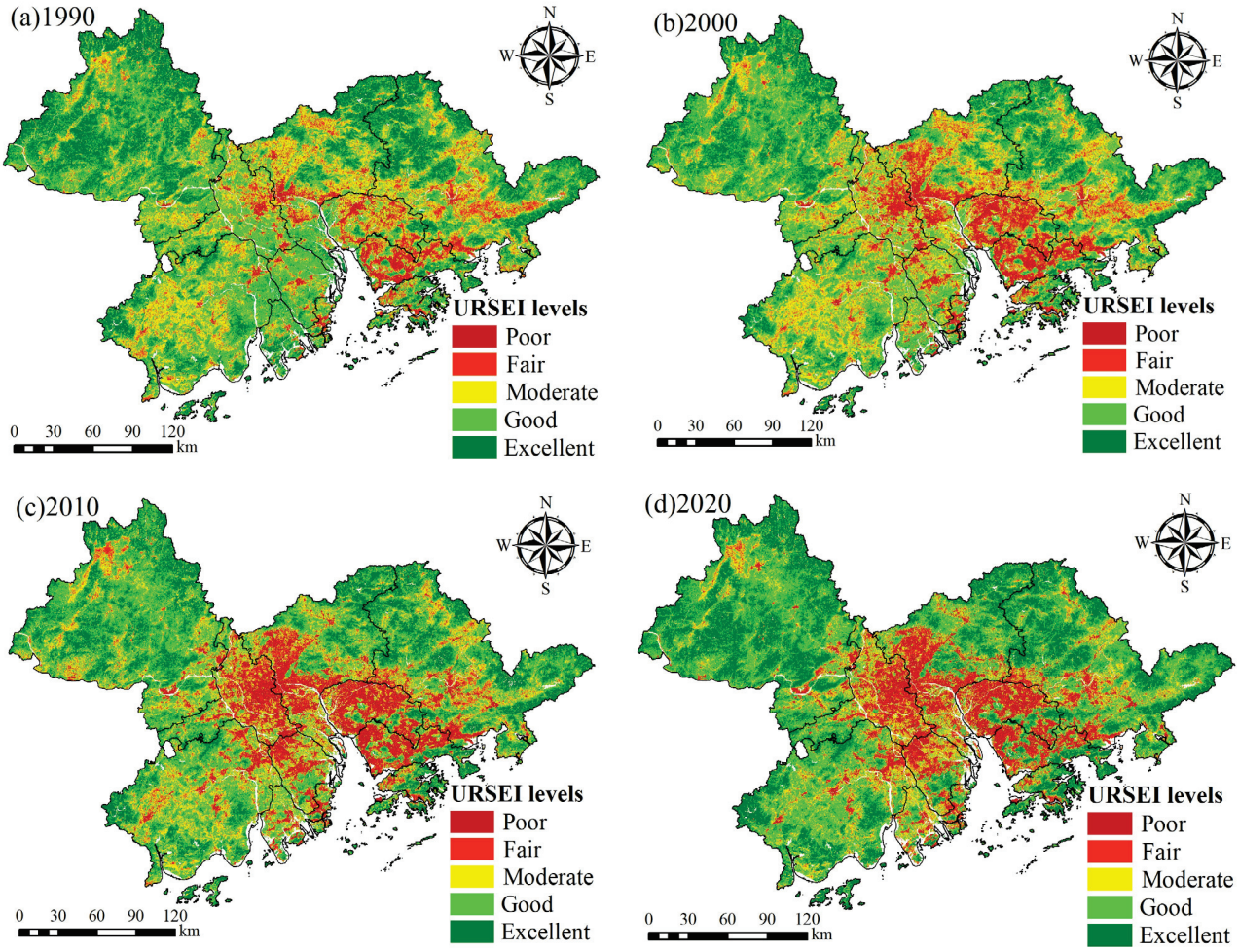

Figure 2. Spatial distribution of the URSEI in the GBA from 1990 to 2020.

Based on the URSEI classification results, the proportion of pixels in different ecological quality levels across the GBA from 1990 to 2020 was calculated, along with the mean URSEI values for the four monitoring periods. The results are shown in Figure 3. Over the past 30 years, the proportion of different URSEI levels has undergone varying degrees of change, with the overall mean URSEI showing a "decline-then-rise" trend. The mean URSEI values for the four years were 0.65, 0.60, 0.60, and 0.63, respectively, decreasing from 0.65 in 1990 to 0.63 in 2020. Compared to 1990, the ecological quality of the GBA in 2020 showed a slight decline. The proportions of areas classified as "excellent" and "good" remained relatively stable, while the proportion of "moderate" areas declined significantly. In contrast, the proportions of "poor" and "relatively poor" areas both increased, with the "poor" category rising notably from 2.54% in 1990 to 8.09% in 2020.

Based on the statistical analysis of the proportion of different ecological quality levels over each period, this study analyzed the ecological quality transitions in the GBA from 1990 to 2020 using transfer pathways (Figure 4). The results indicate that most ecological quality changes occurred between adjacent levels, exhibiting a gradual transition pattern where ecological quality progressively shifted from one level to the next. However, it is also important to note that some changes involved abrupt transitions across multiple levels, leading to significant ecological degradation. Examples include transitions from "moderate"

to "poor", "good" to "poor", and "excellent" to "relatively poor". These areas require particular attention, and efforts should be intensified to strengthen ecological protection and environmental management. This is crucial to mitigating the immense pressure that economic and urbanization developments impose on the ecological environment.

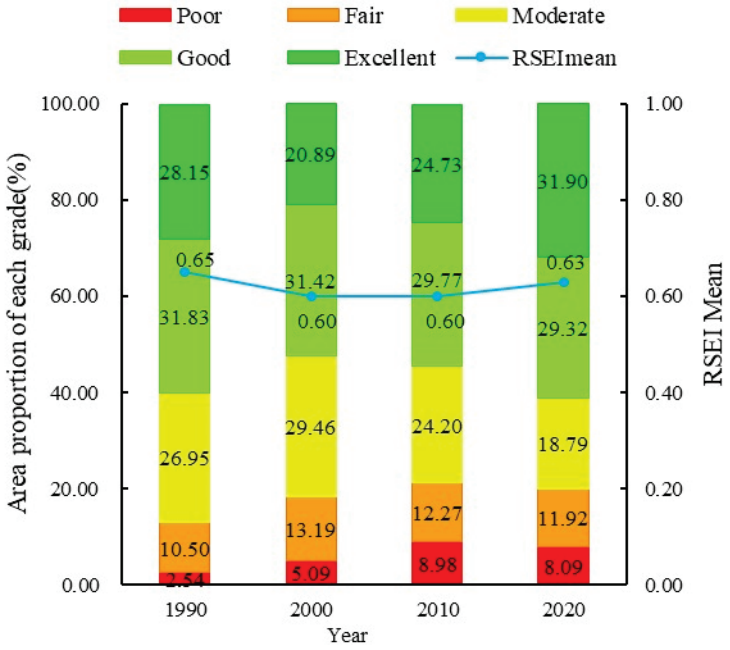

Figure 3. The proportion of area classified by ecological quality.

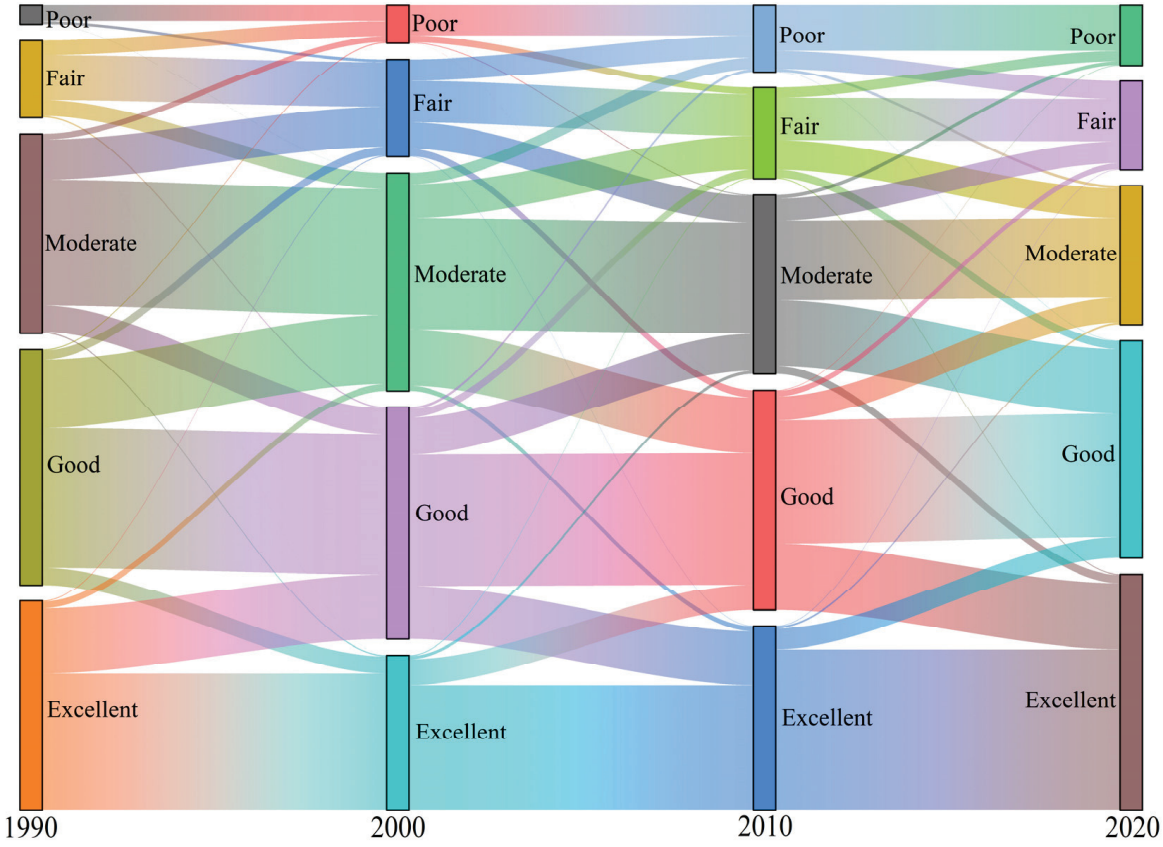

Figure 4. URSEI transfer matrix for the GBA, 1990–2020.

3.3. Ecological Quality Change Detection

To further analyze the spatial and temporal distribution of ecological quality changes, this study applied a differencing method to detect variations in the URSEI across multiple monitoring periods, using its five classification levels (Table 6).

Table 6. Transfer matrix of ecological quality levels.

Level at End Time	Level at Start Time				
	Poor	**Fair**	**Moderate**	**Good**	**Excellent**
Poor	Unchanged	Degraded	Degraded	Degraded	Degraded
Fair	Improved	Unchanged	Degraded	Degraded	Degraded
Moderate	Improved	Improved	Unchanged	Degraded	Degraded
Good	Improved	Improved	Improved	Unchanged	Degraded
Excellent	Improved	Improved	Improved	Improved	Unchanged

Table 7 and Figure 5 present the change detection results. From 1990 to 2000, the ecological quality of the GBA showed a declining trend, with a degradation area of 15,421.23 km^2, accounting for 28.61% of the total area. The spatial distribution of degradation was relatively uniform, affecting every city to varying degrees. Meanwhile, the proportion of improvement was only 8.78%, covering an area of 4730.75 km^2. Between 2000 and 2010, ecological quality exhibited a more balanced trend, with the improvement area reaching 11,386.52 km^2 (21.13%) and the degradation area covering 10,533.77 km^2 (19.55%). The degradation zones were primarily concentrated in Guangzhou, Foshan, Dongguan, Shenzhen, and most parts of Zhongshan. From 2010 to 2020, ecological quality significantly improved, with an improvement area of 14,489.22 km^2, accounting for 26.89% of the total. The improvements were distributed across all cities, while the proportion of degraded areas dropped to 12.13%, mainly concentrated in the central region. Over the entire 30-year period (1990–2020), a total of 13,961.27 km^2 (25.95%) experienced ecological degradation. The most severe declines occurred in Guangzhou, Foshan, Zhongshan, Dongguan, and Zhuhai, while Zhaoqing, Huizhou, Jiangmen, and Shenzhen also exhibited varying degrees of degradation.

Table 7. Ecological quality level transfer matrix of in the GBA from 1990 to 2020.

Start and End Time	Improved		Unchanged		Degraded	
	Area/km^2	**Percentage/%**	**Area/km^2**	**Percentage/%**	**Area/km^2**	**Percentage/%**
1990–2000	4730.75	8.78	33,740.56	62.61	15,421.23	28.61
2000–2010	11,386.52	21.13	31,972.04	59.33	10,533.77	19.55
2010–2020	14,489.22	26.89	32,862.42	60.98	6537.97	12.13
1990–2020	13,068.67	24.29	26,773.19	49.76	13,961.27	25.95

3.4. Ecological Quality Spatial Autocorrelation Analysis

To further explore the spatial aggregation characteristics of ecological quality in the GBA, this study adopts a 5 km × 5 km grid to sample the URSEI values of each period and uses GeoDa software 1.14.0 to conduct spatial correlation analysis on the sampling results.

Global spatial autocorrelation shows (Table 8) that the Moran's I values of the GBA for all four periods are positive, and the significance test *p*-values are all less than 0.01, indicating that the ecological quality in the study area has a significant positive spatial autocorrelation feature, meaning regions with good or poor ecological quality tend to be spatially clustered. Among them, the Moran's I value for 2020 is the highest at 0.614, indicating the strongest spatial clustering of the ecological index in the GBA in 2020. Over the study period, the Moran's I value shows a gradual increasing trend over time.

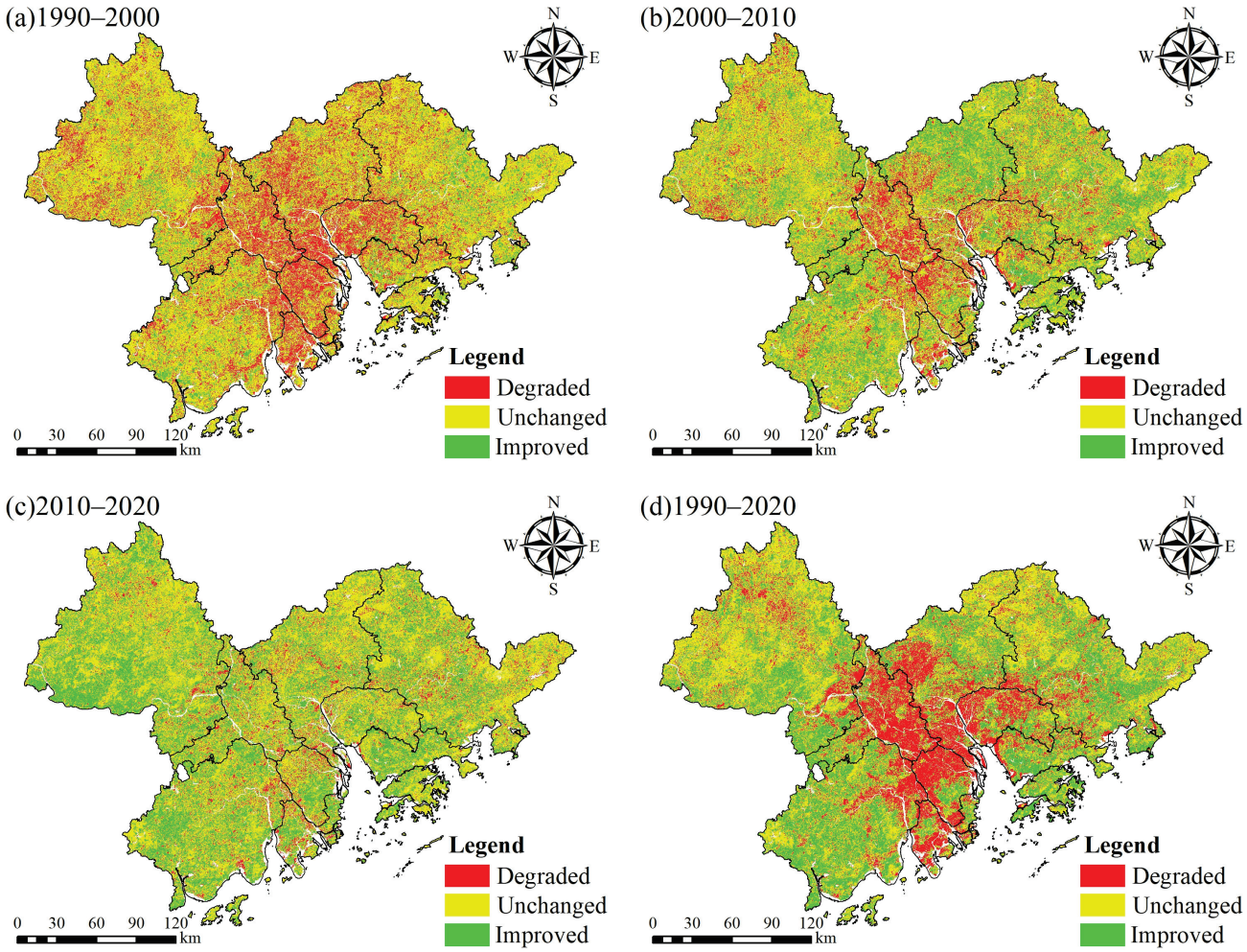

Figure 5. Change detection of ecological quality in the GBA from 1990 to 2020.

Table 8. Global Moran's I value of ecological quality at different times in the GBA.

Year	Moran's I	z	*p*
1990	0.492	44.4	0.001
2000	0.565	50.99	0.001
2010	0.596	52.41	0.001
2020	0.614	54.43	0.001

In order to further investigate the specific locations where the ecological quality in the GBA shows spatial aggregation characteristics, local spatial autocorrelation analysis was conducted to generate LISA clustering maps, which were used to analyze the clustering phenomenon of the URSEI values in the study area. As shown in Figure 6, the high–high cluster areas show a clear high-value aggregation feature, and with the passage of time, the area of these clusters has increased. The high–high cluster areas are mainly distributed in the northwest in Zhaoqing City and in the northeast in Guangzhou and Huizhou Cities. These areas are mostly high-altitude regions, with contiguous forest development, high forest cover, minimal human socio-economic activities, low disturbance and damage to the ecological environment, and thus maintain a good ecological quality foundation with high protection levels, exhibiting well-preserved characteristics. The low–low cluster areas have also shown a clear increasing trend over the past 30 years, primarily located in central Guangzhou, Foshan, Dongguan, Shenzhen, and Zhongshan. In these areas, population density is high, urbanization levels are advanced, and land types are mainly built-up

areas, where human activities intensively affect the ecological environment, leading to poor ecological quality. Overall, except for the insignificant regions, the high–high and low–low clustered areas of the four periods have relatively large and concentrated areas, while the high–low and low–high clustered areas are smaller and more dispersed in distribution.

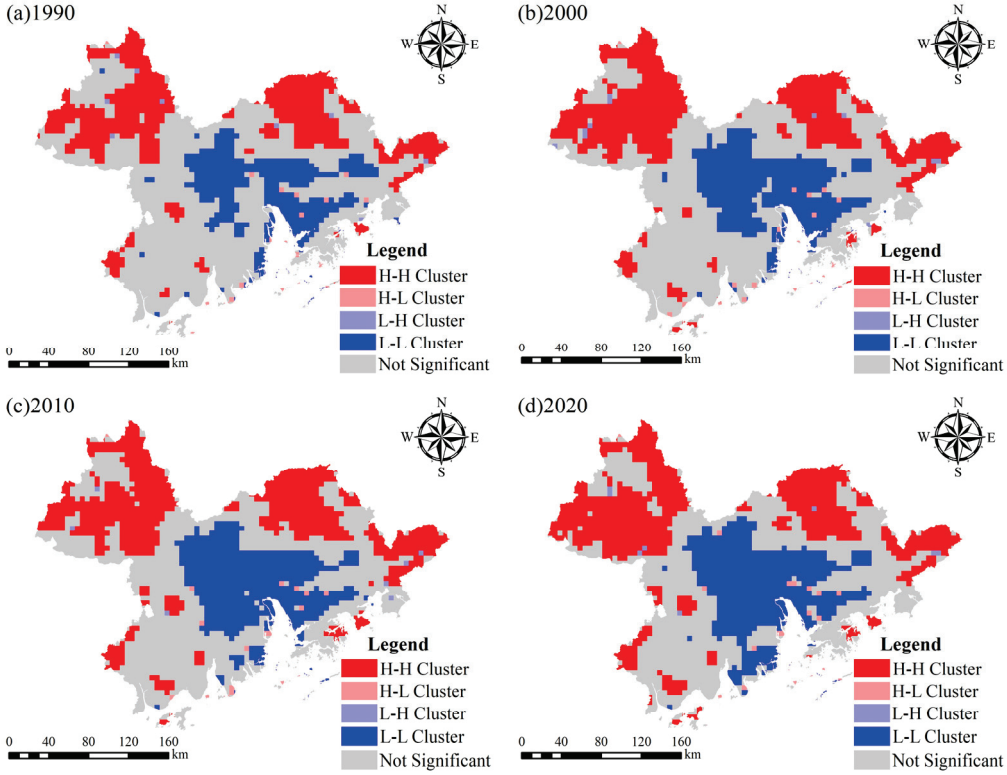

Figure 6. Locally autocorrelated LISA cluster map of ecological index in the GBA.

3.5. Ecological Quality Driving Factors Analysis

3.5.1. Single Factor Detection Results Analysis

The results of the single factor detection are shown in Table 9. The significance test *p*-values of all factors are less than 0.001, indicating that the selected independent variables significantly impact the spatial differentiation of ecological quality in the GBA.

Table 9. The result of single detection from 1990 to 2020.

Factor	1990		2000		2010		2020		1990–2020	
	q Value	Sort	q Value	Sort	q Value	Sort	q Value	Sort	q Value	Sort
Temperature	0.288	1	0.296	2	0.320	3	0.305	4	0.302	3
Precipitation	0.037	8	0.065	8	0.037	8	0.028	8	0.042	8
DEM	0.243	2	0.271	4	0.267	5	0.268	5	0.262	4
Slope	0.181	5	0.208	7	0.232	7	0.256	6	0.219	7
Type of land use	0.145	7	0.218	6	0.282	4	0.328	3	0.243	5
Population density	0.158	6	0.238	5	0.235	6	0.213	7	0.211	6
GDP	0.208	4	0.294	3	0.350	2	0.369	2	0.305	2
Nighttime lights	0.235	3	0.338	1	0.353	1	0.409	1	0.334	1

From the average q-values of the factors for the four monitoring years, nighttime lighting, GDP, and temperature exhibit a strong explanatory power for the spatial differentiation of ecological quality, with average q-values of 0.334, 0.305, and 0.302, respectively, all exceeding 0.3. This suggests that these factors play a dominant role in the spatial differentiation of ecological quality. The next most important factors are elevation, land

use type, population density, and slope, with average q-values ranging from 0.2 to 0.3, indicating a moderate explanatory power for URSEI spatial differentiation. Precipitation has the weakest influence, with an average q-value of only 0.042.

From a temporal perspective, the q-values of the factors fluctuate dynamically, and the relative importance of some factors has significantly changed. In 1990, land use type had a relatively weak explanatory power for ecological spatial heterogeneity, with a q-value of 0.145, ranking seventh. However, by 2020, the q-value increased to 0.328, rising to third place. In 1990, temperature was the dominant factor influencing ecological quality spatial differentiation, while in 2000, 2010, and 2020, the nighttime lighting index became the primary influencing factor, indicating that the dominant factors of ecological quality spatial differentiation in the Greater Bay Area shifted from natural to human factors.

Overall, the spatial differentiation of ecological quality in the GBA is influenced by both natural and human factors. In the early stages of the study period, natural factors had a stronger influence on ecological quality spatial differentiation, while in the later stages, human factors had a greater impact than natural factors, reflecting the profound impact of the rapid urbanization process in the GBA on the ecological environment.

3.5.2. Interaction Detection Results Analysis

An interaction detection analysis was conducted on the influencing factors, and the results are shown in Figure 7. Except for the interaction between precipitation and temperature in 1990 and the nonlinear enhancement effects of precipitation interacting with elevation, land use type, and population density in 2020, all other factor interactions exhibited a bivariate enhancement effect. This indicates that the spatial differentiation of ecological quality in the GBA is not the direct, independent result of a single factor but is instead driven by the synergistic enhancement effect of factor interactions.

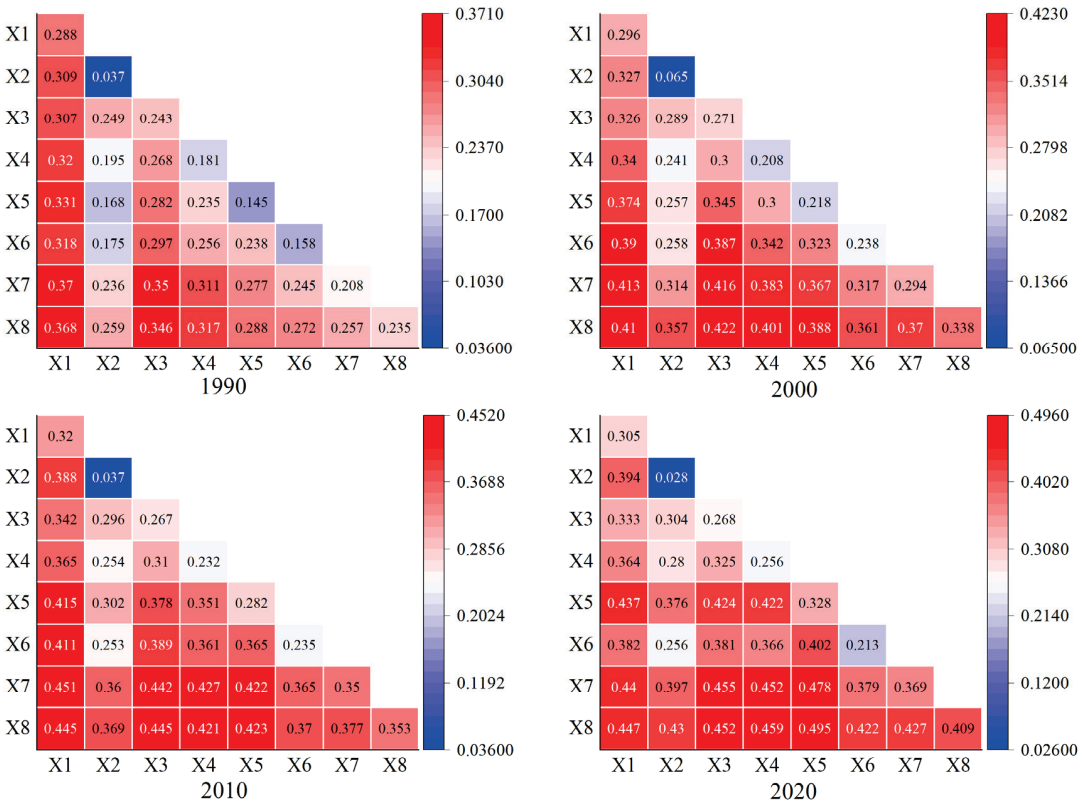

Figure 7. Interactive detection results of driving factors of ecological quality. Note: X1: (temperature), X2: (precipitation), X3: (DEM), X4: (slope), X5: (type of land use), X6: (population density), X7: (GDP), X8: (nighttime lights).

From 1990 to 2020, the highest-ranked interactions in terms of q-value were as follows: temperature ∩ GDP (0.370) in 1990, nighttime light index ∩ elevation (0.422) in 2000, temperature ∩ GDP (0.451) in 2010, and nighttime light ∩ land use type (0.495) in 2020. Over the 30-year period, the interaction q-value steadily increased from 0.370 to 0.495. Before 2010, interactions between natural and human factors had a more pronounced impact on ecological quality. However, in 2020, interactions among human factors had the greatest influence, reflecting the increasing role of socio-economic development and human activities in ecological quality changes.

By combining these findings with the single-factor detection results, it becomes evident that although precipitation had weak explanatory power when acting alone, its q-value increased significantly when interacting with other factors. This suggests that under the influence of factor interactions, single factors with initially low explanatory power can be significantly enhanced through synergistic effects, improving their ability to explain spatial differentiation in ecological quality.

3.5.3. Risk Zone Detection Analysis

Risk zone detection is used to determine whether there are significant differences in the mean attribute values of different partitions of each factor. In this study, the risk zone detection method was applied to identify the optimal range for quantitative factors and the most suitable type for qualitative factors affecting the URSEI. The 2020 risk detection results were selected as an example for analysis.

As shown in Table 10, the 2020 risk detection results indicate a significant negative correlation between the intensity of human factors and the URSEI mean value. Specifically, the three human-related factors—population density, GDP, and nighttime light index—were classified into five levels, with Level 1 representing the lowest value range and Level 5 representing the highest. The analysis results show that for all three factors, the highest URSEI mean values appeared in Level 1, with values of 0.698 (population density), 0.739 (GDP), and 0.8 (nighttime light index). Their optimal ranges were further determined to be 73–1466 people/km^2, 0.04–12.05 million CNY/km^2, and 0–19, respectively. These findings suggest that human activities have a significant impact on the ecological quality of the Guangdong-Hong Kong-Macau Greater Bay Area, with lower human activity intensity corresponding to higher URSEI values, indicating better ecological quality. Additionally, when the land use type was forest, the URSEI mean value was the highest, highlighting the crucial role of forest ecosystems in maintaining high ecological quality.

Table 10. The appropriate type and range of factors.

Factor	Suitability	The Scope or Category Corresponding to the Level of Adaptation	RSEI Mean
Temperature	1	15.52~19.74 °C	0.865
Precipitation	5	1930~2116 mm	0.703
DEM	4	393~651 m	0.863
Slope	5	8.52~18.77°	0.841
Type of land use	4	woodland	0.739
Population density	1	73~1466 people·km^{-2}	0.698
GDP	1	0.04~12.05 million yuan·km^{-2}	0.739
Nighttime lights	1	0~19	0.800

Among natural factors, each variable was similarly classified into five levels (Level 1: lowest, Level 5: highest). temperature also exhibited a negative correlation with the URSEI, with the highest URSEI mean value occurring at Temperature Level 1 (15.52–19.74 °C), suggesting that areas with lower temperatures tend to have better ecological quality. In terms of elevation and slope classifications, the highest URSEI mean values appeared in

Level 4 and Level 5, respectively, indicating that regions with high elevations and steep slopes tend to have better ecological quality, possibly due to lower human disturbance. The precipitation classification results show that the highest URSEI mean value (0.703) was found in Level 5, corresponding to a precipitation range of 1930–2116 mm, suggesting that higher precipitation levels may contribute to maintaining ecological conditions.

4. Discussion

4.1. Applicability Analysis of the URSEI Model

The RSEI has been widely used due to its easy data acquisition, simple calculation, and the absence of manually assigned weights and thresholds. However, when applying the RSEI for long-term ecological quality assessments, the consistency and comparability of time-series evaluation results are often affected by factors such as data acquisition time and weather variations. Additionally, the multiple normalization processes in the RSEI model make the assessment results more dependent on the relative ecological conditions within the study area. In regions with drastic ecological changes, such as the Guangdong-Hong Kong-Macau Greater Bay Area, this dependence further weakens the consistency and comparability of time-series analysis results.

This study proposed multiple improvements to the Remote Sensing Ecological Index (RSEI) to address the challenge of maintaining temporal consistency in ecological quality assessment for cloudy and rainy regions. Given the persistent cloud cover in the Greater Bay Area, our approach moved beyond reliance on single images by selecting imagery from both growing and non-growing seasons within a three-year window (the target year plus one year before and after). Annual indicator factors were generated through median synthesis followed by averaging, which effectively mitigated the impacts of extreme weather and solar altitude variations while enhancing data stability and representativeness. To address thermal data gaps caused by cloud cover, we employed a random forest model using land cover type, NDVI, and elevation as predictors to reconstruct and correct LST data, ensuring spatial consistency.

In terms of indicator normalization, the traditional RSEI normalizes each temporal dataset independently, making it vulnerable to extreme values and temporal incomparability. Our improved method established a land cover invariant reference layer (1990–2020) and extracted indicator values from these stable areas as global normalization thresholds. This approach simultaneously eliminated extreme value effects and maintained consistent normalization baselines across different time periods. For principal component analysis, the conventional RSEI performs PCA separately for each temporal dataset, resulting in inconsistent weights across periods. Our enhanced method merged indicator factors from all four time periods for unified PCA, generating global eigenvectors. The application of fixed weights across all periods ensured the temporal comparability of the URSEI.

The average correlation test revealed that the URSEI's correlation with individual indicators was significantly stronger than any single indicator, confirming its superior comprehensive representation capability. Furthermore, the URSEI classification maps of the Greater Bay Area (Figure 2) showed no apparent edge-matching or mosaic artifacts, with highly consistent spatial patterns of ecological quality across time periods, ensuring result coherence and integrity while improving visualization effectiveness. Similarly, the ecological quality change detection maps (Figure 5) exhibited no anomalous regions, with detected changes closely matching actual conditions, demonstrating the URSEI's effectiveness in maintaining temporal comparability for long-term sequence analysis.

Under the challenging conditions of high cloud cover, frequent rainfall, and rapid ecological changes in the GBA, the URSEI model demonstrates strong applicability and reliability. Its improved normalization method and multi-temporal principal component

fusion analysis technique not only enhance the consistency and comparability of ecological quality assessments but also provide robust support for accurately analyzing long-term ecological evolution trends. In future applications, the URSEI model could be extended to other regions exhibiting similar climatic characteristics and ecological dynamics. Particularly suitable candidates include rapidly urbanizing areas such as the Yangtze River Delta urban agglomeration and Chengdu-Chongqing economic zone, which share with the Greater Bay Area both intensive anthropogenic pressures and frequent cloudy/rainy conditions. The model would also prove valuable for monitoring ecological changes in other southeastern coastal regions where persistent cloud cover and precipitation similarly challenge conventional remote sensing assessments of fast-evolving environments.

4.2. Spatiotemporal Evolution Characteristics and Influencing Factors of Ecological Quality in the GBA

Based on the spatiotemporal variation analysis of the URSEI, this study reveals the significant characteristics and driving mechanisms of ecological quality evolution in the GBA over the past 30 years (1990–2020). The results indicate that ecological quality changes in the GBA exhibit distinct phased characteristics, with 2010 serving as a turning point, dividing the evolution into two stages.

In the first stage (1990–2010), the GBA experienced a significant decline in ecological quality. This trend is closely associated with rapid industrialization and urbanization in the region. During this period, cities on the eastern shore of the Pearl River Estuary, such as Guangzhou, Shenzhen, and Dongguan, served as the frontiers of China's economic reform, where industrial expansion and urban development progressed simultaneously, leading to a substantial increase in human activity intensity. Unregulated land use practices and declining vegetation cover contributed to severe environmental degradation. Between 2000 and 2010, as industrial relocation and upgrading occurred, low-end manufacturing industries gradually shifted to western cities such as Foshan, Jiangmen, and Zhongshan, further exacerbating regional ecological deterioration.

In the second stage (2010–2020), ecological quality in the GBA showed an improving trend. This shift can be attributed to several key factors. First, the pace of urbanization slowed down, and the expansion of industrial land significantly decreased. Second, after 2010, both national and local governments introduced a series of ecological and environmental protection policies, such as the Outline of the Plan for the Reform and Development of the Pearl River Delta Region (2008–2020) and the Guangdong-Hong Kong-Macao Greater Bay Area Development Plan, which explicitly set ecological conservation and green development as key objectives, thereby promoting the implementation of ecological restoration projects. Lastly, the regional industrial system progressively transitioned toward high-tech industries, while traditional high-pollution, high-energy-consumption industries were either phased out or upgraded, effectively reducing industrial pressure on the ecological environment. For instance, cities like Shenzhen vigorously developed high-tech industries and modern service sectors, leading to decreased industrial pollution emissions.

From a spatial perspective, the ecological quality of the GBA exhibits significant spatial heterogeneity. The central urban cluster, including Guangzhou, Foshan, Dongguan, Shenzhen, and Zhongshan, generally shows lower ecological quality due to intensive human activities. In contrast, the northwestern and northeastern regions, such as Zhaoqing and Huizhou, benefit from favorable topographic conditions, high vegetation coverage, and lower human disturbances, maintaining relatively high ecological quality levels. This spatial differentiation pattern is strongly coupled with regional economic development levels and human activity intensity.

Geographical detector analysis results indicate that the spatial differentiation of ecological quality in the GBA is driven by both natural and anthropogenic factors. Among

these, nighttime light intensity, GDP, and temperature are the primary drivers of ecological quality variations. From a temporal perspective, human-activity-related factors, such as land use type, population density, GDP, and nighttime light index, have shown an increasing explanatory power for the URSEI over time, while the influence of natural factors has remained relatively stable. This finding confirms the dominant role of human activities in shaping ecological quality changes in the GBA, reflecting the profound impact of rapid urbanization on the region's ecological landscape.

4.3. Ecological Protection and Sustainable Development Recommendations for theGBA

Based on the assessment results of the URSEI, the ecological quality of the GBA has undergone significant spatiotemporal changes over the past 30 years. Particularly during the rapid urbanization and industrialization processes, some areas have experienced noticeable ecological degradation. To address these challenges and ensure the sustainable development of the regional ecosystem, this study proposes the following ecological protection and sustainability recommendations tailored to the GBA's regional characteristics:

(1) The northwestern and northeastern parts of the GBA (e.g., Zhaoqing and Huizhou) exhibit high ecological quality and a distinct high–high clustering pattern. These areas are predominantly high-altitude regions with dense forest coverage and minimal human disturbance, serving as crucial ecological barriers for the region. It is recommended to strengthen ecological redline management, strictly control the expansion of construction land to prevent ecological degradation and enhance the protection of nature reserves and ecological function zones to improve the stability and resilience of regional ecosystems.

(2) The central urban cluster (e.g., Guangzhou, Shenzhen, Foshan, Dongguan, and Zhongshan) exhibits relatively low ecological quality due to intensive human activities. It is recommended that these cities optimize land use structure, curb the disorderly expansion of construction land, and increase green spaces and water bodies to enhance the stability and resilience of urban ecosystems. Specific measures include promoting urban greening projects by expanding parks and green areas, strengthening water body protection by restoring and rehabilitating wetland ecosystems, and advocating for green buildings and low-carbon city development to mitigate the urban heat island effect.

(3) In industrially intensive areas such as Foshan and Dongguan, ecological degradation is particularly evident. It is recommended to continue promoting industrial upgrading, phasing out outdated production capacities, reducing industrial pollution, and improving ecological environmental quality. Specific measures include encouraging enterprises to adopt clean production technologies to minimize pollutant emissions, strengthening environmental supervision of industrial parks to ensure compliance with emission standards, and promoting green manufacturing and a circular economy to enhance resource efficiency.

(4) The GBA encompasses multiple cities and administrative regions, making cross-regional cooperation and coordination essential for improving ecological quality. It is recommended that cities strengthen collaborative governance in ecological protection, jointly addressing environmental challenges to ensure the integrity and sustainability of the regional ecosystem. Specific measures include establishing a cross-regional ecological protection coordination mechanism, formulating unified ecological protection policies and standards, enhancing the sharing and monitoring of ecological data to improve the scientific precision of regional environmental management, and promoting an ecological compensation mechanism to balance environmental protection with economic development.

4.4. Limitations and Future Works

This study systematically analyzed the spatiotemporal evolution characteristics and driving mechanisms of ecological quality in the Guangdong-Hong Kong-Macao Greater

Bay Area (GBA) from 1990 to 2020 using the Unified Remote Sensing Ecological Index (URSEI) and the geographical detector model. However, several limitations need to be acknowledged, and future improvements are proposed as follows:

Regarding data limitations, due to constraints in historical data availability, the nighttime light and GDP data for 1990 were substituted with data from 1992. While such substitution is common in long-term ecological studies, it may introduce certain biases in the analysis of early-stage driving factors of ecological quality. Future research could employ data interpolation or modeling approaches to optimize the completeness of early-stage data and reduce potential biases caused by direct substitution.

In terms of analytical dimensions, this study primarily relied on remote sensing data and large-scale driving factors for assessment, with relatively insufficient consideration of micro-level socioeconomic elements (e.g., environmental protection investments, specific policy implementation effects, and corporate pollution control measures). Subsequent studies should incorporate field surveys or socioeconomic statistical data to further refine the analysis of driving mechanisms.

5. Conclusions

This study introduces the URSEI as an enhancement of the traditional RSEI. Through optimization of data selection, normalization of invariant region indicators, and multitemporal principal component analysis, the URSEI effectively addresses the challenges of ecological quality assessment in the cloudy and rainy climate of the GBA. The dynamic monitoring results from 1990 to 2020 show significant improvements in the consistency and spatial visualization of ecological assessments.

The findings reveal that the ecological quality of the GBA exhibits a spatial distribution characterized by lower values in the central region and higher values in the northwest and northeast areas. The URSEI values over the years show a trend of decline followed by improvement, with an overall slight degradation of ecological quality, as evidenced by a 24.29% improvement area and a 25.95% degradation area. The spatial analysis indicates a significant positive spatial autocorrelation, with high–high and low–low clustering patterns dominating, which align with the changes in URSEI grades.

The spatial differentiation of ecological quality is influenced by both natural and anthropogenic factors. Key drivers of spatial variation include nighttime light intensity, GDP, and temperature, with human factors having a stronger impact, which has increased over time. This study underscores the importance of considering both natural and human influences in long-term ecological monitoring and provides a reliable method for assessing ecological quality in regions with varying climatic and environmental conditions.

Author Contributions: Conceptualization, F.S. and C.D.; methodology, H.L. and L.Z.; software, L.W.; validation, F.S., C.D. and H.L.; formal analysis, R.J. and L.Z.; investigation, R.J. and H.L.; resources, J.C. and F.S.; data curation, R.J. and H.L.; writing—original draft preparation, R.J. and H.L.; writing—review and editing, F.S. and C.D.; visualization, R.J. and L.Z.; supervision, L.W. and J.C.; project administration, J.C.; funding acquisition, F.S. and H.L. All authors have read and agreed to the published version of the manuscript.

Funding: This research was funded by the Scientific Research Project of the Ecology Environment Bureau of Shenzhen Municipality, grant number SZDL2023001387, the Fundamental Research Foundation of Shenzhen Technology and Innovation Council, grant number JCYJ20220818101617038, the National Natural Science Foundation of China, grant number 42271353, and the Guangdong Basic and Applied Basic Research Foundation, grant number 2024A1515011858.

Data Availability Statement: The data presented in this study are available within the article.

Conflicts of Interest: The authors declare no conflicts of interest.

References

1. Zeng, S.Y.; Ma, J.; Yang, Y.J.; Zhang, S.L.; Liu, G.J.; Chen, F. Spatial assessment of farmland soil pollution and its potential human health risks in China. *Sci. Total Environ.* **2019**, *687*, 642–653. [CrossRef] [PubMed]
2. Mahmoud, S.H.; Gan, T.Y. Impact of anthropogenic climate change and human activities on environment and ecosystem services in arid regions. *Sci. Total Environ.* **2018**, *633*, 1329–1344. [CrossRef] [PubMed]
3. Wang, X.; Lu, B.B.; Li, J.S.; Liu, Q.Y.; He, L.H.; Lv, S.C.; Yu, S.H. Spatio-temporal analysis of ecological service value driven by land use changes: A case study with Danjiangkou, Hubei section. *Resour. Environ. Sustain.* **2024**, *15*, 100146. [CrossRef]
4. Fang, C.L.; Wang, Z.B.; Liu, H.M. Exploration on the theoretical basis and evaluation plan of Beautiful China construction. *Acta Geogr. Sin.* **2019**, *74*, 619–632.
5. Yu, G.R.; Wang, Y.S.; Yang, M. Discussion on the ecological theory and assessment methods of ecosystem quality and its evolution. *Chin. J. Appl. Ecol.* **2022**, *33*, 865–877.
6. Li, J.Q.; Tian, Y. Assessment of Ecological Quality and Analysis of Influencing Factors in Coal-Bearing Hilly Areas of Northern China: An Exploration of Human Mining and Natural Topography. *Land* **2024**, *13*, 1067. [CrossRef]
7. Xu, T.; Wu, H. Spatiotemporal Analysis of Vegetation Cover in Relation to Its Driving Forces in Qinghai-Tibet Plateau. *Forests* **2023**, *14*, 1835. [CrossRef]
8. Wang, R.; Ding, X.; Yi, B.J.; Wang, J.L. Spatiotemporal characteristics of vegetation cover change in the Central Yunnan urban agglomeration from 2000 to 2020 based on Landsat data and its driving factors. *Geocarto Int.* **2024**, *39*, 2316643. [CrossRef]
9. Wang, Y.L.; Zhang, A.; Gao, X.T.; Zhang, W.; Wang, X.H.; Jiao, L.L. Spatial-Temporal Differentiation and Driving Factors of Vegetation Landscape Pattern in Beijing-Tianjin-Hebei Region Based on the ESTARFM Model. *Sustainability* **2024**, *16*, 10498. [CrossRef]
10. Yuan, D.B.; Zhang, L.Y.; Fan, Y.Q.; Sun, W.B.; Fan, D.Q.; Zhao, X.R. Spatio-Temporal Analysis of Surface Urban Heat Island and Canopy Layer Heat Island in Beijing. *Appl. Sci.* **2024**, *14*, 5034. [CrossRef]
11. Chen, X.; Zhang, S.C.; Tian, Z.Y.; Luo, Y.Q.; Deng, J.; Fan, J.H. Differences in urban heat island and its driving factors between central and new urban areas of Wuhan, China. *Environ. Sci. Pollut. Res.* **2023**, *30*, 58362–58377. [CrossRef]
12. Miao, S.; Liu, C.; Qian, B.J.; Miao, Q. Remote sensing-based water quality assessment for urban rivers: A study in linyi development area. *Environ. Sci. Pollut. Res.* **2020**, *27*, 34586–34595. [CrossRef] [PubMed]
13. Zheng, Z.H.; Wu, Z.F.; Chen, Y.B.; Yang, Z.W.; Marinello, F. Exploration of eco-environment and urbanization changes in coastal zones: A case study in China over the past 20 years. *Ecol. Indic.* **2020**, *119*, 106847. [CrossRef]
14. Li, C.; Chen, T.; Jia, K.; Plaza, A. Coupling Analysis Between Ecological Environment Change and Urbanization Process in the Middle Reaches of Yangtze River Urban Agglomeration, China. *IEEE J. Sel. Top. Appl. Earth Observ. Remote Sens.* **2024**, *17*, 880–892. [CrossRef]
15. Wang, C.; Sheng, Q.; Zhu, Z. Exploring Ecological Quality and Its Driving Factors in Diqing Prefecture, China, Based on Annual Remote Sensing Ecological Index and Multi-Source Data. *Land* **2024**, *13*, 1499. [CrossRef]
16. Xu, H.; Wang, Y.; Guan, H.; Shi, T.; Hu, X. Detecting Ecological Changes with a Remote Sensing Based Ecological Index (RSEI) Produced Time Series and Change Vector Analysis. *Remote Sens.* **2019**, *11*, 2345. [CrossRef]
17. Xu, H.Q. A remote sensing index for assessment of regional ecological changes. *China Environ. Sci.* **2013**, *33*, 889–897.
18. Gan, X.T.; Du, X.C.; Duan, C.J.; Peng, L.H. Evaluation of Ecological Environment Quality and Analysis of Influencing Factors in Wuhan City Based on RSEI. *Sustainability* **2024**, *16*, 5809. [CrossRef]
19. Chen, Z.Y.; Chen, R.R.; Guo, Q.; Hu, Y.L. Spatiotemporal Change of Urban Ecologic Environment Quality Based on RSEI-Taking Meizhou City, China as an Example. *Sustainability* **2022**, *14*, 13424. [CrossRef]
20. Zhang, L.; Hou, Q.; Duan, Y.; Ma, S. Spatial and Temporal Heterogeneity of Eco-Environmental Quality in Yanhe Watershed (China) Using the Remote-Sensing-Based Ecological Index (RSEI). *Land* **2024**, *13*, 780. [CrossRef]
21. He, Y.R.; Chen, Y.H.; Zhong, L.; Lai, Y.F.; Kang, Y.T.; Luo, M.; Zhu, Y.F.; Zhang, M. Spatiotemporal evolution of ecological environment quality and its drivers in the Helan Mountain, China. *J. Arid Land* **2025**, *17*, 224–244. [CrossRef]
22. Cai, C.; Li, J.Y.; Wang, Z.Q. Long-Term Ecological and Environmental Quality Assessment Using an Improved Remote-Sensing Ecological Index (IRSEI): A Case Study of Hangzhou City, China. *Land* **2024**, *13*, 1152. [CrossRef]
23. Feng, Z.X.; She, L.; Wang, X.H.; Yang, L.; Yang, C. Spatial and Temporal Variations of Ecological Environment Quality in Ningxia Based on Improved Remote Sensing Ecological Index. *Ecol. Environ. Sci.* **2024**, *33*, 131–143.
24. Cheng, L.L.; Wang, Z.W.; Tian, S.F.; Liu, Y.T.; Sun, M.Y.; Yang, Y.M. Evaluation of eco-environmental quality in Mentougou District of Beijing based on improved remote sensing ecological index. *Chin. J. Ecol.* **2021**, *40*, 1177–1185.
25. Ke, L.N.; Xu, J.H.; Wang, N.; Hou, J.X.; Han, X.; Yin, S.S. Evaluation of Ecological Quality of Coastal Wetland Based on Remote Sensing Ecological Index: A Case Study of Northern Liaodong Bay. *Ecol. Environ. Sci.* **2022**, *31*, 1417–1424.
26. Liu, Y.; Dang, C.Y.; Yue, H.; Lu, C.G.; Qian, J.X.; Zhu, R. Comparison between modified remote sensing ecological index and RSEI. *J. Remote Sens.* **2022**, *26*, 683–697. [CrossRef]

27. Geng, J.; Yu, K.; Xie, Z.; Zhao, G.; Ai, J.; Yang, L.; Yang, H.; Liu, J. Analysis of Spatiotemporal Variation and Drivers of Ecological Quality in Fuzhou Based on RSEI. *Remote Sens.* **2022**, *14*, 4900. [CrossRef]
28. Chen, N.; Cheng, G.; Yang, J.; Ding, H.; He, S. Evaluation of Urban Ecological Environment Quality Based on Improved RSEI and Driving Factors Analysis. *Sustainability* **2023**, *15*, 8464. [CrossRef]
29. Liu, Y.; Zhou, T.; Yu, W. Analysis of Changes in Ecological Environment Quality and Influencing Factors in Chongqing Based on a Remote-Sensing Ecological Index Mode. *Land* **2024**, *13*, 227. [CrossRef]
30. Long, T.; Bai, Z.; Zheng, B. Spatiotemporal Dynamics and Driving Forces of Ecological Environment Quality in Coastal Cities: A Remote Sensing and Land Use Perspective in Changle District, Fuzhou. *Land* **2024**, *13*, 1393. [CrossRef]
31. Yue, H.; Liu, Y.; Li, Y.; Lu, Y. Eco-Environmental Quality Assessment in China's 35 Major Cities Based On Remote Sensing Ecological Index. *IEEE Access* **2019**, *7*, 51295–51311. [CrossRef]
32. He, Y. Construction of qualitative assessment model of ecological environment quality under river safety remediation. *Int. J. Environ. Technol. Manag.* **2024**, *27*, 400–414. [CrossRef]
33. Wang, J.Y.; Chen, G.; Yuan, Y.R.; Fei, Y.; Xiong, J.N.; Yang, J.W.; Yang, Y.M.; Li, H. Spatiotemporal changes of ecological environment quality and climate drivers in Zoige Plateau. *Environ. Monit. Assess.* **2023**, *195*, 912. [CrossRef]
34. Liu, W.M.; Cheng, Z.Y.; Li, J.; Li, G.; Pan, N.H. Assessment of ecological asset quality and its drivers in Agro-pastoral Ecotone of China. *Ecol. Indic.* **2025**, *170*, 113072. [CrossRef]
35. Zeng, J.W.; Dai, X.; Li, W.Y.; Xu, J.P.; Li, W.L.; Liu, D.S. Quantifying the Impact and Importance of Natural, Economic, and Mining Activities on Environmental Quality Using the PIE-Engine Cloud Platform: A Case Study of Seven Typical Mining Cities in China. *Sustainability* **2024**, *16*, 1447. [CrossRef]
36. Liu, Z.; Wang, S.; Fang, C. Spatiotemporal evolution and influencing mechanism of ecosystem service value in the Guangdong-Hong Kong-Macao Greater Bay Area. *J. Geogr. Sci.* **2023**, *33*, 1226–1244. [CrossRef]
37. Ren, Y.F.; He, X.N.; Jiang, Q.N.; Zhang, F.; Zhang, B.T. Advancing high-quality development in China: Unraveling the dynamics, disparities, and determinants of inclusive green growth at the prefecture level. *Ecol. Indic.* **2024**, *169*, 112898.
38. Pharaoh, E.; Diamond, M.; Jarvie, H.P.; Ormerod, S.J.; Rutt, G.; Vaughan, I.P. Potential drivers of changing ecological conditions in English and Welsh rivers since 1990. *Sci. Total Environ.* **2024**, *946*, 174369. [CrossRef]
39. Wang, J.F.; Xu, C.D. Geodetector: Principle and prospective. *Acta Geogr. Sin.* **2017**, *72*, 116–134.
40. Ju, H.; Zhang, Z.; Zuo, L.; Wang, J.; Zhang, S.; Wang, X.; Zhao, X. Driving forces and their interactions of built-up land expansion based on the geographical detector—A case study of Beijing, China. *Int. J. Geogr. Inf. Sci.* **2016**, *30*, 2188–2207. [CrossRef]
41. Tao, S.; Yi, C.; Weidong, L.; Hui, L. Spatial difference and mechanisms of influence of geo-economy in the border areas of China. *J. Geogr. Sci.* **2017**, *27*, 1463–1480.
42. Zuo, S.; Dai, S.; Song, X.; Xu, C.; Liao, Y.; Chang, W.; Chen, Q.; Li, Y.; Tang, J.; Man, W.; et al. Determining the Mechanisms that Influence the Surface Temperature of Urban Forest Canopies by Combining Remote Sensing Methods, Ground Observations, and Spatial Statistical Models. *Remote Sens.* **2018**, *10*, 1814. [CrossRef]
43. Liang, P.; Yang, X. Landscape spatial patterns in the Maowusu (Mu Us) Sandy Land, northern China and their impact factors. *Catena* **2016**, *145*, 321–333. [CrossRef]
44. Huang, J.; Wang, J.; Bo, Y.; Xu, C.; Hu, M.; Huang, D. Identification of Health Risks of Hand, Foot and Mouth Disease in China Using the Geographical Detector Technique. *Int. J. Environ. Res. Public Health* **2014**, *11*, 3407–3423. [CrossRef]
45. Zhang, H.J. Ecological environment change in Guangdong-Hong Kong-Macao Greater Bay Area based on multi-temporal remote sensing ecological index. *Sci. Geogr. Sin.* **2019**, *8*, 8.
46. Yang, C.; Zhang, C.; Li, Q.; Liu, H.; Gao, W.; Shi, T.; Liu, X.; Wu, G. Rapid urbanization and policy variation greatly drive ecological quality evolution in Guangdong-Hong Kong-Macau Greater Bay Area of China: A remote sensing perspective. *Ecol. Indic.* **2020**, *115*, 106373. [CrossRef]
47. Wu, Y.Y.; Luo, Z.H.; Wu, Z.F. Exploring the Relationship between Urbanization and Vegetation Ecological Quality Changes in the Guangdong-Hong Kong-Macao Greater Bay Area. *Land* **2024**, *13*, 1246. [CrossRef]
48. Wang, Y.; Zhao, Y.H.; Wu, J.S. Dynamic monitoring of long time series of ecological quality in urban agglomerations using Google Earth Engine cloud computing:A case study of the Guangdong-Hong Kong-Macao Greater Bay Area, China. *Acta Ecol. Sin.* **2020**, *40*, 8461–8473.
49. Wu, B.F. *ChinaCover*; Science Press: Beijing, China, 2017; p. 397.
50. Liu, J.C.; Xie, T.; Lyu, D.; Cui, L.; Liu, Q.M. Analyzing the Spatiotemporal Dynamics and Driving Forces of Ecological Environment Quality in the Qinling Mountains, China. *Sustainability* **2024**, *16*, 3251. [CrossRef]
51. Ding, X.; Shao, X.; Wang, J.L.; Peng, S.Y.; Shi, J.C. Research on the Spatial-Temporal Pattern Evolution and Driving Force of Ecological Environment Quality in Kunming City Based on Remote Sensing Ecological Environment Index in the Past 25 Years. *Pol. J. Environ. Stud.* **2024**, *33*, 1073–1089. [CrossRef]
52. Wang, X.Y.; Wang, X.D.; Jin, X.; Kou, L.D.; Hou, Y.J. Evaluation and driving force analysis of ecological environment in low mountain and hilly regions based on optimized ecological index. *Sci. Rep.* **2024**, *14*, 24570. [CrossRef] [PubMed]

53. Zhang, S.W.; Wang, Y.; Wang, X.H.; Wu, Y.; Li, C.R.; Zhang, C.; Yin, Y.H. Ecological Quality Evolution and Its Driving Factors in Yunnan Karst Rocky Desertification Areas. *Int. J. Environ. Res. Public Health* **2022**, *19*, 16904. [CrossRef]
54. Zhu, Z.R.; Cao, H.S.; Yang, J.C.; Shang, H.; Ma, J.Q. Ecological environment quality assessment and spatial autocorrelation of northern Shaanxi mining area in China based-on improved remote sensing ecological index. *Front. Environ. Sci.* **2024**, *12*, 1325516. [CrossRef]
55. Wang, S.D.; Si, J.J.; Wang, Y. Study on Evaluation of Ecological Environment Quality and Temporal-Spatial Evolution of Danjiang River Basin (Henan Section). *Pol. J. Environ. Stud.* **2021**, *30*, 2353–2367. [CrossRef]
56. Jiao, K.; Yong, X.Q.; Mao, S.H.; Chen, K.Y. Analysis of the evolution and influencing factors of ecological environment quality after the transformation of resource-exhausted cities based on GEE and RSEI: A case study of Xuzhou City, China. *J. Asian Archit. Build. Eng.* **2024**, 1–19. [CrossRef]
57. Xia, Q.Q.; Chen, Y.N.; Zhang, X.Q.; Ding, J.L. Spatiotemporal Changes in Ecological Quality and Its Associated Driving Factors in Central Asia. *Remote Sens.* **2022**, *14*, 3500. [CrossRef]

Disclaimer/Publisher's Note: The statements, opinions and data contained in all publications are solely those of the individual author(s) and contributor(s) and not of MDPI and/or the editor(s). MDPI and/or the editor(s) disclaim responsibility for any injury to people or property resulting from any ideas, methods, instructions or products referred to in the content.

land

MDPI

Article

Construction and Optimization of the Ecological Security Pattern of Pinglu Canal Economic Zone Based on the InVEST-Circuit Theory Model

Zhanhao Dang [1,2], Baoqing Hu [1,*], Chunlian Gao [1,2], Shaoqiang Wen [1,3], Jinrui Ren [1,2] and Yunfei Liang [2]

[1] Key Laboratory of Environment Change and Resources Use in Beibu Gulf, Ministry of Education, Nanning Normal University, Nanning 530001, China; d972826203@163.com (Z.D.); gaochunlian25@163.com (C.G.); wsq1254191480@163.com (S.W.); 18725186340@163.com (J.R.)
[2] School of Geographical Sciences and Planning, Nanning Normal University, Nanning 530001, China; 13321708240@163.com
[3] School of Natural Resources and Surveying, Nanning Normal University, Nanning 530001, China
* Correspondence: hbq1230@nnnu.edu.cn

Abstract: The strategic delineation of ecological corridors and establishment of robust ecological security frameworks constitute fundamental prerequisites for advancing ecologically balanced growth and premium development within the Pinglu Canal Economic Belt. In this study, a comprehensive framework integrating ecological sources, resistance surfaces, and ecological corridors was developed using the InVEST model combined with circuit theory. The framework was then applied to assess the spatial and temporal dynamics of four major ecosystem services over the period from 2000 to 2020. The main findings are as follows: (1) From 2000 to 2020, the values of the four ecosystem services showed an overall declining trend. Spatially, areas with high ecosystem service importance were mainly concentrated in woodland and grassland areas in the southwest and northwest of the region. (2) The resistance values of the study area's resistance surface ranged from 1 to 4.83. High-resistance areas were primarily located in the central region, corresponding to areas of intense human activity, while low-resistance areas were distributed around the periphery and largely overlapped with ecological source areas, presenting a spatial pattern of "high in the center, low at the edges". (3) In total, 119 ecological barriers, 28 corridors, 8 critical pinch points, and 16 habitat source areas were identified. Building on these results, an enhanced ecological security layout—defined by the 'three belts and three zones' strategy—was formulated to guide restoration efforts and inform ecological management across the Pinglu Canal Economic Region.

Keywords: ecosystem services; ecological corridor; ecological security pattern; InVEST model; circuit theory model; Pinglu Canal Economic Zone

1. Introduction

With the intensification of global environmental problems and the expansion of human activities, ecosystems are under increasing pressure. The problem of ecological degradation is becoming increasingly serious, resources continue to be depleted, and biodiversity is decreasing. These problems continue to threaten the sustainable development of human society [1,2]. Against this backdrop, establishing a scientifically sound and rational ecological security pattern (ESP) has become a crucial approach for ensuring national ecological security, addressing climate change, and preserving biodiversity. By optimizing land use, enhancing the connectivity of ecological protection areas, and improving ecosystem

resilience, an ESP can effectively mitigate ecological risks caused by human activities, provide strong ecological support for socio-economic development, and foster synergistic integration of socioeconomic development and ecosystem functioning [3–5].

An ecological security pattern (ESP) delineates fundamental landscape components, including habitat nodes and connectivity pathways, allocates natural resources rationally, protects critical ecological areas, and enhances the stability and connectivity of ecosystems. This ensures the overall health of regional ecosystems, improves their ability to resist ecological risks, and maintains effective ecological services [6–8]. The evolution of ESP construction techniques has crystallized into a three-phase operational framework: (1) source node identification; (2) resistance surface modeling; (3) corridor network optimization [9–11]. The first step in ESP construction is the identification of ecological sources. These are areas that are highly sensitive to human activities and environmental changes and are of significant importance for regional ecological security, representing the minimum land area required to meet ecological safety needs [12]. The identification of ecological source areas has evolved into three primary methodological branches: (1) quantitative models based on ecosystem service value (ESV) assessments [13,14]; (2) morphological spatial pattern analysis (MSPA) [15]; and (3) landscape network modeling approaches [16]. MSPA and landscape connectivity index methods rely solely on land use data, ignoring environmental factors such as climate, soil, water resources, and vegetation types. In contrast, the ESV assessment models enables a more accurate assessment of multiple functional indicators such as soil and water conservation, carbon storage, water yield, and habitat quality, thereby objectively identifying ecological sources [17,18]. There are two main approaches to constructing resistance surfaces. One is to invert habitat quality as a resistance value [19]; the other involves selecting a set of indicators reflecting human and natural factors and assigning different weights to derive the resistance surface [20–22]. The drawback of the first method is its limited consideration of factors, as resistance is influenced by multiple variables. Using only one factor can result in inaccurate outcomes, while a comprehensive index approach that balances various elements offers more reliable identification of ecological sources. Ecological corridors are one of the key components of an ESP, serving as vital channels for ecological flow and species migration [23]. Common methods for corridor identification include the Minimum Cumulative Resistance (MCR) model, circuit theory, and the gravity model [24–26]. Among these, using the MCR model to extract corridors and the gravity model to assess their importance is more common [27–29], while another method is to apply circuit theory [30,31]. The MCR model assumes that species or ecological flows follow the shortest path with the least resistance from one point to another [32]. However, in reality, species behavior can be random, and this randomness cannot be fully captured by simple cumulative resistance paths. Compared with the first method, the circuit theory model not only effectively extracts ecological corridors but also simulates species migration using the stochastic flow of current over a resistance surface, allowing the identification of ecological pinch points and barriers [33,34].

In summary, although the current ESP research has developed a relatively mature "ecological sources–resistance surface–ecological corridors" framework, there are still limitations in core methodologies. First, ecological source identification tends to overly rely on ecosystem service assessments, which may cause deviations from actual ecological conditions. Second, resistance surface construction often relies on conventional natural factors (e.g., slope, vegetation cover) while neglecting human activity impacts, and the assignment of weights to factors is often subjective. Therefore, this study identifies ecological sources based on ecosystem service assessments and corrects them using nature reserve data. In constructing resistance surfaces, both natural and anthropogenic factors are comprehensively considered, with weights assigned using the analytic hierarchy process

(AHP) to reduce subjectivity. By applying the circuit theory model and analyzing current density thresholds, we systematically examined the spatial configuration of the ecological corridor network and quantitatively identified the distribution patterns of critical ecological pinch points and resistance barriers.

Pinglu Canal begins at the mouth of the Pingtang River in Xijin Reservoir, Hengzhou City, Nanning, and enters the Gulf of Tonkin along the Qin River via Luyu Town, Lingshan County, Qinzhou [35]. Pinglu Canal is a networking project to optimize and enhance the national water transport network. In addition, it is an important component to accelerate the construction of the national comprehensive three-dimensional transportation network. It serves as a landmark project for the construction of a new land and sea corridor in the west, is a practical action to implement the new development concept, and is of great strategic significance for the economic and social development of Guangxi and the southwestern region [36]. Currently, the construction of the Pinglu Canal lacks a comprehensive approach to ecosystem integrity, failing to achieve integrated and coordinated management of key ecological components such as mountains, water bodies, forests, farmlands, lakes, and grasslands. This fragmented ecological governance model compromises the stability and resilience of the ecosystem and increases the risk of ecological degradation and environmental hazards. Therefore, establishing a scientifically sound ecological security pattern for the Pinglu Canal region is of critical importance. Such a framework would facilitate the efficient allocation and protection of regional natural resources, enhance ecosystem service functions, and provide institutional support for ecological restoration, biodiversity conservation, and sustainable resource utilization along the canal. Moreover, it serves as a foundational step toward achieving regional ecological civilization goals, safeguarding ecological security baselines, and promoting the harmonious development of the economy, society, and natural environment. Ultimately, it aligns with the overarching strategy of "ecological priority and green development".

This study aims to construct an ESP in the Pinglu Canal Economic Zone. Specific research objectives include the following: (1) to evaluate four ecosystem services from 2000 to 2020 using the InVEST model and determine ecological sources based on their overall ecological significance; (2) to develop a resistance surface by integrating both natural and anthropogenic factors; and (3) to employ the circuit theory framework to identify ecological corridors, critical nodes, and barrier zones, thereby facilitating the construction and refinement of the ESP for the Pinglu Canal region.

2. Materials and Methods

2.1. Study Area

Pinglu Canal Economic Zone is located in southern Guangxi (20°0′–24°3′ N, 107°19′–110°39′ E), and most of the area is at a low elevation, with the exception of the SW Shiwandashan Mountains and the NW Daming Mountain, which are situated on higher terrain. The core area of the Pinglu Canal Economic Belt involves five cities, including Nanning, Qinzhou, Beihai, Fangchenggang, and Guigang, with an area of about 53,000 km^2 (Figure 1). The Pinglu Canal begins in Nanning and enters the Beibu Gulf after passing through Qinzhou City, with a total length of about 135 km. The climate of the Pinglu Canal Economic Zone is a subtropical monsoon climate with high year-round temperatures and plenty of light hours. In summer, there is a lot of rain, which makes it prone to flooding. In winter, the temperature is favorable compared to the north, which makes it a tourist destination for tourists. As a strategic pivot connecting Nanning's inland shipping hub with the Beibu Gulf International Gateway Port, it has cracked the long-standing water transportation disconnection between the Xijiang River Basin and the Beibu Gulf seaport group. Through the linkage development mode of "port, industry, and city", it promotes

the clustering development of equipment manufacturing, modern logistics, cross-border trade, and other industries and is expected to form a new industrial chain layout covering a population of 50 million people with an annual cargo throughput of over 100 million tons. It is expected to become a key infrastructure leading the China-ASEAN regional economic integration.

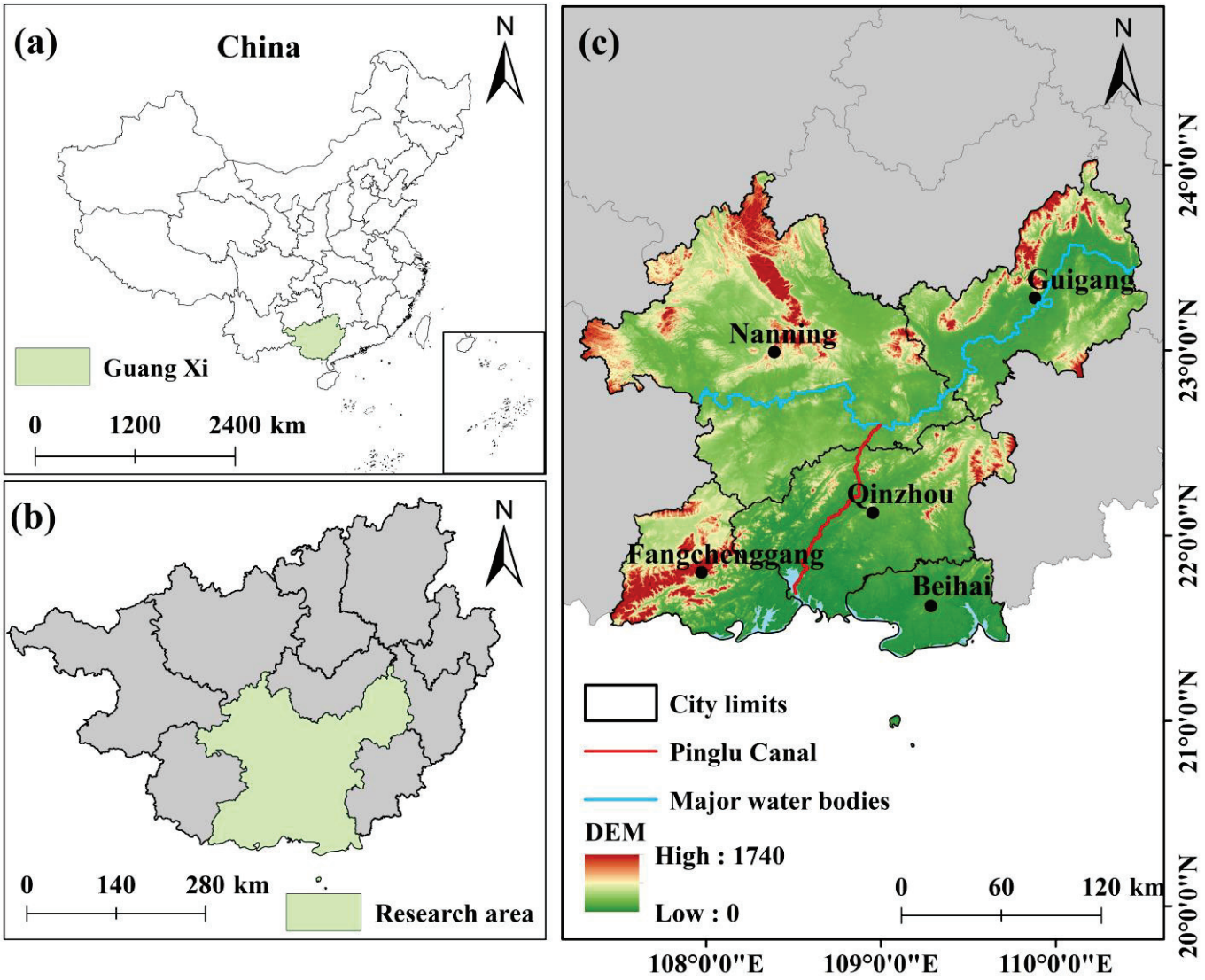

Figure 1. Schematic of the Pinglu Canal Economic Zone. (**a**) Guangxi Geographical Location; (**b**) Geographical location of the study area; (**c**) DEM spatial distribution of Pinglu Canal Economic Zone.

2.2. Data Sources

The data used were obtained from multiple authoritative sources and underwent standardized preprocessing. Land cover datasets from 2000, 2010, and 2020 were derived from the GlobeLand30 land cover database. DEM data were obtained using the geospatial data cloud platform and were used to derive topographic factors such as slope and aspect. Soil data were quoted from the World Soil Database (HWSD v1.2). NDVI data were obtained from the official website of the Loess Plateau SubCenter, and vector data for roads and river networks were extracted from OpenStreetMap. To ensure spatial alignment and model compatibility among heterogeneous multi-source datasets, all data were uniformly projected using the WGS_1984_UTM_Zone_49N coordinate system. Additionally, to eliminate potential spatial scale errors caused by differences in data resolution, all datasets were

resampled to a 30-m spatial resolution using bilinear interpolation. This approach ensured consistency in spatial resolution, the coordinate reference system, and data format across all model inputs, thereby maximizing the scientific rigor and accuracy of the analysis results (Table 1).

Table 1. Data source and description.

Data	Descriptions	Source
2000/2010/2020 land use data	Resolution of 30 m	http://loess.geodata.cn (accessed on 20 August 2024)
2000/2010/2020 precipitation data	1 km resolution monthly mean precipitation dataset	
DEM data	ASTER GODEM elevation data with 30 m resolution	https://www.gscloud.cn/ (accessed on 20 August 2024)
Rainfall erosion factor	Reflecting rainfall intensity in the study area	Precipitation data are obtained by applying the formula
Soil data	Used to calculate soil erosion factors and plant utilization of water	https://gaez.fao.org/pages/hwsd (accessed on 21 August 2024)
NDVI data	For building resistance surfaces	http://loess.geodata.cn (accessed on 21 August 2024)
Road data/river network data	Calculation of distances to roads and rivers	OpenStreetMap Data extract (https://www.openstreetmap.org) (accessed on 22 August 2024)
Railroad data	Calculate the distance to the railroad	

2.3. Methods

First, four ES were assessed using the InVEST model. These services were classified using the natural breaks method and integrated with equal weighting to generate a spatial distribution map of comprehensive ecosystem service importance. Subsequently, this map was overlaid with vector data of nature reserves to identify key ecological sources. For the resistance surface, six resistance factors encompassing both natural (e.g., topography, land use) and anthropogenic (e.g., human disturbance) elements were selected and weighted to construct a composite resistance surface. Utilizing the ecological source areas and resistance surface as inputs, the Linkage Mapper tool—rooted in circuit theory—was applied to delineate ecological corridors, identify critical pinch points, and locate dispersal barriers, ultimately delineating the ecological security pattern. Furthermore, targeted ecological restoration strategies and spatial management and control plans were proposed for identified ecological vulnerabilities, aiming to provide scientific guidance for harmonizing regional development and ecological conservation (Figure 2).

2.3.1. Valuation of Ecosystem Services

Ecosystem services (ES) constitute the environmental foundation for human societal development. They refer to the materials and products provided to humans by ecological components and processes, encompassing both the natural processes that sustain life-support systems and the natural resources that can be directly or indirectly utilized by humans [13]. Among them, the setting of the four ES parameters in the InVEST model is a matter of localization and optimization in the light of the actual situation of the Pinglu Canal Economic Zone. This study fully refers to the parameter setting methods used by scholars who have conducted research in the Pinglu Canal Economic Zone or other similar ecological regions and makes localized corrections and optimization adjustments in combination with the actual situation of the Pinglu Canal Economic Zone. The methods used for the four ES and the parameters used in the relevant literature are shown in the following four sub-points [37].

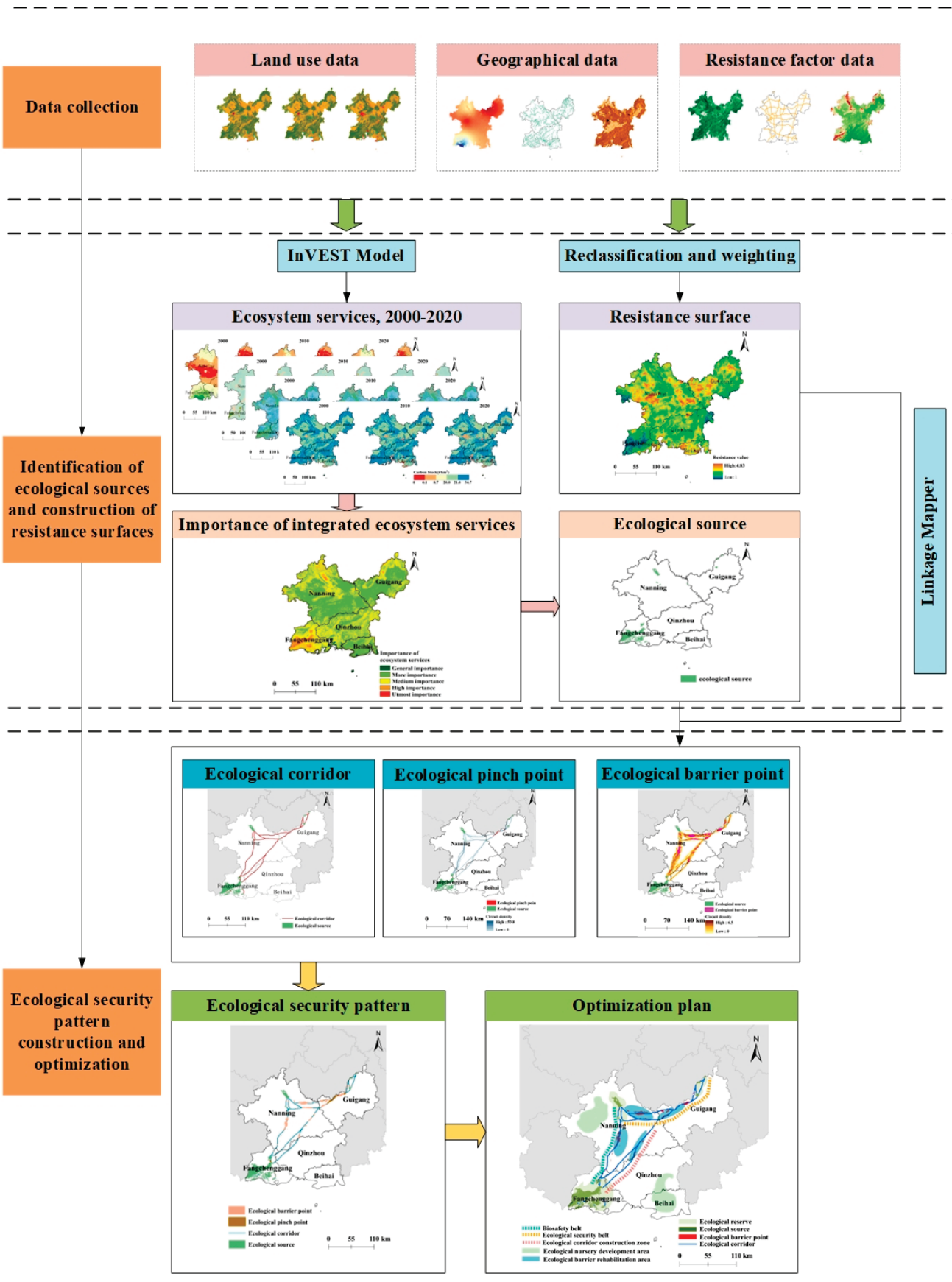

Figure 2. Framework for the study of ecological security patterns.

(1) Soil conservation

The SDR module of the InVEST model quantifies potential and actual soil erosion and soil retention [38,39], providing an important means of assessing soil retention function. The calculation formula is expressed as follows:

$$A = R_{KLS} - U_{SLE} \tag{1}$$

$$R_{KLS} = R \times K \times L \times S \tag{2}$$

$$U_{SLE} = R \times K \times L \times S \times C \times P \tag{3}$$

In the equation, A represents soil retention ($t \cdot hm^{-2} \cdot a^{-1}$), where R_{KLS} indicates theoretical erosion under bare soil conditions, and U_{SLE} represents the adjusted soil erosion amount. The rainfall erosivity factor, R ($MJ \cdot mm \cdot ha^{-1} \cdot h^{-1} \cdot yr^{-1}$), is estimated using mean annual precipitation. The soil erodibility factor, K ($t \cdot ha \cdot h \cdot MJ^{-1} \cdot mm^{-1}$), quantifies the susceptibility of soil to erosion under rainfall impact, estimated according to soil texture composition and organic carbon content [40]. L and S represent slope length and slope gradient factors. C is the cover management factor reflecting vegetation cover and cropping practices, while P denotes the support practice factor used to account for soil and water conservation measures. Specific parameter values are referenced from the relevant literature [41].

(2) Water yield

The InVEST model's Water Yield Module was employed to quantitatively estimate and spatially analyze the annual water yield across the Pinglu Canal Economic Belt. This module is based on a simplified water balance approach and integrates land use/land cover data, climatic variables, and soil characteristics to estimate the water yield capacity of each raster cell over a defined time period. It effectively reflects the spatial pattern of the region's ES function related to water conservation. The calculation formula is expressed as follows:

$$Y(x) = \left(1 - \frac{AET(x)}{P(x)}\right) \times P(x) \tag{4}$$

where $Y(x)$ represents yearly water production (mm) for raster unit x. $AET(x)$ represents the combined soil-vegetation moisture flux (mm), encompassing both edaphic vaporization and phytogenic water release. $P(x)$ indicates the total annual rainfall (mm) received by that grid cell.

(3) Habitat quality

The habitat quality module evaluates ecosystem conditions by spatially overlaying land use types and threat factors, with output values ranging from 0 to 1. The closer the value is to 1, the less human damage to the environment. The closer the value is to 0, the more human damage to the environment [42]. The threat source table and sensitivity table refer to the relevant literature [41]. The calculation formula is as follows:

$$HQ = H \times \left[1 - \left(\frac{D^Z}{D^Z + K^Z}\right)\right] \tag{5}$$

HQ indicates habitat suitability, D denotes the total threat level, K corresponds to the half-saturation constant, a parameter that determines the point at which the threat effect begins to stabilize, and Z is a fixed parameter, commonly set to 2.5 [43].

(4) Carbon storage

The carbon storage assessment module quantitatively evaluates regional carbon storage by integrating carbon density parameters corresponding to different land use types, thereby estimating the amount of carbon stored per unit area for each land category, and generates a spatial distribution map of carbon storage. One of the key input datasets for model operation is the carbon density values corresponding to various land use types. The total carbon storage is calculated using the following equation:

$$C_{tot} = C_{above} + C_{below} + C_{soil} + C_{dead} \quad (6)$$

where C_{tot} stands for the overall carbon storage, C_{above} signifies the carbon content in aboveground biomass, C_{below} denotes the carbon density of underground biomass, C_{soil} refers to the soil organic carbon concentration, and C_{dead} corresponds carbon density of dead organic matter. The carbon density values for each land use category were primarily derived from the existing literature [44] and were adjusted appropriately based on regional ecological characteristics to improve data representativeness and model accuracy.

2.3.2. Ecological Source Area Identification

Based on the ecological characteristics of the Pinglu Canal Economic Zone and the relevant literature, the screening conditions for ecological source sites include the following: (1) they should be in areas with high ecosystem service importance levels; (2) due to the existence of fragmented patches in ecological source sites, the area of the nature reserve in the region should be larger than 10 km^2 [45]. The natural breakpoint (NB) method is a classification method that relies on distribution characteristics of the dataset itself. It classifies the ES based on the "natural distribution breakpoints" in the ES data rather than setting the intervals artificially, so it reflects the importance distribution of ecosystem services more realistically.

Therefore, the NB method was used in ArcGIS software to classify the significance of four ESs, and indicators were categorized into five levels of importance (general importance, more importance, medium importance, high importance and utmost importance). On this basis, four service functions were integrated using the equal-weight spatial superposition method. The natural breakpoint method was then reapplied to divide the overall ecosystem service value into five importance levels, resulting in a comprehensive assessment of the regional ecosystem service significance. In the process of ecological source area identification, the fourth level (high importance) and fifth level (utmost importance) areas in the integrated importance level were selected as alternative ecological source areas [46]. Ultimately, the alternative ecological source sites were combined with the nature reserve data, and ecological core patches exceeding 10 km^2 in area were preserved as the definitive ecological source areas.

2.3.3. Resistance Surface Construction

As a quantitative indicator of landscape connectivity, the resistance surface illustrates relative difficulty of species dispersal between ecological source areas and represents the degree of horizontal resistance experienced by ecological processes across space [47]. In the construction process, the selection of appropriate resistance factors and the assignment of corresponding weights are essential for obtaining accurate results. Drawing on previous studies and integrating relevant findings, this study incorporates both natural and anthropogenic elements. Specifically, six ecological resistance factors were selected: land cover type, NDVI, DEM, slope, distance to roads, and distance to water bodies (Table 2). Each resistance factor was standardized using a five-level classification system ranging from 1 to 5. Using the analytic hierarchy process (AHP) [48], the relative weights of each factor was

evaluated. Finally, the resistance surface was generated by performing a weighted overlay of all resistance factors using the raster calculator within a spatial overlay analysis model.

Table 2. Resistance values and weights.

Resistance Factor	Resistance Value					Weights
	1	2	3	4	5	
LULC	Water	Forest	Grassland	Cropland	Artificial surface	0.06
NDVI	0.67–0.86	0.60–0.67	0.52–0.60	0.39–0.52	0.04–0.39	0.34
DEM	703–1740	399–703	219–399	98–219	0–98	0.11
Slope	32–73	21–32	12–21	5–12	0–5	0.09
Distance to the road (m)	>27,370	16,572–27,370	9683–16,571	4468–9682	<4468	0.18
Distance to the water (m)	<2275	2275–5149	5150–8862	8863–14,851	>14,851	0.22

2.3.4. Extraction of Ecological Corridors, Ecological Pinch Points, and Ecological Barrier Points

Ecological corridors, as structural elements of ecological networks, play a crucial role in maintaining ecosystem service functions. By connecting discretely distributed ecological source areas, they provide spatial carriers for species migration and ecological processes, thereby ensuring the transmission efficiency of ecological flows, material flows, and energy flows at a regional scale [49]. Ecological pinch points refer to critical nodes in the topological structure, often acting as temporary habitats with frequent biological activity or intersections of migration paths, and are essential for maintaining ecological connectivity. In contrast, ecological barrier points are spatial units with significant obstructive effects, whose high resistance characteristics weaken corridor connectivity [46].

In this study, ecological corridors were constructed using the Build Network and Map Linkages modules within the Linkage Mapper tool. Based on this, the Pinchpoint Mapper module of the Linkage Mapper tool was employed to identify ecological pinch points. The 'all-to-one' option was selected, and a weighted cost distance of 1000 m was set to obtain the cumulative current density. The resulting data were classified into five levels using the NB method in ArcGIS 10.8, with the fourth and fifth levels defined as ecological pinch points. To identify ecological barriers, the 'Maximum' mode of the 'Barrier Mapper' module in Linkage Mapper was utilized. After multiple trials and adjustments based on regional conditions, the minimum and maximum detection radii were set to 500 m and 1000 m, respectively, to calculate cumulative current density. The results were then classified into five levels using the natural breaks method, with the fourth and fifth levels designated as ecological barrier areas [48].

The current density derived from the Pinchpoint Mapper module represents the total current density passing through a point among all potential paths; the higher the value is, the more critical the area is as a convergence zone for species migration. Meanwhile, the current density in the Barrier Mapper module represents difference between current density of existing landscape and that of a hypothetical landscape without the barrier. A larger difference indicates a more severe obstruction to corridor connectivity caused by the barrier point.

3. Results

3.1. Spatial and Temporal Evolution of Ecosystem Services

The results indicate a clear spatial differentiation in water yield services. The southwestern region exhibits the highest value distribution, including Fangchenggang City, southwestern Qinzhou City, and western Beihai City. The northern and eastern parts of

the Pinglu Canal Economic Zone exhibit predominantly low values, covering Nanning City, Guigang City, Qinzhou City, and Beihai City. The Shiwandashan Mountain Range, known for its rich biodiversity and extensive vegetation cover, supports a diverse range of flora and fauna, which contributes to its relatively high water yield. A distinct spatial trend is observed, with elevated water production in the southwest and reduced levels in adjacent areas (Figure 3). With inter-annual changes, the water yield service shows a decreasing trend, from 925.2 mm in 2000 to 833.1 mm in 2010 and 789.1 mm in 2020. The habitat quality services in the spatial distribution of the Fangchenggang Shiwandashan Mountains are significantly higher than those in other places, where habitat quality values are relatively low (Figure 4). From a temporal perspective, habitat quality exhibited a fluctuating downward trend: it was 0.096 in 2000, increased to 0.104 in 2010, but declined to 0.084 by 2020. Overall, the values remain low, with the mean below 0.1, indicating poor ecological conditions and the urgent need for enhanced environmental management efforts. High-value areas of soil retention services are primarily concentrated in the northern parts of Nanning and Guigang, as well as in Fangchenggang, while the central region generally shows lower values (Figure 5). The soil and water conservation services decrease from 2000 to 2020, with values of 650.8 t/hm^2, 578.9 t/hm^2, and 550.0 t/hm^2. The area with the most serious decrease in soil and water conservation services is located in Nanning City, where the rapid development of real estate as well as urbanization and the ever-expanding construction land have led to a continuous decrease in the vegetation cover of its development areas. This triggers the problem of soil and water erosion. The most significant reduction in soil retention services was observed in Nanning City. This decline is primarily attributed to the rapid expansion of construction land driven by real estate development and urbanization, which has led to a continuous decrease in vegetation cover and subsequently triggered issues such as soil erosion. In terms of spatial distribution, carbon storage services exhibit higher values in the southern part of the Pinglu Canal Economic Zone, while lower values are observed in the northern regions, demonstrating a spatial pattern characterized as "high in the south and low in the north". The low value zone is located in construction land and bare land, especially in Nanning City and Guigang City, and the values of carbon storage in and around the urban agglomerations are low (Figure 6). From the time dimension, the carbon stock also shows a decreasing trend, with 27.1 t/hm^2 in 2000, 26.7 t/hm^2 in 2010, and 26.2 t/hm^2 in 2020. This is different from the soil and water conservation service, which is decreasing at a more moderate rate, and the value does not change much (Figure 7).

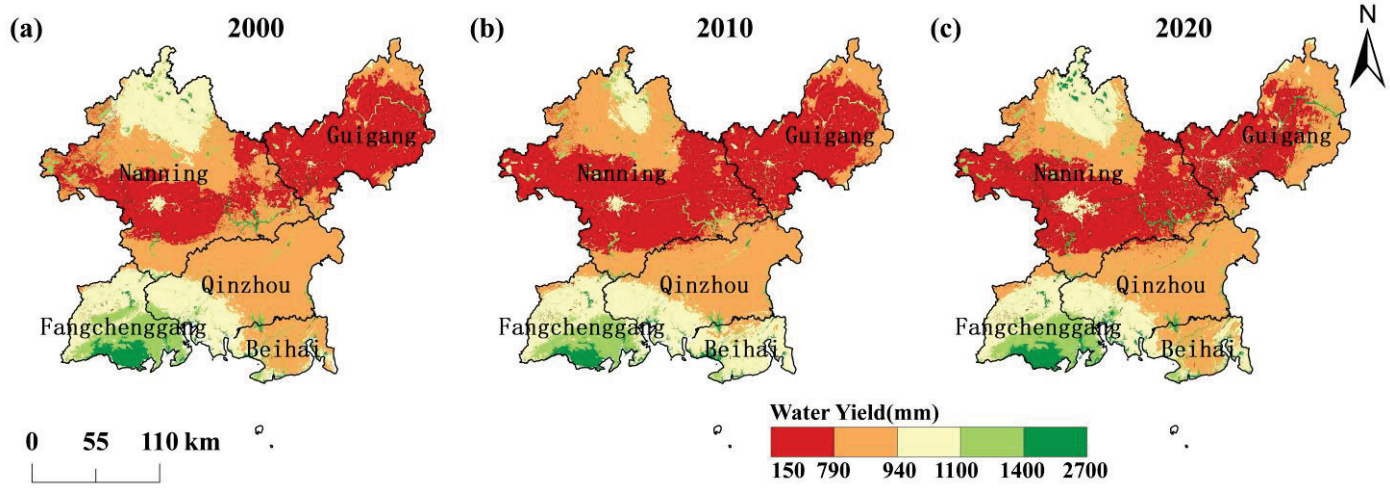

Figure 3. Spatial distribution of water yield, 2000–2020. (**a**) Spatial distribution of water yield in 2000; (**b**) Spatial distribution of water yield in 2010; (**c**) Spatial distribution of water yield in 2020.

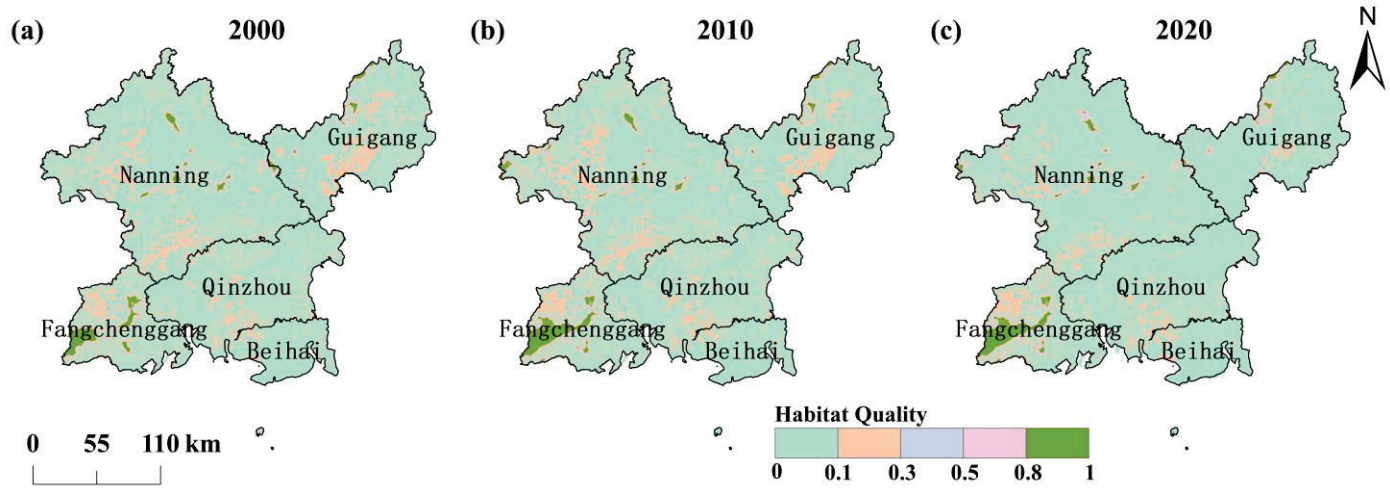

Figure 4. Spatial distribution of habitat quality, 2000–2020. (**a**) Spatial distribution of habitat quality in 2000; (**b**) Spatial distribution of habitat quality in 2010; (**c**) Spatial distribution of habitat quality in 2020.

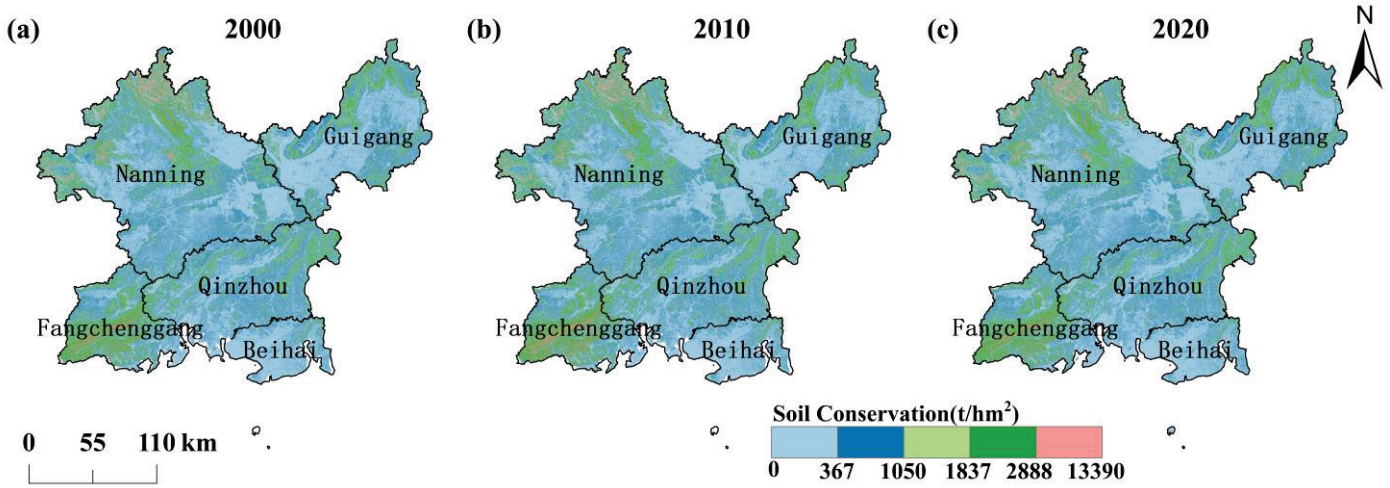

Figure 5. Spatial distribution of soil conservation, 2000–2020. (**a**) Spatial distribution of soil conservation in 2000; (**b**) Spatial distribution of soil conservation in 2010; (**c**) Spatial distribution of soil conservation in 2020.

Regarding the spatial pattern of overall ecosystem service significance, areas of moderate and relatively high importance are primarily located in Nanning, Guigang, and Beihai. Meanwhile, the southwestern and central parts of Fangchenggang City were marked by clusters of highly and extremely important areas, including the northern region of Nanning and the northwest section of Guigang (Figure 8a). The spatial distribution of ES importance levels in the Pinglu Canal Economic Zone is characterized as "lower in the center and higher at the periphery".

Finally, ecological source area was mainly located in Fangchenggang, Nanning, and Guigang, with an area of 1687.6 km^2, i.e., most of the area was located in Fangchenggang Shiwandashan Nature Reserve and Nanning Daming Mountain Nature Reserve, which was consistent with areas of high and very high ecosystem service importance in the comprehensive ecosystem service importance (Figure 8b).

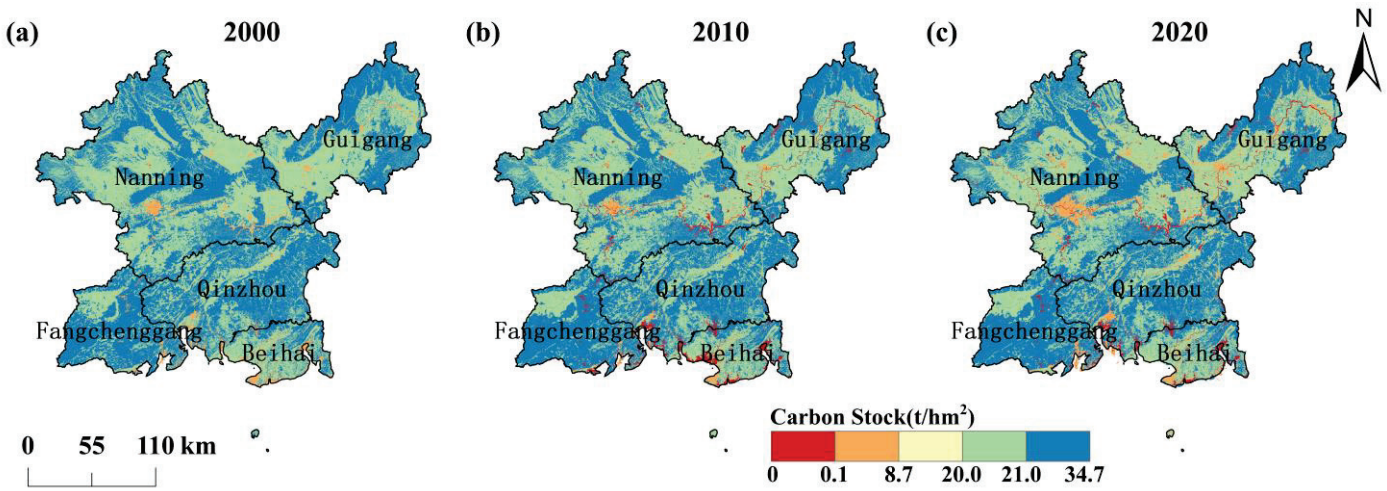

Figure 6. Spatial distribution of carbon stock, 2000–2020. (**a**) Spatial distribution of carbon stock in 2000; (**b**) Spatial distribution of carbon stock in 2010; (**c**) Spatial distribution of carbon stock in 2020.

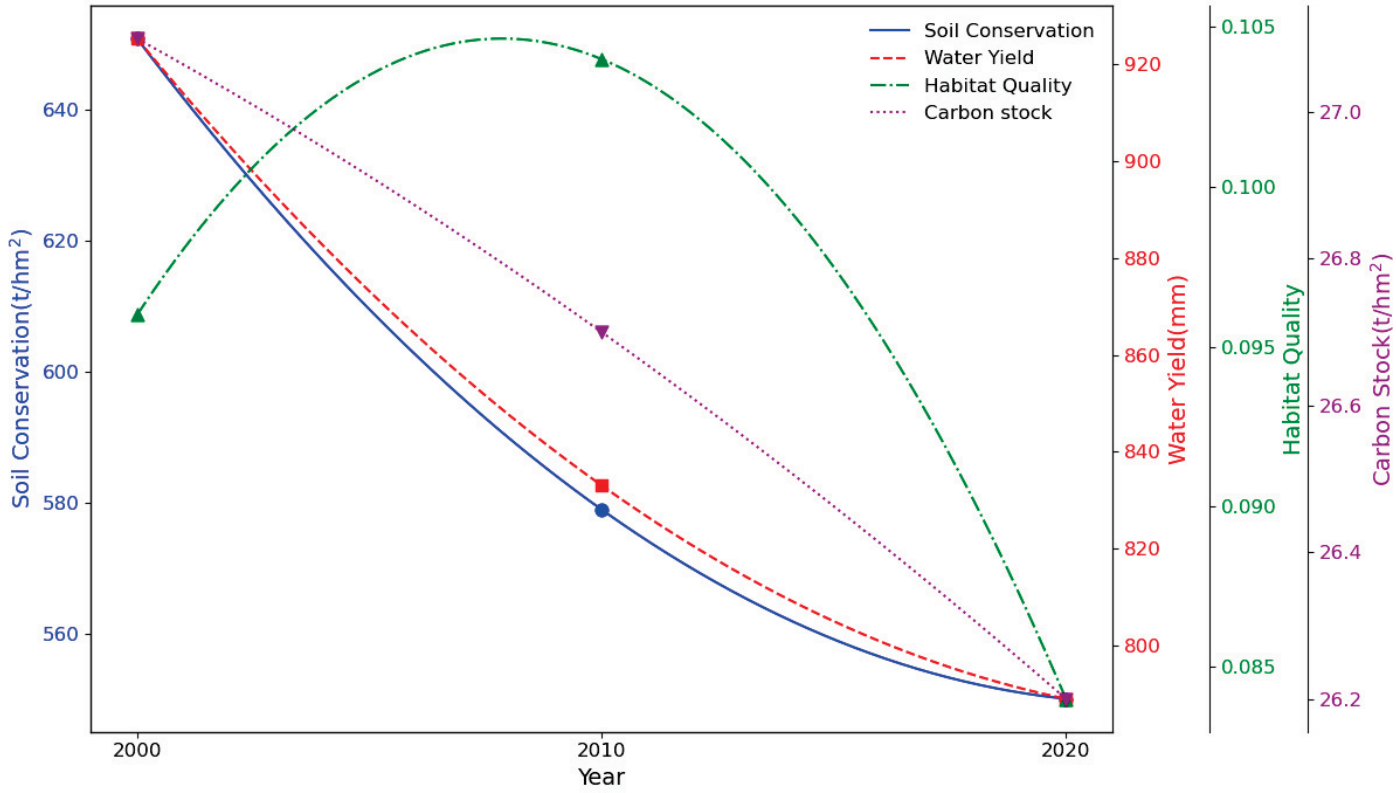

Figure 7. Changes in four ecosystem services in the Pinglu Canal Economic Zone, 2000–2020.

3.2. Resistance Analysis

Based on the figure, the ecological resistance values within the Pinglu Canal Economic Belt range from 1 to 4.83 (Figure 9). Overall, the spatial distribution of resistance values exhibits a decreasing trend from the central areas toward the periphery. High-resistance zones are primarily concentrated in densely built-up urban areas and regions with intense human activity. Notably, the cores of major cities exhibit significantly higher resistance values compared to surrounding areas. These elevated resistance levels are attributed to rapid urbanization and extensive land development, which have severely disrupted natural ecological processes and impeded species migration and ecological flows. In contrast, low-resistance areas are mainly distributed along the outer edges of the study area and largely

coincide with key ecological source locations. These zones are predominantly located in ecologically favorable regions, including Fangchenggang, the northern part of Nanning, and the northeastern part of Qinzhou. Characterized by extensive ecological forest land and low levels of land development, these areas maintain strong ecological connectivity and facilitate the continuity of ecological processes and species dispersal.

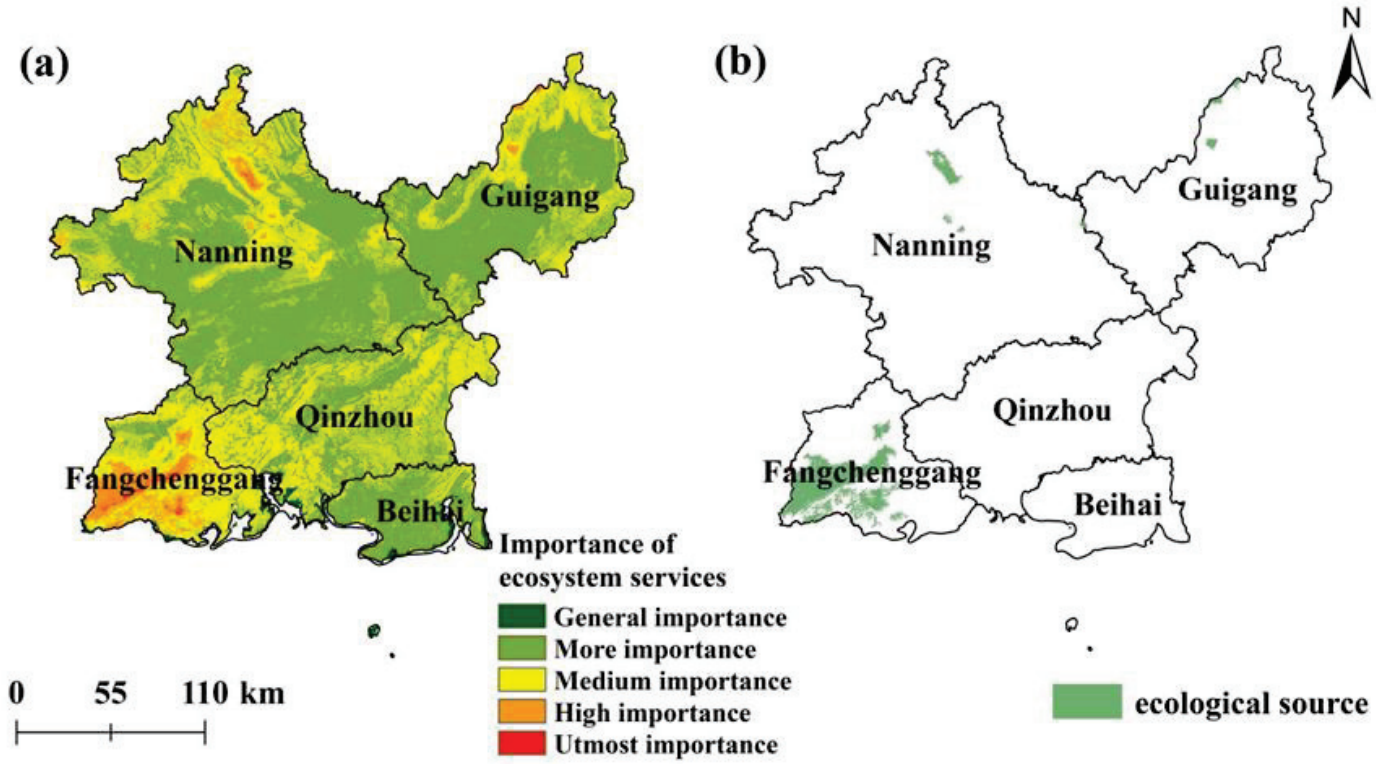

Figure 8. Integrating ecosystem service importance and ecological source. (**a**) Spatial distribution of ecosystem service importance; (**b**) Spatial distribution of ecological source.

3.3. Ecological Corridor Identification

The results indicate that the identified ecological corridors span across Nanning, Guigang, Qinzhou, and Fangchenggang (Figure 10), with a total of 28 corridors extracted, amounting to a combined length of 1426.4 km. Multiple corridors connect each ecological source, significantly enhancing species mobility and overall ecological connectivity. Specifically, the corridors linking ecological sources in Nanning and Guigang primarily extend along the boundary of the study area, while those between Guigang and Fangchenggang run approximately parallel to the Pinglu Canal. The land use along these corridors is predominantly cropland and forest, which helps to mitigate the barrier effect of urban construction land on species migration and supports the functional integrity of the corridors. Overall, the ecological corridors in the study area exhibit a triangular spatial pattern, providing stable and continuous pathways for species migration and dispersal among ecological sources in Nanning, Guigang, and Fangchenggang.

3.4. Ecological Security Pattern Construction

The cumulative current density of ecological pinch points ranges from 0 to 53.8, primarily distributed across western Guigang and the forested northern slopes of the Shiwandashan Mountains in Fangchenggang. These areas are predominantly covered by forest and grassland, providing favorable conditions for ecological connectivity (Figure 11). In contrast, ecological barrier points exhibit a cumulative current density ranging from 0 to 6.5 and are concentrated in the central and northeastern parts of Nanning, as well

as the western urbanized regions of Guigang. Owing to the high ecological resistance in these areas, the formation and connectivity of ecological corridors are impeded, thereby weakening the overall functionality of the regional ecological network (Figure 11). The ESP constructed consists of three key components: ecological corridors, pinch points, and barrier points (Figure 12). Sixteen ecological sources were recognized, covering an area of 1687.6 km^2. Additionally, 28 ecological corridors were delineated, totaling 1426.4 km in length. Eight ecological pinch points were extracted, occupying 44.1 km^2. In total, 119 ecological barrier points were identified, occupying 685.7 km^2. Overall, ecological sources show a generally unbalanced layout, with Nanning, Fangchenggang, and Guigang, emerging as a major cluster area, while no sources were identified in Qinzhou and Beihai. As a result, ecological corridors are mainly distributed among the aforementioned three cities, forming a distinct "triangular" spatial configuration.

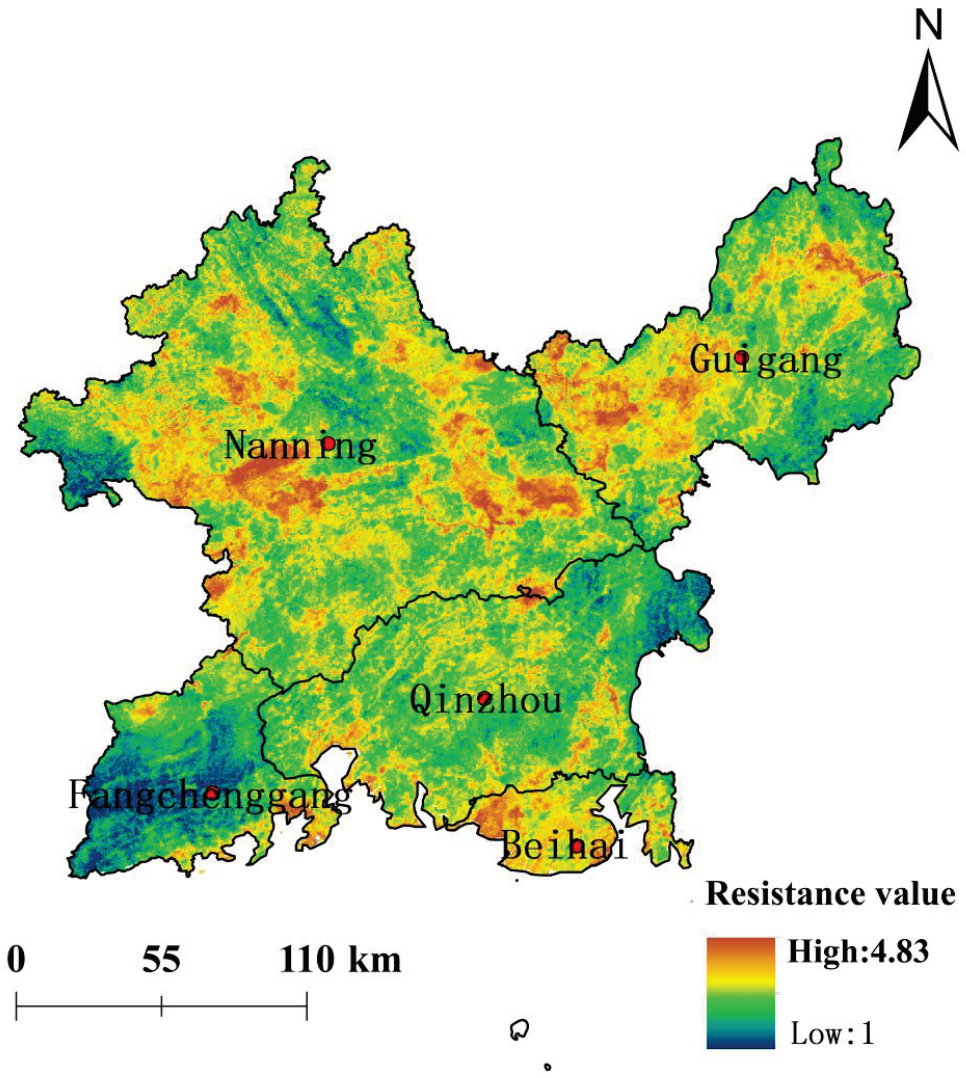

Figure 9. Resistance surface.

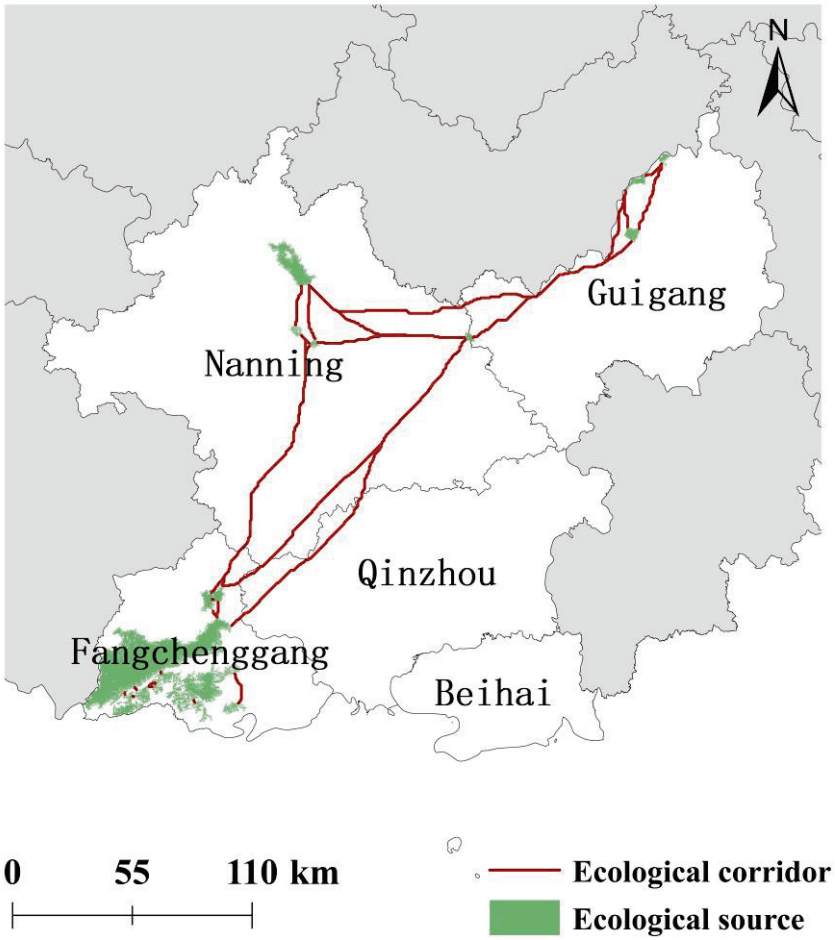

Figure 10. Schematic diagram of the ecological corridor.

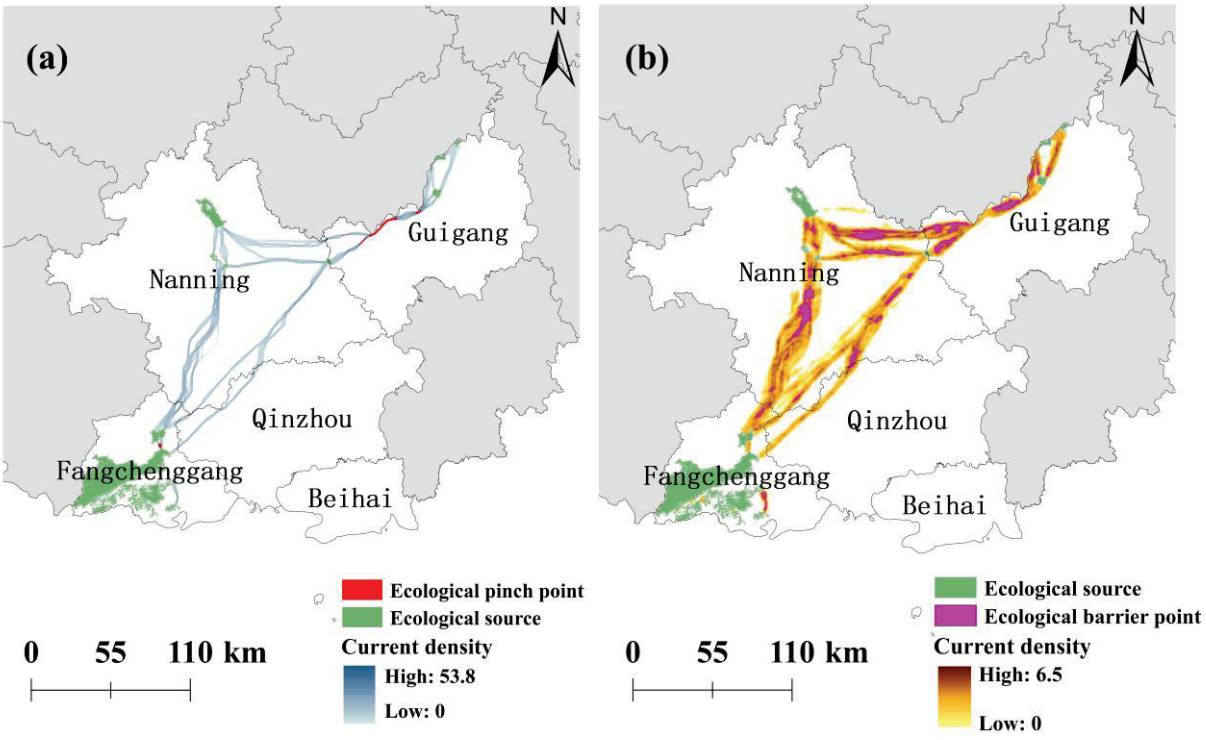

Figure 11. Spatial arrangement of ecological pinch points and ecological barrier points. (**a**) Ecological pinch point extraction results; (**b**) Ecological barrier point extraction results.

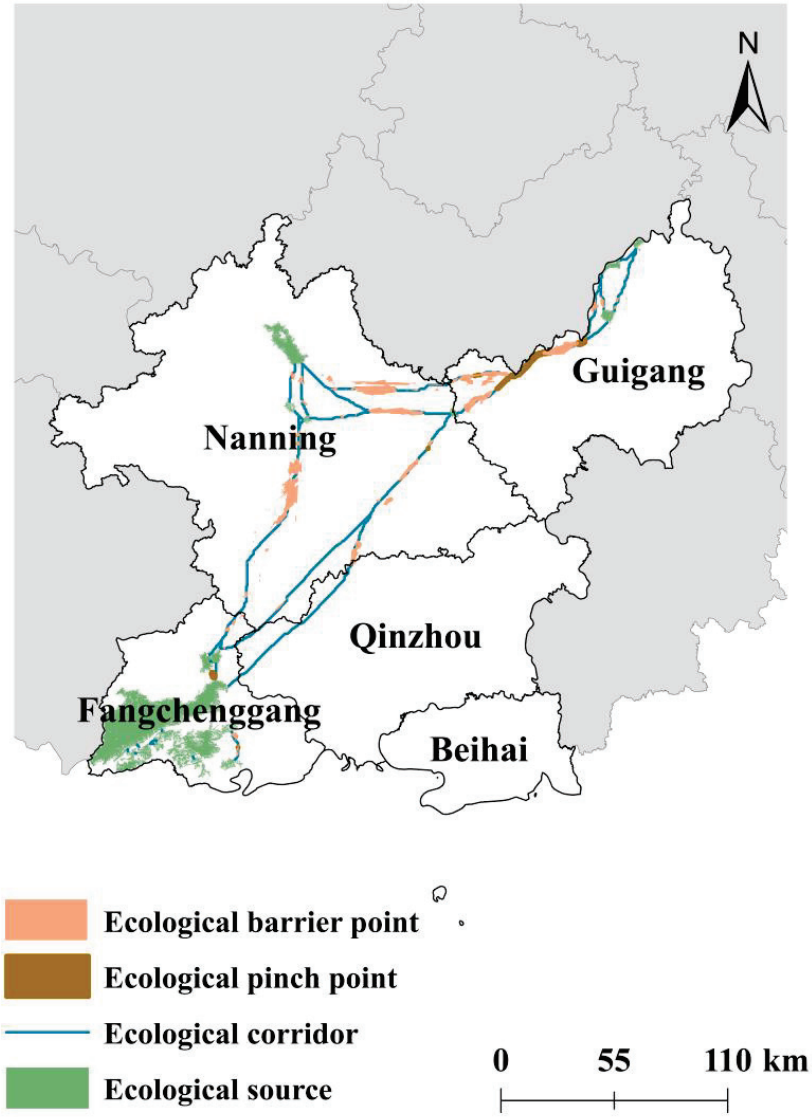

Figure 12. Pinglu Canal ecological security patterns.

4. Discussion

This study employed the InVEST model in conjunction with circuit theory to develop the ESP of the Pinglu Canal Economic Zone. It is worth noting that the habitat quality is poor in most areas of the Pinglu Canal Economic Zone, which also indicates the relatively low vegetation cover. The poor habitat quality also indirectly affects the water yield service, soil and water conservation service, and carbon storage service, which leads to a decreasing trend. The four ecosystem services share the common feature of being higher in the forested and grassland areas and lower in the urban agglomerations and watershed areas. In addition, soil and water conservation, habitat quality, water yield, and carbon storage are also affected by multiple factors such as soil properties, climatic conditions, and human activities. Therefore, corresponding measures should be taken to protect and restore them. First, land use should be rationally planned to reduce unreasonable agricultural and industrial development. Particularly in regions facing a high risk of soil erosion, strategies like reforestation of farmland and restoration of pastures to grassland should be adopted to enhance soil and water conservation capacity in the Pinglu Canal Economic Zone. Second, a monitoring and assessment system for ecosystem services should be established so that protection and restoration measures can be adjusted in a timely manner. In the southeastern part of the study area—coinciding with the location of the Pinglu Canal—ecological corridors are no-

tably absent. Therefore, greater emphasis should be placed on ecological protection during the canal's construction, including the artificial restoration of grassland and forest ecosystems within the affected areas. The presence of ecological pinch points plays a critical role in enhancing corridor connectivity and is vital for conserving biodiversity. Accordingly, ecological protection efforts should be strengthened, particularly for grasslands and forests, to expand the spatial extent of pinch points and further improve the functional connectivity of ecological corridors.

Based on the identified ESP and from the perspective of ecological restoration, protection, and development, this study proposes an ecological optimization framework characterized by the "three belts and three zones", with priority conservation areas as the foundation (Figure 13). Specifically, the "three belts" refer to (1) the ecological security protection belt connecting the Damingshan ecological source area in western Nanning with the Shiwandashan ecological source area; (2) the ecological barrier belt linking Damingshan in Nanning with Pingtian Mountain in Guigang; and (3) the ecological construction belt connecting Pingtian Mountain and Shiwandashan. The ecological safety protection belt in the west and the ecological barrier belt in the north may expand the area of ecological safety buffer zones for the ecological corridors in the west and the north. The construction of animal-specific corridors and fish migration facilities can be used to solve the problem of animal migration and increase the ability of cross-regional exchange of organisms. Constructing an eastern ecological corridor construction zone can increase the number of ecological corridors between the central part of the Pinglu Canal Economic Zone and the southern and northern regions, increasing ecological connectivity. In terms of measures, additional ecological conservation zones can be set up to form a "multi-corridor and multi-zone" ecological pattern. The "three zones" refer to ecological protection zones, ecological conservation development zones, and ecological obstacle restoration zones. Among them, the establishment of ecological protection zones in places where ecological sources are located can provide stable living space for plants and animals in the area. Biodiversity monitoring stations are set up to regularly assess the changes in the number of plants and animals in the ecological reserve, so as to dynamically adjust the protection measures. Since the habitats in northwestern Nanning and Beihai are of relatively low quality and dominated by woodlands and grasslands, the establishment of ecological conservation and development zones around the urban construction sites will contribute to ecological restoration. Regular monitoring of the vegetation cover of the Pinglu Canal Economic Zone can be implemented using remote sensing satellites such as Gaofen-1. When the vegetation cover is greatly reduced, the area of ecological damage can be quickly identified. Areas such as the central part of Nanning City and the northern part of the Pinglu Canal Economic Zone are the main concentration areas of ecological obstacle points. The ecological obstacle restoration area is constructed, and animal activity sensors, cameras, and acoustic recorders are deployed in areas with large ecological obstacle points to grasp the migration of animals in real time, so as to manage the ecological environment.

This study constructed the ESP of the Pinglu Canal Economic Belt. However, the following shortcomings exist: (1) Although the ecological corridors in the Pinglu Canal Economic Zone have been identified using the relevant tools of circuit theory (Linkage Mapper plug-in), the connectivity of the extracted ecological corridors cannot be accurately verified owing to the absence of sustained ecological observation records (e.g., animal migratory paths and biodiversity data) in the Pinglu Canal Economic Zone. (2) The current research only conducted a superficial analysis of four ecological service impact factors and failed to further identify key driving forces. (3) During the construction of the resistance surface, its weight assignment was determined using hierarchical analysis. However, the

measured resistance value in the Pinglu Canal Economic Zone could not be obtained, and the results of the construction of the resistance surface could not be verified. (4) No prediction of the future evolution of the ESP was made because the lack of soil data from past years and DEM data prevented the input of accurate and relevant parameters into the prediction model, which led to the inability to derive and validate the accurate results of the ESP in future scenarios. In future studies, better models and methods should be used to predict future ESPs.

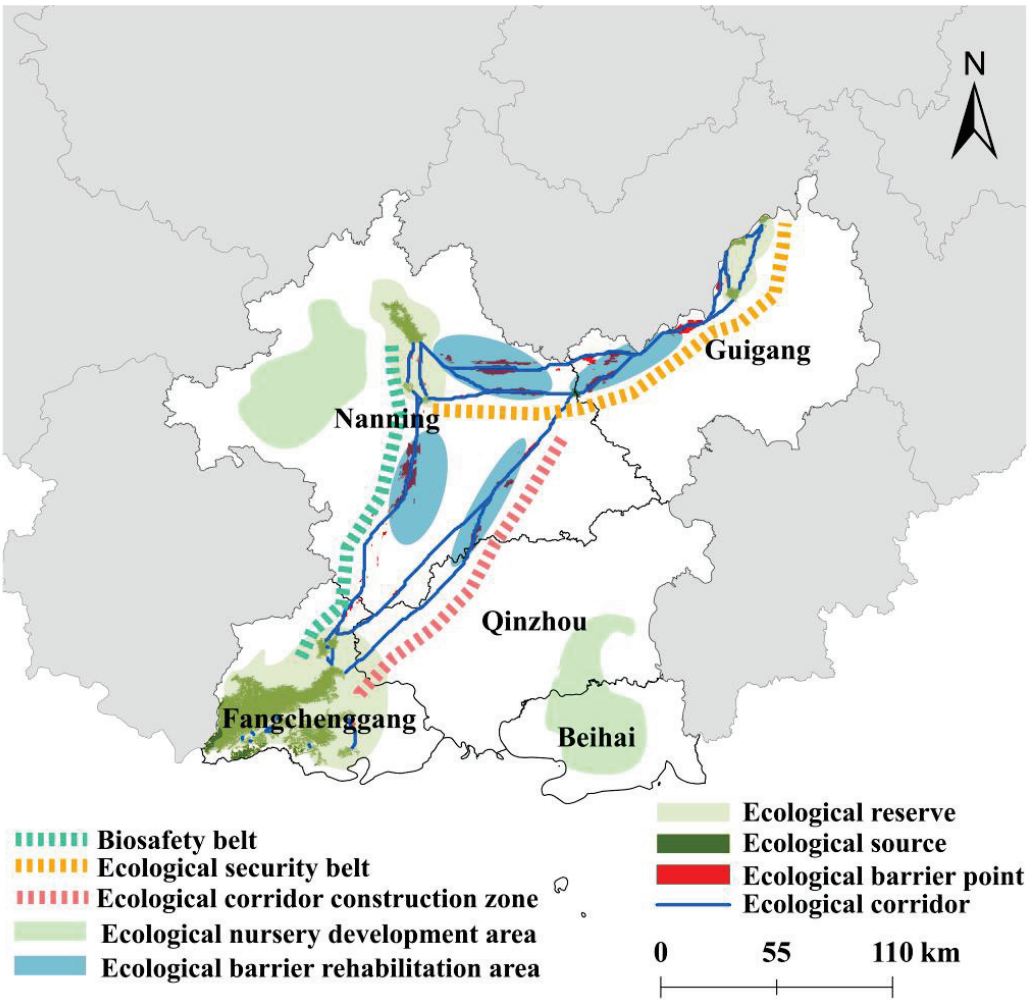

Figure 13. Optimization of the ESP of the Pinglu Canal Economic Zone.

5. Conclusions

(1) The values of the four ecosystem services were relatively high in the southwestern, northwestern, and northeastern regions of the Pinglu Canal Economic Zone but showed an overall declining trend for 2000–2020. Highly and extremely important ecosystem service zones were mainly distributed in woodland and grassland areas in southwestern and central Fangchenggang, northern Nanning, and northwestern Guigang, while moderately and generally important zones were concentrated in urban and construction land areas.

(2) The resistance values of the resistance surface range from 1 to 4.83. The high resistance area is located in the urban agglomeration area, while the low resistance area is located in the boundary of the study area. Most of the ecological source sites overlap, and the overall presentation exhibits a "center of the high, the edge of the low" spatial distribution pattern.

(3) A total of 16 ecological sources (1687.6 km^2), 28 ecological corridors (1426.4 km), 8 ecological pinch points (44.1 km^2), and 119 ecological barriers (685.7 km^2) were identified

in the study area, with ecological corridors exhibiting a roughly triangular spatial distribution. Based on ecological conditions, restoration needs, and development dynamics, an optimized ecological security pattern comprising "three belts" (ecological protection belt, ecological barrier belt, ecological construction belt) and "three zones" (ecological protection zone, ecological maintenance and development zone, ecological barrier restoration zone) is proposed to support the balance between ecological integrity and economic development in the Pinglu Canal Economic Zone.

Author Contributions: Z.D. and B.H. conceived the study; Z.D. developed the methodology and implemented the software; validation was performed by Z.D., C.G. and S.W.; Z.D., J.R. and Y.L. conducted the formal analysis; Z.D. carried out the investigation and curated the data; resources were provided by Z.D.; the original draft was written by Z.D.; Z.D., C.G. and B.H. contributed to the review and editing of the manuscript; visualizations were prepared by Z.D.; B.H. supervised the work; Z.D. managed the project; funding was secured by B.H. All authors have read and agreed to the published version of the manuscript.

Funding: This research was funded by Guangxi Science and Technology Major Project, grant number AA24263011; Guangxi Science and Technology Major Project, grant number AA23062039-2; and National Natural Science Foundation of China, grant number 42071135.

Data Availability Statement: The original contributions presented in the study are included in the article, further inquiries can be directed to the corresponding author.

Conflicts of Interest: The authors declare no conflict of interest.

References

1. Liu, D.; Chang, Q. Ecological security research progress in China. *Acta Ecol. Sin.* **2015**, *35*, 111–121. [CrossRef]
2. Xiao, D.; Xie, F.; Wei, J. Regional ecological construction and mission of landscape ecology. *Ying Yong Sheng Tai Xue Bao* **2004**, *15*, 1731–1736.
3. Xiang, H.; Zhang, J.; Mao, D.; Wang, M.; Yu, F.; Wang, Z.; Li, H. Optimizing ecological security patterns considering zonal vegetation distribution for regional sustainability. *Ecol. Eng.* **2023**, *194*, 107055. [CrossRef]
4. Li, S.; Zhao, Y.; Xiao, W.; Yue, W.; Wu, T. Optimizing ecological security pattern in the coal resource-based city: A case study in Shuozhou City, China. *Ecol. Indic.* **2021**, *130*, 108026. [CrossRef]
5. Nie, W.; Xu, B.; Yang, F.; Shi, Y.; Liu, B.; Wu, R.; Lin, W.; Pei, H.; Bao, Z. Simulating future land use by coupling ecological security patterns and multiple scenarios. *Sci. Total Environ.* **2023**, *859*, 160262. [CrossRef]
6. Cao, C.; Luo, Y.; Xu, L.; Xi, Y.; Zhou, Y. Construction of ecological security pattern based on InVEST-Conefor-MCRM: A case study of Xinjiang, China. *Ecol. Indic.* **2024**, *159*, 111647. [CrossRef]
7. Liu, M.; Peng, J.; Dong, J.; Jiang, H.; Xu, D.; Meersmans, J. Trade-offs of landscape connectivity between regional and interregional ecological security patterns in a junction area of Beijing-Tianjin-Hebei region. *Appl. Geogr.* **2024**, *167*, 103272. [CrossRef]
8. Peng, J.; Zhao, S.; Dong, J.; Liu, Y.; Meersmans, J.; Li, H.; Wu, J. Applying ant colony algorithm to identify ecological security patterns in megacities. *Environ. Model. Softw.* **2019**, *117*, 214–222. [CrossRef]
9. Zhu, Y.; Liu, Y.; Xiao, Y.; Liu, J.; Zhao, Z.; Li, Y.; Hao, Q.; Liu, C.; Li, J. Construction of Ecological Security Patterns Incorporating Multiple Types of Ecological Service Functions for Developed Coastal Regions: A Case Study in Jinjiang Watershed, China. *Land* **2024**, *13*, 1227. [CrossRef]
10. Zheng, Y.; Tang, P.; Dong, L.; Yao, Z.; Guo, J. Evaluation of ecological carrying capacity and construction of ecological security pattern in West Liaohe River Basin of China. *Front. Ecol. Evol.* **2024**, *12*, 1335671. [CrossRef]
11. Zhai, Y.; Zhai, G.; Yu, Z.; Ma, X.; Lu, Z.; Chen, Y.; Liu, J. Constructing the ecological security pattern of the Daqing River Basin for the high-standard ecological construction of Xiong'an New Area, China. *Environ. Dev. Sustain.* **2024**, *6*, 1–24. [CrossRef]
12. Dong, R.; Zhang, X.; Li, H. Constructing the Ecological Security Pattern for Sponge City: A Case Study in Zhengzhou, China. *Water* **2019**, *11*, 284. [CrossRef]
13. Bi, Y.; Zheng, L.; Wang, Y.; Li, J.; Yang, H.; Zhang, B. Coupling relationship between urbanization and water-related ecosystem services in China's Yangtze River economic Belt and its socio-ecological driving forces: A county-level perspective. *Ecol. Indic.* **2023**, *146*, 109871. [CrossRef]
14. Zhang, B.; Cao, J.; Chen, D.; Li, X.; Liu, Y.; Wang, J.; Liu, T. Construction of watershed ecological security patterns with integrated of spatial variability: A case study of the Yellow River Basin, China. *Ecol. Indic.* **2024**, *159*, 111663. [CrossRef]

15. Zhang, F.; Jia, Y.; Liu, X.; Li, T.; Gao, Q. Application of MSPA-MCR models to construct ecological security pattern in the basin: A case study of Dawen River basin. *Ecol. Indic.* **2024**, *160*, 111887. [CrossRef]
16. Chen, W.; Liu, H.; Wang, J. Construction and optimization of regional ecological security patterns based on MSPA-MCR-GA Model: A case study of Dongting Lake Basin in China. *Ecol. Indic.* **2024**, *165*, 112169. [CrossRef]
17. Zhang, Y.; Zhao, Z.; Fu, B.; Ma, R.; Yang, Y.; Lü, Y.; Wu, X. Identifying ecological security patterns based on the supply, demand and sensitivity of ecosystem service: A case study in the Yellow River Basin, China. *J. Environ. Manag.* **2022**, *315*, 115158. [CrossRef] [PubMed]
18. Chen, J.; Wang, S.; Zou, Y. Construction of an ecological security pattern based on ecosystem sensitivity and the importance of ecological services: A case study of the Guanzhong Plain urban agglomeration, China. *Ecol. Indic.* **2022**, *136*, 108688. [CrossRef]
19. Peng, J.; Yang, Y.; Liu, Y.; Du, Y.; Meersmans, J.; Qiu, S. Linking ecosystem services and circuit theory to identify ecological security patterns. *Sci. Total Environ.* **2018**, *644*, 781–790. [CrossRef]
20. Han, P.; Hu, H.; Jiang, M.; Wang, M. Construction of Wetland Ecological Security Pattern in Wuhan Metropolitan Core Area Considering Wetland Ecological Risk. *Land* **2024**, *13*, 1407. [CrossRef]
21. Huang, L.; Chen, Z.; Yang, Z.; Chen, M.; Chen, X.; Zhai, T.; Qiu, T. Integrating "quality-risk-demand" framework and circuit theory to identify spatial range and priority area of ecological security pattern in a rapidly urbanizing landscape. *Ecol. Inform.* **2024**, *82*, 102673. [CrossRef]
22. Ma, J.; Mei, Z.; Wang, X.; Li, S.; Liang, J. Ecological Security Pattern Construction and Multi-Scenario Risk Early Warning (2020–2035) in the Guangdong–Hong Kong–Macao Greater Bay Area, China. *Land* **2024**, *13*, 1267. [CrossRef]
23. Dai, L.; Liu, Y.; Luo, X. Integrating the MCR and DOI models to construct an ecological security network for the urban agglomeration around Poyang Lake, China. *Sci. Total Environ.* **2021**, *754*, 141868. [CrossRef] [PubMed]
24. Liu, X.; Su, Y.; Li, Z.; Zhang, S. Constructing ecological security patterns based on ecosystem services trade-offs and ecological sensitivity: A case study of Shenzhen metropolitan area, China. *Ecol. Indic.* **2023**, *154*, 110626. [CrossRef]
25. Huang, K.; Peng, L.; Wang, X.; Deng, W. Integrating circuit theory and landscape pattern index to identify and optimize ecological networks: A case study of the Sichuan Basin, China. *Environ. Sci. Pollut. Res.* **2022**, *29*, 66874–66887. [CrossRef]
26. Zhou, G.; Huan, Y.; Wang, L.; Zhang, R.; Liang, T.; Han, X.; Feng, Z. Constructing a multi-leveled ecological security pattern for improving ecosystem connectivity in the Asian water Tower region. *Ecol. Indic.* **2023**, *154*, 110597. [CrossRef]
27. Cheng, W.; Ma, C.; Li, T.; Liu, Y. Construction of Ecological Security Patterns and Evaluation of Ecological Network Stability under Multi-Scenario Simulation: A Case Study in Desert–Oasis Area of the Yellow River Basin, China. *Land* **2024**, *13*, 1037. [CrossRef]
28. Fu, Y.; Zhang, W.; Gao, F.; Bi, X.; Wang, P.; Wang, X. Ecological Security Pattern Construction in Loess Plateau Areas—A Case Study of Shanxi Province, China. *Land* **2024**, *13*, 709. [CrossRef]
29. Luo, M.; Jia, X.; Zhao, Y.; Wang, H.; Chen, C.; Li, D.; Yang, S.; Li, J. The Temporal and Spatial Characteristics of Ecological Security Pattern in the Loess Plateau, China. *Land* **2024**, *13*, 570. [CrossRef]
30. Wang, N.; Zhao, Y. Construction of an ecological security pattern in Jiangnan water network area based on an integrated Approach: A case study of Gaochun, Nanjing. *Ecol. Indic.* **2024**, *158*, 111314. [CrossRef]
31. Wang, Y.; Qu, Z.; Zhong, Q.; Zhang, Q.; Zhang, L.; Zhang, R.; Yi, Y.; Zhang, G.; Li, X.; Liu, J. Delimitation of ecological corridors in a highly urbanizing region based on circuit theory and MSPA. *Ecol. Indic.* **2022**, *142*, 109258. [CrossRef]
32. Li, S.; Xiao, W.; Zhao, Y.; Lv, X. Incorporating ecological risk index in the multi-process MCRE model to optimize the ecological security pattern in a semi-arid area with intensive coal mining: A case study in northern China. *J. Clean. Prod.* **2020**, *247*, 119143. [CrossRef]
33. Xu, J.; Fan, F.; Liu, Y.; Dong, J.; Chen, J. Construction of ecological security patterns in nature reserves based on ecosystem services and circuit theory: A case study in Wenchuan, China. *Int. J. Environ. Res. Public Health* **2019**, *16*, 3220. [CrossRef] [PubMed]
34. Dickson, B.G.; Albano, C.M.; Anantharaman, R.; Beier, P.; Fargione, J.; Graves, T.A.; Gray, M.E.; Hall, K.R.; Lawler, J.J.; Leonard, P.B. Circuit-theory applications to connectivity science and conservation. *Conserv. Biol.* **2019**, *33*, 239–249. [CrossRef]
35. Xing, P.; Pan, H. New era canal strategy and practice of Pinglu Canal planning andconstruction. *Port Waterw. Eng.* **2024**, *9*, 1–6.
36. Yao, H.; Li, L.; Hu, Y.; Chen, Z.; Sun, P.; Feng, H.; Jin, Z. River-sea intermodal transportation plan of Pinglu Canal in Beibu Gulf Port. *Port Waterw. Eng.* **2024**, *9*, 14–19.
37. Han, W.; Xia, S.; Zhou, W.; Shen, Y.; Su, X.; Liu, G. Constructing ecological security pattern based on ecological corridor identification in Lhasa River Basin. *Acta Ecol. Sin.* **2023**, *43*, 8948–8957.
38. Jahun, B.; Ibrahim, R.; Dlamini, N.; Musa, S. Review of soil erosion assessment using RUSLE model and GIS. *J. Biol. Agric. Healthc.* **2015**, *5*, 36–47.
39. Liu, Z.; Liu, Z.; Zhou, Y.; Huang, Q. Distinguishing the impacts of rapid urbanization on ecosystem service trade-offs and synergies: A case study of shenzhen, China. *Remote Sens.* **2022**, *14*, 4604. [CrossRef]
40. Xue, Q.; Lu, L.; Niu, R.; Zhang, X.; Du, W. Identification and restoration of key areas of ecological security pattern based on sensitivity to geological disasters: A case study of Jinan City. *Acta Ecol. Sin.* **2021**, *41*, 9050–9063.

41. Huang, X. Study on Land Use Change and Ecosystem Services Trade-Off in Karst-Coastal Zone of Southwest Guangxi. Master's Thesis, Nnaning Normal University, Nanning, China, 2021.
42. Bai, L.; Feng, X.; Sun, R.; Gao, H. Spatial and temporal responses of habitat quality to urbanization: A case study of Changchun City, Jilin Province, China. *Ying Yong Sheng Tai Xue Bao* **2020**, *31*, 1267–1277. [PubMed]
43. Luo, R.; Yang, S.; Wang, Z.; Zhang, T.; Gao, P. Impact and trade off analysis of land use change on spatial pattern of ecosystem services in Chishui River Basin. *Environ. Sci. Pollut. Res.* **2022**, *29*, 20234–20248. [CrossRef] [PubMed]
44. Chen, X. Estimation of soil organic carbon reserves in Guangxi and comparion study with some provinces in China. *Sci. Geogr. Sin.* **2014**, *34*, 1247–1253.
45. Liao, J.; Jiao, J.; Yan, Z.; Li, J.; Zhang, S. Simulation Effect Analysis of RUSLE Model on Slope Soil Erosion Restored by Reclaimed Vegetation in Loess Plateau. *J. Soil Water Conserv.* **2024**, *38*, 97–108.
46. Chen, W.; Liu, X.; Li, H.; Sun, X.; Wang, Y.; Liu, X.; Xing, L.; Wan, R.; Luo, X.; Wan, C.; et al. Ecosystem service function and security pattern of Tianshan Mountains in Xinjiang from 1990 to 2050. *Geol. China* **2024**, *51*, 1644–1663.
47. Spear, S.F.; Balkenhol, N.; Fortin, M.J.; Mcrae, B.H.; Scribner, K. Use of resistance surfaces for landscape genetic studies: Considerations for parameterization and analysis. *Mol. Ecol.* **2010**, *19*, 3576–3591. [CrossRef]
48. Zhang, Z.; Hu, B.; Jiang, W.; Qiu, H. Construction of ecological security pattern based on ecological carrying capacity assessment 1990–2040: A case study of the Southwest Guangxi Karst-Beibu Gulf. *Ecol. Model.* **2023**, *479*, 110322. [CrossRef]
49. Wang, X.; Chen, T.; Feng, Z.; Wu, K.; Lin, Q. Construction of ecological security pattern based on boundary analysis: A case study on Jiangsu Province. *Acta Ecol. Sin.* **2020**, *40*, 3375–3384.

Disclaimer/Publisher's Note: The statements, opinions and data contained in all publications are solely those of the individual author(s) and contributor(s) and not of MDPI and/or the editor(s). MDPI and/or the editor(s) disclaim responsibility for any injury to people or property resulting from any ideas, methods, instructions or products referred to in the content.

MDPI AG
Grosspeteranlage 5
4052 Basel
Switzerland
Tel.: +41 61 683 77 34

Land Editorial Office
E-mail: land@mdpi.com
www.mdpi.com/journal/land

Disclaimer/Publisher's Note: The title and front matter of this reprint are at the discretion of the Guest Editors. The publisher is not responsible for their content or any associated concerns. The statements, opinions and data contained in all individual articles are solely those of the individual Editors and contributors and not of MDPI. MDPI disclaims responsibility for any injury to people or property resulting from any ideas, methods, instructions or products referred to in the content.

Academic Open
Access Publishing

mdpi.com

ISBN 978-3-7258-4594-1